

# Three-Dimensional Free-Radical Polymerization

Gennady V. Korolev · Michael M. Mogilevich

# Three-Dimensional Free-Radical Polymerization

Cross-Linked and Hyper-Branched Polymers

 Springer

Prof. Dr. Gennady V. Korolev<sup>†</sup>

Prof. Dr. Michael M. Mogilevich  
Kaznacheyskaya ulitca  
Dom 13, flat 1  
St. Petersburg 198031  
Russia  
mmmogilevich@mail.ru

Russian edition:

G.V. Korolev, M.M. Mogilevich: Trekhmernaya radicalnaya polimerizatchiya.  
Setchatyae i giperrazvetvlennyae polimerya (2006)  
published by “KhimIzdat Publishing House”, St. Petersburg  
ISBN 5-93808-121-1

ISBN: 978-3-540-87566-6

e-ISBN: 978-3-540-87567-3

DOI 10.1007/978-3-540-87567-3

Library of Congress Control Number: 2008939224

© Springer-Verlag Berlin Heidelberg 2009

This work is subject to copyright. All rights are reserved, whether the whole or part of the material is concerned, specifically the rights of translation, reprinting, reuse of illustrations, recitation, broadcasting, reproduction on microfilm or in any other way, and storage in data banks. Duplication of this publication or parts thereof is permitted only under the provisions of the German Copyright Law of September 9, 1965, in its current version, and permission for use must always be obtained from Springer. Violations are liable to prosecution under the German Copyright Law.

The use of general descriptive names, registered names, trademarks, etc. in this publication does not imply, even in the absence of a specific statement, that such names are exempt from the relevant protective laws and regulations and therefore free for general use.

*Cover design:* WMXDesign GmbH, Heidelberg

Printed on acid-free paper

9 8 7 6 5 4 3 2 1

springer.com

# Preface

At present, three-dimensional free-radical polymerization (TFRP) is a special field of radical polymerization. TFRP is characterized by specific kinetic regularities and mechanisms of processes for the formation of cross-linked or hyper-branched polymers, and they are different from the kinetics and mechanism of classical radical polymerization.

The fundamental studies of kinetics and mechanism of TFRP with formation of cross-linked polymers have been carried out in three stages. The first stage lasted from 1960 until 1983, and the main mechanisms of TFRP of oligo(acrylates) were established during this stage [1–3]. Condensation telomerization, being a universal oligo(acrylate) synthesis procedure, allows us to vary certain molecular parameters, such as length and flexibility of oligomeric blocks, number and type of reactive groups (methacrylic or acrylic groups), and chemical nature of atomic groups of an oligomeric block, which represent the centers of strong intermolecular interactions. For this reason, oligo(acrylates) were very convenient compounds for establishing the main kinetic regularities of TFRP and regularities of formation of polymer three-dimensional cross-linked structures, according to the so-called microheterogeneous mechanism (G.V. Korolev, 1977), at the topological and morphological levels. During the second stage, which lasted from 1983 until 1995, the kinetic regularities of TFRP were studied in depth, and additional evidentiary data in favor of the microheterogeneous mechanism of TFRP were found [4, 5]. The last, or third stage (from 1995 until 2005) involved exploration of TFRP under the “living” chains conditions and identification of new regularities associated with the implementation of these conditions [6], as well as the creation of the new gelation theory applicable to TFRP, investigation into physical and mechanical properties of cross-linked copolymers, and the interpretation of these properties within the framework of the physical network model [6].

The technical value of TFRP is generally known. Industrial use of oligo(acrylates), oligo(estermaleates) in styrene compositions, and oligo-esters modified by fatty acids of vegetable oils (alkyds) is based on TFRP with cross-linked polymer formation. The interest in TFRP throughout the world has markedly increased in the 1990s: by 2000 the number of publications on TFRP had grown tenfold. This growth is explained by the development needs of microelectronics, fiberoptics, and data storage and transmission devices. TFRP makes polymers highly attractive for

applications related to high-tech materials. The radical chain nature of TFRP enables performing curing of fluid polyunsaturated methacrylates in superfast time (seconds!) and an easily controlled mode at normal temperature.

It was found, in the middle of the 1990s, that in addition to cross-linked polymers TFRP can also lead to the formation of hyper-branched polymers (HBP) (non-cross-linked) that have a unique chemical structure and properties which are different from the structure and properties of all known linear and cross-linked polymers. Polymer chains of HBP diverge outward symmetrically in three-dimensional space from the point or linear center of symmetry and look like a branching tree. The unique properties of HBP turned out to be so popular that during the next decade these polymers found use in various applications for polymer materials from microelectronics to medicine. They caused a revolution in polymer materials technology. And, all this gave a new powerful impulse to the development of the entire TFRP field—the intensive and successful investigation into cross-linked polymers synthesized by TFRP conducted for many years did not betoken such a “burst” of interest. Judging by the trends in publications on this issue, this new subfield has developed extremely fast: before 1997, only a few publications appeared per year, during 1997–1998 the number of publications increased to 100, and during 2000–2005 more than 250 articles and patents per year have appeared.

The first part of this book deals with TFRP with formation of cross-linked polymers. It is based mainly on the results of systematic research of the authors and their colleagues.

This part (Chapters 1 through 6) includes all available data (plus analysis of these data) indicating the microheterogeneous character of TFRP. The microheterogeneous mechanism of TFRP includes both polymerization specifics at the initial, intermediate, and final stages (namely, initial formation, growth, and merger of polymer grains performing the function of autonomous micro-reactors) and structural and physical transformations in the course of TFRP (micro-syneresis, microredistribution, and local glass transition).

The interpretation of the main kinetic regularities of polyunsaturated oligomer polymerization in blocks and solutions and kinetic specifics of inhibited TFRP is given taking into account the microheterogeneous mechanism of TFRP. The main regularities of the polymerization of polyunsaturated compounds of vinyl and allyl types in a film under the conditions of oxygen diffusion were explained in the context of the proposed layer-by-layer TFRP model. A model of regular kinetically active associates intended for interpreting kinetic abnormalities of oligo(acrylates) and alkyl methacrylates polymerization is proposed: this model is substantiated both kinetically and via computer simulation. Basic kinetic features of the three-dimensional copolymerization of polyunsaturated (cross-linked) oligomers and monounsaturated (non-cross-linked) vinyl monomers were identified.

The main issues of the new branch in free-radical polymerization—namely, “living” chain three-dimensional free-radical polymerization—are analyzed. Also, exhaustive description is given for all studies on TFRP in the “living” chain mode and the role of this mode for the macromolecular design of cross-linked polymers.

The new theory of gelation in the TFRP process, which was developed by V. I. Irzhak and G.V. Korolev in 2000–2003, is described in depth. This theory is

alternative to the well-known Flory–Stockmayer theory, which is unjustifiably applied to TFRP. Critical conversion (gel point) for various modes of free-radical polymerization is determined in numerical form, and the obtained results are generalized in formulas.

Physical, mechanical, and thermo-mechanical properties of cross-linked (poly) acrylates and cross-linked copolymers of oligomers with vinyl monomers are analyzed in the context of the physical network model (i.e., intermolecular interactions system approximated by network of physical links). The predominant role of the physical network (i.e., a network of physical junctions) in proposed mechanisms for the transition of cross-linked copolymers into high-elastic and forced-elastic states is revealed. Problems of macromolecular design of cross-linked polymers and copolymers are also discussed.

The second part of the book [Chapters 7, 8] is devoted to methods of synthesis, properties, and application of hyper-branched polymers (HBP). An extensive array of information (about 400 publications) is systematized and reviewed. A classification of synthesis methods for HBP, which is based on mechanisms of synthesis reactions, is proposed. Methods for HBP synthesis by three-dimensional free-radical polymerization (with regulation of polymeric chains length due to the variation of initiation rate, employment of chain transfer agents and chain transfer catalysts, and intrachain reactions of radical chain carriers) are discussed in detail with examples. A mathematical model of HBP synthesis by the TFRP method under the conditions of unlimited supply of oxygen is proposed, and results of prediction obtained through the use of this model are presented.

The most successful and representative options of HBP synthesis by “living” chain free-radical polymerization are reviewed in depth because it is in just this case that the topological structure of HBP is distinguished by the maximum degree of regularity, which makes the HBP topological structure similar to the structure of regular HBP dendromers. Also, the method of “living” TFRP makes it possible to synthesize HBP with a sophisticated structure of macromolecules (nanostructured polymers).

Large amounts of information on practical application of HBP are systematized in this book in the form of generalized tables for the sake of convenience for readers. Particular emphasis is placed on HBP that are already produced industrially and on methods for modifying them in the context of specific applications.

Analytical reference materials for the subject matter of this book are given in the Appendix (Chapter 9). A short description of experimental methods that proved to be effective for studying the TFRP kinetics and mechanism, as well as the structure and properties of cross-linked polymers, is also given in the Appendix.

Thus, the authors have tried to give an integral description of scientific and applied aspects of three-dimensional free-radical polymerization with formation of both cross-linked and hyper-branched polymers as well as to outline the current state and trends of the development of this specific area of free-radical polymerization. The readers are to judge whether the authors have succeeded.

*Chapters 1 and 2 were written by G.V. Korolev and M.M. Mogilevich, and Chapters 3, 4, 5, 6, 7, 8, and 9 were written by G.V. Korolev.*

St. Petersburg, July 2008

*Gennady V. Korolev  
Michael M. Mogilevich*

## References

1. Berlin AA, Kefeli TYa, Korolev GV (1967) Poly-esteracrylates. Nauka, Moscow (in Russian)
2. Mogilevich MM (1977) Oxidative polymerization in film-formation processes. Khimia (Chemistry), Leningrad
3. Berlin AA, Korolev GV, Kefeli TYa, Sivergin YuM (1983) Acrylic oligomers and materials on the acrylic oligomers. Khimiya, Moscow (in Russian)
4. Mogilevich MM, Pliss EM (1990). Oxidation and Oxidative Polymerization Unsaturated Compounds. Khimia (Chemistry), Moscow. (in Russian)
5. Korolev GV, Mogilevich MM, Golikov IV (1995) Cross-linked polyacrylates: microheterogeneous structures, physical networks, deformation-strength properties. Khimiya, Moscow (in Russian)
6. Korolev GV (2003) Usp Khim 72: 222–244 (in Russian)

To our deep sorrow one of the authors of the present book – Gennady Vladimirovich Korolev – passed away between its publication in Russian and in English. Therefore, publication of the English version, which was planned by him, is a tribute to the memory of the outstanding scientist he was and a solace for the members of his family and colleagues.

# Contents

## Part I Three-Dimensional Free-Radical Polymerization. Cross-Linked Polymers

<b>1</b>	<b>Microheterogeneous Mechanism of Three-Dimensional Free-Radical Polymerization</b> . . . . .	<b>3</b>
1.1	Microheterogeneous Model of Polymerization Process . . . . .	4
1.2	Polymerization Process: Stages of Formation of the Microheterogeneous Structure for Cross-Linked Polymers . . . . .	5
1.2.1	Formation of Polymer Grains at the Initial Stage of Polymerization . . . . .	5
1.2.2	Growth of Polymer Grains During Polymerization . . . . .	7
1.2.3	Accretion of Polymer Grains at the Final Stages of Polymerization . . . . .	12
1.3	Structural and Physical Processes Taking Place During Three-Dimensional Free-Radical Polymerization . . . . .	17
1.3.1	Microsynthesis of Liquid Components in Reaction Medium . . . . .	17
1.3.2	Microredistribution of Substances Dissolved in Liquid Components . . . . .	20
1.3.3	Local Glass Transition of Highly Cross-Linked Micro-Volumes of Polymer . . . . .	23
1.4	Microheterogeneous Structure of Cross-Linked Polymers . . . . .	25
1.4.1	Interlayers Between Polymer Grains . . . . .	27
1.4.2	Polymer Grains . . . . .	30
	References . . . . .	31
<b>2</b>	<b>Kinetic Features of Three-Dimensional Free-Radical Polymerization</b> . . . . .	<b>33</b>
2.1	Kinetic Features of Individual Stages of Polymerization . . . . .	34
2.1.1	Initial Stage of Polymerization . . . . .	34
2.1.2	Stages of Auto-Acceleration and Auto-Deceleration . . . . .	41
2.2	Inhibited Polymerization . . . . .	46
2.3	Polymerization in Solutions . . . . .	51
2.4	Polymerization in Films Under the Conditions of Oxygen Diffusion . . . . .	54



2.4.1	Vinyl Compounds . . . . .	55
2.4.2	Allyl Compounds . . . . .	66
2.5	Three-Dimensional Free-Radical Polymerization as a Tool for Macromolecular Design of Cross-Linked Polymers . . . . .	75
	References . . . . .	78
<b>3</b>	<b>Living Chain Three-Dimensional Radical Polymerization . . . . .</b>	<b>81</b>
3.1	Living Chains in Free-Radical Polymerization . . . . .	82
3.2	Implementation of Living Chains Conditions in Three- Dimensional Free-Radical Polymerization . . . . .	86
3.2.1	Copolymerization of Styrene with Dimethacrylates in the Presence of Alkoxyamines . . . . .	87
3.2.2	Polymerization of Tri(Ethylene Glycol) Dimethacrylate (tEGdMA) in the Presence of Complex $\text{CuBr}_2$ with Tetramethyl-Tiuramdisulfide . . . . .	93
3.2.3	Polymerization of Dimethacrylates of Poly(Ethylene Glycol)s in the Presence of Complex $\text{CuBr}$ with Organic Ligands . . . . .	97
3.3	Living Chain Three-Dimensional Free-Radical Polymerization as a Tool for Macromolecular Design of Cross-Linked Polymers . . . . .	99
	References . . . . .	109
<b>4</b>	<b>Kinetic Features of Three-Dimensional Free-Radical Copolymerization . . . . .</b>	<b>111</b>
4.1	Kinetic Features of Three-Dimensional Copolymerization of Oligomer and Vinyl Monomers . . . . .	111
4.2	Variation of Copolymer Composition During Three-Dimensional Free-Radical Copolymerization of Oligomers and Vinyl Monomer . . . . .	118
	References . . . . .	127
<b>5</b>	<b>Critical Conversion (Gel Point) in Three-Dimensional Free-Radical Polymerization . . . . .</b>	<b>129</b>
5.1	Inapplicability of Known Critical Conversion Calculation Methods to Three-Dimensional Free-Radical Polymerization . . . . .	131
5.2	Novel Approach to Calculating Critical Conversion in Three- Dimensional Free-Radical Polymerization . . . . .	133
5.3	Results of Critical Conversion Calculation for Different Cases of Three-Dimensional Free-Radical Polymerization . . . . .	136
5.3.1	Living Chains Three-Dimensional Polymerization and Copolymerization (Without Chain Termination) . . . . .	136
5.3.2	Three-Dimensional Polymerization and Copolymerization with Quadratic or Linear Chain Termination . . . . .	143
5.3.3	Three-Dimensional Polymerization with "Pendent" Double Bonds Taken into Account (Chain Termination by Disproportionation) . . . . .	145

5.3.4	Summary of Results of Theoretical Calculations for Critical Conversion . . . . .	150
5.4	Comparison of Results of Theoretical Calculations for Critical Conversion with Experimental Data . . . . .	152
5.4.1	Inhibited Polymerization of Dimethacrylates . . . . .	152
5.4.2	Copolymerization of Divinyl Benzene ( <i>m</i> -DVB) with Styrene . . . . .	154
	References . . . . .	155
<b>6</b>	<b>Properties of Cross-Linked Polymers and Copolymers . . . . .</b>	<b>157</b>
6.1	Cross-Linked Poly(acrylates). Physical and Mechanical Properties . . . . .	157
6.1.1	Influence of Chemical Structure of Oligomers upon Physical and Mechanical Properties of Cross-Linked Poly(acrylates) . . . . .	158
6.1.2	Influence of Physical Network Density upon Physical and Mechanical Properties of Cross-Linked Poly(acrylates) . . . . .	166
6.2	Cross-Linked Copolymers. Physical and Mechanical Properties . . . . .	172
6.2.1	Mechanism of Copolymers Transition into Forced-Elastic State . . . . .	172
6.2.2	Influence of Cyclization on Physical and Mechanical Properties of Copolymers . . . . .	181
6.3	Cross-Linked Copolymers. Thermo-Mechanical Properties . . . . .	185
6.3.1	Mechanism of Copolymers Transition into High-Elastic State . . . . .	185
6.3.2	Comparison of Transitions into High-Elastic State with those into Forced-Elastic State . . . . .	193
6.4	Diffusion-Sorption Properties of Copolymers . . . . .	195
	References . . . . .	199

## **Part II Three-Dimensional Free-Radical Polymerization. Hyper-Branched Polymers**

<b>7</b>	<b>Synthesis of Hyper-Branched Polymers . . . . .</b>	<b>203</b>
7.1	Classification of Reactions for Hyper-Branched Polymer Synthesis . . . . .	203
7.2	Synthesis of Hyper-Branched Polymers Via Three-Dimensional Free-Radical (Co)polymerization with Regulation of Polymer Chain Length . . . . .	205
7.2.1	Regulation of Chain Length Through Initiation Rate Variation . . . . .	206
7.2.2	Regulation of Chain Length by Chain Transfer Agents and Chain Transfer Catalysts . . . . .	211
7.2.3	Regulation of Chain Length Through the Use of Intrachain Reactions of Chain Carrier Radicals . . . . .	226
7.2.4	Regulation of Chain Length Through the Use of Molecular Oxygen as an Inhibitor . . . . .	230

7.3	Synthesis of Hyper-Branched Polymers Via Living Chains Free-Radical Three-Dimensional Polymerization . . . . .	231
7.3.1	Living Chains Free-Radical Three-Dimensional Polymerization as Reaction for Hyper-Branched Polymers Synthesis . . . . .	231
7.3.2	Living Chains Polymerization of Vinyl Monomers with Diethyldithiocarbamate Groups . . . . .	233
	References . . . . .	239
<b>8</b>	<b>Properties and Application of Hyper-Branched Polymers . . . . .</b>	<b>243</b>
8.1	“Structure–Property” Relationship and Purposeful Generation of Hyper-Branched Polymer Properties That Are in Demand in Practice . . . . .	244
8.2	Hyper-Branched Polymers as Modifiers of Polymeric Materials . . . . .	248
8.3	Major Fields for Hyper-Branched Polymers Application . . . . .	250
8.4	HBP: Main Achievements and Problems to Be Solved Without Delay . . . . .	253
	References . . . . .	254
<b>9</b>	<b>Methods for Studying Three-Dimensional Free-Radical Polymerization and Cross-Linked Polymers . . . . .</b>	<b>257</b>
9.1	Calorimetry . . . . .	257
9.2	IR Spectroscopy . . . . .	258
9.3	Other Methods of Kinetic Measurements . . . . .	259
9.4	Light Scattering . . . . .	260
9.5	EPR . . . . .	260
9.5.1	Studying the Kinetics of Free-Radical Accumulation in Nonstationary Mode . . . . .	260
9.5.2	Studying the Kinetics of Decay of Accumulated Free Radicals . . . . .	261
9.5.3	Method of Synchronous Comparison of Continuously Recorded Kinetic Curves $[R^\bullet] = f_1(t)$ and $W = f_2(t)$ . . . . .	262
9.5.4	Structural and Physical Studies Using EPR . . . . .	262
9.6	NMR . . . . .	263
9.7	Physicomechanical and Thermo-Mechanical Methods . . . . .	263
9.8	Volumetric Method . . . . .	264
9.9	Complex Methods . . . . .	264
	References . . . . .	265
	<b>Index . . . . .</b>	<b>267</b>

# Abbreviations

AcN	Acetonitrile
AIBN	2-2'-Azo-bis-isobutyronitrile
ATRP	Atom transfer radical polymerization
BA	Butyl acrylate
BD	Tetra(methylene glycol)
BDOdMA	Buthane diol dimethacrylate
BMA	Butyl(meth)acrylate
BP	Benzoyl peroxide
BPh	Benzophenone
BQ	1,4-Benzoquinone
CEA	Cetyl acrylate
CTA	Chain transfer agent
CTC	Chain transfer catalysis
dAl-EGA	Diallyl ethylene glycol adipate
DB	Degree of branching
DC	<i>N,N</i> -Diethylamino-dithiocarbamates group
DCM	Dichlormethane
DCPD	Dicyclohexyl peroxydicarbonate
DDA	Dodecyl acrylate
DDMA	Dodecyl methacrylate
DDOdMA	Dimethacrylate 1,10-decandiol
dEG	Di(ethylene glycol)
dEGbMAOEC	Oligomers of diethylene glycol bis(methacryloyloxyethyl carbonate) or OCM-2
DHHP	Di(1-hydroxycyclohexyl) peroxide
dMA	Dimethacrylate
dMABDO	Dimethylacrylate-1,4-butandiole
dMA-BGA	Oligomers of dimethacrylate butylene adipate
dMA-BGPh	Oligomers of dimethacrylate butane-1,4-di-ol phthalate, various MW
dMA-BGSb	Oligomers of dimethacrylate butylene glycol sebacate
dMA-dEGPh	Oligomers of dimethacrylate diethylene glycol phthalate
dMAEG	Di(methacrylate) (ethylene glycol)

dMA-EGA	Oligomers of dimethacrylate bis(ethylene glycol) adipate
dMA-EGPh	Oligomers of dimethacrylate ethylene glycol phthalate
dMA-EGSb	Oligomers of dimethacrylate ethylene glycol sebacate
dMAHDO	Dimethylacrylate-1,6-hexandiol
dMAPDO	Dimethylacrylate-1,3-propandiol
dMA-tEGPh	Oligomers of dimethacrylate bis-(triethylene glycol) phthalate
DMFA	Dimethyl formamide
DMPA	2,2-Dimethoxy-2-phenylacetophenone
DSC	Differential scanning calorimetry
DVB	Divinyl benzene
FES	Forced-elastic state
FM	Foreign matter
GPC	Gel-permission chromatography
HBP	Hyper-branched polymer
HDOdMA	Dimethacrylate 1,6-hexanediol
HEMA	(2-Hydroxy)ethyl methacrylate
hMA-PeA	Oligomers of hexamethacrylate (bis-pentaerythritol) adipate
HP	Hydroperoxide
IMI	Intermolecular interactions
IR	Infrared spectroscopy
LALLS	Low angle laser light scattering
LRP	Living radical polymerization
LS	Light scattering
MA	Methyl acrylate
MBP-(1-3)	Oligomers of dimethacrylate tetramethylene glycol phthalate, various MW, is used in Tables 2.1, 2.4, 2.5 only, dMA-BG
MDA	Oligomers of dimethacrylate diethylene glycol adipate, various MW, is used in Tables 2.1, 2.4, 2.5 only
MDP-(1-5)	dMA-dEGPh, is used in Tables 2.1, 2.4, 2.5 only
MDS	Oligomers of dimethacrylate diethylene glycol sebacate, various MW, is used in Tables 2.1, 2.4, 2.5 only
MDU	Oligomers of dimethacrylate diethylene glycol 5,5'-thiodivalerate, various MW, is used in Tables 2.1, 2.4, 2.5 only
MEP	dMA-EGPh, is used in Tables 2.1, 2.4, 2.5 only
MHP	dMA-BGA, is used in Tables 2.1, 2.4, 2.5 only
MMA	Methyl methacrylate
$M_n$	Number average molecular weight
$M_w$	Weight average molecular weight
MWD	Molecular weight distribution
NMP	Nitroxide-mediated radical polymerization
NonA	Nonyl acrylate

NonMA	Nonyl methacrylate
OCA-4	Oligomers of tetraethylene glycol bis(acryloyloxyethyl carbonate)
OCA-6	Oligomers of hexaethylene glycol bis(acryloyloxyethyl carbonate)
OCM-2	dEGbMAOEC
OCM-4	Oligomers tetraethylene glycol bis(methacryloyloxyethyl carbonate)
OCM-6	Oligomers hexaethylene glycol bis(methacryloyloxyethyl carbonate)
PDB	“Pendent” double bonds
PDOdMA	Propane diol dimethacrylate
PMR	<sup>1</sup> H-NMR
polyEGdMA	Poly(ethylene glycol) dimethacrylate
PS	Poly(styrene)
RAFT	Reversible addition fragmentation chain transfer
RTIR	Real-time infrared spectroscopy
teAl-tPA	Tetraallyl of (trimethylol propane adipate)
tEG	Tri(ethylene) glycol
tEGdMA	Tri(ethylene glycol) dimethacrylate
teMA-tEA	Oligomers of tetra(meth)acrylate trimethylolethane adipate (teMA-tEA)
teMA-tPA	Oligomers of tetra(meth)acrylate bis(trimethylolpropane) adipate
TEMPO	2,2,6,6-Tetramethylpiperidiny-1-oxy
TFH	2,4,6-Triphenyl-1-hexene
TFRP	Three-dimensional free-radical polymerization
THF	Tetrahydrofuran
TMTD	Tetramethyl-thiuramdisulfide
TNT	2,4,6-Trinitrotoluene
TS	Breaking tensile strength
VA	Vinyl acetate

**Part I**  
**Three-Dimensional Free-Radical  
Polymerization. Cross-Linked Polymers**

# Chapter 1

## Microheterogeneous Mechanism of Three-Dimensional Free-Radical Polymerization

**Abstract** For the first time, the microheterogeneous mechanism of three-dimensional free-radical polymerization, initially disclosed by the authors in Russian in a number of publications during a period from 1970 to 1995, is here consistently described in English and supported by sufficient proof. This process gives products having complex multilevel cross-linked structure, namely, highly cross-linked polymeric grains and low cross-linked intergrain layers; in their turn, grains of “core-shell” structure and interlayers are also nonuniform in terms of degree of cross-linking of the polymer network at different conversions.

The very concept of the microheterogeneous character of highly cross-linked polymer formation processes was rather precisely presented by Howink as early as in 1934 [1]. Further development of this idea is reflected in works written by Kozlov [2, 3], Gallacher and Bettelheim [4], Korolev and Berlin [5], Notley [6], Bobalek et al. [7], and Dušek [8]. Exploration into the generation and growth of microgel particles during polymerization of unsaturated oligo-esters [4], and the appearance of a hypothesis on the formation [during the polymerization of oligo(acrylates)] of discrete microgel particles, in which a local gel effect is developed [5], contributed to the substantiation of ideas related to the three-dimensional free-radical polymerization (TFRP) mechanism. A TFRP mechanism that includes microheterogeneity [9] was formulated in 1970 based on new experimental data. The phenomenon of microsineresis in the process of highly cross-linked macromolecular structure formation [8] was discovered in 1971. However, only studies that took many years and were focused on polymerization of model objects, with intentionally varied structure, plus exploration into the structure of formed polymers conducted with the use of specially developed methodologies, enabled researchers to obtain strict experimental proofs of the microheterogeneous TFRP mechanism [10]. Only then did the hypothesis turn into a proven concept, and now a TFRP model suitable for quantitative calculations has appeared.



## 1.1 Microheterogeneous Model of Polymerization Process

The essence of the model at the qualitative level consists of the following [10]. The radical polymerization of polyunsaturated compounds leads to formation of polymer coils even at low conversions (i.e., even at pre-gel state) as a result of inter- or intrachain aggregation of polymer chains containing “pendent” double bonds. The diffusion-limited rate of chain termination is decreased in such coils with increasing local viscosity and, as a consequence, the polymerization rate is increased, which, in its turn, leads to further growth of viscosity. Locally (in polymer coils), the polymerization process develops autocatalytically, as a result of which polymer coils turn into highly cross-linked polymer particles (grains). With an increase in the degree of primary macromolecules branching, the probability of intramolecular cross-linking (cyclization) increases, which promotes the formation of microgel particles (grains). The concentration of polymer grains in the reaction medium stops increasing even at the initial stage of conversion, and subsequent polymerization is effected via buildup of new layers of cross-linked polymer from the surface of the grains. Such grains play the role of self-contained micro-reactors, in the surface layers of which the polymerization process is localized. At later stages of polymerization, grains come into contact with one another (as a result of their growth), and the accretion of grains into a monolith in the zones of such contact takes place. The specific character of TFRP process lies in the fact that practically starting from low conversions, a homogeneous reaction system becomes a micro-nonhomogeneous system consisting of highly cross-linked polymer particles that are poorly interconnected with penetrating chains.

The polymerization, i.e., the chemical transformation proper, is accompanied by secondary physical processes, namely, aggregation of polymer chains, microsineresis with isolation of an initial oligomer from quite highly cross-linked micro-volumes of initial oligomer (with certain components dissolved in this initial oligomer—initiators, inhibitors, and other additives), and local glass transition of these highly cross-linked micro-volumes.

The micro-nonhomogeneous reaction medium (in terms of polymer network cross-linking degree) becomes microheterogeneous after the beginning of local glass transition. Also, TFRP and structural physical processes are mutually interconnected. The aggregation of polymer chains accelerates polymerization in cross-linked polymer coils, which, in turn, leads to the accelerated development of local syneresis (microsyneresis) and local glass transition within the coils. In the end, instead of a polymer with macromolecular network uniformly distributed within the volume, a polymer is formed that consists of highly cross-linked volumes (grains) separated by low cross-linked (defective) interlayers.

Thus, according to the microheterogeneous model, in the course of TFRP a set of kinetic, thermodynamic, and topological factors causes structural and physical transformations, which accompany the chemical reaction of polymerization and result in a microheterogeneous structure of cross-linked polymer. Experimental results (presented in Sects. 1.2, 1.3, and 1.4) prove the adequacy of the model; they give grounds for considering that the microheterogeneous mechanism of TFRP is substantiated quite well.

## 1.2 Polymerization Process: Stages of Formation of the Microheterogeneous Structure for Cross-Linked Polymers

### 1.2.1 Formation of Polymer Grains at the Initial Stage of Polymerization

The light-scattering method enables us to study directly the generation and development of micro-nonhomogeneity and microheterogeneity of the reaction medium in the optical range of  $10^{-2}$ – $10\mu\text{m}$  at different conversions  $C$ , including the initial stage of polymerization characterized by  $C \rightarrow 0$ . Micro-nonhomogeneity (microheterogeneity) is quantitatively characterized by the variation of the light-scattering intensity  $R$  at different angles of observation  $\varphi$  and by the variation of characteristic dimensions of scattering centers  $\langle a \rangle$  calculated based on the model of small-angle scattering [11]. Comparison of the dynamics of variation of  $R$ ,  $\langle a \rangle$ , and  $C$  in the course of polymerization enabled the authors to trace the origination of micro-nonhomogeneity and then microheterogeneity of the reaction medium at the initial stage of polymerization in an example of tri(ethylene glycol) dimethacrylate (tEGdMA) oligomer polymerization [12].

From the very beginning of polymerization at  $0 < C < 5\%$  (Fig. 1.1), a certain decrease of characteristic size of scattering centers  $\langle a \rangle$  is observed (Fig. 1.2), accompanied by a concurrent slight increase of light-scattering intensity  $R$  (Fig. 1.3). Most probably, the decrease of  $\langle a \rangle$  is associated with the appearance of a large number of small scatterers in the oligomer against the background of quite large scatterers (foreign inclusions in the oligomer). These scattering centers (which are newly formed after the beginning of polymerization) could be identified with polymer coils that are responsible for the slight growth of light-scattering intensity during this period (Fig. 1.3), which in terms of order of magnitude of  $R$  corresponds to scattering of a diluted solution of polymer in a monomer [13]. At the initial stages of polymerization the reaction medium is homogeneous, although micro-nonhomogeneous: polymer coils and oligomer are not substantially different in terms of refraction index and density, as their volumetric fluctuations are

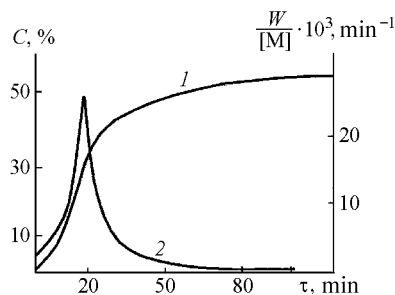
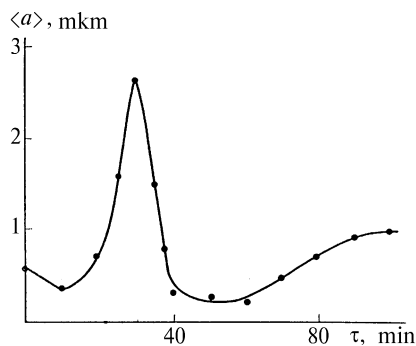


**Fig. 1.1** Integral (1) and differential (2) kinetic curves of tEGdMA photopolymerization. Temperature  $20^{\circ}\text{C}$ :  $[\text{AIBN}] = 0.03\%$  (weight)

**Fig. 1.2** Variation of average size of scattering centers in the course of tEGdMA photopolymerization. Observation angle  $\varphi = 21^\circ$ – $23^\circ$ . Temperature  $20^\circ\text{C}$ :  $[\text{AIBN}] = 0.03\%$  (weight)



responsible for the variation of light-scattering intensity value  $R$ . In the temperature range  $20^\circ$ – $80^\circ\text{C}$ , the tEGdMA oligomer is a thermodynamically good solvent of its own primary products of polymerization (so-called  $\beta$ -polymers) [14–16]. This feature provides swelling of polymer coils in the oligomer and homogenization of the reaction medium.

With the beginning of polymerization auto-acceleration, the situation is radically changed: dramatic growth of size of scattering centers  $\langle a \rangle$  and enhancement of light-scattering intensity  $R$  (see Figs. 1.1, 1.2, and 1.3) are observed. This observation is indicative of mass formation of reaction medium micro-volumes that differ dramatically from the oligomer in terms of density and refraction index. The reason for such large-scale fluctuations in reaction medium polarizability resulting from dramatic growth of  $R$  and  $\langle a \rangle$  most probably lies in mass transition of polymer coils into glass-like polymer grains as a result of local gel effect and growth of such grains. Local glass transition of quite highly cross-linked micro-volumes of

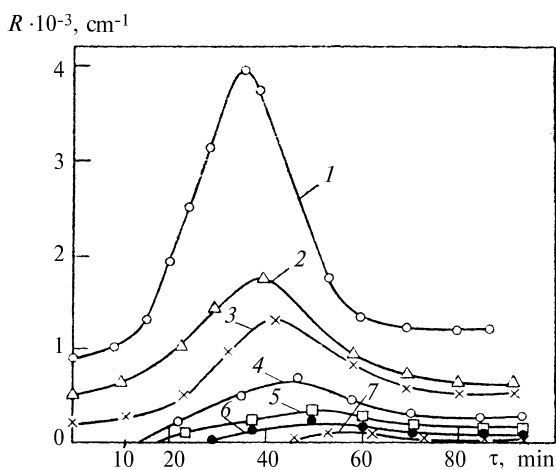


**Fig. 1.3** Variation of reduced intensity of light scattering in the course of tEGdMA photopolymerization. Observation angle  $\varphi$ : 1,  $21^\circ$ ; 2,  $30^\circ$ ; 3,  $40^\circ$ ; 4,  $58^\circ$ ; 5,  $75^\circ$ ; 6,  $80^\circ$ ; 7,  $113^\circ$ . Temperature  $20^\circ\text{C}$ :  $[\text{AIBN}] = 0.03\%$  (by weight)

reaction medium [15] occurs in the same range of conversions, in which dramatic increase of light-scattering intensity is observed. Judging by values of  $R$ , even at low conversions, with just the beginning of polymerization auto-acceleration the micro-nonhomogeneous reaction medium becomes microheterogeneous. Such a medium is, in essence, a nano-dispersion of glass-like microgel particles, weakly bound by penetrating chains in the volume of nonreacted oligomer. The transformation of homogeneous reaction medium into a microheterogeneous one even at the initial stage of polymerization is also shown by the light-scattering method for polymerization of tEGdMA in solutions [16].

### 1.2.2 Growth of Polymer Grains During Polymerization

According to the microheterogeneous model, polymer grains that have formed even at the initial stage of polymerization are in a certain sense self-contained micro-reactors, in the surface layers of which the polymerization process becomes localized. This key point of the model needed thorough experimental substantiation.

Using the method of spectroturbidymetry, it was found (based on turbidity spectra) that actually the accumulation of new isolated particles in the reaction medium stops from the very beginning of oligo(acrylates) polymerization, and subsequent polymerization proceeds with the number of such particles practically unchanged, but with their size increased (Fig. 1.4)[17].

Kinetics of oligo(acrylates) polymerization is described by the Avrami equation (Fig. 1.5) [18], the derivation of which is based on the model of growing heterogeneous particles:

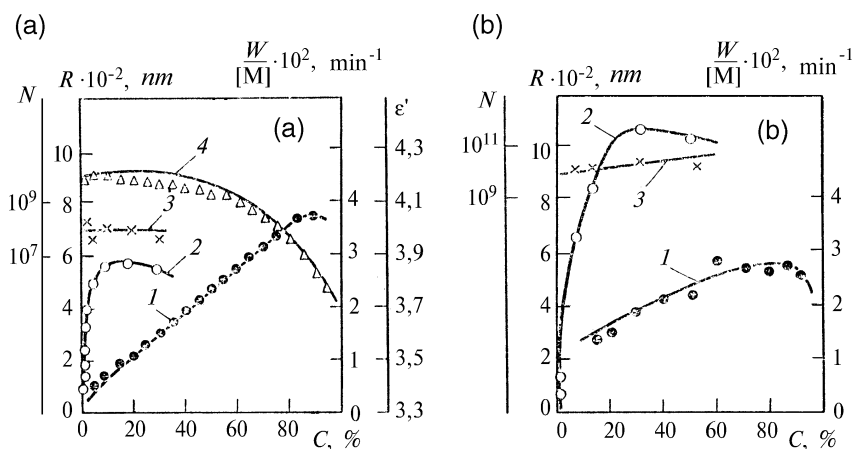
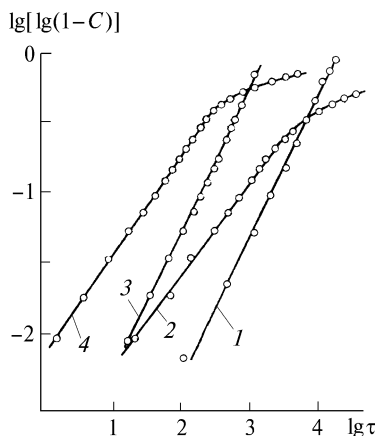


**Fig. 1.4** Variation of reduced polymerization rate  $W/[M]$  (1), size  $R$  (2), concentration of polymer particles  $N$  (3), and dielectric permeability  $\epsilon'$  (4) during polymerization of tEGdMA (a) and dMA-tEGPh (b) in 50% solution of benzene at 50°C

**Fig. 1.5** Dependency of dMA<sub>t</sub>EGPh conversion upon time  $\tau$  in coordinates of Avrami equation.

Polymerization conditions: 1, 2, block; 3, 4, 50% solution in benzene; benzoyl peroxide (BP), % by weight: 1, 3, 1.0; 2, 4, 0.1. Index of Avrami equation  $n$ : 1, 1.6; 2, 1.4; 3, 4, 2.1



$$C = 1 - \exp(-K_t^n) \tag{1.1}$$

where  $C$  = fraction of substance that was subjected to transformation (conversion in terms of double bonds);  $K_t$  = specific rate of transformation process; and  $n$  = index, Fig. 1.6 depending on the geometric shape of growing heterogeneous particles.

An investigation of reaction medium composition as a function of conversion  $C_t$  for different types of oligo(acrylates) [19] led to the following equation:

$$C_t = C_g(1 - V_s) \tag{1.2}$$

where  $C_g$  = conversion in gel fraction and  $V_s$  = volume rating of sol fraction of polymer.

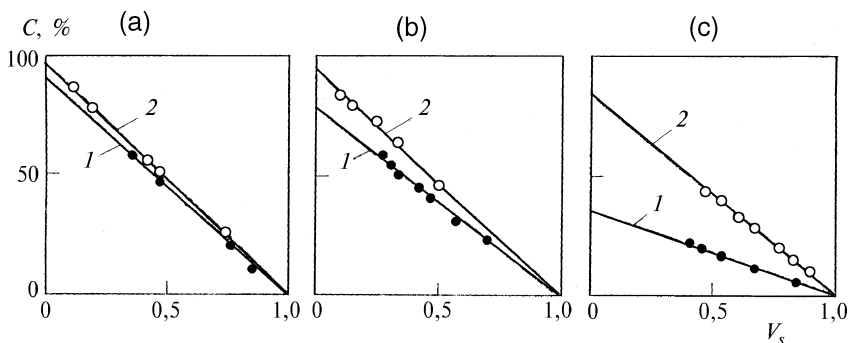


**Fig. 1.6** Dependency of sol yield upon conversion in the case of polymerization of oligo(acrylates) of different functionality  $n$ : (a) tEGdMA ( $n = 2$ ); (b) tMA-tPA ( $n = 4$ ); (c) hMA-PeA ( $n = 6$ ). Temperature °C: 1, 60; 2, 90

Besides, the value of  $C_g$  did not vary in the course of polymerization and was equal to the possible limit value of  $C_t$  at a given temperature:

$$C_g = (C_t)_{\text{lim}} = \text{const} \quad (1.3)$$

The constancy of  $C_g$  in the course of polymerization was stated based on linear character of dependency  $C_t = f(V_s)$ , while equality (1.3) was established based on the section intercepted on the ordinate by direct line in coordinates  $C_t - V_s$  with  $V_s \rightarrow 0$  (Fig. 1.6).

Since

$$C_t = C_s V_s + C_g (1 - V_s) \quad (1.4)$$

(where  $C_s$  = conversion in sol fraction), then it uniquely follows from Eqs. (1.2) and (1.4) that  $C_s = 0$ . It means that the sol fraction consists only of nonreacted initial oligo(esteracrylate) and, hence, the reaction medium during the entire polymerization process contains only two components—namely, insoluble highly cross-linked polymer (gel) with limiting conversion and nonreacted initial oligo(esteracrylate).

Because this conclusion is of key importance for experimental substantiation of the hypothesis implying growing polymer grains, the composition of sol fractions was determined using the gel chromatographic method and then analyzed for non-saturation. Indeed, the sol fraction was represented by a nonreacted oligomer. In the case when  $C_g \neq (C_t)_{\text{lim}}$  during the entire polymerization process, sol fraction also contains only an initial nonreacted oligomer [20]. This regularity is of general character, it is true for oligo(acrylates), which differ in terms of both functionality and structure of oligomer block.

According to the model forecast, polymer grains should consist of highly cross-linked glass-like cores with the limiting conversion degree (at a given temperature) and peripheral surface layers (shell) with uncompleted network structure, i.e., reaction zones, in which polymerization actually proceeds. The auto-deceleration at the final stages of TFRP is interpreted within the framework of the microheterogeneous mechanism as a result of reaction zones overlapping following the contact and accretion of polymer grains (see Sect. 1.2.3). Indeed, during the polymerization of oligo(acrylates) in solutions containing surfactant additives under the conditions excluding aggregation of polymer grains because of overlapping of their peripheral reaction zones, the authors managed to completely eliminate auto-deceleration of polymerization (Fig. 1.7) [21]. Thus, surface reaction zones of polymer grains were kinetically identified.

Information on relative size of reaction zones of polymer grains  $h/r$  (Fig. 1.8) was obtained directly from kinetic characteristics of the oligo(acrylates) polymerization process [22] based on values of  $\gamma$ :

$$\gamma = C_{\text{max.}} / C_{\text{lim}} \quad (1.5)$$

where  $C_{\text{max}}$  = conversion corresponding to maximum polymerization rate; and  $C_{\text{lim}}$  = limiting conversion that could be implemented under given conditions.

Further, the reaction medium filled with polymer grains that are in contact is approximated by a monodisperse set of spheres having radius  $r$  (see Fig. 1.8). In terms of physical meaning,  $\gamma$  is a volume fraction of polymer grains in a reaction medium at the moment of their contact. In the supposition on monodispersiveness of spherical grains, the theoretical value of  $\chi_t$  is equal to 0.64 or 0.72 for tetragonal or hexagonal packing of grains, respectively, while

$$h/r = 1 - (\gamma/\chi_t)^{1/3} \quad (1.6)$$

It follows from the data presented in Table 1.1 that the character of variation of relative size of reaction zones (surface layers) of polymer grains  $h/r$  is determined by oligomer structure, initiator type, and polymerization temperature.

The correlation of yield of sol fraction and TFRP conversion of the type (Eq.(1.2)) enables us to suppose the following mechanism of polymer grains growth. Throughout the entire duration of the polymerization process, i.e., from formation of polymer grains until their contact and accretion (taking the constancy of their concentration in the reaction medium into account), the said process proceeds through buildup of new polymer layers over the periphery of the grains. In this process, a radial gradient of conversion from  $(C_g)_i$  at the internal side of the peripheral layer facing the grain nucleus, with  $(C_g)_i \approx (C_t)_{lim}$  to  $(C_g)_p \approx 0$  at the external side of the layer facing the interlayer of source oligomer with zero degree of transformation (see Fig. 1.8), would obviously exist in the growing peripheral layer with still incomplete network structure (i.e., in the reaction zone of the grain). The average conversion in the entire volume of grain  $C_g$  is described by the following expression (taking the peripheral layer (shell) volume

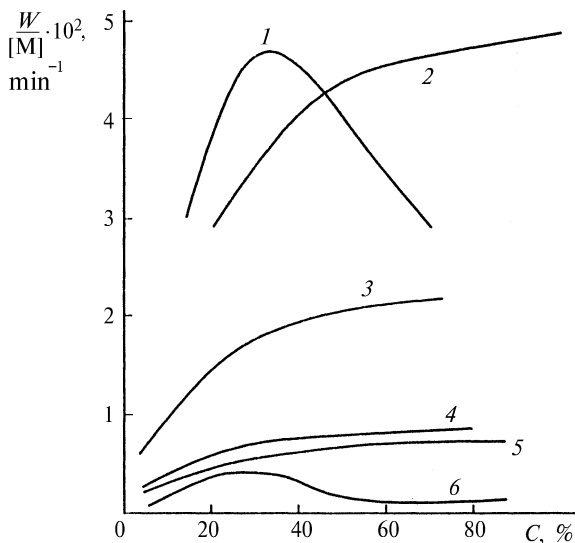


**Fig. 1.7** Kinetics of tEGdMA polymerization in solutions with stabilizing additives: 1–3, 40% solution in acetonitrile; 4–6, 30% solution in heptane. Type and concentration of additive, % (by weight): 1, 6, without additive; 2, colloxylin, 0.1; 3, linoleic acid, 0.2; 4, poly(isoprene), 0.4; 5, surfactants, 0.5

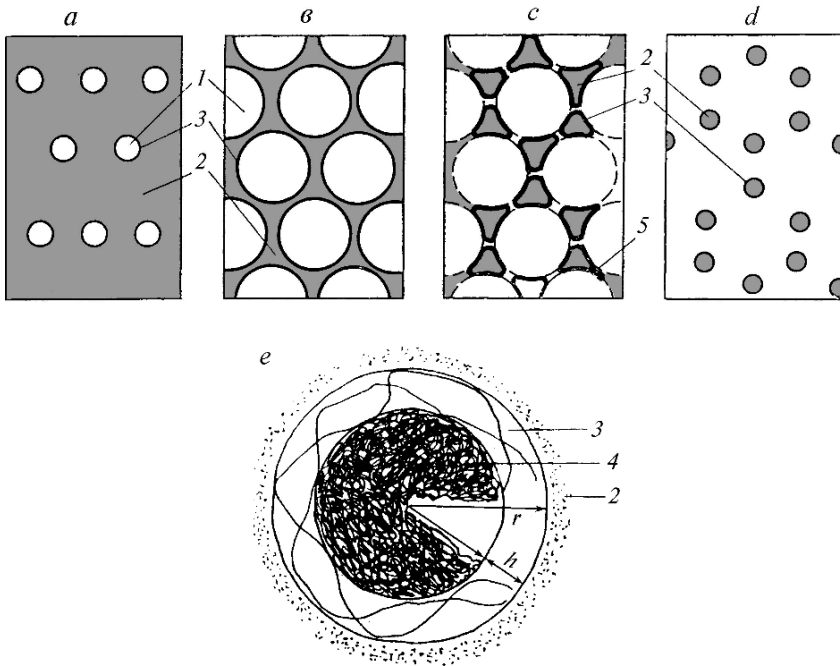


**Fig. 1.8** Formation stages (*a-d*) of microheterogeneous structure of cross-linked polymer in the course of TFRP and schematic diagram of polymer grain (*e*) at stages (*a*) and (*b*) (*e*): (*a*) formation of polymer grains; (*b*) growth of polymer grains; (*c*) contact and accretion of polymer grains; (*d*) microheterogeneous cross-linked polymer. 1, polymer grains; 2, oligomer; 3, surface layer of polymer grain (shell); 4, core of polymer grain; 5, zone of direct contact and accretion of polymer grains

into account):

$$C_g = (C_i)_{lim} \cdot (1 - V_1) + \bar{C}_1 V_1 \tag{1.7}$$

where  $\bar{C}_1$  and  $V_1$  = average conversion in the surface layer and volume of surface layer of the grain, respectively.

It is obvious that at the end of polymerization process (i.e., after the limiting conversion has been reached), the very fact of polymerization cessation is equivalent to the assertion that growing peripheral layers of grains ceased to exist and the value of  $V_1$  became zero. Consequently, at the end of polymerization the ratio of Eq. (1.7) is transformed into that of Eq. (1.4). At earlier stages of polymerization, with  $V_1 > 0$ , ratio (1.7) is true, from which it uniquely follows that  $C_g < (C_t)_{lim}$ .

In the case when the constancy of  $C_g$  and  $C_g = (C_t)_{lim}$  (see Fig. 1.6) is experimentally observed, relationships (1.2) and (1.4) do not contradict one another only on condition that  $V_1 \approx 0$  not only at the end of the polymerization process, but also throughout its entire duration. The physical meaning of this condition is as follows: the buildup of polymer grains occurs in very thin peripheral layers practically only at the very surface of grains when  $h/r < 0.1$  (see Table 1.1). When in the course of



**Table 1.1** Values  $\gamma$  and  $h/r$  for polymerization of tEGdMA and dMA-tEGPh

Oligomer	Initiator concentration, % (by weight)	$\gamma$	$h/r$	Oligomer	Initiator concentration, % (by weight)	$\gamma$	$h/r$
Initiator AIBN, 60°C				Initiator DCPD, 40°C			
tEGdMA	0.010	0.43	0.12	tEGdMA	0.010	0.28	0.24
	0.025	0.46	0.10	tEGdMA	0.050	0.38	0.16
	0.050	0.50	0.08	tEGdMA	0.075	0.42	0.13
	0.075	0.53	0.06	tEGdMA	0.100	0.45	0.11
	0.100	0.55	0.05				
dMA-tEGPh	0.075	0.58	0.03	dMA-tEGPh	0.010	0.38	0.16
				dMA-tEGPh	0.050	0.40	0.14
				dMA-tEGPh	0.075	0.48	0.09
				dMA-tEGPh	0.100	0.62	0.01

*Note.* Given values of  $h/r$  are found from Eq. (1.7) with  $\chi_t = 0.64$  based on the assumption of more probable tetragonal packing of grains [22].

polymerization  $C_g < (C_t)_{\text{lim}}$  and when only at the end of the process, conversion in gel ( $C_g$ ) reaches the limiting value, the buildup of polymer grains occurs in quite voluminous surface layers of grains with  $h/r \geq 0.1$  (see Table 1.1).

Thus, the data set obtained through the use of independent experimental methods completely verifies the hypothesis of growing polymer grains, in the surface layers of which the polymerization process is localized.

### 1.2.3 Accretion of Polymer Grains at the Final Stages of Polymerization

According to the microheterogeneous model, at late stages of polymerization the growing polymer grains come into contact, after which polymerization accretion of discrete grains into a microheterogeneous polymer solid takes place. The monolithization of polymer grains should be accompanied by an abrupt change of properties of the polymer being formed. Indeed, a reaction medium inevitably passes through two states as the polymer grains grow. In the first state, while the size of the grains is quite small, a reaction medium represents a state of dispersion, in which the role of the dispersion phase is performed by solid highly cross-linked strong grains, while the role of continuous dispersion medium is performed by liquid nonreacted oligomer that is thickened by penetrating polymer chains (see Fig. 1.8a,b). The continuous phase should obviously have a level of strength that is close to zero level and which is characteristic of moderately concentrated solutions of polymers. The level of the properties of the polymer material on the whole in this state is preconditioned by the properties of the continuous phase; therefore, the strength should be very low whereas the permeability, in contrast, should be high.

The second state of reaction medium is observed when in the course of polymer grain growth their size is increased to such an extent that they come into contact with one another and start to accrete into a single network structure as a result of polymerization in the contact zones. The oligomer (which served earlier as a continuous phase), separated by grain accretion zones into discrete micro-volumes, becomes a dispersed phase. And, vice versa, polymer grains are transformed from the dispersed phase into the continuous phase during accretion (see Fig. 1.8c). In other words, a certain critical conversion  $C_{cr}$ , which could be regarded as a phase inversion point, is reached in the course of polymerization. After  $C_{cr}$ , the presence of a structural framework composed of accreted solid highly cross-linked grains in the role of continuous phase should inevitably lead to a jump-like alteration of properties of polymer material near  $C_{cr}$ . The strength and elasticity modulus will be dramatically increased in this case, while diffusion permeability, in contrast, will be dramatically reduced; diffusion pathways, which ran over the continuous, easily permeable phase (oligomer) when  $C < C_{cr}$ , would be blocked by barely permeable barriers when  $C > C_{cr}$ .

The monolithization stage is a final stage of polymerization process, the existence of which represents a direct consequence of the microheterogeneous mechanism of TFRP. It was first experimentally discovered as a result of studying the polymerization of studying tEGdMA (triethelenglycol dimethacrylate) oligomer under widely varied conditions [23].

The degree of monolithization was evaluated by elasticity modulus of polymer in compression ( $E_{comp}$ ) and by coefficient of diffusion ( $D$ ) of a number of solvents in the polymer. A quite narrow area of conversion near  $C_{cr} \approx 75\%$ , within which dramatic, almost jump-like variation of cross-linked polymer material properties takes place, is clearly seen in Fig. 1.9 and from data presented in Table 1.2: elasticity modulus is increased almost 3.5 times (from 700 to 2,300 MPa), while the value of the diffusion coefficient is decreased under the same conditions approximately 1,000 times.

The variation of polymerization conditions—initiation method (substantial and irradiation), initiation rate, temperature, or introduction of inhibitors—does not change the above-indicated character of dependency “properties,” i.e., conversion (see also [24], pp. 69–71). It is believed that the described dependency is of universal character and should also be observed in the case of TFRP of polyunsaturated compounds of other types.

It should be pointed out that the observed abrupt change of properties within a narrow interval of conversions could not be explained by conventional gel formation because the gel point under selected conditions of tEGdMA polymerization stays within the area of low conversion values (with  $C < 1\%$ ). An abrupt change of properties is exactly a consequence of monolithization, i.e., accretion of polymer grains. The light-scattering method also records the monolithization stage as a period of sharp decline of light-scattering intensity  $R$  (see Fig. 1.3) and equally sharp reduction of characteristic dimensions of scattering centers  $\langle a \rangle$  (see Fig. 1.2). Such changes of values of  $R$  and  $\langle a \rangle$  are most probably preconditioned by changes in the nature of scattering centers resulting from reaction medium transition from

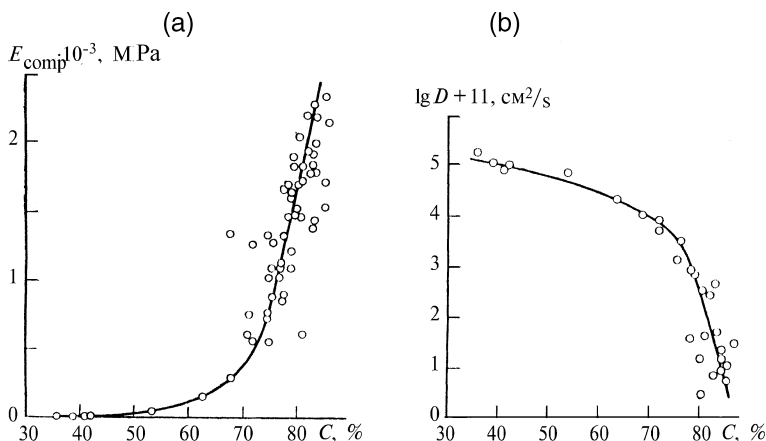


**Fig. 1.9** Dependency of elasticity modulus in case of compression  $E_{\text{comp}}$  (a) and diffusion coefficient of acetone  $D$  (b) upon conversion for tEGdMA polymerization. Polymerization conditions are given in Table 1.2

**Table 1.2** Elasticity modulus in compression  $E_{\text{comp}}$  and diffusion coefficient of acetone  $D$  for different conversion values  $C$  (polymerization of tEGdMA)

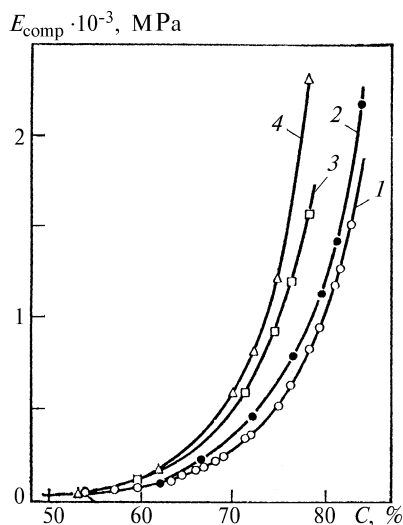
Conditions of polymerization	$C$ , %	$E_{\text{comp}}$ , MPa	$D \times 10^8$ , $\text{cm}^2/\text{s}$
50°C, 240 min	35.8	5.4	180
20°C, 150 min	38.8	10.0	112
60°C, 180 min	42.0	13.3	104
60°C, 240 min	53.3	50.3	74
100°C, 25 h	68.0	297.8	12
60°C, 61 h	75.0	564.0	–
60°C, 180 min + 100°C, 24 h	77.8	928.0	–
60°C, 365 min + 100°C, 24 h	77.0	1047.6	–
60°C, 180 min + $^{60}\text{Co}$ , 1 Mrad during 5 h	80.2	1736.0	–
60°C, 180 min + 100°C, 24 h + $^{60}\text{Co}$ , 1 Mrad during 5 h	79.3	1933.7	1.0
60°C, 61 h + 100°C, 24 h + $^{60}\text{Co}$ , 1 Mrad during 5 h	80.4	2079.0	–
20°C, 150 days + $^{60}\text{Co}$ , 11.5 Mrad during 10 h	79.0	1679.2	–
20°C, 150 days + $^{60}\text{Co}$ , 20 Mrad during 100 h	81.4	2230.6	–

*Note.* Polymerization under conditions indicated in this table was conducted using initiator AIBN ( $[\text{AIBN}] = 2 \times 10^{-2} \text{ mol/l}$ ) and inhibitor 2,4,6-trinitrotolylol (TNT) ( $[\text{TNT}] = 5 \times 10^{-2} \text{ mol/l}$ ).

the state of dispersion of growing polymer grains in a liquid oligomer (Fig. 1.8a,b) to the state at which such oligomer becomes the dispersion phase that is separated into discrete, permanently reducing volumes by zones of polymer grain accretion (see Fig. 1.8c,d).

In-depth study [25] enabled us to find that two chemically identical, but topologically different, polymerization processes proceed at the monolithization stage: one of them (characterized by low efficiency) is localized in wide intergrains layers,

**Fig. 1.10** Dependency of elasticity modulus in compression  $E_{\text{comp}}$  upon conversion: 1, without inhibitor (photopolymerization at 20°C); 2–4, without inhibitor before conversion  $C_{\text{pre}}$ , and later, with an inhibitor for different methods of postpolymerization; 2, postpolymerization for 5 h at 90°C; 3, radiation postpolymerization (dose 1 Mrad, dose rate 166 rad/s); 4, postpolymerization by photoirradiation at 20°C



whereas another (highly efficient) process proceeds in narrow zones of polymer grain contact (see Fig. 1.8). In this case efficiency is understood as an increment of the level of polymer properties that characterize monolithness; e.g., an increment of elasticity modulus  $\Delta E$ , as related to the increment of conversion  $\Delta C$  (Fig. 1.10). The physical meaning of normalizing  $\Delta E/\Delta C$  is an increment of properties level per unit of conversion.

This fundamental topological feature was experimentally determined using the selective (local) inhibition method.

Selective inhibition is based on the different sorption capacity of polymer micro-volumes with respect to molecules of inhibitor that is introduced into a partly formed polymer from the outside (these micro-volumes differ quite significantly in the partly formed polymer in terms of degree of polymer network density) [26]. Selective inhibition was carried out in the following way. The dependency between elasticity modulus at compression  $E_{\text{comp}}$  and conversion  $C$  was determined using polymer samples that were prepared under standard conditions (i.e., at 20°C, with photoinitiation in the absence of inhibitor). Curve  $E_{\text{comp}} = f(C)$  with distinct dramatic growth of value of  $E_{\text{comp}}$ , corresponding to the monolithization stage (see Fig. 1.10, curve 1), served as a reference pattern for identifying the local inhibition effect. Then, under the same standard conditions, samples of prepolymers with different conversions  $C_{\text{pre}}$  and, hence, with different elasticity moduli at compression  $E_{\text{pre}}$ , were prepared. These samples of prepolymers were saturated with vapors of stable nitroxyl radicals of 2,2,6,6-tetramethyl-piperidin-1-oxil (TEMPO), an efficient inhibitor of radical polymerization, which, diffusing into oligo(acrylates) polymers, is incapable of sorption into micro-volumes with quite highly cross-linked polymer network [26]. Following the saturation, postpolymerization of samples was carried out under the conditions of thermal, photo-, or radiation initiation until conversions  $C = C_{\text{pre}} + \Delta C$  and, hence,  $E_{\text{comp}} = E_{\text{pre}} + \Delta E$  (curves 2–4 in Fig. 1.10 and data in Table 1.3).

**Table 1.3** Variation of properties of noninhibited polymers tEGdMA upon completion of post-polymerization in the presence of inhibitor

Prepolymer		Polymer upon completion of postpolymerization				
$C_{pre}, \%$	$E_{pre}, \text{MPa}$	$C, \%$	$E_{comp}, \text{MPa}$	$\Delta C, \%$	$\Delta E, \text{MPa}$	$\Delta E/\Delta C, \text{MPa}/\%$ or $\Delta \text{MPa per } \Delta \%$
Photopolymerization						
53.5	50	53.7	50	0.2	–	–
62.0	100	63.0	170	1.0	70	70
66.0	180	70.4	580	4.4	400	90
67.0	185	73.5	810	6.5	950	153
75.0	510	79.0	2300	4.0	1790	447
Radiation polymerization						
54.0	80	54.1	60	0.1	–	–
59.5	75	59.7	110	0.2	35	175
63.3	115	63.6	220	0.3	105	350
64.4	140	65.0	270	0.6	130	217
68.0	210	71.5	590	3.5	380	109
71.4	350	74.5	910	3.1	560	181
76.5	630	78.5	1560	2.0	930	465
Thermal polymerization						
57.0	60	57.2	60	0.2	–	–
64.6	150	65.4	180	0.8	30	37
66.0	170	67.2	250	1.2	80	67
69.0	200	74.3	580	5.3	320	60
75.0	530	78.1	1040	3.9	510	130
71.8	370	76.1	740	4.3	370	86
81.0	1180	84.5	2150	3.5	970	277

Note. For conditions of postpolymerization, see Fig. 1.10.

The comparison of curves  $E_{comp} = f(C)$  (see Fig. 1.10) shows that starting from a certain critical conversion  $C_{cr} \approx 60\%$ , the elasticity modulus of samples obtained in two stages (prepolymerization without inhibitor and postpolymerization with inhibitor, curves 2–4) is always higher than that of reference samples obtained without using an inhibitor (curve 1). It is indicative of significant structural difference between samples that have been subjected to inhibition, and these structural peculiarities appear only during the postpolymerization process when the increment of conversion  $\Delta C$  is very small as compared to the initial value of  $C_{pre}$  (see Table 1.3). Indeed, the main part of the polymerization process (i.e., before  $C_{pre}$ ) proceeds under the same conditions for the samples being compared and, consequently, results in the formation of identical structures. For instance, the maximum value of  $\Delta C$  during postpolymerization was 6.5%, which was observed for  $C_{pre} = 67.0\%$ . For this sample,  $C = C_{pre} + \Delta C = 73.5\%$ , and elasticity modulus is more than twofold higher than that for the reference sample with similar conversion (curves 1 and 4 in Fig. 1.10 with  $C = 73.5\%$ ). Effects of similar scale were obtained when comparing  $E_{comp}$  of any pairs of inhibited and noninhibited (reference) samples with values of  $C$  being the same.

In other words, a paradoxical effect is observed: inhibition significantly enhances the polymer elasticity, if the comparison is made for equal conversions, or, to be more exact, in the presence of inhibitor, the polymerization process becomes more efficient in terms of structure formation. The trivial influence of inhibitor consists in the chain length reduction in the course of polymerization, and this can in no way contribute to structure formation. An enhancement of structure formation efficiency in the presence of inhibitor is a paradoxical effect if the microheterogeneous model of the polymerization process is not taken into account. Within the framework of the model, this effect appears to be fairly natural.

Indeed, polymerization proceeding in two different zones (2 and 5 in Fig. 1.8c) makes completely unequal contribution into structure formation during monolithization (formation of polymer gel by accretion of polymer grains). The contribution of the process localized in a narrow zone of direct contact of polymer grains (zone 5) into formation of monolith is maximal, while the contribution of the process localized in wide interlayers between grains (zone 2), is, in contrast, minimal. If an inhibitor diffusing into the polymer from outside does not penetrate at all into the zone of direct contact between polymer grains because of diffusion difficulties (or penetrates to a small depth), the inhibition will selectively suppress only polymerization in wide interlayers between grains, which is ineffective in terms of structure formation. Therefore, during postpolymerization in the presence of inhibitor, only such polymerization takes place that is highly efficient for structure formation and which proceeds in narrow zones of direct contact of polymer grains, i.e., in the zones that contain no inhibitor at all or a very small amount of it. The positive influence of inhibitor upon structure formation within the frames of the microheterogeneous model thus acquires a natural explanation. Therefore, the development of two topologically different polymerization processes at later stages of TFRP may be considered as established fact.

### **1.3 Structural and Physical Processes Taking Place During Three-Dimensional Free-Radical Polymerization**

Structural and physical processes of microsineresis, microredistribution, and local glass transition, which take place concurrently with TFRP, precondition its microheterogeneous mechanism and the microheterogeneous structure of cross-linked polymer that is formed thereby. These processes should be necessarily studied together with kinetics of polymerization. This approach was developed and logically implemented in earlier publications by the authors [24, 27].

#### ***1.3.1 Microsineresis of Liquid Components in Reaction Medium***

Microsineresis is preconditioned by thermodynamic incompatibility of highly cross-linked polymers with the liquid phase of a reaction medium. As soon as, with

a given relationship “polymer/liquid phase,” the degree of polymer cross-linking in a certain volume of reaction medium exceeds the value corresponding to the condition of equilibrium swelling [28], separation into layers (syneresis) starts, which is accompanied by the release of fluid-phase surplus from the cross-linked polymer. The most detailed exploration of this phenomenon was conducted by Dušek [8, 29, 30], who demonstrated that in highly cross-linked polymers, as a consequence of strong diffusion difficulties, the process of separation into layers, as a rule, does not reach the stage of macroscopic separation of the medium into two layers, but is terminated at the stage of microseparation into layers (microsyneresis). Drops of fluid of microscopic size (released from the most highly cross-linked micro-volumes) occupy such micro-volumes, which are characterized by the lowest degree of cross-linking, thus forming a metastable, micro-nonhomogeneous system.

Microsyneresis in the course of oligo(acrylates) polymerization was successfully identified on an example of solution polymerization of tEGdMA oligomer [31], using the method of light scattering (for different temperatures of identical samples). This method enables varying the compatibility of highly cross-linked polymer with solution, as well as conditions of equilibrium swelling of polymer networks.

Negative temperature coefficient of light scattering (NTCLS) is observed during polymerization of tEGdMA in 70% solutions of acetonitrile and dimethyl formamide (DMFA) up to a certain critical conversion  $C_{cr}$ : decrease of temperature causes an enhancement of light-scattering intensity  $R$ , while an increase of temperature, on the contrary, leads to dramatic decline of  $R$  (Fig. 1.11a). When  $C_{cr}$  is reached, inversion of the temperature coefficient of light scattering intensity takes place: NTCLS is converted into PTCLS (positive temperature coefficient of light scattering). Control experiments showed that mere variation of temperature does not change the intensity of light scattering of the oligomer, in which no polymerization takes place. The value of  $C_{cr}$  approximately corresponds to a range of

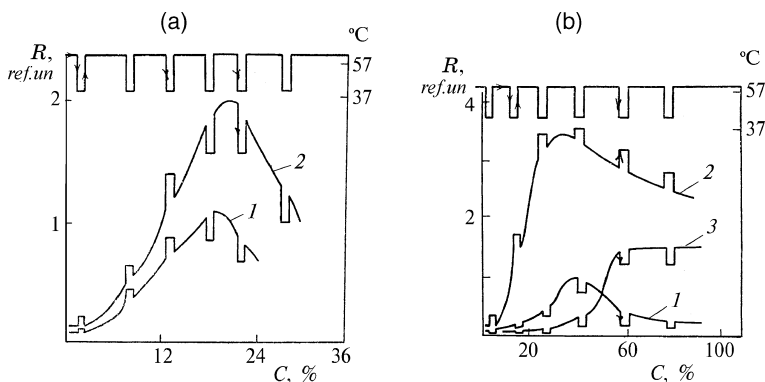


**Fig. 1.11** Variation of reduced light-scattering intensity for polymerization of tEGdMA in solutions of acetonitrile (1) and DMFA (2, 3) at different temperatures  $40^{\circ}$ – $60^{\circ}\text{C}$ : (a) 1, 2, 70% (vol.) tEGdMA,  $[\text{AIBN}] = 3.05 \times 10^{-3} \text{ mol/l}$ ; (b) 2, 40% (vol.) tEGdMA,  $[\text{AIBN}] = 3.05 \times 10^{-3} \text{ mol/l}$ ; 1, 3, 10% (vol.) tEGdMA,  $[\text{AIBN}] = 6 \times 10^{-3} \text{ mol/l}$

conversions, in which auto-acceleration of polymerization is alternated with auto-deceleration. Within the framework of the microheterogeneous mechanism of TFRP, auto-deceleration is interpreted as overlapping of reaction zones (surface layers) during accretion of polymer grains (see Sect. 2.1.2). It is quite certain that the inversion of the temperature coefficient of light scattering after  $C_{cr}$  is caused by transition of reaction medium from the state of polymer grains dispersion in oligomer solution into the state of microheterogeneous polymer solid, when accreted polymer grains become a continuous phase, whereas the nonreacted oligomer and solvent turn out to be in discrete micro-volumes of low cross-linked intergrain layers.

The scale of density fluctuations (refraction index) for each state of reaction medium determines the value of light-scattering intensity  $R = f(\Delta n)$ , in its turn:

$$\Delta n = n_p - n_l \quad (1.8)$$

where  $n_p$  and  $n_l$  are refraction indices of polymer and liquid components, respectively, of reaction medium.

The PTCLS of a microheterogeneous polymer is predetermined by a significant difference in coefficient of thermal expansion of highly cross-linked micro-volumes and that of low cross-linked ones [32]. In a first approximation, it is believed that, with a variation of temperature, only low cross-linked intergrain layers become expanded (compressed), while the volume of highly cross-linked polymer remains unchanged and, hence,  $n_p = \text{const}$ . Expansion of intergrain layers (decline of their density) with an increase of temperature is accompanied by a decrease of  $n_l$  and, hence, by increase of  $\Delta n$  and light-scattering intensity  $R$ .

NTCLS of polymer grain dispersion in oligomer solution before  $C_{cr}$  cannot be interpreted without taking into account microsineresis in surface growing layers of polymer grains: layers with uncompleted cross-linked structure and radial gradient of cross-linking degree. Indeed, as the temperature decreases, the compatibility of cross-linked polymer with polymer solution is impaired and the volume of the surface layers of the polymer grains is reduced (the density increases), with a corresponding increase of refraction index  $n_p$ . In this case, release (microsineresis) of the liquid phase should take place from more highly cross-linked parts of surface layers of polymer grains to less highly cross-linked parts up to a point, when the condition of equilibrium swelling of polymer network at a lower temperature is achieved. The difference in refraction index of polymer grains and that of oligomer solution ( $\Delta n$ ) grows, which leads to an increase in light-scattering intensity  $R$  with a decrease of temperature.

The proposed interpretation of experimental data is confirmed by a variation in the character of temperature dependency of light-scattering intensity as a result of a greater degree of solution dilution. Polymerization of tEGdMA in a 40% solution of DMFA, when contact of polymer grains with overlapping of their surface layers is excluded, is not accompanied by the inversion of temperature coefficient of light scattering: NTCLS is observed from early conversions up to process completion (curve 2 in Fig. 1.11b). Under the conditions of even higher dilution (e.g., in 10% solutions), when the main contribution to the increment of refraction index of the



system  $\Delta n$  is made by the change in solvent density, and not by the polymer degree of cross-linking, the system is characterized by PTCLS throughout the entire duration of polymerization (see curves 1 and 3 in Fig. 1.11b); under these conditions, fluctuations of polarizability (density) of solution continue playing the role of main scatterers, regardless of conversion.

It is believed that microsineresis during polymerization of oligo(acrylates) in the block, because of high thermodynamic affinity of oligomers to intrinsic polymers [16], proceeds not so intensively as during polymerization in solvents; for this reason, it turned out to be impossible to identify this phenomenon using the light-scattering method during block polymerization of oligo(acrylates) [32].

### 1.3.2 *Microredistribution of Substances Dissolved in Liquid Components*

Microsineresis of liquid components of reaction medium should be inevitably followed by micro-volume (local) redistribution of solid substances (initiators, inhibitors) dissolved in liquid substances (oligomers, solvents)<sup>1</sup>.

It became possible to identify microredistribution of initiators in the course of TFRP on an example of polymerization of tEGdMA oligomer [33]. The electronic paramagnetic resonance (EPR) method was used, which enables us to determine the concentration of methacrylate radicals  $R_M^\bullet$ , stabilized in polymer matrix [34 (p. 137), 35]. Radicals  $R_M^\bullet$  are produced as a result of these reactions:



where I = initiator molecule; M = monomer molecule; and  $R_t^\bullet$  = free radical formed as a result of initiator decomposition.

With conversion, which is close to the limiting one, practically all methacrylate groups are interconnected (“pendent”) by chemical bonds with a highly cross-linked rigid polymer frame and, therefore, are characterized by extremely restricted translational mobility. It is natural that the mobility of product of addition of  $R_t^\bullet$  to M radical  $R_M^\bullet$  is also low and, therefore, this product is stabilized in the polymer matrix (does not recombine during the time of observation), and is accumulated up to concentrations that are quite suitable for use of the EPR method. The accumulation of  $R_M^\bullet$  is stopped after the limiting concentration  $[R_M^\bullet]_{lim}$  is reached, with which the average distance between adjacent  $R_M^\bullet$  becomes so small that the characteristic time of their diffusion into one another is decreased to values that are commensurate with

---

<sup>1</sup> In macroscopic scale, volume distribution of dissolved substances in this process remains unchanged; changes are recorded only in case of observation in scaled frame of reference commensurate with the size of polymer grains and intergrains layers.

the time of observation.



The interaction effected as a result of diffusion during reactions 0 and 2 against the background of continuing generation of  $R_M^\bullet$  leads to the establishment of dynamic equilibrium at the level of  $[R_M^\bullet]_{\text{lim}}$ . The content of methacrylate groups in a polymer matrix at any practically achievable degree of polymerization is several orders of magnitude greater than the concentration of radicals  $R_i^\bullet$ . Therefore, formation and stabilization of  $R_M^\bullet$  always take place in the same micro-volume, where  $R_i^\bullet$  appear as a result of initiator decomposition, i.e., in the places of initiator localization.

In case of substance initiation via photolysis of initiators of different nature, the value of  $[R_M^\bullet]_{\text{lim}}$  does not exceed  $2 \times 10^{-3}$  mol/l (Fig. 1.12). Additional irradiation of these samples by a source of  $^{60}\text{Co}$  leads to the growth of value  $[R_M^\bullet]_{\text{lim}}$  no less than three times [up to  $[R_M^\bullet]_{\text{lim}} = (6-7) \times 10^{-3}$  mol/l]. Thus, huge increments of  $\Delta[R_M^\bullet]_{\text{lim}}$ , as compared to source  $[R_M^\bullet]_{\text{lim}}$ , are observed, which is indicative of microredistribution of initiators in the course of tEGdMA polymerization.

Indeed, if microredistribution takes place, then the initiator occupies not the entire volume of the polymer, but only a certain part of it, and methacrylate radicals  $R_M^\bullet$ , generated via photolysis, are also formed only in such micro-volumes, in which initiator is present. Polymer micro-volumes, which are free from  $R_M^\bullet$  (i.e., "empty" micro-volumes), are potentially able to stabilize such numbers of  $R_M^\bullet$ , which is additional for  $[R_M^\bullet]_{\text{lim}}$ . Repeated generation of radicals via  $\gamma$ -irradiation, as a result of which  $R_i^\bullet$  are produced uniformly throughout the entire micro-volume of the polymer, both in "empty" and in completely "filled"  $R_M^\bullet$ , should lead to the growth of a maximum value of  $R_M^\bullet$  up to the value of  $[R_M^\bullet]_{\text{lim}} + \Delta[R_M^\bullet]_{\text{lim}}$ . Increment  $\Delta[R_M^\bullet]_{\text{lim}}$  is proportional to the total share of "empty" polymer volume because dynamic equilibrium is already achieved at the level of  $[R_M^\bullet]_{\text{lim}}$  in the micro-volumes, where the initiator is localized.

**Fig. 1.12** Dependence of concentration of methacrylate radicals stabilized in tEGdMA polymers upon initiation dose. Method for radical generation: 1, irradiation by  $^{60}\text{Co}$ ; 2–5, photochemical initiation. Photoinitiators: 2, methyl benzoate; 3, benzophenone; 4, benzoyl peroxide (BP); 5, AIBN. Conditions of radical generation: temperature  $20^\circ\text{C}$ , samples of polymers with  $C = 79.0\%$

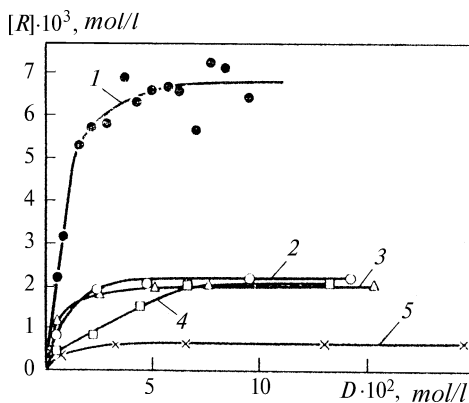
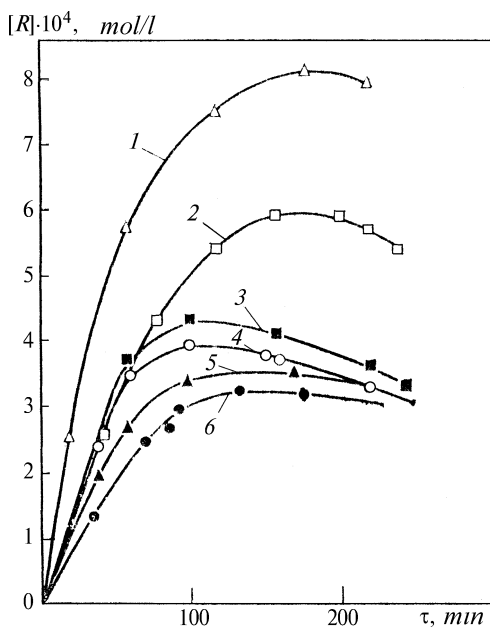


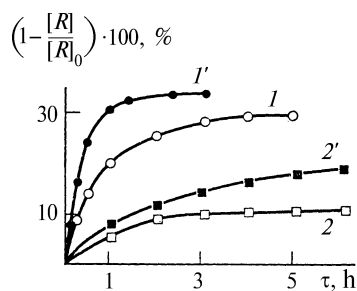
**Fig. 1.13** Dependency of concentration of methacrylate radicals stabilized by polymer matrix upon duration of photoirradiation of tEGdMA polymers obtained at the following temperatures, in °C: 1, 30; 2, 40; 3, 50; 4, 60; 5, 70; 6, 90. [AIBN] = 0.5% (by weight). For all polymer samples,  $C = 78.0\%$



Microredistribution during polymerization of tEGdMA was independently confirmed by detection of dependency of  $[R_M^\bullet]_{lim}$  upon prehistory of the polymer matrix [33]. Value of  $[R_M^\bullet]_{lim}$  decreases 2.5 fold as polymerization temperature increases from 30° to 90°C, despite the equality of compared polymer samples in terms of conversion (Fig. 1.13). As the polymerization temperature increases, the solubility of initiator in the oligomer grows and, therefore, the moment when the interlayer material reaches the state of saturated solution in terms of initiator concentration comes later, at higher conversions. Thus, the share of “empty” volume in the final polymer grows, while the share of volume occupied by initiator decreases proportionally to a decline of  $[R_M^\bullet]_{lim}$ , which, for samples of a given set, depends only upon the share of occupied volume.

During microredistribution, the initiator is forced to penetrate into low cross-linked micro-volumes of polymer, which, in contrast to highly cross-linked micro-volumes, are easy to enter in terms of diffusion [26]. This fact opened a possibility to confirm redistribution of initiator in the course of tEGdMA polymerization via one more independent method, i.e., through diffusion probing of polymer matrix containing stabilized methacrylate radicals  $R_M^\bullet$  [33]. Nitrogen oxide was used as a probe. Nitrogen oxide reacts (during diffusion into polymer samples) with radicals  $R_M^\bullet + NO \rightarrow$  recombination. Polymer samples with conversion level 75.5%, in which  $R_M^\bullet$  were generated via photolysis of initiator (series A) and radiation initiation  $^{60}Co$  (series B), were used as objects of probing. In series A, the share of  $R_M^\bullet$  that were destructed as a result of interaction with NO is much higher than in series B (Fig. 1.14). This fact could be easily interpreted by taking the microredistribution of initiator into account. Indeed, the ratio of accessible volumes to inaccessible vol-

**Fig. 1.14** Kinetics of destruction of methacrylate radicals generated by photoirradiation (1, 1') and irradiation (2, 2') of tEGdMA polymers depending upon NO diffusion time. Polymers were obtained at 20°C: [AIBN] = 0.5% (by weight) during 16 h with conversion  $C = 75.5\%$ . 1, 2, unmilled sample; 1', 2', milled polymer sample



umes for probe molecules in polymers of both series is exactly the same, because polymer samples are absolutely identical. However, as a result of the microredistribution of initiator, the degree of occupation of micro-volumes (inaccessible for NO) with  $R_M^\bullet$  radicals, in the case when radicals were generated via photolysis, is significantly lower than in the case of irradiation generation. This effect is a consequence of microredistribution, which leads to formation of “empty” micro-volumes (not occupied with molecules of initiator and, hence, radicals  $R_M^\bullet$ ) inaccessible for NO cores of polymer grains.

Microredistribution of adduct  $\text{>NO}^\bullet$  (product of interaction of stable nitroxile radical  $\text{>NO}^\bullet$  and cyanizopropile radical  $R_1^\bullet$ ) in the process of tEGdMA and dMA-tEGPh oligomer polymerization was discovered using the EPR method in the spin-probe variant [27 (p. 75); 36].

Thus, based on the example of initiators and adducts of stable nitroxile radicals, microredistribution of substances dissolved in liquid oligomers in the TFRP process could be considered to be a definitely established fact.

### 1.3.3 Local Glass Transition of Highly Cross-Linked Micro-Volumes of Polymer

According to the microheterogeneous model, polymer coils, i.e., particles of micro-gel, are characterized by a higher conversion (because of the local gel effect) than the volume-averaged one. In such cross-linked micro-volumes, segmental mobility of polymer chains deteriorates after the critical concentration of polymer network junctions is reached and local glass transition takes place.

The local glass transition in the TFRP process was identified based on an example of tEGdMA oligomer polymerization by the method of differential scanning calorimetry (DSC) [15]. The presence of the glass phase in polymer samples was found from the increase of differential heat flow  $\partial\Delta H/\partial\tau$ , the so-called heat jump, which is predetermined by the transition of polymer or its part from the glass state into the highly elastic state [37 (p. 164)]. Temperature dependency  $\partial\Delta H/\partial\tau$  was es-

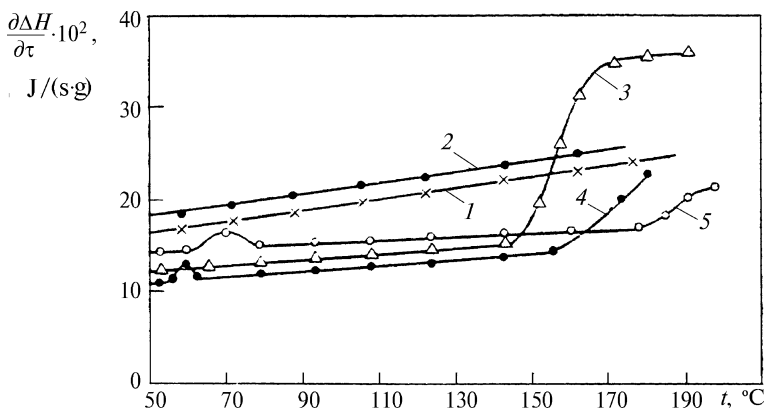


**Fig. 1.15** Variation of differential heat flow in the process of tEGdMA polymers heating. Conversion, %: 1, 0.0; 2, 6.0; 3, 10.0; 4, 27.0; 5, 35.0

established as a result of temperature scanning in the range  $20^{\circ}$ – $200^{\circ}$ C, taking into account the fact that at  $T > 200^{\circ}$ C thermal destruction of oligo(acrylates) polymers occurs [38]. The variation of differential heat flow takes place in a certain temperature range (Fig. 1.15), the average temperature of which was assumed to be equal to the temperature of glass transition  $T_g$ .

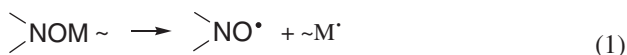
Samples for calorimetric measurements, obtained through polymerization of tEGdMA at  $60^{\circ}$ C, were characterized by conversion  $C$  from 0 to 35.0%. This range of conversions covers initial and intermediate stages of polymerization, when formation and growth of polymer grains occurs (see Sects. 1.2.1, 1.2.2). To prevent polymerization in the process of temperature scanning, samples were saturated with inhibitor, namely, with stable nitroxyl radical.

It follows from the results of differential heat flow measurements taken during temperature scanning (see Fig. 1.15) that a certain part of reaction medium stays in the glass state even at low conversions  $C$  (at  $6 < C \leq 10\%$ ), and glass transition occurs exactly locally in micro-volumes of polymer, which, on the whole, is gel like at  $C < 10\%$ . Most likely, these polymer micro-volumes (capable of glass transition) could be identified with layers with uncompleted cross-linked structure, which adhere to polymer grain cores (see Fig. 1.8). Glass-like polymer grain cores with completed cross-linked structure are incapable of glass transition; therefore, they cannot be identified using the DSC method (see Sect. 1.4.2).

On the whole, the authors believe that structural and physical processes of microsineresis and microredistribution of reaction medium components, as well as local glass transition of quite highly cross-linked micro-volumes of this medium, are established with a high degree of certainty based on the example of oligo(acrylates) polymerization.

## 1.4 Microheterogeneous Structure of Cross-Linked Polymers

The microheterogeneous character of cross-linked polymer structure was established using the EPR method in the variant of spin-probe [26, 39]. The paramagnetic probe 2,2,6,6-tetramethylpiperidin-1-oxyl (TEMPO) was introduced into a polymer via vapor sorption or into the initial oligomer before the beginning of polymerization with subsequent regeneration of probe molecules in the polymer from adduct  $\sim\text{NOM}\sim$  according to the following reactions [40]:



where  $\sim\text{M}\cdot$  = chain-carrier radical.

Sorption of probe molecules by cross-linked polymer occurs selectively, only by low cross-linked interlayers, while highly cross-linked polymer grains remain inaccessible (in terms of diffusion) throughout the time of experiment [25, 26, 39]. In contrast, the regeneration method enables us to introduce spin-probe not only into the interlayers but also into polymer grains [36, 41].

Selectivity of sorption of spin-probe molecules exactly by the interlayer was proved by a set of following results [26]. The maximum sorption of spin-probe decreases with the growth of conversion proportionally to a decrease in the yield of sol fraction identified with the interlayer. Further, proportional dependency holds true at later stages of polymerization in a wide range of conversions (Fig. 1.16). In the case of irradiation of oligo(acrylates) polymers containing absorbed spin-probe, EPR signals are observed (Fig. 1.17), which are a superposition of spin-probe spectra and methacrylate radical spectra. As the methacrylate radical is extremely reactive, its stabilization occurs only during localization in rigid (highly cross-linked) micro-volumes of polymer material, i.e., in grains and in zones of their accretion.

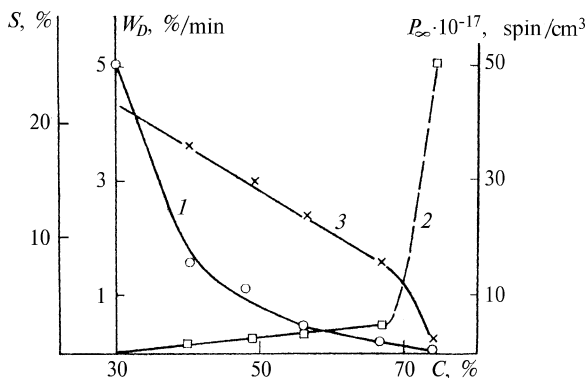


**Fig. 1.16** Influence of conversion upon tMA-tPA polymer properties: 1, sorption of spin-probe [radicals TEMPO at 20°C ( $P_{\infty}$ )]; 2, reduced initial rate of diffusion ( $W_D$ ); 3, content of sol fraction ( $S$ ) in polymer

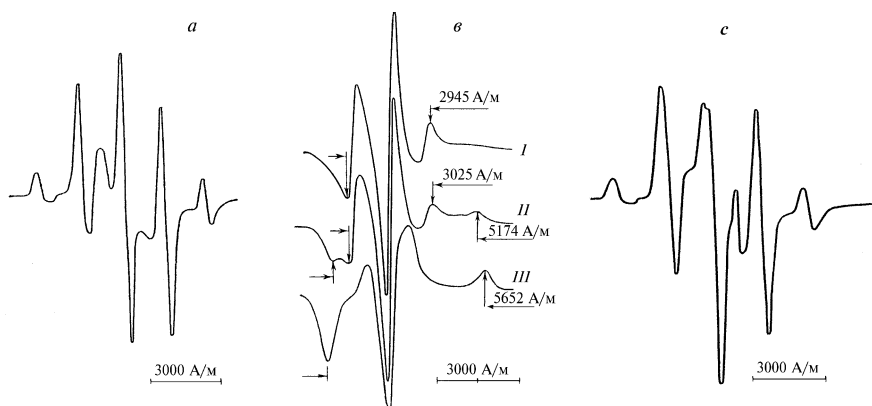


**Fig. 1.17** EPR spectra for poly(methacrylate) and nitroxyl radicals in tMA-tPA polymer [tetramethacrylate of bis(trimethylolpropane) adipate] with conversion 67.0%: (a) spectrum of poly(methylmethacrylate) radicals generated by irradiation of polymers at the  $^{60}\text{Co}$  source (dose, 2 Mrad); (b) spectrum of TEMPO in a polymer saturated with vapors up to  $[\text{NO}^*] = 1 \times 10^{17} \text{ spin/cm}^3$  within the temperature range  $-80^\circ$  to  $+20^\circ\text{C}$ : I, high-temperature region; II, transition region; III, low-temperature region; c superposition of spectra for polymethacrylate and nitroxyl radicals. Polymethylmethacrylate radicals were generated by irradiation by  $^{60}\text{Co}$  source (dose, 2 Mrad). The polymer was saturated with nitroxyl radicals from vapors up to  $[\text{NO}^*] = 1 \times 10^{17} \text{ spin/cm}^3$

Coexistence without recombination of reactive methacrylate radical stabilized by polymer matrix and highly mobile (judging by the value of correlation time  $\tau_c$ ), stable nitroxyl radical within the frame of one and the same polymer substrate is possible only in the case in which they are localized in different micro-volumes. Hence, spin-probe becomes absorbed only in low cross-linked micro-volumes (interlayer material), in which stabilization of methacryl radicals does not take place.

The regeneration method of introducing polymer spin-probe into tEGdMA and dMA-tEPH polymers offered an opportunity to identify both types of micro-volumes—low cross-linked and highly cross-linked—using the EPR method [36, 41]. A spectrum of regenerated spin-probe in tEGdMA polymer is a superposition of two spectra: a narrow one (3600 A/m) and a wide one (5400 A/m) (see Fig. 1.18) [41]. For the narrow spectrum, the spin-probe correlation time  $\tau_c$  was  $1 \times 10^{-9}$  s, while for the wide spectrum it was  $1 \times 10^{-7}$  s. Because the value of  $\tau_c$  is determined by molecular mobility of structural elements in the micro-volume, where the probe molecule is localized [42, 43], such a sharp difference (i.e., by two orders of magnitude!) in values of  $\tau_c$  uniquely indicates on localization of spin-probe in micro-volumes of two types, which are drastically different in terms of molecular mobility. These types of micro-volumes could be reliably identified with low cross-linked interlayers and highly cross-linked polymer grains.

### 1.4.1 Interlayers Between Polymer Grains

Following the accretion of polymer grains, the interlayers between polymer grains that separate the latter at the stage of their growth appear to be included within the structure of cross-linked polymers, thus determining the microheterogeneity of this structure.

An investigation of temperature dependence of the shape of spin-probe EPR spectra selectively absorbed by interlayers material enabled detecting such transitions in the interlayers, which relate to glass transition type, and to establish the structural nonhomogeneity of the interlayers proper by the character of transitions [39].

tEGdMA polymers with different degrees of conversion were subjected to probing. In all cases, irrespective of sample conversion, three characteristic areas of variation in EPR spectra width of nitroxyl spin-probe line were observed during temperature scanning within the range  $-80^{\circ}$  to  $+20^{\circ}\text{C}$  (Fig. 1.17b). A narrow spectrum line (2945–3025 A/m) was observed in the high-temperature area, whereas a wide spectrum line (5413–5650 A/m) was observed in the low-temperature area. Between these two areas, within a certain temperature range  $\Delta T_{1,2} = T_2 - T_1$  (transition area), with increasing temperature, the intensity of the narrow line increases because of the intensity of the wide line, up to complete disappearance of the latter at  $T_2$ .<sup>2</sup> Above  $T_2$ , only the narrow line is observed, while below  $T_1$ , in contrast, only the wide line is seen. The width of transition area  $\Delta T_{1,2}$  between temperatures  $T_1$  and

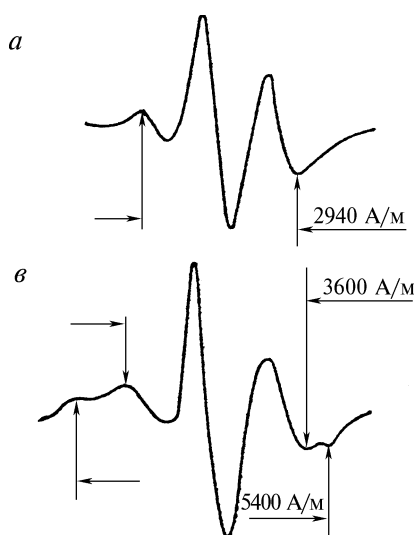
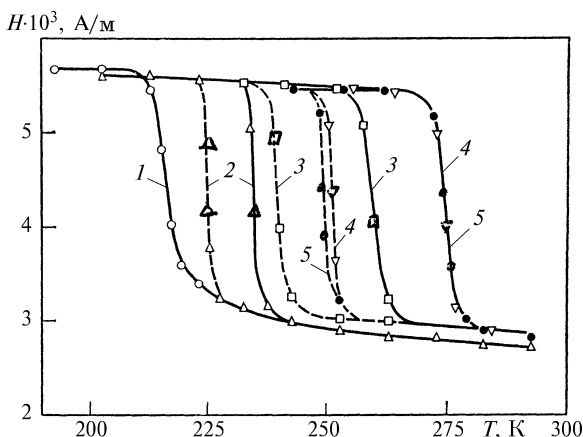


**Fig. 1.18** EPR spectra of nitroxyl radicals TEMPO, regenerated in tEGdMA polymer at  $65^{\circ}\text{C}$ : (a) during 1 h; (b) during 24 h

<sup>2</sup> Special experiments implying the variation of rate of temperature changing in the range  $\Delta T_{1,2}$  showed that the ratio of wide line intensity to narrow line intensity is a unique function of temperature and is not time dependent.



**Fig. 1.19** Dependency of line width of EPR spectra on temperature in tEGdMA polymer with different conversions. Conversion, %: 1, 0.0; 2, 26.0; 3, 51.0; 4, 58.0; 5, 73.0. Transition areas  $\Delta T_{1,2}$  are limited from side  $T_1$  by a continuous line; those from side  $T_2$  are shown by a dotted line



$T_2$  depends upon conversion  $C$  (Fig. 1.19), and it narrows as  $C$  decreases, while in the limit for initial oligomer (i.e., at  $C = 0$ ), the transition area becomes completely deteriorated ( $\Delta T_{1,2} = 0$ ):

$C, \%$	0	25.8	51.1	58.3	72.9
$\Delta T_{1,2}, ^\circ\text{C}$	0	7	20	23	25

Widening of the nitroxyl probe line was observed for a number of polymers when glass-transition temperature  $T_g$  passes into temperature area  $T < T_g$  [42, 43]. It is preconditioned by “freezing-out” of segmental mobility of macromolecules with corresponding deceleration of rotational mobility of the probe. However, in neither of these two cases was a transition area of significant wideness observed, always  $\Delta T_{1,2} \rightarrow 0$ . In microheterogeneous polymer matrices consisting of polymers with different  $T_g$ , we managed to record a temperature range characterizing the coexistence of wide and narrow lines of the nitroxile probe at temperatures higher than  $T_g$  of the first polymer, but lower than  $T_g$  of the second polymer [44, 45]. However, this transition area differs from the one that was observed for the spin-probe selectively absorbed with tEGdMA polymers. In microheterogeneous polymer matrices, the intensity of both coexisting lines (wide lines and narrow ones) remains unchanged in the transition area. In contrast, in interlayers of tEGdMA polymers, a continuous decline of the intensity of the narrow line of the nitroxyl probe occurs when moving from high-temperature limit  $T_1$  to low-temperature limit  $T_2$ .

Taking these results into account, the discussed data could be interpreted as a manifestation of micro-nonhomogeneity of polymer material of interlayers; the narrow line corresponds to defective micro-volumes with low-degree cross-linking (i.e., with reduced concentration of junctions) and, hence, with higher mobility of spin-probe molecules (correlation time  $\tau_c \ll 10^{-7}$  s), while the wide line corresponds to micro-volumes with a higher concentration of junctions (as compared to defective micro-volumes) and, hence, with low molecular mobility ( $\tau_c \geq 10^{-7}$  s). The state corresponding to the wide line is interpreted as glass like, whereas the one corresponding to the narrow line is seen as highly elastic, and  $\Delta T_{1,2}$  is considered to be an area of  $\alpha$ -transition (glass transition). Within the framework of such interpretation, the

ratio of intensity of narrow ( $I_1$ ) and wide ( $I_2$ ) lines in the area of their superposition ( $\Delta T_{1,2}$ ) characterizes the relationship of the total number of micro-volumes staying in highly elastic and glass-like states:

$$\frac{I_1}{I_2} = \frac{\sum_1^m \Delta V_i}{\sum_m^n \Delta V_i} \quad (1.9)$$

where  $\Delta V_i$  = volume of  $i$ th micro-area;  $m$ ,  $(n - m)$ , and  $n$  = number of highly elastic and glass micro-areas and their total number, respectively; and  $\sum_1^n \Delta V_i$  = total volume of the system.

It is obvious that smooth variation of  $I_1/I_2$  in a very broad interval  $\Delta T_{1,2}$  (several dozens of degrees) is possible only in the case when the microheterogeneous system consists of a large set of subsystems (micro-volumes  $\Delta V_i$ ) including  $n$  different types  $\Delta V_i$ , each of which has its own (local) temperature of glass transition  $T_{gi}$ , which varies in the progression  $\Delta V_1, \Delta V_2, \dots, \Delta V_n$ , - e.g.,  $T_{g1} > T_{g2} > \dots > T_{gn}$ . If  $n$  is a sufficiently large number, the variation  $I_1/I_2$  will be smooth (without jumps). It is evident that the value  $\Delta T_{1,2}$  corresponds to the difference  $T_{g1} - T_{gn}$  and, hence, characterizes the degree of micro-nonhomogeneity of cross-linked polymers ( $n$  = number of types of subsystems  $\Delta V_i$ , which differ by values of  $T_{gi}$ :  $\Delta V_i$  with a higher degree of cross-linking is characterized by higher local temperatures  $T_{gi}$ ).

Properties of the interlayer substrate at different degrees of conversion could be characterized by the width of transition area  $\Delta T_{1,2}$ , which serves as a quantitative measure of nonhomogeneity degree, and by the value of average temperature of transition (glass-transition temperature  $T_g = T_2 + 0.5T_{1,2}$ ). Values of  $T_g$ , as well as  $\Delta T_{1,2}$ , increase as the degree of conversion increases (see Fig. 1.19):

$C, \%$	0	25.8	51.1	58.3	72.9
$T_g, ^\circ\text{C}$	-55.0	-42.0	-20.0	-8.0	-4.0

Obviously, the interlayer substrate cannot be uniform in terms of thickness of layer between the grains, because the external peripheral layer of grains is a growing one and is uncompleted in terms of polymerization depth, with a degree of completeness descending in the radial direction (see Sect. 1.2.2). As the degree of conversion grows, grain thickness is increased by the consumption of the interlayer oligomer. Interlayers become thinner, and the contribution of the lowest cross-linked parts of the peripheral layers of grains (accessible for probing) into properties of the interlayer substrate increases accordingly. As a result, as the degree of conversion grows, the degree of nonhomogeneity of the interlayer substrate increases (width of transition zone,  $\Delta T_{1,2}$ ), and a logical shift of averaged temperature of glass transition  $T_g$  of interlayer substrate into a high-temperature area is observed.

### 1.4.2 Polymer Grains

According to kinetic data presented above (see Sect. 1.2.2), polymer grains are well approximated by spherical monodispersed particles consisting of highly cross-linked cores with limiting conversion  $C_{lim}$  (for a given temperature) and growing peripheral layers with uncompleted cross-linked structure and conversion  $C < C_{lim}$ . In turn, the degree of completeness and conversion in peripheral layers declines in the radial direction from the layers adhering to the core surface, from  $C \approx C_{lim}$  to the layers adhering to intergrain layers, with conversion  $C \approx 0$ .

Local glass micro-volumes were detected in samples of tEGdMA polymers through the use of the DSC method (see Sect. 1.3.3), the glass-transition temperatures  $T_g$  of which stay within the high-temperature area (see Fig. 1.15):

$C, \%$	10.0	27.0	35.0
$T_g, ^\circ\text{C}$	160	170	190

Within the framework of the ideas just presented regarding the structure of polymer grains, these polymer micro-volumes (capable of glass transition) were identified with layers adhering to the surface of cores, for which  $T_g$  increases as the degree of conversion increases, while the value of “heat jump” (volume of polymer undergoing glass transition) is decreased (see Fig. 1.15). Such regularity could be preconditioned by an increase in the degree of cross-linking of these layers resulting from growth of conversion degree with concurrent reduction of their thickness (volume). As has been established, upon the completion of polymerization, in peripheral layers of polymer grains, conversion reaches its limit value  $C_{lim}$ , as in the cores of polymer grains. Thus, these layers cease to exist as layers with uncompleted cross-linked structure (see Sect. 1.2.2).

Taking the nonhomogeneity of polymer grain structure into account, their physical (relaxation) states could be presented in the following way.

Highly cross-linked cores of polymer grains with  $C = C_{lim}$  and completed cross-linked structure are in the glass state, and this state is irreversible. Even in the neighborhood of thermal destruction temperature, approximately equal to  $200^\circ\text{C}$ , tEGdMA polymers do not transfer into the highly elastic state [38]. Incapability of  $\alpha$ -transition (glass transition) means for a cross-linked polymer the commensurability of the value of interjunction chains with the value of the kinetic segment and irreversible freezing of segmental mobility.

Peripheral layers of polymer grains with a still uncompleted cross-linking structure, which adhere to cores, are also in the glass state, but, in contrast to core substrate, cross-linked polymers of these layers are capable of  $\alpha$ -transition, although in the high-temperature area  $160^\circ \leq T_g \leq 190^\circ\text{C}$ , close to the thermal destruction temperature for tEGdMA polymers. In contrast to highly cross-linked polymers of cores, polymers of such layers could be related to moderately cross-linked polymers, as the lengths of interjunction chains of such polymers should be greater than the kinetic segment length.

Low cross-linked peripheral layers of polymer grains with  $C \approx 0$  (adhering to intergrain layers) should stay in the highly elastic state, and their glass-transition temperature values probably stay within the low-temperature area, not differing significantly from  $T_g$  of intergrain layers. Indeed, for the material of intergrain layers of tEGdMA polymers, glass-transition temperatures (increasing as degree of conversion  $C$  increases in the range  $0 < C \leq 72.9\%$ ) fall within the range  $-55^\circ \leq T_g \leq -4^\circ\text{C}$  (see Sect. 1.4.1).

Thus, the structure of cross-linked polymers—i.e., the products of TFRP—is complicated at multiple levels: it is microheterogeneous for the polymers proper (being represented by highly cross-linked glass-like polymer grains and low cross-linked intergrain layers) and, in their turn, grains and intergrain layers are also heterogeneous in terms of degree of polymer network cross-linking.

## References

1. Howink R (1934) In: *Physikalische Eigenschaften und Feinbau von Natur und Kunsthharzen* Bd. 119. Leipzig Akademische Verlagsgesellschaft, Leipzig, S 133
2. Kozlov PM (1936) *Org Chem Ind* **2**:581–588 (in Russian)
3. Kozlov PM (1937) *Org Chem Ind* **4**:98–104 (in Russian)
4. Gallacher L, Bettelheim FA (1962) *J Polym Sci* **58**:697–714
5. Korolev GV, Berlin AA (1962) *Vysokomolekul Soedin* **4**:1654–1659 (in Russian)
6. Notley NT (1962) *J Phys Chem* **66**:1577–1582
7. Bobalek EG, Moore ER, Levy CC (1964) *J Appl Polym Sci* **8**:625–657
8. Dušek K (1982) *Polymer networks*. Springer, NY
9. Korolev GV, Smirnov BR, Tvorogov NN (1970) *Papers for jubilee session on high-molecular compounds*. Nauka, Moscow (in Russian)
10. Korolev GV (1977) *Papers for the 1st All-Union Conference on Chemistry and Physical Chemistry of Polymerized Oligomers*, vol 1. Department of the Chemistry and Physics Institute of the USSR Academy of Science, Chernogolovka (in Russian)
11. Eskin VE (1973) *Light scattering by solutions of polymers*. Nauka, Moscow (in Russian)
12. Volkova MV, Belgovskiy IM, Mogilevich MM et al (1987) *Vysokomolekul Soedin A* **29**:435–440 (in Russian)
13. Belgovskiy IM, Enikolopyan NS (1965) *Vysokomolekul Soedin* **7**:2033 (in Russian)
14. Golikov IV, Semyannikov VA, Mogilevich MM (1985) *Vysokomolekul Soedin B* **27**:304–306 (in Russian)
15. Semyannikov VA, Belgovskiy IM, Mogilevich MM et al (1989) *Vysokomolekul Soedin A* **31**:1602–1609 (in Russian)
16. Vasilyev DK, Belgovskiy IM, Mogilevich MM et al (1989) *Vysokomolekul Soedin A* **31**:1233–1237 (in Russian)
17. Roschupkin VP, Ozerkovskiy BV, Kalmykov YuB et al (1977) *Vysokomolekul Soedin A* **19**:699–706 (in Russian)
18. Roschupkin VP, Ozerkovskiy BV, Korolev GV et al (1977) *Vysokomolekul Soedin A* **19**:2239–2245 (in Russian)
19. Berezin MP, Lagunov VM, Korolev GV et al (1981) *Vysokomolekul Soedin A* **23**:422–427 (in Russian)
20. Vasilyev DK, Krasnobayeva VS, Mogilevich MM et al (1989) *Vysokomolekul Soedin B* **31**:430–431 (in Russian)
21. Vasilyev DK, Golikov IV, Mogilevich MM, et al (1987) *Vysokomolekul Soedin B* **29**:563–564 (in Russian)

22. Vasilyev DK, Mogilevich MM, Korolev GV (1986) *Vysokomolekul. Soedin B* **28**:2570–2574 (in Russian)
23. Berezin MP, Korolev GV (1980) *Vysokomolekul. Soedin A* **22**:1872–1878 (in Russian)
24. Berlin AA, Korolev GV, Kefeli TYa, Sivergin YuM (1983) Acrylic oligomers and materials on the acrylic oligomers. *Khimiya, Moscow* (in Russian)
25. Lagunov VM, Golikov IV, Korolev GV (1982) *Vysokomolekul. Soedin A* **24**:131–137 (in Russian)
26. Golikov IV, Berezin MP, Mogilevich MM et al (1979) *Vysokomolekul. Soedin A* **21**:1824–1830 (in Russian)
27. Korolev GV, Mogilevich MM, Golikov IV (1995) Cross-linked polyacrylates: microheterogeneous structures, physical networks, deformation-strength properties. *Khimiya, Moscow* (in Russian)
28. Flory P, Renner J (1943) *J Chem Phys* **1**:521–526
29. Dušek K (1970) *Polym Prepr Am Chem Soc Div Polym Chem* **11**:536–540
30. Sedláček B, Dušek K (1972) *Prepr Int Symp Macromolecules Helsinki* **4**:323–328 (IUPAC, Basel)
31. Vasilyev DK, Belgovskiy IM, Mogilevich MM, et al (1990) *Vysokomolekul. Soedin B* **32**:678–684 (in Russian)
32. Semyannikov VA, Belgovskiy IM, Mogilevich MM (1987) *Vysokomolekul. Soedin B* **29**:315–319 (in Russian)
33. Lagunov VM, Berezin MP, Korolev GV et al (1985) *Vysokomolekul. Soedin A* **27**:2056–2060 (in Russian)
34. Berlin AA, Kefeli TYa, Korolev GV (1967) *Poly-esteracrylates*. Nauka, Moscow (in Russian)
35. Korolev GV, Smirnov BR, Bolkhovitinov AB (1982) *Vysokomolekul. Soedin A* **4**:1660–1664 (in Russian)
36. Ilyin AA, Golikov IV, Mogilevich MM et al (1990) *Vysokomolekul. Soedin B* **32**:243–249 (in Russian)
37. Tager AA (1978) *Physics and chemistry of polymers*. *Khimiya, Moscow* (in Russian)
38. Volkova NN, Berezin MP, Korolev GV, et al (1983) *Vysokomolekul. Soedin A* **25**:871–876 (in Russian)
39. Lagunov VM, Berezin MP, Korolev GV, et al (1981) *Vysokomolekul. Soedin A* **23**:2747–2751 (in Russian).
40. Kovtun GA, Alexandrov AL, Golubev VA (1974) *Izv AN SSSR Khimia No* **10**:2197–2204 (in Russian)
41. Lagunov VM, Smirnov BR, Korolev GV et al (1987) *Vysokomolekul. Soedin A* **29**:1442–1446 (in Russian)
42. Buchanenko AL, Vasserman AM (1973). *Stable radicals*. *Khimiya, Moscow* (in Russian)
43. Vasserman AM, Kovarskiy AL (1986) *Spin labels and spin probes in physics and chemistry of polymers*. Nauka, Moscow (in Russian)
44. Kumler PL, Boyer SF (1976) *Macromolecules* **9**:903–910
45. Kumler PL, Keinath SR, Boyer RF (1977) *Polym Eng Sci* **17**:613–621

## Chapter 2

# Kinetic Features of Three-Dimensional Free-Radical Polymerization

**Abstract** Key results of systematic exploration into three-dimensional free-radical polymerization (TFRP) in blocks, solutions, and films carried out by the authors are described in Chap. 2. An interpretation of TFRP kinetic features takes the microheterogeneous mechanics of polymerization into account. The factors determining the effective reactivity of unsaturated oligomers (allyl and vinyl types) under different conditions and at various TFRP stages were identified. All this enabled the authors to create a scientific basis of control over TFRP needed to produce different-purpose polymeric materials.

The main kinetic features of TFRP were determined in a series of systematic studies conducted by the authors with the use of oligo(acrylates) starting in 1960 [1–5]. Oligo(acrylates) were found to be very convenient oligomers for such experiments because their synthesis method enables us to vary, as targets, chemical composition and oligomer block size in a wide range, with the end methacrylate or acrylate groups able to polymerize being invariable [1, 3].

Processes of TFRP for polyunsaturated oligomers (monomers) of various structures have a similar development pattern. At the initial stage (in nonstructured reaction medium), the polymerization rate  $W_0$  remains constant in a rather narrow range of conversions,  $0 < C < 3 - 4\%$ ; then, in the period of polymerization auto-acceleration, it increases with growing  $C$ , and then with conversion  $C_{\max}$ , it becomes maximal  $W_{\max}$ . Subsequently, polymerization auto-deceleration takes place with complete TFRP process termination when limit conversion  $C_{\lim} < 100\%$ . During periods of auto-acceleration and auto-deceleration, polymerization proceeds in a structured reaction medium. The analysis of main kinetic TFRP features requires identifying factors determining the effective reactivity of oligomers (monomers) at each consecutive stage of the process as well as in different TFRP conditions (in the presence of inhibitors, in solutions, and in films).

## 2.1 Kinetic Features of Individual Stages of Polymerization

### 2.1.1 Initial Stage of Polymerization

Studying the initial stage of polymerization (up to a gel point, in unstructured reaction medium) enables identifying those oligomer-inherent kinetic parameters that at later stages are masked by formation of cross-linked polymer.

#### 2.1.1.1 Influence of Oligomer Viscosity on Initial Polymerization Rate

Table 2.1 contains data showing correlation of initial polymerization rate  $W_0$ , characterizing oligomer reactivity, and macroscopic viscosity of oligomers  $\eta$  [6, 7].

$W_0$  increases with conversions  $C \rightarrow 0$  as the viscosity grows. In its turn, reaction medium viscosity for small conversions is regulated by intensity of intermolecular interactions (IMI) of molecules of initial oligomers. Molecules have centers of strong IMI able to form dipole–dipole and other labile intermolecular bonds. Oligomer molecules (Table 2.1) have strong IMI centers that are systematically varying from two ester groups with intermolecular interaction energy  $E_{\text{IMI}} = 18.4 \text{ kJ/mol}$  for tEGdMA to six ester and two phenyl groups with  $E_{\text{IMI}} = 31.8 \text{ kJ/mol}$  for oligomer MDP-2 [8]. Associated methylene groups  $(-\text{CH}_2-)_n$  may also serve as strong IMI centers. Each of these groups is characterized by very weak dispersion interactions (in case of  $n \geq 4$  these groups enter into IMI with  $E_{\text{IMI}} > 17 \text{ kJ/mol}$  comparable with energy of hydrogen bonds) [9]. Oligomer viscosity grows concurrently with an increase in the number of IMI centers and IMI energy.

**Table 2.1** Initial polymerization rates of (oligo)acrylates  $W_0$  in block and solution at 50°C

Oligomer	Oligomer repeating unit	Kinematic viscosity $\nu$ at 20°C, $\text{mm}^2/\text{s}$	$W_0 \times 10^2, \text{min}^{-1}$		
			In block	In solution, with oligomer <b>ID(PD)<sub>2</sub>DI</b> content, %	
				50	75
tEGdMA	<b>MTM</b>	10	3.0	5.0	8.0
MDA	<b>MDADM</b>	55	3.0	–	7.5
MDP-1	<b>MDPDM</b>	60	4.0	4.3	8.0
MBP-1	<b>MBPBM</b>	115	5.0	6.0	8.0
MDP-2	<b>M(DP)<sub>2</sub>DM</b>	1000	17.5	14.0	–

*Note 1.* Notation conventions for Tables 2.1, 2.4, and 2.5 only: **M, A, I, P**, residues of methacryl, adipine, isobutyric, and *ortho*-phthalic acids, respectively; **D, T, and B**, residues of diethylene glycol, triethylene glycol, and tetramethylene glycol, respectively.

*Note 2.* **I[DP]<sub>2</sub>DI** with  $\nu = 900 \text{ mm}^2/\text{s}$  at 20°C: initiator, dicyclohexylpercarbonate 0.5% (by weight), conversion  $C \rightarrow 0$ .

Dependence  $W_0 = f(\eta)$  is sufficiently universal for oligo(acrylates) polymerization and trivial in terms of its physical sense. Indeed,  $W_0$  is a function of the following kinetic parameters:

$$W_0 = \frac{k_{pr}}{k_{ter}^{1/2}} \cdot [M] \cdot W_i^{1/2} \quad (2.1)$$

where  $W_i$  = initiation rate;  $k_{pr}$  and  $k_{ter}$  = constants of chain propagation rate and chain termination rate; and  $[M]$  = oligo(acrylates) concentration.

Studies were conducted under conditions that were similar in terms of  $W_i$  and  $[M]$ : reduced polymerization rates  $W_0/[M]$  of different oligomers with equal concentrations of one and the same initiator, with similar temperature, and for conversion  $C \rightarrow 0$  were compared. Chain termination constant  $k_{ter}$  [10, 11] should be a parameter that is the most sensitive to viscosity variation in the reaction medium. The authors have found considerable decrease of  $k_{ter}$  as the viscosity grows, under the conditions of diffusion control over reaction of quadratic chain termination. The termination in case of TFRP (even with  $C \rightarrow 0$ ) is limited by diffusion, while the latter is limited by viscosity. The higher is the viscosity, the lower is the value of effective constant  $k_{ter}$  and, therefore, the higher is  $W_0$ .

### 2.1.1.2 Influence of Regular Associates of Oligomer (Monomer) upon Initial Polymerization Rate

Kinetic Anomalies of Oligo(Acrylate) Polymerization: Role of Regular Associates (Hypothesis)

Dependence of initial polymerization rate  $W_0$  on oligo(acrylates) nature comprises not only viscosity influence. In some cases at the initial TFRP stage, abnormal reactivity of oligomers was observed, and this reactivity was interpreted based on the assumption implying the existence of regular kinetically active associates in liquid oligo(acrylates).

For example, when measuring values of chain propagation rate constant  $k_{pr}$  and chain termination rate constant  $k_{ter}$  during polymerization of (alkylene glycol) dimethyl acrylates with different sizes of hydrocarbon chain  $(-\text{CH}_2-)_n$  for conversions  $C \rightarrow 0$ , an abnormally high value of  $k_{pr}$  was found, which increased three-fold as  $n$  increased from 4 to 10 (Table 2.2) [12]. Also, the value of  $k_{pr}$  declines to normal ( $k_{pr} \approx 3001 \cdot \text{mol}^{-1} \cdot \text{s}^{-1}$  at  $25^\circ\text{C}$  for methacrylates [10, 13, 14]) with increasing degree of conversion. The size of the hydrocarbon fragment of (alkylene glycol) dimethyl acrylate molecules does not influence the electron density distribution of double bonds and cannot alter their reactive capacity; hence, the values of  $k_{pr}$  of alkyl (meth)acrylates, differing in terms of size of their alkyl fragments, are quite close [10, 13, 14].

In another case, during polymerization of hexamethacrylate (bis-pentaerythrite) adipate (hMA-PeA) [15], an abnormal influence of viscosity upon initial



**Table 2.2** Values of chain propagation rate constant ( $k_{pr}$ ) and chain termination rate constant ( $k_{ter}$ ) (25°C) for polymerization of alkylene glycol dimethyl acrylates at different conversions

Conversion, %	dMABDO		dMAHDO		dMADDO	
	$k_{pr}$ , 1/(mol·s)	$k_{ter}$ , 1/(mol·s)	$k_{pr}$ , 1/(mol·s)	$k_{ter}$ , 1/(mol·s)	$k_{pr}$ , 1/(mol·s)	$k_{ter}$ , 1/(mol·s)
≈0	≈600	≈8 × 10 <sup>5</sup>	≈1200	≈6.2 × 10 <sup>5</sup>	≈1880	≈4.2 × 10 <sup>5</sup>
2.5	173	7.8 × 10 <sup>4</sup>	690	2.1 × 10 <sup>5</sup>	1660	1.9 × 10 <sup>5</sup>
5	112	2.3 × 10 <sup>4</sup>	245	3.6 × 10 <sup>4</sup>	1400	1.54 × 10 <sup>5</sup>
10	63	5.7 × 10 <sup>3</sup>	102	8.6 × 10 <sup>3</sup>	1900	9.6 × 10 <sup>4</sup>
15	41.5	2.5 × 10 <sup>3</sup>	89	5.8 × 10 <sup>3</sup>	1880	6.7 × 10 <sup>4</sup>
20	33	1.8 × 10 <sup>3</sup>	59	3.1 × 10 <sup>3</sup>	1700	5.4 × 10 <sup>4</sup>
30	17	8.3 × 10 <sup>2</sup>	26	1.3 × 10 <sup>3</sup>	840	2.5 × 10 <sup>4</sup>
40	3.4	1.5 × 10 <sup>2</sup>	9.5	4.3 × 10 <sup>2</sup>	196	5.9 × 10 <sup>3</sup>
50	–	–	–	–	24	6.5 × 10 <sup>2</sup>

Note 1. dMABDO, dimethylacrylate-1,4-butandiole; dMAHDO, dimethylacrylate-1,6-hexandiole; dMADDO, dimethylacrylate-1,10-decandiole.

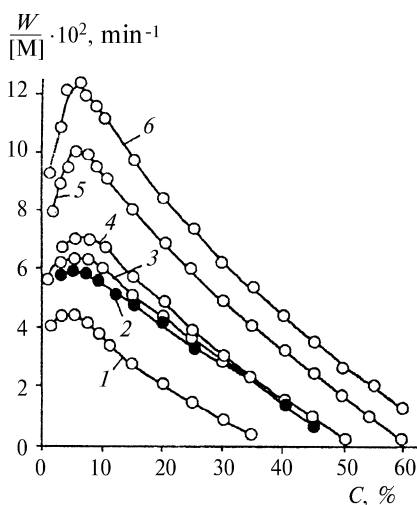
Note 2. Photoinitiator, benzophenone;  $W_i = 7 \times 10^{-9}$  mol/(1·s).

polymerization rate  $W_0$  was found: viscosity decrease after dilution by inert solvents resulted not in the decline of  $W_0$  but, on the contrary, in its increase (Fig. 2.1).

These anomalies suggested the presence of another, specific feature of TFRP for low-degree conversions; namely, influence on polymerization kinetics of regular associates that are sufficiently stable at polymerization temperature and that are formed in initial oligo(acrylates) [16, 17].

Indeed, oligo(acrylates) homo-polymerization in thin films in the air [18] is indicative of oligo(acrylate) ability to form structurally ordered regions (associates) with a long period of structural relaxation even at 65°–80°C. For low-degree

**Fig. 2.1** Influence of solvents on hMA-PeA polymerization rate at 65°C: 1, 4, toluene; 2, butyl acetate; 3, chlorobenzene; 5, dimethyl formamide; 6, formamide. Solvent concentration, % (by weight): 1, 6; 2–6, 24; benzoyl peroxide concentration, 1.5% (by weight)



conversions under the conditions when  $O_2$  diffusion rate into the film from the air is much higher than its utilization rate for the copolymerization reaction of oligomer with oxygen  $\sim M^\bullet + O_2 \rightarrow \sim MO_2^\bullet(1)$  and  $\sim MO_2^\bullet + M \rightarrow \sim MOOM^\bullet(2)$ , homopolymerization develops  $\sim M^\bullet + M \rightarrow \sim MM^\bullet(3)$ ; hence,  $W_3/W_2 = 5-10$ . Under such conditions, normally reaction (1) should prevail over the competing reaction (3) because  $k_1[O_2] > k_3[M]$ . Possibly, the liquid oligomer structure is characterized by such perfect molecule packing in the associates that either diffusion coefficient or oxygen solubility (or both) drop dramatically as compared to conventional weakly associated liquids.

Further accumulation of polymer (as conversion increases) results in structural rearrangement and normal oxidative polymerization with formation of copolymer of oligomer with oxygen  $(-M-O-O-)_n$  with composition 1:1.

Polyfunctional molecules of oligomers with strong IMI centers are characterized by ability to form physical associates, the lifetime  $\tau_{ph}$  of which may go as high as those values that are comparable with characteristic time of polymer chain propagation time  $\tau_{pr}$ . Obviously, if  $\tau_{ph} > \tau_{pr}$  and the association degree of initial oligomer molecules is quite high, the polymer chain propagation proceeds in the associated reaction medium. In this case mutual orientation of molecules in the associate, if it is regular and characterized by correlation time  $\tau_{cor} > \tau_{pr}$ , can be either advantageous or disadvantageous for the polymer chain propagation reaction.

An abnormally high value of  $k_{pr}$  can be explained by the presence of regular associates with mutual orientation of molecules in the associate that is advantageous for polymerization reaction (preformed associate). Increase of  $W_0$  with dilution presumes that mutual orientation of molecules in the associate is disadvantageous (anti-preformed associate). Breakage of such associates with increasing dilution degree provides increase of initial polymerization rates  $W_0$ .

A hypothesis about the presence of kinetically active associates in liquid oligo(acrylates) [15, 16] is based on the fundamental concepts of Academician N.N. Semenov regarding structures with mutual orientation of molecules that is advantageous for the polymerization process. These structures are responsible for abnormal polymerization acceleration of certain vinyl monomers at phase transition temperature "crystal  $\rightarrow$  liquid" [19].

Thus, initial polymerization rate  $W_0$  in nonstructured reaction medium (with  $C \rightarrow 0$ ) is significantly influenced by the initial oligo(acrylates) nature for least by two reasons. First, the existence of fundamental reverse viscosity dependence of chain termination rate constant  $k_{ter} = f(1/\eta)$  leads to direct dependence  $W_0 = f(\eta)$ . Second, presumably the existence of sufficiently stable regular associates in liquid oligo(acrylates) with the advantageous or, in contrast, disadvantageous location of oligomer molecules in associates leads to further propagation of the polymer chain.

### Kinetic Anomalies of Polymerization of Higher Alkyl (Meth)Acrylates. Model of Regular Kinetically Active Associates

Kinetic anomalies of oligo(acrylates) polymerization, presumably related to the formation of regular associates, are especially clearly manifested in polymerization

of higher alkyl (meth)acrylates that could be considered as oligo(acrylates) models containing strong IMI centers in their molecules. Diphilic molecules of monomers with such structure can easily form regular associates of the micellar type, in which hydrophilic and hydrophobic fragments of molecules are segregated and mutually ordered in terms of their position and orientation [20]. An example of alkyl (meth)acrylates polymerization enabled us not only to prove the existence of preformed and anti-preformed associates and their influence on kinetics of polymerization processes but also to propose a quantitative model of polymer chain propagation in regular associates (model of regular kinetically active associates) [21, 22].

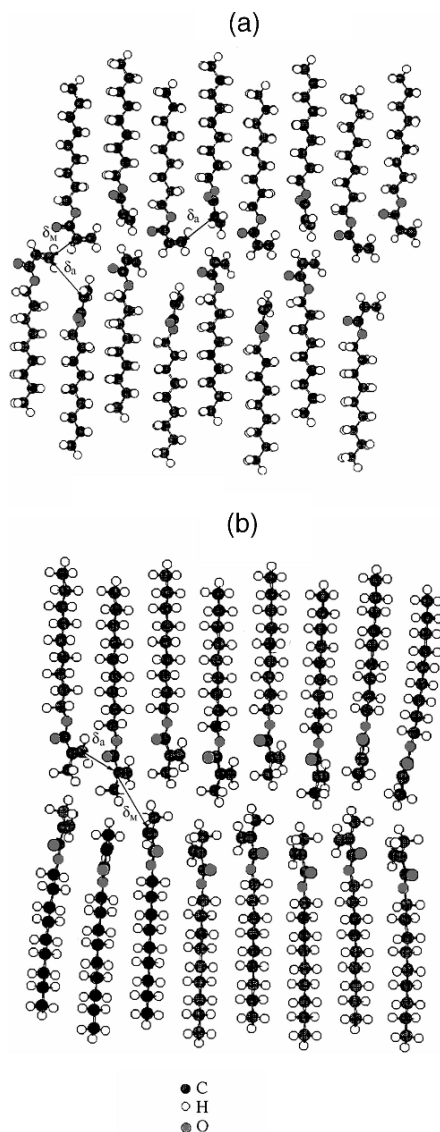
An exploration into the influence upon polymerization rate of small amounts (1–5% mol) of comonomers, which had a similar double bond but different size of alkyl substituent, as compared to the main comonomer, played a crucial role [21, 22]. The quite strong negative impact of such additives in the case of alkyl acrylate polymerization is interpreted based on the assumption that molecules of comonomers-additives are easily built in into preformed associates, but because of the difference of alkyl fragment size, they disturb positional and (or) orientation order of molecules in the associates. Due to the disadvantageous orientation of double bonds, molecules of comonomers-additives interrupt the growth of polymer chain (that develops within the preformed associate) because all reactions of free radical addition are strictly sterically regulated, which is indicated by very low values of the sterical factor:  $10^{-5}$ – $10^{-3}$  [23–25]. Based on these concepts, a calculation system [21, 22] was developed, which enables estimating the average number of molecules in a preformed associate of higher alkyl acrylates and ratio of chain propagation rate constants in the associate and outside it. This ratio was found to increase from 50 to 200 with an increase of  $n$  in a side alkyl fragment  $\text{CH}_3(\text{CH}_2)_n$  from 4 to 12 and, correspondingly, with an enhancement of preformed associates stability.

The positive effect of small additives of congeneric monomers (observed in the case of higher alkyl methacrylate polymerization) is interpreted as an effect of anti-preformed associate breakage (or stability decline) by building in molecules with different positional or orientation order [21, 22, 26].

The model of regular kinetically active associates, although substantiated kinetically [21, 22, 26, 27], [28] p. 48, required direct experimental verification. However, as is well known, there are no direct experimental methods to study the structure and properties of associated structures of liquids [29–31]. At the same time, results of computer modeling for such structures by methods of molecular mechanics and molecular dynamics [32, 33] are not inferior to results of direct experiments in terms of reliability.

The authors conducted computer modeling of associate structures from methyl to cetyl esters in a homologous series of  $n$ -alkyl acrylates and  $n$ -alkyl (meth)acrylates [34] by computing spatial arrangement of associate molecules with minimal potential energy. Equilibrium conformations of associates of  $n$ -alkyl (meth)acrylates were calculated using the molecular mechanics method with parameterization of MM2 [32]. It was shown that higher  $n$ -alkyl acrylates and  $n$ -alkyl (meth)acrylates, starting from butyl esters, are able to form regular associates, in which ester molecules (their hydrocarbonic fragments, ester groups, and double bonds) are mutually ordered in terms of their location and orientation (Fig. 2.2). These regular associates

**Fig. 2.2** Monomolecular section of the middle layer of regulate associate NonA (**a**) and NonMA (**b**)



can be identified with kinetically active associates that earlier were postulated for the interpretation of kinetic anomalies of radical polymerization of higher alkyl (meth)acrylates.

Double bonds in molecules of higher *n*-alkyl acrylates and *n*-alkyl (meth) acrylates are ordered both within the associates and in relationship to double bonds of neighboring associates [35]. In terms of intra-associate ordering of double bonds, the associates of nonyl acrylate (NonA), nonyl methacrylate (NonMA), and other *n*-alkyl acrylates and *n*-alkyl methacrylates are actually identical; in contrast, the

**Table 2.3** Average distance between vinyl carbon atoms ( $\delta$ ) and mutual orientation angle of double bonds ( $\theta$ ) of neighboring molecules within associates ( $\delta_a, \theta_a$ ) of alkyl (meth)acrylates and between associates ( $\delta_{aa}, \theta_{aa}$ )

Associates	$\delta_a, \text{\AA}$	$\theta_a, \text{degrees}$	$\delta_{aa}, \text{\AA}$	$\theta_{aa}, \text{degrees}$
<i>n</i> -Alkyl acrylates				
BA	3.52	3	3.92	81
NonA	3.43	1	3.65	88
DDA	3.40	1	3.58	89
CEA	4.03	0	3.79	92
<i>n</i> -Alkyl (meth)acrylates				
BMA	3.48	3	6.75	177
NonMA	3.78	1	6.84	183
DDMA	3.58	1	6.24	182
CEMA	3.92	1	6.48	182

Note 1. Accuracy of determination of  $\delta$  values in the models is  $\pm 0.01 \text{\AA}$ ;  $\theta$  values,  $\pm 2$ .

Note 2. BA, butyl acrylate; NonA, nonyl acrylate; DDA, dodecyl acrylate; CEA, cetyl acrylate; BMA, butyl methacrylate; NonMA, nonyl methacrylate; DDMA, dodecyl methacrylate; CEMA, cetyl methacrylate.

inter-associate ordering of double bonds of molecules of *n*-alkyl acrylates and *n*-alkyl methacrylates, including NonA and NonMA, differs significantly (Fig. 2.2, Table 2.3).

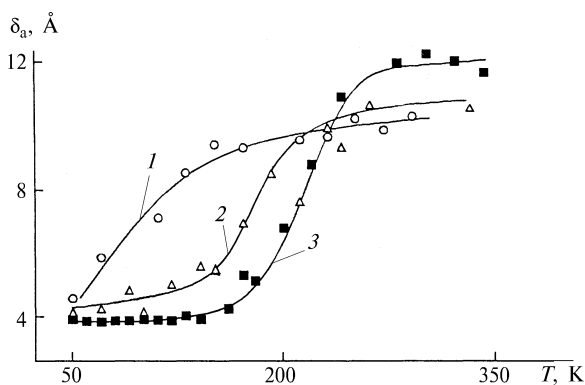
One has grounds to believe that it is precisely these peculiarities of inter-associate ordering of double bonds of associated molecules that represent an advantageous factor for polymerization of higher *n*-alkyl acrylates and, in contrast, a disadvantageous factor for polymerization of higher *n*-alkyl (meth)acrylates. Probably these factors control the addition of polymer radicals to the double bonds of monomer molecules.

It has been established that incorporation of foreign matter molecules (e.g., small amount of comonomer) into associates not only alters the positional ordering of double bonds in sites of additive molecule localization, thus increasing the distance between carbon atoms of neighboring double bonds up to  $5\text{--}9 \text{\AA}$ , but also changes the molecular dynamics of all other molecules of the associate [35]. Modeling of the thermal motion of molecules in regular associates conducted using the molecular dynamics method [33] showed that inclusion of BA (BMA) molecules into a regular associate of NonA (NonMA) results in destabilization of associates (Fig. 2.3), shifting the associate  $\rightleftharpoons$  disassociate equilibrium in favor of nonassociated molecules of monomers.

For *n*-alkyl acrylates, it should result in the decrease of preformed associate concentration and corresponding decline of polymerization rate, while for *n*-alkyl (meth)acrylates it should result in the decrease of anti-preformed associates concentration and growth of polymerization rate.

Results of computer modeling of associative structures of higher alkyl(meth)acrylates permit us to interpret unambiguously kinetic anomalies of radical polymerization of these monomers for low conversions  $C \rightarrow 0$  as kinetic manifestation of their regular associative structures that have such mutual location of double bonds

**Fig. 2.3** Temperature dependencies of average distance between double bonds  $\delta_a$  in various associates: 1, BA; 2, (NonA + BA); 3, NonA



in regular associative structures, which is either advantageous (in case of alkyl acrylates) or disadvantageous [in case of alkyl (meth)acrylates] for polymer propagation reaction.

Thus, the hypothesis implying the existence of regular kinetically active associates [19] proposed to provide explanations for kinetic anomalies of polymerization of crystallizing monomers in the region of their phase transition [36–38] was then expanded in a high-temperature region far from phase transition temperatures by the discovery of kinetic anomalies of oligo(acrylates) polymerization [12, 15–18]. The model of regular kinetically active associates [21, 22] based on the afore-indicated hypothesis and substantiated with results of exploration into kinetic anomalies of polymerization of higher alkyl acrylates and alkyl (meth)acrylates [21, 22, 26] and with computer modeling of structure and temperature stability of associates of these monomers [34, 35] can be considered to be quite valid and reliable as applied to TFRP of polyunsaturated oligomers.

### 2.1.2 Stages of Auto-Acceleration and Auto-Deceleration

The TFRP auto-acceleration and auto-deceleration should be interpreted within the frames of diffusion kinetics: as diffusive mobility of reagents is hindered to a higher and higher degree, at first faster proceeding elementary acts (i.e., chain termination,  $k_{\text{ter}}$ ) and then slower ones (i.e., chain propagation,  $k_{\text{pr}}$ ) become diffusion controlled in the formed network structure of the reaction medium. Therefore, at first auto-acceleration develops because of the declining effective value of  $k_{\text{ter}}$ , and then auto-deceleration starts as a result of the decreasing effective value of  $k_{\text{pr}}$ .

One can draw an analogy with the widely known gel effect phenomenon appearing during conventional linear block polymerization of certain monomers [e.g., methyl methacrylate (MMA)], also resulting in the auto-acceleration – auto-deceleration sequence. Physical reasons are the same here: hindrance of diffusive mobility of reagents to the level where elementary reactions become diffusion controlled and effective values of their elementary rate constants begin diminishing

with a growth in diffusion hindrances. The only difference lies in the mechanism of diffusion mobility hindrance, which leads to considerable quantitative differences for TFRP, with the qualitative analogy being absolute.

In the case of linear polymerization, double bonds stay within monomers until the very end. Therefore, the diffusion control of processes with participation of monomer molecules (chain propagation) appears only at the very late stages of polymerization, when the polymer-monomer mix starts transiting into the glassy state. In the case of TFRP, initial molecules contain two or more double bonds. Addition of one of them to the growing network frame results in the appearance of “pendent” double bonds with extremely limited mobility (Fig. 2.4).

The mobility of double bonds of nonreacted oligomer molecules is probably also limited by incorporation of network fragments with uncompleted structure [39]. Therefore, not only termination, but also propagation, of the chain during TFRP becomes diffusion controlled even at low-degree conversions; this leads to a decrease in auto-acceleration rate. If one compares auto-acceleration development rate for MMA and dimethyl acrylates (DMA), the following could be observed: the  $W_{\max}/W_0$  ratio for MMA is 10–20 times higher than for DMA, and  $dW/dC$  at the section with maximum rate of auto-acceleration development exceeds the same parameter for DMA from 100 to 200 times, while the  $dW/dC$  value proper increases sharply as the conversion degree grows (for DMA,  $dW/dC$  is virtually steady within the entire auto-acceleration range  $0 < C < C_{\max}$ ).

The specific mechanism of diffusion mobility hindrance during TFRP is manifested in specific kinetic regularities related to correlation of effective reactivity

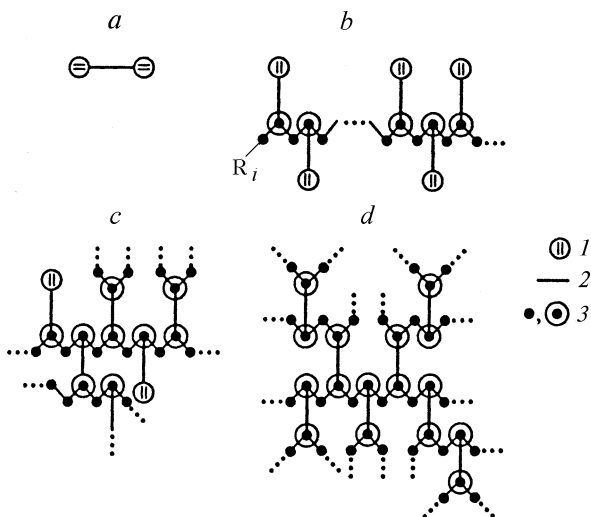


**Fig. 2.4** Successive stages of TFRP for oligomers having two double bonds in their molecules: (a) initial state; (b) primary (nonbranched) polymer chain with “pendent” double bonds; (c) fragment of network with uncompleted structure (conversion  $< 1$ ); (d) fragment of completed network (conversion  $\approx 1$ ); 1, vinyl groups; 2, oligomer blocks; 3, secondary or tertiary carbon atoms with substituents H or R;  $R_i$ , initiator radical

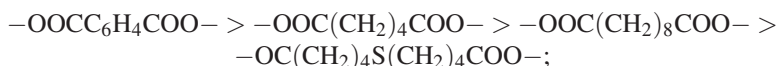
of initial molecules with their physical (conformation) properties (molecule length, size of rotation barrier of constituent atomic groups). These regularities have been followed for large number of oligo(acrylates) of the following structure:



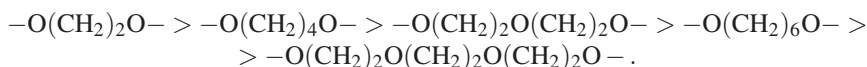
where the  $R_1$  substituent refers to dicarboxylic acids,  $R_2$  refers to glycols, and  $n = 1, 2$  [1 (p. 165); 3 (p. 126); 39]. The oligomer synthesis method allowed varying the length and chemical composition of the oligomer block in a very wide range, with the end group type being the same.

At that, it is possible to separately vary a certain parameter (e.g., oligomer "length"), leaving all other parameters unchanged (nature of reactive groups; nature of groups determining internal rotation barriers and, in the final end, flexibility). Or, in contrast, it is possible to vary only sizes of internal rotation barriers while keeping all other parameters unchanged.

Results of studying the polymerization of oligo(acrylates) of different series, in which the length and chemical composition of the oligomer block changed in regular fashion, are listed in Tables 2.4 and 2.5; typical kinetic curves of polymerization with coordinates "reduced rate  $W/[M]^1$  – conversion  $C$ " are presented in Fig. 2.5. Effective reactive capacity of oligomers at constant temperature was characterized by parameters  $W$ ,  $W_{\max}$ ,  $C_{\max}$ , and  $C_{\text{lim}}$ , where  $W$  = current polymerization rate in the range  $W_0 < W \ll W_{\max}$ ,  $C_{\max}$  = conversion corresponding to the maximum polymerization rate  $W_{\max}$ , and  $C_{\text{lim}}$  = maximum achievable conversion. In each homologous series of oligo(acrylates) with identical structure of oligomer block, the length of the latter varied (Table 2.4); in series I and II, with the length of oligomer block being almost invariable, the nature of diacid (family I) or glycolic (family II) and, hence, oligomer block flexibility, varied (Table 2.5). The internal rotation barriers of atomic groups of oligomer block decrease in series I in the following order:



in family II:



It was found that for identical reaction centers, i.e., end methacrylic groups, the effective reactive capacity of oligomers increases as the length and flexibility of oligomer blocks increase. Also, dependence of the effective reactive capacity on indicated physical (conformation) properties of initial molecules of oligo(acrylates) grows drastically as conversion degree increases; the most sensitive parameters are  $W_{\max}$ ,  $C_{\max}$ , and, especially,  $C_{\text{lim}}$ . For example, curves 1 and 2, and 4 and 5 (see

<sup>1</sup> This relationship is convenient for determining main kinetic regularities of TFRP because  $W/[M] = K_{\text{pr}}\sqrt{W_i/K_{\text{ter}}}$  is an effective constant of polymerization rate at fixed temperature and initiation rate.



**Table 2.4** Homologous series of oligo(acrylates)

Series of (meth)acrylates	General formula	Individual oligo(acrylates)						
		$n = 1$	$n = 2$	$n = 3$	$n = 4$	$n = 5$	$n = 6$	$n = 10$
Alkane diols	$M(CH_2)_nM$	–	dMAEG	dMAPDO	dMABDO	–	dMAHDO	dMADDO
(Diethylene glycol) phthalates	$M(DP)_nDM$	MDP-1	MDP-2	MDP-3	MDP-4	MDP-5	–	–
(Tetramethylene glycol) phthalates	$M(BP)_nBM$	MBP-1	MBP-2	MBP-3	–	–	–	–

Increase of  $W$ ,  $W_{max}$ ,  $C_{max}$  and  $C_{lim}$   $\rightarrow$

Notation conventions for Tables 2.1, 2.4, and 2.5 only. Acidic residues: **M**, methacrylic; **P**, *ortho*-phthalic; alcoholic residues: **D**, diethylene glycol; **B**, tetramethylene glycol

**Table 2.5** Series with various di[acids] and glycols

Series	Notation and repeated unit structure (in brackets) of series member				
I	MDP-1	MDA	MDS	MDU	–
	(MDPDM)	(MDADM)	(MDSDM)	(MDUDM)	–
	MEP	MBP-1	MDP-1	MHP	dMA <sub>t</sub> EGPh
II	(MEPEM)	(MBPBM)	(MDPDM)	(MHPHM)	(MTPTM)

Increase of  $W$ ,  $W_{\max}$ ,  $C_{\max}$  and  $C_{\text{lim}}$

➔

Notation conventions for Tables 2.1, 2.4, and 2.5 only. Acid residues: **M**, methacrylic; **P**, *ortho*-phthalic; **A**, adipinic; **S**, sebacic; **U**, 5,5'-thiodivaleric acid; alcohol residues: **B**, tetramethylene glycol; **H**, hexamethylene glycol; **D**, diethylene glycol; **T**, triethylene glycol; **E**, ethylene glycol.

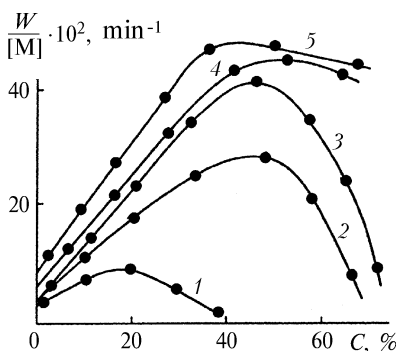


**Fig. 2.5** Kinetics of polymerization of tested dMA series with different length (1 and 2, 4 and 5) and size of internal rotation barriers of molecules with comparable lengths (2 and 3) TFRP substrates:  $M - (\text{CH}_2)_n - M$ ,  $n = 4$  (dMABDO; curve 1),  $n = 10$  (dMADDO; curve 2);  $M(\text{CH}_2)_2\text{O}(\text{CH}_2)_2\text{O}(\text{CH}_2)_2M$  (dMA<sub>t</sub>EG; curve 3);  $M[(\text{CH}_2)_2\text{O}(\text{CH}_2)_2\text{O}(\text{O})\text{C} - \text{Z} - \text{C}(\text{O})\text{O}]_n(\text{CH}_2)_2\text{O}(\text{CH}_2)_2M$ ,  $n = 1$  (MDP-1; curve 4),  $n = 2$  (MDP-2; curve 5).  $M$ , atomic group  $\text{CH}_2 = \text{C}(\text{CH}_3)\text{C}(\text{O})\text{O}$ ;  $Z$ , aromatic fragment of *ortho*-phthalate.  $T = 70^\circ\text{C}$ ; initiator, benzoyl peroxide (1% w.).

Fig. 2.5) refer to the analogous dMA (i.e., dMA having the same set of rotation barriers) with consistently increasing length of oligomer block. The reactive capacity enhances dramatically in the same sequence, especially at final stages of conversion, therefore, the limiting conversion for dMA with the shortest oligomer block  $C_{\text{lim}} \rightarrow 40\%$  (curve 1), and with sufficient chain length (curves 4 and 5), auto-deceleration at the late stages virtually disappears and  $C_{\text{lim}} \rightarrow 100\%$ . Curves 3 and 4 (Fig. 2.5) refer to dMA with close lengths of oligomer blocks, but they are different in terms of sets of internal rotation barriers. In decandiol dimethacrylate (dMADDO, curve 2) only two ester groups are hindered relatively weakly. In tri(ethylene glycol) dimethyl acrylate (tEGdMA, curve 3), weakly hindered rotations of ether bonds are added to ester bonds, and, in the final end, enhancement of effective reactive capacity takes place as a result of transition from dMADDO to tEGdMA.

Parameters associated with the nature of oligomers proper, namely, length of the chain joining end methacrylate groups (oligomer block) and barriers of internal

rotation of atomic groups of the oligomer block, control the mobility of interjunction chains of the macromolecular network that is formed during TFRP. It is only oligomer blocks that become one of three interjunction chains of trifunctional junctions of the polymer network (see Fig. 2.4) after both methacrylate groups of dimethylacrylate react. Because two other interjunction carbon chains  $-\text{CH}_2-$  are maximally short and rigid, it is just the third chain that provides junction relaxation which controls the mobility of elements of structured reaction medium: both the polymer network with pendent double bonds and diffusive mobility of molecules of nonreacted oligomers. As a result, the effective reactive ability of oligomers in TFRP in structured medium (at auto-acceleration and auto-deceleration stages) becomes enhanced as the probability of conformational transitions in the oligomer block of the polymer network increases.

The abnormal kinetic effect of ultrarapid TFRP under the conditions of photochemical initiation should be also interpreted within the framework of diffusion kinetics. In the case of high rates of photochemical initiation, initiating radicals  $\text{R}_1^\bullet$  become main partners in the reaction of quadratic termination of chain  $\sim\text{R}^\bullet + \text{R}_1^\bullet \rightarrow$  termination, where  $\text{R}_1^\bullet$  is a radical small in size and, hence, highly mobile in a structured medium, while  $\sim\text{R}^\bullet$  is a polymeric low mobile radical that is a chain carrier. This fact changes the polymerization kinetics quite dramatically: no auto-acceleration at all, and the order in terms of initiation rate changes from 0.5 (normal value) to 0 (anomaly) [40, 41]. The ultrarapid and easily controlled mode under the conditions of photochemical initiation at normal temperature made TFRP irreplaceable for the purpose of creation of high-tech polymer materials for microelectronics, fiberoptics, and data recording and storage devices [41–44].

Mathematical models of the TFRP process (auto-acceleration and auto-deceleration stages) are discussed in Sect. 2.5.

## 2.2 Inhibited Polymerization

The kinetics and mechanism of polymerization process inhibition, developing under specific conditions of TFRP were studied using inhibited oligo(acrylates) polymerization as an example. These studies are significant not only for understanding the inhibited TFRP mechanism, but also from the technological standpoint. Results of these studies of inhibited oligo(acrylates) polymerization are summarized in publications within the framework of homogeneous approach [1] (p. 194) and with peculiarities of the microheterogeneous TFRP mechanism taken into account [3] (p. 133).

Inhibited polymerization of oligo(acrylates) is of microheterogeneous character. Figure 2.6 shows kinetic dependencies reflecting influence of the quite effective inhibitor (X), benzoquinone (BQ), with  $k_X/k_{pr} = 5.5$  at  $44^\circ\text{C}$  [45], where  $k_X$  and  $k_{pr}$  are reaction rate constants  $\sim\text{M}^\bullet + \text{X} \xrightarrow{k_X}$  and  $\sim\text{M}^\bullet + \text{M} \xrightarrow{k_{pr}}$ , respectively. Because of such differences in rate constants, the inhibitor is mainly consumed at the early TFRP stage. Concentration X was varied, and for each [X] such concentration of

the initiator was selected that the reactive capacity at the initial TFRP stages is the same (curves 1–3 at  $C < 20\%$ ). Dramatic difference in reactive ability with growing  $C$  cannot be explained without taking into account the microheterogeneous pattern of TFRP. Indeed, microheterogenization in the presence of X proceeds in such a way that the higher is the X concentration, the higher is the number of concurrently working self-contained micro-reactors ( $N_{im}$ ) in the reaction system [3, 46]:

$$N_{lim} = \frac{(k_X[X])^2}{(f-1)k_{pr}^2[M]_0} \quad (2.2)$$

where  $f$  = oligomer functionality and  $[M]_0$  = initial concentration of oligomer.

Curves 1–3 in Fig. 2.6 are located correspondingly: the higher is  $[X]$ , the higher is the effective reactive capacity.

The influence of microheterogeneity during inhibited oligo(acrylates) polymerization is demonstrated by comparison of kinetic behavior of one and the same inhibitor in two chemically identical systems that differ only in type of their structure formed sin the course of polymerization. Such comparison was conducted by the example of benzoquinone for chemically identical MMA and dMAtEG polymerizing in accordance with linear and tridimensional mechanisms, respectively. Kinetic parameters of inhibited polymerization are listed in Table 2.6: initial reduced rates  $W/[M]_0$ , fractions of induction period  $\tau_{1/2}$ , during which half of initially introduced inhibitor is consumed, i.e.,  $[X]_{\tau}/[X]_0 = 1/2$ , which is indicated by twofold increase of polymerization rate as compared to the initial rate; the relationship of constant of radical-chain carrier and inhibitor reaction rate to that of radical-chain carrier and monomer reaction rate  $k_X/k_{pr}$  and, finally, stoichiometric coefficient of inhibitor  $\mu$ .

By comparing  $k_X/k_{pr}$  and  $\mu$  for MMA and tEGdMA, it is easy to see that benzoquinone has changed its properties as an inhibitor quite significantly during conversion to tEGdMA: the  $k_X/k_{pr}$  relationship increases approximately 1.5 times, while  $\mu$ , in contrast, decreases almost 4 fold. As from the chemical standpoint both systems, MMA and tEGdMA, are absolutely identical, the observed effect could be explained by structure formation during inhibited polymerization of tEGdMA.

Oligo(acrylates) synthesis and storage, as well as oligo(acrylates) processing via polymerization into finished goods, are possible only through the application of

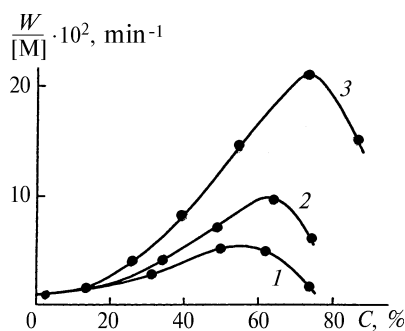


**Fig. 2.6** Polymerization of dMA-tEGPh with fixed molar relationship: initiator (DCPD)/inhibitor (BQ) = 1:1. Initiator and inhibitor concentration, % (by weight): 1, 2; 2, 4; 3, 6.  $T = 35^\circ\text{C}$

**Table 2.6** Parameters of MMA and tEGdMA polymerization inhibited with BQ

Concentrations of initiator and inhibitor $\times 10^3$ , mol/l		MMA				tEGdMA			
AIBN	BQ	$\frac{W}{[M]_0} \cdot 10^3$ , min <sup>-1</sup>	$\tau_{1/2}$ , min	$K_X/k_{pr}$	$\mu$	$\frac{W}{[M]_0} \cdot 10^3$ , min <sup>-1</sup>	$\tau_{1/2}$ , min	$K_X/k_{pr}$	$\mu$
10	2	0.27	310	5.0	2.0	0.41	128	11	0.49
	5	0.14	1030	4.1	2.3	0.16	460	10	0.45
20	2	0.59	149	5.5	1.8	0.74	68	8.5	0.51
	–	0.43	146	6.0	2.0	–	–	–	–
	5	0.26	345	5.4	1.7	0.42	184	6.8	0.50
	–	0.23	400	5.1	2.0	–	–	–	–
40	10	0.18	613	5.6	2.1	0.24	400	7.0	0.40
	2	0.94	92,5	5.6	2.2	1.48	41	8.3	0.57
	–	0.92	90	6.3	2.0	–	–	–	–
	5	0.43	188	6.6	1.7	0.65	115	8.3	0.52
	–	0.46	184	6.0	1.7	–	–	–	–
Mean value				$\approx 5.5$	$\approx 1.9$	–	–	$\approx 8.6$	$\approx 0.5$

Note. Temperature 60°C, initiator, 2,2'-azobis (2-methylpropionitrile) (AIBN). $\mu$ , stoichiometric coefficient of inhibitor

adequate inhibitors that prevent spontaneous polymerization of oligomers. Generalization of data on inhibited oligo(acrylates) polymerization [1, 3] leads to a conclusion that none of the known inhibitors or their combinations have features of the so-called ideally overlapping inhibitors. This term means an inhibitor so highly effective that its presence in a polymerization system decreases the kinetic chain length to the limiting low value (about 1), so that the polymerization process becomes almost completely suppressed for some period of time  $\tau$  (induction period), during which the inhibitor is fully consumed. After lapse of time  $\tau$ , polymerization proceeds as a noninhibited process, i.e., the ideal inhibitor action takes place only during period  $\tau$  without leaving any “traces” in the course of subsequent polymerization, with the exception of influence on stationary concentration of polymer grains. Value  $\tau$  in this case is directly proportional to inhibitor concentration and reversely proportional to the “overlapping” initiator concentration. If the latter parameter value is less compared to the inhibitor concentration (molar concentrations are compared here), value  $\tau$  becomes infinity (i.e., concentration is insufficient for overlapping). The action of inhibitors (that are less effective than the ideal one) differs in the fact that the kinetic chain length during inhibition period  $\tau$  is considerably greater than 1; therefore, a part of the polymerization process (or even the entire polymerization process) proceeds in the presence of inhibitor. The more such nonideal inhibitors complicate the vitrification mode for oligo(acrylates) and impair properties of polymerizates, the more different they are from the ideal ones. The inhibitor efficacy, in other words, the inhibition rate constant  $k_X$ , represents a measure for the approximation to the properties of ideal inhibitors. Information on values of

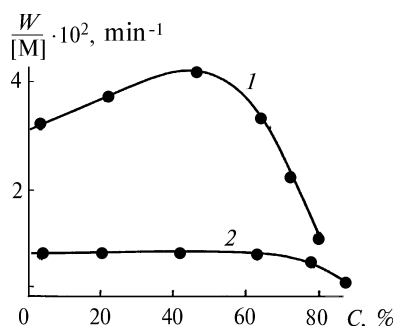
$k_X$  of inhibitors of different classes is given in a monograph [45] and a reference book [47].

The inhibitor ideality degree was suggested to be quantified by an “ideality parameter”  $\theta$  [3] (for ideal inhibitor:  $\theta = 1$ ). Nonideality of behavior ( $\theta < 1$ ) in the case of low-effective inhibitors (the so-called retarding agents) characterized by  $k_X \leq k_{pr}$ , where  $k_X$  and  $k_{pr}$  are reaction rate constants for the reaction of propagation radical with molecule X and oligo(acrylates), respectively, has rather trivial explanation: it follows from  $k_X \leq k_{pr}$  that the inhibitor consumption rate during polymerization conversion does not exceed oligo(acrylates) consumption rate, hence, the inhibitor is present in the reaction system right to the very end of polymerization. In this case quadratic termination of chains  $\sim M^\bullet + \sim M^\bullet$  limited by diffusion due to large size of  $\sim M^\bullet$  (macroradicals, a part of which is linked with the network) is replaced with linear termination  $\sim M^\bullet + X$  with participation of small (highly mobile) molecules X, and the diffusion control over linear termination is expressed to a much lower extent. Therefore, at a certain inhibitor concentration (curve 2, Fig. 2.7), the kinetics characteristic of TFRP (auto-acceleration – maximum – auto-deceleration) transforms in such a way that the auto-acceleration stage disappears completely, while the auto-deceleration stage is shifted to the region of very high conversions.

For effective inhibitors characterized by  $k_X > k_{pr}$ , quite significant deviation from ideality could be explained both by transformation of inhibitors X during the inhibition reaction into secondary products  $X'$  possessing retarding agent properties and by specific features of TFRP proceeding according to the microheterogeneous mechanism. Theoretically, this may happen only in the case when microheterogeneous structures have enough time to be formed during induction period  $\tau$  (i.e. before the introduced inhibitor is fully consumed).

Then, polymerization inhibited by the remaining inhibitor should proceed under specific conditions of complicatedly structured medium, i.e., in a medium consisting of grains or their nuclei surrounded with unreacted initial oligo(acrylates) and having transition zones that consist of peripheral layers of grains and fringe. Under these conditions, inhibitor molecules may turn out to be outside the intensive polymerization conversion zone (for instance, because of microredistribution), and the inhibitor, entering into this zone via diffusion from micro-reservoirs with quasi-constant concentration, would behave as a weaker one, but possessing more expressed prolonged action.

**Fig. 2.7** Polymerization of tEGdMA in the presence of TNT inhibitor (2,4,6-trinitrotoluene) acting throughout the entire TFRP process: 1,  $[TNT] = 5 \times 10^{-3}$  mol/l; 2,  $[TNT] = 3 \times 10^{-2}$  mol/l.  $T = 60^\circ C$ ; initiator, AIBN,  $[AIBN] = 0.02$  mol/l



In other words, the local active mass of inhibitor  $[X]_{loc}$  might turn out to be much lower than its volume-averaged effective concentration  $[X]$ , as a result of which the inhibiting effect proportional to the product of  $k_X[X]_{loc}$  would be diminished, but the time of inhibitor action would be prolonged by feeding of  $[X]_{loc}$  by  $[X]$ . It is obvious that starting from the moment when  $[X]_{loc} \ll [X]$ , the subsequent consumption of inhibitor would also take place in diffusion-limited feeding mode  $[X] \rightarrow [X]_{loc}$ ; the inhibitor would behave as essentially nonideal ( $\theta < 1$ ). Indeed, a reduction of inhibitor active mass caused by structure formation from level  $[X]$  to  $[X]_{loc}$ , on the one hand, would lead to polymerization rate growth during induction period that in practice is similar to reduction of  $\tau$ , and, on the other hand, would result in diminution of polymerization rate after  $\tau$ , as compared to noninhibited polymerization, which is equivalent to an increase in hardening time of three-dimensional structure formation.

Those inhibitors were trial tested for oligo(acrylates) polymerization, the effectiveness of which varied within a very wide range: from low-effective ones, such as 2,4,6-trinitrotoluene with  $k_X/k_{pr} = 0.05$  and  $k_X = 231/(\text{mol} \cdot \text{s})$  at  $44^\circ\text{C}$  [45], to the most highly effective ones, such as stable nitroxyl radicals with  $k_X = 6 \cdot 10^5 1/(\text{mol} \cdot \text{s})$  at  $60^\circ\text{C}$  [45]. In all cases,  $\theta < 1$  and a high value of  $k_X$  in relation to  $k_{pr}$  is only a necessary but not sufficient feature of the ideal inhibitor.

The issue of raising the efficiency of inhibitors (bringing their properties closer to those of the ideal inhibitor) is usually solved through the use of synergists [1, 3]. The application of styrene as a synergist for the inhibited oligo(acrylates) polymerization was suggested and theoretically substantiated [1, 48]. In this case, partial substitution of radical-chain carrier for another radical having higher reactive capacity in relation to a given inhibitor molecule takes place. The substitution is implemented by adding to the reaction system a certain substance, which is able to react easily with the radical-chain carrier, thus forming new free radical.

In the case of styrene added to oligo(acrylates) that contains benzoquinone, the methacrylic radical-chain carrier, after reacting with styrene, is transformed into styrene radical, which is incommensurably more reactive in relation to benzoquinone versus methacrylic radical [styrene radical  $k_X/k_{pr} = 518$  and  $k_X = 1 \times 10^5 1/(\text{mol} \cdot \text{s})$  at  $50^\circ\text{C}$ , and methacrylic radical  $k_X/k_{pr} = 5.5$  and  $k_X = 2.6 \cdot$

**Table 2.7** Effect of styrene additives on benzoquinone (BQ) overlapping for tEGdMA polymerization

BQ concentration, % (by weight)	Styrene concentration, % (by weight)	$\tau$ , min	$\theta$	BQ concentration, % (by weight)	Styrene concentration, % (by weight)	$\tau$ , min	$\theta$
0	0	2	–	0.002	0.13	6	0.30
0.001	–	3.5	0.55	0.002	0.50	10	0.35
0.002	–	4.5	0.38	0.002	1.00	11	0.55
0.004	–	7.5	0.17	–	–	–	–
–	–	–	–	0.004	0.13	8	0.20
0.001	0.50	8	0.55	0.004	0.50	13	0.30
0.001	1.00	8	0.63	0.004	1.00	24	0.39

*Note.* Temperature,  $35^\circ\text{C}$ ; initiator, dicyclohexylperoxydicarbonate (DCPD),  $1.4 \times 10^{-2} \text{mol/l}$ .

$10^3 \text{ l}/(\text{mol} \cdot \text{s})$  at  $44^\circ\text{C}$  when reacting with benzoquinone] [45]. As a result, the inhibitor efficiency (effective value of  $k_X$ ) increases dramatically and, thus, styrene manifests its property as a synergist (Table 2.7).

This is one of the few cases of synergetic effect for which the mechanism has been clearly determined and a quantitative theory has been formulated, enabling one to calculate the effective rate constant  $k_X$  as a function of concentration of inhibitor and styrene [1, 48].

## 2.3 Polymerization in Solutions

Results obtained when studying TFRP in solvents provide valuable data on the polymerization process mechanism both at the very beginning of polymerization and in structured reaction medium. This section presents data related to those polymerization stages, when a microheterogeneous structure consisting of polymeric highly cross-linked grains separated by low cross-linked interlayers serves as a reaction medium.

Typical kinetic results illustrating the solvent effect were obtained by an example of tEGdMA oligomer polymerization in the presence of 0–60% (by volume) various solvents: three good ones (benzene, acetonitrile, DMFA) (Fig. 2.8) and a poor one (heptane) (Fig. 2.9) [5 (p. 109); 49].

It can be seen that the effect of good solvents (thermodynamic quality is meant) is manifested kinetically as an increase in polymerization rate at all conversions, and this increase progresses with growing degree of conversion  $C$ , and at the auto-deceleration stage it becomes total; the rate increases by orders of magnitude with concurrent shift of limiting conversion into the area of high  $C$ . Also, one of the three good solvents, namely, DMFA, exhibits qualitative changes of kinetics pattern at late stages: auto-deceleration at first is shifted to the area of higher  $C$  as solvent concentration grows and then it disappears completely (Fig. 2.8c, curve 5). Limiting (quasi-complete) conversion associated with auto-deceleration also disappears, and polymerization proceeds until complete conversion ( $C \approx 100\%$ ) with auto-acceleration. The poor solvent, i.e., heptane, shows the reverse kinetic effect (Fig. 2.9): as solvent concentration increases, the polymerization rate declines at all conversion stages, and this decline progresses as  $C$  increases, reaching very high values at the auto-deceleration stage, which, in the final step, is manifested as a shift of limiting degree of polymerization to the low-degree conversion area.

It would be well to relate kinetic effects of good solvents, first of all, to an increase in volumes of shell layers or reaction zones of polymer grains (see Fig. 1.8) from additional swelling and, as a consequence of this increase, to the growth of actual total reaction volume with corresponding increase of polymerization rate measured experimentally. Also, it is assumed that possible reduction in the concentration of nonreacted oligomer in the reaction zone (due to dilution) is not sufficient to compensate for this additional increase. Additional swelling of the shell layers may happen because of better affinity of solvent as compared to initial oligomer or higher thinning of macromolecular network in the shell layers



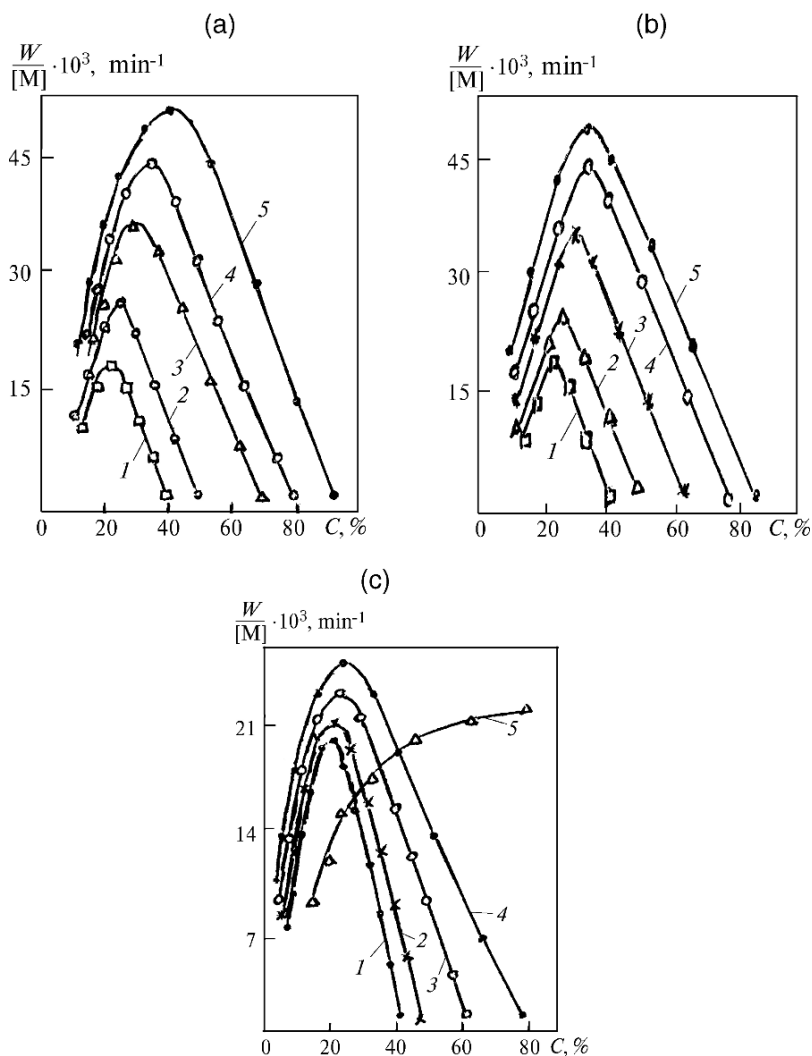
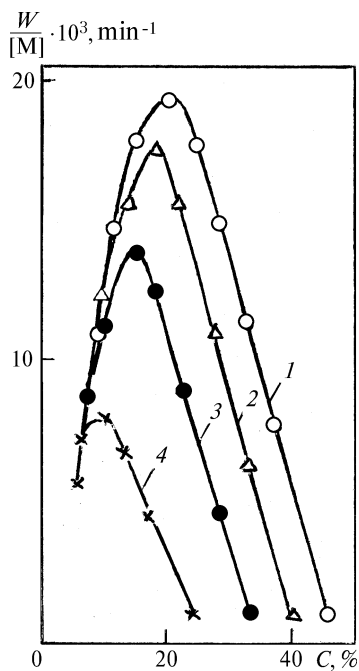


**Fig. 2.8** Dependence of reduced rate of tEGdMA polymerization in solutions of acetonitrile (a), benzene (b), and DMFA (c) upon conversion tEGdMA concentration, % (by volume): 1, 100; 2, 80; 3, 60.0; 4, 50.0; 5, 40.0.  $T = 40^\circ\text{C}$ ;  $[\text{DCPD}] = 2.6 \times 10^{-3} \text{ mol/l}$

resulting from dilution. The first assumption is not true because it is not confirmed by experimentally determined sequences on thermodynamic activity (affinity to tEGdMA polymer), in which the parent oligomer occupies a higher place than other solvents: oligomer > benzene  $\approx$  DMFA > acetonitrile > heptane [50]. In addition, absolute values of maximum reduced polymerization rates  $W/[M]$  attained in case of high-degree dilutions differ quite considerably for selected good solvents: from  $W/[M] = (45-50) \times 10^{-3} \text{ min}^{-1}$  for benzene and acetonitrile to  $W/[M] = 25 \times 10^{-3} \text{ min}^{-1}$  for DMFA; and this sequence of kinetic activity of

**Fig. 2.9** Dependence of reduced rate of tEGdMA polymerization in solutions of heptane upon conversion. tEGdMA concentration, % (by volume): 1, 100; 2, 90.0; 3, 80.0; 4, 70.0.  $T = 40^\circ\text{C}$ ;  $[\text{DCPD}] = 2.6 \times 10^{-3} \text{ mol/l}$



solvents, i.e., benzene  $\approx$  acetonitrile  $>$  DMFA, does not match the thermodynamic activity sequence. Therefore, we have to believe that the reason for additional growth of volume of the near-surface layers in the presence of good solvents is an increased degree of thinning of their network structure.

One of the most probable mechanisms for thinner network at periphery of grains consists in the following. Radial flow of “initial oligomer + solvent” compound is generated by denser packing of network structure of grains, and this denser packing develops successively from grain center to periphery (microsyneresis) (see Sect. 1.3.1). As a result of polymerization, this flow is depleted of the first component, the oligomer, while concurrently enriched with the second component, i.e., the solvent. Specific dynamic concentration of oligomer in the radial flow appears only as a result of counter diffusion flow of nonreacted initial oligomer from the ambient. As initial solvent concentration and conversion degree grow, this dynamic concentration of oligomer may reach indefinitely small values in the shell layers located far enough from highly cross-linked cores of grains. Correspondingly, an indefinitely low cross-linked macromolecular structure will be formed in these layers, which would possess high ability to swell in good solvents. It is well known that such swollen shells [51] prevent aggregation processes by using a mechanism of the so-called polymeric stabilization of dispersion. Therefore, in the presence of good solvents, the probability of grains aggregation is decreased with corresponding diminution of reaction volume and, hence, the tendency for auto-deceleration of polymerization process is degraded at later stages, up to complete disappearance of the auto-deceleration stage. Special experiments showed [52] that introduction of

additives of polymer dispersion stabilizers of different types into a reaction system, such as colloxylin, polisoprene surfactants (see Sect. 1.2.2, Fig. 1.7), results in elimination of auto-deceleration, which may serve as an indirect confirmation of correctness in interpreting the effects of good solvents upon late stages of oligo(acrylates) polymerization. In the case of a poor solvent, i.e., heptane, it is likely that a reduction in the volume of the sparse shell layer of polymer grains takes place due to diminution of swelling degree (precipitation effect) with corresponding kinetic consequences.

A model system was used to evaluate thermodynamic qualities of a reaction medium with respect to cross-linked polymers tEGdMA. The role of polymer in this model system was played by poorly branched soluble products of tEGdMA polymerization (the so-called  $\beta$ -polymers), while the role of reaction medium was played by tEGdMA oligomer or solution of tEGdMA oligomer in benzene or other solvents. The thermodynamic quality of the medium was estimated by the temperature dependence of light-scattering intensity  $R$  during temperature scanning from 20° to 80°C [50]. The presented data indicate that, for the temperature range 20° – 80°C, oligomer, DMFA, and benzene are good solvents for tEGdMA polymers, and, in contrast, heptane is a poor solvent. Acetonitrile, the thermodynamic affinity of which to oligo(acrylates) polymers is higher than that of heptane but significantly lower than that of benzene, DMFA, or tEGdMA oligomer, occupies an intermediate position.

Thus, the presented data verify that kinetic specifics of three-dimensional free-radical polymerization in a structured reaction medium are determined by conformation properties of parent unsaturated oligomers (such as molecule length and internal rotation barriers) and by the action of reaction medium (solvents, surfactants, inhibitor dopes) that influence the aggregation processes of polymer chains (inhibitors with  $k_X > k_{pr}$ ) and the type of chain termination (inhibitors with  $k_X < k_{pr}$ ). The effective reactive capacity of unsaturated oligomers at the initial stage of three-dimensional free-radical polymerization (with initial rate  $W_0$ ) with conversion  $C \rightarrow 0$  (unstructured reaction medium) is determined by other factors, namely, by oligomer viscosity and their capability to produce regular kinetically active associates.

## 2.4 Polymerization in Films Under the Conditions of Oxygen Diffusion

TFRP processes with participation of air oxygen represent a chemical basis for film formation from unsaturated oligomers that are one of the most popular substances among modern industrial-scale film-forming substances [53]. TFRP in liquid oligomers films applied onto substrates and in an oxygen-containing atmosphere is characterized by kinetic specifics that differ significantly from block or solution polymerization<sup>2</sup>. These specifics, as it was found through systematic studies

<sup>2</sup> Results of studying kinetics and mechanism of oxidative polymerization of unsaturated compounds in block and solution are described in monographs [2, 4] and review [58].

[2, 4], are preconditioned by the fact that polymerization (including TFRP) is represented by copolymerization of oligomers with oxygen (oxidative polymerization) and homo-polymerization. The relationship of these conjugated reactions changes in films layer by layer together with changing conversion degree depending on layer-by-layer variation in the concentration of oxygen diffusing into the film. Also, kinetic specifics of TFRP for compounds of vinyl and allyl types<sup>3</sup> in films should be analyzed taking into account the different reactivity of these compounds in reactions of radical addition and radical substitution.

## 2.4.1 Vinyl Compounds

### 2.4.1.1 Kinetic Specifics of Oxidative Polymerization of Vinyl-Type Compounds in Films Under the Conditions of Oxygen Diffusion

These specifics have been studied by an example of polymerization of the following oligo(acrylates)s: dimethyl acrylate of (bis-ethylene glycol)adipate (dMA-EGA), tetra(meth)acrylate of (bis-trimethylolpropane)adipate (teMA-tPA), and hexamethacrylate of (bis-pentaerythrite)adipate (hMA-PeA) [4 (p. 151); 54]. Oligomers were polymerized together with a redox system introduced in concentration of  $2.28 \times 10^{-2} \text{ mol/l}$  (0.55% by weight) of di(1-hydroxycyclohexyl) peroxide (DHHP) and  $1.07 \times 10^{-2} \text{ mol/l}$  (0.05% by weight) of cobalt naphthenate (calculated per metal cobalt) at initiation rates  $W_i$   $8.2 \times 10^{-6}$ ,  $2.0 \times 10^{-5}$ , and  $6.6 \times 10^{-5} \text{ mol/(l}\cdot\text{s)}$ , respectively, at 65°, 80°, and 100°C.

Oxygen absorption was measured by the circulation volumetry method using a specially designed instrument [55]. Kinetic curves of  $O_2$  absorption reflect exactly the kinetics of oxidative polymerization (copolymerization of oligomer with oxygen in reactions  $\sim M^\bullet + O_2 \xrightarrow{k_1} \sim MO_2^\bullet$  (1) and  $\sim MO_2^\bullet + M \xrightarrow{k_1} \sim MOOM^\bullet$  (2), because in identical conditions the oxidation rate of saturated organic compounds that simulate the structures of oligomer blocks dMA-EGA, teMA-tPA, and hMA-PeA is 15–20 times lower than that of these oligo(acrylates)s. This result means that the hydrogen abstraction reaction  $\sim MO_2^\bullet + MH \xrightarrow{k'_2} \sim MOOH + M^\bullet$  (2') can be neglected up to conversion degrees  $C = 90\text{--}95\%$  in terms of double bonds.

The influence of structure for oxidative polymerization is manifested in the fact that oxygen absorption rate  $W_{O_2}$  grows as molecular functionality  $f$  increases, while limiting conversions  $C_{O_2}$  diminish (Figs. 2.10 and 2.11).

Autocatalytic character of oxidative polymerization most likely stems from changes in medium viscosity as a result of polymer product accumulation.

During development of auto-acceleration, soluble polymers [56] with the polymer chain length of  $\approx 10$  oligomer units, the translational diffusion coefficient of

<sup>3</sup> Double bonds of vinyl-type compounds are highly reactive in radical addition reactions. Double bonds in the allyl-type compounds are characterized by low activity in radical addition reactions, while allyl compounds proper are highly reactive in radical substitution reactions.

**Fig. 2.10** Kinetic curves of oxygen absorption during oligo(acrylates) polymerization in films with thickness of 35  $\mu\text{m}$  at  $P_{\text{O}_2} = 21$  kPa: 1 and 2, dMA-EGA, 100° and 80°C; 3 and 4, teMA-tPA, 80° and 65°C; 5, hMA-PeA, 65°C

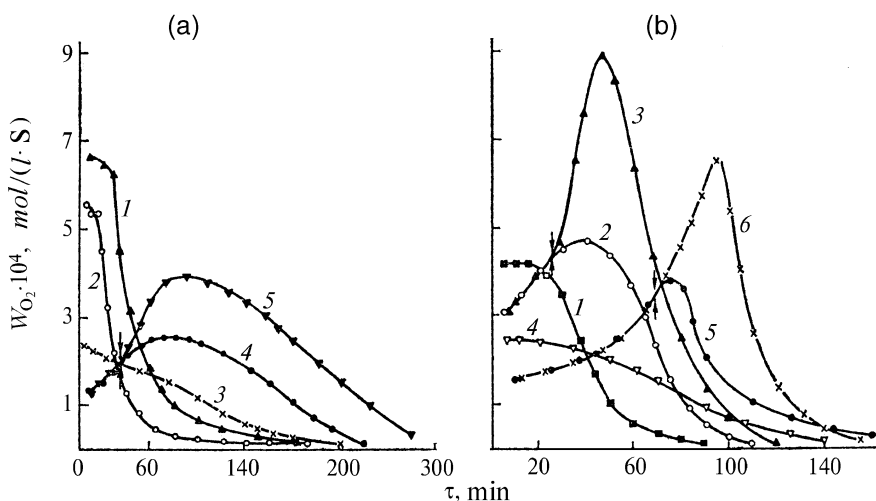
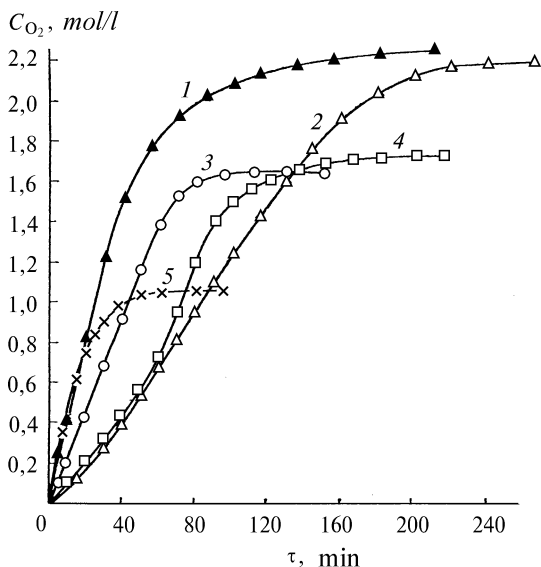
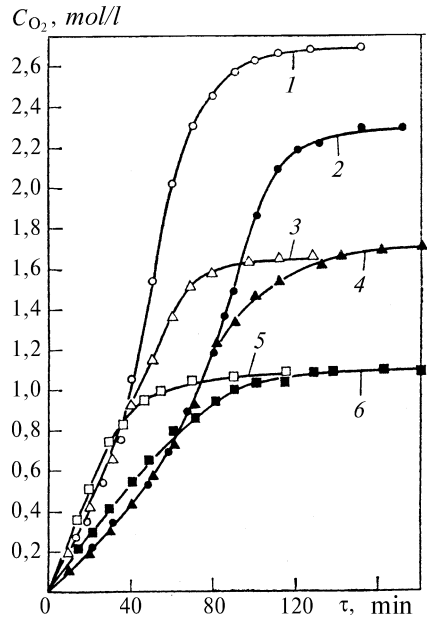


**Fig. 2.11** Dependence of  $W_{\text{O}_2}$  on duration of dMA-EGA (a) and teMA-tPA (b) polymerization in films with different thickness at  $P_{\text{O}_2} = 21$  kPa: (a) 1 and 2, 100°C, 35 and 80  $\mu\text{m}$ ; 3, 4, and 5, 80°C, 80, 35, and 15  $\mu\text{m}$ ; (b) 1, 2, and 3, 80°C, 80, 35, and 15  $\mu\text{m}$ ; 4, 5, and 6, 65°C, 80, 35, and 15  $\mu\text{m}$ . Arrows indicate points corresponding to conversion  $C_{\text{lim}} \approx 1 - 3\%$

which does not exceed  $10^{-7} \text{cm}^2/\text{s}$  [10 (p. 178)], serve as peroxide radical carriers. Under these conditions, quadratic termination should be controlled by diffusion, and auto-acceleration of gel-effect type becomes probable.

However, specifics of oxidative polymerization are not exhausted by trivial development of autocatalysis according to gel-effect mechanism. It was established that process kinetics depends heavily upon film thickness (Figs. 2.11 and 2.12) and

**Fig. 2.12** Kinetic curves of oxygen absorption during teMA-tPA polymerization in films with different thickness when  $P_{O_2} = 21$  kPa: 1, 3, 5, 80°C, 15, 35, and 80 μm; 2, 4, 6, 65°C, 15, 35, and 80 μm



partial pressure of oxygen in the gas phase (Fig. 2.13), namely: as a rule, autocatalysis degree and limiting conversions are inversely dependent upon film thickness, and they grow as partial oxygen pressure  $P_{O_2}$  increases. In some cases, coincident sections of kinetic curves are observed for films of different thickness (Figs. 2.11 and 2.12) and different values of  $P_{O_2}$  (Fig. 2.13), and the length of these sections grows with increasing  $P_{O_2}$ . The reaction in films with the thickness of 80 μm turns out to be sensitive to  $P_{O_2}$  and film thickness practically from the beginning of measurements (Figs. 2.12 and 2.13).

It is impossible to interpret the presented experimental data without using a *layered model of oxidative polymerization in films* [54]. The model is based on the following fundamental notions. Before the beginning of polymerization, oxygen  $[O_2]_0$  concentration is the same in all film layers and is determined by oxygen solubility  $\gamma$  in the oligomer and partial pressure of oxygen  $P_{O_2}$  above the film  $[O_2]_0 = \gamma P_{O_2}$ . With the beginning of polymerization, the diffusion flux of oxygen from the gas phase into the film is generated as a result of oxygen consumption, and positive gradient  $[O_2]$  is observed throughout the film thickness from substrate to surface. Changes of  $[O_2]$  in the  $i$ -th film layer are determined by difference of oxygen consumption rate  $W_{O_2}^i$  and oxygen diffusion  $W_D^i$  into the  $i$ -th layer. Value  $W_D^i$  is derived from the following expression [57]:

$$W_D^i = D_{O_2}^i ([O_2]_o - [O_2]_i) / l_i^2 \quad (2.3)$$

The value of  $W_D^i$  is inversely proportional to squared distance from film surface to the  $i$ -th layer and is determined by gradient  $[O_2]$  and diffusion coefficient  $D_{O_2}^i$ ,

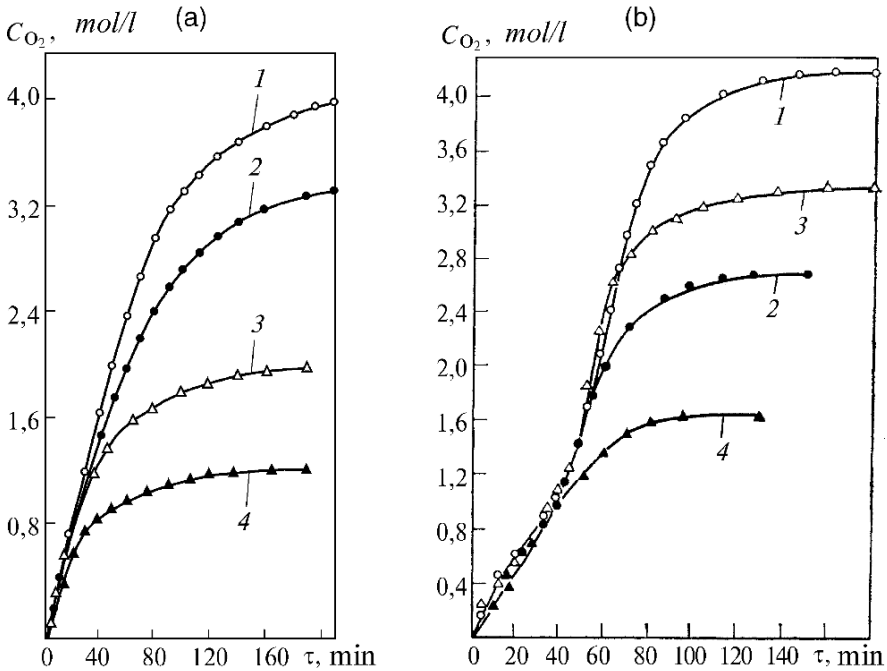


**Fig. 2.13** Kinetic curves of oxygen absorption during dma-EGA polymerization at 100°C(**a**) and teMA-tPA polymerization at 80°C(**b**) with different values of  $P_{O_2}$ : (**a**) 1, 3, 35  $\mu\text{m}$ , 100 and 21 kPa; 2, 4, 80  $\mu\text{m}$ , 100 and 21 kPa; (**b**) 1, 2, 15  $\mu\text{m}$ , 100 and 21 kPa; 3, 4, 35  $\mu\text{m}$ , 100 and 21 kPa

which, in the discussed case, is a function of reaction medium viscosity  $\eta$ , and  $D_{O_2}^i = f(1/\eta)$ . The value of  $W_{O_2}^i$  is found from the following equation:

$$W_{O_2}^i = W_I \cdot v \quad (2.4)$$

where  $W_I$  = initiation rate, and  $v$  = average length of kinetic chains of processes with oxygen participation.

Starting from certain conversion  $C$  (which depends upon film thickness, partial pressure of oxygen above the film, initiation rate, and oligomer oxidability in the film layer, which is farthest from the surface), a situation would inevitably occur when oxidative polymerization rate  $W_{O_2}$  is limited by the rate of oxygen diffusion into film  $W_D$ . The inevitability stems from the fact that  $W_{O_2}$  grows continuously (gel effect) as a result of medium viscosity growth, which results from accumulation of polymer products, while the value of  $W_D$  goes down.

As the polymer accumulation rate in the first layer (adjacent to the substrate) is always higher than that in any of the further layers located above the first one due to lower stationary concentration of inhibitor (i.e. oxygen), the viscosity of the first layer changes the fastest, resulting in a corresponding decrease of the constant of chain termination rate and, therefore, in growth of  $W_{O_2}$ . However, the growth of  $W_{O_2}$  is constrained by the limit of  $W_D$ . This limiting value  $W_{O_2 \text{ lim}}^{(1)} = W_D^{(1)}$  (where

index 1 denotes layer number) is the higher, the closer is the layer to the surface (the value of  $W_D^{(i)}$  is inversely proportional to  $l_i^2$ ).

Then, as the oxidative polymerization process develops further (with corresponding growth of medium viscosity), the oxygen absorption rate in the second layer reaches the limiting value  $W_{O_2 \text{ lim}} = W_D^{(2)}$ , and then the similar situation develops in the third layer:  $W_{O_2 \text{ lim}}^{(3)} = W_D^{(3)}$  and so forth. In this process,  $W_{O_2 \text{ lim}}^{(1)} < W_{O_2 \text{ lim}}^{(2)} < W_{O_2 \text{ lim}}^{(3)} \dots$ , because  $w_D^{(1)} < W_D^{(2)} < W_D^{(3)} \dots$  due to  $l_1 > l_2 > l_3 \dots$ , i.e., the polymerization front, satisfying the requirement  $W_D = W_{O_2 \text{ lim}}$ , moves forward layer by layer from the substrate to the film surface. Each layer passes successively through one and the same set of corresponding viscosity states, but with different and growing degrees of conversion. Starting from the moment when condition  $W_{O_2 \text{ lim}} = W_D$  is satisfied in the lowest film layer with thickness  $l$ , integral rate of oxidative polymerization  $\bar{W}_{O_2}$ <sup>4</sup> for any film with thickness  $l' < l$  turns out to be higher than that for a film with thickness  $l$ . Increasing the partial pressure of oxygen should be equivalent (in terms of its influence on oxidative polymerization development) to film thickness reduction because  $W_D \sim P_{O_2}$ . The value of auto-acceleration for the oxidative polymerization decreases as the polymerization front propagates with  $W_D = W_{O_2 \text{ lim}}$ , and at a certain degree of conversion, auto-deceleration begins, which satisfies condition  $\bar{W}_D < \bar{W}_{O_2}$ . Thus, the autocatalysis degree of the oxidative polymerization according to the layered model (all other factors being equal) should depend upon film thickness and partial pressure of oxygen above the film.

Indeed, in thinner films and in case of higher partial pressures of oxygen, the autocatalysis rates and degrees are higher (see Figs. 2.11, 2.12, and 2.13). Coincident sections of curves  $W_{O_2} = f(\tau)$  (Fig. 2.11) for films that differ in thickness correspond to the reaction medium state, when oxygen consumption rate (even in the deepest layers of thicker film) has not yet reached  $W_{O_2 \text{ lim}}$  and, therefore, does not depend upon thickness value [kinetic mode of oxidative oligo(acrylates) polymerization]. In this mode, the stationary concentration of oxygen in all film layers is virtually equal to oxygen solubility in the substrate. Splitting points of coincident sections of curves correspond to the transition of reaction in lower film layers with thickness of  $35 \mu\text{m}$  into the diffusion mode. Location of splitting points and maximums on curves  $W_{O_2} = f(\tau)$  depend upon oligo(acrylates) structure and film-forming conditions.

Viscosity variation rate  $d\eta/d\tau$  increases as molecular functionality enhances in terms of double bonds and temperature. Therefore, the area of oxidative polymerization development in the kinetic mode in the case of dMA-EGA is larger than for tEMA-tPA. Temperature drop exerts a similar influence upon each of the oligo(acrylates)s. For the same reason, the auto-acceleration period in films with thickness  $80 \mu\text{m}$  ends very quickly, and thus researchers fail to register this period in experiments (Fig. 2.11). Dropping branches of curves  $W_{O_2} = f(\tau)$  are determined by a trivial reason, namely, by dramatic diminution of  $D_{O_2}$  at deep conversions caused by film solidification.

<sup>4</sup> In experiments, it is just the integral process rate (averaged throughout the film volume) that is actually measured.



The afore-described interpretation of experimental data is verified by the character of dependency of kinetics of oligo(acrylates) interaction with oxygen upon partial pressure of oxygen  $P_{O_2}$  (see Fig. 2.13). Rates on coincident sections of curves do not change with increasing  $P_{O_2}$  (kinetic mode of oxidative polymerization); at the same time, the length of these sections increases considerably due to the growth of  $W_D$ , as a result of which  $W_{O_2 \text{ lim}}$  also increases. Increase of  $W_D$  with growing  $P_{O_2}$  also determines an increase of  $C_{O_2 \text{ lim}}$  and maximum rates of oxygen consumption at late stages of reaction, when  $W_{O_2}$  is determined by the value of  $W_D$ . For the same reason, smoothing of differences is observed in kinetics of oligo(acrylates) interactions with oxygen between thin and thick films. Increased film thickness, as well as increased medium viscosity (up to gel consistency), lowers the oxygen diffusion rates to such values that are less or comparable with oxygen consumption rates, thus switching over the oxidative polymerization reaction into diffusion mode. As a rule, switching-over between the modes of oxidative polymerization occurs in the gel-formation area with the content of cross-linked polymer being within 1–3% (see Fig. 2.11).

Thus, the layered model adequately reflects the main kinetic specifics of oxidative polymerization of oligo(acrylates) in films under the conditions of oxygen diffusion.

#### 2.4.1.2 Kinetic Features of TFRP of Vinyl-Type Compounds in Films Under the Conditions of Oxygen Diffusion

Kinetic features of TFRP inhibited by oxygen diffusing into the film were studied taking the polymerization of oligo(acrylates) with different functionality as an example [2, 4]. Oxygen inhibits methacrylate polymerization [including oligo(acrylates)] due to highly effective transfer of chain to oxygen  $\sim M^\bullet + O_2 \xrightarrow{k_1} \sim MO_2^\bullet(1)$  ( $k_1 = 1 \times 10^7 \text{ l} \cdot \text{mol}^{-1} \cdot \text{s}^{-1}$ ) at 50°C for MMA [47]) and slow regeneration of chain by peroxide radicals  $\sim MO_2^\bullet + M \xrightarrow{k_2} \sim MOOM^\bullet$  (2) [4]. The rate of reaction (2) is lower than the chain propagation rate  $\sim M^\bullet + M \xrightarrow{k_3} \sim MM^\bullet$  (3) ( $k_3/k_2 \approx 200$ , MMA at 50°C) [2, 4, 58]. The ratio of rates of competing reactions of chain transfer to oxygen and chain propagation  $\sim M^\bullet + M \xrightarrow{k_3} \sim MM^\bullet$  (3) for oligo(acrylates) polymerization depending on  $[O_2]$  is given in Table 2.8.

**Table 2.8** Dependence of  $\alpha = k_1[O_2]/k_3[M]$  value upon concentration of oxygen  $[O_2]$  dissolved in oligomer

Oligomer	Value of $\alpha$		
	$[O_2] = 1 \times 10^{-2} \text{ mol/l}$	$[O_2] = 2 \times 10^{-3} \text{ mol/l}$	$[O_2] = 3 \times 10^{-4} \text{ mol/l}$
dMA-EGA	40	8	$\approx 1$
teMA-tPA	35	7	$\approx 1$
hMA-PeA	30	6	$\approx 1$

*Note.* Typical values of  $[O_2]$  in monomers for monomer saturation with oxygen under pressure of 100 kPa are  $0.8 \times 10^{-2} \text{ mol/l}$  (25°C) and  $1.0 \times 10^{-2} \text{ mol/l}$  (50°C) [2].

Physically, parameter  $\alpha$  is the number of chain transfer events to oxygen per one event of chain propagation.

Only saturation of oligo(acrylates) with oxygen under pressure of 100 kPa ( $[O_2] = 1 \times 10^{-2}$  mol/l) suppresses the chain propagation reaction practically completely ( $\alpha = 30-40$ ), in the air atmosphere (at  $[O_2]$  in oligomer  $2 \times 10^{-3}$  mol/l)  $\alpha = 6-8$ , and only reduction of  $[O_2]$  to the value of  $3 \times 10^{-4}$  mol/l allows the chain propagation reaction to compete successfully with the reaction of chain transfer to oxygen ( $\alpha \approx 1$ ).

In the context of the *layered model of TFRP of vinyl-type compounds*, it becomes possible to interpret the experimentally found dependence of kinetics of cross-linked polymer formation upon parameters regulating the rate of oxygen diffusion into film. In film, where the reaction with oxygen involvement takes places and where oxygen diffuses concurrently from the gas phase, the oxygen concentration gradient through film thickness appears, with the growth of  $[O_2]$ , from the substrate to the surface:  $[O_2]^{(1)} < [O_2]^{(2)} < [O_2]^{(3)} \dots$  due to  $l_1 > l_2 > l_3 \dots$ , where 1, 2, and 3 are the layer numbers counting from the substrate. At a certain conversion degree, in the film layer adjacent to the substrate,  $[O_2]$  should inevitably fall to a value at which the chain propagation reaction  $\sim M^\bullet + M \xrightarrow{k_3} \sim MM^\bullet$  (3) starts competing successfully with the chain transfer reaction to oxygen  $\sim M^\bullet + O_2 \xrightarrow{k_1} \sim MO_2^\bullet$  (1): increase in viscosity  $\eta$  resulting from accumulation of soluble polymers, i.e., products of oxidative polymerization, leads to the growth of  $W_{O_2}$  (gel effect), while  $W_D$  decreases because  $D_{O_2} = f(1/\eta)$ . Such a situation occurs, first of all, in the layer adjacent to the substrate because the stationary  $[O_2]$ , the polymerization inhibitor, in it is always lower than in any of the upper-lying layers, and the viscosity of this layer grows most rapidly. Homo-polymerization develops as a process with positive feedback: polymerization acceleration from  $[O_2]$  decrease results in increased polymer content in the layer and upgraded viscosity, which, in its turn, would retard oxygen diffusion into the layer still farther and accelerate polymerization. Then, a similar situation will be repeated in the second layer (the one above the first layer) and the TFRP front (originated in the near-the-substrate layer) would propagate layer by layer to the film surface. In this process, each layer successively passes through one and the same set of corresponding viscosity states, but with different, constantly growing degrees of conversions. In the context of the layered model, the TFRP kinetics should depend (with other factors being equal) upon parameters regulating oxygen concentration in each of the film layers: namely, film thickness, partial pressure of oxygen above the film, initiation rate, and oligomer oxidability.

Thus, it has been established that TFRP kinetics (namely, duration of induction period  $\tau$ , polymerization rate  $W_p$ , and maximum yield of cross-linked polymer  $C_p$ ) depends heavily upon film thickness  $l$  (Fig. 2.14) and partial pressure of oxygen in the gas phase  $P_{O_2}$  (Fig. 2.15). According to the forecast derived from the model, increase of  $l$  or decline of  $P_{O_2}$  results in the reduction of  $\tau$  and growth of  $W_p$  and  $C_p$ . The layer-by-layer pattern of TFRP is verified directly: near-the-substrate layers contain a greater amount of cross-linked polymer and are less oxidized compared to film layers near its surface (Table 2.9).

According to the following criterion

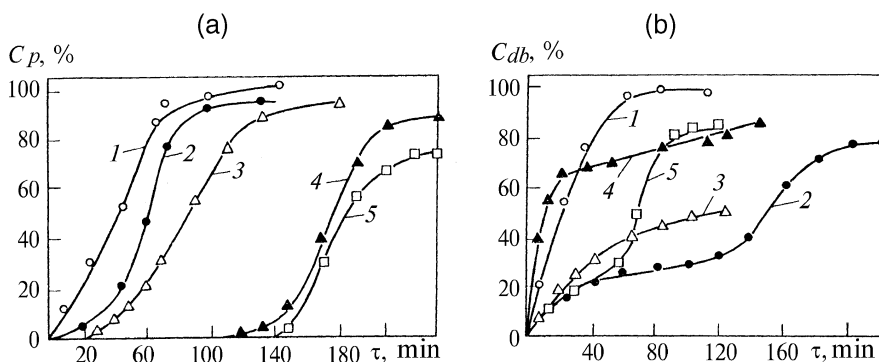


**Fig. 2.14** Kinetic curves of cross-linked polymer formation (a) and consumption of double bonds (b) in oligo(acrylates) films. (a) 1, 2, teMA-tPA, 80°C, film thickness 80 and 35  $\mu\text{m}$ ; 3, 4, 5, dMA-EGA, 80°C, film thickness 80, 35, and 15  $\mu\text{m}$ ; (b) 1, dMA-EGA, 100°C, film thickness 35  $\mu\text{m}$ ; 2, 4, teMA-tPA, 65°C, film thickness 35 and 80  $\mu\text{m}$ ; 3, hMA-PeA, 65°C, 35  $\mu\text{m}$ ; 5, teMA-tPA, 80°C, 35  $\mu\text{m}$

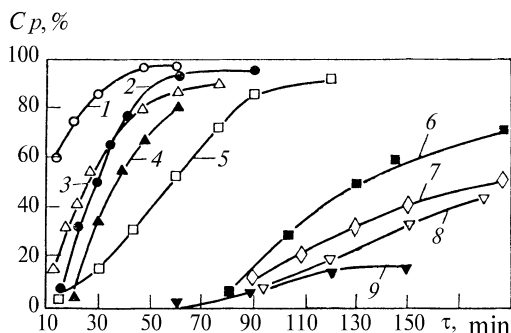


**Fig. 2.15** Kinetic curves of cross-linked polymer formation in oligo(acrylates) films with thickness of 30  $\mu\text{m}$  for various values of  $P_{O_2}$ : 1, 3, 4, hMA-PEA, 65°C, 0, 21, and 100 kPa; 5, 6, 8, teMA-tEA, 65°C, 0, 21, and 100 kPa; 2, 7, 9, dMA-EGA, 100°C, 0, 21, and 100 kPa. Redox system composition, (mol/l)  $\times 10^{-2}$ : [DHHP] = 3.06, [cobalt naphthenate] = 1.07

$$W_{db}/W_{O_2} = 1 - W_H/W_C \quad (2.5)$$

where  $W_{db}$ ,  $W_{O_2}$ ,  $W_H$ , and  $W_C$  = rate of consumption of double bonds, rate of oxygen consumption, rate of homo-polymerization, and rate of copolymerization with oxygen, respectively.

Under given conditions, a cross-linked polymer is formed mainly due to the homo-polymerization reaction (Fig. 2.16). For example, at the maximum of curves  $W_{db}/W_{O_2} = f(\tau)$ , when  $C_p = 50\text{--}80\%$ , from 5 to 50 events  $\sim M^\bullet + M \xrightarrow{k_3} \sim MM^\bullet$  accounted for 1 event  $\sim M^\bullet + O_2 \xrightarrow{k_1} \sim MO_2^\bullet$ . However, oxidative polymerization most likely prevails in the surface layer directly contacting with the air.

**Table 2.9** Changes of acrylic (oligo)esters\* and allylic\*\* (oligo)ethers properties throughout their film thickness

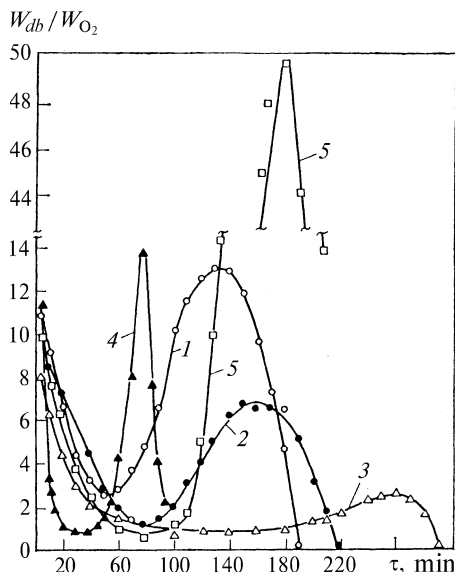
Parameters	dMA-EGA*	teMA-tEA*	dAl-EGA**	teAl-tPA**
Content, % (by weight)				
Cross-linked polymer	63.9/95.1	61.5/92.5	46.7/57.0	58.4/65.3
Double bonds	8.1/7.1	50.3/49.8	28.7/23.3	50.0/44.5
Peroxide number, $gI_2/100g$	0.78/0.19	2.02/0.12	2.9/3.1	19.4/17.0
Acid number, mg KOH/g	22.7/5.1	0.88/0.74	18.3/22.9	29.5/25.8
Number of oxygen atoms attached by oligomer unit	2.08/1.24	3.34/2.64	2.12/1.90	3.25/3.15

Note 1. Numerator, upper layer; denominator, bottom layer.

Note 2. Total film thickness, 70  $\mu m$ ; thickness of upper and bottom layers, 15  $\mu m$  each.

\*, \*\*Polymerization conditions: dMA-EGA, 100°C, 100 min; teMA-tEA, 80°C, 52 min; dAl-EGA, 100°C, 60 min; teAl-tPA, 80°C, 70 min.

**Fig. 2.16** Variation of  $W_{db}/W_{O_2}$  ratio for oligo(acrylates) polymerization: 1, 2, 3, dMA-EGA, 80°C, film thickness 80, 35, and 15  $\mu m$ ; 4, 5, teMA-tPA, film thickness 35  $\mu m$ ; 80° and 65°C



Kinetic anomaly, that is, homo-polymerization in liquid films of oligo(acrylates) ( $W_{db}/W_{O_2} = 5-10$ ) long before gel formation under the conditions of  $W_D > W_{O_2}$ , is discussed in Sect. 2.1.1.

However, specifics of TFRP in oligo(acrylates) films under oxygen diffusion conditions do not consist in layer-by-layer development of the process only. The authors found out that up to rather high-degree conversions, cross-linked polymers are formed from short-chain soluble polymers<sup>5</sup>, and not directly as a result of oligomer polymerization. Soluble polymers are formed in the course of oligo(acrylates) polymerization in films in the air as the main product (before cross-linked polymer

<sup>5</sup> The term "soluble polymers" stands for non-cross-linked products of polyunsaturated compound polymerization.

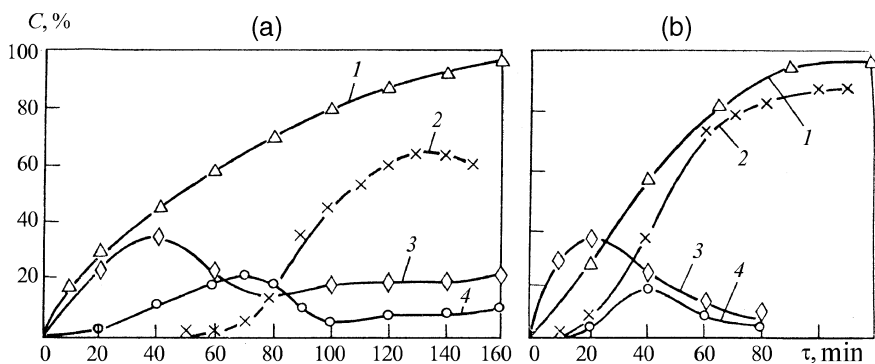


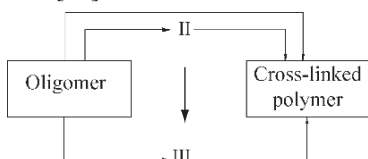
**Fig. 2.17** Kinetic curves of dMA-EGA polymerization at 100°C in films with thickness of 35 (a) and 70  $\mu\text{m}$  (b): 1, conversion in terms of double bonds ( $C_{db}$ ); 2, 3, 4, yield of cross-linked polymer and soluble polymers II and III ( $C_p, C_{II}, C_{III}$ )

formation) during induction period of TFRP with duration  $\tau$ , and as a part of sol fraction after the gel point is reached. In the presence of oxygen, the length of primary polymeric chains decreases approximately by two orders of magnitude, and under given polymerization conditions it should be about 10 oligomer units. This fact raises the stationary concentration of soluble polymers and shifts the beginning of gel formation into the area of high-degree conversions ( $C_{db} = 16\text{--}60\%$  and  $\tau = 20\text{--}100$  min) (see Figs. 2.14 and 2.17). In terms of a set of properties [56], soluble polymers represent unsaturated oxidized compounds with polymerization degree  $\bar{P}_p = 2\text{--}8$  (low molecular fraction denoted as polymers II) and  $\bar{P}_p > 8$  (higher molecular fraction, polymers III). Proton magnetic resonance spectroscopy (PMR) results indicate that chains of soluble polymers consist mainly of  $\sim\text{MOOM}\sim$  units and certain number of  $\text{OK}\sim\text{MM}\sim$  units.

The polymerizing ability of soluble polymers (the inverse values of induction period, formation rate, and maximum yield of cross-linked polymer could be taken as measures for this ability) changes in the following manner [59]:

- Polymers III are always characterized by greater polymerizing ability than polymers II
- Polymerizing ability of both polymers II and polymers III increases as molecular functionality of oligomers enhances
- The later after the beginning of oligomer polymerization the soluble polymers are extracted from films, the lower is their polymerizing ability

The entire set of results on kinetics of polymerization of oligo(acrylates) and their soluble polymers in films under oxygen diffusion conditions enabled the authors to propose and substantiate the following scheme of cross-linked polymer formation [59]:



where II and III are soluble polymers of the II and III types.

It should be pointed out that the main direction of conversion is as follows: oligomer  $\rightarrow$  polymer II  $\rightarrow$  polymer III  $\rightarrow$  cross-linked polymer. The following data could be provided in favor of this conclusion: within the limits of experimental error, the maximum value on accumulation curves for polymer II corresponds (in terms of time) to the highest rate of polymer III accumulation, while the maximum value of accumulation curves for polymer III corresponds to the highest rate of cross-linked polymer formation (Fig. 2.17).

During polymerization auto-acceleration, the relationship  $dC_p/dC_{db} = q$  grows (Fig. 2.18). It means that until a certain degree of conversion, cross-linked polymer is formed mainly not from parent oligomer molecules, but from polymer III blocks that are becoming larger and larger in size.

A certain part of polymer III and cross-linked polymer is likely to be formed directly from the oligomer, which follows from the comparison of the rates of accumulation of these polymers and oligomer consumption. Such direction of TFRP appears to become prevailing for high-degree stages of conversion, in the studied cases, for transformation degrees with  $C_p > 50\text{--}60\%$ .

Thus, the main kinetic specifics of TFRP of vinyl-type oligomers [such as oligo (acrylates)] in films under the conditions of diffusion of oxygen (which serves as polymerization inhibitor) are determined by layer-by-layer development of TFRP and by formation of cross-linked polymers, mainly from short-chain soluble polyunsaturated polymers that represent intermediate products of oligomer polymerization.

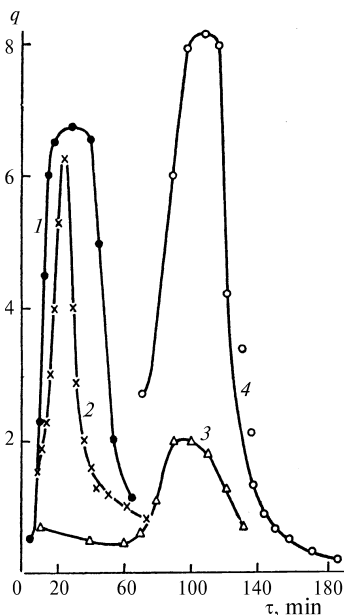


**Fig. 2.18** Variation of parameter  $q$  for teMA-tPA polymerization (1, 3, 4) and hMA-PeA polymerization (2) in films of different thickness and at different temperatures: 1, 80°C, 80 μm; 2, 65°C, 35 μm; 3, 65°C, 80 μm; 4, 65°C, 35 μm

## 2.4.2 Allyl Compounds

### 2.4.2.1 Kinetic Features of Oxidative Polymerization of Allyl-Type Compounds in Films Under the Conditions of Oxygen Diffusion

These features have been mainly studied on oligomer ethers of allyl alcohol (propen-2-ol-1) (OEAl), diallyl(bis-ethylene glycol) adipate (dAl-EGA) and tetra allyl of (bis-trimethylolpropane) adipate (teAl-tPA), which had the identical structure of oligomer block with such oligo(acrylates) as dMA-EGA and teMA-tPA.

These circumstances enabled the authors to identify kinetic patterns of oxidation and oxidative polymerization common for compounds of vinyl and allyl types and made it possible to determine kinetic features of TFRP of oligomer allyl ethers, taking into account different reactive capacity of compounds of allyl and vinyl types in radical addition and radical substitution reactions. Experiments with OEAl in films were performed using a circulation volumetric unit [55] with the same redox system that was introduced in the same concentration as in the case with oligo(acrylates) (see Sect. 2.4.1).

Kinetic curves of oxygen absorption in dAl-EGA and teAl-tPA films (Fig. 2.19), in total, represent kinetics of oxidation and oxidative polymerization of OEAl, because, judging by results of experiments with monomer ethers of allyl alcohol [60], the oxidation and oxidative polymerization proceed as consecutive reactions.

In the case of oxidation of allylpropyl ether and allyl acetate within the range 35°–70°C, before conversion in terms of absorbed oxygen  $C_{O_2} \leq 0.5\%$ , the amount of absorbed oxygen (with accuracy of 5%) corresponds to the amount of formed hydroperoxide with the structure  $HOCH_2-CH=CHOR$  [where R is  $C_3H_7-$  or  $CH_3C(O)-$ ], established using the PMR and infrared (IR) spectroscopy methods.

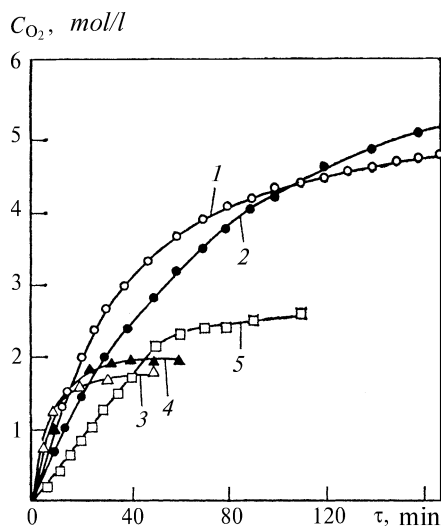
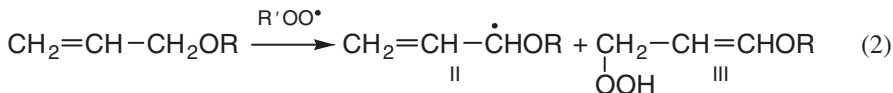
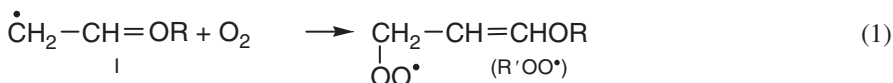


**Fig. 2.19** Kinetic curves of oxygen absorption for OEAl polymerization in films with thickness of 35  $\mu\text{m}$  at  $P_{O_2} = 21$  kPa: 1 and 2, dAl-EGA, 100° and 80°C; 3, 4, and 5, teAl-tPA, 100°, 80°, and 65°C

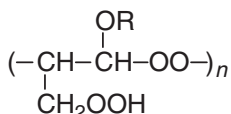
Oxidation proceeds as a chain free-radical process according to the  $\alpha$ -methylene mechanism [2 (p. 134)] with chain propagation stages:



where R is  $\text{C}_3\text{H}_7-$  or  $\text{CH}_3\text{C}(\text{O})-$

Unsaturated hydroperoxide III (i.e., primary product of oxidation) is formed through homolytic elimination of allyl ether  $\alpha$ -methylene by peroxide radical with subsequent isomerization of free radical II into radical I with the transfer of double bond and free valence migration. In this process, the double bond of unsaturated hydroperoxide III (not involved in oxidation) is activated as a result of  $\pi$ - $p$  conjugation of  $\pi$ -electrons of the double bond with  $p$ -electrons of ether oxygen.

Oxidation of monomer allyl ethers to high conversions ( $\text{C}_{\text{O}_2} > 1-2\%$ , in block, at  $50^\circ\text{C}$ ) results in the formation of polymer products with the following structure



(where R:  $\text{C}_3\text{H}_7-$  or  $\text{CH}_3\text{C}(\text{O})-$ ), established using the PMR and IR-spectroscopy methods. This means that it is just unsaturated hydroperoxides III (not allyl ethers) that directly enter in the oxidative polymerization according to the mechanism characteristic for vinyl-type compounds  $\sim\text{M}\cdot + \text{O}_2 \rightarrow \sim\text{MO}_2\cdot(1)$ ,  $\sim\text{MO}_2\cdot + \text{M} \rightarrow \sim\text{MOOM}\cdot(2)$  (where M:  $\text{HOOCH}_2\text{CH}=\text{CHOR}$ ).

Thus, interaction of monomer ethers of allyl alcohol with oxygen for low-degree conversions proceeds in two stages: in the form of consecutive reactions of co-oxidation and oxidative polymerization.

The autocatalytic character of the process of OEAL interaction with oxygen and the dependence of this process upon conditions and oligomer structure (Figs. 2.19, 2.20 and 2.21) is obvious. The influence of structure is manifested in the fact that, with other factors being equal, limiting conversions  $\text{C}_{\text{O}_2\text{lim}}$  decrease as molecular functionality enhances. Most probably the autocatalysis is provided both by degenerate branching on hydroperoxides with participation of cobalt naphthenate and by inhibition of quadratic termination of chain on polyperoxide radicals accompanied by gel-effect development.

However, experimental data indicate that specifics of OEAL oxidation and OEAL oxidative polymerization are not exhausted by trivial development of autocatalysis. The authors also established that the kinetics of OEAL interaction with oxygen diffusing into film depends heavily upon film thickness and partial pressure of oxygen  $P_{\text{O}_2}$  in the gas phase (Figs. 2.20 and 2.21). Similar to the oxidative polymerization of oligo(acrylates), the autocatalysis degree and limiting conversions  $\text{C}_{\text{O}_2\text{lim}}$  are inversely dependent upon film thickness, and they increase as  $P_{\text{O}_2}$  grows.



**Fig. 2.20** Dependence of  $W_{O_2}$  upon duration of teAl-tPA polymerization in films of different thickness at  $P_{O_2} = 21$  kPa: 1, 2, and 3, 80°C, 15, 35, and 70  $\mu\text{m}$ ; 4, 5 and 6, 65°C, 15, 35 and 70  $\mu\text{m}$

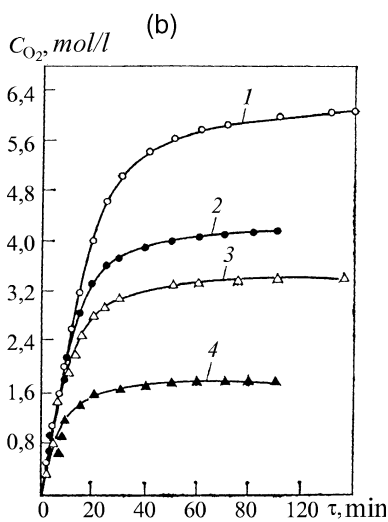
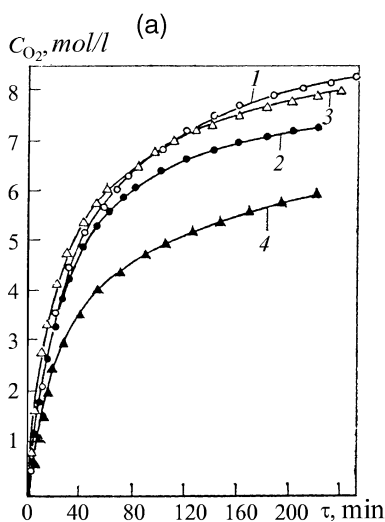
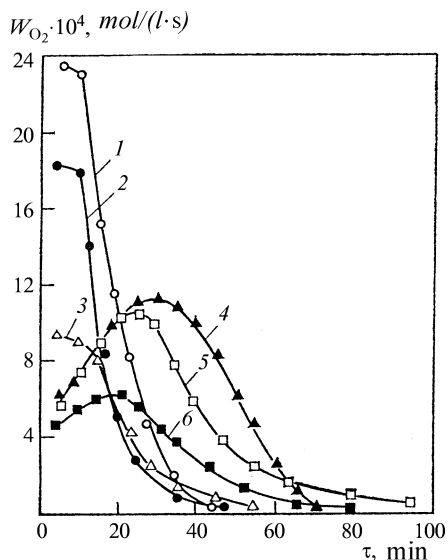


**Fig. 2.21** Kinetic curves of oxygen absorption for dAL-EGA polymerization at 100°C (a) and teAl-tPA at 80°C (b) for different values of  $P_{O_2}$ : a 1, 2, 15  $\mu\text{m}$ , 100 and 21 kPa; 3, 4, 35  $\mu\text{m}$ , 100 and 21 kPa; b 1, 2, 15  $\mu\text{m}$ , 100 and 21 kPa; 3, 4, 35  $\mu\text{m}$ , 100 and 21 kPa

In a number of cases, coincident sections of kinetic curves are observed for films with different thickness and different values of  $P_{O_2}$ , and the length of these sections increases as the value of  $P_{O_2}$  goes up. These regularities were interpreted within the framework of the *layered model for oligo(acrylates) oxidative polymerization* (see Sect. 2.4.1) that give us grounds to extend the layered model on the process of OEAl oxidation and OEAl oxidative polymerization.

### 2.4.2.2 Kinetic Features of TFRP of Allyl-Type Compounds in Films Under Oxygen Diffusion Conditions

These features for oligomer allyl ethers and oligo(acrylates) are very different. In the case of oligo(acrylates), TFRP kinetics depends upon parameters regulating the rate of oxygen diffusion into film as follows: duration of induction period  $\tau$  declines as film thickness  $l$  increases and partial pressure of oxygen  $P_{O_2}$  decreases, while the formation rate  $W_p$  and maximum yield of cross-linked polymer  $C_p C_{lim}$  increase (see Figs. 2.14 and 2.15). In the absence of oxygen, with other conditions being equal, the oligo(acrylates) polymerization proceeds without induction period ( $\tau = 0$ ), with the highest  $W_p$  and  $C_p \geq 95\%$  (see Fig. 2.15). In contrast, in the case of OEAL polymerization in films, the induction period duration grows as the value of  $P_{O_2}$  decreases and the value of  $l$  increases, while formation rate and maximum yield of cross-linked polymer go down (Fig. 2.22). In the absence of oxygen, with other conditions being equal, the OEAL polymerization proceeds at minimal values of  $W_p$  and  $C_p$ . For instance, in teAl-tPA films at 80°C when switching over from polymerization in the air to polymerization in vacuum, the induction period duration grows from 20 to 35 min, and  $C_p$  falls from 85 to 20% (curves 3 and 3' in Fig. 2.22a); polymerization in vacuum stops when approximately 70% of double bonds are still unconsumed (curves 2 and 2' in Fig. 2.22b).

It is highly probable that OEAL oxidation by oxygen diffusing into the film with production of hydroperoxides and concurrent activation of double bonds is a necessary precondition for TFRP of these oligomers.

Indeed, the authors failed to interpret the above-indicated features of TFRP in OEAL films in the context of the layered model without using such an assumption.

Fundamental notions of the layered model of TFRP for allyl-type compounds are as follows. At the moment of time  $t_1$ , with the onset of oligomer oxidation, diffusion

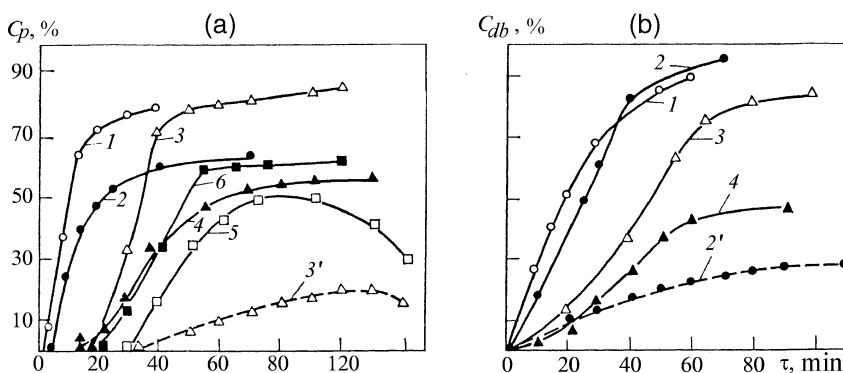


**Fig. 2.22** Kinetic curves of cross-linked polymer formation (a) and consumption of double bonds (b) in OEAL films in the air (—) and in vacuum (---): (a) 1, 2, teAl-tPA, 100°C, 35 and 70  $\mu\text{m}$ ; 3, 3', 4, teAl-tPA, 80°C, 35 and 70  $\mu\text{m}$ ; 5, 6, dAL-EGA, 100°C, 35 and 70  $\mu\text{m}$ ; (b) 1, dAL-EGA, 100°C, 35  $\mu\text{m}$ ; 2, 2', teAl-tPA, 80°C, 35  $\mu\text{m}$ ; 3, 4, teAl-tPA, 65°C, 35 and 70  $\mu\text{m}$

flow of oxygen is generated from the gas phase into the film and gradient  $[O_2]$  is established, with growing, layer after layer  $[O_2]$  from the substrate to the film surface  $[O_2]^{(1)} < [O_2]^{(2)} < [O_2]^{(3)} < \dots$ , where 1, 2, 3 is a layer number counting from the substrate. Variation of  $[O_2]$  in the  $i$ -th film layer is determined by the difference between oxygen consumption rate  $W_{O_2}^i$  and oxygen diffusion rate  $W_D^i$  into the  $i$ -th layer. With high enough thickness of film  $l$ , in a layer adjacent to the substrate, from the very beginning of oxidation  $t_1$   $W_D^{(1)}$  may turn out to be much lower than  $W_{O_2}^{(1)}$ , where index 1 denotes the layer number. Then, by the moment in time  $t_2$ , hydroperoxides HP with concentration  $[HP]^{(1)}$  would accumulate in this layer and certain amount of oxygen with concentration  $[O_2]^{(1)}$  would be left. The following inequality would be a condition for the beginning of polymerization (not inhibited by  $O_2$ ) in any layer

$$[HP]/[O_2] > ([HP]/[O_2])_{cr} \quad (2.6)$$

which follows from the mechanism of oxidation, oxidative polymerization, and polymerization of unsaturated compounds, when these processes are initiated by hydroperoxides produced during oxidation [4]. Depending on oxidation conditions (temperature,  $P_{O_2}$ , initiation rate  $W_I$ , length of oxidation chains), by the moment in time  $t_2$ , in the near-the-substrate layer, into which oxygen does not diffuse, either condition  $[HP]^{(1)}/[O_2]^{(1)} > ([HP]/[O_2])_{cr}$  is fulfilled and polymerization starts, or almost the entire amount of oxygen would be consumed in it without producing such amount of HP that is sufficient for polymerization initiation. Then this layer, where  $[HP]^{(1)}/[O_2]^{(1)} < ([GP]/[O_2])_{cr}$ , will be left nonpolymerized.

In this situation, if the film is thick enough, there always is an  $i$ -th layer located closer to the surface, into which oxygen inflows due to diffusion at rate  $W_D^i$  that is not significantly higher than oxidation rate  $W_{O_2}^i$ ; therefore,  $[HP]$  would definitely reach the stationary concentration  $[HP]_{st}$ , when the oxygen consumption rate is maximum and does not depend upon  $[O_2]$ . At the same time, the oxygen diffusion rate into this layer will continuously decline due to viscosity changes caused by accumulation of polymer products of oxidative polymerization with corresponding decrease of  $[O_2]^i$ . It should be pointed out here that oxidative polymerization most likely proceeds only in conjugated double bonds formed as a result of hydroperoxide oxidation of OEAL without involving nonconjugated double bonds of nonoxidized molecules of oligomers. Hence, starting from a certain moment in time, condition  $[HP]^i/[O_2]^i > ([HP]/[O_2])_{cr}$  will be certainly fulfilled in the  $i$ -th layer and polymerization would start. In layer  $(i+1)$  located above the  $i$ -th layer,  $[HP]$  reaches  $[HP]_{st}$ , somewhat earlier than in the  $i$ -th layer, but  $[O_2]^{i+1} > [O_2]^i$  due to  $l_i > l_{i+1}$ . In the  $(i+1)$ -th layer, the viscosity changes required for fulfillment of polymerization beginning conditions would occur at a more advanced stage of oxidation and oxidative polymerization. The increased viscosity zone (extending from the  $i$ -th layer upward) will diminish the oxygen diffusion rate, thus facilitating the fulfillment of polymerization process condition in the  $(i+1)$ -th layer. Then, the same situation will be repeated in the  $(i+2)$ -th layer and then, in turn, in all upper layers, with each of them passing successively through one and the same set of corresponding viscosity states, but at different, steadily growing degrees of conversion. Thus, after the front

of polymer transformations has been generated in the  $i$ -th layer, it would start extending upward. Extension of this front downward would be attenuated very soon, because the dense film of the  $i$ -th layer would hinder the access of oxygen to lower layers, where the condition (2.6) is not fulfilled in any case,  $[\text{HP}] < [\text{HP}]_{\text{st}}$ ; besides, the deeper the layer is, the lower is  $[\text{HP}]$ . Nonpolymerized lower-located layers will be “immured,” in other words, excluded from the polymerization process.

If by the moment in time  $t_2$ , condition  $[\text{HP}]^{(1)}/[\text{O}_2]^{(1)} > ([\text{HP}]/[\text{O}_2])_{\text{cr}}$  is fulfilled in the layer adjacent to the substrate, then, in accordance with the mechanism described above, it would be successively fulfilled in the second, third, and each of the upper-located film layers, but at increasingly higher degrees of conversion. The front of polymer transformations (i.e., viscosity changes) would extend from the near-the-substrate layer (as it does from the  $i$ -th layer) to the film surface and no unpolymerized (“immured”) layers would be left in the film.

Hence, for each of the specific conditions upon which  $[\text{HP}]$  and  $[\text{O}_2]$  depends, namely, temperature, values of  $P_{\text{O}_2}$ ,  $D_{\text{O}_2}$ , and  $W_l$ , oxidation chain length, a critical film thickness  $l_{\text{cr}}$  exists, which is characterized by the fact that in films with  $l < l_{\text{cr}}$ , not-oxygen-inhibited polymerization would not proceed at all, whereas in films with  $l > l_{\text{cr}}$  it would proceed only partially to a depth that is approximately equal to  $l_{\text{cr}}$ , counting from the film surface. In films with thickness  $l > l_{\text{cr}}$ , such TFRP parameters as  $1/\tau W_p$ , and  $C_{\text{lim}}$  would depend directly upon partial pressure of oxygen  $P_{\text{O}_2}$  above the film and film thickness, and these parameters, in the end, regulate  $[\text{O}_2]$  and  $[\text{HP}]$  in each film layer.

Indeed, in OEAL films with thickness of 35–70  $\mu\text{m}$ , the induction period duration  $\tau$  declines under oxygen diffusion conditions, while rate  $W_p$  and limiting conversion of cross-linked polymer  $C_{\text{lim}}$  grows with increasing  $P_{\text{O}_2}$  and reducing film thickness (Fig. 2.22). With the distance from the surface of the  $i$ -th layer, where polymerization is originated, being equal for two films with different thickness, the part of the film (cut off from oxygen access by this layer) is larger in the thicker film. This leads to a decrease of measured integral values  $W_p$  and  $C_p$  (averaged throughout the film volume) because condition (2.6) is not fulfilled in the “immured” layers and polymerization does not take place. In terms of its influence on TFRP kinetics, the decrease of  $P_{\text{O}_2}$  is equivalent to film thickness growth. The authors managed to identify nonpolymerized film layers “immured” near the substrate (and forecast by the layered model of TFRP) with polymerization of *cis*-oligobutadiene, the allyl-type oligomer (Table 2.10).

**Table 2.10** Changes of features in *cis*-oligobutadiene films throughout their thickness

Indices	Upper layer	Lower layer
Cross-linked polymer content, %	25.7	0.0
Double bonds content, %	59.2	90.0
Peroxide number, g I <sub>2</sub> /100 g	15.6	3.8
Acid number, mg KOH/g	33.2	1.5
Oxygen content, %	7.01	2.07

*Note.* Total film thickness, 70  $\mu\text{m}$ ; thickness of upper and lower layers, 15  $\mu\text{m}$  each; polymerization temperature, 20°C; exposure time, 4 h.

The authors also obtained experimental data that are indicative of the presence of films with thickness  $l < l_{cr}$ , in which OEAl polymerization (not inhibited by oxygen) does not take place at all. For instance, for dAL-EGA at 100°C,  $W_I = 2 \times 10^{-5} \text{ mol}/(1 \cdot \text{s})$ ,  $P_{O_2} = 21 \text{ kPa}$  (in the air), a cross-linked polymer is not formed at all in films with thickness 15  $\mu\text{m}$ , despite the fact that more than 95% of double bonds have reacted. Probably for this oligomer, the value of  $l_{cr} > 15 \mu\text{m}$  under given conditions.

This assumption could be substantiated in the following way. For polymerization in films under oxygen diffusion conditions, the number of cross-links per film volume unit is determined by the ratio of rates of the following competing polymerization reactions:  $\sim M^\bullet + M \rightarrow \sim MM^\bullet$  (3) with formation of one cross-link per each reacted double bond and oxidative polymerization:  $\sim M^\bullet + O_2 \xrightarrow{k_1} \sim MO_2^\bullet$  (1) and  $\sim MO_2^\bullet + M \xrightarrow{k_2} \sim MOOM^\bullet$  (2), with the number of cross-links being less than one for each reacted double bond due to destructive transformations for bonds  $-\text{COOC}-$ . Under identical conditions in terms of temperature, film thickness and  $P_{O_2}$ , dAL-EGA polymerization proceeds with much higher contribution of reactions (2.1) and (2.2) versus dMA-EGA polymerization (Figs. 2.23 and 2.16) and, hence, dAL-EGA films contain a considerably lower amount of cross-linked polymer than dMA-EGA films (Table 2.9). Polymers of upper layers of OEAl and oligo(acrylates) films, judging by diminished content of cross-linked polymer versus their lower layers (Table 2.9), are subjected to oxidative destruction the most. Probably a cross-linked polymer is formed in the upper layers of oligomers of vinyl and allyl types with thickness  $l > l_{cr}$  mainly because of oxidative polymerization. In the limiting case, with  $l < l_{cr}$  under the conditions when polymerization process is represented by oxidative polymerization only, while oxidative destruction is developed quite considerably, a cross-linked polymer is not formed at all in all layers of the dAL-EGA film.

However, specifics of TFRP in OEAl films under oxygen diffusion conditions are not confined to layer-by-layer development of the process. The authors found out that a significant part of cross-linked polymers is formed not directly during polymerization of oligomers, but from short-chain soluble polyunsaturated polymers that represent intermediate products of the TFRP process. Soluble polymers

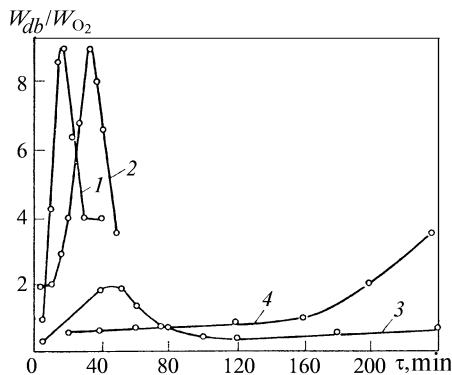


**Fig. 2.23** Variation of  $W_{db}/W_{O_2}$  ratio for OEAl polymerization. 1, teAl-tPA, 100°C, 70  $\mu\text{m}$ ; 2, teAl-tPA, 80°C, 70  $\mu\text{m}$ ; 3, dAL-EGA, 100°C, 15  $\mu\text{m}$ ; 4, dAL-EGA, 80°C, 35  $\mu\text{m}$

are formed during OEAl polymerization as the main product before the beginning of TFRP (during TFRP induction period  $\tau$ ) and as a part of sol-fraction after reaching the gel point. Oxidative polymerization by double bonds activated by  $\pi$ - $p$  conjugation under the conditions of strongly developed chain transfer to oligomer by  $\alpha$ -methylene groups inevitably results in quite short-chain polymers, the polymerization degree of which  $\bar{P}_p$  increases slightly (in average, up to  $\bar{P}_p \approx 10$ ) due to homo-polymerization. The formation of just short-chain polymers upgrades their stationary concentration and shifts the beginning of gel formation to the area of higher conversions ( $C_{db} = 20$ –50%,  $\tau = 20$ –30 min; Figs. 2.22 and 2.24).

In terms of a set of properties [2 (p. 120)], soluble OEAl polymers are unsaturated compounds with polymerization degree  $\bar{P}_p = 2$ –8 (low molecular fraction denoted as polymers II) and  $\bar{P}_p > 8$  (higher molecular fraction, polymers III). PMR results show that the ratio of  $\sim$ MOOM $\sim$  and  $\sim$ MM $\sim$  units in chains of soluble dAl-EGA and teAl-tPA polymers lies in the range from 4:1 to 3:1, which indicates that in addition to oxidative polymerization, homo-polymerization also proceeds under the above-described conditions ( $t = 65^\circ$ – $100^\circ\text{C}$ ,  $P_{O_2} = 21\text{kPa}$ ,  $l = 35$ – $70\mu\text{m}$ ).

Polymerizing capacity of soluble polymers in films was studied under the conditions taken for parent oligomers [2 (p. 124); 61]. The obtained results could be summarized as follows:

- Polymerizing capacity that was estimated based on polymerization rate and limiting yield of cross-linked polymers is always higher for polymer III vs. polymer II.
- Polymerizing capacity of polymers II and III grows as molecular functionality of oligomer enhances.
- The later from the beginning of oligomer polymerization that soluble polymers are isolated from films, the lower is their polymerizing capacity.

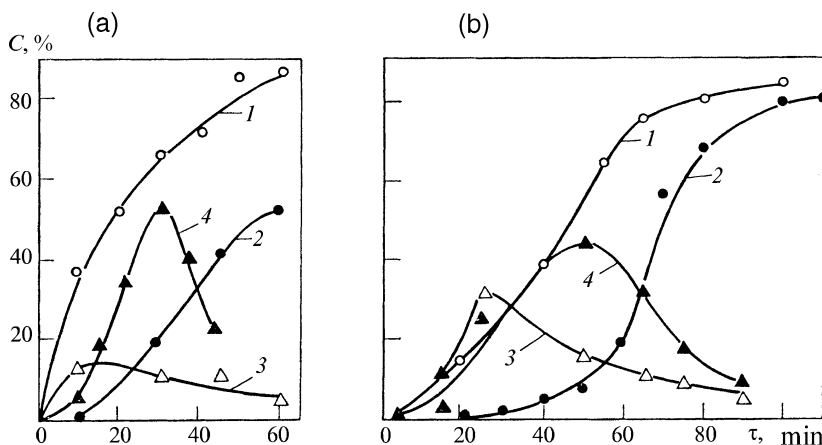


**Fig. 2.24** Kinetic curves for dAl-EGA polymerization at  $100^\circ\text{C}$ (a) and teAl-tPA polymerization at  $65^\circ\text{C}$ (b) in films with thickness  $35\mu\text{m}$ : 1, double-bond conversion ( $C_{db}$ ); 2,3,4, yield of cross-linked polymer and soluble polymers II and III ( $C_p, C_{II}, C_{III}$ )

A total set of results on kinetics of OEAl and their soluble polymer polymerization in films under oxygen diffusion conditions gives grounds for us to consider the following direction of polymerization transformations as the main one: oligomer  $\rightarrow$  polymer II  $\rightarrow$  polymer III  $\rightarrow$  cross-linked polymer. The following data could be provided in favor of this conclusion:

- Within the limits of experimental error, the maximum value on accumulation curves for polymer II corresponds (in terms of time) to the highest rate of polymer III accumulation, while the maximum value on accumulation curves for polymer III corresponds to the highest rate of cross-linked polymer formation (see Fig. 2.24).
- During the polymerization auto-acceleration period, polymer yield per each reacted double bond  $q = dC_p/dC_{db}$  (Fig. 2.25) increases; this means that until a certain degree of conversion is reached, the cross-linked polymer is formed mainly not from molecules of parent oligomer, but from polymer III volumes that are becoming larger and larger in size.

Probably a certain part of polymer III and cross-linked polymer is still formed directly from oligomer during high-degree conversions with  $C_p \geq 50\%$ . On the whole, the scheme proposed earlier for oligo(acrylates) polymerization could be also applied for the formation of OEAl polymers (see Sect. 2.4.1).

Thus, main kinetic features of TFRP for oligomer allyl ethers in films under oxygen diffusion conditions are determined by the layer-by-layer development of TFRP and formation of cross-linked polymers mainly from short-chain soluble polyunsaturated polymers that represent intermediate products of polyunsaturated oligomer polymerization. It should be also pointed out here that the mechanisms of layer-by-layer development of TFRP and causes of formation of soluble polymers for OEAl and oligo(acrylates) (as compounds of allyl and vinyl types) are totally different (see Sects. 2.4.1 and 2.4.2).

The role of oxygen (diffusing into the film) in TFRP of compounds of allyl type is also fundamentally different from its role in TFRP of vinyl-type compounds. For OEAl and other allyl-type compounds with double bonds that are not so active in radical addition reactions and with strongly developed reaction of chain transfer on oligomer, oxidation is a necessary condition for TFRP development.

Oxidative polymerization and polymerization (which are responsible for TFRP) are most likely initiated mainly by hydroperoxides, which are formed during OEAl

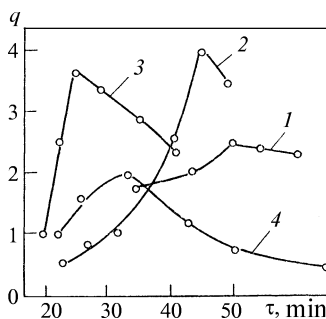


**Fig. 2.25** Variation of parameter  $q$  during dAl-EGA polymerization (1, 2) and tAl-tPA polymerization (3, 4) in films of different thickness and at different temperatures: 1 and 2, 100°C, 35 and 70  $\mu\text{m}$ ; 3 and 4, 80°C, 15 and 35  $\mu\text{m}$

oxidation caused by oxygen diffusing into the film. In contrast, TFRP of vinyl-type compounds [including oligo(acrylates)] with double bonds that are highly reactive in radical addition reactions, the oxygen diffusing into the film is, first of all, an inhibitor, and oxidation is just an inevitable secondary process.

## 2.5 Three-Dimensional Free-Radical Polymerization as a Tool for Macromolecular Design of Cross-Linked Polymers

Actually, a final goal of any kinetic or structural and physical study in the field of polymers is gaining basic data for macromolecular design. These data include kinetic regularities, mechanism of macromolecule formation process, and patterns of formation of supermolecular structures regulating properties of polymer solids (materials). In the case of linear (non-cross-linked) macromolecules, the final structure of polymer solids is influenced both by polymerization process parameters regulating molecular mass characteristics of macromolecules and by conditions of supermolecular structure formation process, which include purposeful technological action, such as thermal, mechanical (pressing, calendaring, rolling, etc.), and introduction of modifying additives. In the case of cross-linked (linked) and especially highly cross-linked polymers, the polymerization process parameters exert decisive influence upon the formation of polymer solids and, hence, final polymer properties, because opportunities for special technological action on these are dramatically limited by to infusibility, insolubility, and weakly expressed relaxation capacity of highly cross-linked polymers.

Macromolecular design of cross-linked polymers (that are TFRP products) is implemented based on results of fundamental studies that enable determining specifics of kinetic regularities and TFRP mechanism, the main peculiarity of which consists in microheterogeneity (see Chaps. 1 and 2). To use these results as an effective tool for macromolecular design, they should be transformed into a mathematical (computer) TFRP model. Currently existing TFRP models can be classified into two groups: the microheterogeneous model and homogenous models.

The *microheterogeneous model*, which is based on kinetic interpretation of simplified concepts of the microheterogeneous mechanism of TFRP, was developed from the end of the 1970s to the beginning of the 1980s [3]. In summary, it could be presented as follows. Microgel particles, operating in the mode of self-contained micro-reactors, are approximated with spheres of averaged radius  $r$ . It is assumed that the polymerization process is localized in the peripheral layer of such sphere (with thickness  $h$  that does not change as degree of conversion increases) (see Fig. 1.8). Computations showed that the number of micro-reactors during transformation is virtually constant, so the growth in the conversion degree of occurs due to the increase of  $r$ . After  $r$  reaches a value at which spheres begin contacting each other, their loose peripheral layers (playing roles of effective reactors) partially overlap, and their cores, consisting of highly cross-linked polymers with limiting conversion and, therefore, incapable of mutual penetration, are packed as a tetragonal or (which is less probable) a hexagonal structure. Cavities of the structure



made of spheres (more precisely, internal near-the-surface layer of these cavities with thickness  $h$ ) serve as the place of polymerization process localization (reaction zone) at this stage. With sufficiently high conversion, the spherical shape of these cavities (with average radius  $r'$ ) is assumed. It is obvious that in the course of subsequent polymerization the value of  $r'$  declines.

Within the framework of such a model (the percolation model), the constants of rates of all elementary acts (initiation, propagation, termination) do not change with conversion changes because, during polymerization, conditions in the reaction zone (in loose near-the-surface layers over dense highly cross-linked polymer) remain the same, and only the total volume of the reaction zone changes: at first it grows (until the moment when spheres come into contact), and then declines. Correspondingly, the overall (experimentally observed) reduced rate of polymerization  $W/[M]$  at first increases (auto-acceleration stage), and then decreases (auto-deceleration). Both stages in this case could be described with simple mathematical expressions:

Auto-acceleration:

$$W = W_0 \left( 1 - \frac{C}{C_{\text{lim}}} \right) + W_r (4\pi N)^{1/3} h \left( \frac{3C}{C_{\text{lim}}} \right)^{2/3} \quad (2.7)$$

where  $W_0$  and  $W_r$  = polymerization rates in the initial reaction medium and in spherical layers with thickness  $h$ ;  $C$  = current conversion;  $C_{\text{lim}}$  = limiting conversion; and  $N$  = concentration of spherical micro-reactors (microgel particles, grains).

Auto-deceleration:

$$W = W_0 \left( 1 - \frac{C}{C_{\text{lim}}} \right) + W_r (4\pi N)^{1/3} h^3 2^{2/3} \left( 1 - \frac{C}{C_{\text{lim}}} \right)^{2/3} \quad (2.8)$$

However, an interval between auto-acceleration and auto-deceleration cannot be described with such simple relationships.

The number of micro-reactors (microgel particles) formed in the reaction system reaches constant value  $N_{\text{lim}}$  already at early TFRP stages (with  $C < 1\%$ ); it depends on both kinetic parameters and reaction conditions.

In the absence of inhibiting additives:

$$N_{\text{lim}} = \frac{W_1 k_{\text{ter}}}{(f-1) k_{\text{pr}}^2 [M]_0} \quad (2.9)$$

where  $W_1$  = initiation rate;  $f$  = monomer functionality; and  $[M]_0$  = initial monomer concentration.

In the presence of inhibitor X, the value of  $N_{\text{lim}}$  is derived from Eq. (2.2), in which  $k_X$  = constant of acceptance rate of radical-chain carriers.

Equations ( 2.2, 2.7, 2.8, and 2.9) show how one can control TFRP kinetics and morphology of highly cross-linked polymers being formed. For instance, increasing  $W_1$  or/and introducing additives of inhibitor X makes it possible to transform a large-grain structure into a fine-grain one. An advantage of this model consists in the fact that it takes the microheterogeneous pattern of TFRP into account.

Homogeneous mathematical (computer) models imply more complicated formulas [42–44, 62–64]. Elementary TFRP acts (initiation, chain propagation, and termination) are assumed to proceed under the conditions of diffusion control. Therefore, effective values of their rate constants are dependent in certain manner upon conversion and vary in the course of polymerization. Type of functions  $k = f(C)$  depends on selection of a particular physical model of diffusion control of elementary acts: either the Smolukhovsky one, or within the framework of the free volume theory, or with involvement of concepts on “reaction” diffusion. It should be pointed out that certain physical constants remain undefined and subsequently (i.e., during comparison of calculation results with experimental data) they play the role of adjustable parameters. From the applied science standpoint, such a semiempirical theory has certain advantages: obtained formulas are applicable for forecasting macromolecule design, but only under limited conditions because of the empirical character of parameters.

The most developed model is the one [62] where expressions for constants of elementary act rates are obtained in the following form:

$$k_{pr} = \frac{k_{pr0}}{1 + \exp[A_{pr}(1/v - 1/v_{av})]} \quad (2.10)$$

$$k_{ter} = \frac{k_{pr0}}{1 + \{R_d k_{pr}[M]/k_{ter0} + \exp[-A_{ter}(1/v - 1/v_{av})]\}^{-1}} \quad (2.11)$$

Here  $k_{pr0}$  = true kinetic propagation constant, i.e., value of  $k_{pr}$  in the absence of diffusion control;  $A$  = parameter determining how fast the diffusion-controlled kinetic constant decreases with growing hindrances for diffusion;  $V$  = average partial free volume of the system;  $v_{cr}$  = critical free volume for chain propagation reaction determined as a value, with which  $k_{pr} = (1/2)k_{pr0}$ ;  $R_d k_{pr}[M]$  = member representing the contribution of the “reaction diffusion” mechanism;  $[M]$  = instantaneous concentration of double bonds; and  $R_d$  = a parameter characterizing “reaction diffusion.”

To calculate the partial free volume for a given conversion, it is necessary to know six parameters of a material: monomer and polymer density ( $\rho_m$  and  $\rho_p$ ), their glass-transition temperatures ( $T_{gm}$  and  $T_{gp}$ ), and the difference of expansion coefficients in high-elastic and glass states ( $\alpha_m$  and  $\alpha_p$ ). Parameter  $R_d$  is determined [40] based on results of nonstationary experiments (post effect) as follows:

$$R_d = \frac{k_{ter}}{k_{pr}[M]} \quad (2.12)$$

Such an approach does not take microheterogeneity of the reaction medium into account (in an explicit form), and it is little different from known gel effect theories developed for the case of linear polymerization of conventional (monofunctional) vinyl monomers in high-viscosity media [11]. Trivial kinetic regularities of TFRP (autocatalysis at early stages, auto-deceleration at high-degree conversions, type of dependence  $W/[M]$  upon initiation rate with fixed values of  $C$ ), as well as results of nonstationary kinetic measurements of “elementary” (but, actually, effec-

tive) constants of chain propagation rates and chain termination rates agree quite satisfactorily with results obtained through the use of models that are based on dependence of diffusion-regulated constants of rates upon the reaction medium state determined by conversion.

However, during TFRP, nontrivial processes and phenomena (described in detail and analyzed in monographs [3, 5], as well as presented in Chaps. 1 and 2) are observed, which cannot be interpreted based on homogenous models with constants  $k = f(C)$ : that is why a microheterogeneous model of TFRP was developed.

It is obvious that both models—a homogenous model and a microheterogeneous one—represent extreme (limiting) cases of TFRP. Actually, the TFRP microheterogeneity is most expressed for oligomers with short and/or hard oligomer blocks in the case of polymerization with low rates of initiation (no higher than  $10^{-7} \text{ mol} \cdot \text{l}^{-1} \cdot \text{s}^{-1}$ ). For oligomers with long and/or flexible blocks or in the case of polymerization with very high initiation rates (above  $10^{-6}$ – $10^{-5} \text{ mol} \cdot \text{l}^{-1} \cdot \text{s}^{-1}$ ), microheterogeneity becomes less expressed. Recently when conducting TFRP in the “living” chain mode, during copolymerization with appropriately selected comonomers, as well as during polymerization in the mode of formation of very short chains (inhibition, chain transfer, catalytic chain transfer), researchers managed to minimize sources of heterogeneity origination to such an extent that for these cases the homogeneous model of radical polymerization is quite applicable.

We would like to especially emphasize here that considerable efforts by researchers are focused on issues of computer modeling of TFRP [41–44, 62–64]. Rapid development of this research area is important for extending the opportunities for macromolecular design of cross-linked polymers.

## References

1. Berlin AA, Kefeli TYa, Korolev GV (1967) Poly-esteracrylates. Nauka, Moscow
2. Mogilevich MM (1977) Oxidative polymerization in film-formation processes. Khimia (Chemistry), Leningrad
3. Berlin AA, Korolev GV, Kefeli TYa, Sivergin YuM (1983) Acrylic oligomers and materials on the acrylic oligomers. Khimiya, Moscow (in Russian)
4. Mogilevich MM, Pliss EM (1990) Oxidation and oxidative polymerization of unsaturated compounds. Khimia (Chemistry), Moscow (in Russian)
5. Korolev GV, Mogilevich MM, Golikov IV (1995) Cross-linked polyacrylates: micro-heterogeneous structures, physical networks, deformation-strength properties. Khimiya, Moscow (in Russian)
6. Korolev GV, Berlin AA, Kefeli TYa (1962) *Vysokomolek Soedin* **4**:1520–1527 (in Russian)
7. Kefeli TYa, Korolev GV, Filippovskaja YuM (1961) *J Polym Sci* **52**:169–177
8. Korolev GV, Berezin MP (1997) *Vysokomolek Soedin A* **39**:242–249 (in Russian)
9. Korolev GV, Boichuk IN, Mogilevich MM et al (2001) *Vysokomolek Soedin A* **43**:713–721 (in Russian)
10. Bagdasaryan XS (1966) Radical polymerization theory. Nauka, Moscow (in Russian)
11. Gladyshev GP, Popov VA (1974) Radical polymerization at deep conversion degrees. Nauka, Moscow (in Russian)

12. Tvorogov NN (1967) Synopsis of thesis for Ph.D. degree in chemistry. Institute of Chemical Physics of the USSR Academy of Science, Moscow (in Russian)
13. Plate NA, Ponomarenko AG (1974) *Vysokomolek Soedin A* **16**:2635–2645 (in Russian)
14. Lipatov YuS, Nesterov A.S., Gritsenko TM, Veselovskiy RA (1971) Reference book on chemistry of polymers. Naukova Dumka, Kiev (in Russian)
15. Berlin AA, Samarin EF (1969) *Vysokomolek Soedin B* **9**:530–533 (in Russian)
16. Berlin AA, Tvorogov NN, Korolev GV (1966) *Dokl Akad Nauk* **170**:1073–1076 (in Russian)
17. Berlin AA, Tvorogov NN, Korolev GV (1966) *Izv AN SSSR Khimia No. 1*:193 (in Russian)
18. Mogilevich MM, Sukhanov GA, Korolev GV (1975) *Vysokomolek Soedin A* **17**:2487–2492 (in Russian)
19. Semenov NN (1960) *Chemistry and technology of polymers 1960, No. 7*:8196–198 (in Russian)
20. Plate NA, Shibayev VP (1980) *Comb polymers and liquid crystals. Khimiya, Moscow* (in Russian)
21. Korolev GV, Perepelitsyna EO (2000) *Dokl Akad Nauk* **371**:488–492 (in Russian)
22. Korolev GV, Perepelitsyna EO (2001) *Vysokomolek Soedin A* **43**:774–783 (in Russian)
23. Semenov NN (1958) *Certain issues of chemical kinetics and reactive capacity. Publishing House of USSR Academy of Science, Moscow* (in Russian)
24. Salem L (1985) *Electrons in chemical reactions. Mir, Moscow* (Russian translation)
25. Minkin VI, Simkin Vya, Minyayev RM (1986) *Quantum chemistry of organic compounds: reaction mechanisms. Khimiya, Moscow* (in Russian)
26. Korolev GV, Ilyin AA, Mogilevich MM et al (2002) *Izv Vuz Khim Khim Tekh* **45**:33–38
27. Korolev GV, Ilyin AA, Mogilevich MM et al (2003) *Vysokomolek Soedin A* **45**:883–890 (in Russian)
28. Korolev GV, Mogilevich MM, Ilyin AA (2002) *Association of liquid organic compounds. Mir, Moscow* (in Russian)
29. Krestov GA (ed) (1995) *Experimental methods of solution chemistry: spectroscopy and calorimetry. Nauka, Moscow* (in Russian)
30. Kutepov AM (ed) (1997) *Experimental methods of solution chemistry. Nauka, Moscow* (in Russian)
31. Durov VA (2002) In: *Concentrated and saturated solutions. Nauka, Moscow* (in Russian), p 170
32. Burkert U, Allinger NL (1986) *Molecular mechanics. Mir, Moscow* (Russian translation)
33. Heerman DV (1990) *Computer simulation methods in theoretical physics. Moscow* (Russian translation)
34. Korolev GV, Ilyin AA, Solovyev NE, Mogilevich MM et al (2001) *Vysokomolek Soedin A* **43**:1822–1827 (in Russian)
35. Korolev GV, Ilyin AA, Solovyev NE, Mogilevich MM et al (2002) *Vysokomolek Soedin A* **44**:1947–1954 (in Russian)
36. Kargin VA, Kabanov VA, Papisov IM, Zubov VP (1961) *Dokl Akad Nauk SSSR* **141**:389–392 (in Russian)
37. Papisov IM, Kabanov VA, Kargin VA (1965) *Vysokomolek Soedin* **7**:1779–1785 (in Russian)
38. Kabanov VA, Papisov IM, Gvozdetskiy AN, Kargin VA (1965) *Vysokomolek Soedin* **7**:1787–1791 (in Russian)
39. Korolev GV, Smirnov BR, Zhiltsova LZ et al (1967) *Vysokomolek Soedin* **9**:9–14 (in Russian)
40. Yong JS, Bowman CN (1999) *Macromolecules* **32**:6073–6081
41. Decker C (1998) *Polym Int* **45**:133–141
42. Tobita H (1998) *Macromol Theory Simul* **7**:225–232
43. Wen M, McCormick AV (2000) *Macromolecules* **33**:9247–9254
44. Okay O (1999) *Polymer* **40**:4117–4129
45. Denisov ET, Azatyan VV (1997) *Inhibition of chain reactions. Institute of Chemical Physics, Chernogolovka* (in Russian)
46. Korolev GV (2003) *Usp Khim* **72**:222–244 (in Russian)

47. Denisov ET (1971) Liquid-phase reaction rate constants. Nauka, Moscow (in Russian)
48. Korolev GV (1965) Synopsis of thesis for doctor of science degree in chemistry. Institute of Chemical Physics of the USSR Academy of Science, Moscow (in Russian)
49. Golikov IV, Vasilyev DK, Mogilevich MM (1990) *Izv Vuz Khim Khim Tekh* **33**:94–99 (in Russian)
50. Vasilyev DK, Belgovskiy IM, Mogilevich MM (1989) *Vysokomolek Soedin A* **31**:1233–1237 (in Russian)
51. Lipatov YuS (1980) Interphase phenomena in polymers. Naukova Dumka, Kiev (in Russian)
52. Vasilyev DK, Golikov IV, Mogilevich MM et al (1987) *Vysokomolek Soedin B* **29**:563–564 (in Russian)
53. Brock T, Groteklaes M, Mischke P (2004) European coatings handbook: paint media. Moscow (Russian translation)
54. Mogilevich MM, Sukhanov GA, Korolev GV et al (1975) *Vysokomolek Soedin A* **17**:2390–2395 (in Russian)
55. Mogilevich MM, Sukhanov GA (1973) *J LKM* **2**:53–55 (in Russian)
56. Mogilevich MM, Sukhanova NA, Yablonskiy OM et al (1973) *Izv Vuz Khim Khim Tekh* **16**:1898–1903
57. Frank-Kamenetskiy DA (1966) Diffusion and mass transfer in chemical kinetics. Nauka, Moscow (in Russian)
58. Mogilevich MM (1979) *Usp Khim* **48**:362–386 (in Russian)
59. Mogilevich MM, Sukhanova NA, Korolev GV (1973) *Vysokomolek Soedin A* **15**:1478–1482 (in Russian)
60. Mogilevich MM, Sukhov VD, Yablonskiy OP et al (1977) *Dokl Akad Nauk SSSR* **232**:1355–1358 (in Russian)
61. Mogilevich MM, Krasnobaeva VS (1976) *Izv Vuz Khim Khim Tekh* **19**:105–108
62. Goodner MD, Bowman CN (1999) *Macromolecules* **32**:6552–6559
63. Elliot IE, Bowman CN (1999) *Macromolecules* **32**:8621–8628
64. Platkowski K, Reichert K-H (1999) *Polymer* **40**:1057–1066

## Chapter 3

# Living Chain Three-Dimensional Radical Polymerization

**Abstract** Based on analysis of the mechanism of anion polymerization in the living chains mode, the authors have formulated necessary and sufficient conditions for the implementation of the living chains conditions for radical polymerization. Also, achievements in the field of controlled radical polymerization (CRP) and mechanisms of these processes for obtaining linear polymers [nitroxide-mediated polymerization (NMP) and atom transfer radical polymerization (ATRP)] are briefly described in Chap. 3. Different options for producing cross-linked polymers under three-dimensional free-radical polymerization (TFRP) in the living chains conditions are described in detail and supported by experimental results obtained by the authors. Kinetics of cross-linked polymer formation plus mechanical and diffusion properties of obtained cross-linked polymers are compared with relevant results of conventional TFRP. Comparison of results enabled the author to formulate tactics for macromolecular design of cross-linked polymers and areas of application for polymeric materials with modified topology and morphology.

Living radical polymerization, living chains in radical polymerization, or, to be more exact, radical polymerization in the living chains conditions<sup>1</sup>, is a new and rapidly developing area in the field of radical polymerization, which appeared in the beginning of the 1990s<sup>2</sup> as a result of the discovery (during the previous decade) of a new elementary act of the polymerization process that involves the participation of chain carrier radicals  $\sim R^\bullet$ : the reversible addition of  $\sim R^\bullet$  to stable free radicals or to certain metal complexes. No less than 400–500 publications devoted to living radical chains appeared annually in 2004–2007, and this fact serves as evidence of the high scientific and applied significance, as well as of the promising character, of this new area of scientific research. Of course only key publications related to living chains in linear radical polymerization are analyzed in this chapter, while publications on three-dimensional free-radical polymerization in the living chains conditions are represented exhaustively, and special attention is given to living chains

---

<sup>1</sup> The term “controlled radical polymerization (CRP)” is generally accepted in publications in English, but we believe that this term covers a wider range of phenomena than radical polymerization in the living chains conditions. Thus, we will use the latter from now on.

<sup>2</sup> The history of discovery of living free-radical polymerization and stages of its evolution are described in reviews [1, 2].

three-dimensional free-radical polymerization as a tool for macromolecular design of cross-linked polymers.

### 3.1 Living Chains in Free-Radical Polymerization

The notion of living polymer chains was introduced by Michael Szwarc in the middle of the 1950s in the course of studying anionic polymerization [3]. Since polymer anions  $\sim R^-$  are incapable of quadratic chain termination reaction, in the absence of reactive foreign matter (FM) that terminates the chains linearly,  $\sim R^- + FM \rightarrow$  termination, the anion polymerization proceeds as unteminated. Polymer anions remain dormant not only in the course of the polymerization process but also upon its completion: polymerization restarts after the addition of a fresh portion of the same monomer or any other monomer capable of anion polymerization at the same centers  $\sim R^-$ . That is, the lifetime of living polymer chains  $\tau$  exceeds the period of complete polymerization  $t$  ( $\tau > t$ ).

Another remarkable peculiarity of anion polymerization in the living chains conditions—namely, molecular weight distribution of formed polymer—practically reaches the monodisperse level (parameter of polydispersion  $M_w/M_n \rightarrow 1.0$ ). The stage of polymer chain generation in anion polymerization develops rapidly during time  $\tau_i$ , which is significantly shorter than the time of complete polymerization  $t$ . The condition  $\tau_i \ll t$  means that all polymer chains that were generated practically simultaneously grow synchronously, so that the number-averaged molecular weight  $M_n$  of the polymer being formed is proportional to time, and molecular weight distribution of the polymer narrows continuously (even with the number of polymer chains being equal to several tens of links  $M_w/M_n \rightarrow 1.0$ ).

Thus, anion polymerization in the living chains conditions proceeds under the conditions when  $\tau > t$ , and  $\tau_i \ll t$ .

The fundamental distinction of radical polymerization from anion polymerization in terms of kinetics consists in the quadratic termination of radicals that are carriers of polymer chains:  $\sim R^\bullet + \sim R^\bullet \rightarrow$  termination; this means that the lifetime of polymer chains  $\tau$  is significantly shorter than the time of complete polymerization  $t$  ( $\tau \ll t$ ). Consequently, to ensure the fulfillment of the main condition for living radical polymerization implementation  $\tau > t$ , it is necessary to prolong the lifetime of chain carriers radicals  $\sim R^\bullet$ , thus preventing their quadratic termination, but retaining the high reactive capacity of  $\sim R^\bullet$  in the propagation reaction in relation to monomer molecules  $\sim R^\bullet + M \rightarrow \sim RM^\bullet$ . This problem seemed to be unsolvable one.

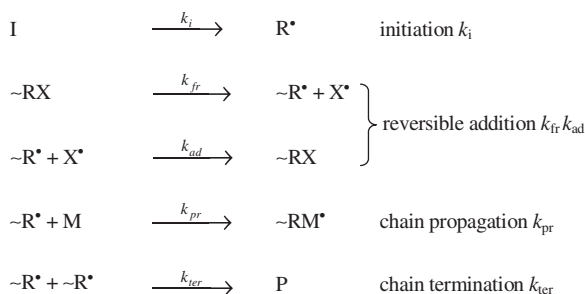
The second condition, i.e.,  $\tau_i \ll t$ , is also not fulfilled in the case of radical polymerization. This condition is necessary for the realization of the main advantage of living polymerization, namely, monodispersiveness of the polymer being formed. In the case of radical polymerization, generation of new chains (initiation) takes place throughout the entire polymerization process (it is not restricted by a short initial period  $\tau_i$ ), which fact disturbs the synchronous character of polymer chain growth and inevitably raises the degree of polymer polydispersity. As is well known,

in radical polymerization, the minimum polymer polydispersity characterized by parameter  $M_w/M_n$  is equal either to 1.5 or to 2 depending upon the type of chain termination reaction (recombination and disproportionation) [4].

For this reason, it was believed that the mechanism of radical polymerization made it impossible to implement the living chains conditions. However, the discovery of a new elementary act in radical polymerization, namely, temporary capture of chain carrier radicals  $\sim R^\bullet$  by acceptor A ( $\sim R^\bullet + A \rightleftharpoons \sim RA$ ) with subsequent regeneration of  $\sim R^\bullet$  (so-called degenerative transfer)<sup>3</sup> [5, 6], allowed us to solve this problem. This solution made it possible to prolong the lifetime of  $\sim R^\bullet$  to such an extent that it became greater than the time of complete conversion ( $\tau > t$ ), and also to attain the synchronous propagation of polymer chains after fulfilling condition  $\tau_i \ll t$ .

Stable nitroxyl radicals  $\text{>NO}^\bullet (X^\bullet)$  [7] or  $\sim R^\bullet$  alkoxyamines with a weak bond  $\text{>NO}-C$  formed in situ during acceptance of polymer radicals were initially proposed as acceptors<sup>4</sup>. If  $\sim R^\bullet$  are polystyrene radicals, then even at 100°C a quite high rate of dissociation of this bond is provided. As a result, as was rigorously proven first by Georges et al. [7], growing polystyrene chain  $\sim R^\bullet$  exists in the reaction system in two alternating states: in a passive state (in the form of adduct  $\sim RX$ ) and in an active one (as polymer radical  $\sim R^\bullet$ ).

Researchers started using alkoxyamines as agents of living radical polymerization as such [7–11], or they were synthesized in the reaction system proper from introduced nitroxyl radicals and radical initiators [12–14]. The mechanism of action of alkoxyamines as agents of living radical polymerization could be presented as shown in Scheme 3.1 [1]:



**Scheme 3.1** Reversible deactivation (including nitroxide-mediated) polymerization

where I, M, and P are molecules of initiator, monomer, and polymer, respectively;  $k_i$ ,  $k_{pr}$ , and  $k_{ter}$  are constants of rates for reactions of initiation, propagation, and termination, respectively;  $\sim\text{RX}$  = adduct;  $\text{X}^\bullet$  = stable free radical; and  $k_{fr}$  and  $k_{ad}$  are constants of rates of adduct fragmentation and addition, respectively.

<sup>3</sup> In Russian, the term reversible inhibition is sometimes used.

<sup>4</sup> This branch of radical polymerization in the living chains conditions is named nitroxide-mediated polymerization (NMP).



Stages of reversible addition are the key stages; they make it possible for growing chains  $\sim R^\bullet$  to avoid termination during quadratic termination reaction because of competing capture of radical  $\sim R^\bullet$  by stable free radical  $X^\bullet$ . In this process, in the time interval between generation (or regeneration) of chains,  $\sim R^\bullet$  have enough time to react with monomers, thus implementing the propagation of the polymer chain. With the proviso that  $k_{\text{ter}}[\sim R^\bullet]^2 \ll k_{\text{ad}}[X^\bullet]$ , the prevailing reaction  $\sim R^\bullet + X^\bullet$  simply transfers the chain into temporarily inactive state  $\sim RX$  (dormant state), in which it stays until the next act of dissociation  $\sim RX$ . Thus, the condition  $\tau > t$  is fulfilled. At the end of polymerization, after the initial monomer is completely depleted, practically all chains (with the exception of a small fraction of them, which were terminated according to the quadratic mechanism with the formation of conventional, statistical polymer P) appear to be in the latent state  $\sim RX$ . Obviously, addition of a fresh portion of initial or other monomer (during synthesis of block copolymer) would “develop” active centers  $\sim R^\bullet$ ; i.e., the present situation will be quite adequate for living polymerization.

For the provision of another important condition, namely, simultaneity of chain generation ( $\tau_i \ll t$ ), it is sufficient that the half-life value of adduct  $\sim RX$ , equal to  $0.69/k_{\text{fr}}$ , is significantly (10–100 times) less than the time of complete polymerization  $t$ . It is obvious that with the proviso that  $0.69/k_{\text{fr}} \ll t$ , each growing chain has enough time to multiply (tens and hundreds of times) both in the active state and in the sleeping one. This fact synchronizes the growth of chains, thus providing the monodispersiveness of the polymer.

Research into radical polymerization of styrene in the living chains condition enabled the authors to identify the following regularities [15]:

- Polymerization rate  $W$  is proportional to the concentration of monomer M (the first order with respect to monomer concentration) and does not depend upon concentration of alkoxyamine (zero order) or upon concentration of stable nitroxyl radical, if the synthesis of alkoxyamine is performed in situ.
- The molecular weight of a polymer grows linearly with increasing degree of polymerization (i.e., with increasing conversion). This regularity is observed at least up to  $M_n \approx (2-3) \times 10^4$ .
- Polydispersity of polymer varies depending upon process conditions, but, as a rule, the value of  $M_w/M_n \leq 1.3$ .
- Concentration of stable nitroxyl radical throughout the entire duration of polymerization process constitutes 0.1–1.0% of initial concentration of alkoxyamine.

In steady-state approximation, the rate of living radical polymerization (proceeding according to Scheme 3.1) is given by expression  $W = k_{\text{pr}}[M](W_i/k_{\text{ter}})^{1/2}$ , which coincides with the expression describing the rate of conventional radical polymerization without reversible addition. Under steady-state conditions, reversible addition reactions make zero contribution to stationary concentration of propagating polymer chains and, hence, to value  $W$ , because all radicals generated at stage  $\sim RX \rightarrow \sim R^\bullet + X^\bullet$  are removed from a reaction system at stage  $\sim R^\bullet + X^\bullet \rightarrow \sim RX$ .

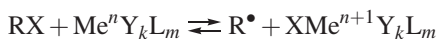
Thus, the use of stable nitroxyl radicals or alkoxyamines makes it possible to theoretically solve the problem of implementing the living chains conditions in radical polymerization.

The most important disadvantage of alkoxyamines as agents of living polymerization consists in the fact that they are effective only for polymerization of styrene and its derivatives [16–18]; they appeared to be ineffective when other monomers are used. It should be pointed out that alkoxyamines have limited application in copolymerization of polar monomers (acrylates, methacrylates) with styrene [14, 19–23]. The most probable reason for the reduced efficiency of alkoxyamines for polymerization of polar monomers consists of the too high strength of bond C–ON in appropriate alkoxyamines. In the case with styrene polymers, styrene derivatives, and copolymers of styrene with polar monomers, the presence of a phenyl substitute in the  $\alpha$ -position as related to bond  $\text{>NO-C}$  makes this bond more labile, able to dissociate at a sufficient rate at a temperature that is lower than 150°C [24, 25].

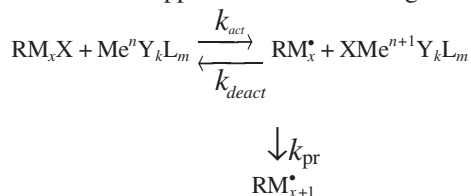
On the whole, results of detailed quantitative analysis [15, 26–28] of polymerization processes proceeding in the presence of alkoxyamines or other compounds with similar properties may serve as a theoretical basis for designing various processes of living polymerization.

Halogenide complexes of transition metals with organic ligands [29] of the general formula  $\text{Me}^n\text{Y}_k\text{L}_m$  (where Me is a transition metal,  $n$  is metal valence, Y are anions of  $\text{Cl}^-$  or  $\text{Br}^-$ , and L is organic ligand) were proposed for use as agents for living radical polymerization somewhat later than stable nitroxyl radicals or alkoxyamines. This kind of living radical polymerization acquired the name of atom transfer radical polymerization (ATRP) [1, 30].

The action of  $\text{Me}^n\text{Y}_k\text{L}_m$  compounds as agents of living radical polymerization is based on the M.S. Kharasch reaction [31], reversible oxidation-reduction interaction of halogenide complexes of transition metals with alkyl halogenides RX with the formation of alkyl radical  $\text{R}^\bullet$ :



The fact that this reaction proceeds in the medium of monomer M leads to initiation of polymerization  $\text{R}^\bullet + x\text{M} \rightarrow \text{RM}_x^\bullet$ , where  $x$  is the number of monomer molecules that have enough time to add to alkyl radical  $\text{R}^\bullet$  before the moment of  $\text{RM}_x^\bullet$  deactivation as a result of reaction with  $\text{XMe}^{n+1}\text{Y}_k\text{L}_m$ . Because such deactivation is of temporary character due to periodically repeated activation, the radical polymerization in the presence of  $\text{MeY}_k\text{L}_m$  and alkyl halogenides proceeds in essence under living chains conditions at a first approximation according to Scheme 3.2 [32, 33]:



**Scheme 3.2** Scheme of atom transfer living radical polymerization

where  $\text{RM}_x^\bullet$  = the growing polymer chain; X = halogen; and  $k_{\text{act}}$ ,  $k_{\text{deact}}$ , and  $k_{\text{pr}}$  are constants of activation, deactivation, and chain propagation, respectively.

Indeed, the cycle activation  $\rightleftharpoons$  deactivation proceeds in a somewhat more complicated way than in the simplified scheme presented above. Reverse reaction includes an intermediary stage, namely, addition of free radical  $R^\bullet$  to  $Me^{n+1}Y_kL_m$  with formation of intermediate  $R-Me^{n+1}Y_kL_m$ . The stepwise growth of the polymer chain takes place exactly due to this intermediate. The chain grows not because of monomer insertion into bond  $R-Me^{n+1}$  but as a consequence of addition of this monomer to radical  $R^\bullet$  formed during reversible fragmentation of the afore-indicated intermediate. This intermediate is deactivated as a result of its fragmentation into alkyl halogenide  $RX$  and the initial complex  $Me^nY_kL_m$ .

In the majority of cases initiation is conducted using alkyl halogenides  $RX$  and complexes  $Me^nY_kL_m$  [29, 32–38], but it has been reported that [39–41] polymerization was initiated by AIBN in the presence of complexes  $Me^{n+1}Y_kL_m$ .

Merits that compare complexes  $Me^nY_kL_m$  favorably to stable free radicals (alkoxyamines) served as an impetus for rapid development of studies of living radical polymerization controlled by these complexes [1, 2]:

- Action of compounds of type  $Me^nY_kL_m$  is characterized by a universal character, which extends to radical polymerization of all known monomers.
- Alkyl halogenide complexes of transition metals with organic ligands act as agents of living radical polymerization at significantly lower temperature ( $50^\circ\text{--}90^\circ\text{C}$ ), which is important from the standpoint of energy consumption reduction and diminution of secondary reactions probability.
- Compounds of type  $Me^nY_kL_m$  enable obtaining polymers with significantly narrower MWD including practically monodisperse ones ( $M_w/M_n = 1.04\text{--}1.05$ ).
- An important merit of compounds of the  $Me^nY_kL_m$  type consists in the possibility of conducting living radical polymerization in ecologically friendly aqueous medium (in water emulsions and suspensions).

Systematization and analysis of works in all directions in the field of living radical polymerization are presented in general publications [1, 2, 30, 42–48].

### 3.2 Implementation of Living Chains Conditions in Three-Dimensional Free-Radical Polymerization

Complexities arising during implementation of the living chains conditions in three-dimensional free-radical polymerization (TFRP) are associated mainly with the following circumstances. The first is the deficit of information on behavior of living radical polymerization agents under the conditions of strongly structured reaction media. One can reasonably suppose that diffusion hindrances and specific phenomena (such as micro-syneresis and microredistribution of initiation systems components) will influence the elementary stages of reversible acceptance of radicals—chain carriers that represent the essence of living radical polymerization mechanism. Second, as methacrylates represent the most numerous group of objects for TFRP and the action of many agents of living radical polymerization is limited by styrene, its derivatives, and styrene-containing reaction media, the search

for new agents of TFRP or for ways for adapting them to the TFRP conditions is required. The problem is that the majority of agents suitable for TFRP of methacrylates contain (as basic components) halogenides of copper, iron, cobalt, and other metals of variable valence, which are insoluble or partially soluble in structured reaction media. And, finally, a nonconventional system of proofs for the fact of implementation of living chains conditions is required for TFRP. In linear radical polymerization, testing of such conditions is based on measuring the molecular and weight characteristics of a polymer being formed [1].

Most meaningful results of the investigation of TFRP proceeding under living chains conditions are given below. The publications on this issue are scanty [49–60].

### 3.2.1 *Copolymerization of Styrene with Dimethacrylates in the Presence of Alkoxyamines [49]*

It is least difficult to implement TFRP in the living chains conditions for polyunsaturated analogues of styrene [2,2-bis-(4-vinylphenyl)propane] [52, 53], isomers of divinyl benzene [57, 58], and mixtures of dimethacrylates with styrene [49, 50]. In the latter case, alkoxyamines served as agents of living radical polymerization because alkoxyamines are well studied and have been successfully tested in polymerization of styrene and its monounsaturated substitutes [1]. Alkoxyamines are usually synthesized in situ from equimolar complexes of benzoyl peroxide (or other substances that generate free radicals under the conditions of polymerization) and from nitroxyls [2,2,6,6-tetramethyl-piperidiny-1-oxyl (TEMPO) di-*tert*-butylnitroxyl, etc.]. Alkoxyamines are inefficient in the medium of other monomers, except for styrene-like ones. However, it has been demonstrated [61] that addition of styrene in the concentration of no less than 50% (mol) to network-forming (polyunsaturated) monomers with methacryl double bonds makes alkoxyamines quite effective in such copolymer systems.

Copolymerization of styrene and dimethyl acrylates was conducted at 120°C; alkoxyamines were synthesized in situ from benzoyl peroxide or dicyclohexyl peroxydicarbonate (DCPD) and TEMPO with mole ratio 1:1.1. Because the synthesis of alkoxyamines was completed under these conditions for time period  $\Delta\tau = 5$  min by 90% [1], while polymerization time  $t$  exceeded hundreds of minutes, the necessary condition for implementation of living radical polymerization  $\Delta\tau \ll t$  (simultaneity of polymer chain generation) during synthesis of alkoxyamines in situ was certainly fulfilled.

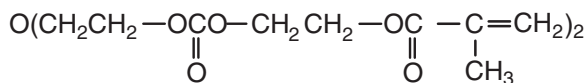
Kinetics of copolymerization of styrene with dimethacrylates was studied using precision isothermal calorimetry at 120°C. Averaged values of homo-polymerization molar heat,  $\bar{Q} = 0.5(Q_1 + Q_2)$ , where  $Q_1$  and  $Q_2$  are known molar heat of styrene homo-polymerization ( $Q_1 = 72.85$  kJ/mol [62]) and methylmethacrylate (MMA) ( $Q_2 = 58.82$  kJ/mol [63]), were used to calculate the copolymerization rate. The justification for such averaging is based on known values of copolymerization constants  $r_1$  and  $r_2$ , which are less than 1 ( $r_1 \approx r_2 \approx 0.5$  [64]), which ensures constancy

of  $\bar{Q}$  in the course of copolymerization with the proportion of components in the initial mixtures being 1:1.

Concurrently with copolymerization kinetics, the kinetics of accumulation of nitroxyl radicals (TEMPO) in the reaction system was recorded synchronously using the EPR method.

Synchronous rheokinetic measurements (capillarity viscosity) were taken to determine the gel point  $C_{gp}$ , i.e., the conversion, at which a continuous macromolecular network appears within the volume of the entire reaction system. It has been shown that  $C_{gp}$  (corresponding to no flow of reaction medium in a capillary) coincides with the gel formation point determined by other [53], more reliable methods.

Ethylene glycol dimethacrylate (dMEG), diethylene glycol bis (methacryloyloxyethyl) carbonate, commonly named oligo(carbonate)methacrylate OCM-2 of the following structure, and styrene were purified according to described methods [65].



Results of kinetic studies presented in Figs. 3.1, 3.2, and 3.3 enabled us to draw a conclusion on the implementation of living chains conditions under given

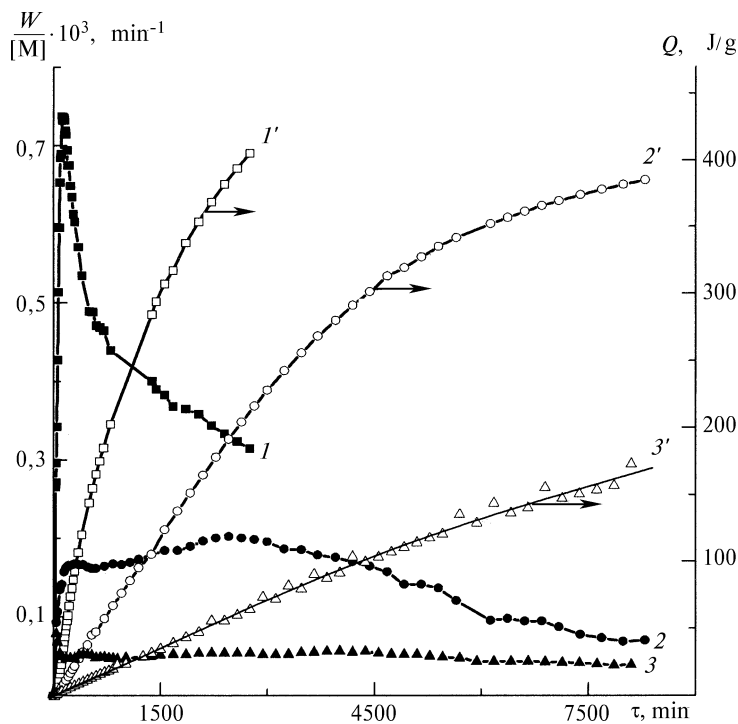


**Fig. 3.1** Kinetics of copolymerization of styrene and dMAEG Molar content of comonomers: 1:1 (*I*, *I'*); 1:3 (*2*, *2'*); 1:9 (*3*, *3'*).  $T = 120^\circ\text{C}$ .  $[\text{BP}] = 0.03 \text{ mol/l}$ ;  $[\text{TEMPO}] = 0.036 \text{ mol/l}$

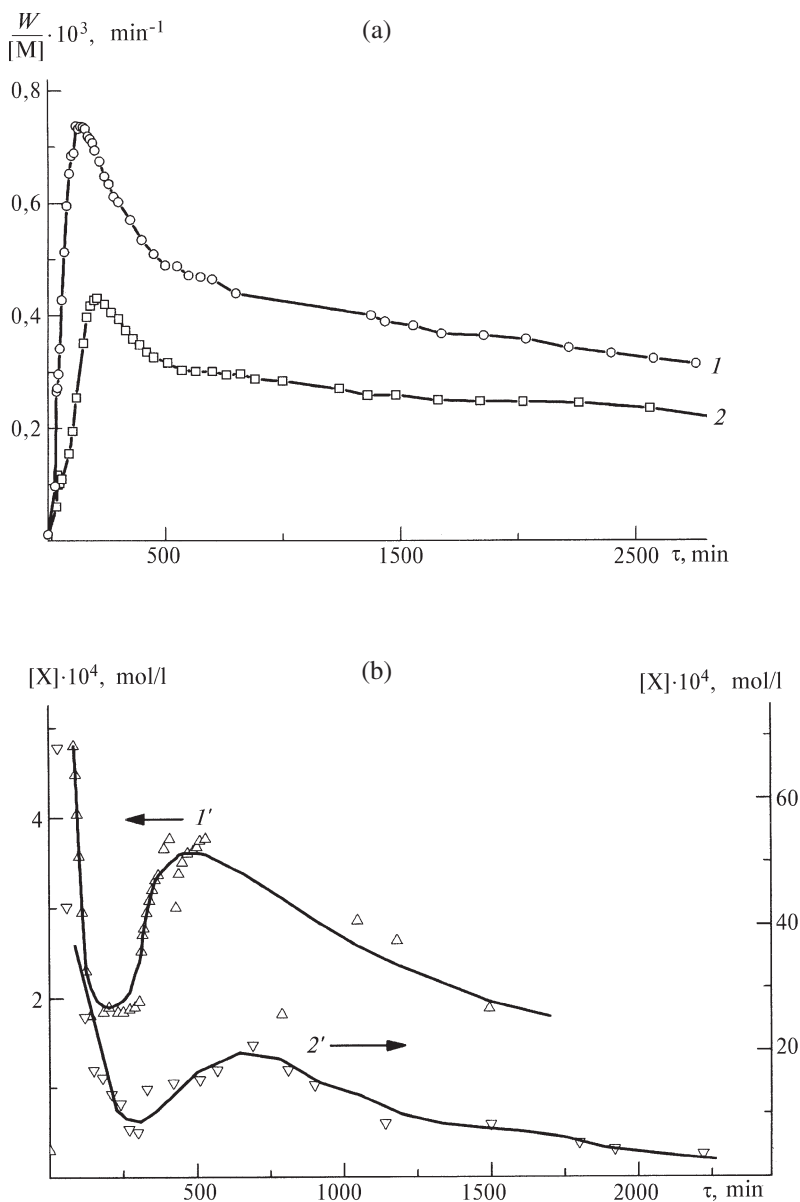


**Fig. 3.2** Kinetics of copolymerization of styrene and dMAEG (1) and OCM-2 (2) (1:1 ratio) (a) and kinetics of  $[X^\bullet]$  accumulation (1', 2') (b)  $T = 120^\circ\text{C}$ .  $[\text{BP}] = 0.03 \text{ mol/l}$ ;  $[\text{TEMPO}] = 0.036 \text{ mol/l}$  (synthesis of living radical polymerization agents in situ)

circumstances. The main argument is the comparison between reduced (reduction by current concentration of total content of double bonds  $[\text{M}]$ ) polymerization rate  $W/[\text{M}]$  (Fig. 3.2a) and concentration of stable nitroxyl radicals  $[X^\bullet]$  (Fig. 3.2b) in the reaction system. Indeed, such a high level of inhibited polymerization rate ( $X^\bullet$  is

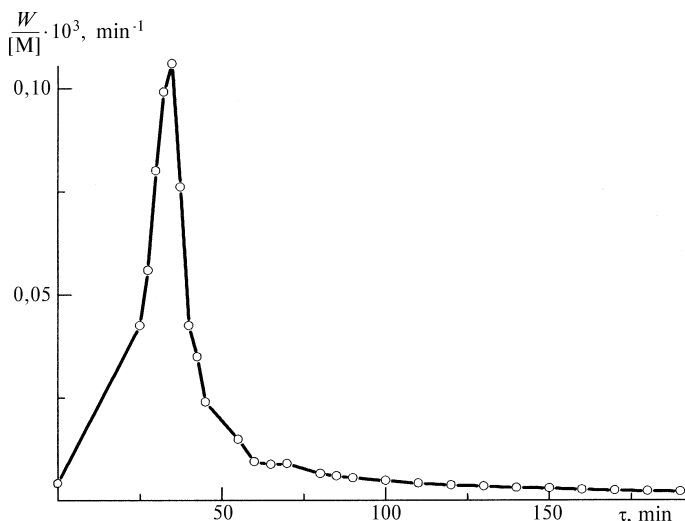


**Fig. 3.3** Kinetics of copolymerization of styrene and dMAEG (1:1 ratio) at 120°C in the absence of alkoxyamines

a strong inhibitor),  $(W/[M]) \times 10^3 = 0.25\text{--}0.45 \text{ min}^{-1}$  ( $t = 500\text{--}1000 \text{ min}$ ) with such a high concentration of inhibitor ( $[X^\bullet] \times 10^4 = 3\text{--}20 \text{ mol/l}$ ) could only be the case when the elementary act of addition-fragmentation is a reversible reaction. According to the concepts presented above (see Sect. 3.1), the reversibility of inhibition in the case of radical polymerization is exactly a mechanism transforming a conventional mode into the living chains conditions. If the inhibition act were irreversible, the polymerization rate estimated according to the following relationship:

$$W/[M] = k_{pr}W_i/k_x[X] \quad (3.1)$$

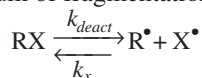
with known numeric values (l, mol, s) at  $T = 120^\circ\text{C}$ ,  $k_{pr} = 2 \times 10^3$ ,  $k_x = 10^7$ , and  $W_i = 10^{-7}$  (from data on thermal initiation for styrene) and  $[X^\bullet] = (3\text{--}20) \times 10^{-4}$  would have been equal to  $(1\text{--}6) \times 10^{-8} \text{ s}^{-1} = (0.6\text{--}3.6) \times 10^{-6} \text{ min}^{-1}$ , i.e., it would have been  $10^2\text{--}10^3$  times (!) less than experimentally observed values  $(2.5\text{--}4.5) \times 10^{-4} \text{ min}^{-1}$ .

It must be pointed out that the test for living chains conditions, which is nowadays universally accepted in worldwide practice and which consists of the fact that the growth of polymerization degree  $\bar{P}_n$  (measured by the value of number-averaged molecular weight  $M_n$ ) is proportional to the increase of conversion in the course of polymerization process, is unsuitable for the case of three-dimensional polymerization because of the impossibility of direct measurement of  $M_n$ .

As the ratio of components in initial dimethyl acrylate–styrene mixtures varies in favor of higher content of dimethacrylates, the polymerization rate goes down in compliance with the known fact of inefficiency of alkoxyamines as agents of living radical polymerization in the medium of methacrylates [1] (Fig. 3.1).

The comparison of numeric values of  $W/[M]$  and  $[X^\bullet]$  at  $t = \text{const}$  allows also to calculate (using data given in Fig. 3.1) the combination of constant values of rates

$k_{deact}k_{pr}k_x$ , including such an important parameter as the constant of homolytic decomposition rate of alkoxyamine formed in situ. Indeed, it is known [1] that the time during which the equilibrium of fragmentation-addition is established



lies within the less-than-second interval, i.e.,  $[\text{X}^\bullet] = k_{deact}[\text{RX}]/k_x[\text{R}^\bullet]$ , where  $[\text{RX}]$  is the current concentration of alkoxyamine, which is practically constant during the entire polymerization process and which is close to the concentration of  $3 \times 10^{-2}$  mol/l of initial precursor substances (benzoyl peroxide and TEMPO).

Instantaneous value  $[\text{R}^\bullet]$  is derived from  $W/[M]$  in compliance with the known relationship  $W/[M] = k_{pr}[\text{R}^\bullet]$  as  $[\text{R}^\bullet] = W/([M]k_{pr})$ , which in the end leads to the following relationship:

$$k_{deact}k_{pr}/k_x = \frac{W}{[M]} \frac{[\text{X}^\bullet]}{[\text{RX}]} \quad (3.2)$$

Combinations of rate constants  $\alpha = k_{deact}k_{pr}/k_x$  given in Table 3.1 were calculated using this relationship.

It follows from Table 3.1 that for equimolar mixtures “dimethacrylate–styrene” numeric values of  $\alpha$  stay within the same interval as for the case of homopolymerization of styrene with alkoxyamines under living chains conditions; the value of  $\alpha$  dramatically declines as the content of dimethacrylate in the initial mixture increases. It seems likely that it is an indication of the change in the mechanism in the direction of deviation from the living chains conditions at high content of methacrylates. Estimation of  $k_{deact}$  from  $\alpha$  by values of  $k_{pr} = 2 \times 10^3$ ,  $k_x = 10^7$  l/(mol · s) gives the value of  $k_{deact} = (2-5) \times 10^4 \text{s}^{-1}$  at 120°C, which agrees well with data of independent measurements of  $k_{deact}$  taken using direct methods for alkoxyamines of this type [1].

Thus, judging by the value of  $\alpha$ , one has grounds to believe that during the three-dimensional polymerization process under the living chains conditions, despite formed structures of highly cross-linked network type, homolytic cleavage of alkoxyamines is not hindered significantly by the potential danger of cage effect increase, in contrast to conventional three-dimensional polymerization, for which manifold decrease (10–100 times) of probability of initiator radicals yield from Frank-Rabinovich cage under the influence of structure formation was observed [66]. Such difference could be explained by the different character of structure formation: it is believed that the living chains conditions significantly diminish the degree of microheterogenization of the reaction system in the polymerization process with the respective decrease in rigidity of highly cross-linked macromolecular structure being formed. Indeed, the comparison of features of dimethyl acrylate–styrene copolymers obtained by conventional three-dimensional polymerization with those obtained by living radical three-dimensional polymerization confirms that the latter have a more elastic structure with the values of conversion being close. The comparison of features at similar conversions is a necessary condition in this case, because the features themselves strongly depend upon conversion (see Sect. 3.3).



**Table 3.1** Kinetic parameters of three-dimensional copolymerization of di(methyl) acrylates and styrene ( $T = 120^\circ\text{C}$ )

Polymerization system	$\frac{W}{[M]} \cdot 10^3$ , $\text{min}^{-1}$	$t$ , min	$[X^*] \cdot 10^6$ , $\text{mol/l}$	$t$ , min	$\frac{k_{deact}k_{pr}}{k_x} \cdot 10^8$ , $\text{s}^{-1}$	$C_{lim}$ , %	$t_{lim}$ , min	$C_{gp}$ , %	$t_{gp}$ , min
Styrene	1.5–1.8	100–500	–	–	–	85	2100	–	–
Styrene [BP] = 0.03 mol/l [TEMPO] = 0.036 mol/l	1.3–1.1	200–800	170–87	200–800	10.4–4	90	3160	–	–
Styrene:dMAEG=1:1 [BP] = 0.03 mol/l [TEMPO] = 0.036 mol/l	0.9–0.4	200–1400	290–190	200–1400	12–3.3	75	4000	33	700
Styrene:dMAEG = 1:3 [BP] = 0.03 mol/l [TEMPO] = 0.036 mol/l	0.16	150–1470	43	1470	0.35	57	4400	22	1470
Styrene:dMAEG = 1:9 [BP] = 0.03 mol/l [TEMPO] = 0.036 mol/l	0.05	90–5000	17	3800	0.04	45	19000	17	3800
Styrene: OCM-2 = 1:1 Without additives	10–1	50–200	–	–	–	89	2700	<1	20
Styrene: OCM-2 = 1:1 [BP] = 0.03 mol/l [TEMPO] = 0.036 mol/l	0.3–0.26	300–1500	700–800	300–1500	10	66	4300	16	620
Styrene : OCM-2 = 1:1 [TEMPO] = 0.036 mol/l	0.4–0.2	300–1500	–	–	–	50	4560	11	470

Notes.  $W/[M]$ , reduced rate in a certain time interval;  $[X^*]$ – current TEMPO concentration in a certain time interval;  $C_{gp}$ – critical conversion of gel formation (gel point);  $t_{gp}$ – gel formation time;  $C_{lim}$ – limiting conversion, at which polymerization rate becomes virtually zero.

Rheokinetic measurements also verify the conclusion that the living chains conditions are actually implemented in three-dimensional radical copolymerization of styrene with dimethacrylates (composition 1:1) in the presence of alkoxyamines. The value of  $C_{gp}$ , which is extremely low in the case of conventional radical polymerization of dimethacrylates [66] ( $C_{gp} = 10^{-4} - 10^{-3}$ ), grows dramatically after transfer to the living polymerization conditions ( $C_{gp} > 10^{-2}$ ) [67]; conversion  $C_{gp}$  is expressed in fractions of  $C = ([M]_0 - [M])/[M]_0$ , where  $[M]_0$  and  $[M]$  are initial and current concentration, respectively, of vinyl groups. For copolymerization of styrene with dimethacrylates (composition 1:1) in the presence of alkoxyamines (see Fig. 3.2), the value of  $C_{gp}$  exceeds  $10^{-4}$ .

### **3.2.2 Polymerization of Tri(Ethylene Glycol) Dimethacrylate (tEGdMA) in the Presence of Complex $CuBr_2$ with Tetramethyl-Tiuramdisulfide [51]**

In the process of searching for agents for living radical polymerization that are efficient in methacrylate media (without styrene additives), it was found that when using a three-component system of additives — dinitryl of azo-izobutyric acid (AIBN) + tetramethyl-tiuramdisulfide (TMTD) +  $CuBr_2$ , — at  $90^\circ C$ , polymerization proceeds in two stages: the first (initial) stage lasts for a period of time equal to the time during which the initiator is consumed completely ( $\approx 5$  periods of half-life of AIBN), while the second (main) stage lasts until monomer exhaustion. Also, the ratio of conversions corresponding to each stage, i.e.,  $C_1$  to  $C_2$ , is determined by the relationship of components AIBN, TMTD, and  $CuBr_2$  and can be optimized for the purpose of conducting the entire polymerization process predominantly in the mode of the second stage, which was qualified as the living chains conditions (mode). The fact of the presence of prolonged (tens of hours and even days) “after-effect” (development of polymerization process in the absence of already consumed initiator) and changes of characteristic features of polymerizates identified by comparison with polymerizates obtained through the use of the standard method served as the grounds for such qualification. Indeed, transformation of propagating polymer chains during the initial stage into living chains via reversible acceptance in the form of adducts with TMTD and  $CuBr_2$  is the most probable explanation for the existence of the after-effect in this case.

Results of kinetic exploration into the process of three-dimensional polymerization in the presence of the three-component system AIBN + TMTD +  $CuBr_2$  in an example of tri(ethylene glycol) dimethacrylate (tEGdMA) are given below.

tEGdMA and AIBN were purified according to a known procedure [60]. Impurities were removed from TMTD and  $CuBr_2$  via recrystallization (from solutions in acetone), and the degree of purification was controlled according to  $T_m$ . Kinetics of tEGdMA polymerization was studied by the method of isothermal calorimetry at  $90^\circ C$ . Molar heat of MMA polymerization ( $Q = 58.82 \text{ kJ/mol}$  [63]) was used to calculate the polymerization rate.

Figure 3.4 (curves 1 and 4) shows the influence of AIBN additives, which is commensurable with TMTD in terms of concentration. These additives appeared to be capable of raising the polymerization rate far beyond the limits of time interval characterizing their exhaustion. For instance, the period of AIBN half-life at 90°C is equal to 23 min (constant of decay rate  $k_{dc} = 5 \times 10^{-4} \text{s}^{-1}$ ); hence the time of AIBN consumption is  $\approx 100$  min. Further, the lifetime of active products of AIBN decomposition (i.e., free radicals) is less than 1 s. Therefore, the significant increase of polymerization rate under the action of AIBN at  $t > 100$  min [rate at  $t = 300\text{--}400$  min increases 3–5 times (Fig. 3.4, curves 1, 4)] is absolutely unexplainable if we do not take into account the possibility of reversible addition of chain carriers radicals in the presence of TMTD, which is a necessary and sufficient feature of living radical polymerization. It is obvious that during the initial stage of polymerization process, AIBN does not vanish into thin air, but is transformed into sulfur-containing adducts capable of chain reinitiation.

A possible option of a mechanism for addition of initiator radicals and chain reinitiation in the presence of TMTD is given in Korolev et al. [51].

As applied to practical implementation of the living radical polymerization conditions, it is obvious that the use of TMTD only (or together with AIBN) could give only a partial solution of the problem. In any case, the contribution of the first stage of polymerization process proceeding according to the conventional radical chain mechanism remains quite significant because of the necessity to synthesize in the reaction system living radical polymerization agents  $\text{RS}_2\text{P}$  (where P is a polymer

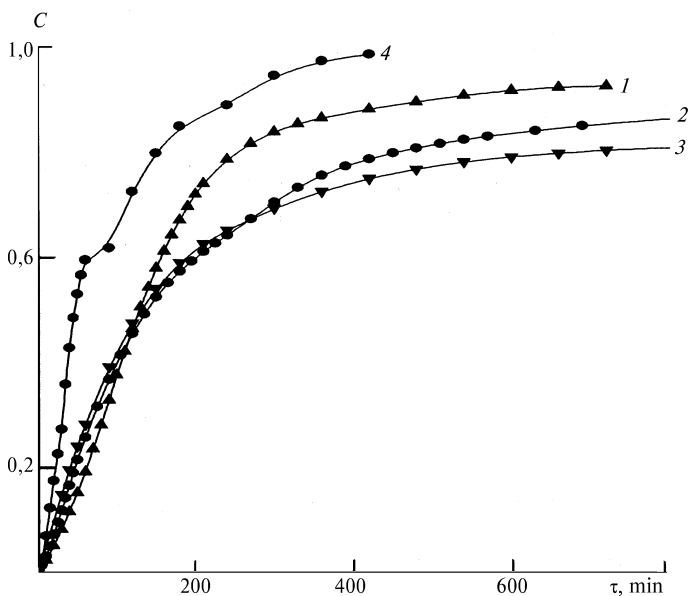


**Fig. 3.4** Kinetics of tEGdMA polymerization in the presence of TMTD and influence of AIBN additives.  $T = 90^\circ\text{C}$ .  $[\text{TMTD}] = 1 \times 10^{-2}$  (1, 4) and  $2 \times 10^{-2}$  mol/l (2, 3);  $[\text{AIBN}] = 1 \times 10^{-3}$  (1) and  $1 \times 10^{-2}$  mol/l (4)

chain) and, possibly, some other agents, which are not taken into account by the proposed mechanism [51]. And, until sufficient concentration of living radical polymerization agents is attained as a result of this synthesis, the conventional radical polymerization takes place.  $\text{CuBr}_2$  was used for conventional polymerization suppression, which is known, on the one hand, as an efficient radical-chain inhibitor, and on the other hand as a main component for the synthesis of agents for living radical polymerization (see Sect. 3.1).

Indeed, metals haloids with variable valence  $\text{Me}^n\text{X}_k$  are known [1, 2] as highly efficient agents of living radical polymerization. They are used in the form of complexes  $\text{Me}^n\text{X}_k\text{L}_m$  with organic ligands L. Compound  $\text{CuBr}_2$  is most widely used as metal halogenide, while 2,2'-bipyridine usually serves as ligand L, and AIBN serves as a source of free radicals.

Results demonstrating the action of  $\text{CuBr}_2$  in conventional radical polymerization initiated by AIBN are presented in Fig. 3.5. A distinct period of induction  $\tau = 50$  min. is observed, and the duration of this period corresponds to the calculated one ( $\tau = 53$  min), estimated according to the formula that takes into account the consumption of AIBN during time  $\tau$ :

$$\tau = -(k_{dc})^{-1} \ln \left( 1 - \frac{\mu [\text{CuBr}_2]_0}{2f[\text{AIBN}]_0} \right) \quad (3.3)$$

where  $\mu$  is a stoichiometric coefficient of inhibitor (for  $\text{CuBr}_2$ ,  $\mu = 1$ );  $k_{dc}$  = constant of AIBN decay rate at  $90^\circ$ , equal to  $5 \times 10^{-4} \text{s}^{-1}$ ;  $[\text{CuBr}_2]_0$  and  $[\text{AIBN}]_0$  = concentration at the initial moment;  $f$  = initiation efficiency equal to  $\approx 0.6$ .

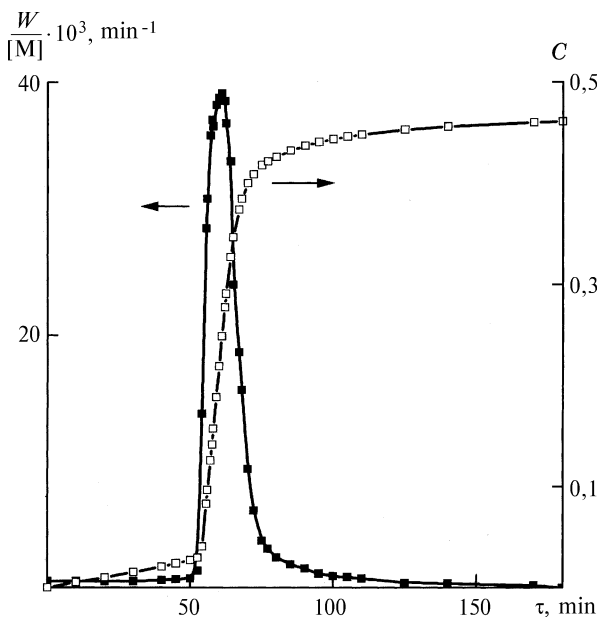


**Fig. 3.5** Dependence of reduced rate of polymerization  $W/[M]$  and conversion  $C$  upon time for tEGdMA polymerization  $T = 90^\circ\text{C}$ .  $[\text{AIBN}] = 1 \times 10^{-2} \text{mol/l}$ ;  $[\text{CuBr}_2] = 1 \times 10^{-2} \text{mol/l}$

Therefore, there are no grounds to believe that addition of radicals carriers by  $\text{CuBr}_2$  molecules possesses (at least to a certain extent) reversibility, which is characteristic of organic complexes of  $\text{CuBr}_2$ . However, in the case of polymerization initiated by TMTD, the situation changes profoundly (Fig. 3.6). Addition of  $\text{CuBr}_2$  no longer results in the appearance of an induction period. Polymerization proceeds at quite a high rate, and the value of  $W/[M]$  does not rise in time, as it should (because of inhibitor consumption), but, on the contrary, it goes down, and only with a very long time  $t$  does the process become intensified and self-acceleration start (second stage). In this case, the main part of the polymerization process proceeds under second-stage conditions: the first stage develops to conversions  $C \leq 0.1$ , while the second stage proceeds from  $C \approx 0.1$  to  $C > 0.8$  (see Fig. 3.6, curve 3).

To determine the nature of the second stage of the process initiated by TMTD in the presence of  $\text{CuBr}_2$ , the method of introducing additives of quickly decomposing additional initiator AIBN was used once again (the time of full transformation at  $90^\circ\text{C}$  is  $\approx 100$  min). It can be clearly seen in Fig. 3.7 that the “outburst” of initiation at  $t \leq 100$  min does not disappear completely, as it should (taking into account that the lifetime of the most long-living radicals carriers of the chain  $\sim\text{RS}^\bullet$  or  $\sim\text{RS}_2^\bullet$  does not exceed 10 s in this reaction system), but leads to dramatic intensification of the polymerization process at the second stage at  $t \gg 100$  min. Also, the higher is the AIBN concentration, the more efficiently the second stage proceeds (the value of  $W/[M]$  in its maximum increases more than fivefold as a result of [AIBN] increase from 0 to  $10^{-2}$  Mol/l; see Fig. 3.7, curves 1, 3). It should be emphasized here that in the presence of  $\text{CuBr}_2$  the activation of the second stage does not lead to the increase of the duration of the first stage, which remains within the limits  $C \leq 0.1$ . At the same time, in the absence of  $\text{CuBr}_2$ , AIBN additives, which also activate the second stage, also dramatically increase the contribution of the first stage. In other words, it appeared that a three-component system (TMTD +  $\text{CuBr}_2$  + AIBN) makes

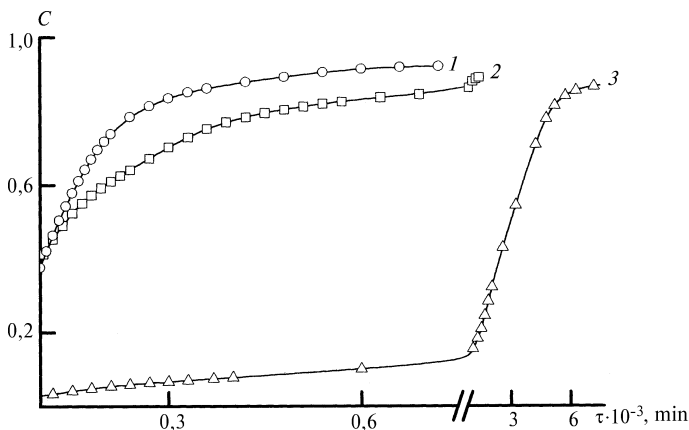


**Fig. 3.6** Influence of  $\text{CuBr}_2$  on kinetics of tEGdMA polymerization in the presence of TMTD.  $T = 90^\circ\text{C}$ .  $[\text{TMTD}] = 1 \times 10^{-2}$  (1) and  $2 \times 10^{-2}$  mol/l (2, 3)

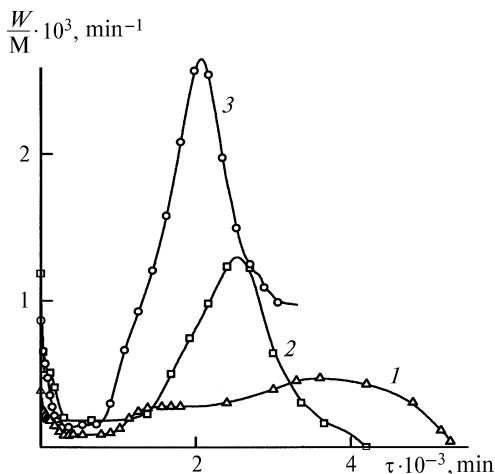
**Fig. 3.7** Influence of AIBN + CuBr<sub>2</sub> additive upon kinetics of tEGdMA polymerization in the presence of TMTD.

$T = 90^\circ\text{C}$ .

$[\text{TMTD}] = 2 \times 10^{-2} \text{ mol/l}$

(1-3);  $[\text{CuBr}_2] = 1 \times 10^{-2} \text{ mol/l}$  (1-3);

$[\text{AIBN}] = 1 \times 10^{-3}$  (2) and  $1 \times 10^{-2} \text{ mol/l}$  (3)



it possible to conduct polymerization almost entirely under the second-stage conditions and, besides, it proceeds at an increased rate (as compared to the situation when  $[\text{AIBN}] = 0$ ).

Judging by obtained results, the nature of the second stage is determined by accumulation of propagating polymer chains that temporarily exist in the form of  $\sim\text{RS}_2\text{P}$  (and, possibly, other sulfur-containing products) and copper-containing labile adducts  $\text{Cu} \cdots \text{P}$ . These  $\text{RS}_2\text{P}$  and adducts  $\text{Cu} \cdots \text{P}$  should be regarded as agents of living radical polymerization that are capable of multiple repetition of reversible addition cycles. Hence, it is possible to assert with a high degree of probability that polymerization of dimethacrylates in the presence of TMTD + CuBr<sub>2</sub> + AIBN proceeds according to the living chains mechanism.

### 3.2.3 Polymerization of Dimethacrylates of Poly(Ethylene Glycol)s in the Presence of Complex CuBr with Organic Ligands [60]

Research into polymerization of dimethacrylates of poly(ethylene glycol)s in the presence of CuBr complexes with organic ligands showed that this system could be an efficient agent of TFRP of methacrylates under the living chains conditions starting from  $70^\circ\text{C}$ . In this case, the objects of comparison were kinetic regularities of polymerization, critical conversions (gel point), molecular weight characteristics of sol fractions, and kinetics of accumulation of stable radicals—chain carriers for conventional and living TFRP. It was found that the character of kinetic curves (which is typical for conventional TFRP “auto-acceleration – maximum rate – auto-deceleration”) is transformed after transferring to the living chains conditions into a curve with the maximum rate at the very beginning of transformation ( $C \rightarrow 0$ ). The subsequent decline of rate proceeds quicker than it should, if the first order of monomer is meant, i.e., with features of auto-deceleration. A characteristic kinetic feature of living chains conditions, namely, linear character of dependence

$\ln([M]_0/[M])$  upon time (where  $[M]_0$  and  $[M]$  are initial and current monomer concentration, respectively), is observed only up to conversion level  $C \approx 40\%$ . This finding gives grounds to believe that later stages of TFRP ( $C > 40\%$ ) proceed in the conventional mode due to the influence of the highly cross-linked macromolecular structure of the reaction medium. Critical conversion  $C_{cr}$  shifted as a result of transition to the living chains conditions from  $C_{cr} < 1\%$  to  $C_{cr} \geq 5\%$ , which agrees well with other experimental data [49] and with a new theory of gel formation [67]. Gel Permeation Chromatography (GPC) analysis performed in the course of TFRP showed that sol fraction in the course of conventional TFRP is a pure monomer at all stages of polymerization process, starting from  $C \rightarrow 0$  and up to  $C > 50\%$ , which agrees well with the microheterogeneous mechanism of TFRP (see Chap. 1). As a result of switching over to the living chains conditions, the value of  $M_n$  of the sol fraction linearly grows with the conversion increase (a characteristic feature of living radical polymerization [1]) up to  $C_{cr}$ , and then in the range of  $10\% \leq C \leq 40\%$  slightly decreases (from  $M_n = 8000$  in the point of maximum at  $C = 10\%$  to  $M_n = 6000$  at  $C = 40\%$ ). The value of  $M_w/M_n$  stays at the level of  $\approx 2.5$  throughout this entire range of  $C$ .

It is possible to use data of EPR measurements [60] for quantitative estimates, which has not been done by the authors of this publication. It was found out that kinetics of accumulation of free methacrylate radicals  $[R^\bullet] = f(t)$ , where  $t$  is time of polymerization, for both cases, i.e., for conventional and living TFRP, takes the form of curves with maximum  $[R^\bullet]_{max}$  attainable with conversion  $C \approx 50\%$ . When the temperature changes from  $70^\circ$  to  $90^\circ\text{C}$ , the value of  $[R^\bullet]_{max}$  decreases 3.5 times in the case of conventional TFRP, and in the case of living polymerization it decreases by more than one order of magnitude. However, quantitative evaluations that could be made by comparing data on reduced rates of polymerization with  $[R^\bullet]$  at identical  $t$  in the course of TFRP are of highest interest:

$$W/[M] \equiv W' \quad (3.4)$$

where  $[M]$  = current monomer concentration. Indeed, from

$$W = k_{pr}[R^\bullet][M] \quad (3.5)$$

the current value of constant of chain propagation rate will be written as

$$k_{pr} = W'/[R^\bullet] \quad (3.6)$$

where  $[R^\bullet]$  = concentration of radical-chain carriers, i.e., chains capable of adding the molecules of M.

Overall radicals concentration  $[R^\bullet]_\Sigma$  measured by the EPR method also includes, in addition to  $[R^\bullet]$ , inactive methacrylate radicals fixed in highly cross-linked structure in micro-areas with frozen mobility of both partners  $R^\bullet$  and M [74]; therefore:

$$k_{pr} \geq W'/[R^\bullet]_\Sigma \quad (3.7)$$

Using the value of  $[R^\bullet]_\Sigma$  measured by the EPR method instead of unknown value of  $[R^\bullet]$ , it is possible to obtain the bottom limit

$$k_{pr} \equiv k'_{pr} (k_{pr} \geq k'_{pr} = W'/[R^\bullet]_\Sigma) \quad (3.8)$$

Values of  $k'_{pr}$  estimated by such a method based on data from Yu et al. [60] are given below.

In the case of conventional TFRP at 70°C in the range  $55 \leq C \leq 75\%$ , the value of  $k'_{pr}$  ( $1 \cdot \text{mol}^{-1} \cdot \text{s}^{-1}$ ) goes down from 9800 to 380. In the case of living TFRP at the same temperature and in the same range of  $C$ , the value of  $k'_{pr}$  stays within the ranges 60–70. If we do not have any doubts about the truthfulness of the experimental data in Yu et al. [60], this is an unexpected and nontrivial result. It is known [69] that the value of  $k_{pr}$  in the course of conventional TFRP goes down from  $300\text{--}500 1 \cdot \text{mol}^{-1} \cdot \text{s}^{-1}$  at  $C \rightarrow 0$  to  $k_{pr} < 10$  at  $C > 50\%$ . Because  $k_{pr} > k'_{pr}$ , we get  $k_{pr} > 9800$  (!?) at  $C = 55\%$ . The value of  $k'_{pr} = 60\text{--}70$  ( $k'_{pr} > 60\text{--}70$ ) in the case of living polymerization at 70°C appears to be quite normal, if compared with data from Ivorogov et al. [69] because the level of molecular mobility of cross-linked macromolecular medium increases when TFRP transfers to the living chains conditions. However, available data [60] for living TFRP at higher temperatures once again lead to nontrivial results: at  $C \geq 50\%$  with the growth of  $C$  up to the limiting values, the value of  $k'_{pr}$  at 80°C stays within the range 250–500 ( $k_{pr} > 250\text{--}500$ , which is absolutely inconsistent with the forecast).

Thus, it has been established with a high degree of certainty that the three-dimensional free-radical copolymerization of dimethacrylates with styrene (with the use of alkoxyamines) and TFRP of dimethacrylates (with complexes of  $\text{CuBr}_2$  or  $\text{CuBr}$  with organic ligands) is implemented under the living chains conditions. However, our work should be regarded only as the first steps in the creation of independent direction in the field of TFRP—polymerization of polyunsaturated oligomers (monomers) under the living chains conditions.

### 3.3 Living Chain Three-Dimensional Free-Radical Polymerization as a Tool for Macromolecular Design of Cross-Linked Polymers

Specific mechanism of three-dimensional free-radical polymerization (TFRP) that includes microheterogenization of the polymerization system with formation of microgel particles (playing the role of local micro-reactors) is extremely sensitive to factors controlling the conditions of micro-gel formation. One of the major factors of this kind is the formation, even at the earliest stages of polymerization ( $C < 1\%$ ), of long ( $10^2\text{--}10^4$  units) primary polymer chains with “pendent” double bonds (one or several depending upon the functionality of initial polyunsaturated monomer) capable of intrachain cross-linking due to the pendent bonds (cyclization) with subsequent aggregation in the form of a microgel. A reaction system consisting of polymer chains (branched, cross-linked, and aggregated) is thermodynamically and



kinetically unstable in the medium of initial oligomer. Separation into micro-phases intensified by local gel effect starts within this medium. In the end, this leads to the formation of topological and morphological defects, which adversely affects physical and mechanical characteristics of polymers of this type and materials produced on the basis of these polymers.

The fact that TFRP proceeds under living chains conditions changes the character of kinetic regularities and process mechanism. “Instantaneous” chain growth of macromolecules (which takes place in the case of conventional TFRP) is transformed, in the case of TFRP under the living chains conditions, into a stepwise “slow” process. The term “instantaneous” is understood as “meeting the condition  $\tau \ll t$ ” (where  $\tau$  = time from the moment of propagating chain generation until its termination as a result of quadratic or linear termination, and  $t$  = polymerization time), while the term “slow” is understood as “meeting the condition  $\tau \geq t$ .” The main factor leading to the generation of microheterogeneity is leveled as a result of such transformation. Because all growing chains are generated in a polymerization system practically concurrently and their propagation is synchronous, long chains are missing at early stages of conversion: their length increases in proportion to the growth of conversion. And, since the main specific features of TFRP are preconditioned by microheterogeneity, leveling of such kind (even partial leveling) should serve as a source of radical changes of physical and mechanical, thermo-mechanical, sorption-related, and other properties of polymers.

Indeed, the cycle of research [49–51] has enabled us to show (in an example of tEGdMA polymerization and copolymerization) that transition from conventional TFRP to the TFRP under living chains conditions upgrades the molecular mobility and, hence, changes the properties of copolymers that are controlled by molecular mobility. Purposeful comparison of characteristic features of polymers and copolymers obtained via conventional TFRP [(co)polymers I] and TFRP under the living chains conditions [(co)polymers II] was carried out within these research studies [50, 51]. Characteristic features were understood as features that are most sensitive to the transformation of conventional TFRP into the living chains conditions. Physical and mechanical, thermodynamic, diffusion, and sorption properties, as well as kinetics of termination of free radicals stabilized in polymer matrices, appeared to be characteristic features for (co)polymers I and II.

Copolymers of styrene and tEGdMA of type I were obtained via conventional polymerization at 70°C,  $[\text{BP}] = 1 \times 10^{-3}$  mol/l with the ratio of initial comonomers being 1:1; copolymers II via polymerization of mixtures of comonomers of the same composition with the BP-TEMPO system ( $[\text{BP}] = 1 \times 10^{-3}$  mol/l and  $[\text{TEMPO}] = 3.3 \times 10^{-3}$  mol/l).

tEGdMA polymers of type I were obtained via conventional TFRP at 90°C and  $[\text{AIBN}] = 1 \times 10^{-3}$  mol/l, while polymers II were obtained via TFRP under the living chains conditions at 90°C with catalytic system “TMTD –  $\text{CuBr}_2$  – AIBN” with the concentration of components  $2 \times 10^{-2}$ ,  $1 \times 10^{-2}$ , and  $1 \times 10^{-2}$  mol/l, respectively. For all polymer samples, conversion  $C$  was controlled by densitometric and calorimetric methods, and for copolymers by these methods plus by infrared (IR) spectroscopy [70]. It is obvious that comparison of properties of copolymer

samples of types I and II makes sense only in the case of identical conversions  $C$  (Figs. 3.8 and 3.9). Only such samples were selected for subsequent studies of properties, for which the convergence in terms of  $C$  (measured by different methods) was better than 3% (if  $C \approx 90\%$ ) or 5% (if  $C \leq 80\%$ ).

Thermo-mechanical features of copolymers were determined using a precision device, and physical and mechanical properties were determined in the uniaxial compression mode. Sorption experiments were carried out in the atmosphere of saturated vapor at  $20^\circ\text{C}$ .

Diagrams of uniaxial compression (at the rate of  $10^{-3}\text{s}^{-1}$ ) of tEGdMA polymers and copolymers with different conversions are shown in Figs. 3.8 and 3.9.

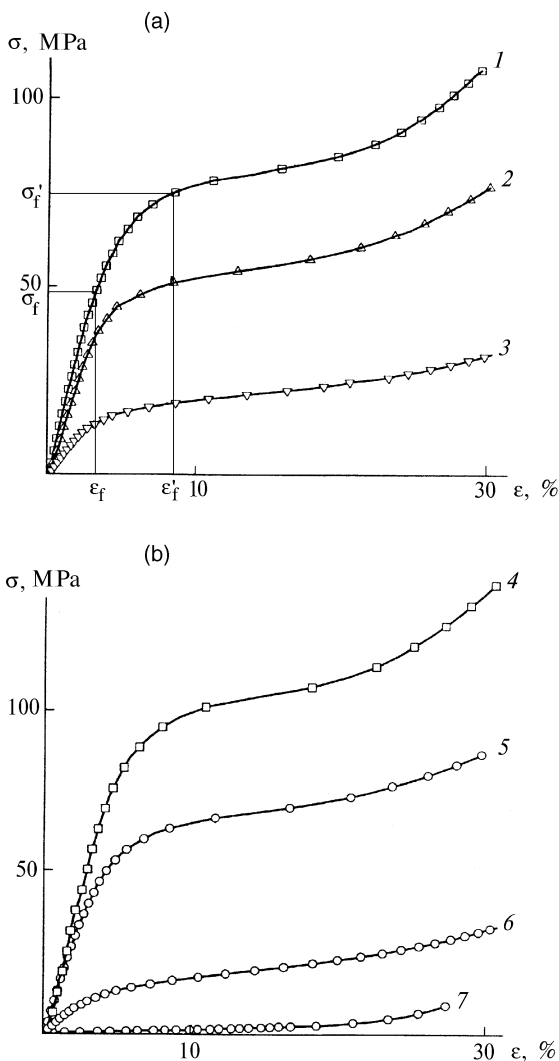
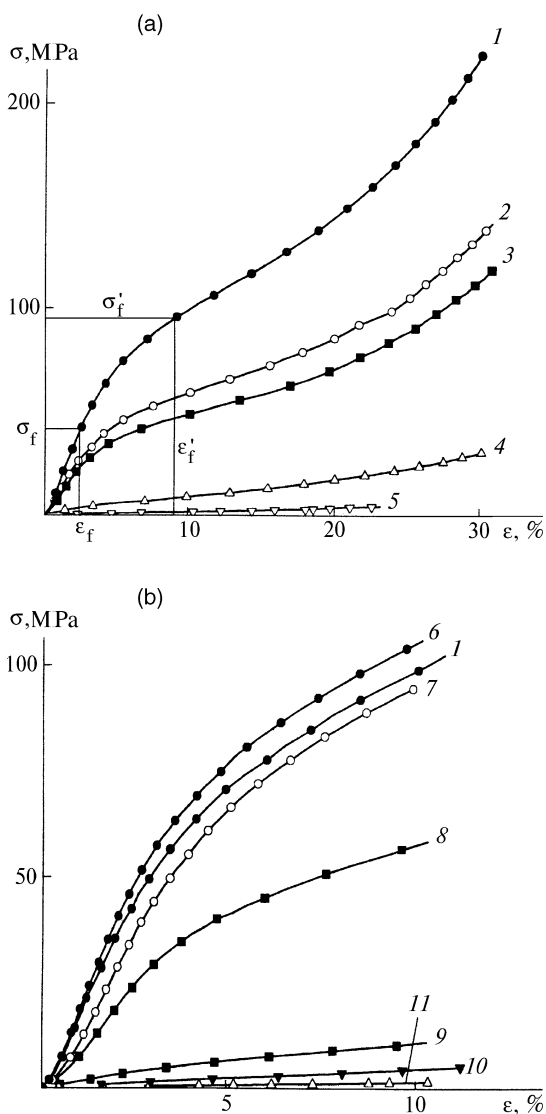


**Fig. 3.8** Dependence of compressive strain  $\epsilon$  upon stress  $\sigma$  for copolymers of type I (1–3) (a) and II (4–7) (b) at  $20^\circ\text{C}$  and different values of conversion  $C = 0.72$  (1);  $0.78$  (2);  $0.85$  (3);  $0.71$  (4);  $0.79$  (5);  $0.86$  (6); and  $0.95$  (7). Deformation rate is  $10^{-3}\text{s}^{-1}$

**Fig. 3.9** Dependence of compressive strain  $\epsilon$  upon stress  $\sigma$  for polymers I (1, 6–11) and II (2–5) at 20°C and different values of conversion.  $C = 0.77$  (1); 0.80 (2); 0.79 (3); 0.62 (4); 0.47 (5); 0.81 (6); 0.79 (7); 0.79 (8); 0.64 (9); 0.53 (10); and 0.40 (11). Deformation rate is  $10^{-3}\text{s}^{-1}$



Characteristic parameters in this case are the slope of the initial linear section (elasticity modulus  $E_1$ ), the beginning of deviation from linearity (points  $\sigma_f$ ,  $\epsilon_f$ ) – transition area from glassy state to forced-elastic state, the end of transition area (points  $\sigma'_f$ ,  $\epsilon'_f$ ), and the slope of the second linear section (forced elasticity modulus  $E_2$ ). For highly cross-linked glass-like polymers, points  $\sigma_f$ ,  $\epsilon_f$ , as a rule, correlate with the strength and rupture with uniaxial tension [71].

Comparison of samples of copolymers of types I and II with close values of  $C$  (Fig. 3.8) shows that more elastic structures (with lower resistance to deformation)

are formed as a result of TFRP under the living chains conditions: when  $C = 0.85$ , the initial elasticity moduli  $E_1$  are practically identical, but later the development of the deformation process in the direction of forced elasticity for samples II proceeds more actively; deviation from linear dependency  $\sigma(\varepsilon)$  starts at lower values of  $\sigma_f$  (index “f” denotes the beginning of the transition area to forced elasticity).

Correspondingly, as  $\varepsilon$  grows, effective elasticity modulus  $\sigma/\varepsilon$  in area  $\sigma > \sigma_f$  decreases significantly faster for samples II also. It can be seen from the comparison of curves  $\sigma = f(\varepsilon)$  for polymers of type I and II with close values of  $C$  (see Fig. 3.9) that samples II are characterized by a higher level of molecular mobility (lower rigidity): both elasticity moduli  $E_1$  and  $E_2$  at similar values of  $C$  for samples of type II are significantly lower than those for samples of type I.

Thermo-mechanical curves of copolymers of types I and II (Fig. 3.10) differ sharply both in terms of glass-transition temperature, which for copolymers I is shifted to high-temperature area by  $40^\circ\text{--}50^\circ\text{C}$ , and in terms of elasticity of high-elastic state: compliance (it is directly proportional to the value of deformation  $\varepsilon$ ) is a plateau on thermo-mechanical curves that, for polymers II, was obtained via TFRP under living chains conditions, and is two times higher than that for copolymers I synthesized via conventional TFRP. TFRP under the living chains conditions noticeably transforms the profile of the thermo-mechanical curve for tEGdMA polymers (see Fig. 3.11 near here.): the curve section approaching the high elasticity plateau becomes steeper (in the region of  $25^\circ\text{C}$ ) and the height of the plateau is increased (the elasticity modulus in highly elastic state declines). However, in this process, the main peculiarity of highly cross-linked polymers formed in radical-initiated

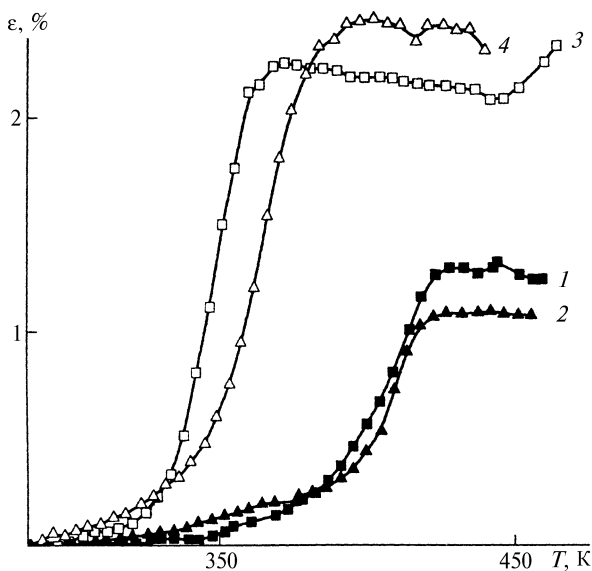


**Fig. 3.10** Thermo-mechanical curves for copolymers of type I (1, 2) and II (3, 4).  $C = 0.78$  (1); 0.85 (2); 0.79 (3); and 0.86 (4)

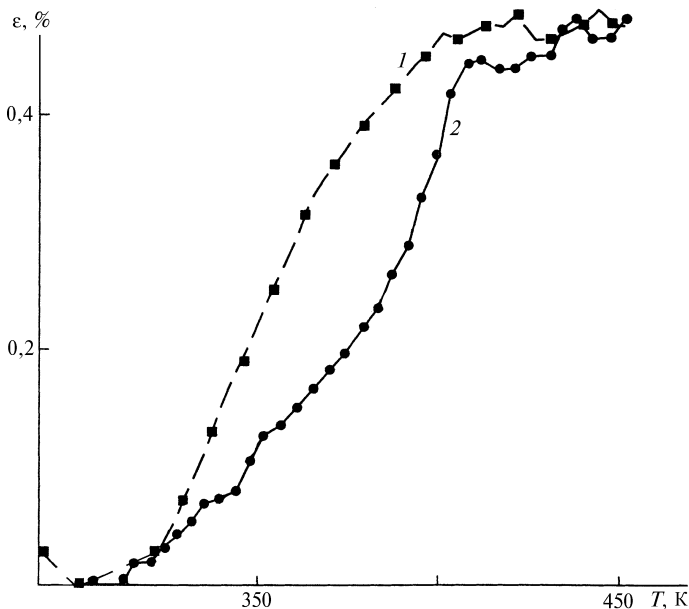
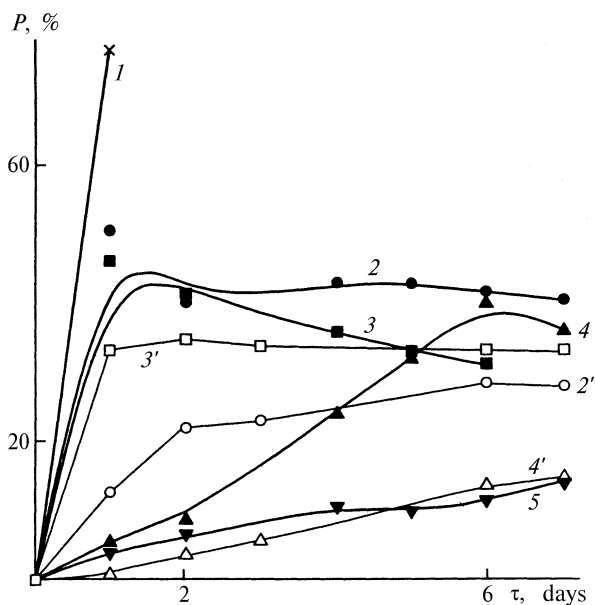


Fig. 3.11 Thermo-mechanical curves for polymers I (1) and II (2).  $C = 0.77$  (1) and 0.80 (2)

processes is retained: width ( $\Delta T$ ) of the transition area from glassy state to highly elastic state ( $\alpha$  transition) stays extremely high ( $\Delta T = 75^\circ\text{C}$  for samples II and I; for comparison, for highly cross-linked polyepoxides,  $\Delta T = 10^\circ\text{--}20^\circ\text{C}$ ).

If we assume that the living chains conditions actually lead to considerable modification of highly cross-linked structure both at the topological level (decline of cyclization probability) and at the morphological level (decline of graining degree), then in this case a too high value of  $\Delta T$  should be considered to be a manifestation of certain structural peculiarities, which are not associated with micro-nonhomogeneity. It is not improbable that these peculiarities are determined by specifics of spatial localization of network junctions: they are rather rigidly bonded by carbo-chains into “strands” (one junction is separated from another by a short link,  $-\text{CH}_2-$ ). Besides, the links of such strands serve as  $\alpha$ -relaxants (fragments of structure, the unfreezing of which is responsible for  $\alpha$ -transition). As pendant groups of units contain interchain bridges (cross-links) and cycles of different size, their relaxation ability is different and hence, a set of  $\alpha$ -relaxants of different type is formed, and these relaxants provide sufficient width of transition area  $\Delta T$ .

The method of diffusion (sorption) probing of (co)polymers with molecules of low molecular substances [72, p. 82] also detected a difference in the structure of copolymers of types I and II. It appeared that both the diffusion rate and the limiting sorption of benzene vapors for copolymers of type II are incomparably higher than those for copolymers I (Fig. 3.12). It should be pointed out that thermodynamic affinity of sorbate molecules strongly influences the value of limiting sorption (sorption equilibrium), while the size of molecules influences the diffusion rate. As



**Fig. 3.12** Kinetic curves of benzene sorption by copolymers of type II (1–5) and I (2'–4').  $T = 20^\circ\text{C}$ .  $C = 0.5$  (1); 0.71 (2); 0.72 (2'); 0.79 (3); 0.78 (3'); 0.86 (4); 0.85 (4'); and 0.95 (5)

for acetone (degraded affinity as compared to benzene, lower size of molecules), it appeared that diffusion and sorption parameters of polymers I and II are less characteristic in structural and physical testing (Fig. 3.13). Results of diffusion and sorption probing with benzene molecules are indicative of higher level of molecular mobility in tEGdMA polymers II (Fig. 3.14); the rate of diffusion of benzene vapors

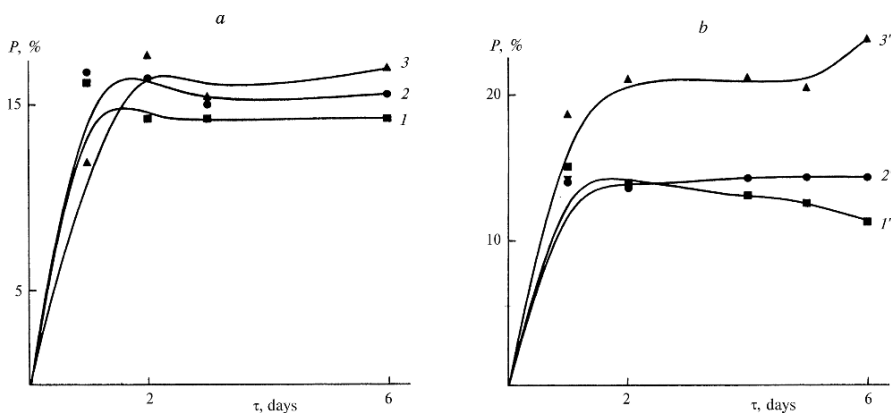


**Fig. 3.13** Kinetic curves of acetone sorption by copolymers of type I (a) and II (b).  $T = 20^\circ\text{C}$ .  $C = 0.72$  (1); 0.78 (2); 0.85 (3); 0.71 (1'); 0.79 (2'); and 0.86 (3')

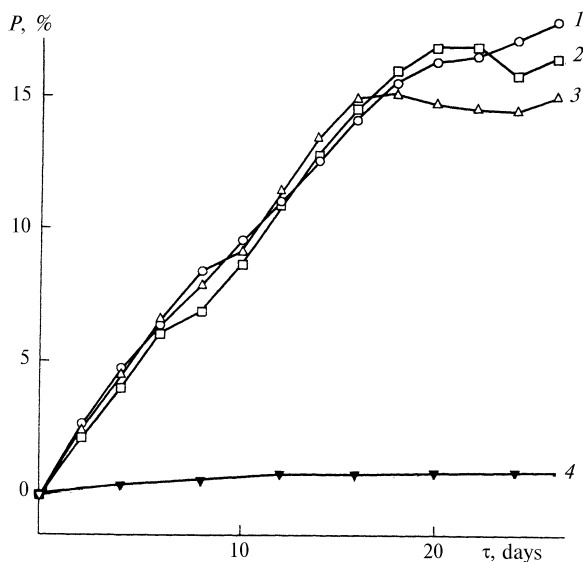


**Fig. 3.14** Kinetic curves of benzene sorption by polymers II (1-4).  $T = 20^{\circ}\text{C}$ .  $C = 0.82$  (1); 0.83 (2); 0.80 (3); and 0.85 (4)

and limiting sorption for polymers I is incomparably lower than those for polymers II (compare a group of curves 1-3 with curve 4).

Based on data obtained as a result of diffusion and sorption probing, one can draw a conclusion that the effective density of macromolecular network after transition of TFRP into the living chains conditions declines. This conclusion correlates well with the results of physical-and-mechanical and thermo-mechanical testing: decrease of values of elasticity moduli in forced-elastic state and in highly elastic state for copolymers II is a reflection of reduced density of the network.

This result (i.e., a higher level of molecular mobility in ATRP, and NMP-obtained highly cross-linked structures) could seem to be paradoxical because the transformation of the chain mechanism of cross-linked macromolecules growth into a stepwise mechanism during transition to the living chains conditions dramatically decreases the cyclization probability [73]. We mean the formation of small cycles owing to neighboring pendent double bonds in the main carbo-chains.

Probably, this paradox could be explained by the following.

Most probably, the difference in properties of copolymers of types I and II is associated with their structural peculiarities at the morphological level. It is unlikely that the difference between copolymers I and II at the topological level represents a reason for the differences in properties of these copolymers. In contrast, topological defects of highly cross-linked copolymers in TFRP under the living chains conditions are diminished because the probability of cyclization (it is a side process that reduces the volume concentration of interchain cross-links) declines. Improvement of network topology (decreasing the concentration of defects of small cycle type) is preconditioned by incorporation of styrene links that decrease the probability of cyclization.

The chain nature of conventional TFRP represents the reason for the formation of a special morphological structure of highly cross-linked polymers, namely, nanodispersion of microgel particles (grains), which accrete at the final stage of polymerization into a microheterogeneous grain monolith (see Chapter 1). Grains in such structure can play the role of reinforcing filler, as does soot in rubber. It is known that introduction of reinforcing fillers leads to a steep rise of effective density of the polymer network by the interaction of filler particles with polymer matrix, and this interaction manifests itself in the form of additional junctions that connect polymer chains. That is why, in a polymer of type I, the network density appears to be abnormally high. And, probably, the abnormal exceedance of network density is so high that it outweighs the loss of network junctions caused by cyclization. In transition from the chain mechanism of conventional TFRP to the stepwise mechanism of TFRP under living chains conditions, the grain effect (microheterogeneity) of copolymers is leveled with corresponding reduction of effective density of polymer network in copolymers of type II.

Molecular mobility of tEGdMA polymers of type I and II was also studied by a radiation probing method [72, p. 44; 74] in terms of kinetics of termination of methacrylate radicals, chain carriers stabilized in polymer matrices. Radicals were generated by irradiating polymer samples with  $\gamma$ -radiation with  $^{60}\text{Co}$  (dose 2 Mrad, equal for polymers I and II). It can be seen from Fig. 3.15 that temperature dependences of constants of quadratic termination rates  $k_{\text{ter}}$  for stabilized methacrylate radicals (in the coordinates of the Arrhenius equation) are different for polymers I and II: for polymers II, the Arrhenius equation does not hold true.

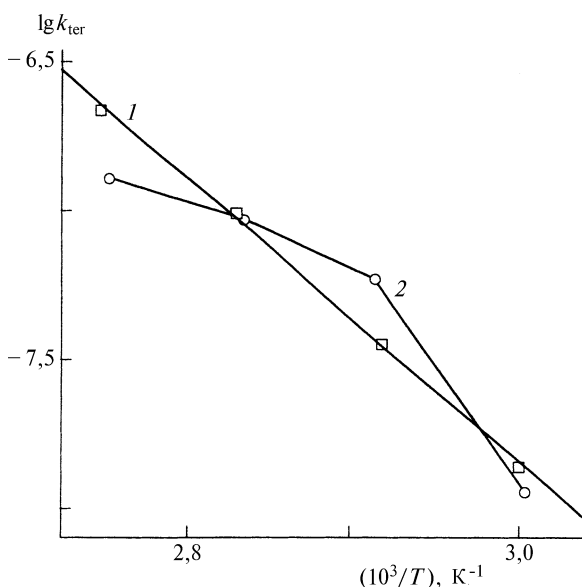


**Fig. 3.15** Temperature dependence of constant of termination rate  $k_{\text{ter}}$  for methacrylate radicals in polymers I (1) and II (2) irradiated with  $^{60}\text{Co}$ .  $D = 2$  Mrad



It means that as the temperature varies, the restructuring of those elements of network structure takes place, the molecular mobility of which controls the translation diffusion of stabilized radicals. It seems likely that a less stable structure is formed in the course of TFRP under the living chains conditions, a structure that is more sensitive to thermal action.

Characteristic features of polymers of tri(ethylene glycol) dimethacrylate and its copolymers with styrene (of types I and II) are conveniently presented in Table 3.2. It can be seen from this table that transformation of conventional TFRP into TFRP under living chains conditions leads to drastic changes of specific characteristics: the elasticity modulus decline both in glassy state and in highly elastic state, the glass-transition temperature decreases by  $40^\circ - 50^\circ$ , the rate of diffusion of solvents and their sorption equilibrium grow, and the regularity (type of function) of temperature dependence of quadratic termination rate constant of network-stabilized free radicals is also changed.

Thus, the method of TFRP under the living chains conditions as a tool for macromolecular design is efficient for obtaining cross-linked macromolecular structures with an upgraded level of macromolecular mobility (used, for example, in gel chromatography or as materials with enhanced relaxation ability). It seems likely that the absence of reinforcing micro-volumes or low concentration of these micro-volumes plus the very high density of network (grains) in cross-linked polymers obtained via TFRP under the living chains conditions represents the reason for the changes in features.

The synthesis of hyper-branched polymers (HBP) represents another direction in macromolecular design in the field of TFRP under the living chains condition.

**Table 3.2** (Co)polymers tEGdMA – styrene characteristics (type I and II)

Characteristics of polymers and copolymers	Polymer types		Copolymer types	
	I	II	I	II
Elasticity modulus $E$ , MPa	2120	1330	$\frac{1650}{1310}$	$\frac{1490}{400}$
Stress $\sigma$ at deformation $\varepsilon = 10\%$ , MPa	104	59.0	$\frac{77.1}{52.3}$	$\frac{62.8}{17.0}$
Rate $W_S$ of benzene vapor sorption at $25^\circ\text{C}$ , during 1 h	$1.24 \times 10^{-3}$	0.42	$\frac{0.14}{1.38}$	$\frac{0.22}{2.00}$
Sorption of benzene vapors during 24 h at $25^\circ\text{C}$ , %	<1	16.5	$\frac{15}{35}$	$\frac{38}{46}$
Temperature dependence of recombination rate constant	Linear	Nonlinear	–	–

*Note 1.* Polymers (copolymers) of type I and II were obtained via conventional TFRP and TFRP under living chains conditions, respectively.

*Note 2.* Physical and mechanical tests were conducted in the mode of uniaxial compression at the deformation rate of  $\varepsilon^\bullet = 10^{-4} \text{ s}^{-1}$  on polymer samples with conversion  $C = 80 \pm 2\%$ . For copolymers, the value above the line is obtained at  $C = 85 \pm 2\%$ ; the value below the line is obtained at  $C = 78 \pm 2\%$ .

Extremely important results were obtained for this direction, which has been successfully developed during the past decade, because it appeared that the living chains conditions provide the highest degree of structural regularity of HBP macromolecules, which brings statistical HBP closer to ideally regular dendrimers to the maximum extent. These results are described in Chap. 7.

## References

1. Korolev GV, Marchenko AP (2000) *Usp Khim* **69**:447–475 (in Russian)
2. Carnegie Mellon Department of Chemistry site. Page of Research areas of the Matyjaszewski Polymer Group. <http://www.chem.cmu.edu/groups/maty/about/research/index.html>. Accessed 5 May 2008
3. Szwarc M, Levy M, Milkovich R (1956) *J Am Chem Soc* **78**:2656–2657
4. Bagdasaryan XS (1966) Radical polymerization theory. Nauka, Moscow (in Russian)
5. Lagunov VM, Smirnov BR, Korolev GV et al (1987) *Vysokomolekul Soedin A* **29**:1442–1446 (in Russian)
6. Nair CPR, Clouet G, Brossas J (1988) *J Macromol Sci Part A* **25**:1089–1126
7. Georges MK, Veregin RPN, Kazmaier PM, Hamer GK (1993) *Polym Mater Sci Eng* **68**:6–11
8. Hawker CJ (1994) *J Am Chem Soc* **116**:11185–11186
9. Gatala JM, Rubel F, Hammouch SO (1995) *Macromolecules* **28**:8441–8443
10. Puts RD, Sogah DY (1996) *Macromolecules* **29**:3323–3325
11. Hawker CJ (1995) *Angew Chem Int Ed Engl* **34**:1456–1459
12. Georges MK, Veregin RPN, Kazmaier PM, Hamer GK (1993) *Macromolecules* **26**:2987–2988
13. Georges MK, Kee RA, Veregin RPN, Hamer GK et al (1995) *J Phys Org Chem* **8**:301–305
14. Matyjaszewski K, Gaynor S, Gresta D et al (1998) *J Phys Org Chem* **8**:306–315
15. Greszta D, Matyjaszewski K (1996) *Macromolecules* **29**:7661–7670
16. Barclay GG, Hawker CJ, Ito H et al (1998) *Macromolecules* **31**:1024–1031
17. Kazmaier PM, Daiton K, Georges MK et al (1997) *Macromolecules* **30**:2228–2231
18. Ide N, Fukuda T (1997) *Macromolecules* **30**:4268–4271
19. Listigovers NA, Georges MK, Odel PG, Keoshkerian B (1996) *Macromolecules* **29**:8992–8993
20. Bohrisch J, Wendler U, Jaeger W (1997) *Macromol Rapid Commun* **18**:975–982
21. Baethge H, Butz S, Schmidt-Naake G (1997) *Macromol Rapid Commun* **18**:911–916
22. Fukuda T, Terauchi T, Goto A et al (1996) *Macromolecules* **29**:3050–3052
23. Marestin C, Noel C, Guyot A, Claverie J (1998) *Macromolecules* **31**:4041–4044
24. Vedeneyev VI, Gurvich LV, Kondratiyev VN et al (1962) Energy of chemical bond breakage. Publishing House of the USSR Academy of Science, Moscow (in Russian)
25. Fukuda T, Terauchi T, Goto A et al (1996) *Macromolecules* **29**:6393–6398
26. Fischer H (1997) *Macromolecules* **30**:5666–5672
27. Greszta D, Matyjaszewski K (1996) *Macromolecules* **29**:5239–5240
28. He J, Zhang H, Chen J, Yang Y (1997) *Macromolecules* **30**:8010–8018
29. Wang J-S, Matyjaszewski K (1995) *J Am Chem Soc* **117**:5614–5615
30. Grishin DF, Semyoncheva LL (2001) *Russ Chem Rev* **70**:496–510
31. Curran DF (1991) In: Trost BM, Fleming T (eds) *Comprehensive organic synthesis*, vol 4. Pergamon Press, Oxford
32. Ship DA, Matyjaszewski K (1999) *Macromolecules* **32**:2948–2955
33. Wang J-L, Grimaud T, Matyjaszewski K (1997) *Macromolecules* **30**:6507–6512
34. Qiu J, Gaynor SG, Matyjaszewski K (1999) *Macromolecules* **32**:2872–2875
35. Percec V, Barboiu B (1995) *Macromolecules* **28**:7970–7972
36. Percec V, Barboiu B, Neumann A et al (1996) *Macromolecules* **29**:3665–3668

37. Tang W, Tsarevsky NV, Matyjaszewski K (2006) *J Am Chem Soc* **128**:1598–1604
38. Yamada K, Miyazaki M, Ohno K, Fukuda T et al (1999) *Macromolecules* **32**:290–293
39. Xia J, Matyjaszewski K (1997) *Macromolecules* **30**:7692–7696
40. Percec V, Kim H-J, Barboiu B (1997) *Macromolecules* **30**:8526–8528
41. Patten TE, Xia J, Abernathy TA, Matyjaszewski K (1996) *Science* **272**:866–868
42. Otsu T, Matsumoto A (1998) *Adv Polym Sci* **136**:75–137
43. Matyjaszewski K (1998) *Controlled radical polymerisation*. University Press, Oxford
44. Korolev GV, Matyjaszewski K (2000) *Controlled/living radical polymerisation*. Oxford University Press, Oxford
45. Tsarevsky NV, Matyjaszewski K (2007) *Chem Rev* **107**:2270–2299
46. Braunecker WA, Matyjaszewski K (2007) *Prog Polym Sci* **32**:93–146
47. Hawker CJ, Bosman AW, Harth E (2001) *Chem Rev* **101**:3661–3688
48. Goto A, Fukuda T (2004) *Prog Polym Sci* **29**:329–385
49. Korolev GV, Kochneva IS, Bakova GM et al (2001) *Vysokomolekul Soedin A* **43**:784–792 (in Russian)
50. Korolev GV, Kochneva IS, Bakova GM et al (2002) *Vysokomolekul Soedin A* **44**:1484–1489 (in Russian)
51. Korolev GV, Bakova GM, Berezin MP et al (2003) *Vysokomolekul Soedin A* **45**:33–44 (in Russian)
52. Ide N, Fukuda T (1997) *Macromolecules* **30**:4268–4271
53. Ide N, Fukuda T (1999) *Macromolecules* **32**:95–99
54. Kannurpatti AR, Lu SX, Bunker GM, Bowman CN (1996) *Macromolecules* **29**:7310–7315
55. Kannurpatti AR, Anderson KJ, Anseth JW, Bowman CN (1997) *J Polym Sci B Polym Phys* **35**:2297–2307
56. Kannurpatti AR, Anseth JW, Bowman CN (1998) *Polymer* **39**:2507–2513
57. Tsoukatos T, Pispas S, Hadjichristidis N (2001) *J Polym Sci A Polym Chem* **39**:320–325
58. Pasquale AJ, Lomg TEJ (2001) *Polym Sci A Polym Chem* **39**:216–223
59. Amosova SV, Biryukova EI, Brodskaya EI et al (2004) *Vysokomolekul Soedin A* **46**:484–490 (in Russian)
60. Yu Q, Zeng F, Zhu S (2001) *Macromolecules* **34**:1612–1618
61. Fukuda T, Kubo K, Ma Y-D (1992) *Prog Polym Sci* **17**:875–916
62. Beresniewicz A (1959) *J Polym Sci* **39**:63–79
63. Karapetyan ZA, Smirnov BA (1987) *Vysokomolekul Soedin* **29**:2102–2109 (in Russian)
64. Ham D (1971) *Copolymerization*. Khimia, Moscow (Russian translation)
65. Korolev GV, Makhonina LI (1968) *Vysokomolekul Soedin* **10**:245–251 (in Russian)
66. Berlin AA, Kefeli TYa, Korolev GV (1967) *Poly-esteracrylates*. Nauka, Moscow
67. Korolev GV, Irzhak TF, Irzhak VI (2001) *Polymer J Ser A* **43**:970–976 (in Russian)
68. Korolev GV, Smirnov BR, Bolkhovitinov AB (1962) *Vysokomolekul Soedin* **4**:1660–1664
69. Tvorogov NN, Korolev GV (1964) *Vysokomolekul Soedin* **6**:1006–1001 (in Russian)
70. Kurmaz SV, Rostchupkin VP, Kochneva IS (2002) *Plasticheskie Massy* **3**:34–38 (in Russian)
71. Moloney AC, Kausch HH, Stieger HR (1983) *J Mater Sci* **18**:208–216
72. Berlin AA, Korolev GV, Kefeli TYa, Sivergin YuM (1983) *Acrylic oligomers and materials on the acrylic oligomers*. Khimiya, Moscow (in Russian)
73. Korolev GV, Irzhak TF, Irzhak VI (2002) *Russ J Phys Chem B* **21**:58–68
74. Lagunov VM, Berezin MP, Korolev GV et al (1985) *Vysokomolekul Soedin A* **27**:2056–2060 (in Russian)

## Chapter 4

# Kinetic Features of Three-Dimensional Free-Radical Copolymerization

**Abstract** Chapter 4 is concerned with those specific features of three-dimensional free-radical copolymerization that allow synthesizing cross-linked copolymers with prespecified structure and properties, i.e., to implement macromolecular design. Experiments staged for four oligo(meth)acrylates and various vinyl monomers showed that commonly used copolymerization constants are unsuitable for planning cross-linked copolymer structure. The authors propose new approaches for cross-linked copolymer design.

Radical copolymerization of polyunsaturated oligomers and vinyl monomers has been used extensively and successfully for a long time to produce cross-linked copolymers [1]. Copolymerization eliminates a range of shortcomings inherent to cross-linked homo-polymers. During the past decade cross-linked copolymers are noted to be used more extensively, including hi-tech applications (see surveys [1–3]). This fact intensified research of three-dimensional free-radical copolymerization, bringing to the fore the issue of macromolecular design of cross-linked copolymers, i.e., a controlled synthesis of such copolymers with forecasted structure and properties required for a specific field of application.

A set of systematic studies [4–7] allowed exploring copolymerization and properties of polyunsaturated (network forming) oligomers and vinyl monomers. It enabled establishing kinetic features of three-dimensional free-radical copolymerization and properties of cross-linked copolymers that are basic for the macromolecular design. The kinetic results of this set of studies are presented in detail in this chapter; basic properties of cross-linked copolymers are discussed in Chap. 6.

### 4.1 Kinetic Features of Three-Dimensional Copolymerization of Oligomer and Vinyl Monomers

To ensure sufficient generalization of kinetic basic data, it is necessary to form a representative set of subjects to be studied. Such a set was formed as follows [4]. Tri(ethylene glycol) dimethacrylate (i.e., widely used tEGdMA oligomer was selected as polyunsaturated oligomer  $M_1$ , and vinyl monomers providing various sets of copolymerization constants  $r_1$  and  $r_2$  were used as  $M_2$ . This approach provided

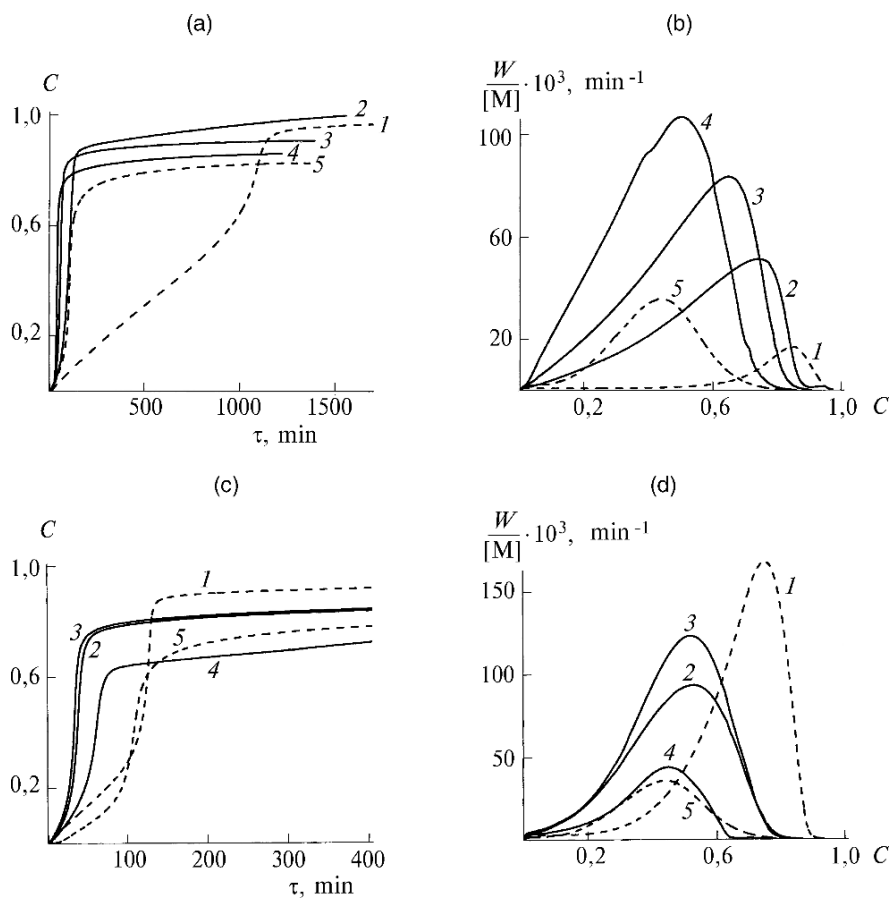
different types of chain microstructure of produced copolymers, namely, alternating microstructure (styrene,  $r_1 \approx 0.5 < 1$ ,  $r_2 \approx 0.5 < 1$ ), microstructure with a tendency for block formation [butyl acrylate (BA),  $r_1 \approx 2 > 1$ ,  $r_2 \approx 0.5 < 1$ ] and a block-grafted one [vinyl acetate (VA)  $r_1 \approx 20 \gg 1$ ,  $r_2 \approx 0.05 \ll 1$ ]. Besides, the volume of steric hindrance group was varied in  $M_2$  [from  $-\text{CH}_3$  in MMA to  $-\text{C}_{12}\text{H}_{25}$  in dodecylmethacrylate (DDMA)], with the double bond nature being invariable (methacrylate).

Copolymerization kinetics was studied using the isothermal microcalorimetry method [60°C: initiator AIBN and highly effective inhibitor 2,2,6,6-tetramethyl piperidine-1-oxyl (TEMPO) to prevent spontaneous polymerization of the initial mixture] [4]. To calculate the polymerization rate and conversion, we used molar heat of polymerization  $Q_2 = 58.8 \text{ kJ/mol}$  for methyl-, butyl-, and dodecylmethacrylates;  $71.6 \text{ kJ/mol}$  for styrene;  $77.4 \text{ kJ/mol}$  for BA; and  $89.2 \text{ kJ/mol}$  for VA [8, 9]. Heat of tEGdMA polymerization  $Q_1$  was assumed to be equal to that of MMA ( $58.8 \text{ kJ/mol}$  calculated per one double bond). Values of  $Q_{1,2}$  for copolymerization were calculated using an additive scheme:  $Q_{1,2} = \alpha_1 Q_1 + 4\alpha_2 Q_2$ , where  $\alpha_1$  and  $\alpha_2$  are molar fractions of components 1 and 2, respectively, in the initial mixture. Conversion was controlled in terms of density using the flotation method (its densitometric titration version) [10].

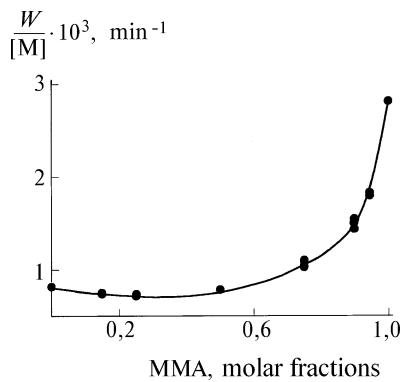
Figures 4.1, 4.2, 4.3, 4.4, and 4.5 show results of kinetic measurements taken by the calorimetric technique. Obviously, copolymerization heat averaging by the additive scheme introduces a certain error, which increases with the growth of difference  $Q_2 - Q_1$ . This fact should be taken into account when analyzing data for  $M_2 = \text{styrene}$   $Q_2 - Q_1 = (71.6 - 58.8) \text{ kJ/mol}$ ,  $M_2 = \text{BA}$   $Q_2 - Q_1 = (77.4 - 58.8) \text{ kJ/mol}$ , and especially for  $M_2 = \text{VA}$   $Q_2 - Q_1 = (89.2 - 58.8) \text{ kJ/mol}$ . In the case of  $M_2 = \text{styrene}$ , the least error is observed in the region of mixture compositions  $[M_1]: [M_2]$  close to equimolar ones; in the case of  $M_2 = \text{VA}$ , the error is quite large with any ratio  $[M_1]: [M_2]$ . Figures 4.1, 4.2, 4.3, 4.4, and 4.5 show the kinetic results as coordinates “conversion ( $C$ ) – time ( $\tau$ )” and “reduced rate ( $W/[M] - C$ .” The rate was reduced using averaged current concentration of the monomer mixture.

Figure 4.1a,b shows kinetic results for  $M_2 = \text{styrene}$ . It is clearly seen that the increase in content of network-forming agent  $M_1$  in copolymer exerts quite significant influence at both the auto-acceleration and auto-deceleration stages: beginning of auto-acceleration ( $C_g$ ) and maximum position  $W/[M]C_{\text{max}}$  shift systematically to lower values of  $C$ . It is obvious that as  $[M_1]$  increases, higher structuring of the reaction medium leads to decline of molar mobility level in the system, and molar mobility level regulates quadratic termination of chains when  $C \geq C_g$  and growth of chains when  $C > C_{\text{max}}$  [11–15]. Hence, hindering of mobility of propagating chains accelerates three-dimensional free-radical copolymerization (auto-acceleration stage), whereas freezing the mobility of double bonds, in contrast, decelerates this process (auto-deceleration stage).

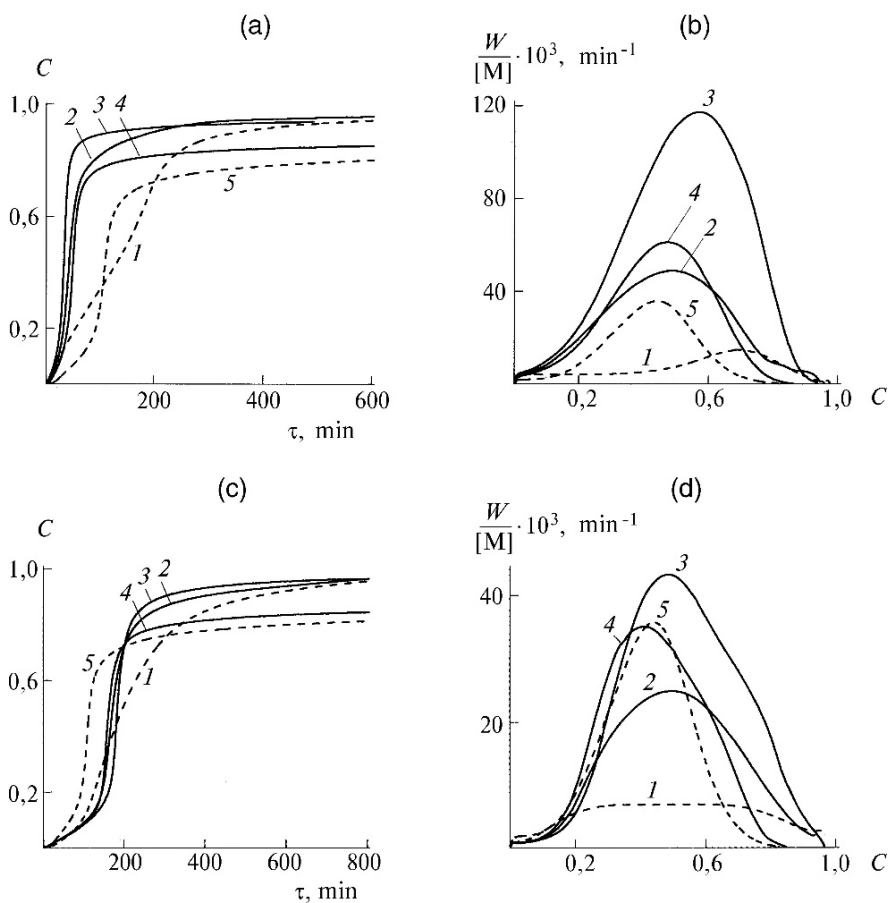
Within range  $C_g < C < C_{\text{max}}$ , the most favorable situation for three-dimensional free-radical copolymerization is observed: chain termination progressively slows down as  $C$  increases, while the chain propagation has not yet begun decelerating because an elementary event of growth is limited by mobility of low molecular (and



**Fig. 4.1** Kinetics of copolymerization of tEGdMA ( $M_1$ ) and styrene ( $M_2$ ) (a, b) and MMA ( $M_2$ ) (c, d). Molar ratio  $[M_1]/[M_2]$ : 0 : 1 (1); 1 : 3 (2); 1 : 1 (3); 3 : 1 (4); and 1 : 0 (5).  $T = 60^\circ\text{C}$ ;  $[\text{AIBN}] = 2 \times 10^{-2} \text{ mol/l}$

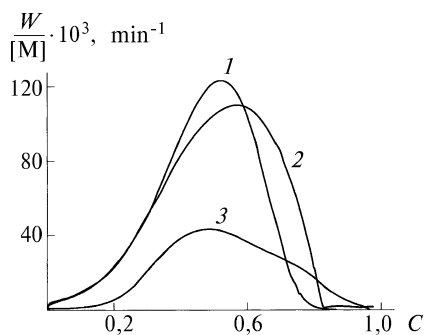


**Fig. 4.2** Kinetics of copolymerization of MMA and styrene.  $T = 60^\circ\text{C}$ ;  $[\text{AIBN}] = 2 \times 10^{-2} \text{ mol/l}$



**Fig. 4.3** Kinetics of copolymerization of tEGdMA (M<sub>1</sub>) and BMA (M<sub>2</sub>) (a, b) and DDMA (M<sub>2</sub>) (c, d). Molar ratio  $[M_1]/[M_2]$ : 0 : 1 (1); 1 : 3 (2); 1 : 1 (3); 3 : 1 (4); and 0 : 1 (5).  $T = 60^\circ\text{C}$ ;  $[\text{AIBN}] = 2 \times 10^{-2} \text{ mol/l}$

**Fig. 4.4** Kinetics of copolymerization of tEGdMA (M<sub>1</sub>) and vinyl monomers (M<sub>2</sub>). Molar ratio  $[M_1] : [M_2] = 1 : 1$ . Monomers M<sub>2</sub>: 1, MMA; 2, BMA; 3, DDMA.  $T = 60^\circ\text{C}$ ;  $[\text{AIBN}] = 2 \times 10^{-2} \text{ mol/l}$



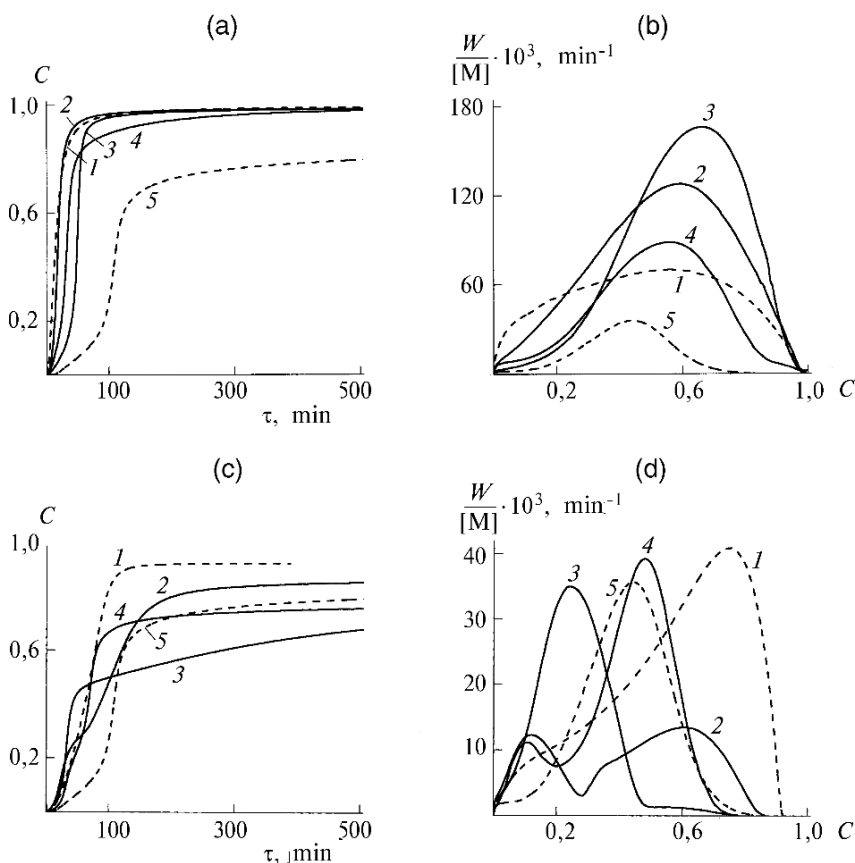


**Fig. 4.5** Kinetics of copolymerization of tEGdMA ( $M_1$ ) and BA ( $M_2$ ) (a, b) and VA ( $M_2$ ) (c, d). Molar ratio  $[M_1] : [M_2]$ : 0 : 1 (1); 1 : 3 (2); 1 : 1 (3); 3 : 1 (4); and 0 : 1 (5).  $T = 60^\circ\text{C}$ ;  $[\text{AIBN}] = 2 \times 10^{-2} \text{ mol/l}$

hence, more mobile than the chain) monomer. To freeze the mobility, it is necessary to attain significantly higher  $C = C_{\max} \gg C_g$ . We would like to point out here that the value of  $C_g$  was conditionally defined as conversion, at which the reduced rate  $W/[M]$  is doubled.

To be sure that enhanced reactive capacity resulting from increased fraction of network-forming monomer  $M_1$  in the initial reaction mixture is indeed associated with purely physical factors, Fig. 4.2 presents similar results with the only difference being that a non-network-forming (monounsaturated) analogue of tEGdMA monomer (methyl methacrylate, MMA) was used as  $M_1$ . The value of initial copolymerization rate  $(W/[M])_0$  in this case is a measure of "actual" (chemical) reactive capacity of mixture  $M_1 + M_2$ . It is seen that addition of 0.25 and even 0.5 molar fractions of MMA to styrene does not practically influence the reactive capacity, in contrast to tEGdMA (cf. Fig. 4.1a,b). Also, it is known that the reactive capacity of



the methacrylic group in dimethyl acrylates and MMA is almost the same, which allows considering them as analogue monomers.

Substitution of  $M_2 = \text{MMA}$  for  $M_2 = \text{styrene}$  (Fig. 4.1c, d) results in a qualitatively similar pattern, but with certain quantitative differences: the highest auto-acceleration rate (being measured by the value of  $(W/[M])_{\max}$ ) is reached at  $[M_1] : [M_2] = 1 : 1$ , but not 3 : 1 as for styrene. In this case interpretation of results using physical effects only seems to be the only one because, from the standpoint of reactive capacity, tEGdMA and MMA are analogue monomers.

Both alkyl(meth)acrylates – BMA and DDMA – are chemical analogues of tEGdMA (Fig. 4.3), because reactive capacity of the double bond in a homologous series of alkyl(meth)acrylates is known to change slightly as the alkyl group length grows starting from  $-\text{CH}_3$  (MMA) [9, 16].

To assess the effectiveness of alkyl substituent as a factor influencing the kinetics of three-dimensional free-radical copolymerization process, Fig. 4.4 presents data for the comparison of fixed ratio of monomers in the initial mixture  $[M_1] : [M_2] = 1 : 1$  for  $M_2 = \text{MMA}$ , BMA, and DDMA.

It is seen that with increasing content of alkyl substituent in  $M_2$ , the influence of  $M_2$  at the auto-deceleration stage grows dramatically: the longer is the alkyl chain, the higher are the  $C$  values, at which complete “freezing” of chain growth events occurs ( $W/[M] \rightarrow 0$ ). It can be related to the action of links  $M_2$  as internal plasticizer enhancing molecular mobility.

An expressed two-stage pattern of the process represents a distinctive feature of three-dimensional free-radical copolymerization for the case of  $M_2 = \text{VA}$  (Fig. 4.5c,d). The first stage is conventional: it includes auto-acceleration followed by auto-deceleration. The second stage starts for equimolar mixture at  $C \approx 0.5$  and continues with virtually constant rate up to  $C > 0.7$ . The second stage seems to be nothing more than a process close to VA polymerization proceeding in a structured highly cross-linked matrix (according to  $r_1 \gg 1$  and  $r_2 \ll 1$ ). Taking the microheterogeneity into account [12–15], the matrix is a structure that includes microregions with low concentration of junctions (or low cross-linking) network (structural defects). Possibly, VA polymerization at the second stage of three-dimensional free-radical copolymerization proceeds in the defects, thus “curing” them. Then, at the first stage of three-dimensional free-radical copolymerization, VA plays the role of temporary plasticizer (solvent), and a highly cross-linked matrix is formed in unusual conditions.

When  $M_2 = \text{BA}$  (Fig. 4.5a,b), the tendency of departure from statistical distribution of  $M_1$  and  $M_2$  in chains in favor of block formation should be expressed to a lesser extent versus  $M_2 = \text{VA}$ , judging by values of  $r_1$  and  $r_2$ . Hence, the two-stage pattern of three-dimensional free-radical polymerization is not observed.

The obtained kinetic data agree well with an assumption of negative influence of monounsaturated monomers upon the secondary process of intrachain cross-linking (cyclization). Indeed, cyclization during three-dimensional free-radical polymerization is one of the reasons for microheterogeneity development in a reaction system in the form of microgel particles playing a role of self-contained microreactors [12–15]. Besides, auto-acceleration at initial and intermediate stages of the

polymerization process develops according to a particular regularity related to the reaction system specifics. This regularity implies that optimal conditions for maximum rate polymerization (in the gel-effect mode) are arranged in peripheral layers of microgel particles. Therefore, polymerization rate at the auto-acceleration stage is proportional to the total volume of all peripheral layers and, hence, auto-acceleration develops due to an increase of this total volume resulting from the growth of microgel particles in size during the polymerization process until the moment the growing particles begin contacting each other. After that, the total reactive volume starts diminishing, the polymerization rate passes its maximum, and the auto-acceleration mode transforms into the auto-deceleration one (see Sects. 1.2.2 and 1.2.3).

Therefore, as a result of cyclization and microheterogenization generated by it, the polymerization process takes place only in a certain part of a reaction medium, being a certain fraction  $\beta < 1$ ; it is equal to a ratio of the sum of volumes  $V_i$  of the peripheral layers of microgel particles to full volume  $V$  of the polymerization system. Obviously, complete suppression of cyclization accompanied by complete homogenization of the reaction system should lead to the growth of transformation rate at the auto-acceleration stage in  $\beta^{-1}$  times. Because the thickness of the peripheral layers of microgel particles is sufficiently small [12–15] (according to the most reliable estimates  $0.1 \leq \beta \leq 0.3$ ; see Table 1.1, Sect. 1.2.2), the suppression of cyclization should be accompanied by a 3- to 10-fold increase in polymerization rate.

Considerable increase of  $W/[M]$  at the auto-acceleration stage (up to the maximum point) is observed in Figs. 4.1 and 4.3 for minimal ( $[M_1] : [M_2] = 3 : 1$ ) additive of monounsaturated monomer  $M_2$  for the case  $M_2 =$  styrene (more than 3 fold; and with conversion  $C < 0.1$ , even 10 fold) and for higher additives ( $[M_1] : [M_2] = 1 : 1$ ) for MMA and BMA (more than 2 fold, and with  $C < 0.1$ , more than 3 fold). Styrene links building into copolymer chains were found to be an incommensurably more serious hindrance for the intrachain cross-linking (cyclization) than MMA and BMA links. It is likely to be related both to the type of distribution of  $M_2$  in chains ( $r_1 \leq 1, r_2 \leq 1$ , a tendency to alternating) and to the steric crowding effect of phenyl groups. The role of alkyl substituent volume for steric crowding is clearly seen when comparing curves 4 and 5 in Fig. 4.1c, d and Fig. 4.3a,b: when a minimal amount of  $M_2$  is added (curves 4), the increase of  $W/[M]$  at the auto-acceleration stage in case of the considerably bulky substituent  $-C_4H_9$  (for BMA) is significantly higher compared to  $-CH_3$  (for MMA). An overly high volume of group  $-C_{12}H_{25}$  (for DDMA) appears to provoke structure complications of the micelle formation type and, therefore, kinetic data in Fig. 4.3c, d are not consistent with the above-described regularity.

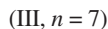
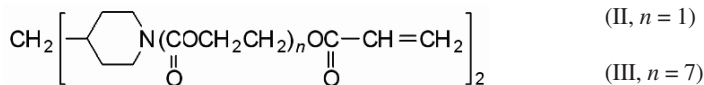
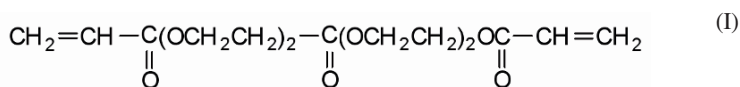
In conclusion, we emphasize once again that the nontrivial character of obtained kinetic results consists in the fact that in a certain range of compositions  $[M_1] : [M_2]$ , dilution of network-forming monomer  $M_1$  with non-network-forming monomer  $M_2$  results in variation of effective reactive capacity of mixture  $M_1 + M_2$  in a direction that is contradictory to the variation of its true (chemical) reactive capacity. For instance, the effective reactive capacity of the mixture increases in the range  $[M_1] : [M_2] = 1 : 0 - 3 : 1$  as styrene content grows, while the chemical reactive capacity, in contrast, declines; in the case of mixture “di(meth)acrylate – methacrylates,” the

effective reactive capacity within the range  $[M_1] : [M_2] = 1 : 0 - 1 : 1$  grows, while the chemical reactive capacity remains unchanged.

## 4.2 Variation of Copolymer Composition During Three-Dimensional Free-Radical Copolymerization of Oligomers and Vinyl Monomer

The current section presents results of detailed study of copolymerization of methyl (meth)acrylate ( $MMA = M_1$ ) and diacrylates ( $M_2$ ) [5]. To apply the obtained results for macromolecular design, special attention was paid to identification of dependencies of copolymer composition (instantaneous and average) upon conversion and values  $r_1$  and  $r_2$  evaluation at different stages of copolymerization process, as well as to studying the kinetic regularities of the latter.

Oligodiacylates I, II, and III were chosen as  $M_2$ :



Copolymerization kinetics was studied by the isothermal microcalorimetry method at 60°C using AIBN initiator and by IR spectroscopy at 20°C [photo-initiation with irradiation from a UV source in the presence of additives of 2,2-dimethoxy-2-phenylacetophenone (DMPA)]. To calculate the polymerization rate, we have used molar heat of MMA polymerization ( $Q = 58.82 \text{ kJ/mol}$ ) [8] and that of butyl acrylate polymerization ( $Q = 77.87 \text{ kJ/mol}$ ) [9] having constant values in homologous series  $\text{CH}_2=\text{C}(\text{CH}_3)\text{COOR}_1$  and  $\text{CH}_2=\text{CH}-\text{COOR}_2$  when varying  $R_1$  and  $R_2$  [9, 16]. Values  $Q_{1,2}$  for copolymerization were calculated according to the additive scheme:  $Q_{1,2} = \alpha_1 Q_1 + \alpha_2 Q_2$ , where  $\alpha_1$  and  $\alpha_2$  are molar fractions of components 1 and 2 in the initial mixture. Obviously, this scheme reflects exactly the situation for “azeotropic” copolymerization only, which proceeds without changes in the composition of mixture  $M_1 + M_2$  during the transformation. In all other cases, an error appears, the value of which is determined by numeric values of copolymerization constants  $r_1$  and  $r_2$  and by composition of copolymerizing mixture.

For IR spectroscopy measurements, we used not conventional MMA as  $M_1$ , but completely deuterated MMA (d-MMA) because mixtures of oligodiacylates I–III and MMA do not contain spectral lines suitable for individual quantitative analysis of double bonds of acrylate and methacrylates groups during copolymerization. When substituting d-MMA for MMA, such spectral lines appear: frequencies

of deformation vibrations of hydrogen double bonds in acrylate ( $810\text{ cm}^{-1}$ ) and d-MMA ( $747\text{ cm}^{-1}$ ) are clearly differentiated. Frequencies of valence vibrations of double bonds of  $1638\text{ cm}^{-1}$  (acrylate) and  $1592\text{ cm}^{-1}$  (d-MMA) are also differentiated quite sufficiently, but, in this case, the spectrum in the area of  $1638\text{ cm}^{-1}$  has a sophisticated shape (splitting) and, therefore, frequencies of  $810$  and  $747\text{ cm}^{-1}$  were mainly used for separate quantitative analysis of acrylic and methacrylic double bonds during copolymerization [17]. Special experiments on MMA and d-MMA copolymerization showed that influence of the isotopic effect in the case of d-MMA during copolymerization is negligible: separately measured kinetic curves for MMA and d-MMA practically coincide; measurements were taken for frequencies  $1638\text{ cm}^{-1}$  (MMA) and  $1592\text{ cm}^{-1}$  (d-MMA) corresponding to valence vibrations of bonds  $\text{C}=\text{C}$  [17].

Representative kinetic curves obtained through the use of calorimetry method are shown in Figs. 4.6a, 4.7a, and 4.8a (in “conversion  $C$  – time  $\tau$ ” coordinates) and in Figs. 4.6b, 4.7b, and 4.8b (in “reduced polymerization rate  $W/[M]$  – conversion” coordinates, where  $[M]$  is current concentration of double bonds in a copolymerization system). Despite possible distortions of kinetic curve shapes associated with the influence of  $r_1$  and  $r_2$  values and changes of mixture composition  $M_1 + M_2$  in the course of polymerization, data in Figs. 4.6, 4.7, and 4.8 enable us to draw quite specific conclusions (especially when we take into account published values [9] of  $r_1 = 2$ ,  $r_2 = 0.5$ , and chosen composition of mixture  $[M_1]/[M_2] > 1$  for experiments, which ensure minimal distortions caused by the use of the additive scheme).

It follows from Figs. 4.6a, 4.7a, and 4.8a that regardless of initial mixture composition  $M_1 + M_2$ , copolymerization proceeds to high conversions ( $C > 0.9$ ) that are virtually indistinguishable from limiting conversion ( $C_{\text{lim}}$ ) of MMA under given conditions ( $T = 60^\circ\text{C}$ , initiation rate  $W_1 = 2 \times 10^{-7}\text{ mol} \cdot \text{l}^{-1} \cdot \text{s}^{-1}$ ). Therefore, we believe that the cross-linked structure formed as a result of cross-linking of

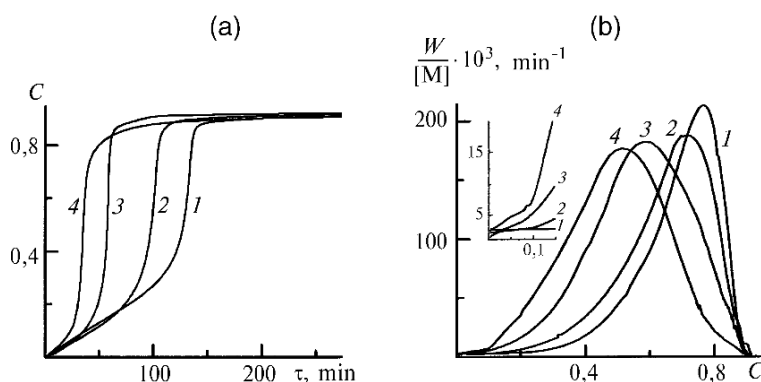


**Fig. 4.6** Kinetics of MMA copolymerization and oligodiacylate II. Content of oligomer II in initial composition, % (by weight): 1, 0; 2, 0.5; 3, 22.0; 4, 49.0.  $T = 60^\circ\text{C}$ ;  $[\text{AIBN}] = 2 \times 10^{-2}\text{ mol/l}$

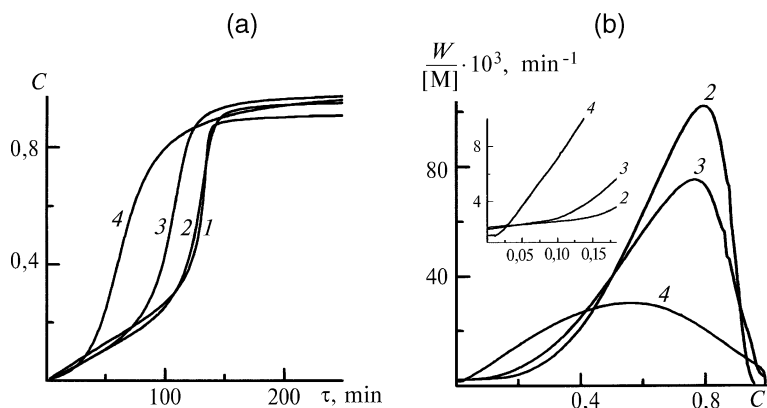


**Fig. 4.7** Kinetics of MMA copolymerization and oligodiacylate I. Content of oligomer I in initial composition, % (by weight): 1, 0; 2, 11.4; 3, 19.2; 4, 49.7.  $T = 60^{\circ}\text{C}$ ;  $[\text{AIBN}] = 2 \times 10^{-2} \text{ mol/l}$

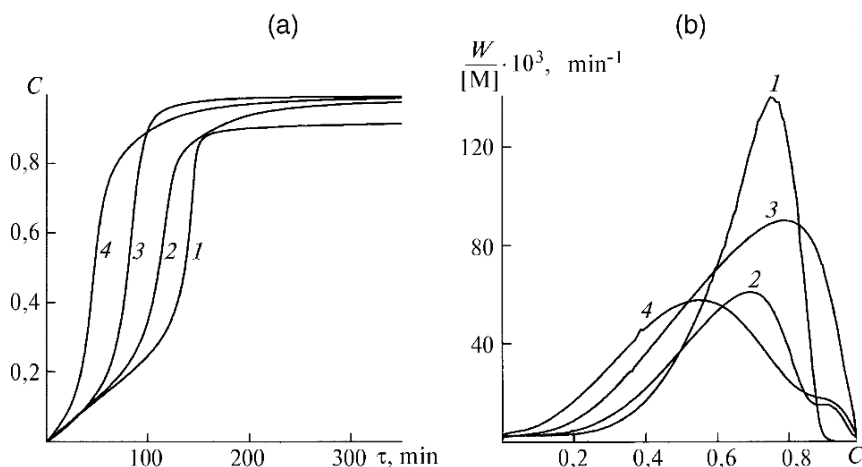


**Fig. 4.8** Kinetics of MMA copolymerization and oligodiacylate III. Content of oligomer III in initial composition, % (by weight): 1, 0; 2, 19.3; 3, 33.7; 4, 47.6.  $T = 60^{\circ}\text{C}$ ;  $[\text{AIBN}] = 2 \times 10^{-2} \text{ mol/l}$

poly(meth)acrylate chains by diacrylates does not shift the glass-transition temperature ( $T_g$ ) of the polymer–monomer mixture P+M to higher temperatures.

Indeed, it is well known [18 (p. 187)] that the reason for the existence of  $C_{\text{lim}} < 1$  in the case of MMA polymerization is glass transition of P + M at a given temperature ( $T_{\text{pol}} = 60^{\circ}\text{C}$ ) that freezes mobility M and, hence, prevents growth of polymer chains  $\sim\text{R}^{\bullet} + \text{M} \xrightarrow{k_{pr}} \sim\text{R}^{\bullet}$  (the mobility of radicals carriers of chain  $\sim\text{R}^{\bullet}$  is frozen even earlier with  $C \ll C_{\text{lim}}$ ). In other words, mixture P + M at the time of the polymerization process cessation ( $C \rightarrow C_{\text{lim}}$ ) containing  $(1 - C_{\text{lim}}) [\text{M}]_0$  (where  $[\text{M}]_0$  is initial concentration of monomer) of residual monomer has glass-transition temperature  $T_g = T_{\text{pol}} = 60^{\circ}\text{C}$ . One can expect that cross-linking of polymer chains during copolymerization with oligomers I–III would result in even greater freezing

of mobility and, hence, to decrease of the  $C_{lim}$  value. However, it does not happen, which is a remarkable fact, because in other cases, when di(ethylene) and tri(ethylene)glycol dimethyl acrylates were used instead of oligomers I–III, the value of  $C_{lim}$  declined quite considerably. The reason for such a difference consists in either enhanced flexibility of molecules of oligomers I–III or particularities of formation of cross-linked structure associated with  $r_1 > 1$  and  $r_2 < 1$  ( $r_1 = 2$ ,  $r_2 = 0.5$  [9]) vs.  $r_1 = r_2 = 1$ , which takes place when di(ethylene)- and tri(ethylene glycol) dimethyl acrylates are used. These particularities are as follows: with low values of  $C$ , the copolymer is enriched with MMA units (and, therefore, it is weakly cross-linked), and then, as  $C$  grows, the cross-linking degree increases more and more. Highly cross-linked copolymer formed only at high  $C$ , obviously, would turn out to be dispersed in weakly cross-linked matrix and would not exert a significant influence upon  $T_g$ , reflecting  $T_g$  of the matrix. It should be pointed out here in the case of oligomer III, addition of diacrylate results in notable growth of  $C_{lim}$  (see Fig. 4.8).

Another conclusion is related to the influence of oligomers I–III additives upon the beginning of the auto-acceleration stage (gel effect). In this case, the cross-linking degree is manifested rather dramatically: a natural shift of conversion  $C_g$  (where “g” means gel effect) to lower values occurs as the amount of oligomers I–III grows (see Figs. 4.6 to 4.8). This regularity is rather trivial because auto-acceleration is associated with freezing of translation mobility of growing chains  $\sim R^\bullet$ , which results in decrease of quadrate termination rate  $\sim R^\bullet + \sim R^\bullet \xrightarrow{k_{ter}} P$  and, hence, in growth of  $W/[M]$ . It can be seen (Figs. 4.6b, 4.7b, and 4.8b) that maximal  $W/[M]$  is shifted to lower values of  $C$  as the content of oligodiacrylates in the initial mixture grows. At that, the value of  $(W/[M])_{max}$  behaves differently for oligomers I–III: with oligomer II, it is virtually constant and equal to  $(W/[M])_{max}$  for MMA polymerization. With oligomers I and III, it is considerably lower and decreases with increasing content of diacrylate in the initial mixture. The authors encountered difficulties when interpreting this result.

Kinetic results of separate determination of rates ( $V = dC/dt$ ) of consumption of each of the comonomers  $M_1$  and  $M_2$  during copolymerization of d-MMA ( $M_1$ ) and oligodiacrylates I and III ( $M_2$ ) are presented in Figs. 4.9 and 4.10. It can be seen from these figures that for all compositions of initial mixture  $[M_1]_0/[M_2]_0 = 0.58\text{--}4.47$  selected for studying, the rate of d-MMA transformation is higher as compared to oligomers I and III during the entire copolymerization process or within limited range of conversions.

One can see a trend to dramatic increase of copolymerization rate  $dC_1/dt + dC_2/dt = V$  as MMA content in the initial mixtures goes down (see Fig. 4.9c). When  $[M_1]_0 = 0$ , a stepwise and more than twofold increase of  $V$  vs.  $V$  in the presence of 7% (by weight) MMA (which approximately corresponds to 0.07 of volume dilution) is observed. Obviously, such a low-degree dilution of the highly viscous reaction system  $M_1 + M_2$  and low-viscosity component  $M_1$  cannot provide so high an extent of  $V$  decrease due to the growth of diffusion-controlled constant of rate ( $k_{ter}$ ) of quadrate chain termination. This finding gives us grounds to believe that the abnormally high reactive capacity of oligomer I during polymerization is related

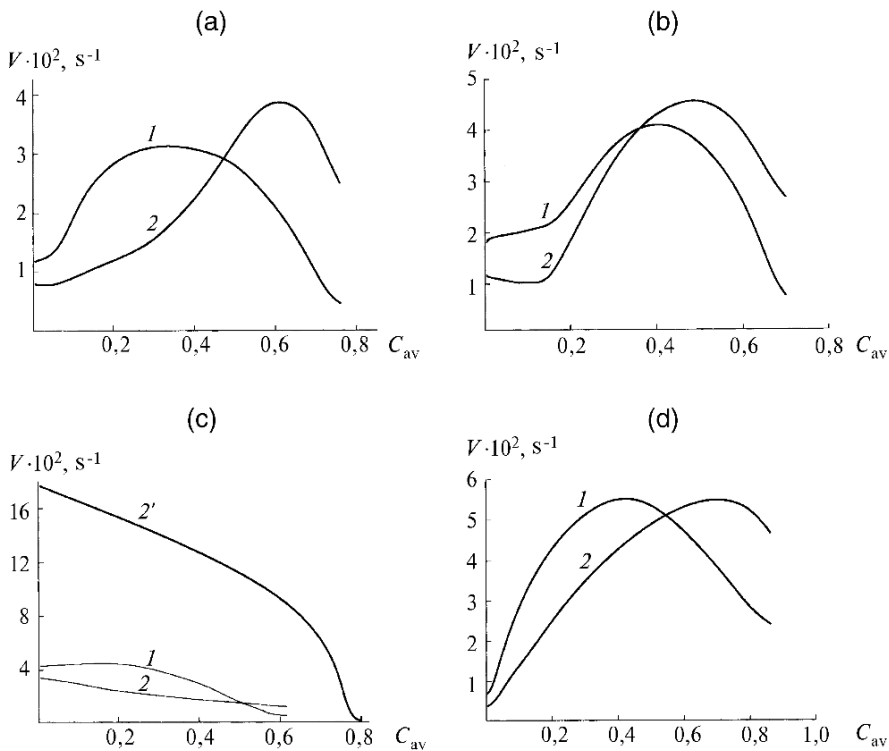


**Fig. 4.9** Kinetics of consumption of components  $M_1 = \text{d-MMA}$  (1) and  $M_2 = \text{oligomer I}$  (2) for different compositions of initial mixture  $[M_1]_0/[M_2]_0$ : (a) 1.75; (b) 1.5; (c) 0.58; (d) 1.5. Photoinitiator: DMPA 0.5% (by weight).  $T = 20^\circ\text{C}$ . For cases a–c, analytical bands at 810 and 747  $\text{cm}^{-1}$ ; for d, at 1638 and 1592  $\text{cm}^{-1}$ . Curve 2', polymerization of oligomer I under similar conditions. For  $C_{av}$ , see Eq. (4.9).

to the ability of this oligomer (characterized by high-degree intermolecular interaction) to form associates, similar to the previously observed situation for higher alkyl acrylates [19 (p. 147); 20].

Figures 4.11 and 4.12 show results of variation (during copolymerization) of reaction mixture composition  $[M_1]/[M_2]$  and copolymer composition  $m_1/m_2$  (molar ratio of links  $M_1$  and  $M_2$ ), of instantaneous averaged

$$(m_1/m_2)_{av} = ([M_1]_0 dC_1/dt) / ([M_2]_0 dC_2/dt) \quad (4.1)$$

and averaged integral:

$$(m_1/m_2)_\Sigma = C_1 [M_1]_0 / C_2 [M_2]_0 \quad (4.2)$$

where  $[M_i]_0$  and  $[M_i]$  = initial and current concentration of a  $i$ -th comonomer in reaction mixture; and  $C_i$  = conversion, calculated by the following formula:

$$C_i = ([M_i]_0 - [M_i]) / [M_i]_0$$

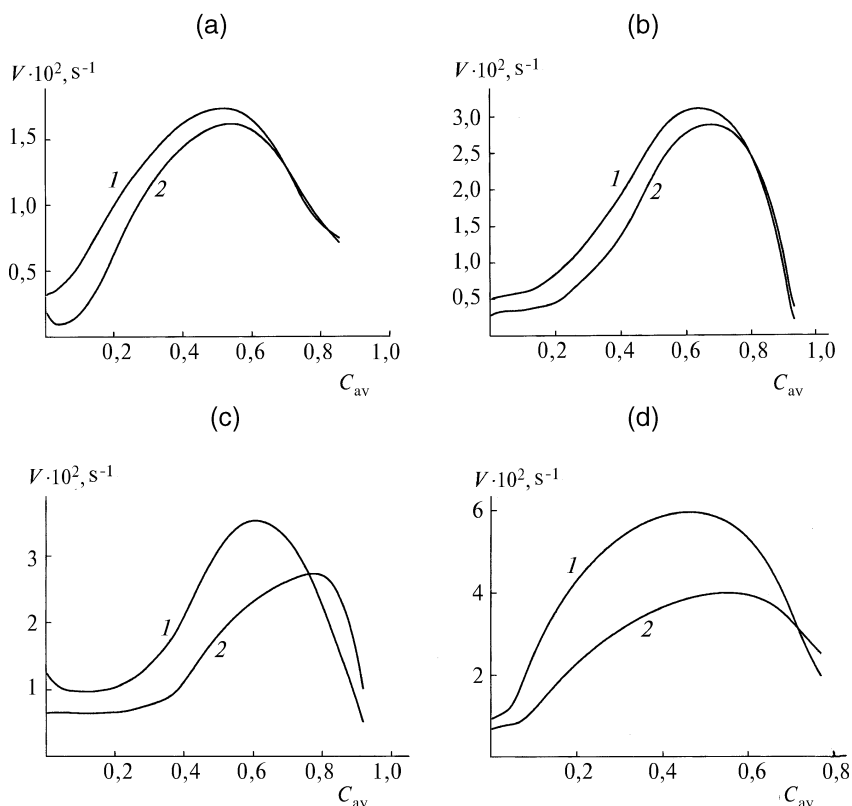


**Fig. 4.10** Kinetics of consumption of components  $M_1 = \text{d-MMA}$  (1) and  $M_2 = \text{oligomer III}$  (2) for different compositions of initial mixture  $[M_1]_0/[M_2]_0$ : (a) 4.47; (b) 3.73; (c) 3.28; (d) 1.5. Photoinitiator, DMPA 0.6–0.8% (by weight).  $T = 20^\circ\text{C}$ . Analytical bands at  $810$  and  $747\text{ cm}^{-1}$ . For  $C_{av}$ , see Eq. (4.9).

To analyze these data, we will use the copolymer composition equation [21, 22], which serves as the basis for calculations for all known copolymerization constants  $r_1$  and  $r_2$  presented in reference publications [9, 22]:

$$\frac{d[M_1]}{d[M_2]} = \frac{[M_1]}{[M_2]} \cdot \frac{r_1[M_1] + [M_2]}{r_2[M_2] + [M_1]} \quad (4.3)$$

Then we will write it using other symbols that are more relevant to the procedure of subsequent analysis:

$$\frac{[M_1]_0 dC_1/dt}{[M_2]_0 dC_2/dt} = \frac{[M_1]}{[M_2]} \cdot \frac{r_1 \cdot \frac{[M_1]}{[M_2]} + 1}{r_2 + \frac{[M_1]}{[M_2]}} \quad (4.4)$$



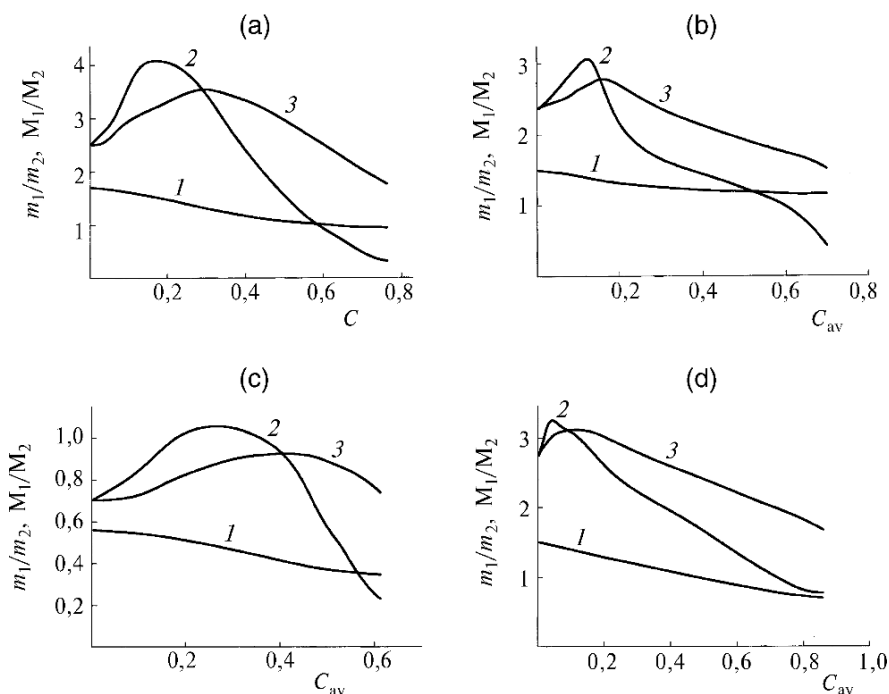


**Fig. 4.11** Variation of monomer mixture composition  $[M_1]/[M_2]$  (I) of instantaneous  $m_1/m_2$  (2) and integral  $(m_1/m_2)_\Sigma$  (3) copolymer composition during copolymerization of d-MMA ( $M_1$ ) and oligomer I ( $M_2$ ). Initial mixture composition  $[M_1]_0/[M_2]_0$ : (a) 1.75; (b) 1.4; (c) 0.58; (d) 1.5. Photoinitiator DMPA 0.6% (by weight).  $T = 20^\circ\text{C}$ . Calculation of  $m_1/m_2$ ,  $(m_1/m_2)_\Sigma$  and  $C_{av}$  by formulas (4.1), (4.2), and (4.9), respectively

or, after substituting  $V_1 = dC_1/dt$ ,  $V_2 = dC_2/dt$  and denoting  $[M_1]/[M_2] \equiv \alpha$  and  $[M_1]_0/[M_2]_0 \equiv \alpha_0$ , we will obtain an expression that is more convenient for comparison with data from Figs. 4.9, 4.10, 4.11, and 4.12:

$$V_1/V_2 = \frac{\alpha}{\alpha_0} \cdot \frac{r_1\alpha + 1}{r_2 + \alpha} \quad (4.5)$$

In linear form convenient for calculation of  $r_1$  and  $r_2$ , instead of Eq. (4.5), we have:

$$Y_{av} = r_1 - r_2 X_{av} \quad (4.6)$$

where:

$$X_{av} = (m_1/m_2)_{av} (M_2/M_1)_{av}^2 \quad (4.7)$$

$$Y_{av} = (m_1/m_2)_{av} (M_2/M_1)_{av} - (M_2/M_1)_{av} \quad (4.8)$$

$(m_1/m_2)_{av}$  calculated by Eq. (4.1).

Index “av” designates relationships of reacted and unreacted comonomers for averaged conversion calculated using the following equation:

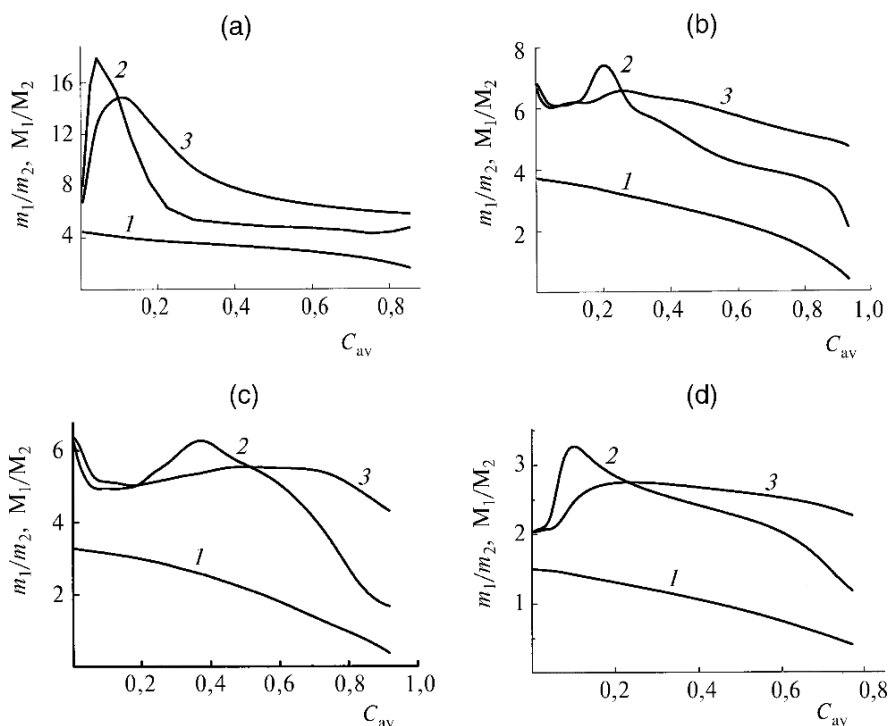


**Fig. 4.12** Variation of monomer mixture composition  $[M_1]/[M_2]$  (1) of instantaneous  $m_1/m_2$  (2) and integral  $(m_1/m_2)_\Sigma$  (3) copolymer composition during copolymerization of d-MMA ( $M_1$ ) and oligomer III ( $M_2$ ). Initial mixture composition  $[M_1]_0/[M_2]_0$ : (a) 4.47; (b) 3.73; (c) 3.28; (d) 1.5. Photoinitiator DMPA 0.6% (by weight).  $T = 20^\circ\text{C}$ . Calculation of  $m_1/m_2$ ,  $(m_1/m_2)_\Sigma$  and  $C_{av}$  by formulas (4.1), (4.2), and (4.9), respectively

$$C_{av} = (C_1[M_1]_0 + C_2[M_2]_0)/([M_1]_0 + [M_2]_0) \quad (4.9)$$

Current values of  $X_{av}$  and  $Y_{av}$  at any polymerization stage are easy to calculate based on data from Figs. 4.11 and 4.12 using formulas (4.7) and (4.8):

Integrating Eq. (4.5) in the region of low conversions, when  $\alpha$  can be assumed to be constant and equal to  $\alpha_0$ , we would obtain:

$$(m_1/m_2)_\Sigma \approx \frac{r_1 \alpha_0 + 1}{r_2 + \alpha_0} \cdot \alpha_0 \quad (4.10)$$

or

$$Y_i = r_1 - r_2 X_i \quad (4.11)$$

where  $X_i = (m_1/m_2)_\Sigma (M_2/M_1)_{i=0}^2$ ; and  $Y_i = (m_1/m_2)_\Sigma (M_2/M_1)_{i=0} - (M_2/M_1)_{i=0}$ .  $(m_1/m_2)_\Sigma$  is calculated using Eq. (4.2)

Using relationship (4.6) for determining  $r_1$  and  $r_2$  appears to be the most preferable, as this can be done based on data of a single experiment choosing any composition of initial mixture  $\alpha_0$ . However, it is necessary in this case that values  $r_1$

and  $r_2$  do not change with conversion. Attempts to construct linear dependence (4.5) based on data from Figs. 4.9, 4.10, 4.11, and 4.12 led to curves of complex shape. Only certain fragments of these curves (being rather long in some cases, within the range of  $C_i$  up to several dozen percent) had linear sections with absolute term  $r_1 = 1.5\text{--}2.5$  and slope  $r_2 = 0.2\text{--}0.8$  [published values averaged by several sources:  $r_1 = 2 \pm 0.5$  and  $r_2 = 0.5 \pm 0.2$  [9, 22] for the pair  $M_1 = \text{MMA}$ ,  $M_2 = \text{methyl acrylate (MA)}$ ]. The complex pattern of dependences  $Y_{\text{av}} = f(X_{\text{av}})$  indicates that values  $r_1$  and  $r_2$  in this case are not permanent in the course of the entire copolymerization process.

As a rule, relationship (4.10) is used to calculate  $r_1$  and  $r_2$ . The experiment in this case is interrupted at conversion  $C \approx 0.1$ , the copolymer is extracted, and its composition is analyzed. Then, the experimentally determined value  $(m_1/m_2)_\Sigma$  and initial value  $\alpha_0$  are placed in Eq. (4.10), the procedure is repeated for another composition of the initial mixture  $\alpha_0$ , and, thus, a system of two equations with two unknowns –  $r_1$  and  $r_2$  – is written down (obviously, for higher reliability one should not be limited with only two variants of  $\alpha_0$ ). Using this procedure for data from Figs. 4.11 and 4.12 [for each initial mixture having  $\alpha_0$  composition, we were choosing values  $(m_1/m_2)_\Sigma$  with  $C_{\text{av}} = 0.1\text{--}0.15$ ], we obtained values  $r_1$  and  $r_2$  that were also very close to published data ( $r_1 = 1.8\text{--}2.4$  and  $r_2 = 0.3\text{--}0.6$ ). In other words, if we use the commonly accepted method for  $r_1$  and  $r_2$  determination only, we would obtain values corresponding to data published in reference books. Within the framework of the method enabling us to monitor the copolymer composition continuously during the entire process, one would find inconsistency of  $r_1$  and  $r_2$  values in the course of polymerization process disturbing our confidence in the reliability of reference values of  $r_1$  and  $r_2$  as a macromolecular design tool. Results presented in Figs. 4.11 and 4.12 give grounds to question the practical importance of efforts spent on determination of  $r_1$  and  $r_2$ .

As applied to issues of macromolecular design of copolymers (and, specifically, cross-linked copolymers), data such as those presented in Figs. 4.11 and 4.12 are the most useful and informative. Indeed, if one averages data of two concurrent measurements (made at different IR frequencies; see Fig. 4.10b,d), then within the limits of experimental error, it would appear that the composition of the initial mixture  $[M_1]_0/[M_2]_0 \equiv \alpha_0 \approx 1.6$  meets the “azeotropicity” requirements, according to which the initial mixture composition is not different from copolymer composition  $\alpha_0 \approx m_1/m_2$  and, therefore, at all transformation stages within range  $0 < C_{\text{av}} < 1$  the composition of copolymer and that of reaction mixture should remain constant (of course, only subject to the condition that is often taken for granted, groundlessly, that in this case  $r_1$  and  $r_2$  keep constant numeric values). It can be seen from Fig. 4.10(b,d) that in our case copolymerization system “azeotropicit” does not ensure constancy of copolymer composition: the latter starts changing according to complex regularity even at low conversions. From Eq. (4.4) we derive that the azeotropic composition of initial mixture  $(\alpha_0)_a$  is described with the following relationship:

$$(\alpha_0)_a = \sqrt{0,25(r_2 - r_1)^2 + 1} + 0,5(r_2 - r_1) \quad (4.12)$$

Value  $(\alpha_0)_a = 1.6$ , found from averaging data from Fig. 4.10b,d, corresponds, according to Eq. (4.10), to value  $|r_2 - r_1| \approx 1$ , which conforms rather well with published data  $r_1 = 2 \pm 0.5$ ,  $r_2 = 0.5 \pm 0.2$ .

Therefore, when using conventional approaches, the obtained results for low conversions ( $C \rightarrow 0$  and  $C \approx 0.1$ ) agree well with known values of  $r_1$  (methacrylate), and  $r_2$  (acrylate). However, the full system of data presented in Figs. 4.9, 4.10, 4.11, and 4.12 strongly suggests that values of copolymerization constants for chemical design of macromolecular structures could be used only if they are actually constants. Otherwise, one would require the information such as that provided in Figs. 4.9, 4.10, 4.11, and 4.12. It should be borne in mind that virtually all  $r_1$  and  $r_2$  indicated in published sources [9, 22] were not tested as constants truly retaining constant value during copolymerization. Also, in many cases available data indirectly prove the contrary.

It follows from the above-presented results that data on kinetics of individual consumption of reaction mixture components  $M_1$  and  $M_2$  represent the most reliable basis for macromolecular design of copolymers (in particular, cross-linked copolymers), rather than the  $r_1$  and  $r_2$  values presented in reference publications. The authors believe that an extremely minimized program for obtaining basic kinetic data for macromolecular design of cross-linked copolymers should include kinetic studies, enabling us to make judgments about both overall conversion and individual conversion of each of the comonomers.

## References

1. Rostchupkin VP, Kurmaz SV (2004) *Russ Chem Rev* **73**:247–274
2. Matsumoto A (1995) *Adv Polym Sci* **123**:41–80
3. Dušek K (1993) *Collect Czech Chem Commun* **58**:2245–2265
4. Korolev GV, Bubnova ML, Makhonina LI, Bakova GM (2005) *Vysokomolekul Soedin A* **47**:1086–1097 (in Russian)
5. Korolev GV, Baturina AA, Berezin MP, Kurmaz SV (2004) *Vysokomolekul Soedin A* **46**:656–667 (in Russian)
6. Korolev GV, Bubnova ML, Makhonina LI, Bakova GM. (2005) Deformation and fracture of materials #11:2–7 (in Russian)
7. Korolev GV, Bubnova ML, Makhonina LI, Bakova GM (2006) *Vysokomolekul Soedin A* **48**:632–645 (in Russian)
8. Karapetyan ZA, Smirnov BR (1987) *Vysokomolekul Soedin A* **29**:2102–2109 (in Russian)
9. Lipatov YuS, Nesterov AE, Gritsenko TM, Veselovskiy RA (1971) Reference book on chemistry of polymers. Naukova Dumka, Kiev (in Russian)
10. Houben-Weyl. (1955) *Methoden der Organischen Chemie*. Georg Thieme Verlag, Stuttgart B 3/1:S188
11. Berlin AA, Kefeli TYa, Korolev GV (1967) *Poly-esteracrylates*. Nauka, Moscow (in Russian)
12. Berlin AA, Korolev GV, Kefeli TYa, Sivergin YuM (1983) *Acrylic oligomers and materials on the acrylic oligomers*. Khimiya, Moscow (in Russian)
13. Korolev GV, Mogilevich MM, Golikov IV (1995) *Cross-linked polyacrylates: micro-heterogeneous structures, physical networks, deformation-strength properties*. Khimiya, Moscow (in Russian)

14. Korolev GV (1977) Papers for the 1st All-Union Conference on Chemistry and Physical Chemistry of Polymerized Oligomers, vol. 1. Department of the Chemistry and Physics Institute of the USSR Academy of Science, Chernogolovka (in Russian)
15. Korolev GV (2003) *Russ Chem Rev* **72**:222–244 (in Russian)
16. Plate NA, Ponomarenko AG (1974) *Vysokomolek Soedin A* **16**:2635–2645 (in Russian)
17. Kurmaz SV, Tarasov VP, Berezin MP, Rostchupkin VP (2000) *Vysokomolek Soedin A* **42**:1637–1646 (in Russian)
18. Berlin AA, Volfson SA, Enikolopyan NS (1978) Kinetics of polymerization processes. Khimia, Moscow (in Russian)
19. Korolev GV, Mogilevich MM, Ilyin AA (2002) Association of liquid organic compounds. Mir (World), Moscow (in Russian)
20. Korolev GV, Boichuk IN, Ilyin AA, Mogilevich MM (2001) *Vysokomolek Soedin A* **43**:713–721 (in Russian)
21. Bagdasaryan XS (1966) Radical polymerization theory. Nauka, Moscow (in Russian)
22. Ham G (1971) Copolymerization. Khimia, Moscow (Russian translation)

# Chapter 5

## Critical Conversion (Gel Point) in Three-Dimensional Free-Radical Polymerization

**Abstract** A new approach for the calculation of critical conversion for three-dimensional free-radical polymerization (TFRP) is proposed and described in Chap. 5. This approach implies the use of moments in numeric form and generalization of obtained results as formulas for different conditions of TFRP. Derived formulas enabled the authors to present actual TFRP processes (that differ by constants of elementary acts) as master curves with generalized coordinates. Calculation results are compared both with the author's data and published experimental data on inhibited polymerization of dimethacrylates and on copolymerization of divinyl benzene and styrene. The authors also clarified and substantiated a conclusion on incorrect application of TFRP critical conversion calculation methods using the Flory and Stockmayer formulas for critical conversion in the case of polycondensation.

Gel formation theory developed in the work of Flory and Stockmayer [1, 2] as applied to network formation processes proceeding according to the polycondensation mechanisms was groundlessly extended to network formation processes that develop according to the mechanisms of radical polymerization. The observed discrepancy between theoretically calculated values of critical conversion  $\alpha_{cr}$  (also called gel point) and experimentally measured values  $(\alpha_{exp})_{cr}$  was usually explained by secondary process of minor cycles formation (cyclization), the contribution of which is especially high in the case of three-dimensional free-radical polymerization (TFRP) for certain reasons. However, only in very recent times have researchers managed to implement such TFRP processes, to which the contribution of cyclization is negligibly small: these are TFRP in the living chains mode and copolymerization of network-forming (polyunsaturated) monomers,  $M_p$ , and with monounsaturated (non-network-forming) monomers  $M_m$ , with the proportion of components  $M_p$  to  $M_m$  exceeding a certain critical value  $(M_m/M_p)_{cr}$ . The discrepancy between theoretical and experimental data observed in these processes could no longer be explained by cyclization; it became evident that these discrepancies represent the result of wrongly extending the Flory–Stockmayer approaches to the field of TFRP.

This situation gave rise to the necessity of developing new approaches intended specifically for TFRP. One of such approaches was proposed and developed in

2001–2002 [3–7]. The task was accomplished using the method of moments in numeric form with subsequent generalization of obtained results as formulas relating the value of  $\alpha_{cr}$  with constants of initiation rate, propagation rate, transfer rate, and termination rate (linear and quadratic) of chains, with initial concentrations of initiator, transfer agent, and functionality of monomer mixture. The case of polymerization with varying reactivity of functional groups in the course of reaction was analyzed. Limits of applicability of analytical expressions are specified. A comparison of  $\alpha_{cr}$  values calculated based on these expressions,  $(\alpha_1)_{cr}$  values and  $(\alpha_2)_{cr}$  values concurrently calculated according to Flory–Stockmayer with experimental data,  $(\alpha_{exp})_{cr}$ , showed that when the conditions of the experiment were changed toward minimization of contribution made by secondary processes of cyclization, the values of  $(\alpha_1)_{cr}$  become closer and closer to those of  $(\alpha_{exp})_{cr}$ , becoming in the end equal to them. Also, the values of  $(\alpha_2)_{cr}$  at first become close to those of  $(\alpha_{exp})_{cr}$ , and then the discrepancy is observed again; this indicates the higher degree of reliability of the new approach as compared to the known Flory–Stockmayer approach as applied to the processes of network forming that develop according to the TFRP mechanism.

The value of critical conversion  $\alpha_{cr}$  in the case of formation of cross-linked polymers (the so-called gel point) characterizing the transition of the system from the fluid state to the state with an equilibrium elasticity modulus represents an important parameter of the system from both the technological and theoretical standpoints [8–10]. Formation of an insoluble gel could lead to difficulties in technological processes for polymer production, and contrariwise, association of the critical conversion value with structural and kinetic parameters of the process determines the possibility of obtaining a cross-linked polymer with required physical and mechanical characteristics. From the theoretical standpoint, the gel point determines the percolation threshold in a polymer system being formed, and identification of the dependency of this value upon kinetic and structural characteristics is an important problem.

Calculations intended for finding  $\alpha_{cr}$  became especially important most recently, when starting from the beginning of the 1990s a specific trend in the field of three-dimensional polymerization—namely, synthesis, studying of properties, and extensive technological application of hyper-branched polymers (HBP), which are analyzed in detail in Chaps. 7 and 8—started developing quite rapidly. In this case, when optimizing the HBP synthesis processes, one should be able not only forecast numeric values of  $\alpha_{cr}$  in each particular case (when conversion exceeds  $\alpha_{cr}$ , HBP molecules lose their specific topological structure and their previous features preconditioned by it, being transformed into cross-linked macromolecules), but also to purposefully change the conditions of synthesis toward increasing  $\alpha_{cr}$  (ideally up to 1, which ensures the highest possible yield of HBP, equal to 100%). It is evident that such purposefulness is possible only in the case when quantitative relationships are known, which associate the experimentally regulated parameters (initiation rate, concentration of chain transfer agents, ratio of concentration of mono- to polyunsaturated monomers in the initial mixture, and the like) with the value of  $\alpha_{cr}$ . Of special value in this case are the analytical expressions obtained by the authors [3–7], the results of which are given below in generalized form.

## 5.1 Inapplicability of Known Critical Conversion Calculation Methods to Three-Dimensional Free-Radical Polymerization

The problem of finding the critical conversion value  $\alpha_{cr}$  was solved by Flory and Stockmayer [1, 2] for polycondensation reactions that could be presented by the following scheme:



where a bond is formed as a result of reaction between functional groups A and B. This reaction could be accompanied (or not accompanied) by the release of by-products, and groups A and B could be different or identical. If the number of functional groups per one molecule of initial reagents exceeds two [i.e., if  $R_1A_n$  and  $R_2B_m$  will be in formula (5.1) instead of  $AR_1A$  and  $BR_2B$ ], the formation of branched and cross-linked polymers is possible. At a certain conversion, the highest (starting from the second) moments of macromolecule distribution according to molecular weight are converted into infinity. This value of conversion is mathematically defined as critical. Experimentally it is obtained from data on viscosimetry (viscosity tends to infinity) or relaxation measurements (appearance of equilibrium elasticity modulus). Recently, a method for finding the gel point that uses data of frequency dependence of the relaxation modulus became very popular [11]: it is thought that the equality of values  $G'(\omega)$  and  $G''(\omega)$  corresponds to critical conversion.

The value of critical conversion and network structure is determined by the character of initial reagent distribution with function groups [12]. This character could be expressed by values of number-averaged functionality  $\bar{f}_n$  and weight-averaged functionality  $\bar{f}_w$  [9–12]:

$$\bar{f}_n = \frac{\sum_i i m_i}{\sum_i m_i}, \quad \bar{f}_w = \frac{\sum_i i^2 m_i}{\sum_i i m_i}$$

where  $m_i$  is the concentration of initial reagents having  $i$  functional groups.

For polycondensation with uni-type functional groups, the theory yields [1, 2]:

$$\alpha_{cr}(\bar{f}_w - 1) = 1 \quad (5.2)$$

In the case of functional groups of different types:

$$\alpha_{cr}^2 r (\bar{f}_{Aw} - 1)(\bar{f}_{Bw} - 1) = 1 \quad (5.3)$$

where  $r$  = relationship of concentrations of mutually interacting functional groups:

$$r = \frac{\sum_i i m_{ai}}{\sum_j j m_{bj}} < 1$$

Indices  $A$  and  $B$  refer to functional group type.



A special case is the reaction of cross-linking of polymer chains. Usually critical conditions are expressed in the following way:

$$\alpha_{cr}(\bar{P}_w - 1) = 1 \quad (5.4)$$

where  $\bar{P}_w$  is the weight-averaged degree of polymerization of cross-linked macromolecules.

It is assumed in this case (implicitly) that any polymer chain unit could take part in the cross-linking reaction.

Formulas (5.2)–(5.4) were obtained both by statistic method and by kinetic calculation method [8–10], and later they were verified experimentally. The absence of intramolecular reactions (reactions between groups belonging to one and the same macromolecule) represents a condition of their applicability.

To describe the three-dimensional polymerization processes that could be schematically presented in the following form,



where M is monomer;  $\sim R_i^\bullet$  is the active chain (index  $i$  stands for the number of monomer units in the chain), formula (5.4) is usually used.

In this case,  $\alpha_{cr}$  is understood as the value of critical branching introduced by Flory and Stockmayer [1, 2]. The relationship between  $\alpha_{cr}$  and conversion is found via solving kinetic equations for consumption of monomer functional groups [13]. Thus, the calculation is based on probabilistic considerations, which have quite restricted applicability to polymerization processes [8–10]. Kinetic calculation of gel point was proposed earlier reports [10, 14–16]. In these publications, the calculation of gel point was based on the condition  $dN/dt = 0$ , or, to be more exact, the number of chains  $N$  is practically equal to 0. It is evident that increased values should be obtained in this case, because (as with polycondensation) the infinite value of second moments of distribution with molecular weights (and, consequently, with functional groups) is attained at lower conversions than attainment of zero concentrations of polymer chains [1, 9, 10].

The correct condition of requirement for infinity of second moment in molecular weight distribution has been reported [10, 17]. Similar expressions were obtained in this case, the form of which appeared to be close to (5.4)

$$\alpha_{cr} = \frac{(k_{ter}W_i)^{1/2}}{(n-1)k_{pr}M_0} \quad \text{and} \quad \alpha_{cr} = \frac{[(k_{ter} + k_{ter1})R + k_{trM}M]^2}{k_{pr}M[(3k_{ter} + 2k_{ter1})R + 2k_{trM}M]}$$

However, the chain length in this case was found through kinetic parameters of the polymerization process: initiation rate  $W_i$ , constant of propagation reactions  $k_{pr}$ , constant of chain termination through disproportioning  $k_{ter1}$  and recombination  $k_{ter}$ , and chain transfer  $k_{trM}$  through monomer and monomer functionality  $n$ . We emphasize that in the second case the conversion is understood as conversion depth in terms of a monomer, not in terms of functional groups. Besides, it was noted that the reduced analytical form could be obtained only under special conditions.

These formulas were not verified experimentally, but their truthfulness was not questioned because it is well known that conditions of their agreement with three-dimensional polymerization are not implemented [9, 10]: due to rapid propagation of the chain with the radical mechanism and low concentration of chains at initial stages of the process, the intramolecular cyclization reaction proceeds quite intensively [9, 18]. In this case, repeated cross-linking within one and the same pair of chains (formation of multiplet junctions and ladder macromolecular structures) is considered to be the factor, which reduces the effective concentration of interchain cross-links, thus increasing the value of critical conversion. Because of this, the microheterogeneous character of the process is typical for radical polymerization [19–24].

At the same time, from the kinetics standpoint, the polymerization reaction differs quite radically from the polycondensation reaction [9]. As can be seen from comparison of schemes (5.1) and (5.5), in the first case two functional groups are consumed during the reaction, while in the second case only one is consumed, and the concentration of active centers is not changed in this reaction. Therefore, it is sufficient to have one functional group in the monomer molecule to obtain a polymer chain via polymerization, while the monofunctional monomer terminates the chain in the polycondensation reaction. This circumstance raises doubts about the applicability of approaches developed for polycondensation to polymerization processes.

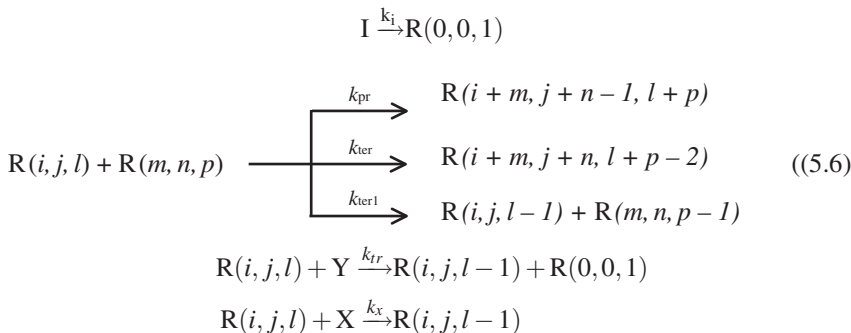
On the other hand, the research in living free-radical three-dimensional polymerization [24] showed that in this case the relationship (5.4) is also not satisfied [25], although the cyclization reaction does not play a significant role and the microheterogeneous character of the process does not manifest itself [25, 26].

These considerations served as a ground for formulating the problem, namely, finding critical conditions (gel point) for three-dimensional free-radical polymerization [3–7]. The solving of this problem is given below.

## 5.2 Novel Approach to Calculating Critical Conversion in Three-Dimensional Free-Radical Polymerization

Polymer chain in linear polymerization could be characterized by a single value, i.e., by degree of polymerization, distinguishing thereby between living (active) and terminated chains. With three-dimensional polymerization, the formed macromolecule has a certain number of nonreacted functional groups (pendent double bonds) and two or more active centers in addition to a certain number of monomer units. Thus, any chain should be described at least using three values:  $i$  monomer units,  $j$  functional groups, and  $l$  active centers, i.e., the vector notation  $R(i, j, l)$  should be introduced for such chains.

The next scheme represents a process of radical polymerization in its simplest case, which takes into account only initiation, propagation, transfer on agent X, and quadratic and linear (on agent Y) termination of chains:



where I = initiator; R(0,0,1) = primary radical; monomer units  $k_i, k_{pr}, k_{ter}, k_{ter1}, k_{tr}, k_x$  = constants of rate of reactions for initiation, propagation, termination through recombination and termination through disproportioning, transfer of chain on agent Y, and linear termination on inhibitor X, respectively.

The system of differential equations describing the process takes the following form:

$$\begin{aligned}
 \frac{dI}{dt} &= -k_i I \\
 \frac{dR(0,0,1)}{dt} &= k_i I - R(0,0,1)(k_{pr}F + k_{tr}Y + k_{ter}R + k_x X) + k_{tr}YR \\
 \frac{dR(i,j,l)}{dt} &= -R(i,j,l)[k_{pr}(IF + jR) + l(k_{tr}Y + k_{ter}R)] + \\
 & R(i,j, l+1)(k_x X + k_{tr}Y) + k_{pr} \sum_{m,n,p}^{i,j,l} [n(k-p)R(i-m, j-n+1, l-p) \\
 & - p(j-n-1)R(i-m, j-n-1, l-p)]R(m,n,p) \quad (5.7)
 \end{aligned}$$

where  $i, j, l = 0,1,2,3, \dots$ ; F = overall concentration of functional groups in the system; and R = overall concentration of active centers.

For the sake of simplicity, an assumption was made that initiation is carried out via monomolecular decomposition of initiator I, and the reactivity of functional groups does not depend upon macromolecular size and chemical complexity. The reactivity of active centers in the reactions of propagation, transfer, and termination of chain is also independent upon this factor. Only the termination through recombination is taken into account in the scheme.

To solve the system (5.7), it is convenient to use the method of generating functions [9, 10]. The generating function in the case under consideration takes the following form:

$$F(\vec{q}) = \sum_i \sum_j \sum_l q_1^i q_2^j q_3^l R(i,j,l) \quad (5.8)$$

where vector,  $\vec{q} \equiv \{q_1, q_2, q_3\}$ ,  $q_i$  = arbitrary variables, and  $q_1$  characterizes the macromolecule by its monomer units,  $q_2$  by functional groups, and  $q_3$  by active centers.

Differentiation of Eq. (5.8) by  $q_i$  with subsequent equating of all  $q_i$  to 1 gives the moments of generating function (5.8):

$$N = F(\vec{1}) = \text{overall concentration of chains (zero moment)}$$

first moments:

$$M = \frac{\partial F(\vec{1})}{\partial q_1} = \sum_{i,j,l} iR(i,j,l) = \text{overall concentration of monomer units in the system}$$

$$F = \frac{\partial F(\vec{1})}{\partial q_2} = \sum_{i,j,l} jR(i,j,l) = \text{overall concentration of functional groups}$$

$$R = \frac{\partial F(\vec{1})}{\partial q_3} = \sum_{i,j,l} lR(i,j,l) = \text{overall concentration of active centers}$$

and second moments =  $F_{ij} \equiv F_{ij}(\vec{1}) = \frac{\partial^2 F(\vec{q})}{\partial q_i \partial q_j}$  when  $\vec{q} = \vec{1}$ .

$$F_{11} = \sum i(i-1)R(i,j,l); F_{12} = \sum ijR(i,j,l); F_{13} = \sum ilR(i,j,l);$$

$$F_{22} = \sum j(j-1)R(i,j,l); F_{23} = \sum jlR(i,j,l); F_{33} = \sum l(l-1)R(i,j,l).$$

Substitution of (5.7) into (5.8) gives:

$$\begin{aligned} \frac{\partial F(\vec{q})}{\partial t} = & k_i q_3 I + k_{pr} \left[ q_3 \cdot \frac{\partial F(\vec{q})}{\partial q_2} \cdot \frac{\partial(\vec{q})}{\partial q_3} - q_3 F \cdot \frac{\partial F(\vec{q})}{\partial q_3} - q_2 R \cdot \frac{\partial F(\vec{q})}{\partial q_2} \right] \\ & + (k_x X + k_{tr} Y)(1 - q_3) \frac{\partial F(\vec{q})}{\partial q_3} + k_{ter} \left[ \frac{1}{2} \cdot \frac{\partial F(\vec{q})}{\partial q_3} - q_3 R \right] \frac{\partial F(\vec{q})}{\partial q_3} \end{aligned} \quad (5.9)$$

Differentiation of Eq. (5.9) for all  $q_i$  with subsequently equating them to 1 gives a system of differential equations for moments of generating function and, hence, for moments of distribution of macromolecules in terms of length, chain functionality, and number of active centers. It is obvious that all these values are functions of time.

The system of differential equations for the moments has the following form:

$$\begin{aligned} dI/dt &= -k_i I \\ dN/dt &= k_i I - k_{pr} FR - 1/2 k_{ter} R^2 - k_x X \\ dM/dt &= 0 \\ dF/dt &= -k_{pr} FR \\ dR/dt &= k_i I - k_{ter} R^2 - k_x X \\ dY/dt &= -k_{tr} YR \\ dF_{11}/dt &= 2k_{pr} F_{12} F_{13} + k_{ter} (F_{13})^2 \\ dF_{12}/dt &= k_{pr} (F_{13} F_{22} + F_{12} F_{23} - R F_{12}) + k_{ter} F_{13} F_{23} \\ dF_{13}/dt &= k_{pr} (F_{13} F_{23} + F_{12} F_{33} + R F_{12}) - (k_{tr} Y + k_x X) F_{13} + k_{tr} (F_{33} - R) F_{13} \end{aligned} \quad (5.10)$$

$$\begin{aligned}dF_{22}/dt &= 2k_{pr}(F_{22}F_{23} - RF_{22}) + k_{ter}(F_{23})^2 \\dF_{23}/dt &= k_{pr}((F_{23})^2 + F_{22}F_{33} - RF_{23} + RF_{22}) - (k_X X + k_{TR} Y)F_{23} \\&\quad + k_{ter}(F_{33} - R)F_{23} \\dF_{33}/dt &= 2k_{pr}F_{23}(F_{33} + R) - 2(k_X X + k_{tr} Y)F_{33} + k_{ter}(F_{33} - 2R)F_{33}\end{aligned}$$

Solving the system (5.10) enables us to obtain full information on the course of polymerization process, including the value of critical conversion.

As mentioned above, the conversion into infinity of the second moment of molecular weight distribution represents a mathematical criterion for network polymer formation. However, as can be seen from formulas (5.2) and (5.3) and as follows from the physical meaning of the gel formation process, functionality distribution is the determining factor. In terms of moments of generating function, it will be the value of the second moment of generating function in terms of functionality,  $F_{22}(t) = \sum_{i,j,l} j(j-1)R(i,j,l)$ .

Results of calculations for specific TFRP processes are given below.

### 5.3 Results of Critical Conversion Calculation for Different Cases of Three-Dimensional Free-Radical Polymerization

#### 5.3.1 Living Chains Three-Dimensional Polymerization and Copolymerization (Without Chain Termination) [5]

Figure 5.1 shows curves of variation of value  $F_{22}(t)^1$  in the course of the living polymerization process (no reactions of initiation, chain transfer, and termination,  $k_i = k_{tr} = k_{ter} = k_X = 0$ ) on the condition of instantaneous initiation. As can be seen,  $F_{22}(t)$  increases by orders of magnitude in an extremely narrow range of conversions, demonstrating that it tends to infinity. Thus, without any risk of significant error, the value, which is marked on the abscissa by the asymptote to the curve  $F_{22}(t) - \alpha$ , could be taken as the critical conversion value. As computations show (Table 5.1), the critical conversion value  $\alpha_{cr}$  (thus obtained) for the selected value of concentration of active centers  $I_0$  is a single-value function of the initial value of parameter  $F_{22}(0)$  and does not depend upon initial concentration of functional groups  $F(0)$ .

Dependence of  $\alpha_{cr}$  upon  $F_{22}(0)$  for the case of living polymerization with instantaneous initiation is presented in Fig. 5.2.

As is seen, this dependence adheres to the root law, and straight lines relating to different values of active centers concentration are parallel to one another. Analysis

<sup>1</sup>  $F_{22}$  – second moment of functionality distribution of initial monomer molecules at time moment  $t = 0$ ,  $F_{22} \equiv F_{22}(0) = \sum_i i(i-1)m_i$ , where  $m_i$  – initial molar concentration of  $i$ -functional monomer,  $i$  – number of double bonds in  $i$ -monomer molecule. For example, for copolymerization of dimethacrylates  $M_2$  with methacrylates  $M_1$ ,  $F_{22} = 2(2-1)[M_1] + 1(1-1)[M_1] = 2[M_1]$ .

**Fig. 5.1** Kinetic curves for variation of the second moment of functionality distribution  $F_{22}(t)$  in living polymerization at instantaneous initiation.

$I_0 = 10^{-3}$  mol/l.

$F_{22}(0) = 20(1); 5(2); 1(3); 0.5(4);$  and  $0.1$  mol/l(5)

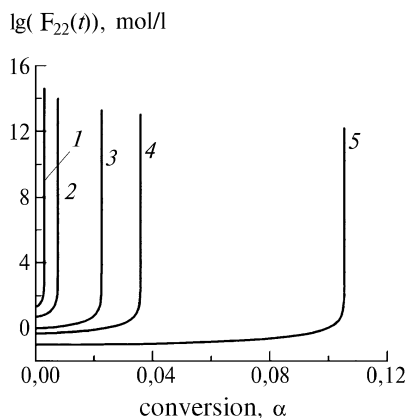


**Table 5.1** Dependence of critical conversion value upon monomer functionality distribution

$F(0)$ , mol/l	$F_{22}(0)$ , mol/l	$\alpha_{cr}$	$F(0)$ , mol/l	$F_{22}(0)$ , mol/l	$\alpha_{cr}$
20	0.2	0.0708	10	20	0.0071
20	2.0	0.0224	2	0.2	0.0708
20	20	0.0071	2	2.0	0.0224
10	0.2	0.0708	2	20	0.0071
10	2.0	0.0224	—	—	—

Note 1. Living polymerization with instantaneous initiation;  $I_0 = 10^{-3}$  mol/l.

Note 2.  $F(0)$  = initial concentration of functional groups.

Note 3.  $F_{22}(0)$  = second moment of functionality distribution of initial monomer molecules.

shows that the value of critical conversion in the case under consideration is described by the following formula:

$$\frac{\alpha_{cr}^2 F_{22}(0)}{I_0} = 1 \quad (5.11)$$

To a certain extent, the truthfulness of relationship (5.11) is verified by experimental data obtained by Ide and Fukuda [26] (Fig. 5.2):  $(\alpha_{cr}^2 F_{22}(0))/I_0 \approx 0.2$ . A certain discrepancy is probably explained by the fact that first, Ide's publication [26] deals with radical living polymerization and there are no data about the concentration of the chains (if it is equal to initiator concentration), and second, according to the critical conversion determination method, the value of critical conversion found experimentally could be lower than the theoretical value [27].

In terms of external view, formulas (5.11) and (5.2) look similar. Indeed, if we take into account that  $F_{22}(0)/F(0) = \bar{f}_w - 1$ , formula (5.11) can be transformed into the following:

$$\alpha_{cr}^2 r (\bar{f}_w - 1) = 1 \quad (5.11a)$$

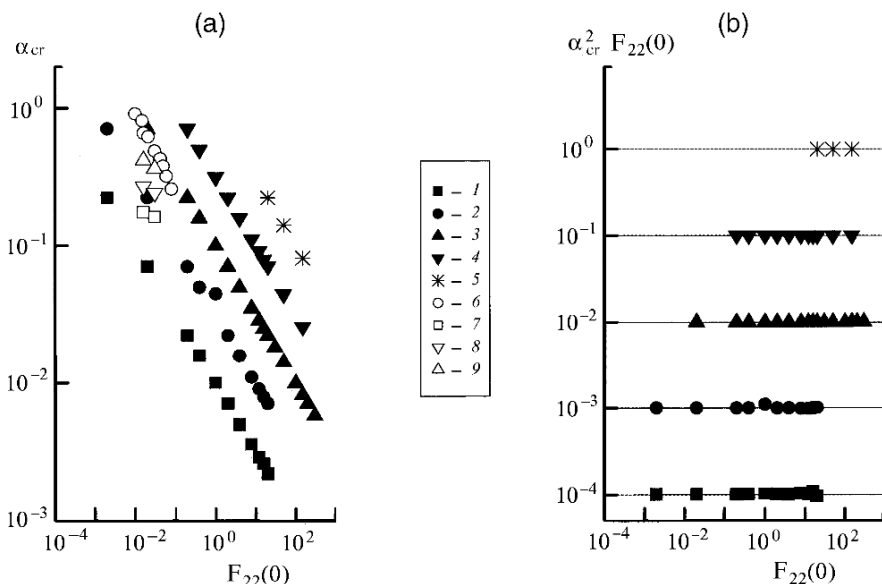


**Fig. 5.2** Dependence of critical conversion value  $\alpha_{cr}$  (a) and function  $\alpha_{cr}^2 F_{22}(0)$  (b) upon  $F_{22}(0)$  in living polymerization with instantaneous initiation.  $I_0 = 10^{-4}$  (1);  $10^{-3}$  (2);  $10^{-2}$  (3); 1 (5); 0.023 (6); 0.0061 (7); 0.0099 (8); and 0.034 mol/l (9). 1–5, calculation results; 6–9, data from Ide and Fukuda [26]

However, in this case we have similarity of appearance because the value of  $r$  (which is the ratio of concentration of functional groups to that of active centers) is much higher than 1; in formula (5.3), in contrast,  $r < 1$ . Besides, a multiplier is missing, which characterizes the functionality distribution of the second reagent (active centers). Taking into account the aforementioned circumstance that initial molecules of active centers are multifunctional [ $(R(0,0,1)/I_0 = 1)$ ] and are not consumed in the polymerization reaction process, this multiplier cannot be found. Thus, the origin of the second degree with critical conversion value from formula (5.11) is determined not by the fact that two functional groups react simultaneously, as in Eq. (5.3), but is most likely associated with the fact that a condition for critical point attainment consists in the necessity that a reaction of at least two groups belonging to polyfunctional monomers (i.e., monomers that produce branching molecules) should take place per one chain. Certainly this criterion is essentially different from condition (5.3).

An empirical relationship that is close to Eq. (5.11) in terms of form was obtained after solving the problem on radical copolymerization of mono- and bifunctional monomers using the Monte Carlo method [28]. The difference lies in the fact that the exponent was somewhat different from 2, and the value of relative concentration of a branching (i.e., bifunctional) comonomer was used instead of the second moment of functionality. The first distinction can be easily explained by the fact that polymerization process modeling allows taking the cyclization reaction

into account. Therefore, gel point should be shifted in the direction of higher conversions as compared to the gel point calculated analytically. As for the second value, i.e., molar fraction of branching comonomer, its use has no substantiation at all. Price [28] came to the conclusion that the obtained relationship conforms to Flory–Stockmayer ideas. However, quite to the contrary, the calculation given in this publication attests that the conformity is lacking.

Analysis of polymerization processes proceeding by a more complex mechanism confirms the latter conclusion. Figure 5.3 shows the results for living polymerization subject to condition of slow initiation ( $k_i \neq 0$ ,  $k_X = k_{ter} = k_{tr} = 0$ ) [5]. As can be seen, the relation between  $\alpha_{cr}$  and  $F_{22}(0)$  is expressed in the form of parallel straight lines in the logarithmic scale, thus demonstrating the presence of relationship  $\alpha_{cr} \approx [F_{22}(0)]^{-0.67}$  with a shift along the axis of ordinates depending upon the initiation rate. All results are described by relationship (5.12) with a high degree of accuracy:

$$\alpha_{cr}^3 \cdot \frac{k_{pr} F_{22}^2(0)}{k_i I_0} = 1 \quad (5.12)$$

However, it is obvious that this result is in no way interrelated with formulas (5.2) and (5.3). At the same time both formulas, namely, (5.11) and (5.12), correlate the critical conversion value with the weight-averaged functionality of the initial mixture of monomers assigned to the concentration of chains (Eq. (5.11)) or rate of chains accumulation (Eq. (5.12)). This regularity also manifests itself in the case

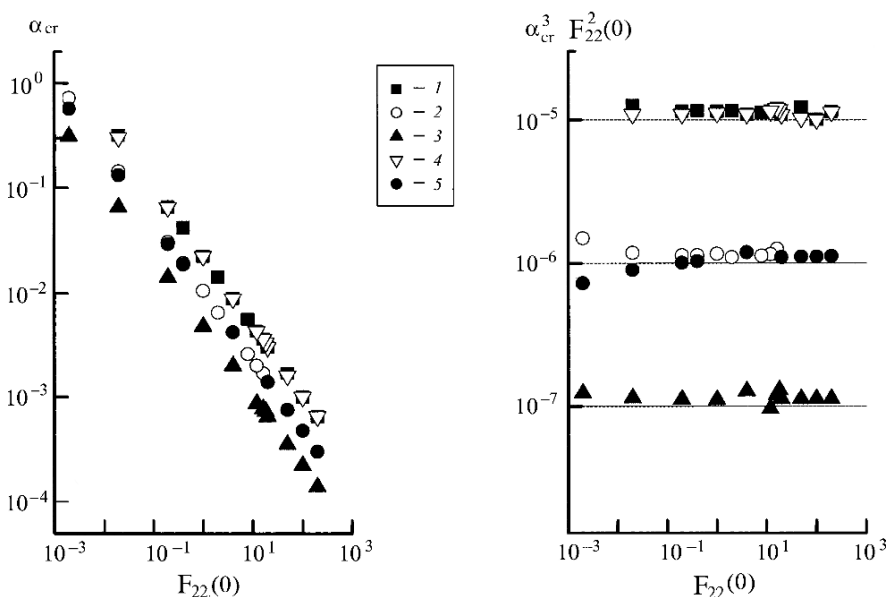


**Fig. 5.3** Dependence of critical conversion value  $\alpha_{cr}$  (a) and function  $\alpha_{cr}^3 F_{22}^2(0)$  (b) of  $F_{22}(0)$  in living polymerization for the case of slow initiation  $I_0 = 1$  (1);  $10^{-1}$  (2);  $10^{-2}$  (3,4); and  $10^{-3}$  mol/l (5).  $k_i/k_{pr} = 10^{-5}$  (1–3) and  $10^{-3}$  mol/l (4,5)



when the chains concentration is determined by a more complex mechanism, i.e., by chain transfer reaction or chain termination reaction.

It should be pointed out that both formulas (5.11) and (5.12) represent examples of limiting cases obtained from a more general expression for  $W_i \rightarrow \infty$  (instantaneous initiation) or  $W_i \rightarrow 0$  (slow initiation).

The following formula could be an example of this:

$$\frac{\alpha_{cr}^2 F_{22}(0)}{I_0} = 1 - \exp \left[ - \frac{k_i}{k_{pr} \alpha_{cr} F_{22}(0)} \right] \rightarrow \begin{cases} 1 & \text{at } k_i \rightarrow \infty \\ \frac{1}{k_{pr} \alpha_{cr} F_{22}(0)} & \text{at } k_i \rightarrow 0 \end{cases}$$

However, the absence of analytical solution for system (5.10) does not give the possibility to obtain this result in explicit form. The numeric calculation [4], the results of which are given in Fig. 5.4, shows that formula (5.11) is true when  $k_i / (k_{pr} \alpha_{cr} F_{22}(0)) \geq 6$ . If  $k_i / (k_{pr} \alpha_{cr} F_{22}(0)) < 1$ , the critical conversion value is found from expression (5.12). The term “instantaneous initiation” should be assigned to the case when ratio  $k_i / k_{pr} > 0.1 \text{ mol/l}$ .

Kinetic solution of the problem on living polymerization with slow initiation is given by Dušek and Somvarsky [29]. It is shown in this publication that the proposed approach leads to results that are different from those provided by statistic solution. However, calculations carried out with the use of system (5.10) (taking into account that initiation proceeds with interaction between initiator and functional group) give a different result, as it is seen from the data listed in Table 5.2.

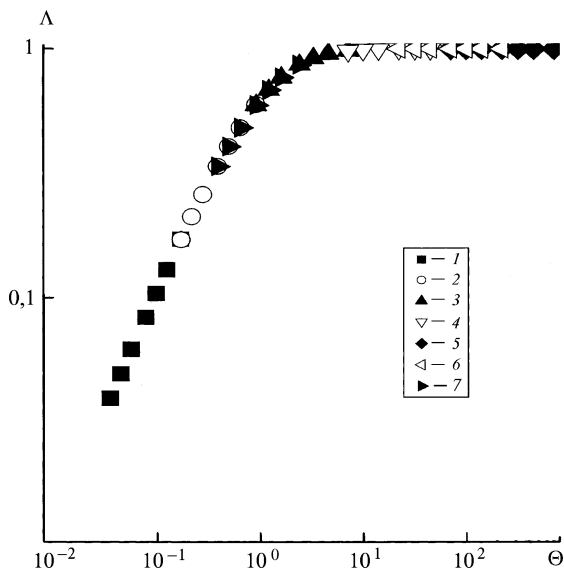


**Fig. 5.4** Dependence of critical conversion value  $\alpha_{cr}$  upon initiation rate in living polymerization in generalized coordinates. The curve shows areas of validity of dependences (5.10) and (5.11).  $\Lambda = \alpha_{cr}^2 F_{22}(0) / I_0$ ;  $\Theta = (k_i / k_{pr}) \alpha_{cr} F_{22}(0)$ ;  $\lg(k_i / k_{pr}) = -5$  (1);  $-4$  (2);  $-3$  (3);  $-2$  (4);  $-1$  (5);  $0$  (6); and  $1$  (7)

**Table 5.2** Comparison of results obtained in reference [29] with calculations performed according to the modified scheme (5.9a)

$k_i/k_{pr}$	0.01		0.1		1.0		10	
	[29]	(5.9a)	[29]	(5.9a)	[29]	(5.9a)	[29]	(5.9a)
$I_0/m_0$								
0.001	0.020	0.020	0.030	0.031	0.032	0.033	0.032	0.033
0.01	0.046	0.048	0.083	0.089	0.100	0.108	0.105	0.109
0.1	0.102	0.112	0.204	0.236	0.316	0.367	0.332	0.385
0.5	0.177	0.204	0.375	0.448	0.707	0.758	0.864	0.855

Note.  $F(0) = 10$ ,  $F_{22}(0) = 20$ ; monomer concentration  $m_0 = 5 \text{ mol/l}$ .

In this case the equation for generating function takes the following form:

$$\begin{aligned}
 \frac{\partial F(\vec{q})}{\partial t} = & k_1 q_3 I F + k_{pr} \left[ \frac{\partial F(\vec{q})}{\partial q_2} \cdot \frac{\partial F(\vec{q})}{\partial q_3} - q_3 F \cdot \frac{\partial F(\vec{q})}{\partial q_3} - q_2 R \cdot \frac{\partial F(\vec{q})}{\partial q_2} \right] \\
 & + k_{tr}(1 - q_3) \cdot \frac{\partial(\vec{q})}{\partial q_3} + k_{ter} \cdot \left[ \frac{1}{2} \cdot \frac{\partial F(\vec{q})}{\partial q_3} - q_3 R \right] \cdot \frac{\partial F(\vec{q})}{\partial q_3} \\
 & + q_3 k_i I \cdot \frac{\partial F(\vec{q})}{\partial q_2} - q_2 k_i I \frac{\partial F(\vec{q})}{\partial q_2}
 \end{aligned} \quad (5.9a)$$

The system (5.10) will also change to a certain extent.

Critical conversion values obtained after solving the modified system (5.10) in all cases appear to be somewhat higher than the ones obtained in [29]. Even if we take into account that conversion in [29] is understood as consumption of monomer  $\alpha_m$ , rather than consumption of functional groups, i.e.,  $\alpha_m = (m_0 - m)/m_0 = 2\alpha + \alpha^2$ , where  $\alpha$  is conversion in terms of functional groups, no agreement is observed. These discrepancies are possibly stem from the method of divergent process construction in [29] to take into account the reaction of interaction of active centers with “pendent” functional groups and from obtaining the generating function  $G_1(z_a)$  (Eqs. (5.15) and (5.16) in [29]).

Figure 5.5 shows the relationship between critical conversion,  $F_{22}(0)$ , and rate of chain transfer reaction for instantaneous (Fig. 5.5a) and slow (Fig. 5.5b) initiation [23]. In both cases the invariants characteristic of processes in the absence of transfer are plotted on the ordinate axis. Selection of appropriate coordinates for the abscissa axis allows presenting the entire array of “experimental” data on generalized curves. The left branch in both cases demonstrates the presence of dependence:

$$\alpha_{cr} \approx \frac{1}{2} \cdot \frac{k_{tr} Y_0}{k_{pr} F_{22}(0)} \quad (5.13)$$

Thus, critical conversion in this range of kinetic parameters is defined as a ratio of the chain transfer rate to the propagation rate on functional groups belonging to polyfunctional (branching) monomers. In a certain sense this ratio is

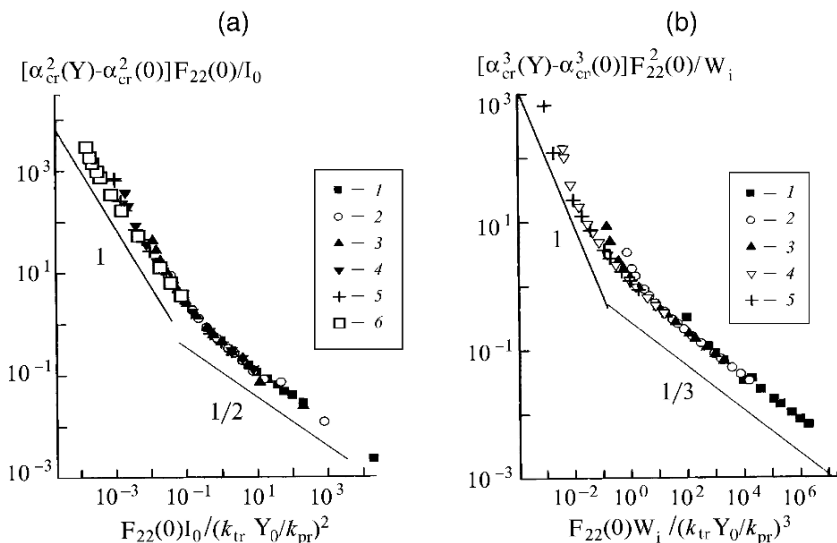


**Fig. 5.5** Dependence of critical conversion value  $\alpha_{cr}$  upon  $F_{22}(0)$  in living polymerization for instantaneous (a) and slow (b) initiation and chain transfer:  $I_0 = 10^{-4}$  mol/l. (a)  $X_0 = 0$  (1);  $1$  (2–4, 6), and  $10^{-1}$  mol/l (5).  $k_{tr}/k_{pr} = 10^{-3}$  (2);  $10^{-2}$  (3);  $10^{-1}$  (4–6). (b)  $W_i = 10^{-4}$  (mol/l) $^2$ .  $X_0 = 0$  (1);  $1$  (2–4), and  $10^{-1}$  mol/l (5).  $k_{tr}/k_{pr} = 10^{-3}$  (1, 2);  $10^{-2}$  (3);  $10^{-1}$  (4, 5). The initiation rate in this figure and in the next one is related to the chain propagation constant; therefore, it is expressed in (mol/l) $^2$ . Numbers near the curves represent values of the tangent of straight line slope angle

close to formula (5.3). However, the right branches of the curves are described by relationships (5.11) and (5.12), for the cases of instantaneous and slow initiation, respectively.

Crossover points for both cases are described by the following relationships:

$$\frac{k_{pr}F_{22}(0)}{k_{tr}Y_0} \approx \begin{cases} \frac{k_{tr}Y_0}{k_{pr}I_0} & \text{for instantaneous initiation} \\ \frac{(k_{tr}Y_0)^2}{k_{pr}k_iI_0} & \text{for slow initiation} \end{cases} \quad (5.14)$$

Therefore, if  $k_{tr}/k_{pr} \approx 1$  and  $Y_0 \approx I_0$ , it is necessary to use formula (5.13), if  $F_{22}(0) < Y_0$ , relationship (5.11) or (5.12) should be used. However, it is evident that if  $F_{22}(0) < Y_0$ ,  $\alpha_{cr}$  would exceed 1, i.e., the gel point will be unattainable. Thus, for practically significant conditions of polymerization, specifically formulas (5.11) and (5.12) are meaningful, i.e., chain transfer reaction (and, hence, the actual length of polymer chain) does not play any role for finding the critical conversion value. In other words, the concentration of active centers in the first case and initiation rate in the second case are important not as factors prescribing the chain length [as it is necessary on condition that formula (5.4) is valid], but they determine the concentration of the second reagent participating in the formation of the macromolecule, the active center. In this sense formulas (5.11) and (5.12) are close to condition (5.2). It has to be noted that all these obtained relationships are applicable not only to

homo-polymerization processes, but also to copolymerization processes, if we are dealing with comonomers with similar reactive ability, which differ only by the number of multiple bonds in the molecule (e.g., monomethacrylates with dimethacrylates). In this case the numeric value of  $F_{22}(0)$  will be uniquely determined by composition of comonomer mixture:  $F_{22}(0) = \sum_i i(i-1)m_i$ .

### 5.3.2 Three-Dimensional Polymerization and Copolymerization with Quadratic or Linear Chain Termination [3,4]

Let us now analyze three-dimensional polymerization with quadratic chain termination: ( $k_{ter} \neq 0, k_X = k_{tr} = 0$ ). Calculation results are presented in Fig. 5.6, and the invariant, which is similar to the one that determines dependence (5.13), is used as a variable on the axis of ordinates, namely:

$$\alpha_{cr} \frac{k_{pr} F_{22}(0)}{k_{ter} R} = \frac{k_{pr} \alpha_{cr} F_{22}(0)}{\sqrt{k_{ter} W_i}}$$

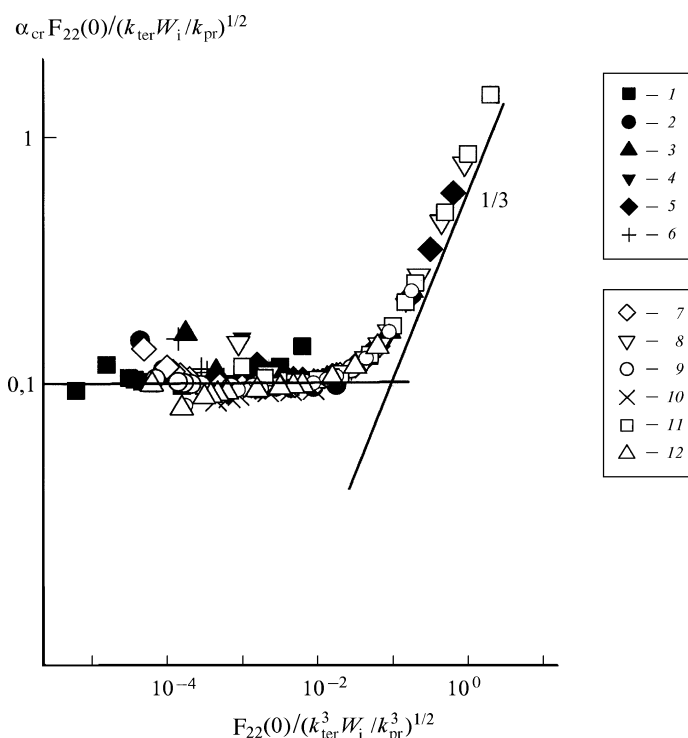


**Fig. 5.6** Dependence of critical conversion value  $\alpha_{cr}$  upon conditions of radical polymerization for the case of chain termination through recombination  $W_i = 10^{-5}(1-4, 11, 12)$ ;  $5 \times 10^{-5}(8-10)$ ; and  $10^{-4}(\text{mol/l})^2(5-7)$ .  $k_i/k_{pr} = 10^3(4, 5, 8)$ ;  $2 \times 10^3(11, 12)$ ;  $5 \times 10^3(3, 6)$ ;  $10^4(1, 7, 9)$ ;  $5 \times 10^4(2)$ ; and  $10^5(10)$

In choosing the appropriate coordinates for the abscissa, all results form a single curve that is also broken down into two sections. The first one determines the dependence of critical conversion: upon kinetic parameters of polymerization reaction similar to relationship (5.13):

$$\alpha_{cr} \approx 0,33 \cdot \frac{\sqrt{k_{ter}W_i}}{k_{pr}F_{22}(0)} \quad (5.15)$$

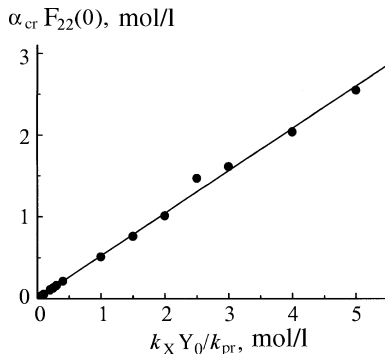
The value of critical conversion is proportional to the ratio of chain termination and chain propagation rates on branching functional groups (belonging to polyfunctional monomers). The value of proportionality coefficient is determined by the fact that termination through recombination was analyzed. As is shown below, disproportionation and linear termination lead to a coefficient that is equal to 0.5. Relationship (5.12) is strictly satisfied at the second section, and the crossover point is determined by this equality:

$$\frac{k_{pr}F_{22}(0)}{\sqrt{k_{ter}W_i}} \approx \frac{k_{ter}}{k_{pr}} \quad (5.16)$$

For conventional values of kinetic parameters, namely,  $W_i \approx 10^{-5} \text{ mol} \times \text{l}^{-1} \cdot \text{s}^{-1}$ ,  $k_{ter} \approx 10^5$  and  $k_{pr} \approx 10^3 \text{ l} \cdot \text{mol}^{-1} \cdot \text{s}^{-1}$  [30], relation (5.15) is satisfied, if  $F_{22}(0) < 1 \text{ mol/l}$ ; in the opposite case, the dependence of critical conversion upon polymerization conditions is described by formula (5.11). For instance, in the case of three-dimensional polymerization of dimethyl acrylates,  $F_{22}(0) \approx 20 \text{ mol/l}$ . Consequently, only relationship (5.12) could be analyzed. Thus, with polymerization involving chain termination, critical conditions are also independent of chain length, but are determined by the same parameters as in the case with living polymerization, namely, by the weight-averaged functionality of monomer mixture and by initiation rate.

Results obtained after solving the system of equations (5.10) for linear termination (i.e., for inhibited polymerization,  $k_{ter} = 0, k_X \neq 0$ ) are given in Fig. 5.7. Within a wide, but reasonable, range of initiation rate values, termination constants  $k_X$ , and constants of termination agent concentration, dependence of critical conversion

**Fig. 5.7** Dependence of critical conversion value  $\alpha_{cr}$  upon inhibited polymerization conditions  $W_i/k_{pr} = 10^{-9} \div 10^{-1} (\text{mol/l})^2$



upon polymerization conditions is described by a relationship similar to (5.13), namely:

$$\alpha_{\text{cr}} = 0,5 \cdot \frac{k_X X}{k_{\text{pr}} F_{22}(0)} \quad (5.17)$$

This result is determined (with selected values of kinetic constants (see Table 5.5, below) by a critical relationship of type (5.14):

$$\Psi = \frac{(k_X X)^3}{k_{\text{pr}}^2 F_{22}(0) W_i} > 1 \quad (5.14a)$$

In other words, in the case of linear termination, the produced chains are too short to be a factor determining the gel point; in this case, the moment of gel formation is regulated by the branching rate, which is also typical for living polymerization.

### 5.3.3 *Three-Dimensional Polymerization with “Pendent” Double Bonds Taken into Account (Chain Termination by Disproportionation) [6]*

Formation of primary macromolecules in diluted solution in the monomer at early stages is usual with three-dimensional free-radical polymerization. A consequence of polyunsaturation of initial molecules of the monomer (oligomer) is that certain links of the chain contain “pendent” double bonds (PDB), subsequent conversion of which is determined by two factors. On the one hand, their local concentration near the active end of the macroradical could be significantly higher than the average one in terms of volume-average double bond concentration, which leads to increased consumption of these bonds with formation of intrachain cross-links instead of interchain ones. For this reason, the apparent reactive ability of PDB is enhanced, while the critical conversion increases [9]. On the other hand, shielding of PDB by the polymer chain proper (especially during the aggregation of PDB) leads to impairment of reactive ability by the steric factor. Finally, the reactive ability of the double bond could change depending upon whether this double bond belongs to the monomer molecule or to the monomer unit of the macromolecule. The combined impact of all these factors makes elucidation of the true pattern of the mechanism for cross-links formation with three-dimensional free-radical polymerization difficult.

Indeed, the authors of studies [26, 31–34] devoted to kinetics of three-dimensional free-radical polymerization monitored common conversion of double bonds ( $C_1$ ) and “pendent” double bonds ( $C_{\text{PDB}}$ ) separately. It appeared that at the initial stages of the reaction, when  $C_1$  was close to zero,  $C_{\text{PDB}}$  attained values within  $0.2 \div 0.4$ . In terms of value of relative reactive ability  $\epsilon$  ( $\epsilon = k_{\text{prPDB}}/k_{\text{pr1}}$ , where  $k_{\text{pr1}}$  and  $k_{\text{prPDB}}$  are constants of the chain propagation reaction rate at initial and “pendant” double bonds), it gives  $\epsilon \gg 1$ . A mixture of styrene with  $0.2 \div 2\%$  (mol) 2,2-bis-(4-vinyl-oxy-phenyl)propane was used as the copolymerization system in

these studies [26, 35–37], whereas a mixture of MMA with 1 ÷ 2% (mol) DMAEG was used as the copolymerization system by Matsumoto et al. [38]. In both cases there are no grounds to suppose that the reactive ability of the vinyl groups could enhance in the case of fixing them to a polymer chain. Obviously in this case growth of local concentration of “pendant” groups near the active end of the macroradical represents a determining factor. Three-dimensional free-radical polymerization in the living chains conditions [25, 26] showed that in this case  $k_{prPDB}/k_{pr1} \approx 0.3$ , i.e., in the case of living polymerization, when the concentration of macromolecules is high at the very beginning of the reaction, and the chains are small in terms of their length and therefore the effect of local concentration of pendent double bonds disappears, impaired reactive ability of double bonds is observed as compared to that of double bonds in initial monomers. It is likely that steric restrictions are decisive in the indicated system. Impairment of reactive ability of PDB as compared to initial double bonds leads to the formation of “sparse” interpenetrating clusters, whereas enhancement of this reactive ability leads to the formation of compact and densely packed “grains” [39].

The appearance of approaches enabling us to truthfully evaluate the variation of reactive ability of polyunsaturated monomers (oligomers) in the course of three-dimensional free-radical polymerization and data indicating that such variation actually takes place served as an impetus for the formulation of the calculation problem [6].

Taking the variation in reactive ability of double bonds into account within the proposed calculation scheme means that it is necessary to single out initial (monomer) reagents from the overall number of polymer chains and to introduce a special generating function for these reagents:

$Z(\vec{q}) = \sum_i q_1 q_2^i m_i$  ( $m_i$  = concentration of the  $i$ -functional monomer). Thus, in the case with bifunctional oligomers (e.g., dimethyl acrylates),  $Z(\vec{q}) = q_1 q_2^2 m_2$

The kinetic pattern of  $m_i$  consumption is expressed by this equation:

$$\frac{dm_i}{dt} = -k_{pr1} i m_i R$$

where  $k_{pr1}$  = constant of propagation rate on double bonds belonging to monomers leads to an ordinary differential equation in partial derivatives for generating function:

$$\frac{\partial Z(\vec{q})}{\partial t} = k_{pr1} q_2 \frac{\partial Z(\vec{q})}{\partial q_2} R \quad (5.18)$$

Solving of this equation using the method of characteristics gives

$$Z(\vec{q}) = \sum_i q_1 (q_2 e^{-k_{pr1} \tau})^i m_i(0) \quad (5.19)$$

where  $\tau = \int_0^t R(\xi) d\xi$ ;  $m_i(0)$  = initial concentration of the  $i$ -functional monomer.

Equation (5.19) could be presented in the form of a system for moments that take distribution by double bonds into account (index 2):

$$\begin{aligned}
 \frac{dZ}{dt} &= -k_{pr1}RZ_2 \\
 \frac{dZ_2}{dt} &= -k_{pr1}R(Z_2 + RZ_{22}) \\
 \frac{dZ_{22}}{dt} &= -k_{pr1}R(2Z_{22} + RZ_{222}) \\
 \frac{dZ_{222}}{dt} &= -k_{pr1}R(3Z_{222} + RZ_{2222})
 \end{aligned}
 \tag{5.20}$$

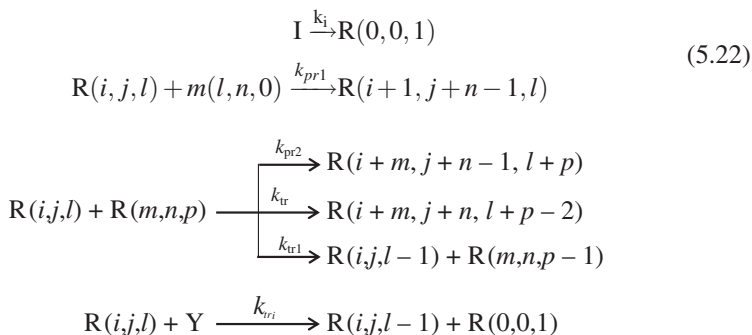
and so forth; i.e., the obtained system is not a closed one.

However, it is necessary to take into account that the initial reaction mixture consists of monomer molecules of restricted functionality. This circumstance makes it possible to cut the equation system. Indeed, since

$$\begin{aligned}
 Z_2(\vec{q}) &= q_1 \cdot \sum_{i=1}^n i q_2^{i-1} m_i \\
 Z_{22}(\vec{q}) &= q_1 \cdot \sum_{i=1}^n i(i-1) q_2^{i-2} m_i \\
 Z_{222}(\vec{q}) &= q_1 \cdot \sum_{i=1}^n i(i-1)(i-2) q_2^{i-3} m_i
 \end{aligned}
 \tag{5.21}$$

and so on, then  $Z_{22}(1) = 0$  for linear polymerization,  $Z_{222}(1) = 0$ , if functionality is no higher than 2 ( $n = 2$ ), and  $Z_{2222} = 0$ , if  $n$  is no higher than 3.

The pattern describing the process of radical polymerization becomes more complicated as compared to Eq. (5.2):



The system of differential equations for the concentration of macromolecules and moments of generating functions is changed accordingly. Initial conditions also change in this case: at  $t = 0$   $m(l, i, 0) = m_i(0)$ , all  $R(i, j, l) = 0$ .

Calculations show [6] that the above-obtained result is attained with a high degree of accuracy (Table 5.3), namely, that the critical conversion value depends only



**Table 5.3** Dependence of critical conversion value upon the relationship of constants of chain propagation rate  $\epsilon$  on “pendent” double bond and monomer double bond for living polymerization

$Z_2(0)$	$Z_{22}(0)$	$Z_{222}(0)$	$\alpha_{cr}$			
			$\epsilon = 1$	$\epsilon = 0.5$	$\epsilon = 0.2$	$\epsilon = 0.1$
10	1	3	31.44/4.68	44.80/7.36	71.70/13.56	101.06/21.67
10	5	15	14.12/1.58	19.92/2.56	31.62/4.67	44.75/7.47
10	10	30	9.99/1.01	14.11/1.60	22.23/3.00	31.64/4.68
1	20	114	6.93/0.63	9.98/1.00	13.55/1.85	21.86/2.94
5	20	90	7.07/0.63	9.98/1.00	15.43/1.85	21.86/2.94
10	20	60	7.07/0.63	9.99/1.00	15.66/1.85	21.83/2.94
20	20	0	7.07/0.63	9.99/1.00	15.66/1.85	21.88/2.94

Note 1. In the numerator, for values  $k_i/k_{pr} = 1$  mol/l, and in the denominator, for values  $k_i/k_{pr} = 10^{-4}$  mol/l,  $I_0 = 10^{-3}$  mol/l.

Note 2. In terms of formulation of initial composition for a three-component mixture of mono-functional (concentration  $m_1$ ), bifunctional ( $m_2$ ), and trifunctional ( $m_3$ ) monomers,  $Z_2(0) = m_1 + 2m_2 + 3m_3$ ,  $Z_{22}(0) = 2m_2 + 6m_3$ , and  $Z_{222}(0) = 6m_3$  (see formulas (5.21)).

upon the second moment of initial molecules distribution in terms of functionality  $Z_{22}(0)$ . Also, formulas of type (5.11) and (5.12) appear to be valid for living polymerization, namely:

$$\alpha_{cr}^2 \cdot \frac{\epsilon F_{22}(0)}{I_0} = 1 \quad \text{and} \quad \alpha_{cr}^3 \cdot \frac{\epsilon^2 F_{22}^2(0)}{k_i I_0} \cdot k_{pr1} = 1 \quad (5.23)$$

where  $\epsilon = k_{PDB}/k_{pr1}$ .

Results of calculation of radical polymerization (with chain termination) are given in Fig. 5.8. As in the example described above, depending upon the relationship of kinetic parameters, critical conversion is determined by different relationships. If  $k_{pr1} Z_{22} / \sqrt{k_{ter} W_i} < k_{ter} / k_{PDB}$  the expression for gel point takes the following form:

$$\alpha_{cr} = \frac{1}{2} \cdot \frac{\sqrt{k_{ter} W_i}}{k_{PDB} Z_{22}} \quad (5.24)$$

In the opposite case, the relationship describing the process of living polymerization with slow initiation appears to be valid for critical conversion.

We would like to point out that coefficient 0.5 in expression (5.24) is determined by the fact that termination through disproportioning was taken into account in the calculation. For the purpose of recombination (as has already been stated), the coefficient of 0.33 appears to be true.

As has been shown above, an estimate of the relative constant of chain propagation  $\epsilon$  given in [25] seems to be the most correct. This value was estimated directly based on kinetic measurements of consumption of comonomers and “pendent” groups, and the final estimate was  $\epsilon = 0.38$ . Let us analyze this value according to formula (5.23), assuming that (as it was specified in the initial conditions for calculation scheme) the constants of copolymerization of copolymers are equal. As the living polymerization in [25] was conducted by introducing an adduct of oligomer

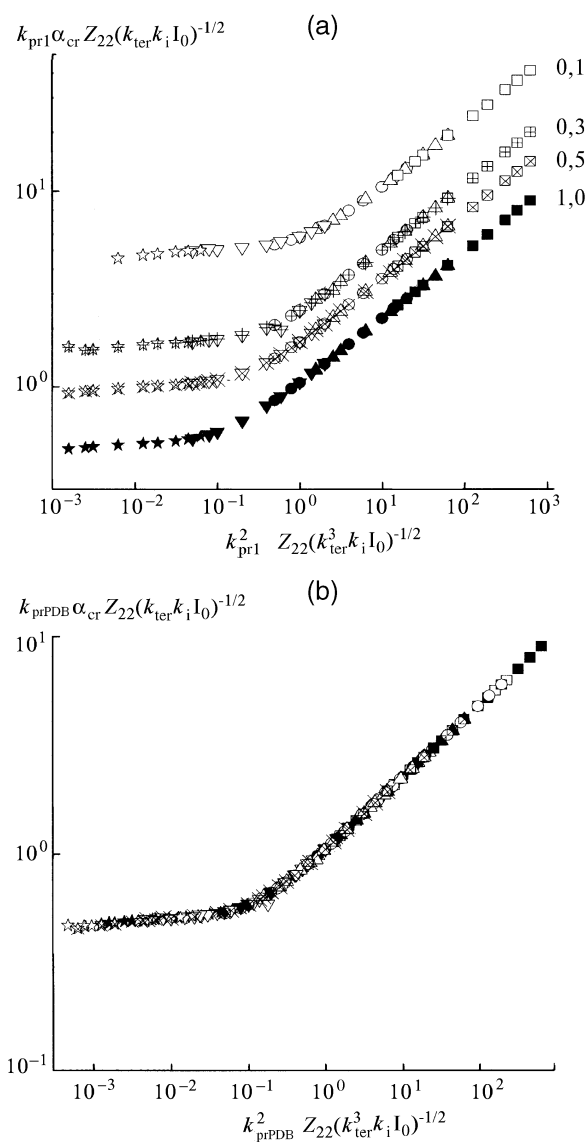


**Fig. 5.8** Dependence of critical conversion value in radical polymerization with chain termination upon second moment of initial monomer mixture distribution in terms of functionality  $Z_{22}(0)$  without taking the value of  $\epsilon$  into account (a) and taking it into account (b). Numbers on curves in (a) are values of  $\epsilon$ .  $I_0 = 10^{-4}$  (1,2) and  $10^{-2}$  (3,4,5) mol/l.  $k_i/k_{pr1} = 10^{-5}$  mol/l;  $k_{ter}/k_{pr1} = 10^3$  (1);  $10^4$  (2,5); and  $10^2$  (3, 4)

**Table 5.4** Calculated values of relative constant of chain propagation on “pendent” double bond according to data from [25]

$Z_{22}$ , mol/l	$\alpha_{cr}$				$\varepsilon = k_{PDB}/k_{pr1}$			
	$I_0 \times 10^3$ , mol/l				$I_0 \times 10^3$ , mol/l			
	34	23	9.9	6.1	34	23	9.9	6.1
0.17	0.91	–	–	–	0.24	–	–	–
0.255	0.81	–	–	–	0.20	–	–	–
0.272	0.66	0.42	0.27	0.20	0.29	0.48	0.50	0.56
0.356	0.62	–	–	–	0.25	–	–	–
0.513	0.49	0.36	0.24	0.16	0.27	0.34	0.33	0.45
0.714	0.43	–	–	–	0.26	–	–	–
0.85	0.38	–	–	–	0.28	–	–	–
1.02	0.32	–	–	–	0.32	–	–	–
1.36	0.27	–	–	–	0.34	–	–	–

Note.  $k_{pr1}$  and  $k_{PDB}$  are constants of chain propagation on free (in monomers) and pendent double bonds.

polystyrene and nitroxile (TEMPO) into the system, the initiation could be considered to be instantaneous. Thus:

$$\varepsilon = \frac{I_0}{\alpha_{cr} Z_{22}(0)} \quad (5.23a)$$

Calculation results are listed in Table 5.4. As is seen, as a result of averaging all 15 values obtained for different conditions of experiments,  $\varepsilon = 0.35 \pm 0.1$ , which practically coincides with the value  $\varepsilon = 0.38$  obtained from independent kinetic measurements described by Ide and Fukuda [25].

Consequently, the use of a critical conversion value for evaluating the reactive ability of PDB is possible, but it should be based on formulas that were derived in this publication. It is obvious that experimental determination of  $\alpha_{cr}$  should be carried out under such conditions that exclude localization of PDB near active ends of growing chains, i.e., either under the conditions providing the living polymerization mode or with small enough concentrations of polyunsaturated comonomer [37, 40]. Also, it was recently found that three-dimensional free-radical polymerization in the presence of high concentrations of chain transfer agents [3] or inhibitors [4, 5], decreasing the average length of chains to several links (instead of the usual  $10^2$ – $10^3$  links), also refers to such conditions.

### 5.3.4 Summary of Results of Theoretical Calculations for Critical Conversion

Analysis of solutions presented in Sects. 5.3.1–5.3.3 shows that the critical conversion value is related to kinetic conditions of three-dimensional free-radical

polymerization process in a complicated way. Depending upon the relationship of initiation reaction rate to the rate of material chain termination (conditions (5.12) or (5.15)), gel point is determined either by initiation rate only or by termination rate only. The first condition is realized in the case when opportunities for chain branching are good, i.e., when the concentration of polyunsaturated monomer is high. Then, kinetics of active center accumulation represents an important factor.

In the second case, the length of the material chain plays an important role, because with a low concentration of polyunsaturated monomer, the number of pendent double bonds (probable points of branching) per polymer chain becomes a limiting factor. However, in any case the weight-averaged functionality of initial monomer mixture is a critical factor.

Generalized results of calculations described in Sects. 5.3.1–5.3.3 and published in [3–7] are listed in Table 5.5 in the form of formulas with critical conditions of their satisfiability.

**Table 5.5** Formulas for critical conversion ( $\alpha_{cr}$ )

Type of process	$F_{22}$ is low	$F_{22}$ is high	Critical conditions
LTFRP, instantaneous initiation		$\frac{\alpha_{cr}^2 F_{22}}{I_0} \approx 1$ (5.11)	$\frac{k_i}{k_{pr} \alpha_{cr} F_{22}} > 6$
The same + chain transfer	$\alpha_{cr} \approx 0,5 \cdot \frac{k_{tr} Y_0}{k_{pr} F_{22}}$ (5.13)	$\frac{\alpha_{cr}^2 F_{22}}{I_0} \approx 1$ (5.11)	$F_{22} > < \frac{(k_{tr} Y_0)^2}{k_{pr}^2 I_{22}}$
LTFRP, slow initiation		$\frac{\alpha_{cr}^3 F_{22}^2 k_{pr}}{W_i} \approx 1$ (5.12)	$\frac{k_i}{k_{pr} \alpha_{cr} F_{22}} < 1$
The same + chain transfer	$\alpha_{cr} \approx 0,5 \cdot \frac{k_{tr} Y_0}{k_{pr} F_{22}}$ (5.13)	$\frac{\alpha_{cr}^3 F_{22}^2 k_{pr}}{W_i} \approx 1$ (5.12)	$F_{22} > < \frac{(k_{tr} Y_0)^3}{k_{pr}^2 k_i I_0}$
Ordinary TFRP (slow initiation, termination through recombination)	$\alpha_{cr} \approx 0,33 \cdot \frac{\sqrt{k_{tr} W_0}}{k_{pr} F_{22}}$ (5.15)	$\frac{\alpha_{cr}^3 F_{22}^2 k_{pr}}{W_i} \approx 1$ (5.12)	$F_{22} > < \frac{\sqrt{i_1^3 W_i}}{k_{pr}^2}$
Ordinary TFRP (slow initiation, linear termination)	$\alpha_{cr} \approx 0,5 \cdot \frac{k_X X}{k_{pr} F_{22}}$ (5.17)	–	–
Ordinary TFRP (taking PDB into account, termination through disproportioning)	$\alpha_{cr} \approx 0,5 \cdot \frac{\sqrt{k_{ter} W_i}}{k_{pr} Z_{22}}$ (5.24)	–	$\frac{k_{pr} Z_{22}}{\sqrt{k_{ter} W_i}} < \frac{k_{ter}}{k_{PDB}}$

Note 1. TFRP, three-dimensional free-radical polymerization.

Note 2. LTFRP, TFRP in the mode of living chains ("nonterminated" TFRP).

Note 3.  $F_{22}(0) = \sum_i (i-1)m_i$ , where  $i$  = number of multiple bonds in a molecule of  $i$ -monomer, and  $m_i$  = molar concentration of  $i$ -monomer.

Note 4.  $Z_{22} \equiv Z_{22}(0) = \sum_i i(i-1)m_i$ .

Note 5. In the case of termination through recombination, 0.33 will be used in formula (5.24) instead of numerical coefficient 0.5.

## 5.4 Comparison of Results of Theoretical Calculations for Critical Conversion with Experimental Data

The majority of experimental data in the field of three-dimensional free-radical polymerization were obtained from an example of oligomers of acryl series of the RM<sub>n</sub> type, where M is the acryl or methacryl group ( $n = 2-6$ ), their mixtures with monomers ( $n = 1$ ), and divinylbenzoles and their mixtures with styrene and other comonomers.

In the case of conventional radical polymerization with quadratic termination of chains according to formulas (5.12) and (5.15), the value of  $\alpha_{cr}$  increases with growing initiation rate  $W_i$ . However, even with maximum achievable values  $W_i \approx 10^{-2} \text{ mol} \cdot \text{l}^{-1} \cdot \text{s}^{-1}$ , the value of  $\alpha_{cr}$  does not exceed  $10^{-2}$  (taking into account that  $F_{22}(0) \approx 20 \text{ mol/l}$ , and  $k_{pr} \approx 10^2 - 10^3 \text{ l} \cdot \text{mol}^{-1} \cdot \text{s}^{-1}$ ). Such data are unsuitable for comparison with the experimental data because the error of critical conversion measurement in the area  $\alpha_{cr} \leq 10^{-2}$  is commensurate with the value being measured. Our measurements (carried out for a large set of dimethacrylates RM<sub>2</sub> of different chemical origin of R with  $W_i = 10^{-8} - 10^{-6} \text{ mol} \cdot \text{l}^{-1} \cdot \text{s}^{-1}$ ) make it possible to experimentally evaluate only the upper limit of  $\alpha_{cr} \leq 10^{-2}$ . The forecast according to formula (5.11) yields an estimate of  $10^{-4} \leq \alpha_{cr} \leq 10^{-2}$ . The value of  $\alpha_{cr} = 2.9 \times 10^{-2}$ , staying outside the error limits, was observed only in one case—for ethylene glycol dimethyl acrylate [41]; it is significantly higher than the theoretically forecasted value ( $\alpha_{cr} = 2 \times 10^{-4}$ ). The shift of experimentally obtained value by two decimal exponents in the direction of increase is interpreted by Funke et al. [41] (see also Irzhak et al. [9]) as a manifestation of cyclization and dramatic impairment of reactive ability of pendent double bonds as compared to initial double bonds of dimethacrylate.

The most productive method for comparison of the theory with experimental data is represented by the case implying a shift of  $\alpha_{cr}$  to the area of high values, which is attained either from reduction of  $F_{22}(0)$  by diluting the system with a monofunctional comonomer, or by using sufficient amounts of highly efficient inhibitors of radical polymerization.

### 5.4.1 Inhibited Polymerization of Dimethacrylates

Radical polymerization of tri(ethylene glycol) dimethacrylate initiated by dicyclogexyl peroxidicarbonate (DCPD) in the presence of large amounts of inhibitors of benzoquinone (BQ) or trinitrotoluene (TNT) was conducted in cylinder-shaped vials evacuated of air and sealed (vial height, 250 mm; diameter, 3–3.5 mm) [3]. Conversion was determined based on contraction (shift of meniscus was tracked with accuracy of up to 0.1 mm; overall shift by the moment of gel formation in selected inhibition range was 3–10 mm). The gel formation point was determined based on loss of fluidity. Comparison with other methods [25] showed that this

**Table 5.6** Comparison of experimentally obtained and calculated values of  $\alpha_{cr}$  for inhibited polymerization of tri(ethylene glycol) dimethyl acrylate

Inhibitor		$K_{XX}, s^{-1}$	Critical conversion		
Substance	Concentration, mol/l		Experiment	Calculation using formula(5.4a)	Calculation using formula(5.17)
TNT	0.05	5	$\approx 0.01$	$3.6 \times 10^{-3}$	$8.9 \times 10^{-4}$
	0.1	10	0.06	$7.2 \times 10^{-3}$	$1.8 \times 10^{-3}$
	0.2	20	0.08	$1.4 \times 10^{-2}$	$3.6 \times 10^{-3}$
	0.5	50	0.11	$3.6 \times 10^{-2}$	$9 \times 10^{-3}$
BQ	0.005(4)*	10	0.065	$7.2 \times 10^{-3}$	$1.8 \times 10^{-3}$
	0.005(2)*	10	0.055	$7.2 \times 10^{-3}$	$1.8 \times 10^{-3}$
	0.005(1)*	10	0.045	$7.2 \times 10^{-3}$	$1.8 \times 10^{-3}$
	0.01	20	0.085	$1.4 \times 10^{-2}$	$3.6 \times 10^{-3}$
	0.05	100	0.125	$7.2 \times 10^{-2}$	$1.8 \times 10^{-2}$
	0.01	200	0.135	$1.4 \times 10^{-1}$	$3.6 \times 10^{-2}$
	0.03	600	0.16	$4.3 \times 10^{-1}$	$7.2 \times 10^{-2}$
	0.05	1000	0.19	$7.2 \times 10^{-1}$	$1.8 \times 10^{-1}$

Note 1. TNT ( $k_x \approx 10^2 l \cdot mol^{-1} \cdot s^{-1}$ ), BQ ( $k_x \approx 2 \times 10^3 l \cdot mol^{-1} \cdot s^{-1}$ )  $k_{pr} \approx 350 l \cdot mol^{-1} \cdot s^{-1}$  [30],  $M_0 \approx 4 mol/l$   $F_{22}(0) \approx 8 mol/l$

Note 2. Molar “initiator/inhibitor” ratio = 2, initiator =DCPD.

Note 3. In the series marked with a “\*” sign, kinetics of polymerization was recorded using the precision calorimetry method; numbers in brackets are initiation rate,  $W_i \times 10^{-7} mol \cdot l^{-1} \cdot s^{-1}$ .

method yields sufficiently accurate value of critical conversion. Obtained results are listed in Table 5.6.

It follows from the table that in the area of longest lengths of propagating polymer chains (with lowest values of  $k_{XX}$  parameter) a very dramatic discrepancy (by orders of magnitude) between calculated and experimentally obtained values of critical conversion is observed, but then, as the molecular weight decreases (with growing  $k_{XX}$ ), the experimental and calculated values become closer. The best coincidence is observed when formula (5.17) is used for calculating  $\alpha_{cr}$ . As the main reason for too high experimental values of  $\alpha_{cr}$  is cyclization [9] that represents intrachain cross-linking of “pendent” double bonds, the authors suppose that the probability of cyclization is declining as the length of growing polymer chains decreases with increasing  $k_{XX}$ . Therefore, a comparison with experimental data specifically in the area of highest values of  $K_{XX}$  enables us to identify the actual advantage of formula (5.17) as the most exact one. At the same time, the obtained result means that the proposed calculation gives a correct estimate of critical conversion value not only in the area of parameters, where formula (5.17) is true, but also in an area where the ratio of Eq. (5.12) can be satisfied.

It is all the more important that very often [42] the deviation of experimental values of  $\alpha_{cr}$  from calculated values is looked upon as a test enabling estimation of the contribution of cyclic structures into polymeric networks, and the calculation of  $\alpha_{cr}$  is based on the Flory–Stockmayer formula (5.4). It is obvious that the use of ratio (5.17) in this case will allow avoiding erroneous conclusions.

### 5.4.2 Copolymerization of Divinyl Benzene (*m*-DVB) with Styrene

It was anticipated that with decreasing content of polyfunctional agent (*m*-DVB) in an initial (co)monomer mixture [40], the probability of cyclization would fall to a negligibly small value, which would provide an “ideal” structure of polymer network. A proof for this conclusion was sought for in the coincidence of calculated and experimental values of  $\alpha_{cr}$ , and the Flory–Stockmayer formula was used for the said calculation:

$$\alpha_{cr} = \frac{1}{\rho(\bar{P}_w - 1)} \quad (5.4a)$$

where  $\rho$  = molar fraction of cross-linking agent (*m*-DVB);  $\bar{P}_w$  = weight-averaged degree of polymerization of initial polymer chains, i.e., the chains that would be formed in the absence of cross-linking agent by the moment, which corresponds to the gel formation point.

The value of  $\bar{P}_w$  was found using the GPC method for conversions that are lower than  $\alpha_{cr}$ , with subsequent extrapolation to zero conversion. The results are presented in Table 5.7. As for selected values of kinetic constants (see note to Table 5.7) the critical condition for estimating  $\alpha_{cr}$  determines the selection of formula (5.15), it was just this formula that was used in the calculations.

It follows from data listed in Table 5.7 that the conclusions of Matsumoto et al. [40] stating that at low concentrations of *m*-DVB (the last line in the table) the state of “ideal” network is attained casts strong doubts. The conclusion regarding the attainment of the ideal network state that was drawn by Mitomi et al. [35] dealing with copolymerization of dimethyl acrylates with monomethacrylates also casts strong doubts. In this case, similarity of experimentally obtained values of  $\alpha_{cr}$  and values of  $\alpha_{cr}$  calculated based on formula (5.4a) was observed at still lower values of bifunctional component at 0.03%(mol) dimethyl acrylate. Recalculation according to formula (5.15) in this case also leads to significantly lower values of  $\alpha_{cr}$  and thus points to the fact that despite the conclusions made by Soper et al. [37], the contribution of cyclic structures is high enough.

**Table 5.7** Comparison of experimental and calculated values of  $\alpha_{cr}$  for copolymerization of *m*-DVB with styrene

<i>m</i> -DVB, %(mol)	$\bar{P}_w \cdot 10^{-3}$	F <sub>22</sub> (0)	$\alpha_{cr}$		
			Experiment	Calculation using formula (5.4a)	Calculation using formula (5.15)
1	1.19	0.154	0.215	0.0425	0.032
0.5	0.79	0.077	0.333	0.133	0.065
0.25	0.74	0.039	0.488	0.271	0.128
0.17	0.67	0.026	0.549	0.435	0.192

*Note.* Copolymerization in the block initiated by AIBN ( $4 \times 10^{-2}$  mol/l) at 60°C;  $W_i = 4 \times 10^{-7}$  mol · l<sup>-1</sup> · s<sup>-1</sup>,  $k_{pr} = 200$  l · mol<sup>-1</sup> · s<sup>-1</sup>,  $k_{ter} = 10^7$  l · mol<sup>-1</sup> · s<sup>-1</sup>, and F<sub>22</sub>(0) = 15.4 mol/l for *m*-DVB.

Also, the contribution of cyclization remains quite significant in those cases, when the length of “primary” chains is decreased by several orders of magnitude as a result of intensive chain transfer in the course of polymerization process [35], although the tendency to cyclization suppression is clearly manifested in this process. For example, in the case with polymerization of dimethacrylates, the ratio of experimental value of critical conversion to calculated value decreases from 100 (at  $\bar{P}_w = 1000$  in the absence of chain transfer agent) to 13 ( $\bar{P}_w = 142$ ) and to 7–8 ( $\bar{P}_w = 64$ ) in the presence of highly efficient chain transfer agents (dodecylmerkaptanes).

In the case of diallyl monomers that are active chain transfer agents, at lowest values of  $\bar{P}_w = 39$ –49, this ratio falls to 5.2–5.5. This tendency manifests itself not only when chain length decreases, but also when chain rigidity is enhanced [36].

In the case of inhibited polymerization of dimethacrylates (which was analyzed above; see Table 5.6), similarity of calculated and experimentally obtained values of critical conversion is observed for  $\bar{P}_w$ , which is approximately equal to several units. Apparently, this is the main reason for the fact that contribution of cyclization is close to zero and the “ideal” network structure is obtained thereby.

## References

1. Flory PJ (1953) Principles of polymer chemistry. Cornell University Press, Ithaca, NY
2. Stockmayer W (1943) J Chem Phys **11**:45–51
3. Korolev GV, Irzhak TF, Irzhak VI (2001) Vysokomolek Soedin A **43**:2106–2111 (in Russian)
4. Korolev GV, Irzhak TF, Irzhak VI (2002) Russ J Phys Chem **21**:58–68 (in Russian)
5. Korolev GV, Irzhak TF, Irzhak VI (2001) Vysokomolek Soedin A **43**:970–976 (in Russian)
6. Korolev GV, Irzhak TF, Irzhak VI (2002) Vysokomolek Soedin A **44**:5–9 (in Russian)
7. Irzhak VI, Irzhak TF, Korolev GV (2002) Critical conversion in three-dimensional polymerization. Institute of Chemical Physics, Chernogolovka (in Russian)
8. Irzhak VI (2004) Usp Khim **73**:275–2291 (in Russian)
9. Irzhak VI, Rozenberg BA, Enikolopyan NS (1979) Cross-linked polymers. Synthesis, structure, and properties. Nauka, Moscow (in Russian)
10. Kuchanov SI (1978) Methods of kinetic calculations in polymer chemistry. Khimiya, Moscow (in Russian)
11. Chambon F, Winter HH (1985) Polymer Bull **13**:499–503
12. Entelis SG, Evreinov BB, Kuzayev AI (1985) Reactive oligomers. Khimiya, Moscow (in Russian)
13. Gordon M (1954) J Chem Phys **22**:610–613
14. Tvorogov NN (1976) Vysokomolek Soedin A **18**:1919–1927 (in Russian)
15. Tvorogov NN, Berlin AA (1976) Vysokomolek Soedin A **19**:1274–1282 (in Russian)
16. Tvorogov NN, Kondratyeva AG (1978) Vysokomolek Soedin A **20**:1550–1559 (in Russian)
17. Pismen LM, Kuchanov SI (1971) Vysokomolek Soedin A **13**:791–802 (in Russian)
18. Dušek K (1993) Collect Czech Chem Commun **58**:2245–2265
19. Korolev GV (1977) Papers for the 1st All-Union Conference on Chemistry and Physical Chemistry of Polymerized Oligomers, vol. 1. Department of the Chemistry and Physics Institute of the USSR Academy of Science, Chernogolovka (in Russian)
20. Berlin AA, Korolev GV, Kefeli TYa, Sivergin YuM (1983) Acrylic oligomers and materials on the acrylic oligomers. Khimiya, Moscow (in Russian)



21. Korolev GV, Mogilevich MM, Golikov IV (1995) Cross-linked polyacrylates: micro-heterogeneous structures, physical networks, deformation-strength properties. *Khimiya, Moscow* (in Russian)
22. Anseth KS, Bowman CN (1995) *J Polym Sci Part B Polym Phys* **33**:1769–1780.
23. Okay O, Kurz M, Lutz K et al (1995) *Macromolecules* **28**:2728–2737
24. Sun X, Chiu YY, Lee J (1997) *Ind Eng Chem* **36**:1343–1351
25. Ide N, Fukuda T (1999) *Macromolecules* **32**:95–99
26. Ide N, Fukuda T (1997) *Macromolecules* **30**:4268–4271
27. Djavadyan EA, Irzhak VI, Rozenberg BA (1999) *Vysokomolek Soedin A* **41**:624–632 (in Russian)
28. Price FP (1968) *J Polym Sci C* **25**:3–10
29. Dušek K, Somvarky J (1985) *Polym Bull* **13**:313–319
30. Denisov ET (1971) *Liquid-phase reaction rate constants*. Nauka, Moscow (in Russian)
31. Holdway J, Haward RN, Parsons W (1978) *Makromol Chem* **179**:1939–1950
32. Mrkvichkova L, Kratochvil P (1981) *J Polym Sci Polym Phys Ed* **19**:1675–1686
33. Landlin DT, Macosco CW (1988) *Macromolecules* **21**:846–851
34. Matsumoto A, Okuno S, Aota H (1995) *Macromol Symp* **93**:1–10
35. Mitomi D, Matsumoto A, Aota H, et al (2000) *Polymer* **41**:1321–1324
36. Matsumoto A, Yamashita Y, Oiwa M (1993) *J Thermoset Plast Jpn* **14**:139.
37. Soper B, Haward RN, White EFT (1972) *J Polym Sci Polym Chem Ed* **10**:2545–2564
38. Matsumoto A, Ueda A, Aota H, et al (2002) *Eur Polym J* **38**:1777–1782
39. Salnikov VA, Bolbit NM (1985) *Vysokomolek Soedin A* **30**:2551–2555 (in Russian)
40. Matsumoto A, Okuno S, Aota H (1996) *Angew Makromol Chem* **240**:275–284
41. Funke W, Okay O, Yoos-Müller (1998) *Adv Polym Sci* **136**:139–234.
42. Matsumoto A, Kitaguchi Y, Sonoda O (1999) *Macromolecules* **32**:8336–8339

# Chapter 6

## Properties of Cross-Linked Polymers and Copolymers

**Abstract** The productive efficiency of the strength model developed by the authors is demonstrated in an example of experimental data on physical, mechanical, thermo-mechanical, and sorption properties of cross-linked polymers [on the basis of 23 polyfunctional oligo(acrylates)] and copolymers (on the basis of oligomeric dimethacrylate with five vinyl monomers). The strength model describes a cross-linked polymeric solid (obtained through TFRP) as superposition of interacting networks of physical and chemical bonds, taking into account the microheterogeneous environment of networks that is created in the course of polymerization. The authors established that the network of physical bonds exerts the prevailing influence upon strength characteristics in the forced-elastic state and that the network of chemical bonds exerts the prevailing influence upon strength characteristics in the glassy state. The value of information presented in Chap. 6 is upgraded by the description of the properties of those copolymers, the specifics of formation of which were analyzed in Chap. 4.

### 6.1 Cross-Linked Poly(acrylates). Physical and Mechanical Properties

Results of systematic research into the physical and mechanical properties of cross-linked poly(acrylates) synthesized via three-dimensional free-radical polymerization (TFRP) of oligomers of different classes are presented in articles and reviews [1–5], in which an attempt is made to establish a dependence of measurement of these properties upon the chemical structure of initial oligomers. This problem was successfully solved by one of the authors [6 (p. 148)] in the context of dominating influence of network of physical bonds on elastic and strength properties of cross-linked polymers. The term “network of physical bonds” implies a system of intermolecular interactions (IMI) that form a continuous spatial network of labile physical bonds (junctions).<sup>1</sup>

<sup>1</sup> Various types of intermolecular interactions in polymers and the possibility to approximate IMI systems in the form of network of physical bonds (physical network model) are discussed in two monographs [6, 7] and a survey [8].

Properties of polymers including cross-linked polymers (i.e., elastic, strength, and relaxation properties) for which time of the application of mechanical load or any other force field plays an important role, are, in essence, kinetic properties [7–10]. It is obvious that resistance to deformation (elasticity), and resistance to breaking (strength) in case a certain force is applied, as well as ability to restore initial state after the action of force field is eliminated (relaxation), are determined by the degree of the link of material components with one another. The concentration of chemical junctions and physical junctions ( $v_{\text{ch}}$  and  $v_{\text{ph}}$ ) in a unit of polymer volume serves as a quantitative measure of linkage degree. Effective concentration of physical junctions is not a constant of a given material (in contrast to concentration of chemical network junctions). It depends upon the conditions in which the measurement of a property is taken (namely, upon testing time and temperature). The shorter is the time of force action and the lower is the temperature of conducted experiment, the greater is the portion of physical network junctions that exhibits resistance to the said force action (see Sect. 6.2.1).

The combination of chemical and physical junctions of the network determines the molecular mobility responsible for the properties of cross-linked polymers. Elastic, strength, and relaxation properties of cross-linked poly(acrylates) should be considered as a function of the integral network that includes two components: the constant chemical network of covalent bonds and the variable network of intermolecular interactions (physical network, which is superimposed on chemical network). The chemical network is a constant for a given cross-linked polymer, and the degree of cross-linking of this network is determined by the structure of the initial oligomer and the three-dimensional polymerization mode. The density of the physical network is variable. As mentioned above, it depends on the intermolecular interaction (IMI) linkage dissociation energy  $E_a$ , and conditions of the experiment, plus the spatial arrangement of atomic groups that form physical junctions.

Hence, the contribution of the physical network to deformation resistance is determined by the degree of formation of potential junctions of the physical network in the form of IMI linkages, and this degree, along with values of  $E_a$  and conditions of the experiment, depends also upon the type of molecular packing of a given polymer.

Key experimental data on physical and mechanical properties of cross-linked poly(acrylate)s of different classes are also discussed within the framework of the network model [6, p. 166].

### ***6.1.1 Influence of Chemical Structure of Oligomers upon Physical and Mechanical Properties of Cross-Linked Poly(acrylates)***

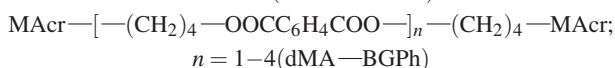
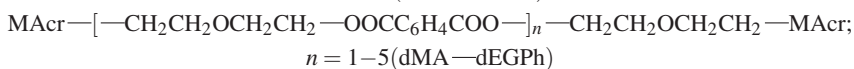
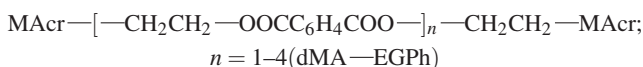
The chemical structure of oligomer molecules includes the following main elements influencing the physical and mechanical properties of cross-linked poly(acrylates):

- Potential junctions of the polymer chemical network [double bonds of acrylate and meth(acrylate) groups] that are formed in the course of polymerization either in full or partially
- Potential junctions of the physical network (atomic groups, centers of intermolecular interactions) that are formed only partially because of steric hindrances and freezing of mobility resulting from formation of the chemical network
- Bonds with a low potential rotation barrier, which ensures a high level of molecular mobility, thus facilitating the dissipation of mechanical energy
- Bulk atomic groups, the source of steric hindrances

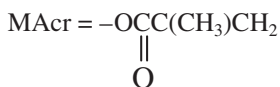
All this should be taken into account when comparing the physical and mechanical properties of cross-linked poly(acrylates) that differ in their chemical structure.

One of the popular methods used for comparative studying of physical and mechanical properties of cross-linked poly(acrylates) consists in selecting a series of polymers obtained via polymerization of oligomers (members of the so-called oligomer-homologous series) as objects of study. Every oligomer-homologous series is made up of oligomers with gradually increasing number of units  $n$  in the oligomeric block. Cross-linked polymers of an oligomer-homologous series of oligo(acrylates) and oligo(carbonate-acrylates) were analyzed [6 (p. 166)].

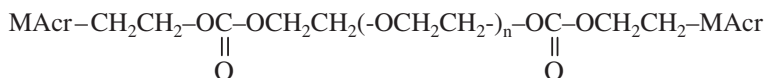
Oligo(methacrylates) are represented by an oligomer-homologous series of dMA-EGPh, dMA-dEGPh, and dMA-BGPh based on *o*-phthalic acid and dimethacrylates of ethylene glycol, diethylene glycol, and butylene glycol (butane-1,4-di-ol), respectively:



where MAcr is methacrylate:

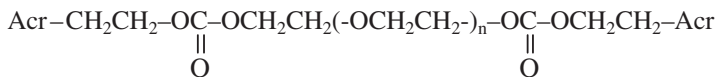


Oligo(carbonate-methacrylates) are represented by series OCM-2-OCM-4-OCM-6:



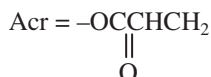
$$n = 1(\text{OCM} - 2); n = 2(\text{OCM} - 4); n = 3(\text{OCM} - 6)$$

Oligo(carbonate-acrylates) are represented by series OCA-2 - OCA-4 - OCA-6 characterized by variation of  $n$  within a wider range:

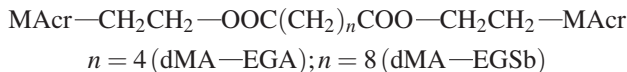


$$n = 2(\text{OCA} - 2); n = 4(\text{OCA} - 4); n = 6(\text{OCA} - 6)$$

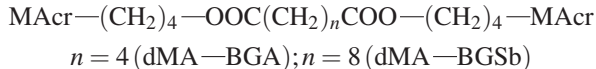
when Acr = acrylate.



dMA-EGA and dMA-EGSb are classified with oligo(methacrylates) on the basis of ethylene glycol and adipinic or sebacic acids, respectively:



Oligo(methacrylates) with longer-chain dMA-BGA and dMA-BGSb were obtained on the basis of the same acids and butylene glycol:



Physical and mechanical characteristics of cross-linked poly(meth)acrylates systematized according to oligomer-homologous series are listed in Tables 6.1, 6.2, 6.3, and 6.4.

Figure 6.1 shows the dependence of breaking tensile strength (TS) upon extent of chemical network cross-linking ( $v_{\text{ch}}$ ). The reverse value of the molecular weight of initial oligo(acrylates) is taken as a measure for the extent of chemical network cross-linking. An error is introduced when using such a measure for the extent of chemical network cross-linking ( $v_{\text{ch}}$ ) because of the difference between experimentally obtained and theoretical values of conversion, which is insignificant because of the semiquantitative level of discussion. It can be seen that when a sufficient body of data is available (e.g., for series dMA-EGPh and dMA-dEGPh),  $\sigma$  increases quite rapidly as the extent of chemical network cross-linking grows, and then  $\sigma$  declines steeply.

The position of the maximum of curves  $\sigma = f(v_{\text{ch}})$  depends on oligomer-homologous series nature, while the maximum breaking strength is practically constant and almost equals the limiting value of strength attained for cross-linked poly(acrylates) in the course of variation of all possible parameters, including testing conditions (see Fig. 6.1).

**Table 6.1** Variation of properties of cross-linked poly(meth)acrylates in homologous series dMA-EGPh and dMA-dEGPh [2]

Initial oligomer	Oligomer MW	Polymerization shrinkage, %	Stress at break, MPa		Breaking elongation, %	Impact resilience, kJ/m <sup>2</sup>	Brinell hardness, MPa	Tg, °C ± 2
			Under static flexure	Under compression				
dMA-EGPh-1	390	10.05	100	208	1.5	4.8	200	-
dMA-EGPh-2	582	7.66	120	-	2.1	5.6	170	-
dMA-EGPh-3	774	6.45	80	160	2.6	6.4	130	-
dMA-EGPh-4	960	4.63	65	120	3.0	8.2	110	-
dMA-dEGPh-1	478	7.5	115	-	11.0	5.0	135	60
dMA-dEGPh-2	714	4.8	160	220	15.0	10.0	86	46
dMA-dEGPh-3	950	4.3	155	-	20.0	11.4	69	32
dMA-dEGPh-4	1186	3.7	90	-	26.0	16.0	10	24
dMA-dEGPh-5	1422	-	74	-	32.0	19.0	90	20

**Table 6.2** Physical and mechanical properties of cross-linked poly(meth)acrylates [1]

Polymer	MW	$v_{ch} = 10^3/MW$ , mol/kg	$\sigma$ , MPa	$\epsilon$ , %
dMA-EGPh-1	390	2.57	43	1.4
dMA-EGPh-2	582	1.72	81	2.3
dMA-EGPh-3	774	1.29	48	2.9
dMA-EGPh-4	966	1.04	35	3.7
dMA-dEGPh-1	478	2.09	62	2.2
dMA-dEGPh-2	714	1.4	86	3.1
dMA-dEGPh-3	950	1.05	83	4.2
dMA-dEGPh-4	1186	0.84	45	5.2
dMA-dEGPh-5	1422	0.70	37	7.5
dMA-EGA	370	2.70	49	2.2
dMA-EGSb	426	2.34	12	3.5

Note 1. Rate of tension strain,  $\bar{V}_\epsilon = 0.5 \text{ min}^{-1}$ ; temperature, 20°C.

Note 2.  $\sigma$ , breaking strength;  $\epsilon$ , breaking elongation; MW, molecular weight of oligomer.

**Table 6.3** Physical and mechanical properties of cross-linked poly(meth)acrylates [1]

Polymer	MW	$v_{ch} = 10^3/MW$ , mol/kg	$\sigma$ , MPa	$E$ , MPa	$\epsilon$ , %	$\sigma/E$
dMA-dEGPh-1	478	2.09	76	3200	3.8	0.024
dMA-dEGPh-2	714	1.40	64	2450	4.7	0.026
dMA-BGPh-1	446	2.24	36	3350	1.1	0.011
dMA-BGPh-2	666	1.50	64	3150	2.4	0.020
dMA-EGA	370	2.70	50	2100	2.4	0.024
dMA-EGSb	426	2.35	10	450	3.0	0.022
dMA-BGA	426	2.35	16	500	4.3	0.032
dMA-BGSb	474	2.11	2	–	4.3	–

Note 1. Rate of tension strain,  $\bar{V}_\epsilon = 0.07\text{--}0.09 \text{ min}^{-1}$ ; temperature, 20°C.

Note 2.  $\sigma$ , breaking strength;  $\epsilon$ , breaking elongation;  $E$ , elasticity modulus; MW, molecular weight of oligomer.

**Table 6.4** Physical and mechanical properties of cross-linked poly-carbonate(meth)acrylates [1]

Polymer	MW	$v_{ch} = 10^3/MW$ , mol/kg	$\sigma$ , MPa	$E$ , MPa	$\epsilon$ , %	$\sigma/E$
OCM-2	374	2.67	75	3910	2.5	0.019
OCM-4	388	2.58	70	–	4.4	–
OCM-6	402	2.49	61	2480	4.7	0.025
OCA-2	346	2.89	75	3150	3.0	0.024
OCA-4	374	2.67	55	2300	3.7	0.024
OCA-6	398	2.51	34	1400	13.1	0.024

Note 1. Rate of tension strain,  $\bar{V}_\epsilon = 0.007\text{--}0.009 \text{ min}^{-1}$ ; temperature, 20°C.

Note 2.  $\sigma$ , breaking strength;  $\epsilon$ , breaking elongation;  $E$ , elasticity modulus; MW, molecular weight of oligomer.

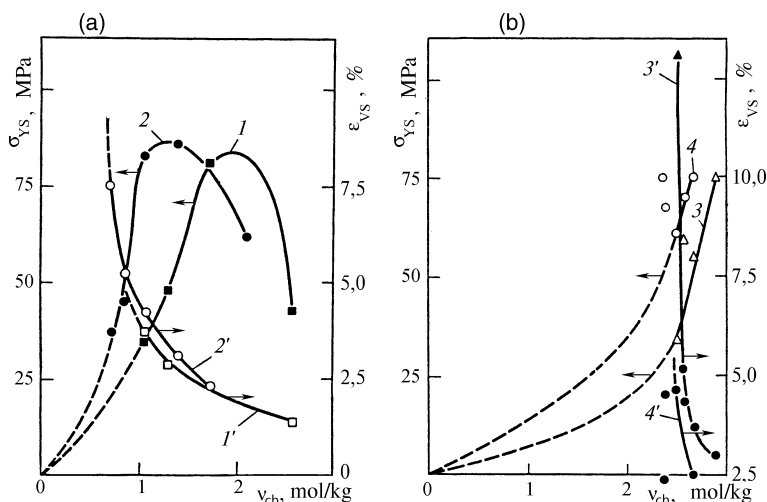


**Fig. 6.1** Dependence of physical and mechanical properties of cross-linked poly(meth)acrylates upon extent of chemical network cross-linking (based on data listed in Tables 6.2 and 6.4). **a** Oligomer-homologous series of cross-linked poly(meth)acrylates: dMA-dEGPh (1, 1') and dMA-EGPh (2, 2'). **b** Oligo-carbonate(meth)acrylates (4, 4') and oligo-carbonate-acrylates (3, 3')

It is obvious that the growth of cross-linked polymer strength (when moving from higher members of a homologous series to lower ones) on ascending branches of curves  $\sigma = f(v_{ch})$  cannot be a result of a simple increase in the density of physical network or chemical network.

Indeed, judging by values of molar constants of attraction of different atomic groups contained in cross-linked poly(acrylates) [6, p. 176], the physical network density  $v_{ph}$  (when moving from higher members of a homologous series to lower ones) not only does not increase, but declines slightly. The increase of  $v_{ch}$  by itself also cannot give the observed enhancement of strength because the additive contribution of the chemical network into the integral network  $v_{\Sigma} = v_{ch} + v_{ph}$  is insignificant; this is confirmed by a decrease (of more than 10 fold) of the elasticity modulus of oligo(acrylates) polymers after breaking of physical network junctions (e.g., in the case of a temperature rise). Hence, with the background of high values of  $v_{ph}$  ( $v_{ph}/v_{ch} > 10$ ), the 2-fold increase of  $v_{ch}$  (for cross-linked polymers belonging to dMA-EGPh and dMA-dEGPh series) certainly cannot lead to the observed 2-fold growth of strength, with the proviso of additivity of contribution of both networks (i.e., chemical and physical) into the resulting (integral) network of a polymer, that is, with the proviso that equality  $v_{\Sigma} = v_{ch} + v_{ph}$  is satisfied. The dependence of  $\sigma$  upon  $v_{ch}$  is even stronger for the OCA-2-OCA-6 series (see Fig. 6.1): increase of  $v_{ch}$  by only 15–20% results in 2-fold enhancement of strength. The strongest influence of  $v_{ch}$  was observed for the dMA-EGSb-dMA-EGA series of cross-linked polymers; an insignificant increase of  $v_{ch}$  (by about 15%) leads to an increase of  $\sigma$  of more than 4-fold (!) (see Table 6.2).

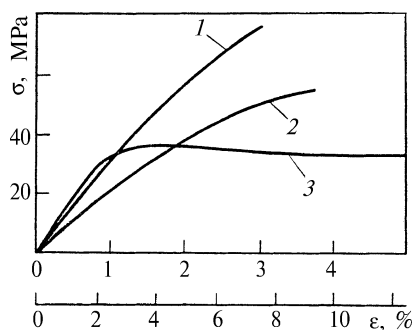


Observed nonadditivity of the  $v_{\text{ch}}$  contribution could be preconditioned by freezing of molecular mobility (resulting from formation of chemical network junctions) and corresponding enhancement of stability of physical junctions that are located in the freezing zone, the size of which depends upon the flexibility of oligomeric chains (i.e., upon the presence of “hinged” groups in them). The restriction of mobility (i.e., freezing) of chain fragments that carry physical junctions leads to a sharp increase in the lifetime of physical junctions (resulting from connection of chains by covalent bonds) according to the mechanism of the cage effect type. Indeed, in the freezing zone, breaking of intermolecular bonds by the action of energy fluctuation does not necessarily result in breaking of physical junctions because bringing the intermolecular interaction centers (that became free) away from one another is hindered by the restriction of mobility. That is why the probability of restoration of the same physical junction is very high, which is equivalent to the enhancement of its stability. Hence, the increase in the concentration of chemical junctions (cross-links) is accompanied by the formation of physical junctions characterized by enhanced stability. In other words, what takes place is not a simple addition but a synergistic interaction of two networks—namely, chemical and physical—which leads to the nonadditive effect  $v_{\Sigma} > v_{\text{ch}} + v_{\text{ph}}$ , where  $v_{\text{ph}}$  is the calculated value of concentration of physical junctions, with freezing effect not taken into account. Obviously, the length of the freezing zone along the chain is determined by the presence (or absence) of atomic groups with a low internal rotation barrier of type  $-\text{CH}_2-\text{O}-\text{CH}_2-$  in the chain. If the oligomeric chain contains atomic groups with a high internal rotation barrier of type  $-(\text{CH}_3)\text{C}(\text{CH}_3)-$ , the freezing (i.e., stabilization) zone can extend over the entire oligomeric chain.

The comparison of series dMA-EGPh, dMA-dEGPh, oligo(carbonate)-acrylates and oligo(carbonate)methacrylates shows that the effect of physical junction stabilization by chemical junctions diminishes in the indicated sequence of these series (see Fig. 6.1). For instance, when  $v_{\text{ch}} = 2.5 \text{ mol/kg}$ , the strength in the first two series is already higher than the maximum value, while for the last series the value of strength is still far from the maximum value. Thus, freezing of mobility of oligomeric chains of carbonate methacrylates becomes more difficult as  $v_{\text{ch}}$  increases.

The physical meaning of maxima on curves  $\sigma = f(v_{\text{ch}})$  (see Fig. 6.1) is obvious. As soon as the major part of the physical junctions has been stabilized through freezing, which is caused by increasing  $v_{\text{ch}}$ , the mechanical stress redistribution mechanism, the function of which is performed by the network of labile intermolecular bonds (i.e., by the physical network), turns out to be completely disabled. The stress concentration in defective zones of microheterogeneous structure of polymers leads to local overstresses that do not have enough time to relax (in other words, to become redistributed) and, as a consequence, to formation and propagation of microcracks. As a result of this, brittle transition of material occurs. Transfer to brittle transition is clearly manifested on tensile stress-strain diagrams (Fig. 6.2) and is expressed in the disappearance of the curvilinear section on curves  $\sigma = f(\epsilon)$ , which is related to forced elasticity. Only the initial linear section  $\sigma = f(\epsilon)$  remains if the

**Fig. 6.2** Representative strain curves for tension of cross-linked poly(carbonate-acrylates):  $T = 20^\circ\text{C}$ ; rate of extension,  $V_{\dot{\epsilon}} = 7 \times 10^{-3} \text{min}^{-1}$ . 1, OCA-2; 2, OCA-4; 3, OCA-6 (use the lower axis of abscissa)



brittle transition takes place, and in this case ultimate breaking strength  $\epsilon$  declines very steeply.

A data analysis method that is based on comparison of strength values reduced by elasticity modulus  $\sigma' = \sigma/E$  (instead of comparison of absolute values of strength) could be employed to evaluate the role of atomic groups of different chemical nature in redistribution processes. Selection of  $E$  as the reduction parameter is quite evident, as the elasticity modulus is proportional to the total extent of cross-linking (i.e., density) of the polymer network  $v_{\text{ch}} + v_{\text{ph}}$ , and, hence, values of  $\sigma'$  represent strengths that are reduced to identical extents of cross-linking of effective networks. It should be pointed out here that the value of  $v_{\text{ph}}$  includes only those physical junctions the lifetime of which exceeds the observation time (i.e., time of mechanical load action during experimental measurements of physical and mechanical parameters, in this case, strength).

It can be seen from Tables 6.3 and 6.4 that, depending on the chemical nature of oligomer molecules, the reduced strength varies from 0.011 to 0.032, and for the majority of cross-linked poly(acrylates), the value of  $\sigma'$  varies within the range 0.015–0.026. The authors believe that the higher is the degree of manifestation of stress redistribution processes in a polymer, the higher is the value of reduced strength. Brittle transition corresponds to lower values of  $\sigma'$ . The comparison of tensile stress-strain diagrams confirms this conclusion (Fig. 6.2).

Thus, it is possible to trace two different mechanisms of formation of cross-linked poly(acrylate) strength depending on their chemical structure. One mechanism is trivial, and according to this mechanism, strength enhances symbate to the growth of elasticity modulus simply by the increase in the extent of effective network cross-linking  $v_{\Sigma} = v_{\text{ch}} + v_{\text{ph}}$ . This mechanism is characteristic of those polymers, the chemical structure of which facilitates freezing of molecular mobility owing to high values of  $v_{\text{ch}}$  (with molecular weights of oligomers being low) because of inclusion of such atomic groups into the oligomeric chain that are potentially strong junctions of the physical network, for instance,  $-\text{C}_6\text{H}_4-$ ,  $-\text{C}_6\text{H}_4-\text{C}(\text{CH}_3)_2-\text{C}_6\text{H}_4-$ , and the like (see Tables 6.3 and 6.4).

Another mechanism of strength enhancement consists in intensification of stress redistribution processes. In this case, elasticity moduli are characterized by relatively low values, while strength values are, in contrast, quite high. It can be seen

from Tables 6.3 and 6.4 that the highest degree of redistribution process intensification is observed after introduction of “hinged” groups such as  $-\text{CH}_2\text{OCH}_2-$  into oligo(acrylates) molecules (compare dMA-dEGPh-1 with dMA-BGPh-1, etc.) or after extension of oligomeric chains owing to the increase of length or number of hydrocarbon sections of type  $-(\text{CH}_2)_n-$  (compare OCM-2 with OCM-6, dMA-BGPh-1 with dMA-BGPh-2, and so forth). However, with a too large number of “hinged” groups or too significant increase of  $n$  (compare dMA-EGA with dMA-EGSb), the reduced strength starts decreasing, having passed through its maximum. Obviously, this takes place because of excessive decline of the  $v_{\text{ph}}$  value. Indeed, the physical network efficiency in the stress redistribution processes is determined by its density  $v_{\text{ph}}$ , but with the proviso that a necessary level of molecular mobility in the overstress zone has been attained. Hence, the decline of  $v_{\text{ph}}$  does not adversely affect the efficiency of overstress relaxation only until this efficiency is limited by mobility restriction (i.e., by freezing).

### ***6.1.2 Influence of Physical Network Density upon Physical and Mechanical Properties of Cross-Linked Poly(acrylates)***

The influence of the chemical structure of initial oligomers upon the physical and mechanical properties of polymers of cross-linked poly(acrylates) was discussed in the previous section. It was shown that this influence is manifested via participation of elements of the chemical structure of oligomer molecules in the formation of stable covalent and labile intermolecular bonds, which represent the junctions of chemical and physical networks, respectively. Also, the concentration of physical network junctions  $v_{\text{ph}}$  (i.e., network density) represents the immediate factor for the generation of physical and mechanical properties, while the role of the chemical network consists of stabilization of physical junctions.

From this point of view, it is extremely interesting to consider the influence of rate of mechanical action application and testing temperature upon physical and mechanical properties of cross-linked poly(acrylates). These parameters enable one to vary  $v_{\text{ph}}$  without changing the chemical nature of the initial oligomer.

The lifetime of physical junction  $\tau_{\text{lifc}}$  under loading is determined by parameters given below in relationship (6.2). Only those junctions exhibit resistance to the mechanical action that exists during the time of experiment  $\tau_{\text{ex}}$ . Therefore, effective density of physical network  $v_{\text{ph}}$  includes concentrations of only those junctions that satisfy  $\tau_{\text{lifc}} > \tau_{\text{ex}}$ . As a set of physical junctions with different  $\tau_{\text{lifc}}$  is present in a polymer, then as  $\tau_{\text{ex}}$  decreases, the increasingly greater number of junctions would satisfy the condition  $\tau_{\text{lifc}} > \tau_{\text{ex}}$ . In other words,  $v_{\text{ph}}$  should increase as  $\tau_{\text{ex}}$  declines. Results of  $v_{\text{ph}}$  variation in response to changing strain rate  $\bar{V}_{\text{e}}$  within 3–4 decimal exponents are presented in Table 6.5 and Fig. 6.3. Obviously,  $v_{\text{ph}}$  increases as  $\bar{V}_{\text{e}}$  grows and  $\tau_{\text{ex}}$  declines.

Variation of testing temperature represents another method for changing the physical network density  $v_{\text{ph}}$ . It follows from relationship (6.2) that as the temperature increases, the lifetime of physical junctions  $\tau_{\text{lifc}}$  goes down, and, therefore, with

**Table 6.5** Influence of strain rate ( $\bar{V}_\epsilon$ ) upon physical and mechanical properties of cross-linked poly(acrylates) at 20°C [1]

$\bar{V}_\epsilon$ 10 <sup>2</sup> , min <sup>-1</sup>	$\sigma_{ys}$ , MPa	$\epsilon_{ys}$ , %	$E_1$ , MPa	$\sigma/E_1$	$\bar{V}_\epsilon$ 10 <sup>2</sup> , min <sup>-1</sup>	$\sigma_{ys}$ , MPa	$\epsilon_{ys}$ , %	$E_1$ , MPa	$\sigma/E_1$
OCM-2					dMA-EGA				
0.08	67	2.6	3250	0.021	0.06	50	3.8	1760	0.028
0.77	75	2.6	3710	0.020	0.31	53	4.0	1920	0.027
1.5	76	2.5	3810	0.020	–	–	–	–	–
7.1	79	2.4	4000	0.019	3.1	50	2.3	2120	0.024
87	78	2.4	4300	0.018	51	49	2.2	2140	0.023
880	11	0.2	4850	0.002	–	–	–	–	–
dMA-EGSb					dMA-dEGPh				
0.03	5.0	1.7	306	0.016	0.11	55	5.1	2490	0.022
0.30	9.0	2.5	360	0.025	0.96	58	4.3	2170	0.022
–	–	–	–	–	9	76	3.8	3200	0.024
3.2	10	3.0	455	0.022	18	79	3.6	3300	0.024
40	12	3.5	462	0.026	90	74	2.4	3400	0.022
–	–	–	–	–	–	–	–	–	–
OCM-6									
0.1	57	5.8	2370	0.024	18	71	3.7	2570	0.028
0.9	61	4.7	2480	0.025	33	71	3.6	2630	0.027
1.7	63	4.3	2490	0.025	84	72	3.8	2760	0.026
8.1	68	3.8	2520	0.027	–	–	–	–	–

the fixed value of  $\tau_{ex}$ , the lesser number of junctions will satisfy condition  $\tau_{life} > \tau_{ex}$ , that is, the value of  $v_{ph}$  should decrease as the temperature increases. Data of such kind are given in Table 6.6 and Fig. 6.4.

The analysis of data listed in Tables 6.5 and 6.6 and in Figs. 6.3 and 6.4 leads to conclusion that, regardless of the method by which the variation of physical network density was obtained, the increase of  $v_{ph}$  at first would give the enhancement of strength of highly cross-linked poly(acrylates) and then, starting from certain values of  $v_{ph}$ , as  $v_{ph}$  continues growing, the strength is diminished, i.e., the regularity is repeated, which was observed during stabilization of physical junctions by superimposition of the chemical network.

On curves showing variation of parameters of physical and mechanical properties  $\sigma$ ,  $E$ , and  $\epsilon$  depending on strain rate  $\bar{V}_\epsilon$  in all cases (see Fig. 6.3), one can clearly see two regions: a region of rapid changes of properties resulting from growth of  $\bar{V}_\epsilon$  (with  $\bar{V}_\epsilon \times 10^2 < 10 - 25 \text{ min}^{-1}$ ) and a region where properties change only slightly, almost a plateau (with  $25 < \bar{V}_\epsilon \times 10^2 < 100 \text{ min}^{-1}$ ). The third region, namely, the region of  $\sigma$  and  $\epsilon$  decline with increase in  $\bar{V}_\epsilon$ , is observed only in a very wide range of  $\bar{V}_\epsilon \times 10^2$  variation (with  $\bar{V}_\epsilon \times 10^2 > 100 - 500 \text{ min}^{-1}$ ). It seems likely that the presence of this plateau is connected with the nature of physical junction lifetime distribution function  $\tau_{life}$  or, in other words, function of distribution of junctions in terms of bond energy. The percentage of physical junctions, the value of  $\tau_{life}$  for which stays within the range  $25 < (1/\tau_{life}) \times 10^2 < 100 \text{ min}^{-1}$ , is close to zero, that is, the distribution function has something like a “dip” in this region at times.

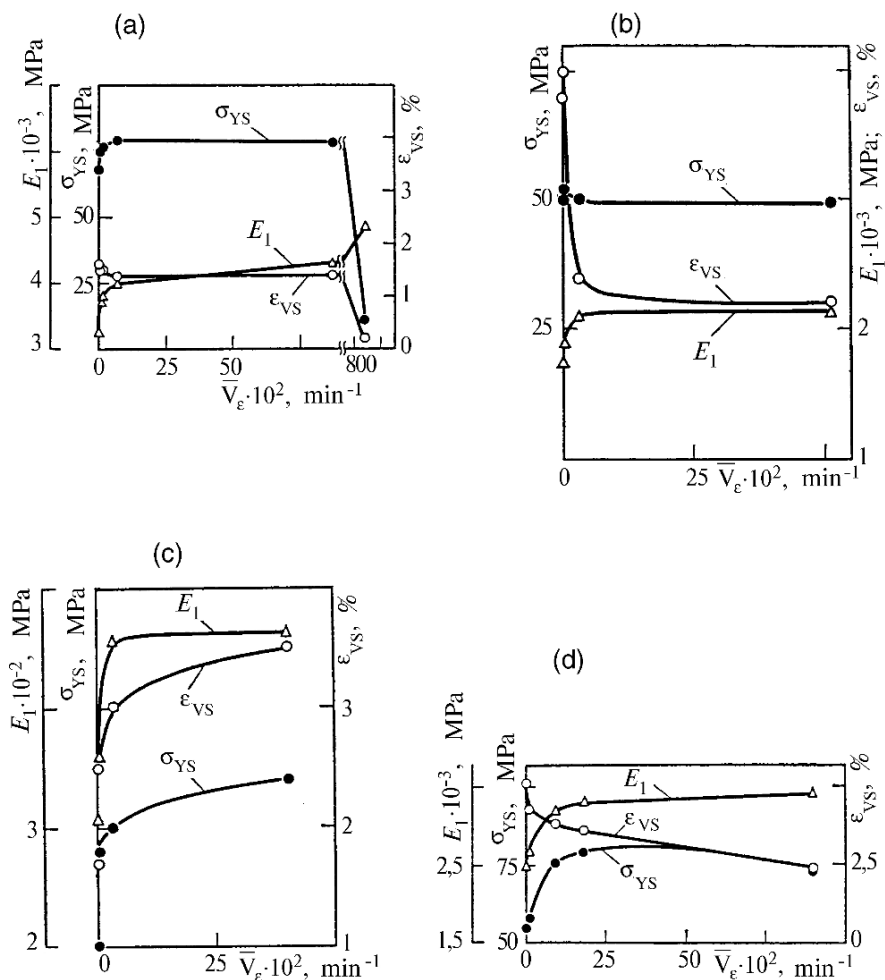


**Fig. 6.3** Dependence of physical and mechanical properties of cross-linked poly(meth)acrylates upon strain rate (based on data listed in Table 6.5). **(a)** OCM-2 polymer; **(b)** dMA-EGA polymer; **(c)** dMA-EGSb polymer; **(d)** dMA-DEGPh-1 polymer

Temperature dependences of parameters of physical and mechanical properties (Fig. 6.4) are so constructed that the direction of temperature variation by axis of the abscissa coincides with the direction of increase in  $v_{ph}$ . In all cases, for small values of  $v_{ph}$ , a region of symbate increase of  $\sigma$  and  $\epsilon$  is observed, whereas for high values of  $v_{ph}$ , a region of antibate increase of  $\sigma$  and  $\epsilon$  is observed. Most probably, the difference of temperature method for  $v_{ph}$  varying from the method connected with changes of  $\bar{V}_e$  consists, first of all, in the fact that a much wider range of  $v_{ph}$  is covered (especially in the direction of low values of  $v_{ph}$ ).

Besides, temperature variation may cause side disturbances in a micro-nonhomogeneous polymeric material. These side disturbances take the form of local

**Table 6.6** Influence of temperature upon physical and mechanical properties of cross-linked polymer dMA-EGA for different strain rates  $\bar{V}_e$  [1]

$\bar{V}_e = 0.30 \times 10^{-2}, \text{min}^{-1}$					$\bar{V}_e = 0.06 \times 10^{-2}, \text{min}^{-1}$				
T, K	$\sigma_{ys}, \text{MPa}$	$\epsilon_{ys} \times 10, \%$	$E_1, \text{MPa}$	$\sigma/E_1$	T, K	$\sigma_{ys}, \text{MPa}$	$\epsilon_{ys} \times 10, \%$	$E_1, \text{MPa}$	$\sigma/E_1$
—	—	—	—	—	243	47	19	2700	0.017
253	55	32	2940	0.019	252	58	29	2580	0.022
273	62	52	2500	0.025	270	44	35	1800	0.024
280	60	59	2300	0.026	—	—	—	—	—
293	50	40	1920	0.026	293	50	38	1760	0.028
323	30	35	1100	0.027	333	29	67	1120	0.026
343	25	40	1050	0.024	351	17	46	550	0.031
363	19	37	1000	0.019	365	15	42	520	0.029
385	12	33	625	0.019	—	—	—	—	—
393	9	28	340	0.027	392	4	19	300	0.013
421	4	18	250	0.016	—	—	—	—	—

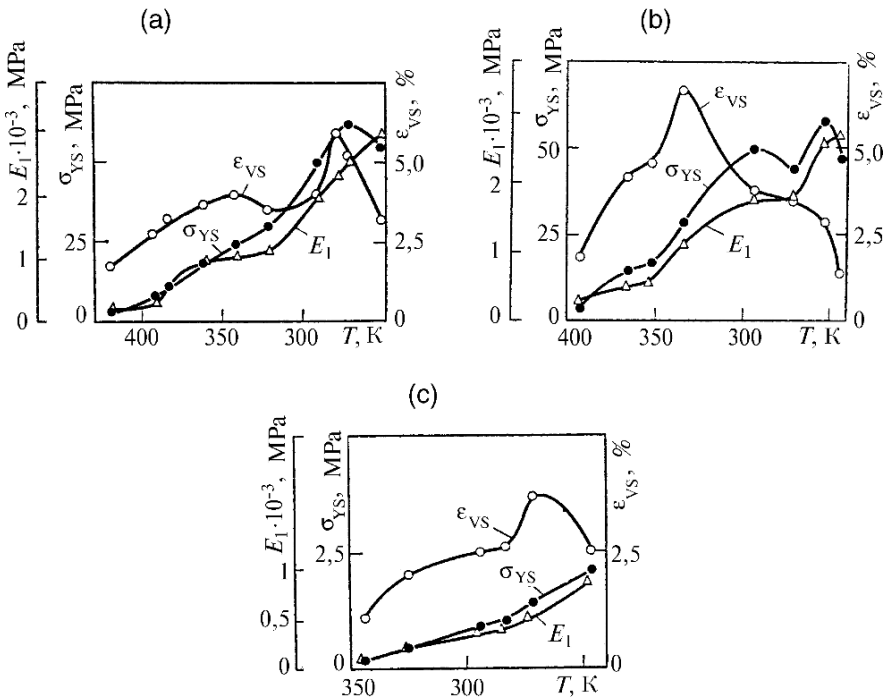


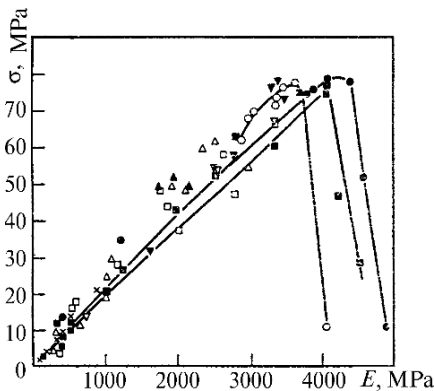
**Fig. 6.4** Dependence of physical and mechanical properties of cross-linked poly(meth)acrylates upon temperature for different strain rates (based on data listed in Table 6.6). (a) dMA-EGA polymer,  $\bar{V}_e = 3.0 \times 10^{-3} \text{min}^{-1}$ ; (b) dMA-EGA polymer,  $\bar{V}_e = 6 \times 10^{-4} \text{min}^{-1}$ ; (c) dMA-EGSb polymer,  $\bar{V}_e = 3.0 \times 10^{-3} \text{min}^{-1}$

micro-stresses resulting from the difference between the thermal expansion coefficient of grain material and that of the interlayer material.

The reduced strength grows with increase in  $v_{ph}$ , passes through its maximum, and then decreases again. The value of  $v_{ph}$  (corresponding to the maximum) provides the best conditions for redistribution of stresses in a material. At lower values of  $v_{ph}$ , the centers of intermolecular interactions (that provide for redistribution) are characterized by sufficient mobility, but their number is too small, whereas at higher values of  $v_{ph}$  the number of such centers is sufficient, but their mobility is frozen. The abnormal “splash” in reduced strength near the glass-transition temperature of oligo(acrylates) polymers is noteworthy. Although the absolute values of strength in this region are very small, values of  $\sigma/E$  are abnormally high. It is not improbable that in this temperature region orientation self-hardening is possible because of local glass transition in those micro-regions, in which orientation processes develop [3].

So, the dependence of strength of all types of studied cross-linked poly(acrylates) upon the cross-linking degree of effective network  $v_{\Sigma} = v_{ch} + v_{ph}$  [elasticity modulus  $E = f(v_{ch}, v_{ph})$ ] serves as a measure for cross-linking degree of effective network is reflected by curves with maxima (Fig. 6.5), while all points below the maximum point fall quite well onto a single master curve, despite the fact that the increase of  $E$  was effected by absolutely different methods: by increase in  $v_{ch}$  (resulting from decrease of molecular weight of initial oligo(acrylates)), or by increase of  $v_{ph}$  resulting from test temperature decrease or from strain rate growth. In a first approximation, the level of strength properties depends relatively weakly upon specific features of the chemical structure of oligo(acrylates) molecules and is determined mainly by the overall degree of cross-linking of polymer chains, by its effective network  $v_{\Sigma} = v_{ch} + v_{ph}$ . When a certain value of  $v_{ch} + v_{ph}$  is reached (let us denote the critical value of the elasticity modulus corresponding to this certain value as  $E_{crit}$ ), the strength reaches its maximum  $\sigma_{max} = 70\text{--}80\text{ MPa}$  [which is the same for oligo(acrylates) of different chemical nature] and only the value of  $E_{crit}$  [varying from 3500 to 4500 MPa for different series of oligo(acrylates)] reflects the chemical individuality of initial oligomers to a certain extent. When  $E > E_{crit}$ , the strength drops very steeply for all studied oligomer-homologous series.

**Fig. 6.5** Generalized dependence of breaking strength upon overall concentration of junctions of chemical and physical networks expressed in elasticity modulus units (based on data listed in Tables 6.2, 6.3, 6.4, 6.5, and 6.6)



The physical network in polymer structure always functions as a tool that redistributes mechanical stresses in material inner space in the process of deformation. Indeed, if the essentially reversible character of the process of disintegration and formation of physical junctions is taken into account, a quite obvious conclusion could be drawn that the junctions, which have disintegrated in local centers of stress concentration, are restored after release (relaxation) of over stresses, thus blocking the onset of micro-cracking and preventing it from growing extremely intensively. Hence, the physical network is a strength factor operating according to mechanism of stress redistribution in the direction of stresses equalization. The higher is the degree of material nonhomogeneity (i.e., the higher is the degree of material defectiveness), the more nonuniformly stresses are distributed in it during deformation and the higher is the reinforcing role of the physical network in such materials as a tool for redistribution and equalization of the stress field. Microheterogeneous cross-linked poly(acrylates) are characterized by a particular need for reinforcement by the physical network, but excessive densification of the physical network leads to strength deterioration (Fig. 6.5).

However, the physical network can effectively function as a stress redistributor only in the case if, upon junction disintegration under the action of overstress, network chain sections carrying fragments of the former junction can quickly move to a new position suitable for junction restoration. Therefore, the concurrent "activation" (freezing, stabilization) of all intermolecular interactions occurring when  $T$  goes down or  $\bar{V}_e$  grows (as well as when  $v_{ch}$  increases) leads to such deceleration in relaxation of chain sections carrying fragments of physical junctions that the junctions characterized by the greatest bond energy do not have enough time to be restored. It is just these junctions that play the most important role in stress redistribution and reinforcement.

Hence, the fact that in the region of high values of elasticity modulus  $E$  curve  $\sigma = f(E)$  starts falling as  $E$  increases (Fig. 6.5) can be explained not by the growth of physical network degree, but by a change of the kind of function for distribution of network junctions over bond energies. This change results in the appearance of a large number of low-energy junctions that "densely populate" relaxing sections of chains and prevent relaxation (and, thereby, restoration of high-energy junctions) and do not bring significant contribution to blocking of micro-cracking centers. In other words, physical junctions characterized by low bond energy are strong enough to inhibit the displacement (relaxation) of unloaded sections of chains, and, at the same time, are too weak to prevent the micro-destruction center growth taking place under the action of overstress.

In all cases described in this section, the centers of intermolecular interactions in oligomer molecules are apparently not strong enough to provide a high level of  $v_{ph}$ . And in the case of  $v_{ph}$  excitation resulting from superimposition of  $v_{ch}$ , weak junctions that impair the capability of strong centers for regeneration are stabilized also (especially if they are located near chemical junctions). The introduction of "hinged" groups improves the situation a little, but such improvement has strictly limited character due to destabilization of strong junctions in addition to weak ones. Probably, the introduction of ionogenic groups having  $E_{IMI} \approx 85$  kJ/mol



in combination with hinged groups of the ether types into oligomer molecules would enable obtaining values  $\sigma = 100\text{--}150\text{ MPa}$  with  $E = 5000\text{--}6000\text{ MPa}$ .

## 6.2 Cross-Linked Copolymers. Physical and Mechanical Properties [11]

Structural and physical properties of systematic series of synthesized cross-linked copolymers were identified based on results of measurements of thermo-mechanical, physico-mechanical, and diffusion-sorption properties [11]. Further, measurements of density also served as a supplementary method [in addition to infrared (IR) spectroscopy] for monitoring the final conversion of samples after their non-isothermal annealing upon removal from a calorimetric cell, in which kinetically controllable copolymerization was conducted under isothermal conditions (at  $60^\circ\text{C}$ ) up to limiting conversion  $(C_{\text{lim}})_{\text{iso}} < 1$ . Annealing (after polymerization) under non-isothermal conditions (stepwise conditions, with a step =  $10^\circ$ ) at  $60^\circ\text{--}130^\circ\text{C}$  makes it possible to increase the limiting conversion up to  $(C_{\text{lim}})_{\text{ni}} \approx 1$  (the subindex “iso” means isothermal conditions and subindex “ni” means non-isothermal conditions). This is a very important matter because equality of conversion for objects being compared represents a mandatory requirement for the comparison of properties of (co)polymers in systematic series of samples and for the identification of regularities and trends (because of very strong dependence of properties on conversion in the region of high conversions).

The method of physico-mechanical testing under axial compression conditions with the use of mini-samples weighing  $\approx 0.1\text{ g}$  appeared to be a very effective tool for structural and physical exploration into macromolecular networks characterized by a high degree of cross-linking. Under these conditions, the probability of premature fracture of material via generation of a main crack on an incidental defect is minimized. As a result of this, the authors managed to implement high-degree deformation (strain) including transition into the forced-elastic state.

### 6.2.1 Mechanism of Copolymers Transition into Forced-Elastic State

Representative curves of deformation (strain) in coordinates “stress ( $\sigma$ ) – strain ( $\epsilon$ )” are presented in Fig. 6.6.

In all cases, Hooke’s law is obeyed in a quite wide range of deformations from 0 to  $\epsilon_1$  (linear section with slope  $E_1$ ). A deviation from Hooke’s law (beginning in point  $\sigma_1$ ) represents the beginning of a region of transition into the forced-elastic state, and this transition ends in point  $\sigma_2$ ,  $\epsilon_2$ . Further the second linear section with slope  $E_2$  is observed. In terms of physical meaning,  $E_1$  is the elasticity modulus for the glassy state, while  $E_2$  is the elasticity modulus for the forced-elastic state.

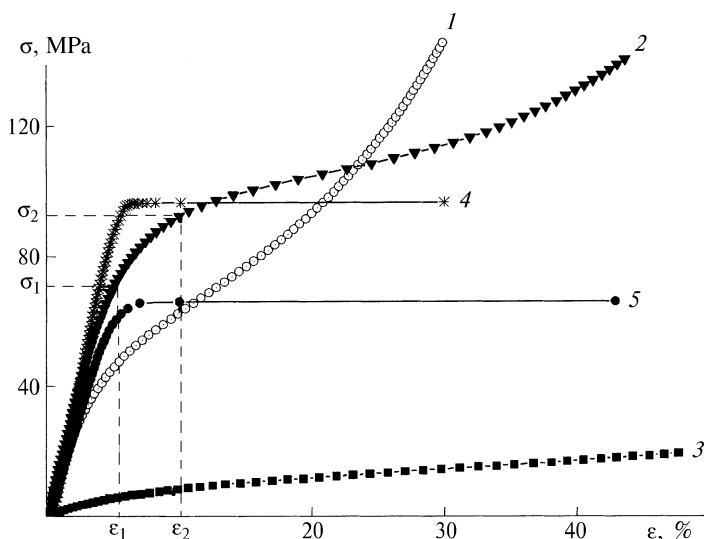


**Fig. 6.6** Representative curves of strain in coordinates “stress ( $\sigma$ ) – strain ( $\epsilon$ )” in the case of axial compression for samples with maximum value of concentration of chemical network junctions for tEGdMA polymer (1) and for samples of copolymer tEGdMA and MMA (2), BMA (3), styrene (4), and VA (5), with minimal value of concentration of physical network junctions.  $T = 23 \pm 1^\circ\text{C}$ ;  $\dot{\epsilon} = 10^{-4} \text{ s}^{-1}$

All above-indicated parameters— $E_1$ ,  $E_2$ ,  $\sigma_1$ ,  $\sigma_2$ , critical stress  $\sigma_{\text{cr}} = \sigma_1 + 0.5 \times (\sigma_2 - \sigma_1)$ , and width of transition into the forced-elastic state (FES)  $\Delta\sigma = \sigma_2 - \sigma_1$  (Table 6.7)—were analyzed as the reflection of certain structural and physical features in the given systematic series of copolymers. For this purpose, all of these are presented as a function of copolymer composition in Figs. 6.7 and 6.8.

Before proceeding to the discussion of data given in Figs. 6.7 and 6.8, let us briefly review the basic structural and physical concept on which the discussion logic would be based. The concept is based on a network model of a polymeric solid [6, 12, 13], according to which the chemical network of covalent bonds with volume concentration of junctions equal to  $v_{\text{ch}}$  and physical network of bonds with concentration of junctions  $v_{\text{ph}}$  of intermolecular interactions (IMI) are responsible for resistance to deformation. And, due to the lability of physical network junctions, they can exhibit resistance to deformation only in the case when their lifetime ( $\tau_{\text{life}}$ ) is commensurable with characteristic time of mechanical action (i.e., with time of experiment  $\tau_{\text{exp}}$ ), i.e., if the following condition is met:

$$\tau_{\text{life}} \geq \tau_{\text{exp}} \quad (6.1)$$

According to Eyring et al. [14]:

$$\tau_{\text{life}} = \tau_0 \exp[(E_{\text{dis}} - \gamma\sigma)/RT] \quad (6.2)$$

**Table 6.7** Physical and mechanical properties of copolymers tEGdMA,  $M_2$ :  $T = 23^\circ\text{C}$ 

$M_2$	$[M_1]$ , % (mol)	$C^*$ , %	$E_1 \times 10^{-2}$ , MPa	$E_2 \times 10^{-2}$ , MPa	$E_1/E_2$	$\epsilon_1$ , %	$\sigma_1$ , MPa	$\epsilon_2$ , %	$\sigma_2$ , MPa	$\sigma_{cr}$ , MPa	$\Delta\sigma_{cr}$ , MPa
MMA	0	95	15.5	0.91	17.0	3.51	51.8	16.8	101.1	76.4	49.3
	26	92	15.7	1.32	11.9	2.35	37.0	13.3	93.1	65.0	56.1
	50	87	14.0	2.01	6.96	2.36	32.9	11.4	82.6	57.7	49.7
	75	84	14.6	2.64	5.53	1.70	24.7	10.2	78.6	51.6	53.9
	100	82	13.8	2.74	5.05	1.31	16.9	9.62	60.8	38.8	43.9
BMA	0	100	1.53	0.27	5.73	1.45	2.22	24.7	13.8	8.0	11.6
	25	97	9.08	0.54	16.8	2.03	17.3	12.5	37.1	27.2	19.8
	52	87	10.7	1.35	7.93	1.72	18.1	11.1	52.6	35.3	34.5
	75	85	11.5	1.91	6.02	1.91	22.0	9.61	55.0	38.5	33.0
	100	82	13.8	2.74	5.05	1.31	16.9	9.62	60.8	38.8	43.9
DMA	25	95	0.061	–	–	1.77	0.27	–	–	–	–
	50	94	1.46	0.43	3.39	1.61	2.22	9.85	8.29	5.25	6.07
	75	92	7.45	1.38	5.40	2.03	14.2	9.63	37.1	25.6	22.9
	100	82	13.8	2.74	5.05	1.31	16.9	9.62	60.8	38.8	43.9
Styrene	0	97	20.7	0.002	8821	3.27	68.8	6.3	96.0	82.4	27.2
	25	89	18.4	0.27	68.1	2.72	49.3	11.8	88.8	69.0	39.5
	50	90	17.3	1.17	14.8	2.2	38.0	11.6	90.7	64.3	52.7
	75	84	14.7	1.94	7.58	1.54	22.1	9.90	70.7	46.4	48.6
	100	82	13.8	2.74	5.05	1.31	16.9	9.62	60.8	38.8	43.9
BA	25	89	0.11	–	–	–	–	–	–	–	–
	51.5	93	5.73	1.06	5.41	1.14	6.08	9.08	24.7	15.4	18.6
	75	87	12.3	1.75	7.03	1.69	19.4	10.1	55.7	37.5	36.3
	100	82	13.8	2.74	5.05	1.31	16.9	9.62	60.8	38.8	43.9
VA	0	95	14.0	0.002	8218	3.12	43.6	9.7	65.8	54.7	22.2
	25	89	3.89	0.72	5.40	1.75	6.8	8.86	16.9	11.8	10.1
	50	88	12.5	1.49	8.37	1.35	16.2	9.63	51.6	33.9	35.4
	75	88	18.8	3.61	5.21	1.22	21.6	10.3	90.3	55.9	68.7
	100	82	13.8	2.74	5.05	1.31	16.9	9.62	60.8	38.8	43.9

Note.  $C^*$  obtained by densitometry.

where, as applied to the process of dissociation of IMI bonds in the field of mechanical forces,  $E_{dis}$  = dissociation energy;  $\tau_0$  = frequency of atomic oscillation  $\sigma$  = mechanical stress; and  $\gamma$  = numerical factor.

Therefore, only those IMI bonds would make a contribution in  $v_{ph}$ , the value of  $E_{dis}$  for which (at given value of  $\sigma$  and selected strain rate  $\epsilon$ ) exceeds  $E_{dis}$  defined by the following inequality:

$$\tau_0 \exp[(E_{dis} - \gamma\sigma)/RT] \geq \tau_{exp} \quad (6.3)$$

Values of  $E_{dis}$  for IMI of different types are summarized in a monograph [15]; IMI energy estimation and calculation methods are also described in this monograph.

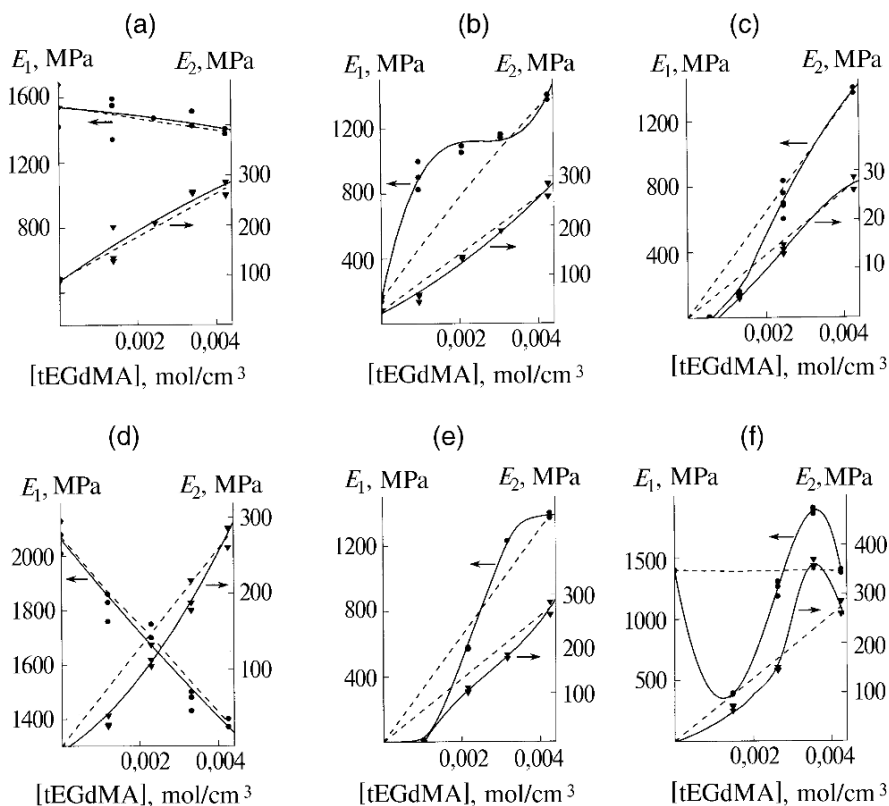


**Fig. 6.7** Dependences of elasticity moduli in glassy ( $E_1$ ) and forced-elastic ( $E_2$ ) states under strain in the mode of axial compression for different copolymers of tEGdMA and  $M_2$ :  $M_2 = \text{MMA}$  (a);  $M_2 = \text{BMA}$  (b);  $M_2 = \text{DDMA}$  (c);  $M_2 = \text{styrene}$  (d);  $M_2 = \text{BA}$  (e);  $M_2 = \text{VA}$  (f).  $T = 23^\circ \pm 1^\circ\text{C}$ .  $\epsilon^* = 10^{-4} \text{ s}^{-1}$ . *Dotted lines*, calculated values; *solid lines*, experimental dependences

In our case, the carriers of  $v_{\text{ch}}$  are only those tEGdMA molecules that have two multiple bonds, which form chemical junctions: ester groups and ether groups in tEGdMA molecules capable of dipole–dipole IMI serve as carriers of  $(v_{\text{ph}})_{M_1}$ . Comonomer molecules  $M_2$  form  $(v_{\text{ph}})_{M_2}$  owing to appropriate IMI centers. In certain cases, cooperation of physical junctions is possible [15 (p. 147);16], which results in the formation of such strong bonds that under the conditions of the experiment they manifest themselves as chemical bonds. Let us denote the network consisting of such junctions as  $v_{\text{ch}}'$ . In the case of MMA, it is known [17] that short syndio- and isotactic unit sequences (that are always present in the chains of atactic PMMA synthesized via radical polymerization) behave as complementary sequences. Because of this fact, IMI centers in them become cooperated, which results in the formation of physical junctions of type  $v_{\text{ch}}'$  (these junctions are referred to as stereocomplexes). The mechanisms of  $v_{\text{ph}}$  formation are described in detail in a monograph [12] and a review [13].

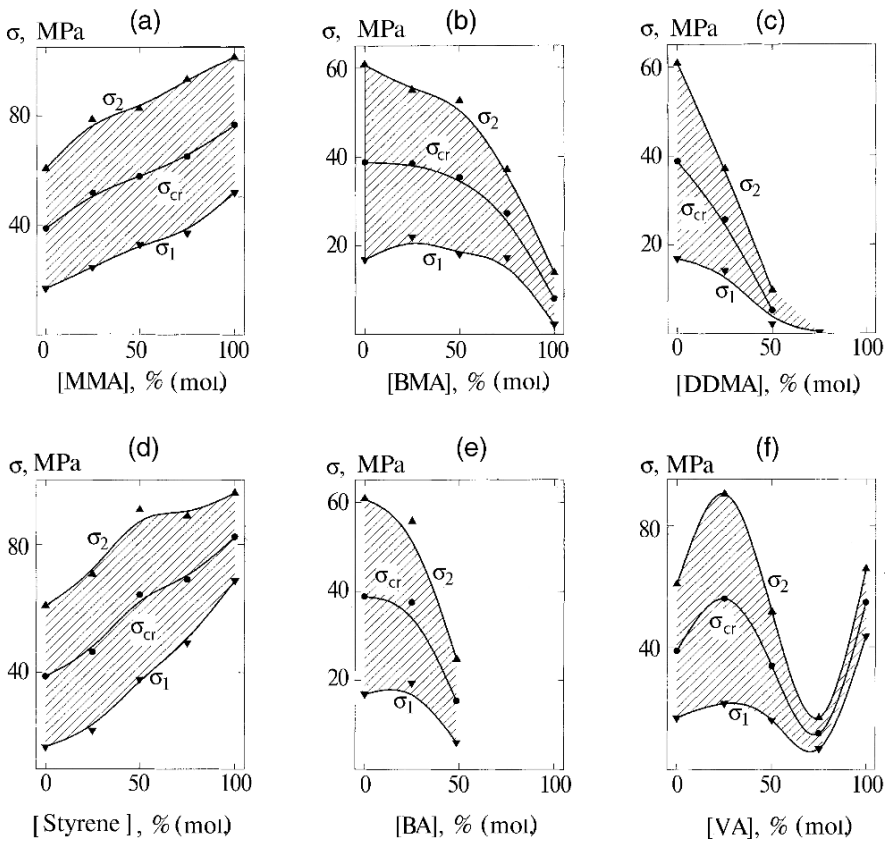


**Fig. 6.8** Dependences of critical stress ( $\sigma_{cr}$ ), lower ( $\sigma_1$ ), and upper ( $\sigma_2$ ) boundaries of  $\alpha$ -transition region under strain in the mode of axial compression upon copolymer composition tEGdM-M<sub>2</sub> and different M<sub>2</sub>: MMA (a), BMA (b), DDMA (c), styrene (d), BA (e), and VA (f).  $T = 23^\circ \pm 1^\circ\text{C}$ ;  $\dot{\epsilon} = 10^{-4} \text{S}^{-1}$

Another kind of very strong IMI bonds having  $\tau_{\text{life}} \geq \tau_{\text{exp}}$  at  $\sigma > \sigma_2$  are the so-called physical junctions stabilized by nearby chemical junctions (Kraus was the first to discover these junctions in the 1960s [18]). In the general case the effect of stabilization of weaker junctions by stronger ones located nearby is observed not only in combined network  $v_{\text{ch}} + v_{\text{ph}}$ , but also in a purely physical network. Therefore, in homopolymeric M<sub>2</sub> as well, which do not have the chemical network but do have a physical network component consisting of cooperated junctions with high values of  $E$ , the value of residual  $v_{\text{ph}}'$  in the forced elastic state will be higher than the concentration of these strong junctions by the number of adjacent junctions located in “stabilization” zones.

Within the framework of the network model, the carrier network (i.e., network exhibiting resistance to deformation) in the glassy state includes all three components,  $v_{\Sigma} = v_{\text{ch}} + v_{\text{ch}}' + v_{\text{ph}}$ ; and, at that,  $v_{\text{ch}} + v_{\text{ch}}' < v_{\text{ph}}$ , i.e., mainly the physical network functions, and its contribution is, of course, determined not only by volume

concentration of atomic groups (that are carriers of strong IMI centers), but also by the degree of realization of these potential junctions of the physical network in the form of IMI bonds, which, in its turn, is predominantly determined by the type of molecular packing characteristic of a given polymeric solid. Therefore,  $v_{ph}$  and  $v_{ch}'$  are effective values, which implicitly include additional factors also (at least, the influence of molecular packing).

During deformation,  $v_{ph}$  remains constant only until the moment when, according to condition (6.3), lifetime  $\tau_{life}$  of labile physical junctions would decline to a value commensurable with time of experiment  $\tau_{exp}$  due to increase of  $\sigma$ . As soon as this occurs, junctions with  $\tau_{life} < \tau_{exp}$  would cease to perform the function of carriers, which is adequate to  $v_{ph} \rightarrow 0$  ("breaking" of the physical network). Because  $v_{ph}$  consists of a set of physical junctions of different stability (which differ by value of  $E_{dis}$ ), with  $\sigma \rightarrow \sigma_1$ , the "weakest" junctions (characterized by lowest  $E_{dis}$ ) would start disintegrating, followed by stronger and stronger junctions and, finally, with  $\sigma \rightarrow \sigma_2$ ,  $v_{ph} \rightarrow 0$  would occur, and the carrying network  $v_{\Sigma} = v_{ch} + v_{ch}' + v_{ph}$  would be transformed into  $v_{FES} = v_{ch} + v_{ch}'$ . After that, within a quite wide range of  $\sigma > \sigma_2$ , the lifetime of most stable physical junctions (characterized by volume concentration  $v_{ch}'$ ) would stay within the limits of fulfillment of condition  $\tau_{life} > \tau_{exp}$  as  $\sigma$  increases, that is,  $v_{FES} = v_{ch} + v_{ch}' = \text{const}$  would be observed within this range. The constancy of inclination of strain curves in region  $\sigma > \sigma_2$  represents a reflection of this fact.

Hence, within the framework of the network model of polymeric solids, the essence of transition into the forced-elastic state (FES) consists in transition (at fixed temperature) from glassy state characterized by value  $v_{net} = v_{ch} + v_{ch}' + v_{ph}$  and maintained in the range  $0 \leq \sigma \leq \sigma_1$  (where  $v_{net} = \text{const}$ ) to a state characterized by value  $v_{FES} = v_{ch} + v_{ch}'$  and maintained in the region  $\sigma \geq \sigma_2$ , where  $v_{FES} = \text{const}$ . The role of the "driving force" of this transition is played by mechanical stress  $\sigma$ , which functions according to regularity (6.3): transition mechanism = "breaking" of physical junctions network, while the transition width reflects the difference between dissociation energies of physical junctions of different nature  $\Delta E_{dis} = (E_{dis})_{max} - (E_{dis})_{min}$  and, probably, a set of possible types of molecular packing (for microheterogeneous polymeric solids) if the packing is able to significantly influence the degree of realization of potential IMI centers as IMI bonds.

Further, let us analyze the relationship between effective carrier network  $v_{eff}$  and elasticity modulus within the framework of the network model. Theoretically, a quantitative relationship between network  $v_{ch} + v_{ph}$  in polymeric solid and elasticity modulus  $E$  was established only for the highly elastic state and only for the subclass of very low cross-linked networks  $(v_{ch} + v_{ph}) \leq 10^{-1} \text{ mol/l}$ :

$$E = f v R T \quad (6.4)$$

where  $v$ , in terms of physical meaning, is integral network  $v_{ch} + v_{ph}$ , while proportionality factor  $f$  has the numerical value 1–3 depending on topological singularities of the network. Later it was found [19] that proportionality of  $E$  and  $v$  is preserved also for the subclass of highly cross-linked networks  $10^{-1} \leq v \leq 10 \text{ mol/l}$ .

For instance, Katz and Tobolsky [19] experimentally established, on an example of (co)polymers of methyl(meth)acrylate and di(meth)acrylates, that as  $\nu$  grows [ $\nu$  value was changed by varying the fraction of di(meth)acrylate in the binary mixture] this regularity holds true for the subclass of most highly cross-linked networks  $3 \leq \nu \leq 10$  mol/l, but in this case the numerical value of  $f$  increases up to 10–12. Nominal concentration  $\nu_{\text{ch}}$  equal to molar concentration of di(meth)acrylate is taken as the value of  $\nu$ . Tobolsky conducted his experiments in the field of highly elastic state at  $T > T_g$ .

The authors failed to find published data on the relationship between  $E$  and  $\nu$  for the forced-elastic state at  $T = 23^\circ\text{C} < T_g$  as well as for the glassy state. This relationship is obvious at the qualitative level; the value of  $E$  should change symbate as a result of  $\nu$  variation because it is just the integral carrier network that exhibits resistance to deformation. In our case, implying studying of copolymers, only the nominal value of  $\nu_{\text{ch}}$  is known with certainty (it is equal to the true value of  $\nu_{\text{ch}}$  with a precision to the error due to secondary reaction of small cycle formation, in other words, cyclization). The nominal value of  $\nu_{\text{ph}}$  could be estimated by calculation described in [20] (in some cases [21], such calculations give reliable results). Also, it is practically impossible to estimate values of  $\nu_{\text{ch}}'$ . Therefore, a dependence upon molar concentration of di(meth)acrylate, which is equal to the half of nominal value of  $\nu_{\text{ch}}$  [each di(meth)acrylate molecule forms two trifunctional junctions as a result of copolymerization] has been accepted as the basis for systematization of data presented in Figs. 6.7 and 6.8.

In Fig. 6.12a composition of copolymers (in molar fractions) was used for data systematization, which is convenient for characterizing the composition of initial mixtures and copolymers being formed, but does not correspond to the physical meaning of  $\nu$ . Conversion of molar fractions  $a$  to volume concentrations  $[M_1]$  and  $[M_2]$  was carried out by the following formulas:

$$[M_1]_{\text{cp}} = \frac{\rho_{\text{cp}}}{M_{M_1} - M_{M_2} + \frac{M_{M_2}}{\alpha_1}} \quad (6.5)$$

where  $[M_1]$  and  $[M_2]$  are expressed in mol/cm<sup>3</sup>, copolymer density  $\rho_{\text{cp}}$  in g/cm<sup>3</sup>, and molar weights of monomers  $M_{M_1}$  and  $M_{M_2}$  are expressed in g/mol. Values of  $\rho_{\text{cp}}$  in (6.5) were derived by the densitometric titration method.

Reference (calculated) lines were drawn in Figs. 6.7 and 6.9 (shown as dotted lines). The physical meaning of these reference lines is based on the assumption that during (co)polymerization links  $M_1$  and  $M_2$  would be the carriers of the same network junctions ( $M_1$  = chemical junctions and  $M_2$  = physical junctions), which took place in homopolymers. Then, if we denote integral networks (chemical + physical) in homopolymers as  $(\nu_\Sigma)_{M_1}$  and  $(\nu_\Sigma)_{M_2}$ , integral network  $\nu_\Sigma$  in the copolymer would consist of  $(\nu_\Sigma)_{M_1}$  and  $(\nu_\Sigma)_{M_2}$  represented in fraction relationship with respect to volume concentrations of units  $M_1$  and  $M_2$  in (co)polymer. That is:

$$\nu_\Sigma = (\nu_\Sigma)_{M_1} \cdot \frac{[M_1]_{\text{cp}}}{[M_1]_{\text{hp}}} + (\nu_\Sigma)_{M_2} \cdot \frac{[M_2]_{\text{cp}}}{[M_2]_{\text{hp}}} \quad (6.6)$$

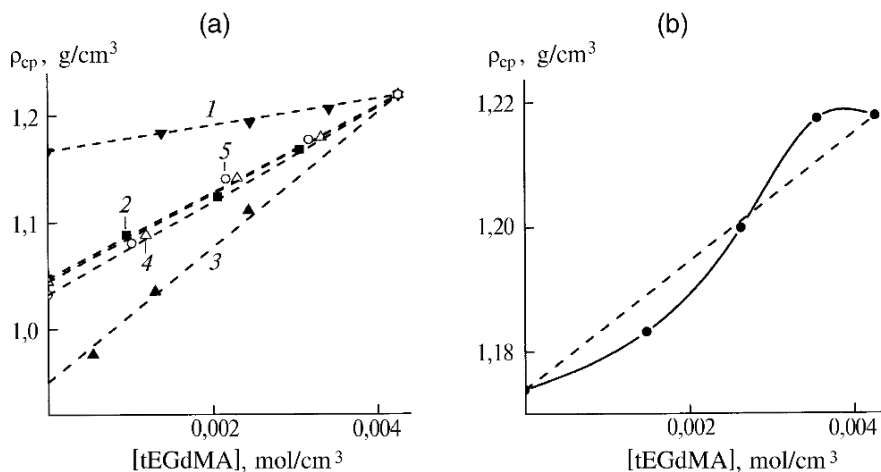


**Fig. 6.9** Experimental dependences (points) and calculated dependences with additivity taken into account (*dotted curves*) of copolymers density (tEGdMA- $M_2$ ) upon composition for different  $M_2$ . (a) MMA (1); BMA (2); DDMA (3); styrene (4); BA (5); (b) VA

where  $(v_{\Sigma})_{M_1}$  and  $(v_{\Sigma})_{M_2}$  = volume concentrations of effective junctions network (chemical network plus physical network) in homopolymers  $M_1$  and  $M_2$ ;  $[M_1]_{cp}$ ,  $[M_2]_{cp}$ ,  $[M_1]_{hp}$ , and  $[M_2]_{hp}$  = volume concentrations of units  $M_1$ ,  $M_2$  in copolymers and homopolymers (subindex “cp” means copolymer and subindex “hp” means homopolymer).

If we also assume that elasticity moduli in homopolymers  $(E_{hp})_{M_1}$  and  $(E_{hp})_{M_2}$  and in copolymers  $E_{cp}$  are proportional to  $v$ , then  $E_{cp}$  could be expressed as a function of elasticity moduli of homopolymers  $(E_{hp})_{M_1}$  and  $(E_{hp})_{M_2}$  in the form of the following additive relationship:

$$E_{cp} = (E_{hp})_{M_1} \cdot \frac{[M_1]_{cp}}{[M_1]_{hp}} + (E_{hp})_{M_2} \cdot \frac{[M_2]_{cp}}{[M_2]_{hp}} \quad (6.7)$$

We emphasize that it is just volume concentration of units  $[M]_{cp}/[M]_{hp}$  that should be used in equations (6.6) and (6.7), not the molar fractions of these units. Hence, the physical meaning of reference lines (dotted lines in Figs. 6.7 and 6.9) consists in fulfillment of additivity in respect of effective network  $v$  (relationship (6.6)) provided that elasticity modulus is proportional to the value of  $v$ .

Let us now analyze data presented in Fig. 6.7. It can be seen that elasticity modulus  $E_1$  (glassy state) and  $E_2$  (forced elasticity state) in some cases obey the additive law quite accurately (6.7): MMA = both elasticity moduli, BMA =  $E_2$ , and styrene =  $E_1$ . In the other two cases, additivity is observed in a limited range of copolymer composition: BMA =  $E_2$  and DDMA =  $E_1$  and  $E_2$ . In all these cases the experiment is consistent with the assumption that  $E \sim v$  even in glassy state, that is, the empirical law discovered by Tobolsky for the case of very low cross-linked (meth)acrylates in highly elastic state, probably, in some cases, covers the glassy state also.



Another noteworthy feature consists in the fact that, first, the value of  $E_2$  for homopolymer  $M_1$  is incommensurably higher in all cases than that for homopolymers  $M_2$ . If interpreted within the framework of the network model, this fact is indicative of an incommensurability of  $v_{ch}$  and  $v_{ph}$  contributions into an integral effective network, that is,  $v_{ch} \gg v_{ph}$  in the region of forced-elastic state. Second, an increase in  $E_2$  is observed as molar concentration  $M_1$  grows. Deviations from additivity in Fig. 6.7 have a different nature for different copolymerization systems. In the case  $M_2 = \text{styrene}$ , only deviation of  $E_2$  is observed outside the experimental error limits (and this deviation is insignificant). In the case  $M_2 = \text{DDMA}$ , a deviation (with a minus sign) appears in the region of copolymer compositions with low content of network-forming monomer  $M_1$ , which could be associated with high-degree microheterogenization of copolymers that was visually observed in the form of turbidity. In the case  $M_2 = \text{BA}$ , significant negative deviations from additivity of both elasticity moduli in the region of copolymer compositions enriched with  $M_2$  units are, probably, associated with depression of lower value of  $\alpha$ -transition value (Fig. 6.12e) to a temperature below 23°C, i.e., the temperature at which measurements of  $E_1$  and  $E_2$  were taken. It is not improbable that significant positive deviation from additivity of  $E_1$  value for BMA is related to the positive influence of copolymer composition by value of  $T_g$  (Fig. 6.12b) that was observed in the same range of compositions and, that was, probably, caused by the same reasons, which were analyzed when  $T_g$  was discussed (diminution of cyclization contribution due to the shadow effect of bulk substitutes  $C_4H_9$  with all ensuing topological and morphological consequences).

Of particular interest are data for  $M_2 = \text{VA}$ : deviations from additivity take place through inversion point and they are accompanied by the change of the minus sign (in the region of compositions with high content of VA-VA units) for plus sign (when the content of VA in copolymer is low). A remarkable circumstance in this case is the fact that the character of deviation of curves  $E_1$  (glassy state) faithfully reproduces the character of deviation of corresponding curves for  $E_2$  (forced elasticity state). This finding suggests that VA and tEGdMA polymers have common structural and physical features, which is characteristic of both states, the more so as anomalies of  $\alpha$ -transition were expressed to the maximum extent exactly in the case  $M_2 = \text{VA}$  (Fig. 6.12f). Anomaly  $T_g$  for  $M_2$  consists in the existence of copolymer composition range, in which  $T_g$  of copolymers is higher (!) than  $T_g$  of each of the homopolymers. A similar anomaly is also observed for both modules  $E_1$  and  $E_2$ : a range exists, in which the value of  $E$  is higher (!) than  $E$  of each of homopolymers. These strongly pronounced features of copolymer properties is, apparently, connected, first of all, with topological peculiarities of their network structure of the “snake-cage” type (network of tEGdMA with long grafted VA chains). This network structure is formed due to specific set of constants of copolymerization  $r_1 \approx 20 \gg 1, r_2 \approx 0.05 \ll 1$ .

Measurements of copolymer density (Fig. 6.9) also indicate exclusiveness of VA copolymers: deviations from additivity correlate with features showed in Figs. 6.7 and 6.8f and 6.12f.

Additive densities of copolymers were calculated by the following formula:

$$\rho_{\text{adcp}} = \frac{M_{M_1} (\rho_{\text{hp1}} - \rho_{\text{hp2}})}{\rho_{\text{hp1}}} \cdot [M_1] + \rho_{\text{hp2}} \quad (6.8)$$

where  $\rho_{\text{hp1}}$  and  $\rho_{\text{hp2}}$  = densities of homopolymers consisting of units  $M_1$  and  $M_2$ , respectively;  $[M_1]$  = volume concentration of  $M_1$  units; and  $M_{M_1}$  = molecular weight of monomer  $M_1$ .

It should be specially pointed out here that the gross composition of all synthesized copolymers is practically the same as the composition of the initial binary mixture of monomers  $M_1 + M_2$ , because the copolymerization process via annealing at  $T > T_g$  was conducted in all cases to high conversions (82–97%), which were controlled through the use of densitometric and IR spectroscopy methods.

It is obvious that from the standpoint of the network model, or within the framework of any other approaches existing nowadays, it is impossible to correctly interpret a set of systematic data presented in Figs. 6.7, 6.8, 6.9 and Table 6.7, especially data so complex as for the case  $M_2 = \text{VA}$ . However, one of the most significant advantages of the network model in this case consists in the fact that it enables us to rigorously and logically describe the mechanism of transition from the glassy state into the forced-elastic state and to formulate the structural and physical essence of the highly elastic state. All this offers an opportunity to build quite reasonable assumptions within the framework of the same logic. Also, these assumptions plus the full set of basic data given in Figs. 6.7, 6.8, 6.9 and Table 6.7 enable the authors to draw more or less substantiated conclusions regarding specific features of topological and morphological structure of the systematic set of copolymers presented herein.

### 6.2.2 *Influence of Cyclization on Physical and Mechanical Properties of Copolymers*

Formation of small cycles (cyclization) by the linking together of double bonds pendent to adjacent units of primary polymeric chains during three-dimensional free-radical polymerization is a secondary reaction that leads to reduction of the numerical value of  $v_{\text{ch}}$  as compared to the nominal value in the topological aspect and to microheterogenization of the polymeric solid being formed in the morphological aspect. Usually the influence of various factors upon cyclization is estimated based on deviation of experimentally obtained values of critical conversion of gel formation  $(C_{\text{cr}})_{\text{exp}}$  from theoretical (calculated) values  $(C_{\text{cr}})_{\text{th}}$ . In this case, the difference  $\Delta C = (C_{\text{cr}})_{\text{th}} - (C_{\text{cr}})_{\text{exp}}$  serves as a measure of cyclization contribution. According to the opinion of many authors [22–24], copolymerization of network-forming monomers ( $M_1$ ) with monounsaturated monomers ( $M_2$ ) that get embedded between adjacent units  $M_1$  into primary polymeric chains, thus reducing the probability of interaction of adjacent pendent double bonds, represents one of the factors that reduce  $\Delta C$ . Obviously, the efficiency of  $M_2$  in this case should depend upon the type of function of distribution of  $M_1$  and  $M_2$  units in chains (statistical, alternation,

block), as well as upon the presence of bulk substituents in  $M_2$  molecules that exert a shadow effect.

In our case, values of  $v_{ch}$  are so high (even with minimal content of network-forming  $M_1$  in copolymers, 25% mol) that the value of  $C_{cr}$  is too small ( $C_{cr} < 0.01$ ) and therefore cannot be measured with a sufficient degree of accuracy. However, both the topological and morphological consequences of cyclization (reduction of  $v_{ch}$  and microheterogenization) undoubtedly serve as factors that influence the properties of copolymers. Let us try to discover features indicating the influence of cyclization upon physical and mechanical properties that are presumably associated with a reduction of cyclization contribution to the growth of  $M_2$  content in copolymers.

In the glassy state, the physical network makes the main contribution to the carrier network,  $v_{\Sigma} = v_{ch} + v_{ch}' + v_{ph}$ . Therefore, the topological consequences of cyclization (reduction of  $v_{ch}$ ) cannot exert a direct influence upon  $E_1$ . However, morphological features “provoked” by cyclization (microheterogenization) can be reflected in the value of  $E_1$ . In the forced elasticity state, the contribution of  $v_{ch}$  to the value of  $v_{\Sigma}$  increases drastically, and the topological consequences of cyclization should appear to be clearly expressed exactly in the forced-elastic state. Therefore, let us begin exploring the influence of cyclization upon physical and mechanical properties of copolymers with the analysis of curves  $E_2$  in Fig. 6.7 and data in Fig. 6.8 and Table 6.7.

Based on data given in [23], we believe that with low content of network-forming monomer  $M_1$  in copolymers having alternating or statistically distributed units  $M_1$  and  $M_2$ , cyclization does not practically take place and, hence, the effective network in the forced-elastic state is equal to nominal  $v_{ch}$  plus  $v_{ch}'$ . In its turn,  $v_{ch}'$  is composed of a highly stable physical network having cooperated junctions<sup>2</sup> and physical network with junctions stabilized by adjacent junctions of chemical network. Now, let us compare  $E_2$  at any fixed value of nominal network  $v_{ch}$  chosen in the region of low concentration of  $M_1$  (e.g.,  $v_{ch} = 4 \times 10^{-3}$  mol/cm<sup>3</sup>, which corresponds to [tEGdMA] =  $2 \times 10^{-3}$  mol/cm<sup>3</sup>), in the first place, for copolymers having alternating or statistical distribution of units:  $M_2 =$  styrene, MMA, BMA, or DDMA. For  $M_2 =$  styrene or DDMA with [tEGdMA] =  $2 \times 10^{-3}$  mol/cm<sup>3</sup>, the value of  $E_2 \approx 95$  MPa. For BMA and especially MMA,  $E_2 > 95$  MPa, but if we introduce a correction for  $v_{ch}'$  and subtract value  $E_2$  for homopolymers (the difference of  $E_2$  value of which from zero is caused by the presence of  $v_{ch}'$ ) from the value  $E_2$  for copolymers, then in all four cases (styrene, MMA, BMA, DDMA) the values of  $E_2$  would appear to be practically equal ( $E_2 \approx 95$  MPa). Such a coincidence cannot be casual and, apparently, points to the fact that, first, when the content of tEGdMA is [tEGdMA] =  $2 \times 10^{-3}$  mol/cm<sup>3</sup> (and lower), the contribution of cyclization can be neglected, and, second, the type of functional dependence of elasticity modulus  $E_2$  in the forced-elastic state upon volume concentration of junctions of the effective network is a direct proportionality. If we assume any other type of functional dependence  $E = f(v)$ , then in this case it would be impossible to introduce a correction

<sup>2</sup> Published data on the presence of such networks are verified by highest value of  $E_2$  in homopolymer (Table 6.7) and are available for  $M_2 =$  MMA only [17].

for  $v_{ch}'$  by simple subtraction of  $E_2$  for the homopolymer. Having chosen point  $[tEGdMA] = 2 \times 10^{-3} \text{ mol/cm}^3$  as a starting point and reasonably believing that at this point effective values of  $v_{ch}$  are the same as nominal values for all four copolymers, let us analyze the rates of  $E_2$  growth with increasing tEGdMA concentration, taking into account the fact that cyclization (while reducing the effective value of  $v_{ch}$ ) should exert a corresponding influence on  $E_2$  growth rates, a measure for which is the slope of curves  $E_2$  in Fig. 6.7,  $\frac{dE_2}{d([tEGdMA])} \equiv \beta$ . It can be seen that the lowest value of  $\beta$  is when  $M_2 = \text{MMA}$ , while in the other three cases the values of  $\beta$  are higher and close to one another. If it is really possible to believe that  $\beta$  decreases because of reduction of effective value of  $v_{ch}$  as compared to the nominal value, then the obtained correlation of  $\beta$  values could be easily explained: a tendency to alternation of units in copolymers takes place in the case  $M_2 = \text{styrene}$ , while in the case  $M_2 = \text{BMA}$  and  $\text{DDMA}$ , the profound shadow effect of bulk substituents  $\text{C}_4\text{H}_9$  and  $\text{C}_{12}\text{H}_{25}$  represents those advantages obtained by more effective suppression of cyclization, which distinguish these monomers from MMA.

Now let us analyze more complex cases of copolymers characterized by a tendency to blocking in chains ( $M_2 = \text{BA}$ ), which is so expressed in the case of  $M_2 = \text{VA}$  that long grafted PVA chains are formed in the network structure. It can be seen from Fig. 6.7e,f that in a point chosen as a starting point (with  $[tEGdMA] = 2 \times 10^{-3} \text{ mol/cm}^3$ ), values of  $E_2$  in both cases are close to the value of 95 MPa obtained earlier for other monomers. From the network model standpoint, it means that the effective value of  $v_{ch}$  for these copolymers is also the same as that for other cases. And, as all copolymers differ in terms of the nature of IMI centers, in terms of type of distribution of units in chains, and in terms of volume of substituents in the pendent groups of main polymeric chains, then the total number of units of network-forming monomer (i.e.,  $[tEGdMA] = 2 \times 10^{-3} \text{ mol/cm}^3$ ) serves as the only common parameter for all of them. Therefore, there are strong grounds to believe that it is exactly the equality of nominal values of  $v_{ch}$  that serves as a reason for equality of  $E_2$  values, whence it follows that the value of  $E_2$  is uniquely determined by the nominal chemical network until formation of factors influencing the effective carrying network of forced-elastic state  $v = v_{ch} + v_{ch}'$  starts at higher  $[tEGdMA]$ . One of such factors, namely, cyclization, acts in the direction of  $v$  decline due to fall of  $v_{ch}$ . Another factor, namely, stabilization of such junctions by chemical network [18], in contrast, increases  $v$  due to the growth of  $v_{ch}'$ . Sharp growth of  $E_2$  after the starting point (incommensurable with values of  $\beta$  for all others monomers) observed in the case of  $M_2 = \text{VA}$  (Fig. 6.7f) probably points to the existence of one more potential factor that increases  $v_{ch}'$ , and this factor is a nontrivial one, as the attainment of the maximum and subsequent decline of  $E_2$  is observed later. Stabilization of interchain IMI bonds (of dipole–dipole type) of adjacent PVA chains or their sections with formation of long enough (and, hence, having high total energy of bonds), probably, even regular (mutually oriented) sequences, by the chemical network may serve as such a factor. The growth of  $v_{ch}'$  resulting from this factor may take place only in the limited range of concentration of chemical network junctions: with low values of  $v_{ch}$ , stabilization is still weakly expressed, and with too high values of  $v_{ch}$ , mobility of grafted PVA chains appears to be so frozen

that their orientation with formation of cooperated IMI bonds becomes impossible. From the foregoing discussion it follows that in the case of  $M_2 = VA$ , the value of  $\beta$  does not carry information on cyclization process due to masking by another, more powerful factor. The same could be said for the case of  $M_2 = BA$ , despite the fact that in this case the tendency to blocking (judging by  $r_1$  and  $r_2$  values) is expressed incommensurably more weakly.

Data on  $E_1$  in glassy state in terms of cyclization influence should be analyzed with great caution because the contribution of the chemical network to the carrier network  $v_\Sigma = v_{ch} + v'_{ch} + v_{ph}$  in this case is negligibly small, and only indirect influence at the morphological level (i.e., influence on microheterogeneity degree of glass-like polymeric solids) can serve as the direction of cyclization influence on  $E_1$ , because it is known [24] that cyclized structures serve as nuclei of microgel particles. Apparently, in those cases when  $E_1$  varies according to the trend close to additivity (Fig. 6.7a, c, d), no specific features appear that are associated with changes in the degree of microheterogeneity. When  $M_2 = BA$  and  $VA$ , these specific features are most likely determined not by cyclization influence, but by a special type of molecular packing of  $M_2$  chains or their sections in the di(meth)acrylate network (once again we would like to point out here an extraordinary peculiarity for the case when  $M_2 = VA$ : dependence of elasticity modulus on copolymer composition is not trivial, and the inversion point with respect to the reference point for glassy and forced-elastic states is qualitatively identical). However, the fact that curve  $E_1$  flattens out as a plateau in the case of  $M_2 = BMA$  (this plateau is located much higher than the additivity line) could be explained with a certain degree of probability by stabilization at a certain level of microheterogeneity degree of copolymers in the range of composition corresponding to the plateau. Indeed, in the case of  $M_2 = BMA$ , the tendency to micro-immiscibility of phases with the formation of microgel is much more expressed than for the case of other monomers, with the exception of DDMA [for which this tendency, due to even greater length of hydrophobic fragment (alkyl substitutor) than the length of BMA hydrophobic fragment, is expressed so strongly that turbidity is observed]. However, the ability for shielding of adjacent double bonds susceptible to cyclization is also high. Therefore, the plateau on curve  $E_1$  may represent a consequence of compensation for cyclization factor growing with increasing tEGdMA content by the intensity of micro-immiscibility of phases decreasing in the same direction due to reduction of BMA component content characterized by poor thermodynamic compatibility. Therefore, the microheterogeneity degree related to  $E_1$  by antipate dependence most likely remains unchanged in the range of copolymer compositions, for which  $E_1 \approx \text{const}$ .

It should be also pointed out here that when discussing the results, the authors did not consider approaches implying taking the thermodynamic parameters into account, which control the compatibility of polymer and monomer components of polymerization systems at different stages of polymerization. It is obvious that consideration of these parameters would give deeper insight into the reasons for the regularities observed both in kinetics of  $M_1 + M_2$  copolymerization [21] and in properties of formed copolymers. Indeed, it is just the thermodynamic features of

polymer-monomer mixtures in highly cross-linked polymerization systems that represent one of the main reasons for the occurrence of microheterogeneity, according to the mechanism of the microsineresis phenomenon discovered by Dušek [25]. However, inclusion of thermodynamic approaches in the discussion of results is apparently impossible at present because of the lack of information on thermodynamic parameters controlling compatibility of components in copolymerizing systems  $M_1 + M_2$ . It is only known at this point that obtaining such information is a very challenging task, as it has been shown [in an example of Huggins constant ( $\chi$ ), which is the most commonly used of such parameters] that for highly cross-linked polymer networks the value of  $\chi$  is a function of not only the nature of components but also of network junctions concentration. Therefore, the authors thought it expedient to leave the problems of thermodynamic compatibility of components during copolymerization aside, except for one case, namely,  $M_2 = \text{DDMA}$ , when copolymerization was accompanied by obvious separation of the reaction system, which was manifested, depending on the composition of initial mixture  $M_1 + M_2$ , either as microseparation of layers (opalescence or turbidity) or as typical macroscopic layer separation with the formation of a “curdy” mass.

In conclusion, the authors would like to emphasize that the observed influence of copolymer composition on physical and mechanical properties is not trivial (from the standpoint of additivity) and unpredictable, as well as the evolution of copolymer composition during copolymerization. It is obvious that this nontriviality is related to specific features of the microheterogeneous mechanism for the formation of highly cross-linked, macromolecular structures in radical chain processes [6, 12]. However, as yet the authors have failed to identify this relationship in the form of trends suitable for forecasting. Therefore, macromolecular design of such systems has to be based on empirical data, which gives rise to the problem of minimization of an array of required source data. The authors believe that an extremely minimized program for the obtaining of such data should include kinetic studies enabling us to estimate both the gross transformation [21] and individual transformation of each of the comonomers [26], as well as exploration into physical and mechanical properties of copolymers as described in the present section.

### **6.3 Cross-Linked Copolymers. Thermo-Mechanical Properties [11, 27]**

#### **6.3.1 *Mechanism of Copolymers Transition into High-Elastic State***

Thermo-mechanical studies were conducted in the penetration mode on samples  $\approx 2$  mm in height and  $\approx 4$  mm in diameter at a constant rate of heating,  $5^\circ/\text{min}$ , under constant loading  $\sigma = \text{const}$  and in dilatometric mode ( $\sigma \approx 0$ ) using a special installation intended for thermo-mechanical studies of polymers [28]. The temperature

corresponding to the maximum on differential curves  $d\varepsilon/dT$  was taken as the value of  $T_g$ . Physical and mechanical studies of polymers were conducted on cylindrical samples in the axial compression mode  $T = 23^\circ \pm 1^\circ\text{C}$  and strain rate  $\dot{\varepsilon} \approx 10^{-4} \text{ s}^{-1}$  using a custom-designed installation for mini-samples  $\approx 0.1 \text{ g}$  in weight equipped with a precision dynamometer of lever type in a thermostatically controlled chamber.

The transition from glassy state into highly elastic one ( $\alpha$ -transition) in the case of highly cross-linked polymers synthesized via radical polymerization is characterized by an extremely wide transition region (sometimes more than  $100^\circ$ ). For polycondensation highly cross-linked polymers produced on the basis of epoxy resins, the width of this region does not exceed  $10^\circ$ – $15^\circ$ ; this gives grounds for asserting that the mere fact of the presence of highly cross-linked structure cannot serve as a reason for widening of the  $\alpha$ -transition region. It is still unclear what factors determine the transition region width. Probably, microheterogeneity at the topological and morphological levels that inevitably arises during three-dimensional free-radical polymerization represents one of these factors. The authors believe that the presence of topological heterogeneity (such as cycles of different size that are produced as a result of intrachain cross-linking) leads to a wide set of topological  $\alpha$ -relaxants, each of which is characterized by its own temperature  $T_{gi}$ . Besides, it is believed that the existence of morphological heterogeneity leads to even greater augmentation of the number of  $\alpha$ -relaxants, as topologically identical  $\alpha$ -relaxants (located in morphologically different micro-regions) can have different values of  $T_{gi}$  due to different molecular packing density in these regions, which can influence the molecular mobility of a given  $\alpha$ -relaxant. This supposition agrees well with data from Lagunov et al. [29], in which it was found (using the paramagnetic probing method) that the EPR spectrum of nitroxyl probe in highly cross-linked methacrylates represents a superposition of two signals, broad and narrow line widths, inherent to glassy and high elastic states of the probed polymeric matrix, respectively. Transfer of intensity from one signal to another occurs during temperature scanning, which was interpreted within the framework of the microheterogeneous model of the highly cross-linked methacrylate structure, which allows for the coexistence of micro-regions that are in glassy state (broad line width) and high elastic state (narrow line width) in a wide temperature range  $\Delta T = (50^\circ$ – $100^\circ)\text{C}$ . In this case, the width of  $\Delta T$  is determined by a set of local glass transition temperature  $T_{gi}$  of micro-regions (see Sect. 1.4.1).

Therefore, it is not improbable that  $\alpha$ -transition region width for highly cross-linked macromolecular structures synthesized via radical polymerization may serve as a characteristic parameter reflecting structural and physical properties to a certain extent, which fact served as incentive for experimental studies of  $\Delta T_g$ .

Typical thermo-mechanical curves in coordinates “strain – temperature,” both initial curves  $\varepsilon'(T)$  (Fig. 6.10 a) and corrected curves  $\varepsilon(T)$  (Fig. 6.10 b) with thermal expansion taken into account, are shown in Fig. 6.10. Integral curves  $\varepsilon(T)$  were then differentiated, and lower ( $T_{g1}$ ) and upper ( $T_{g2}$ ) boundaries of that  $\alpha$ -transition were determined based on obtained differential curves  $d\varepsilon/dT$  (Fig. 6.11). The temperature corresponding to the maximum of curves was taken to be the value of  $T_g$  that corresponds to the point of inflection on integral curves. Parameters  $T_{g1}$ ,  $T_{g2}$ ,  $T_g$ , and

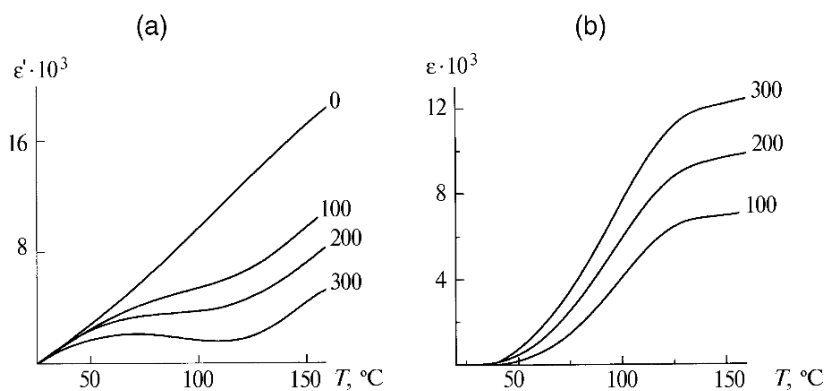


**Fig. 6.10** Typical integral thermo-mechanical curves (by the example of tEGdMA homopolymer) at constant rate of heating  $dT/dt = 5^\circ/\text{min}$  and constant load. **(a)**  $\sigma = \text{const}$  (numbers near curves represent conventional units); **(b)**  $\sigma = 0$  (negligibly small load, which provides only for the contact of rod with sample) corresponding to thermal expansion curve and used for the correction of values of apparent strain  $\epsilon'$  by the formula  $(\epsilon)_{\sigma} = (\epsilon')_{\sigma} - (\epsilon')_{\sigma=0}$

$\alpha$ -transition region width  $\Delta T_g = T_{g2} - T_{g1}$  are presented in Fig. 6.12 as functions of copolymer composition.

Narrowing of the transition region with increasing content of  $M_2$  in copolymers represents a general trend clearly observed in Fig. 6.12a–f. However, the rate of this narrowing (slope of curves  $\Delta T_g$ ) is specific for each  $M_2$ : monotonous narrowing proportional to composition is observed only for  $M_2 = \text{styrene}$  ( $d\Delta T_g/d[M_2] \approx \text{const}$ ).

For  $M_2 = \text{MMA}$ , monotonous narrowing occurs up to  $[M_2] \approx 50\%(\text{mol})$ , and then a sharp rise of  $d\Delta T_g/d[M_2]$  is observed; for  $M_2 = \text{BMA}$  with  $[M_2] \leq 25\%(\text{mol})$ , no narrowing is practically observed and then rapid narrowing takes place within the

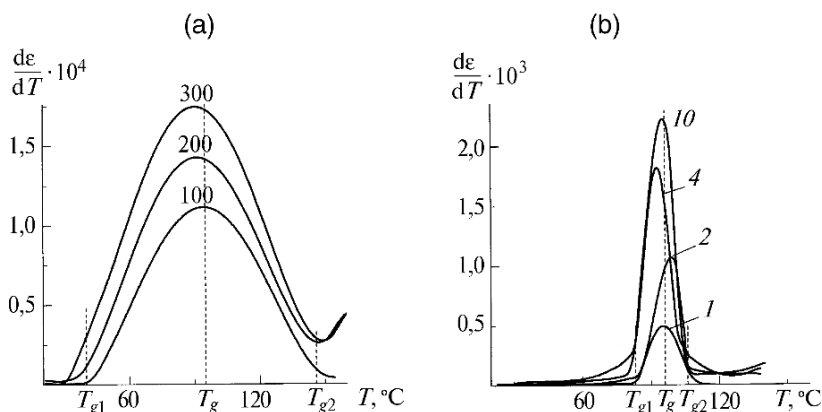


**Fig. 6.11** Typical differential ( $d\epsilon/dT = f(T)$ ) thermo-mechanical curves at constant rate of heating  $dT/dt = 5^\circ/\text{min}$  and constant load  $\sigma = \text{const}$  (numbers near curves represent conventional units) for samples with maximum (100%) and minimum (0%) content of network-forming comonomer ( $M_1$ ): **(a)** tEGdMA homopolymer; **(b)** MMA homopolymer



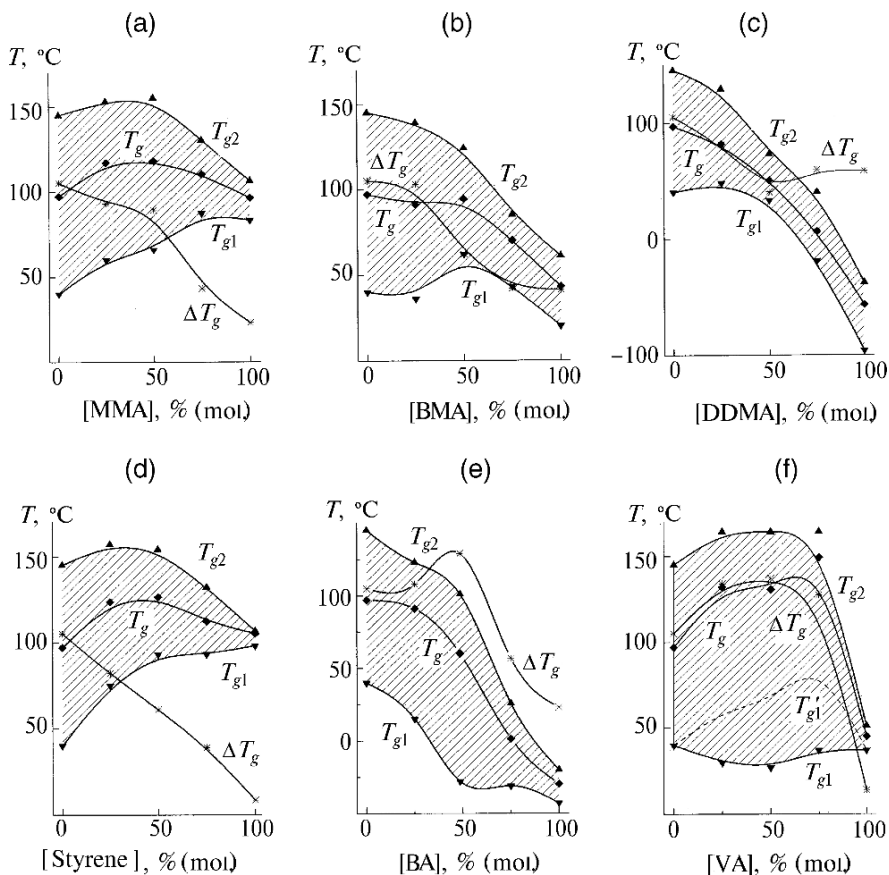


**Fig. 6.12** Dependence of lower ( $T_{g1}$ ) and upper ( $T_{g2}$ ) boundaries of  $\alpha$ -transition, glass transition temperature ( $T_g$ ), and transition region width ( $\Delta T_g = T_{g2} - T_{g1}$ ) upon composition of copolymer tEGDMA- $M_2$  for different  $M_2$ : MMA (a), BMA (b), DDMA (c), styrene (d), BA (e), and VA (f)

range  $25\% < [M_2] < 75\%$ (mol) up to the limiting value corresponding to homopolymer BMA.

For  $M_2 =$  DDMA (as well as for BMA), at a certain content of  $M_2$  in copolymer (at 50%mol for DDMA and at 75%mol for BMA), complete narrowing of the  $\alpha$ -transition region is observed to the value corresponding to homopolymer  $M_2$ ; for BA and VA, there is a region of copolymer compositions ( $25\% \leq [M_2] \leq 50\%$  mol for BA and  $0\% \leq [M_2] < 50\%$ mol for VA), in which broadening (!) of  $\alpha$ -transition region occurs as the content of  $M_2$  in copolymers increases, instead of its narrowing. It is noteworthy that the tendency to “blocking” of  $M_2$  units in copolymer chains should be observed precisely for these copolymers, judging by copolymerization constants ( $r_1 = 2 > 1$ ;  $r_2 \approx 0.5 < 1$  for BA and  $r_1 \approx 20 \gg 1$ ,  $r_2 \approx 0.05 \ll 1$  for VA). This tendency, apparently, extends (in the case of VA) to the stage of formation of poly(vinyl acetate) chains that are grafted to the cross-linked (meth)acrylate structure with generation of specific block copolymers of the “snake-cage” type.

That is, for VA copolymers, one can expect the appearance of an additional source for the formation microstructural heterogeneity both on topological (long grafted chains) and on morphological (isolation of polyvinyl acetate chains aggregates in the form of included polymer) levels. It is not improbable that it is precisely this factor that represents the reason for  $\alpha$ -transition region expansion as the content of VA units in the network increases.

Another general regularity consists in nonadditivity of values of  $(T_g)_{M_1M_2}$  of copolymers in relation to values of  $(T_g)_{M_1}$  and  $(T_g)_{M_2}$  homopolymers. In the case of copolymers with MMA and styrene, values of  $(T_g)_{M_1}$  and  $(T_g)_{M_2}$  are quite close to one another, and value of  $(T_g)_{M_1M_2}$  of copolymers grows as the content of  $M_2$  in copolymers increases (reaching the maximum with at  $M_2 = 25\text{--}50\%$ mol) up to values exceeding the temperature of glass transition of  $M_1$  and  $M_2$  homopolymers by  $10^\circ\text{--}20^\circ$ . This effect is especially expressed for VA copolymers when  $(T_g)_{M_1} \gg (T_g)_{M_2}$ : the maximum value of  $(T_g)_{M_1M_2} \approx 140^\circ\text{C}$  (with  $[M_2] = 75\%$ mol) is almost  $40^\circ\text{C}$  higher (!) than the highest glass transition temperature for the first homopolymer  $(T_g)_{M_1} \approx 100^\circ\text{C}$  and exceeds the glass transition temperature for the second homopolymer  $(T_g)_{M_2} \approx 45^\circ\text{C}$  almost by  $100^\circ\text{C}$ . In the case of additivity, the inverse effect should be observed just for VA because of  $(T_g)_{M_1} \gg (T_g)_{M_2}$ ; namely, the steep decline of  $(T_g)_{M_1M_2}$  as  $[M_2]$  grows. In another case (i.e., BMA) when  $(T_g)_{M_1} \gg (T_g)_M$  also takes place, nonadditivity is also manifested in a wide enough range,  $0\% < [M_2] \leq 50\%$ (mol): the value of  $(T_g)_{M_1M_2}$  in this range does not decline with growing content of BMA in copolymer, although BMA is characterized by a low value of  $(T_g)_{M_2} \approx 43^\circ\text{C}$ . Thus, a not trivial phenomenon is observed, namely, enhancement of “thermostability”<sup>3</sup> of copolymers as the content of polymer units characterized by lower thermostability in these copolymers increases (!).

Analysis of obtained results from the standpoint of structural and physical peculiarities of highly cross-linked macromolecular structures formed in the processes of three-dimensional free-radical copolymerization was conducted taking the following considerations into account.

It is yet unclear what factors determine the width of  $\alpha$ -transition. In our case, a hypothesis implying that very wide  $\alpha$ -transition ( $\Delta T_g \approx 100^\circ\text{C}$ ) for highly cross-linked tEGdMA homopolymer is determined by a corresponding wide set of  $\alpha$ -relaxants (i.e., elementary fragments of the macromolecular network, the mobility of which is necessary for the transition from glassy state into high elastic state) demonstrates the highest degree of consistency with experimentally obtained data. This set includes relaxants of different type, each of which has inherent transition temperature  $T_{gi}$  corresponding to a certain point in the glass transition range from  $T_{g1}$  to  $T_{g2}$ . The least “heat resistant” (i.e., most easily defrosted) relaxants become defrosted beginning from  $T_{g1}$ , while the most heat resistant (hard to defrost) are defrosted beginning from about  $T_{g2}$ . The value of  $d\varepsilon/dT$  (see Fig. 6.11) in this case can serve as a measure of population of each point in the glass transition range with relaxants and, hence, selection of abscissa of maximum point on curves  $d\varepsilon/dT = f(T)$  as  $T_g$  means that selected value refers to the most occupied region in the  $\alpha$ -transition

<sup>3</sup> From here on the term “thermostability” is used not as a characteristic of a macroscopic property, but as a submolecular property. Hereinafter, this term is used without quotation marks.

range. Specific structural peculiarities of topological and morphological levels apparently serve as a source of a wide set of  $\alpha$ -relaxants for the tEGdMA polymer (which is a typical representative of highly cross-linked macromolecular structures formed in the course of three-dimensional free-radical polymerization). At the morphological level, it is microheterogeneity [6, 12], and at the topological level, intrachain cycles of various configurations formed during three-dimensional free-radical polymerization (as secondary process) as a result of intrachain joining of pendent double bonds in primary carbo-chains [30]. There are good grounds to believe that copolymerization of polyfunctional monomers of  $M_1$  type with conventional vinyl monomers  $M_2$  with a single multiple bond in the molecule should exert suppressing action upon both the above-indicated sources of the wide set of  $\alpha$ -relaxants, thus narrowing the range of  $\alpha$ -transition. Indeed, formation of small cycles (cyclization) occurs as a result of joining of adjacent multiple bonds pendent to  $M_1$  units. During copolymerization,  $M_2$  units (penetrating between adjacent  $M_1$  units) increase the distance between pendent bonds and, hence, decrease the probability of cyclization. And, because cyclized macromolecules serve as nuclei of microgel particles, the level of microheterogeneity also becomes degraded.

In view of the above-indicated reasons, let us analyze data presented in Fig. 6.12a–f. In two cases (for styrene and MMA), values of  $T_g$  for homopolymers  $M_1$  and  $M_2$  are very close. Hence, the most representative  $\alpha$ -relaxants are characterized by approximately similar thermostability (temperature regions of highest occupation coincide). Further, the  $\alpha$ -transition region for  $M_2$  homopolymer is so narrow (especially for the case of styrene) as compared to  $M_1$  homopolymer that all  $\alpha$ -relaxants in this case could be considered to be practically of the same type (let us denote them by the symbol  $P_{M_2}$ ). In addition to relaxants of  $P_{M_2}$  type, the  $M_1$  homopolymer contains much higher thermostable relaxants (denote the most thermostable of them as  $P_{M_1}^{\max}$ ) and considerably lower thermostable relaxants ( $P_{M_1}^{\min}$ ). Data presented in Fig. 6.12a,d enable us to evaluate the influence of copolymerization on thermostability of relaxants of  $P_{M_1}^{\min}$  type (curves  $T_{g_1}$ ) and  $P_{M_1}^{\max}$  type (curves  $T_{g_2}$ ). It can be seen that the thermostability of  $P_{M_1}^{\min}$  grows steeply with increasing content of  $M_2$  in the copolymer (especially for styrene), and this growth continues up to equimolar composition for styrene and up to composition of 75% (mol)  $M_2$  for MMA. Because the ratio of copolymerization constants  $r_1$  and  $r_2$  is such that styrene has a tendency for alternation of units in chains ( $r_1 \approx r_2 \approx 0.5 < 1$ ), and MMA has a tendency for statistical distribution ( $r_1 \approx r_2 \approx 1$ ), growth of thermostability  $P_{M_1}^{\min}$  can be assigned to the topological effect of separation of  $M_1$  units carrying pendent double bonds, with corresponding decrease of intrachain cyclization probability. Indeed, in the case of alternation of chains, they are separated more effectively than in the case of statistical distribution. If this is true, then  $\alpha$ -relaxants of  $P_{M_1}^{\min}$  type could be identified with structural fragments of the network that include small cycles.

Thermostability of  $\alpha$ -relaxants of  $P_{M_1}^{\max}$  type (curves  $T_{g_2}$  in Fig. 6.12a,d) also increases as the content of  $M_2$  units in copolymers increases, although it grows not so intensively as in the case of  $P_{M_1}^{\min}$ . This fact cannot be explained from the purely topological standpoint only, because formally a new group of  $\alpha$ -relaxants is produced and the thermostability of these  $\alpha$ -relaxants is higher than that of the

most thermostable  $\alpha$ -relaxants of both homopolymers. The topological effect should be quite the contrary; namely, the nominal degree of cross-linking of the network should decrease and molecular mobility should become enhanced as the content of  $M_2$  increases. It was shown that the extent of influence of degree of network cross-linking upon the  $T_g$  value is high enough [20]. It seems likely that in this case effective degree of network cross-linking is significantly lower than the nominal degree due to cyclization and, hence, copolymerization (that prevents cyclization to a certain extent) can lead even to an increase in effective degree of network cross-linking (at least, in micro-volumes occupied with  $\alpha$ -relaxants of type  $P_{M1}^{\max}$ ). Besides, following the logic of the above-indicated initial considerations, it is believed that starting from a certain content of  $M_2$  (when the cyclization contribution becomes insignificant), reduction in volume concentration of network junctions due to dilution of network-forming monomer  $M_1$  with non-network-forming monomer  $M_2$  would become a prevailing effect, and thermostability would begin declining.

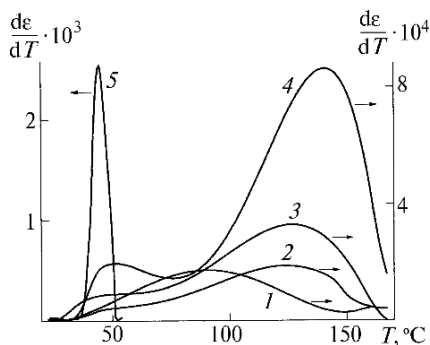
Taking the morphological specifics [6, 12, 30] of objects under study into account, the authors believe that  $\alpha$ -relaxants of the  $P_{M1}^{\min}$  and  $P_{M1}^{\max}$  types are located in structurally different micro-regions:  $P_{M1}^{\max}$  is in more highly cross-linked regions (microgel particles), while  $P_{M1}^{\min}$  is in gaps with low cross-linked network (structural defects). In the case of alternation or statistical distribution of units, copolymerization smoothes out these structural differences by the decrease of cyclization probability and, hence, reduction of microheterogeneity degree; this also facilitates narrowing of the  $\alpha$ -transition area. In this case it is impossible to separate the topological from the morphological contribution and therefore both should be taken into account. An attempt was made [31, 32] to assess the value of the morphological contribution by transferring the three-dimensional free-radical polymerization process into the living chains mode. Structural differences are smoothed out in this case (as in the case of copolymerization). It was found that this had practically no impact on glass-transition area width, which gives grounds to believe that the topological factor, namely, the variety of cycle configurations, serves as the main source of the wide set of  $\alpha$ -relaxants in this case.

For  $M_2 = \text{BMA}$  (Fig. 6.12b),  $T_g$  values for homopolymers differ so dramatically that regularities that were clearly manifested for  $M_2 = \text{styrene}$  and  $M_2 = \text{MMA}$  appear to be masked by the contribution of  $\alpha$ -relaxants of  $P_{M2}$  type having very low thermostability associated with bulk group  $-\text{C}_4\text{H}_9$ . That is why  $T_{g2}$  starts declining even at a low content of  $M_2$ , and for  $T_{g1}$ , there is a region in which copolymerization liquidates  $\alpha$ -relaxants of  $P_{M1}^{\min}$  type having the lowest thermostability (supposedly because of liquidation of the smallest cycles).

It is seen from Fig. 6.12c that for  $M_2 = \text{DDMA}$ , the masking contribution of  $P_{M2}$  relaxants increases even more due to an even lower value of  $T_g$  than for BMA, and hence, the supposed effect of small cycle liquidation because of the shielding action of DDMA units is noticeable only in the range  $0\% < [\text{DDMA}] < 25\%$  (mol) and at the lower boundary only: within this range,  $T_{g1}$  does not decline with increasing [DDMA].

In the case of  $M_2 = \text{VA}$  (Fig. 6.12f), the network structure is transformed dramatically by the combination of copolymerization constants ( $r_1 \approx 20 \gg 1$ ;

**Fig. 6.13** Differential thermo-mechanical curves at constant rate of heating  $dT/dt = 5^\circ/\text{min}$  and constant load for tEGdMA-VA copolymers with different content of VA. 1, 0; 2, 25; 3, 50; 4, 75; 5, 100% (mol)



$r_2 \approx 0.05 \ll 1$ ). With this combination,  $M_1$  is polymerized at first with very weak participation of  $M_2$  (homopolymerization of  $M_1$  takes place actually, while  $M_2$  performs the function of inert diluent), and only at deep stages of conversion (when  $M_1$  is almost exhausted) does polymerization of  $M_2$  start. As a result, the topological structure of the “snake-cage” type is formed: a network of tEGdMA polymer and long grafted chains of PVA.

The presence of the latter is manifested on thermo-mechanical curves as a separate glass-transition region corresponding to PVA homopolymer (Fig. 6.13). From our standpoint, the concurrence of the two facts, namely, formation of unusual topological structure and appearance of unusual features in tEGdMA-VA copolymer, is not coincidental. Possibly, it is indicative of a decisive role of a specifically topological factor in this case.

As might be expected, another topological effect is practically missing in this case, namely, the influence of copolymerization on the cyclization process that was observed for styrene and methacrylates. This difference is attested by the absence of a glass-transition area narrowing up to the highest content of  $M_2$  in the copolymer (Fig. 6.12f). Moreover, extension of the  $\Delta T_g$  range was observed. This extension resulted both from  $T_{g1}$  reduction and from  $T_{g2}$  increase.  $T_{g1}$  reduction can be explained only by nontrivial reasons: if the assumption is made that the appearance of a new group of  $\alpha$ -relaxants having very low temperature of transition ( $\approx 10^\circ\text{C}$  lower than the transition temperature for PVA) is related to special packing of PVA chains in the tEGdMA polymer matrix (which is more sparse as compared to PVA homopolymer). As the content of BA in copolymer grows, the size of micro-areas (consisting of PVA) increases and packing of PVA chains in the matrix becomes the same as the one in the homopolymer: the value of  $T_{g1}$  grows (Fig. 6.12f) to a value corresponding to the lower limit of the glass-transition area of PVA homopolymer. The validity of such interpretation is confirmed by the path of curve  $T_{g1}$ , which represents the lower limit of the glass-transition area of copolymers (with said limit measured with dropping of the low-temperature part of the glass-transition range associated with mobility of PVA chains) (Fig. 6.12f, dashed line). Physically,  $T_{g1}$  is the lower limit of the glass-transition range of the tEGdMA homopolymer matrix, and this limit goes up with increasing content of VA. Concurrently, the upper limit  $T_{g2}$  also goes up. Hence, VA somehow modifies the matrix to a significant

extent despite the copolymerization inertness of VA. Most likely, in the course of copolymerization VA performs the function of temporary plasticizer, facilitating the relaxation processes during formation of the highly cross-linked structure, thus providing more perfect molecular packing of its fragments. In contrast, the packing of PVA chains (that are formed under conditions of rigid matrix) turns out to be incompletely realized.

The case when  $M_2 = \text{BA}$  (Fig. 6.12e) is qualitatively similar to  $M_2 = \text{VA}$  in terms of the tendency to formation of  $M_2$  units (quantitatively, this tendency is expressed much more weakly judging by values of  $r_1$  and  $r_2$ ), but it is distinguished by considerably lower value of  $T_g$  for the homopolymer. Therefore, dependences  $T_g$ ,  $\Delta T_g$ ,  $T_{g1}$ , and  $T_{g2}$  upon comonomer composition in Fig. 6.12e are qualitatively closer to those shown in Fig. 6.12f for  $M_2 = \text{VA}$  (the effect of  $\alpha$ -transition area extension is also observed with increasing content of  $M_2$  in copolymer) than to data for the monomer, which is an analogue for BMA (in terms of the amount of alkyl substituent  $-\text{C}_4\text{H}_9$ ) shown in Fig. 6.12b, which is logically consistent with a unified system of considerations used by us as the basis for interpreting the above-analyzed results.

Of course our approach represents only one of the possible options and does not preclude the use of alternative approaches. Nevertheless, it enables one to clearly see manifestations (in a variety of regularities shown in Fig. 6.12a–f) of the influence of specific topological and morphological factors instead of chaos.

### 6.3.2 Comparison of Transitions into High-Elastic State with those into Forced-Elastic State

Data shown in Figs. 6.8 and 6.12 allow comparing the regularities inherent to transitions to highly elastic and forced-elastic (FE) states (i.e.,  $\alpha$ -transitions and FE transitions) and enable us to identify certain structural and physical features of copolymers being studied. When  $M_2 = \text{MMA}$  or styrene, the width of FE transition, in contrast to  $\alpha$ -transition (see Fig. 6.12a,d), is practically independent of copolymer composition, and the value of  $\sigma_{cr}$  increases monotonically with growing content of  $M_2$  units. Most likely, so sharp a distinction from  $\alpha$ -transition (see Fig. 6.8a,d) is explained by the influence of temperature: FE transition was studied at a significantly lower temperature (23°C). Indeed, the set of relaxants controlling this transition is determined by relationship  $\tau_i > t_{obs}$ , where  $t_{obs}$  = observation time (i.e., time of experiment), and  $\tau_i$  = time of life of  $i$ -th relaxant in the set that grows exponentially with decreasing temperature ( $\tau_i = \tau_0 \exp[E_i/RT]$  in the absence of field of mechanical forces or  $\tau_i = \tau_0 \exp[(E_i - \gamma\sigma)/RT]$  in the field of forces with intensity  $\sigma$ ). Because the value of  $\tau_{exp}$  determined by experiment methodology is constant in this case, a certain fraction of relaxants would fall outside the relationship  $\tau_i > \tau_{exp}$  due to growth of temperature resulting from decreasing values of  $\tau_i$ . The set of transition-controlling relaxants would be reduced, and the transition width would decline. It seems likely that this constitutes the difference of  $\alpha$ -transition from FE transition for  $M_2 = \text{MMA}$  or styrene. The mere fact of higher resistance to FE transition (higher

value of  $\sigma_{cr}$ ) of non-cross-linked MMA and styrene homopolymers (as compared to highly cross-linked tEGdMA homopolymer) is indicative of the relatively higher contribution of the IMI physical network ( $v_{ph}$ ) at 23°C into the integral network  $v_{\Sigma} = v_{ch} + v_{ph}$  that regulates physical and mechanical properties (according to the polymer networks theory [12, 13]).

For  $M_2 = \text{BMA}$ , regularities of  $\alpha$ -transition and FE transition are virtually similar (see Figs. 6.8b and 6.12b). Most likely, this is explained by significantly lower temperature of glass transition for BMA homopolymer as compared to MMA or styrene homopolymers.

For  $M_2 = \text{VA}$ , similarity of  $\alpha$ -transition and FE transition (see Figs. 6.8f and 6.12f) is expressed in the presence of maximums on curves for dependence  $T_g$  (for  $\alpha$ -transition) and  $\sigma_{cr}$  (for FE transition) upon copolymer composition. These maximums are indicative of existence of copolymer structure having abnormally high resistance both to thermal and mechanical action. However, an important distinction is observed in the FE transition area, namely, appearance of minimum of  $\sigma_{cr}$  when the content of VA in copolymer is high (75%mol). This difference means that copolymer containing 75%(mol) VA is characterized by ability to change qualitatively with decreasing temperature from  $\approx 100^\circ$  to 23°C temperature at which FE transition was measured): at 100°C, resistance to external action (to the thermal one) is abnormally high (the value of  $T_g$  for copolymer is higher than for any of homopolymers), while at 23°C resistance to external action (to the mechanical one) is abnormally low (the value of  $\sigma_{cr}$  for copolymer is lower than for any of homopolymers). And once again we draw attention to structural specifics of copolymer containing 75%(mol) VA: judging by values of  $r_1$  and  $r_2$ , as well as by data shown in Fig. 6.13 (curve 4), this copolymer represents a topologically unusual version of cross-linked copolymer having long grafted polyvinyl acetate chains (“snake-cage”).

In conclusion, a certain analogy of forced-elastic and highly elastic states should be pointed out. Within the framework of the physical network model, the essence of  $\alpha$ -transition consists in “destruction” of  $v_{ph}$  and  $v_{ch}$  (possibly  $v_{ch}$  would not be completely destroyed), again according to relationship (6.3), but with one difference; namely,  $T$  operates in this case instead of  $\sigma$ . Possibly it is just this factor, namely, significant drop of volume concentration of physical network junctions, that is the reason for the change in the trend of free volume growth with increasing  $T$  in the case of  $T > T_g$ . The analogy consists, first, in the fact that high deformations develop in both cases (in our case, these are 30–40% deformations), and, second, these deformations are reversible: after load is removed, deformations are brought back to zero level (i.e., the elasticity observed is virtually no different from elasticity in the highly elastic state). In our case, full reversibility of deformation was observed for all samples on sections of curves  $\sigma$ – $\epsilon$  with constant slope  $E_2$ , and for the most highly cross-linked samples (namely, for tEGdMA and for its copolymers with  $M_1$  units content being no higher than 50% mol), the reversibility was observed in the area of higher deformations, outside  $E_2 = \text{const}$ , on sections where the slope of curves started increasing.

It should be specially emphasized that the authors managed to observe the transition of highly cross-linked polymers into the forced-elastic state at temperature

$T_{\text{exp}} = T_g - \Delta T$  (where  $\Delta T > 50^\circ\text{C}$ ) only in the axial compression mode owing to hydrostatic component of mechanical force field. This hydrostatic component prevents propagation of micro-cracks generated on structural defects when  $\sigma \approx \sigma_1$ . On stretching, breaking occurs in the very beginning of the transition area. Comparison of a large array of  $\sigma_1$  values obtained in the axial compression mode with the values of tensile strength  $\sigma_{\text{el}}$  carried out by many authors on an example of highly cross-linked methacrylates (see, for instance, [33]) showed that  $\sigma_{\text{el}} \approx \sigma_1$  is observed. This approach allows replacing labor-consuming (shaping specimens as “vanes” or “dumbbells”) and material-consuming (hundreds of grams of polymers) measurement of  $\sigma_{\text{el}}$  with a simple measurement of  $\sigma_1$ .

Development of significant reversible deformations could be regarded as a factor of analogy of the highly elastic state with the forced elasticity state. This analogy becomes even more expressed if we take into account results of Poisson coefficient ( $\delta$ ) measurements for axial compression of highly cross-linked poly(meth)acrylates with an oligomeric block of a different nature [34]. In transitional area, with  $\sigma > \sigma_1$  the value of  $\delta$  becomes less than 0.5, and as it declines further, with  $\sigma > \sigma_2$  it reaches a value within 0.38–0.45 (in some cases even lower, 0.30) depending on the chemical nature of poly(meth)acrylate, which is indicative of increasing specific volume of samples, and this is equivalent to the growth of free volume, if formation of pores and micro-cracks is excluded. Special experiments (namely, interruption of loading at the stage when  $\sigma = \sigma_{\text{cr}}$  and repetition of loading after the sample stays in rest state during a time period that is sufficient for deformation relief and return into initial state) showed that curve  $\sigma$ – $\varepsilon$  is well reproduced in the case of repetition, which excludes the increment of free volume due to formation of macroscopic pores and cracks; they are “healed” in the course of relaxation and, hence, they are nano-sized, corresponding to the notion of free volume. It is likely that relatively main modes of molecular motions (segmental type motions) become active unfrozen in a polymeric body staying in the forced-elastic state because of the sharp reduction of  $v_{\text{ph}}$ , and, judging by declining values of Poisson coefficient, this mobility is possibly accompanied by corresponding increment of free volume.

## 6.4 Diffusion-Sorption Properties of Copolymers

Using the diffusion-sorption probing method, the authors managed to identify a number of important features of highly cross-linked poly(acrylate) microstructure. Probing was carried out in acetone or water vapors at  $20^\circ\text{C}$  and atmospheric pressure. It was shown earlier for tEGdMA polymers using  $\text{H}_2\text{O}$  (saturated vapor at room temperature) as sorbate [6(p.82)] that noticeable sorption starts only at high enough conversion  $C$ : with  $C = 0$ , limiting (equilibrium) sorption  $p$  is only  $\approx 0.5\%$ (by weight), and it stays at this level until  $C \approx 0.36$ , and then it grows step-wise to  $p = 2.1\%$ (by weight); the maximum value of  $p$  is observed in the area of very high  $C \geq 0.8$ . Since the concentration of hydrophilic centers (determined by chemical structure of tEGdMA molecules) remains constant in the course of



polymerization, the growth of  $p$  with increasing  $C$  (i.e., enhancement of effective hydrophily with increasing conversion) can be explained only by the formation of micro-cavities able to sorb water (using capillary mechanism) and related to microheterogenization of the polymerization system during polymerization. Thus, diffusion-sorption probing with the use of  $H_2O$  as a sorbate can serve as a test of microheterogeneity.

Data on limiting sorption values of  $H_2O$  for copolymers of different composition with high conversion ( $C \geq 0$ ) are shown in Fig. 6.14. Dashed straight lines are lines of additive sorption, i.e., calculated values of  $p$  for each composition, and these values were derived based on the assumption that the  $a$  value is proportional to the overall concentration of hydrophilic centers contained in  $M_1$  and  $M_2$  units of copolymer of a given composition. In all cases (with the exception of  $M_2 = MMA$ )

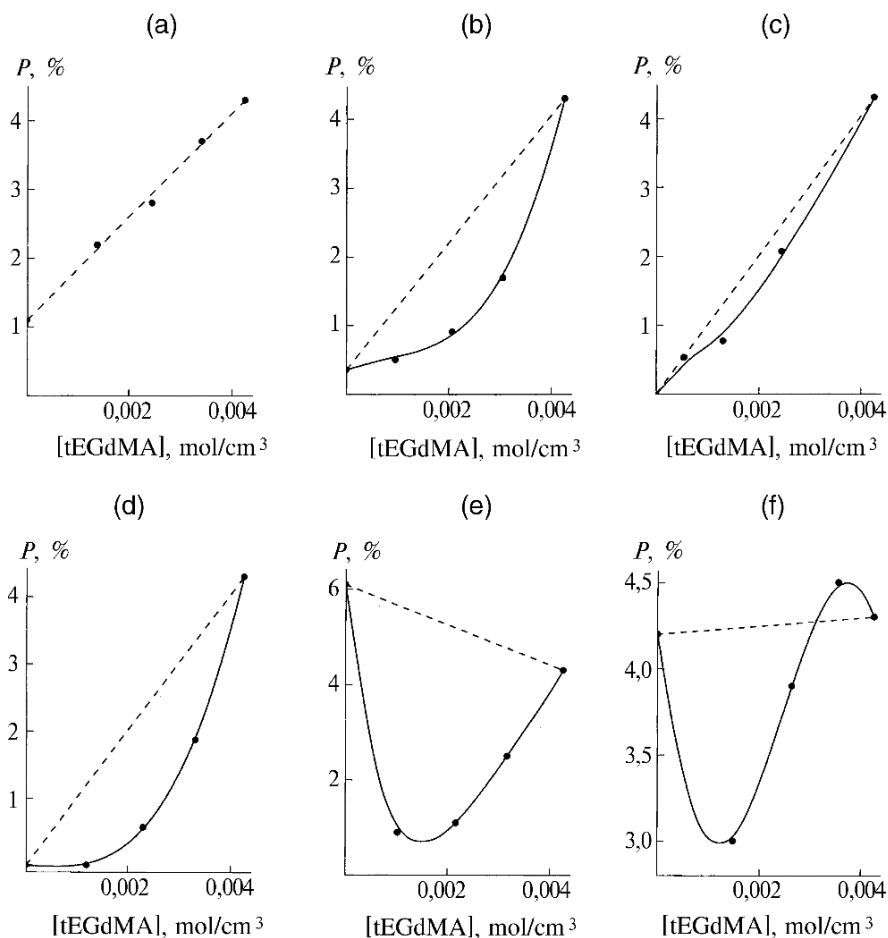


**Fig. 6.14** Dependence of limiting sorption  $p$  of water vapor at  $23^\circ\text{C}$  upon tEGdMA- $M_2$  copolymer composition for  $M_2 = \text{MMA}$  (a), BMA (b), DDMA (c), styrene (d), BA (e), and VA (f). Dashed straight lines, additivity calculation

experimental curve are located below calculated (additive) lines, which could be interpreted as an indication of microstructural homogenization when transferring from microheterogeneous tEGdMA homopolymer to copolymers that were progressively enriched with  $M_2$  units, and the homogenization proper, as a consequence of cyclization suppression.

The latter agrees well with the kinetic argument presented above. Minor deviation from additivity in the case of  $M_2 = \text{VA}$  (observed for low content of VA in copolymer) can be explained as follows: because  $r_1 = 20 \gg 1$  and  $r_2 = 0.05 \ll 1$ , with low VA content, tEGdMA polymerization proceeds virtually in the homopolymerization conditions, and VA becomes polymerized only at deep conversions forming local centers of VA homo-polymerization in the structure of the tEGdMA polymer, which upgrades the structural micro-nonhomogeneity.

The least deviation from additivity in the case of  $M_2 = \text{MMA}$  (experimental lines virtually coincide with calculated line) correlates well with kinetic data, according to which monomers with alternating and statistically distributed units in copolymer chains form the following sequence in terms of cyclization suppression efficiency: styrene > BMA > MMA.

Data for another sorbate (acetone) are shown in Fig. 6.15. In contrast to water, acetone possesses expressed thermodynamic affinity to  $M_2$  and  $M_1$  units

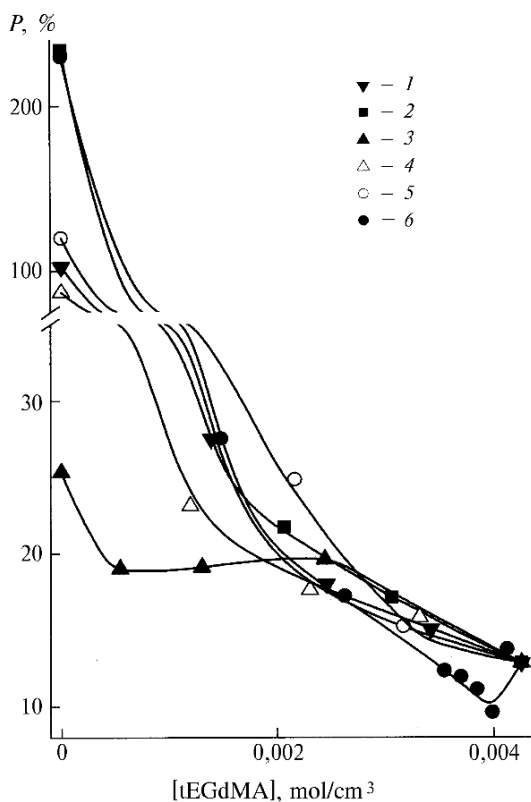


**Fig. 6.15** Dependence of limiting sorption  $p$  of acetone vapor at 23°C upon composition of copolymers tEGdMA:  $M_2$  for  $M_2 = \text{MMA}$  (1), BMA (2), DDMA (3), styrene (4), BA (5), and VA (6)

(when water is used as sorbate, a noticeable level of affinity is observed only for  $M_2 = \text{BA}$  and  $\text{VA}$ , when  $p$  of homopolymers are equal to 6% and 4.2%, respectively). Indeed, the value of  $p$  of acetone for the case of  $M_2$  homopolymers lies within  $25\% < p < 230\%$ , and for  $M_1$  homopolymer,  $p \approx 13\%$ . The application of sorbate of this type enables us to track the evolution of integral network  $v_\Sigma = v_{\text{ch}} + v_{\text{ph}}$  in copolymers when varying their composition.

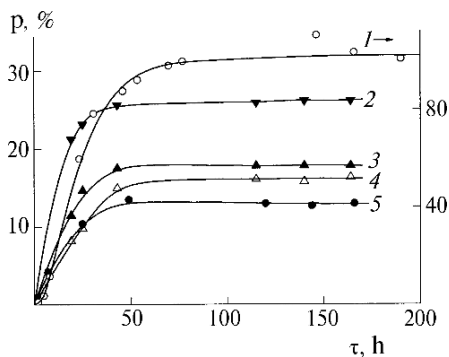
Here,  $v_{\text{ch}}$  = concentration of chemical network junctions (which is theoretically equal to doubled concentration of  $M_1$  because each double bond in the di(meth)acrylate molecule is converted into a chemical network junction in the course of polymerization);  $v_{\text{ph}}$  = concentration of physical network junctions, i.e., network of labile bonds of intermolecular interactions with the lifetime exceeding observation time (the nature and features of physical junctions in polymers, as well as methods for  $v_{\text{ph}}$  determination are described in a monograph [12]). Indeed, it is just the degree of cross-linking of integral network  $v_\Sigma$  that serves as a factor restricting the value of limiting sorption.

Therefore, when copolymer composition is varied, the values of  $p$  and  $v_\Sigma$  change in opposite directions.

It is seen from Fig. 6.15 that  $v_\Sigma$  value declines monotonously with decreasing [tEGdMA] (i.e., with decreasing  $v_{\text{ch}}$ ) in all cases, with the exception of DDMA. The nonmonotonous character of dependence of  $p$  upon tEGdMA content for  $M_2 = \text{DDMA}$  verifies the assumption (made earlier based on kinetic data) that tEGdMA copolymers with diphilic DDMA molecules may have an unconventional structure conditioned by micelle formation in the course of copolymerization. Obviously, the diphility associated with the presence of this alkyl substituent of  $\text{C}_{12}\text{H}_{25}$ , in the case of DDMA, is expressed much more strongly than when other alkyl(meth)acrylates are used, namely, BMA and BA with relatively small groups  $\text{C}_4\text{H}_9$ . Very low value of  $p$  ( $p = 25\%$ ) for DDMA homopolymer (for PBA and PBMA,  $p = 120\%$  and  $230\%$ , respectively) is indicative of a relatively high value of  $v_{\text{ph}}$ , which could be related to a high degree of cooperation of centers of very weak (dispersion type) intermolecular interactions in groups  $\text{C}_{12}\text{H}_{25}$  and, as a consequence, to formation of strong physical junctions of cooperative type. A high degree of mutual orientation of interacting atomic groups  $\text{C}_{12}\text{H}_{25}$  is required for the action of such junctions. Therefore, we believe that formation of the chemical network during copolymerization with tEGdMA would impede the mutual orientation process, thus reducing the value of  $v_{\text{ph}}$ . It seems likely that it is just for this reason that the value of  $v_\Sigma = v_{\text{ch}} + v_{\text{ph}}$  does not grow with increasing tEGdMA content—as it does in all other cases—but remains virtually constant in the range [tEGdMA] = 0–2.5 mol/l. It is not improbable that increase of  $v_{\text{ch}}$  in this range caused by the increment of [tEGdMA] is compensated by decrease of  $v_{\text{ph}}$  resulting from progressing impediment of mutual orientation of groups  $\text{C}_{12}\text{H}_{25}$  as the degree of chemical network cross-linking goes up.

Sharp increase of  $v_\Sigma$  (decline of  $\alpha$ ) with increasing  $v_{\text{ch}}$  for all other copolymers is indicative of a situation  $v_{\text{ph}} \ll v_{\text{ch}}$  arising at least starting from [tEGdMA] > 1 mol/l (i.e., nominal  $v_{\text{ch}} > 2$  mol/l). In the opposite case, the value of  $v_\Sigma = v_{\text{ch}} + v_{\text{ph}}$  would not have been so sensitive a function of [tEGdMA]. However, we can

**Fig. 6.16** Representative kinetic curves for sorption at 23°C in an example of acetone vapor sorption by tEGdMA-MMA copolymers depending on molar ratio.  $[M_1]:[M_2] = 0:1$  (1), 1:3 (2), 1:1 (3), 3:1 (4), and 1:0 (5)



suppose that an alternative version is responsible for the high sensitivity of  $v_{\Sigma}$  to variation of  $v_{ch}$ . This version is based on the known effect implying generation of new physical junctions when cross-links are formed [18]. In this case, the mobility of the polymeric chain section adjacent to the chemical junction being formed is frozen, which leads to a sharp growth in stability of weak, actually nonfunctioning physical junctions (their lifetime is shorter than observation time).

This fact transforms them into strong, actually existing junctions. The small non-monotonous section of the curve in Fig. 6.15 verifies the structural peculiarity of tEGdMA and VA copolymers once again. This peculiarity is determined by virtually separate polymerization of  $M_1$  and  $M_2$  instead of copolymerization with formation of a specific structure.

Rough estimates of diffusion coefficients  $D$  of water and acetone are derived from data on sorption kinetics (representative curves are given in Fig. 6.16). The high error of these estimates is associated with poor straightening of kinetic data in coordinates of Fick's equation. Values of  $D$  for water fall within  $2 \times 10^{-8}$ – $3 \times 10^{-6}$   $\text{cm}^2/\text{s}$ , and those for acetone are from  $1 \times 10^{-8}$  to  $5 \times 10^{-7}$   $\text{cm}^2/\text{s}$ . The authors failed to determine the dependence of  $D$  values upon copolymer composition and nature of  $M_2$  because the measurement error was too high.

## References

1. Unpublished results of Berlin AA, Kireeva SM, Sivergin YuM. Reported to the authors in 1974
2. Matveeva NG (1977) Papers for the 1st All-Union Conference on Chemistry and Physical Chemistry of Polymerized Oligomers 2:276. Department of the Chemistry and Physics Institute of the USSR Academy of Science, Chernogolovka (in Russian)
3. Sivergin Yu M, Kireyeva SM, Grachev AA et al (1980) Dokl Akad Nauk SSSR **254**:931–934 (in Russian)
4. Berlin AA, Sukhareva LA, Kefeli TYa (1976) Vysokomolekul Soedin A **18**:2542–2547 (in Russian)
5. Berlin AA, Matveeva NG (1970) Successes of chemistry and physics of polymers. Khimia, Moscow (in Russian)

6. Berlin AA, Korolev GV, Kefeli TYa, Sivergin YuM (1983) Acrylic oligomers and materials on the acrylic oligomers. Khimiya, Moscow (in Russian)
7. Regel VG, Slutsker AI, Tomashevskiy EE (1974) Kinetic theory of solid body strength. Nauka, Moscow (in Russian)
8. Bartenev GM (1984) Polymer strength and mechanism of polymer breaking (in Russian). Khimiya, Moscow
9. Gul' VV, Kuleznev VN (1979) Structure and mechanical properties of polymers (in Russian). Vysshaya Shkola, Moscow
10. Ward I (1975) Mechanical properties of solid polymers. Khimia, Moscow (Russian translation)
11. Korolev GV, Bubnova ML, Makhonina LI, Bakova GM (2006) *Vysokomolekul. Soedin. A* **48**:632–645 (in Russian)
12. Korolev GV, Mogilevich MM, Golikov IV (1995) Cross-linked polyacrylates: micro-heterogeneous structures, physical networks, deformation-strength properties. Khimiya, Moscow (in Russian)
13. Irzhak VI, Korolev GV, Soloviev ME (1997) *Usp. Khim.* **66**:179–200
14. Glasstone S, Laidler K, Eyring H (1948) The theory of absolute rates of reaction. IL, Moscow (Russian translation)
15. Korolev GV, Mogilevich MM, Ilyin AA (2002) Association of liquid organic compounds. Mir, Moscow (in Russian)
16. Korolev GV, Boichuk IN, Ilyin AA, Mogilevich MM (2001) *Vysokomolekul. Soedin. A* **43**:713–721 (in Russian)
17. Gons J, Vorenkamp EJ, Challa G (1977) *J. Polym. Sci. Chem. Ed.* **15**:3031–3038
18. Kraus Y (1963) *J. Appl. Polym. Sci.* **7**:1257–1263
19. Katz D, Tobolsky AV (1964) *J. Polym. Sci. A* **2**:1595–1605
20. Irzhak VI, Rosenberg BA, Enikopyan NS (1979) Cross-linked polymers. Synthesis, structure and properties. Nauka, Moscow (in Russian)
21. Korolev GV, Bubnova ML, Makhonina LI, Bakova GM (2005) *Vysokomolekul. Soedin. A* **47**:1086–1097 (in Russian)
22. Dušek K (1993) *Collect. Czech. Chem. Commun.* **58**:2245–2265
23. Matsumoto A (1995) *Adv. Polym. Sci.* **123**:41–80
24. Rostchupkin VP, Kurmaz SV (2004) *Usp. Khim.* **73**:247–274 (in Russian)
25. Dušek K (1982) Polymer networks. Springer, NY
26. Korolev GV, Baturina AA, Berezin MP, Kurmaz SV (2004) *Vysokomolekul. Soedin. A* **46**:656–667 (in Russian)
27. Korolev GV, Bubnova ML, Makhonina LI, Bakova GM (2005) Deformation and fracture of materials #11:2–7 (in Russian)
28. Berezin MP, Korolev GV (1977) Papers for the 6th World Conference on Chemistry and Physical Chemistry of Oligomers **1**:69. Chernogolovka (in Russian)
29. Lagunov VM, Berezin MP, Korolev GV et al (1981) *Vysokomolekul. Soedin. A* **23**:2747–2751 (in Russian)
30. Korolev GV (2003) *Usp. Khim.* **72**:222–244 (in Russian)
31. Korolev GV, Bakova GM, Berezin MP et al (2003) *Vysokomolekul. Soedin. A* **45**:33–44 (in Russian)
32. Korolev GV, Kochneva IS, Bakova GM et al (2002) *Vysokomolekul. Soedin. A* **44**:1484–1489 (in Russian)
33. Moloney AC, Kausch HH, Stinger HR (1983) *J. Mater. Sci.* **18**:208–216
34. Rabinovich AP (1970) Introduction into mechanics of reinforced polymers. Nauka, Moscow (in Russian)

## Part II

# Three-Dimensional Free-Radical Polymerization. Hyper-Branched Polymers

A new (non-network) direction has developed rapidly in the field of three-dimensional polymerization since the mid-1990s: synthesis, study of properties, and application of hyper-branched polymers (HBP). The reason for exceptional interest in HBP consists in their valuable, often unique, properties as determined by the specific topological structure of the macromolecules.

Polymeric chains of HBP diverge symmetrically in three-dimensional space from a point or linear center of symmetry, and they are shaped as a branching tree (Fig. Part II.1). Progressively branching chains of HBP could be arranged in space in many different ways: as a sphere, cylinder, or topologically more complex shape consisting of spheres or cylinders connected by penetrating chains (see Fig. Part II.1). HBP with such topologically complex macromolecules are called nanostructured polymers. Scientists distinguish the core and the shell in an HBP macromolecule: the shell is a peripheral layer of end nonbranched chains and the core is the remaining volume of macromolecule filled with branched chains.

The final degree of HBP branching is characterized by the DB parameter (i.e., degree of branching) determined by the following relationship:

$$DB = (D + T)/(D + T + L)$$

where D, L, and T are the number of branched, linear, and terminal units in the HBP molecule, respectively.

For dendrimers having a strictly regular topological structure of macromolecules,  $DB \rightarrow 1$ , while for all other HBP,  $DB < 1$ . As a rule, the remarkable properties of HBP, distinguishing them from linear and cross-linked polymers, manifest themselves when DB parameter = 0.4–0.8. Among these properties are high solubility and thermodynamic compatibility, low viscosity of solutions, absence of dependence of hydrodynamic volume of macromolecules upon molecular weight, and, finally, ability of macromolecules to function as nano-containers for “guest” molecules absorbed by the core [see 1–10 (Chap. 7)].

HBP with statistical structure of branched macromolecules, while preserving unique properties of dendrimers that have a strictly regular topological structure, in contrast to the latter are synthesized in a much simpler way and, hence, are more accessible and comparatively inexpensive.

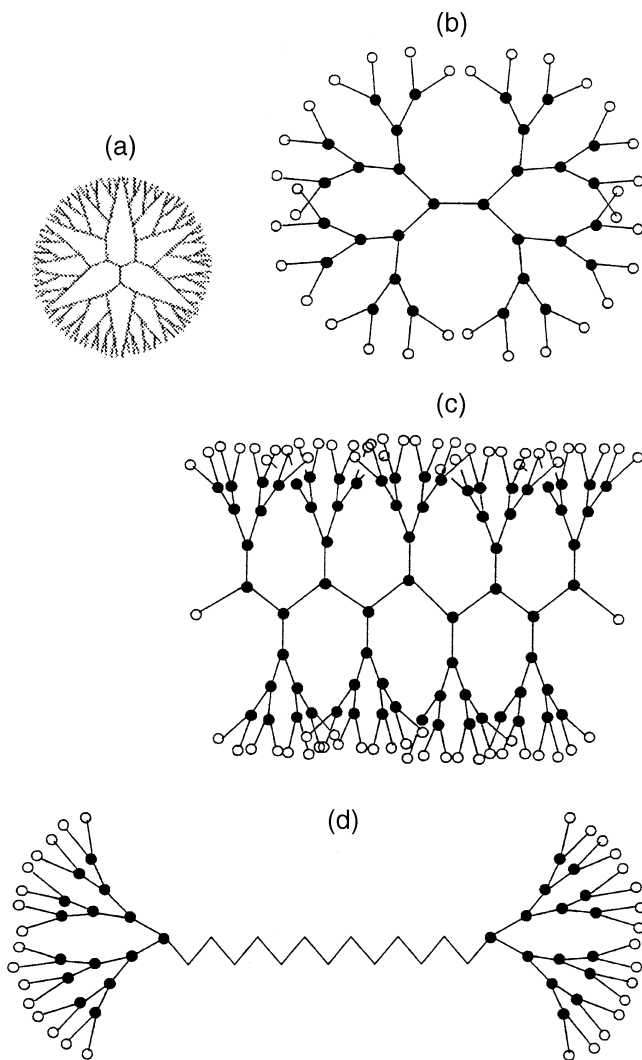


**Fig. Part II.1** Different types of macromolecules of hyper-branched polymers: (a) dendrimer macromolecule; (b) spherical macromolecule; (c) cylinder-shaped macromolecule; (d) two spherical macromolecules connected by penetrating chain (nanostructured macromolecule). o, functional group; •, branching points; •—•, interjunction chains; •—o, terminal chains with identical or different functional groups. Structure of macromolecules: (a) regular; (b–d) statistical

Let us consider in greater detail the main reactions of HBP synthesis via three-dimensional free-radical copolymerization under the conditions of polymer chain branching in the following chapter, Chap. 7.

# Chapter 7

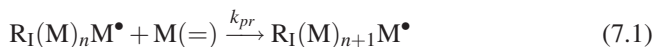
## Synthesis of Hyper-Branched Polymers

**Abstract** Chapter 7 is concerned with synthesis of hyper-branched polymers (HBP) by the radical polymerization method. It also describes theoretical potentialities of this method including several practical approaches to HBP synthesis, namely, HBP synthesis via regulation of chain length (initiation rate, agents and catalysts of chain transfer, inhibitors) and HBP synthesis via living chain polymerization. In this discussion, experimental results obtained by the authors and published data are compared with calculation results, including results related to the new developed gel formation theory. The most successful options of HBP synthesis in the living chains mode (including nanostructured polymers) are also discussed in Chap. 7. The main significance of the data obtained consists in their suitability for use as base data for targeted synthesis of HBP with predictable properties—HBP design.

### 7.1 Classification of Reactions for Hyper-Branched Polymer Synthesis

The problems arising during synthesis of HPB with specified properties (molecular weight, degree of branching, shape of macromolecules) are of different nature depending upon the type of selected synthesis reaction. Analysis of these problems leads to the following, apparently the most rational classification of HBP synthesis reactions, which found application in this field.

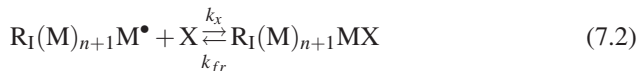
1. Polymerization according to the mechanism of *stepwise* polyaddition of the polycondensation type.
2. Radical polymerization according to mechanism of *chain* polyaddition.
3. Radical polymerization in the living chains conditions, which is a special case of polyaddition because the propagation of polymer chains develops according to the same radical chain mechanism as it does in the case of conventional radical polymerisation.





where  $R_I$  is the initiator radical;  $M(=)$  is the double bond in the molecule of initial monomer;  $M$  is units of polymer chain; and  $M^\bullet$  is the terminal unit with free valence.

However, degeneration of chain polyaddition into the stepwise one as a result of the act of reversible inhibition represents a significant distinction from the conventional radical polymerization



This act provides for the existence of the living chains conditions: the propagation of the polymer chain according to reaction (7.1) is inevitably preceded by the act of homolytic decomposition  $R_I(M)_{n+1}MX$  (reinitiation 7.2) with activation energy  $E_{fr} = 105\text{--}126\text{ kJ/mol}$ , close to initiation activation energy  $E_i = 117\text{--}126\text{ kJ/mol}$ , when organic peroxides and azodinitriles are used as initiators. That is, in contrast to conventional radical polymerization, when after a single act of initiation the polymer chain grows during a very short period of time,  $\tau_{pr} < 1\text{ s}$ , from the value of  $n_0 = 0$  to  $n = n_{lim}$  (where the final length of chain  $n_{lim} > 10^2\text{--}10^3$  units is limited by the chain termination act), in the case of living radical polymerization each act of initiation is accompanied only by a restricted increment of polymer chain and the next act of reinitiation is required for subsequent polyaddition. As  $E_{fr} \approx E_i$ , the macromolecule propagation reaction (which is essentially chain like) is identical to stepwise polymerization of the polycondensation type and the time of polymer chains propagation,  $\tau_{pr} \geq t_{lim}$ , where  $t_{lim}$  is the full time of the polymerization process; in conventional radical polymerization, the propagation time (or lifetime) of polymer chains  $\tau_{pr} < 1\text{ s} \ll t_{lim}$ . Therefore, it is reasonable to consider living radical polymerization as a special case, which has the features of both stepwise and conventional radical polymerization.

The above-described classification according to the principle of “instantaneous” (chain,  $\tau_{pr} \ll t_{lim}$ ) or “slow” (stepwise,  $\tau_{pr} \geq t_{lim}$ ) propagation of polymer chains plus free radical or molecular character of the polyaddition reaction is apparently the most reasonable for the following considerations.

1. Formation of small cycles from the interaction of reactive groups of adjacent chains or due to interchain interaction represents a secondary reaction preventing the branching of chains. As is shown below, the minimization of cyclization in the case of stepwise and radical chain polyaddition reactions is attained through the use of methods that are fundamentally different.
2. The highest possible yield ( $C_{lim}$ ) of target product, i.e., HBP, in synthesis reactions is determined by a number of parameters (functionality of initial reagents, ratio of their concentrations, etc.) and is forecasted by calculation according to gel formation formulas (Chap. 5). In the case of stepwise polyaddition reactions, a widely known Flory–Stockmayer equation is used. A completely different approach is required in the case of radical chain polyaddition: a new theory of gel formation (Chap. 5), especially intended for three-dimensional free-radical polymerization, is employed here.

3. Methods for controlling the reaction of HBP synthesis in the case of stepwise and radical chain polyaddition are also fundamentally different. With stepwise formation of propagating polymer chains, only the temperature and sometimes additives of catalysts serve as controlling factors. In the case of radical chain reactions, this set of factors is augmented with “inertia-free” control via external irradiation by light or ionizing radiation (photoinitiation or radiation initiation of chains), as well as via introducing additives of special regulating substances (inhibitors, decelerators, chain transfer agents, and chain transfer catalysts).

## 7.2 Synthesis of Hyper-Branched Polymers Via Three-Dimensional Free-Radical (Co)polymerization with Regulation of Polymer Chain Length

Synthesis of HBP via radical polymerization occupies a special place, because nowadays the latter is characterized by high technological significance [11–13]. Groups of English [14–18], German [19–22], and Japanese [23–31] researchers are the most advanced in HBP synthesis via radical polymerization. The main advantage of radical polymerization, i.e., chain mechanism of macromolecule propagation, is at the same time the main hindrance for HBP synthesis. Indeed, on the one hand, the chain mechanism ensures high rates of the process, high controllability through varying the concentrations of additives of initiators, inhibitors, and chain transfer agents, extremely good predictability based on large array of constants of rates characterizing the elementary stages accumulated by the present time [32–35], and the presence of a number of universal regularities, which are particularly characteristic of radical reactions [36, 37], taking into account the development of a new theory of gel formation specially intended for three-dimensional free-radical polymerization (see Chap. 5). However, on the other hand, the chain mechanism of three-dimensional free-radical polymerization preconditions a rather prominently manifested tendency of transition from the formation of branched polymerization products (such as soluble HBP) to network ones (such as microgel and macrogel) that are infusible and insoluble. Thus, for example, critical conversion  $C_{cr}$  (gel point), at which the polymerization system is transformed into gel, in the case of radical polymerization of (meth)acrylic monomers  $M_2$  containing two double bonds in each molecule, at ordinary rates of initiation  $W_i \approx 10^{-6} - 10^{-8} \text{ mol}/(1 \cdot \text{s})$  is so shifted to the area of low conversions  $C \rightarrow 0$  that it can be measured experimentally only with an accuracy to the upper boundary of  $C_{cr} < 0.01$ . Refining the  $C_{cr}$  value via calculation by formulas of the gel formation theory gives the value  $C_{cr} \approx 10^{-4}$  (!). In other words, under normal conditions the synthesis of HBP from di(meth)acrylates via radical polymerization is possible only with the yield lower than 1%. If  $M_m$  (where  $m > 2$ ) is used as a initial monomer for HPB synthesis, the value of  $C_{cr}$  is decreased still further.

Based on gel formation theory formulas, two main directions for changing the conditions of three-dimensional free-radical polymerization (leading to the increase

in  $C_{cr}$ , and, hence, to the increase in HBP yield) are seen; namely, decline in average functionality (F) of initial monomers and reduction of the average length ( $\bar{P}$ ) of propagating polymer chains (in this case  $\bar{P}$  is the number of units).

To reduce F in the case of  $M_2$  molecules, it is necessary to dilute  $M_2$  with monounsaturated (non-network-forming) monomer  $M_1$ , which has only one double bond capable of polymerization. However, in this case there is a limiting condition concerning the composition of mixture  $M_2/M_1$ : as soon as the dilution with monomer  $M_1$  reaches a level at which the content of  $M_2$  becomes lower than 3 in the chains consisting of  $\bar{P}$  units, the coefficient of branching in HBP being formed becomes less than 2 and further dilution would lead to the formation of poorly branched polymers that do not possess the HBP properties.

It is easy to demonstrate using an example of a mixture of monomers  $M_1 + M_2$  of the (meth)acrylate type that with ordinary  $W_i \approx 10^{-7} \text{ mol}/(1 \cdot \text{s})$ , the value of  $\bar{P} \approx 10^4$  units, while  $C_{cr} \rightarrow 1$  (and, hence, the yield of HBP  $\rightarrow 100\%$ ) with molar composition of mixture  $M_2/M_1 \rightarrow 10^{-5}$ . Consequently, if the dilution with monomer  $M_1$  is brought to such a degree that the yield of dissolvable product of polymerization would be increased to 100%, this product would appear to be practically unbranched (each chain of  $10^4$  units will contain on average 0.1 units of branching monomer  $M_2$ ). If the dilution degree is reduced to the level  $M_2/M_1 = 3 \times 10^{-4}$  giving the branching coefficient equal to 2, the value of  $C_{cr}$  would be reduced to 0.1 (yield of HBP is only 10%! ). However, even if so small a yield is accepted as sufficient, it should be borne in mind that the HBP formed thereby will be significantly different in terms of topology from typical HBP synthesized and widely tested by the present time. This topological difference consists in rather significant length of chain sections between adjacent branchings (the so-called interjunction chains): on average, two branchings per chain, the length of which is  $\bar{P} = 10^4$  units, i.e., the length of interjunction chains will be close to  $10^3$  units. Synthesis and exploration of HBP with variable length of interjunction chains showed [38] that with the length exceeding several dozen units, the HBP properties are becoming closer to the properties of conventional linear polymers of similar molecular weight.

Therefore, to successfully solve the problem of HBP synthesis via radical polymerization, the approach based on diluting polyfunctional monomers  $M_m$  with monofunctional ones  $M_1$  is used only as supplementary, while the main approach consists in the development of methods for reducing the length of polymer chains  $\bar{P}$  to several units.

The most efficient approaches of this kind, enabling us to successfully solve the problems of HBP synthesis via radical polymerization, are given below.

### **7.2.1 Regulation of Chain Length Through Initiation Rate Variation**

The average length of polymer chains  $\bar{P}$  in the case of radical polymerization, in compliance with the theory of chain nonbranched reactions, is related to kinetic parameters of the polymerization process by the following relationship [36, 37]:

$$\bar{P} = \frac{\text{chains propagation rate}}{\text{chains termination rate}} = \frac{k_{pr}[M]}{\sqrt{W_i k_{ter}} + k_{tr}[Y] + k_x[X]} \quad (7.3)$$

where  $k_{pr}$ ,  $k_{tr}$ ,  $k_x$ , and  $k_{ter}$  are constants of rates of propagation, transfer, linear, and quadratic termination of chains, respectively;  $[M]$ ,  $[Y]$ , and  $[X]$  = concentrations of monomer, chain transfer agent, and inhibitor;  $W_i$  = initiation rate (in the case of substantial initiators;  $W_i = k_i[I]$ , where  $k_i$  = initiation rate constant;  $[I]$  = initiator concentration; and, in the case of photoinitiation or radiation initiation,  $W_i = k'_i[i]$ , where  $[i]$  = radiation intensity).

It is obvious that in the case of TFRP the relationship (7.3) refers only to *primary chains* initiated by a given single act of radical generation by initiator  $R_1^\bullet (I \xrightarrow{k_i} R_1^\bullet)$ . It follows from Eq. (7.3) that  $\bar{P}$  decreases with growing  $W_i$ . When chain transfer agents and inhibitors are missing from a polymerization system, this decrease adheres to the following law:

$$\bar{P} = \frac{k_{pr}[M]}{\sqrt{W_i k_{ter}}} \quad (7.4)$$

Taking into account that numeric values of  $k_{pr}$ ,  $k_{ter}$  ( $l \cdot \text{mol}^{-1} \cdot \text{s}^{-1}$ ),  $k_i$  ( $\text{s}^{-1}$ ), and  $[M]$  ( $\text{mol/l}$ ) in the case of polymerization of vinyl monomers stay within  $10^2 \leq k_{pr} \leq 10^4$ ,  $10^6 \leq k_{ter} \leq 10^8$ , and  $10^{-5} \leq k_i \leq 10^{-7}$  [32–34, 36], the condition of successful synthesis of HBP from monomer  $M_2$ ,  $\bar{P} \approx 3$ , will be fulfilled only when very high concentrations of initiator are used, commensurable with monomer concentration, that is,  $[I] \geq 1 \text{ mol/l}$  instead of the usually used  $[I] \leq 10^{-2} \text{ mol/l}$ .

A hundredfold increase  $[I]$  gives rise to a number of additional factors that do not manifest themselves with small  $[I]$  under conventional conditions of polymerization:

1. Quadratic termination of chains with participation of radicals  $R_1^\bullet$  and, hence, existence of limiting rate of polymerization  $W \leq W_{lim} = \text{const}$ , which stops increasing with the growth of  $W_i$ , starting from a certain critical value of  $W_i \geq (W_i)_{cr}$
2. Chain transfer with participation of initiator molecules
3. Considerable increase of contribution of chain mechanism of initiator decomposition for initiators, which are susceptible to chain decomposition

It is obvious that HBP synthesized under these conditions would inevitably contain a large number of initiator fragments both in interjunction chains (i.e., in the “core”) and in end chains (i.e., in the “shell”).

Successful synthesis of HBP by this method was first implemented by a group of Japanese researchers headed by T. Sato [39–43] from monomers  $M_2$  of dimethacrylates and divinyl benzene (in certain cases with dilution with  $M_1$ ) in the presence of AIBN as initiator (with addition of inhibitor in certain cases). The developed process of HBP synthesis was called by the authors “initiation-fragment incorporation radical polymerization.”

### 7.2.1.1 Synthesis of HBP Via Copolymerization of Divinyl Benzene ( $M_2$ ) with Ethyl Styrene ( $M_1$ ) Initiated by AIBN (I) in the Presence of Benzyl-oxyimino-acetate (X) as a Decelerator<sup>1</sup> [39]

Copolymerization was carried out in a benzene solution with concentration of components indicated in brackets (mol/l) at 70° and 80°C:  $M_2$  (0.25),  $M_1$  (0.25), X (0.5), and I (0.5). The yield of copolymer and its molecular weight ( $M_n$ ) grew in the course of the process until the moment of initiator exhaustion, and then they became constant at times  $t \approx 4\tau_1$ , where  $\tau_1$  = the period of initiator half-life. The value of  $\tau_1 = 2\text{--}6\text{ h}$  at 70°C and 2 h at 80°C (which corresponds to values of  $k_i = 3.2 \times 10^{-5}$  and  $9.6 \times 10^{-5} \text{ s}^{-1}$  and  $W_i = 1.6 \times 10^{-5}$  and  $4.8 \times 10^{-5} \text{ mol} \cdot \text{l}^{-1} \cdot \text{s}^{-1}$ ). Upper value of yield was equal to 47% (70°C) and 48% (80°C) at  $M_n = 23,200$  ( $M_w/M_n = 3.4$ ) and 26,400 ( $M_w/M_n = 3.4$ ). At the moment of attainment of upper limit values of copolymer yield and  $M_n$  value, the total content of reacting double bonds in copolymerization system approaches zero. Thus, the limit yield occurs not because of complete consumption of initiator but due to exhaustion of double bonds in  $M_2$  and  $M_1$ . Unfortunately, the authors do not describe the procedure for copolymer yield determination, and therefore we can only suppose that low molecular substances (products of quadratic termination of initiator radicals  $R_1^\bullet + R_1^\bullet \rightarrow$  products of quadratic termination of initiator radicals  $\sim R^\bullet + X \rightarrow$  other products of interaction) account for approximately half of reaction products. No author's comments are provided for a very interesting regularity: in the course of copolymerization, the parameter of polydispersity at 70°C grows from 1.7 (6) to 3.2–3.5 (46–47), and at 80°C, contrariwise, goes down from 5.0 (26) to 3.4 (44–48); current yields of copolymers are given in parentheses.

The proof of the presence of hyper-branching of copolymer structure, as well as determination of characteristic parameters of synthesized HBP, was carried out using a modern methodological complex specially developed for these purposes during the past decade [6, 9, 44]. This complex includes both the methods for analysis of fragments of macromolecules chemical structure (NMR of high resolution on protons and  $^{13}\text{C}$ , chemical and elemental analysis for the identification of chemical groups), and gel chromatography (using two and three detectors) in combination with laser light scattering under different angles and with electron microscopy. All these methods enable researchers to identify the degree of branching and concentration of interjunction and terminal chains, set of functional groups in the core and in the shell of HBP macromolecules, size of macromolecules, hydrodynamic radius  $R_h$  and gyration radius  $R_g$ , Mark–Houwink parameter  $\alpha$  in the known relationship  $\eta = KM^\alpha$  (for HBP  $\alpha < 0.5$ , in contrast to conventional linear polymers, for which  $\alpha \geq 0.5$ ). And, finally, special comparative testing of solubility and thermodynamic compatibility (which are incommensurably higher in the case of HBP) was

<sup>1</sup> Inhibitors X are usually classified into strong inhibitors (simply inhibitors) and weak inhibitors (decelerators) [36]. The ratio of constant of chain linear termination rate at molecules of X,  $k_X$ , to the constant of chain propagation rate  $k_{pr}$  serves as classification feature: when  $k_X/k_{pr} > 1$ , X is an inhibitor, while when  $k_X/k_{pr} \leq 1$  X is a decelerator.

carried out (comparison with linear analogues characterized by approximately similar molecular weight).

It was found as a result that copolymer composition evolves in the course of the process in the following way. The content of initiator fragments grows from 28% to 42% during period  $t$  from 2 to 18 h (for  $T = 70^\circ\text{C}$ ), and then it remains invariable (the final time is 24 h). The total content of  $M_2$  and  $M_1$  units goes down from 59% to 42% (mol) during time interval from  $t = 0$  to  $t = 12$  h, attaining then the constant value. At that the content of unreacted double bonds drops from 16% (mol) ( $t = 2$  h) to 0 ( $t = 12$  h). Since each macromolecule of HBP copolymer being formed grows continuously in the course of polymerization process (the value of  $M_n$  goes up with increasing  $t$  according to law that is close to linear one), the variation of composition is recorded in macromolecules in the form of copolymer composition gradient.

Specific features of HBP (distinguishing this class of macromolecules from conventional linear polymers) clearly manifest themselves in comparative study of polystyrene (PS) and HBP using two methods: namely, gel-permeation chromatography (GPC) and GPC in combination with multiangle light scattering (laser source of light). The results of this study (presented in Table 7.1) show that starting from a certain value  $M_n$ , hydrodynamic radius of HBP macromolecules ( $R_h$ ) and radius of gyration ( $R_g$ ) cease to grow with increasing  $M_n$ , and these limiting values (in nm)  $R_h = 10.5$  and  $R_g = 13.2$  are lower than  $R_h = 14.3$  and  $R_g = 27.5$  for linear analogue (PS). Correspondingly, values of  $M_n$  and  $M_w$  determined with the use of the GPC method appear to be dramatically lower as compared with “true” values measured by a combination of the GPC method and the light-scattering method.

Viscosimetry (solution in benzene, use of Ubbelohde viscosimeter,  $30^\circ\text{C}$ ) identifies one more remarkable property, which represents a distinguishing feature of HBP—independence of viscosity ( $\eta$ ) upon HBP concentration in solution: when increasing [HBP] from 2 to 10 g/l, the value  $\eta = \text{const} = 0.008$  l/g, while viscosity of PS in the same interval of polymer concentrations increases from 0.02 to 0.025 l/g. The reference sample in viscosimetric experiments (PS) was selected with  $M_n = 30,000$  and  $M_w = 54,000$  being lower than  $M_n = 74,500$  and  $M_w = 336,000$  for HBP, but the viscosity in this case is two times higher than that for HBP having any fixed concentration of polymer in the solution.

**Table 7.1** Comparison of data obtained using two methods for HBP and polystyrene (PS)

	GPC method			Combination of GPC method and light-scattering method				
	$M_n \times 10^{-4}$	$M_w \times 10^{-4}$	$M_w/M_n$	$M_n \times 10^{-4}$	$M_w \times 10^{-5}$	$M_w/M_n$	$R_g$ (nm)	$R_h$ (nm)
HBP-1	1.19	2.38	2.0	3.19	0.74	2.3	5.4	5.1
HBP-2	1.69	5.41	3.2	7.45	3.36	4.5	13.8	10.6
HBP-3	2.02	6.07	3.0	7.25	3.36	4.6	13.2	10.5
HBP-4	2.32	7.89	3.4	7.33	3.41	4.6	13.2	10.5
PS	—	—	—	12.3	2.96	2.4	27.5	14.3

Values of  $\eta$  used as characteristic ones and extrapolated to the zero value of polymer concentration are equal to 0.008 and 0.018 l/g for HBP and PS, respectively. As such difference is typical of all HBP synthesized and studied up to the present time irrespective of their chemical nature, it is used in the practice of research work as the simplest express test for hyper-branching.

It also appeared that macromolecules of synthesized HBP are characterized by sufficiently high level of micro-viscosity that provides matrix stabilization of free radicals formed from decelerator (X) in the course of copolymerization. The EPR method enabled researchers to record nitrogen-centered radicals  $X^\bullet$ , the concentration of which (mol/l) continuously grows from  $10^{-6}(70^\circ\text{C})/2 \times 10^{-6}(80^\circ\text{C})$  in the course of copolymerization during 5 h to  $3.5 \times 10^{-6}(70^\circ\text{C})/6.3 \times 10^{-6}(80^\circ\text{C})$ . After cooling the reaction system to  $20^\circ\text{C}$ , the concentration of  $X^\bullet$  is significantly reduced ( $\approx 10$  times), but not to the zero value. Quite high residual value  $[X^\bullet] = 3.7 \times 10^{-7}$  mol/l at  $20^\circ\text{C}$  is indicative of formation of rigid polymer structures. These structures capture some  $X^\bullet$  in the molecules of HBP formed in the course of copolymerization proceeding under the conditions of quite high dilution by benzene, inert dilutor, which enhances the molecular mobility and, hence, hinders capturing of  $X^\bullet$ . Therefore, the fact of stabilization of at least a certain part of  $X^\bullet$  after cessation of initiation (at  $20^\circ\text{C}$  initiator practically ceases to generate radicals) indicates the existence of micro-volumes in HBP macromolecules, with these micro-volumes being characterized by a very high level of micro-viscosity and being inaccessible for the plasticizing action of benzene.

Transmission electron microscopy (Hitachi 800, 200 kV) of synthesized HBP gives an image in the form of densely packed discrete spherical particles of approximately the same size (diameter 2–3 nm), which is less than that of  $R_g$  and  $R_h$ . Attempts made by the authors to raise the concentrations of  $M_1$ ,  $M_2$ , X, and I in the solution 1.2–2 times, while preserving the selected relationship of components  $2[M_1] = 2[M_2] = [X] = [I]$ , led to an increase in the yield of HBP from 47–48% to 51–59%, but gel formation was observed in this case.

Next, the data obtained by Sato et al. [39] are compared with theoretical estimates for relationships (7.3) and (7.4). Substituting known values ( $1 \cdot \text{mol}^{-1} \cdot \text{s}^{-1}$ )  $k_{\text{pr}} = 150$  and  $k_{\text{ter}} = 10^7$  (practically identical for  $70^\circ$  and  $80^\circ\text{C}$ ) and  $W_i = 1.6 \times 10^{-5}$  (at  $70^\circ\text{C}$ ) and  $W_i = 4.8 \times 10^{-5}$  mol/(l·s) (at  $80^\circ\text{C}$ ) into (7.4), we obtain  $\bar{P} = 6(70^\circ\text{C})$  and  $\bar{P} = 3(80^\circ\text{C})$  without taking into account the inhibiting action of additive X. To take X into account, it is necessary to know the value of  $k_X$ , which is not indicated by these authors [39]. Taking into account that X is a decelerator, i.e.,  $k_X < k_{\text{pr}}$ , and having selected the maximum value of  $k_X \approx 10^2$  l/(mol·s), we obtain a decrease in values of  $\bar{P} = 2$  and  $\bar{P} = 1$  according to formula (7.4), respectively. If these values were true, HBP formation would not take place, because the value  $\bar{P} > 2$  is necessary for the formation of HBP from equimolar mixture  $M_1 + M_2$  (only in this case would the branching coefficient exceed 1). Apparently, in reality  $k_X < 10^2$  l/(mol·s) and actual values of  $\bar{P}$  at  $70^\circ$  and  $80^\circ\text{C}$  stay within ranges  $2 < \bar{P} \leq 6$  and  $2 < \bar{P} \leq 3$ . It means that, in terms of length of polymer chain, the data provided by the authors match the theory quite well.

However, in terms of critical conversion of gel formation ( $C_{cr}$ ) a critical discrepancy is observed with the theoretical estimate for relationships given in Chap. 5.

Indeed, the value of  $C_{cr}$  in this case is derived from a theoretical relationship:

$$C_{cr} = 0,33 \frac{\sqrt{W_i k_{ter}}}{k_{pr} F_{22}}$$

where  $F_{22} = 2[M_2] = 0.5 \text{ mol/l}$ , while the values of  $k_{pr}$ ,  $k_{ter}$ , and  $W_i$  are the same as the those given above. Substituting their numeric values, we obtain  $C_{cr} < 0.1 \equiv 10\%$  for both temperatures; this is significantly lower than the experimental yield of HBP, which is  $\approx 50\%$ . Such a significant discrepancy between the experimental value and theoretical one most probably indicates a high degree of cyclization in HBP macromolecules, which is inherent to the processes of three-dimensional free-radical polymerization. It is known that cyclization shifts the value of  $C_{cr}$  to the region of higher numeric values. This explanation agrees well with observed stabilization of free radicals  $I^\bullet$ , as cyclization leads to formation of cross-linked micro-areas of micro-gel type in the core of HBP macromolecules.

In other publications by Japanese scientists belonging to the group of T. Sato [40–42], HBP synthesis by a similar method is described (at very high rates of initiation  $W_i \geq 10^{-5} \text{ mol} \cdot \text{l}^{-1} \cdot \text{s}^{-1}$ ) using divinyl benzene [41], ethylene glycol di(methacrylate) [40], and divinyl adipinat [42] as branching monomers  $M_2$ .

At present it is not possible to evaluate the perspectives of the T. Sato method from the standpoint of its application and its competitiveness, because it is not clear from their publications [39–43] to what extent the procedure for isolating HBP from a 50% mixture of by-products is labor intensive and complicated. The necessity for conducting synthesis in highly diluted solutions and the very high consumption of initiator represent obvious disadvantages of the method. Unquestioned advantages of the method are its universality and high rate of synthesis process. The universality consists in the possibility of using this method for obtaining HBP with any type of functional groups, which are available in a wide variety of components for radical copolymerization of  $M_1$  and  $M_2$ . For instance, only for one class of  $M_1$  monomers, i.e., methacrylates with formula  $\text{CH}_2=\text{C}(\text{CH}_3)\text{COOR}$ , many compounds are known with different R: from R-alkyl with a widely variable length and degree of carbo-chains branching to R containing atomic groups hydroxy, amino, plus also methacrylates, carriers of atomic groups (methacrylamid and methacryl acid).

### 7.2.2 Regulation of Chain Length by Chain Transfer Agents and Chain Transfer Catalysts

Relationship (7.3) indicates possible ways for regulating chain length. Such regulation is necessary for the implementation of HBP synthesis via three-dimensional free-radical polymerization. One such way consists of the increase of initiation rate



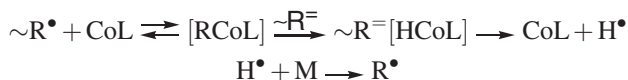
$W_i$  to very high values  $W_i > 10^{-5} \text{ mol} \cdot \text{l}^{-1} \cdot \text{s}^{-1}$ , enabling us to reduce the length of material chains to values  $\bar{P}$  amounting to several units (instead of hundreds or thousands of units at conventional rates of initiation). This approach was successfully implemented by a group of Japanese scientists (see Sect. 7.2.1). Another approach that consists in intensification of chain transfer acts for the purpose of attaining the same goal. It was widely used by a group of English scientists headed by D. C. Sherrington [14–18]. In this case the chain transfer was carried out in two ways. First, through the use of conventional method: introduction of additives of substances (Y) capable of reacting with chain carrier radical  $\sim\text{R}^\bullet$  with formation of new, also active radical  $\sim\text{R}_Y^\bullet$  that initiates a new material chain. In this process, molecules Y are expended and, hence, the consumption of Y is one molecule per one chain. It follows from relationship (7.3) that for realization of  $\bar{P} = 3\text{--}5$  units such values of  $k_{tr}[\text{Y}]$  are necessary that are only three to five times lower than values of  $k_{pr}[\text{M}]$  (at conventional rates of initiation,  $W_i = 10^{-7} \text{ mol} \cdot \text{l}^{-1} \cdot \text{s}^{-1}$ , in the absence of inhibitors, when  $k_X[\text{X}] = 0$ ). It means that it is necessary that either  $k_{tr} < k_{pr}$ , or that  $[\text{Y}]$  should be high (commensurable with  $[\text{M}]$ ). The variant  $k_{tr} > k_{pr}$  is rather inconvenient for HBP synthesis. It is easy to show<sup>2</sup> that consumption of Y in this case will be higher than consumption of M and that continuous addition of Y would be required during the polymerization process for maintaining  $\bar{P} = \text{const}$ . Consequently, an option remains that implies using the unusually high concentrations of Y or the unconventional approach that is based on using the phenomenon of chain transfer catalysis, which was discovered by us [45, 46] more than two decades ago and which currently has found extensive application in the world of science and in practice.

D.C. Sherrington and his colleagues employed both approaches for HBP synthesis via three-dimensional free-radical copolymerization: the conventional approach implying high concentrations of Y and chain transfer catalysis (CTC).

The phenomenon of CTC was discovered by us in an example of polymerization of methyl(meth)acrylate in the presence of very small (catalytic) additives of compounds such as organic macrocyclic complexes of cobalt CoL (porphyrins, phthalocyanines, and oximes of cobalt) [45, 46]. It appeared that CoL additives in the amount of  $10^{-6}$  to  $10^{-5} \text{ mol/l}$  reduce the chain length 10–100 times (!), which corresponds in this case to relationship  $k_{tr} \gg k_{pr}$ . However, with  $k_{tr} \gg k_{pr}$ , the action of CoL should cease at the very early stages of polymerization because of quicker consumption of CoL as compared to consumption of M. However, this did not occur, and CoL was acting throughout the entire polymerization process without being expended (which was proved by measurements of  $M_n$  of polymers at various stages of polymerization process) and, hence, it behaved as a catalyst.

In-depth exploration [47] into the CTC process using different methods (GPC, NMR, IR and UV spectroscopy, etc.) enabled us to identify the following mechanism of catalysis:

<sup>2</sup> Solving the system of differential equations  $-d[\text{M}]/dt = k_{pr}[\text{M}][\text{R}^\bullet]$  and  $-d[\text{Y}]/dt = k_{tr}[\text{Y}][\text{R}^\bullet]$  gives  $[\text{Y}] = [\text{Y}]_0 - (1-C)^{k_Y/k_{pr}}$ , where  $C = ([\text{M}]_0 - [\text{M}])/[\text{M}]_0$  – monomer conversion.



Polymethacrylate chain  $\sim R^\bullet$  with the end double bond of the  $\sim\text{CH}_2\text{—C}(\text{COOCH}_3)=\text{CH}_2$  type, which is different from the methacrylate double bond, is formed as a result of disproportioning of chain carrier radical  $\sim R^\bullet$  accepted by CoL in the form of a complex [RCoL] followed by transformation into hydride HCoL, which is extremely unstable. It decomposes practically instantaneously, releasing atomic hydrogen and initial CoL. The formed  $\text{H}^\bullet$  is exceptionally active and immediately generates new chain  $\sim R^\bullet$ .

Further development of the CTC concept, mainly by researchers from other countries [48], has led to creation of new, still more efficient CoL complexes and to development of multiple options of practical application of CTC.

The first researcher, who experimentally proved the possibility of shifting critical conversion (gel point)  $C_{\text{cr}}$  into the region of very high values  $C_{\text{cr}} \rightarrow 1$  during copolymerization of divinyl monomers,  $M_2$ , and monovinyl monomers,  $M_1$ , was A. Matsumoto [49–51]. He showed that under the conditions of intensive chain transfer (in the presence of alkylmerkaptans functioning as transfer agent) in copolymerization systems  $M_1 + M_2$  (where  $M_2 =$  dimethacrylates or divinyl benzene, while  $M_1 =$  monomethacrylates or styrene), gel formation is not observed at all if molar ratio  $M_1 : M_2$  exceeds 100. However, this result was obtained before the beginning of the HBP boom, and that is why it was not developed further at that time.

Only in 2000, when the “triumphant march” of HBP was in full blast, did D.C. Sherrington and his colleagues use the approach that is based on suppression of gel formation by intensive chain transfer for synthesizing one more class of HBP, namely, copolymers of methylmethacrylate ( $M_1$ ) and branching monomers  $M_m$  di- and tri(meth)acrylates and divinyl benzene [14–18].

### 7.2.2.1 Synthesis of HBP Via Copolymerization of Methyl Methacrylate and Di(meth)acrylates in the Presence of Chain Transfer Agent [14, 17]

Synthesis strategy consists in the use of sufficiently concentrated solutions ( $\approx 40\%$  volume of comonomers; solvent is weakly polar toluene), but with very low content of branching monomer  $M_2$  (1–2% mol) with equimolar additive of quite active chain transfer agent (1-dodecantiol, 1–2% mol,  $k_{tr}$ ,  $1 \cdot \text{mol}^{-1} \cdot \text{s}^{-1}$ , for methacrylates  $\approx 300$ , while for acrylates  $\approx 3500$ ). Besides, using conventional initiator AIBN ( $\approx 5 \times 10^{-2} \text{ mol/l}$ ) at  $80^\circ\text{C}$  ( $W_i = 5 \times 10^{-2} \text{ mol} \cdot \text{l}^{-1} \cdot \text{s}^{-1}$ ), it is possible to obtain HBP with the yield of  $\approx 90\%$  ( $t = 16\text{h}$ ). HBP is isolated through precipitation (with methanol or heptane as precipitation agents). Polarity of the precipitation agent slightly influences the yield of overprecipitated HBP as well as its molecular and weight characteristics, which points to a certain complexity of fractional and

**Table 7.2** Results of studying methyl methacrylate (MMA) and tri(propylene glycol) di(acrylate) copolymers using GPC-1 and GPC-3 methods

Analysis method	[Y], % (by weight)	[M <sub>2</sub> ], % (by weight)	$\bar{M}_w$	$\bar{M}_n$	$M_w/M_n$	$g'$	$\alpha$
GPC-1	2.0	1.5	18,029	6,745	2.67	–	–
GPC-3	2.0	1.5	21,850	11,750	1.86	0.59	0.56
GPC-1	2.0	3.0	27,330	8,380	3.16	–	–
GPC-3	2.0	3.0	32,800	13,800	2.36	0.54	0.50

chemical composition of synthesized product. Increase of [M<sub>2</sub>] or decrease of [Y] in the initial reaction mixture inevitably results in gel formation.

Several samples of copolymers MMA and di(butylene glycol) or (tripropylene glycol) diacrylates were synthesized using this strategy. Then, these samples were studied by the method of conventional GPC-1 (using a refractometric detector) and the GPC-3 method implying the employment of three detectors (laser differential refractometer, diffraction viscosimeter, and photometer for measuring light scattering with a laser source). Typical results are presented in Table 7.2.

It can be seen from Table 7.2 that “true” molecular and weight characteristics of copolymers obtained from light-scattering data differ quite significantly from the characteristics determined by the GPC-1 method, which is based on hydrodynamic volumes of macromolecules. Because macromolecules become more densely packed as the branching degree grows, a discrepancy between hydrodynamic volumes and results of the GPC-1 method application is observed (molecular weights are underrated); this is an indirect proof of hyper-branching of synthesized copolymers. A more direct proof is a decrease of the Mark–Houwink parameter  $\alpha$  from the value 0.7 (measured for reference specimen of linear PMMA) to 0.50–0.56 for copolymers, and decrease of parameter  $g' = (R_g)_h / (R_g)_l$  to 0.59 and 0.54 ( $R_g$  = gyration radius; indices “h” and “l” mean hyper-branched and linear, respectively). The physical meaning of decreasing  $\alpha$  and  $g'$  consists in increasing the compactness (density of molecular packing) of macromolecules. It is seen from Table 7.2 that an increase in content of branching monomer M<sub>2</sub> in the initial system logically correlates with a decrease of  $\alpha$  and  $g'$ .

When using ethylene glycol dimethacrylate as M<sub>2</sub>, the synthesis strategy was corrected in the direction of raising the degree of initial reaction system dilution with a dilutor (toluene): fourfold dilution was used in addition to twofold dilution. Molar relationship of components was M<sub>1</sub> : M<sub>2</sub> : Y = 100 : 5 : 5, concentration of initiator was 1% (mol) per total content of double bonds, temperature = 80°C, and  $t = 5$  h. The role of inert solvent is demonstrated on an example of copolymerization system having low content of branching monomer M<sub>2</sub> (Table 7.3).

It is seen from Table 7.3 that dilution influences the yield nonmonotonously: at first the yield is reduced, and then it grows dramatically. Also, the solubility in the series of solvents selected for testing is enhanced. Especially astounding is the transition from dilution of 20 to 25 cm<sup>3</sup> (from 3.3 fold to 4.2 fold): a certain similarity to

**Table 7.3** Effect of diluting the reaction system with toluene on an example of composition  $M_1 : M_2 : Y = 100 : 2 : 2$  (total volume  $\approx 6\text{cm}^3$ )

Toluene volume, $\text{cm}^3$	Consistency of reacted mixture	Copolymer yield, %	Copolymer solubility (test: $0.5\text{g}/\text{cm}^3$ )
0	g	–	Insoluble
5	g	92	Insoluble
10	vl	92	Insoluble in DMSO
15	vl	75	Insoluble in DMSO
20	vl	51	Soluble
25	lvl	74	Soluble

*Note.* g, gel; vl, viscous liquid; lvl, low-viscous liquid. Testing solvents: THF, chloroform, dichloromethane, DMSO.

the critical phenomenon is observed, judging by a jump in yield from 51% to 74% and dramatic variation in mixture consistency.

MWD curves for this series of experiments (presented against the background of reference curve for linear PMMA) point to a rather strong broadening of MWD as the content of dilutor goes down (from molecular weights of  $10^3$ – $10^6$  for  $25\text{cm}^3$  of toluene to  $10^2$ – $10^7$  for  $10\text{cm}^3$ ). Also, all curves are polymodal. In transition from 20 to  $25\text{cm}^3$  of dilutor, in contrast to data from Table 7.2, no dramatic variation of MWD is observed: both curves are bimodal and an increase in degree of dilution leads only to insignificant narrowing of MWD.

In another series of experiments, where the relationship of components was  $M_1 : M_2 : Y = 100 : 15 : Z$  (with fivefold dilution with toluene), the value of  $Z$  varied from 4 to 15. In this series an attempt was made to compensate for high content of  $M_2$  via corresponding increase in the content of  $Y$ . It was found that after  $Z$  is increased from 4 to 9, expressed gel formation takes place, then at  $Z = 10$ , viscous liquid with gel particles is formed, and at  $Z = 11$  a low viscous liquid with gel particles is formed, and, finally, starting from  $Z = 12$ , a transparent low viscous liquid is formed. When  $Z$  increases from 12 to 15, the yield of copolymers drops from 86% to 61%, and copolymers are soluble in a number of solvents that are chosen for testing (see note to Table 7.3), with the exception of DMSO. MWP of copolymers is rather broad and polymodal.

As a result, the following optimum option of HBP synthesis was chosen: relationship of components  $M_1 : M_2 : Y = 100 : 5 : 5$ , a two- to fourfold dilution of mixture of components with inert solvent. Variation of copolymer composition during copolymerization at different stages of the process determined using NMR and chemical analysis method is presented in Table 7.4.

Additional information on the above-described HBP synthesis process could be derived by analyzing the results obtained by the authors within the scope of general chain reactions theory (relationship 7.1) and gel formation theory (Chap. 5) using the following relationships:

$$\bar{P} = \frac{k_{\text{pr}}([M_1] + [M_2])}{\sqrt{W_1 k_{\text{ter}}} + k_{\text{tr}}[Y]} = \frac{k_{\text{pr}}[M_1]}{k_{\text{tr}}[Y]} \quad \text{and} \quad C_{\text{cr}} = 0.5 \frac{k_{\text{pr}}[Y]}{k_{\text{pr}}F_{22}(0)} = \frac{0.5k_{\text{tr}}[Y]}{k_{\text{pr}}2[M_2]}$$

taking into account  $\sqrt{W_1 k_{\text{ter}}} \ll k_{\text{tr}}[Y]$  and  $[M_2] \ll [M_1]$ .

**Table 7.4** Composition of copolymer at various stages of copolymerization for system  $M_1 : M_2 : Y = 100 : 5 : 5$ 

Time, h	Total content of $M_2$ units, % (mol)	$\overline{M}_2/M_2 =$ fraction of $M_2$ units having pendent double bonds, % (mol)	Time, h	Total content of $M_2$ units, % (mol)	$\overline{M}_2/M_2 =$ fraction of $M_2$ units having pendent double bonds, % (mol)
0.5	7.8	87	3	4.3	43
1	6.7	72	4	3.1	32
2	4.2	63	5	2.8	24

*Note.* Content of Y fragments in copolymer is 9.8% (by weight); it coincides with the calculated one (10.0%, by weight).

For methacrylates,  $k_{pr} = 500$ ,  $k_{tr} = 300 \text{ l}/(\text{mol} \cdot \text{s})$  at  $80^\circ\text{C}$ ; using the base relationship of the authors  $M_1 : M_2 : Y = 100 : 5 : 5$ , we obtain:  $\overline{P} = 30$  units,  $C_{cr} = 0.15$  for any degree of dilution, because the molar relationship of components was kept constant by the authors.

It follows from the estimate  $\overline{P} = 30$  units that topological structure of the synthesized copolymer differs dramatically from standard topology of typical HBP, synthesized by methods of stepwise polymerization, the features of which are well studied.

Further, these features turned out to be required in the application aspect. In typical HBP, interjunction and terminal chains are quite short; their length usually does not exceed 10–20 interatomic bonds. With  $\overline{P} = 30$  units and molar relationship  $M_1/M_2 = 100 : 5$ , there are only  $\approx 1.5$  units of branching monomer  $M_2$  per 30 units, instead of 3, which are necessary to provide a branching coefficient equal to 2. Hence, a rather weakly branched polymer is formed with very long interjunction and end chains. Judging by other data [38], in which the dependence of HBP properties upon the lengths of interjunction and end chains was studied in detail, the longer are the chains, the more weakly are the distinctive features of HBP manifested, and the closer are these features to those inherent to linear analogues. It should be emphasized here that the authors of [14, 17] give convincing proof of hyper-branching of synthesized products only in one case (see Table 7.4), for which incomplete data on synthesis conditions are provided. It follows from the estimate of  $C_{cr} = 15\%$  that high copolymer yields (which are significantly higher than  $C_{cr}$ ) obtained by the authors represent a consequence of large contribution of cyclization, which shifts the value of  $C_{cr}$  in the direction of high conversions.

Thus, additional information obtained through comparison of analyzed experimental data with relevant theoretical relationship gives grounds to suppose that HBP synthesized by the proposed method are characterized by nonstandard topology (elongated chains plus high contribution of cyclized fragments).

### 7.2.2.2 Synthesis of HBP Via Copolymerization of Methyl(meth)acrylate and Various Branching Comonomers in the Presence of Chain Transfer Agents of Different Types [15, 16, 18]

HBP were synthesized from a mixture with molar relationship of components  $M_1 : M_2 : Y = 100 : 1.7 : 1$  in 40% toluene at 80°C for  $M_1 =$  methyl(meth)acrylate,  $M_2 =$  tri(propylene glycol) di(acrylate),  $Y =$  dodecylmerkaptan, after which HBP properties were studied. For comparison, a conventional chain transfer agent, i.e., dodecylmerkaptan, was substituted with chain transfer catalyst cobalt (II) bis(boron difluoro dimethylglyoxime) (abbreviation, CoBF), the concentration of which varied, and HBP were synthesized under the same conditions with subsequent expansion into properties. AIBN,  $3 \times 10^{-2}$  mol/l (at 80°C  $k_i = 8 \times 10^{-5} \text{ s}^{-1}$ ,  $W_i = 2.4 \times 10^{-6} \text{ mol} \cdot \text{l}^{-1} \cdot \text{s}^{-1}$ ) was selected as initiator I.

Kinetics of copolymerization is described by linear dependence until conversion  $C = 50\%$  ( $t = 1$  h), and then it is described by a convex curve with continuously decreasing slope (with decreasing rate) up to  $C \geq 85\%$  ( $t = 6$  h).

The composition of copolymer (i.e., the number of  $M_2$  units) as well as its glass-transition temperature  $T_g$  (Table 7.5), was also determined for different stages of conversion.

MWD of copolymers listed in Table 7.5 was measured using the GPC-3 method, and it was found that unimodal and quite narrow MWD (molecular weights stay within  $10^{3.5} - 10^{4.5}$ , with maximum at  $10^{4.2}$ ) broadens and becomes bimodal (with maxima at  $10^{4.4}$  and  $10^{4.8}$ ) as  $t$  increases. This copolymer was fractioned, and properties of its individual fractions with different value of  $M_w$  were studied (fractions I, II, III, IV, V, and VI, respectively) (Table 7.6).

Studying copolymer properties (described above) gives rather convincing evidence of hyper-branched character of copolymers. First, values of  $\alpha$  and  $g'$  are considerably lower than those for nonbranched analogues (linear PMMA); second, the growth of molecular weights of macromolecules during copolymerization is another argument; and third, growth of  $M_2$  units number per macromolecule (which is equivalent to an increase in the degree of branching) because it is just  $M_2$  that perform the function of branching agents represents one more argument.

**Table 7.5** Conversion ( $C$ , %), composition of copolymer, and its properties at different stages of copolymerization

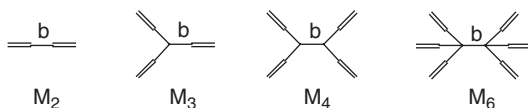
$t$ , h	$C$ , %	$M_2$ , % (by weight)	$T_g$ , °C	$\alpha$
0.5	24.2	5.2	96.8	0.60
1.0	50.6	5.5	77.4	0.55
2.0	69.5	5.0	80.6	0.50
4.0	81.1	5.3	96.9	0.47
6.0	87.0	5.4	95.6	0.45

*Note.* Content of  $M_2$  units was determined using the NMR method,  $T_g$  using the scanning calorimetry method, and  $\alpha$  using the GPC-3 method. For control specimen of PMMA (nonbranched analogue),  $\alpha = 0.7$ ;  $T_g = 100^\circ\text{C}$ .

**Table 7.6** Properties of individual fractions of copolymer isolated at deep stages of copolymerization (at  $C = 87\%$ )

Fraction	$M_w \times 10^{-3}$	Content of $M_2$ units		$\alpha$	$g'$
		Percent (%) (by weight)	Number of $M_2$ units in macromolecule		
I	7	4.5	$\approx 2$	0.70	0.98
II	25	4.7	$\approx 6$	0.68	0.90
III	75	5.7	15	0.55	0.75
IV	250	6.0	50	0.53	0.55
V	450	6.0	90	0.37	0.50
VI	1100	—	—	0.33	0.35

Analysis of very important factors has been presented [15, 16]; namely, functionality ( $m$ ) of branching monomer ( $M_m$ ), and length and flexibility of  $M_m$  molecules between terminal functional groups (double bonds). This fragment is denoted with letter “b” in the schematic presentation of  $M_m$  molecules. The value of  $m$  was varied in the following series of di-, tri-, tetra-, and hexa-acrylates: tri(propylene glycol) di(acrylate) ( $M_2$ ), tri(methylol propane) tri(acrylate) ( $M_3$ ), penta(eritrit) tetra(acrylate) ( $M_4$ ), and di(pentaeritrit) hexa(acrylate) ( $M_6$ ), schematically presented as follows:



Five polyethylene glycol methacrylates characterized by different lengths of poly(ethylene glycol) chain, i.e., mono-, di-, tri-, and tetra(ethylene glycol) di(methacrylate) and di(methylacrylate) on the basis of poly(ethylene glycol) PEG-400 with the number of polyoxyethylene units significantly exceeding 4, were selected as a series of objects with variable fragment “b.”

Two more objects were studied to determine the role of chemical nature of double bond in  $M_2$ : ethylene glycol di(acrylate) and divinyl benzene with very short and rigid fragments “b.” In combination with the first member of the previous series, i.e., ethylene glycol di(methacrylate), a rather representative set is obtained consisting of three objects with variable chemical nature of double bond in molecules that are quite of the same type in terms of “b.”

MMA was selected as the main (nonbranching) comonomer, and copolymerization was carried out under one and the same conditions at  $80^\circ\text{C}$  in toluene solution (with double or triple dilution) in the presence of AIBN (I) as an initiator and dodecylmercaptan (Y) as a chain transfer agent.

Results related to the influence of functionality ( $m$ ) of  $M_m$  molecules are listed in Table 7.7.

It follows from Table 7.7 that molecular weight of copolymers grows in the general case with increasing concentration of acrylate groups [Acr] (potential centers of

**Table 7.7** Influence of functionality  $m$  of branching comonomer  $M_m$  upon properties of copolymers MMA- $M_m$ 

No.	$m$	[ $M_m$ ], % (mol)	[Acr], % (mol)	$C(M_1)$ , %	GPC-1			GPC-3			$\alpha$	$T_g, ^\circ\text{C}$
					$M_n \times 10^{-3}$	$M_w \times 10^{-3}$	$M_w/M_n$	$M_n \times 10^{-3}$	$M_w \times 10^{-3}$	$M_w/M_n$		
1	2	0.50	1.0	88.0	6.74	18.0	2.67	11.7	21.8	1.86	0.56	80.5
2	3	0.50	1.5	88.0	7.18	26.5	3.89	11.2	28.3	2.53	0.48	104.3
3	4	0.50	2.0	88.0	9.07	65.5	7.22	26.3	142.5	5.42	0.40	109.4
4	6	0.50	3.0	82.0	9.48	200	21.1	6.02	684	11.3	0.26	111.8
5	3	0.33	1.0	85.0	7.17	22.1	3.08	11.7	28.2	2.41	0.50	73.8
6	4	0.25	1.0	88.0	7.12	21.7	3.04	13.8	32.1	2.33	0.51	78.9
7	6	0.17	1.0	86.0	7.27	22.1	3.05	8.67	35.4	4.08	0.36	81.6
8	2	1.00	2.0	91.0	8.38	27.3	3.26	13.8	32.8	2.38	0.50	75.4
9	2	1.50	3.0	89.0	8.40	46.0	5.48	12.7	68.4	5.39	0.44	71.9
10	2	2.00	4.0	89.0	9.53	103	10.84	6.07	92.4	15.2	0.40	83.5

Note 1. Copolymers were synthesized at  $80^\circ\text{C}$  in toluene (dilution  $\approx 2$  times) in the presence of  $3 \times 10^{-2}$  mol/l I and  $5 \times 10^{-2}$  mol/l Y at  $[M_1] = 5$  mol/l.

Note 2. [Acr], concentration of acrylate double bonds;  $C(M_1)$ , conversion of monomer  $M_1$ .

Note 3. Parameter of Mark-Houwink equation  $\alpha$  for nonbranched analogue of PMMA is equal to 0.72.

Note 4. Value of  $T_g$  was found using the method of scanning calorimetry.

branching) in the initial copolymerization system. With a fixed value of [Acr] (series of objects 1, 5–7; 3, 8; 4, 9), it is possible to evaluate the role of functionality: at  $[Acr] = 1\%$  (mol) the increase of  $m$  from 2 to 6 (objects 1, 5–7) leads to the increase of  $M_w$  (GPC-3) from  $22 \times 10^3$  to  $35 \times 10^3$ ; at  $[Acr] = 2\%$  (mol) (objects 3 and 8), the influence of  $m$  is still stronger:  $M_w$  (GPC-3) grows from  $33 \times 10^3$  to  $142 \times 10^3$  as  $m$  increases from 2 to 4; at  $[Acr] = 3\%$  (mol) such growth takes place from  $68 \times 10^3$  to  $684 \times 10^3$  (!) as  $m$  increases from 2 to 6. In this case, the correlation between  $M_n$  and  $m$  is indistinct, which is especially true for values  $M_n$  for objects 4, 7, and 10 (they are characterized by very low values, which, unfortunately, is not commented upon by the authors at all).

The value of  $T_g$  either weakly depends upon [Acr] (at low  $m = 2$ , objects 1, 9–10), or (at  $m > 2$ ) grows noticeably as [Acr] increases (objects 5 and 2; 6 and 3; 7 and 4). At fixed [Acr] (objects 1, 5–7; 3 and 8; 4 and 9)  $T_g$  either weakly depends upon  $m$  (at small [Acr] = 1% mol, objects 1, 5–7), or (at [Acr] > 1% mol, objects 3 and 8; 4 and 9) grows with increasing  $m$ .

The most important parameter  $\alpha$ , the degree of declining of which as compared to  $\alpha = 0.72$  (for nonbranched analogue of PMMA) characterizes hyper-branching (as it is now believed by all researchers working in the field of HBP), has the best numeric value  $\alpha = 0.26$  for the case of object 4 (which has high values of parameters  $m$  and [A]: 6 and 3). At fixed  $m$  ( $m = 2$ , objects 1, 8–10;  $m = 3$ , objects 2, 5;  $m = 4$ , objects 3 and 6;  $m = 6$ , objects 4, 7) improvement is observed (decline of  $\alpha$  with increasing [A]) in all cases. At fixed [Acr] (see corresponding sets of objects in Table 7.7), parameter  $\alpha$  goes down (hyper-branching is more clearly expressed) as the functionality of branching comonomers  $M_m$  enhances. Quantitative depen-



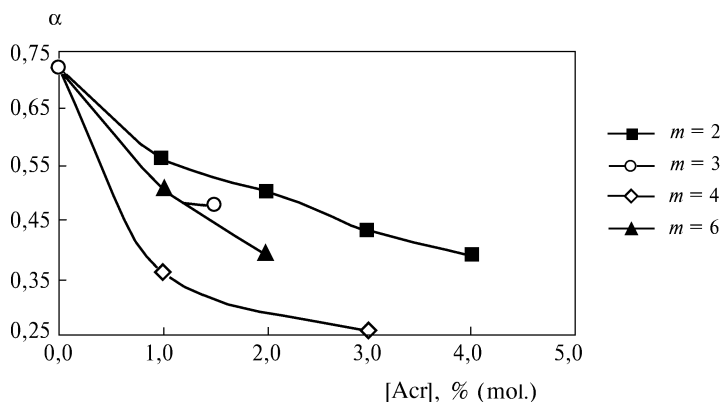


**Fig. 7.1** Influence of functionality  $m$  of branching comonomers  $M_m$  upon the type of dependence  $\alpha = f([Acr])$

dence in coordinates “ $\alpha - [Acr]$ ” for each of the fixed values of  $m$  obtained by the authors directly based on the readings of viscosimetric detector of GPC-3 device is presented in Fig. 7.1.

The extremely low degree of branching of the above-described copolymers and direct positive test on hyper-branching according to the Hovink parameter plus also a number of indirect positive tests give grounds to search for additional hidden branching factors efficiently functioning during copolymerization under given conditions. One of such factors could be the local mechanical and chemical destruction of interjunction chains of macromolecules in micro-areas with very sparse network structure under the action of swelling. Such a destruction mechanism implying the formation of free radicals was discovered more than 50 years ago as a phenomenon of  $\omega$ -polymerization [36 (p. 181); 52–54] and until nowadays is used for the synthesis of the so-called  $\omega$ -polymers having practical significance [e.g.,  $\omega$ -poly(vinyl pyrrolidone), used in wine making]. This version is described in greater detail in the next section.

Let us now consider data on variation of length and flexibility of “b” block and the chemical nature of double bonds in  $M_2$  molecules during copolymerization with methylmethacrylate  $M_1$  [18]. A systematic set of objects of study was indicated above. Let us designate dimethacrylates with 1, 2, 3, and 4 and  $p$ -ethylene glycol units in chain “b” as  $M_{2-1}$ ,  $M_{2-2}$ ,  $M_{2-3}$ ,  $M_{2-4}$ , and  $M_{2-p}$ , respectively (here,  $p > 4$  corresponds to the chain length in polyethylene glycol PEG-400, on the basis of which  $M_{2-p}$  was synthesized). Let us designate ethylene glycol di(acrylate) as  $M_{2-1A}$  and divinyl benzene as  $M_{2-B}$ . The series  $M_{2-1} \dots M_{2-p}$  is intended for determining the role of length and flexibility of “b,” whereas series  $M_{2-1}$ ,  $M_{2-1A}$ ,  $M_{2-B}$  is intended for determining the influence of the chemical nature of double bonds.

Results of exploring the first series of objects are presented in Table 7.8. MWD characteristics were determined using the GPC-2 method (two detectors were employed: a refractometric one and a multi-angle light-scattering detector with laser source of 680 nm). Sulfur-containing fragments (S) of chain transfer agent

**Table 7.8** Influence of length of oligomer chains of  $M_2$  molecules upon the copolymerization process with MMA and properties of copolymers

Sample	$M_2$	Yield, %	[S], %	$M_n \times 10^{-3}$	$M_w \times 10^{-3}$	$M_w/M_n$	Solubility (0.5 g/cm <sup>3</sup> )
PMMA	0	–	–	52.3	115	2.20	Soluble in all solvents
PMMA-1	0	70	–	27.9	37.8	1.35	Soluble in all solvents
PMMA-2	0	70	–	11.2	17.7	1.58	Soluble in all solvents
HBP-1	$M_2$ -1	67	2.3	21.9	58.2	2.65	Soluble in all solvents
HBP-2	$M_2$ -2	62	2.4	6.57	18.2	2.76	Insoluble in DMSO and DCM
HBP-3	$M_2$ -3	65	2.5	5.87	20.2	3.44	Insoluble in DMSO
HBP-4	$M_2$ -4	61	2.2	6.60	98.4	10.4	Insoluble in DMSO
HBP-p	$M_2$ -p	62	2.6	–	–	–	Insoluble in all solvents

Note. PMMA, commercial sample, Aldrich Chemical. PMMA-1 was synthesized under the same conditions as HBP, without adding  $M_2$  and  $Y$ ; PMMA-2 was synthesized under the same conditions as HBP, with addition of  $[Y] = 2 \times 10^{-2}$  mol/l

were identified by means of elemental analysis. Toluene, tetrahydrofuran (THF),  $CHCl_3$ , dichloromethane (DCM), and dimethyl sulfoxide (DMSO) were used as testing solvents. Conditions of copolymerization were as follows:  $T = 80^\circ C$  ( $t = 5$  h), in toluene solution (fourfold dilution), molar relationship of components  $M_1 : M_2 : Y = 100 : 12 : 12$ ,  $[I] = 2 \times 10^{-2}$  mol/l ( $W_i = 1.6 \times 10^{-6}$  mol $\cdot$ l $^{-1}$  $\cdot$ s $^{-1}$ ).

Reference samples of nonbranched PMMA will be first used for comparing their  $M_n$  with theoretical value of  $\bar{P}$  (with the exception of the first commercial sample, for which the polymerization conditions are unknown):

$$\bar{P} = \frac{k_{pr}[M]}{\sqrt{W_i k_{tr} + k_{tr}[Y]}}$$

For PMMA-1  $[M] = 2$  mol/l,  $k_{pr} = 5001/(\text{mol}\cdot\text{s})$ ,  $[Y] = 0$ ,  $W_i = 1.6 \cdot 10^{-6}$  mol/(l $\cdot$ s),  $k_{tr} = 10^7$  l/(mol $\cdot$ s) and, hence,  $\bar{P} = 250$  units; in terms of  $M_n$  we obtain  $M_n = 2.5 \times 10^4$  (agrees very well with the experimental value of  $M_n = 2.8 \times 10^4$ ). For PMMA-2  $[Y] = 2$  mol/l,  $k_{tr} = 3001/(\text{mol}\cdot\text{s})$  and, hence,  $\bar{P} = 100$  or  $M_n = 10^4$  (excellent agreement with experimental  $M_n = 1.12 \times 10^4$ ). Thus, this polymerization system operates in full agreement with the theory.

For branched sample of HBP-1, theoretical length of primary polymeric chain  $\bar{P} = 13$  ( $[Y] = 0.25$  mol/l), the value of  $M_n$  for primary polymeric chain is  $\approx 1300$ . Comparing it with  $M_n = 2.2 \times 10^4$  for HBP-1 from Table 7.8, we obtain that synthesized macromolecule includes  $\approx 17$  primary chains, each of which contains 1.6  $M_2$  units that represent centers of branching (we assume that copolymer composition is equal to the composition of initial mixture  $M_1 : M_2$  because due to identity of methacrylic double bonds in  $M_1$  and  $M_2$ , the values of both copolymerization constants,  $r_1$  and  $r_2$ , are apparently close to 1). Thus, the HBP-1 macromolecule should contain  $\approx 28$  branchings.

From the standpoint of gel formation theory ( $C_{cr} = \frac{0.5k_{tr}[Y]}{k_{pr}F_{22}(0)} = 15\%$ ), the discrepancy between calculated value of  $C_{cr} = 15\%$  and experimental value  $C_{cr} \geq 67\%$

is indicative of the high degree of cyclization of HBP-1 macromolecules. Also, these macromolecules are soluble in solvents that were selected as the testing ones (Table 7.8).

The composition of macromolecules of the entire HBP series was studied using the methods of elemental analysis and NMR (400 MHz). No quantitative data are given, but it is asserted on the qualitative level that all macromolecules consist of the same atomic groups (including centers of branching) and that all of them contain pendent methacrylic groups, S atoms, and fragments of  $C_{12}H_{25}$ , chain transfer agent dodecyl merkaptan. Generally speaking, there are no qualitative differences. The version presented in the next sections clarifies the paradoxical results given in Table 7.8 to a certain extent.

Now let us address the results of studies of HBP synthesis process in the presence of branching comonomers  $M_2$  that differ by the nature of double bonds. The objects of comparison were di(methacrylates) ( $M_2-1$ ), di(acrylates) ( $M_2-1A$ ), and divinyl benzene ( $M_2-B$ ). When they are copolymerized with methyl methacrylate ( $M_1$ ), they differ by a set of copolymerization constants  $r_1$  and  $r_2$ :  $r_1 = r_2 = 1$  for  $M_2-1$ ;  $r_1 = 2$ ,  $r_2 = 0.5$  for  $M_2-1A$ ; and  $r_1 = r_2 = 0.5$  for  $M_2-B$ . Copolymerization conditions are the same:  $80^\circ C$  in toluene solution (fourfold dilution); initiator, AIBN,  $[I] = 2 \times 10^{-2} \text{ mol/l}$  ( $W_i = 1.6 \times 10^{-6} \text{ mol} \cdot \text{l}^{-1} \cdot \text{s}^{-1}$ ); Y, dodecylmerkaptan ( $k_{tr}$ ,  $1 \cdot \text{mol}^{-1} \cdot \text{s}^{-1}$ :  $\approx 300$  for  $M_2-1$ ,  $\approx 3500$  for  $M_2-1A$ , and  $\approx 2250$  for  $M_2-B$ ), polymerization time  $t = 5 \text{ h}$  ( $\approx 2$  period of initiator half-life). Unfortunately, patterns of research into each of the three  $M_2$  were somewhat different and therefore the comparison seems to be possible only as applied to a restricted interval of compositions of initial mixtures. Main results (suitable for comparison) are presented in Table 7.9. Comparison of compositions of initial mixtures  $M_1 : M_2 : Y$  (that ensured absence of gel formation during copolymerization) is given in Table 7.8.

It follows from the data listed in Tables 7.9, 7.10, and 7.11 that at a certain relationship of initial components no gel formation takes place in the copolymerization system. Also, this relationship varies depending on the nature of the double bond in  $M_2$ . In all cases the increase of  $M_2$  content should necessarily be accompanied by a respective increase in Y content in the initial mixture. As a rule, with equimolar ratio of  $M_2$  to Y, gel formation is not observed. Obviously of highest interest are the systems with a high content of  $M_2$ , because it is just in this case that highly branched copolymers are formed. According to the data of Table 7.11, the highest content of  $M_2$  is observed in mixtures  $M_1 : M_2 : Y = 100 : 15 : Z$  where Z is the Y content required for suppression of gel formation during copolymerization. In this case, the value of Z will be one of the characteristic parameters of influence exerted by the chemical nature of the double bond in  $M_2$ .

For  $M_2-1$ ,  $Z = 12$  (see Table 7.9) with copolymer yield amounting to 86%; for  $M_2-1A$ , the value of  $Z = 8$  is significantly lower (see Table 7.10) than for  $M_2-1$ , while the yield is slightly lower, 72%. For  $M_2-B$ , it is difficult to accurately estimate Z using data from Table 7.11; it is only clear that with  $Z = 15$  no gel formation is observed, but the yield in this case is significantly lower (49%) than in the first two cases. Judging by the yield, it makes sense to prefer  $M_2-1$  as a more significant (from the practice standpoint) branching comonomer. However, obviously this fac-

**Table 7.9** Copolymerization of MMA (M<sub>1</sub>) and ethylene glycol dimethacrylate (M<sub>2</sub>) at 80°C

Molar relationship M <sub>1</sub> /M <sub>2</sub> /Y	Yield, %	Consistency of final copolymerization system	Solubility (0.5 g/cm <sup>3</sup> )	Sulfur content, %	
				Calculated	Found
100/15/15	61	lvl	Soluble	3.1	2.4
100/15/14	88	lvl	Soluble	2.9	2.0
100/15/13	83	lvl	Soluble	2.7	2.0
100/15/12	86	lvl	Soluble	2.5	1.9
100/15/11	73	lvl + g	Soluble	2.4	1.7
100/15/10	83	vl + g	Soluble	2.2	1.4
100/15/9	80	g	Insoluble	2.0	1.6
100/15/8	88	g	Insoluble	1.8	1.9
100/15/7	77	g	Insoluble	1.6	1.8
100/15/6	86	g	Insoluble	1.4	1.7
100/15/5	74	g	Insoluble	1.2	1.2
100/15/4	88	g	Insoluble	1.0	0.5

*Note.* Toluene solution (fourfold dilution) in the presence of  $2 \times 10^{-2}$  mol/l AIBN ( $W_i = 1.6 \times 10^{-6}$  mol · l<sup>-1</sup> · s<sup>-1</sup>) and different concentrations of dodecylmerkaptan (Y). g, gel; lvl, low viscous liquid; vl, viscous liquid. Testing solvents: toluene, tetrahydrofuran, chloroform, dichlor-methane, and dimethyl-sulfoxide (DMSO). All copolymers are insoluble in DMSO. Copolymerization time,  $t = 5$  h.

**Table 7.10** Copolymerization of MMA (M<sub>1</sub>) and ethylene glycol di(acrylate) (M<sub>2</sub>) at 80°C

Molar relationship M <sub>1</sub> /M <sub>2</sub> /Y	Yield,%	Consistency of final copolymerization system	Solubility (0.5 g/cm <sup>3</sup> )	$M_n \times 10^{-3}$	$M_w \times 10^{-3}$	$M_w/M_n$	Content of Y fragments, %	
							Calculated	Found
100/15/15	60	vl	Soluble	5.28	15.5	2.94	29.0	17.0
100/15/14	62	vl	Soluble	6.14	21.9	3.57	27.0	18.5
100/15/13	61	vl	Soluble	7.84	44.5	5.68	25.0	14.0
100/15/12	71	vl	Soluble	7.14	59.3	8.30	22.8	17.0
100/15/11	68	vl	Soluble	8.14	87.4	10.7	21.0	6.8
100/15/10	84	vl	Soluble	5.03	159.7	31.7	19.7	16.7
100/15/9	78	vl	Soluble	6.83	206.3	30.2	17.1	13.8
100/15/8	72	vl	Soluble	6.02	133.8	22.2	15.6	11.6
100/15/7	70	g	Insoluble	—	—	—	13.6	8.5
100/15/6	74	vl	Soluble	15.8	377.4	238.2	12.7	5.8
100/15/5	77	g	Insoluble	—	—	—	9.4	9.8

*Note.* The same conditions as in Table 7.9. Content of Y fragments was determined using the elemental analysis, % S.

tor is not important enough, because one should also take other important factors into account, including branching degree, contribution of cyclization, and number of terminal chains (including end double bonds). For this purpose, it is necessary to conduct comparative study of all three options of copolymers according to the pattern of the same type.

The most convincing quantitative data on branching degree were obtained for M-1A (Table 7.12).

**Table 7.11** Copolymerization of MMA (M<sub>1</sub>) and divinyl benzene (M<sub>2</sub>) at 80°C

Molar relationship, M <sub>1</sub> /M <sub>2</sub> /Y	Yield, %	Consistency of final copolymerization system	Solubility (0.5 g/cm <sup>3</sup> )	M <sub>n</sub> × 10 <sup>-3</sup>	M <sub>w</sub> × 10 <sup>-3</sup>	M <sub>w</sub> /M <sub>n</sub>	Content of fragments, %			
							M <sub>2</sub>		Y	
							Calculated	Found	Calculated	Found
100/1/0	68	g	Insoluble	—	—	—	1	4.6	0	0
100/1/1	79	vl	Soluble	55.5	62.1	11.2	1	6.3	1	2.3
100/2/2	77	lf	Soluble	7.39	97.7	13.2	2	3.5	2	2.8
100/5/5	69	vl	Soluble	10.2	130.2	12.8	5	6.4	5	5.8
100/8/8	61	vl	Soluble	9.18	111.1	12.1	8	9.5	8	8.6
100/12/12	51	vl	Soluble	12.7	102.7	8.09	12	13.7	12	12.7
100/15/15	49	vl	Soluble	13.0	84.7	6.50	15	16.5	15	13.2
100/5/3	66	g	Insoluble	—	—	—	5	8.0	3	3.7

*Note.* The same as in Table 7.9. Toluene solution (twofold dilution) in the presence of  $4 \times 10^{-2}$  mol/l AIBN ( $W_i = 3.2 \times 10^{-6}$  mol  $\cdot$  l<sup>-1</sup>  $\cdot$  s<sup>-1</sup>) and different concentrations of dodecylmercaptan (Y). Divinyl benzene is a mixture of 55% *m*-DVB, 25% *n*-DVB, and  $\approx 20\%$  *m*- and *n*-ethyl styrene. Content of Y fragments was determined by elemental analysis, % S. Content of M<sub>1</sub> was determined under the condition [Y] = 0. Content of M<sub>2</sub> fragments was determined based on difference ( $\pm 2\%$ ).

Based on the above-analyzed data, the authors draw the following conclusions from the comparison of di(methacrylates)  $M_2$ -1, di(acrylates)  $M_2$ -1A, and divinyl benzene  $M_2$ -B as branching comonomers [of course, as applied to the compositions with the highest concentration of  $M_2$  ( $M_1 : M_2 : Y = 100 : 15 : Z$ )]. In the presence of  $M$ -1A, the lowest tendency of copolymerization system to gel formation is observed, which allows to have the highest concentration of branching monomer (mixture  $M_1 : M_2 : Y = 100 : 15 : 8$ ), while for two other branching comonomers it is necessary to have  $Z = 15$ .

Further, for  $M_2$ -1A we obtain the highest content of pendent double bonds in the final copolymer (16% mol of total content of  $M_2$  fragments in macromolecules, while in the case with  $M_2$ -1, only 4% was obtained, and the result obtained for  $M_2$ -B was  $\approx 0\%$ ).

Molecular weight characteristics of respective polymers also differ rather strongly for all three monomers (Table 7.13).

It follows from Table 7.13 that for dimethacrylates MWD is the worst, and it is so broad that the copolymer in this case should represent a very wide set of molecules

**Table 7.12** Content of branchings, chain transfer agent fragments, and end double bonds in copolymers of MMA and ethylene glycol diacrylate

Molar relationship $M_1/M_2/Y$ in an initial mixture	Molar relationship $M_1/Y$ in a copolymer	Molar relationship $M_1/M_2$ in a copolymer	Molar relationship $M_1/M_2^*$ in a copolymer	Content of $M_2^-$ to $M_2$ in a copolymer, %	$N_c$
100/15/15	100/10.8	100/13.0	100/10.9	16.0	1.01
100/15/14	100/11.5	100/14.8	100/10.6	28.5	0.92
100/15/13	100/10.0	100/13.0	100/9.0	30.7	0.90
100/15/12	100/9.9	100/12.9	100/9.7	25.0	0.98
100/15/11	100/9.8	100/13.6	100/10.1	25.6	1.03
100/15/10	100/10.6	100/12.1	100/8.9	26.6	0.84
100/15/9	100/9.5	100/12.7	100/10.6	16.6	1.12
100/15/8	100/8.7	100/12.8	100/8.4	35.0	0.97
100/15/6	100/6.3	100/12.4	100/7.9	36.6	1.25

*Note.*  $M_2^*$  are  $M_2$  units that have reacted by both their double bonds (of branching);  $M_2^-$  are  $M_2$  units that have reacted only by their one double bond (pendent double bonds).  $N_c = [M_2^*]/[Y]$ ; in terms of physical meaning this is the number of branchings per one primary polymeric chain (each chain contains one Y fragment at its end).

**Table 7.13** Comparison of MWD parameters of polymers for  $M_2$  characterized by different chemical nature of double bond

$M_2$	$M_n$	$M_w$	$M_w/M_n$
Divinyl benzene $M_2$ -B	13,020	84,750	6.5
Dimethacrylates $M_2$ -1	4,159	383,600	92.2
Diacrylates $M_2$ -1A	5,280	15,550	2.9

*Note.* Initial mixture  $M_1 : M_2 : Y = 100 : 15 : 15$ .

having different molecular weights. The best MWD is observed for diacrylates, but the value of  $M_n$  is higher for that in the case of divinyl benzene. Besides, the latter case is also characterized by the highest value of macromolecule compactness (defined as the highest molecular weight for fixed hydrodynamic volume of macromolecules). Therefore, the authors have grounds to believe that the highest degree of macromolecules branching is achieved in the case when divinyl benzene is used.

It is obvious that attributes such as “the best” and “the worst” are fairly conventional in this case. The main significance of obtained data consists in the fact that they are quite suitable for use as base data for targeted synthesis of HBP with predictable properties (HBP design). The practical application of HBP will depend on their function; in some cases, the MWD width would be a decisive property, while in other cases, the presence of reacting double bonds would be most important, and so forth.

In conclusion, the authors would like to emphasize that the cycle of systematic studies analyzed in Sect. 7.2.2 and related to HBP synthesis using the method of radical copolymerization in the presence of chain transfer agents represents a completed initial stage enabling us to substantiate the perspectives of further development of this direction in terms of both scientific and technological aspect.

### ***7.2.3 Regulation of Chain Length Through the Use of Intrachain Reactions of Chain Carrier Radicals***

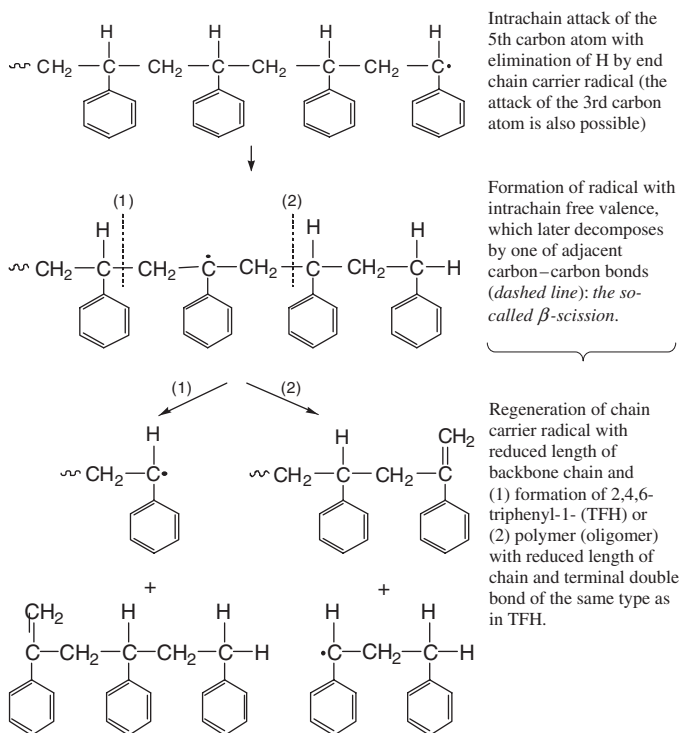
It has been established recently that in addition to known chain transfer reactions, other nontrivial radical reactions leading to restriction of polymeric chains could be used in radical polymerization processes.

For the first time, features indicating the existence of such reactions were identified during exploration into thermal polymerization (i.e., polymerization in the absence of initiators) of styrene. It appeared that a mathematical model of polymerization process developed [55, 56] on the basis of generalization of a large body of kinetic data and data of MWD measurements at high temperature (200–230°C) gives increased values of molecular weights of polymers. Later, a new body of experimental data was obtained for higher temperature: for 300°C [57]. An attempt to adjust the mathematical model with the use of these data led to a conclusion that secondary reactions of polymeric chain destruction proceed concurrently with polymerization, after which some researchers made an attempt to identify these reactions [58].

However, only recently have scientists managed to determine the detailed mechanism of these reactions (it was used later for HBP synthesis [59]) via employment of a complex methodological set of tools, which included GPC,  $^{13}\text{C}$ -NMR (300 MHz), and the latest version of mass spectroscopy (called matrix-assisted laser desorption/ionization time-of-flight mass spectrometry). This approach enabled researchers to measure MWD of products in the course of styrene polymerization at 260–343°C and identify both terminal groups of oligomeric chains. Polymeriza-

tion was carried out in flow reactor with regulated residence time  $\tau = 5\text{--}90$  min of reagents in the reaction zone. Products for testing were selected in two series: at  $T = \text{const} = 260^\circ\text{C}$ , but for different values of  $\tau = 5/15$  min and at  $\tau = \text{const} = 15$  min, but for different values of  $T = 260\text{--}343^\circ\text{C}$ .

After interpretation of chemical structure of all polymerization products (including identification of terminal groups of oligostyrenes), it was shown that in the case of high-temperature polymerization of styrene the main mechanism for restriction (the authors used the term “backbiting”) of propagating polymeric chain length is as follows:



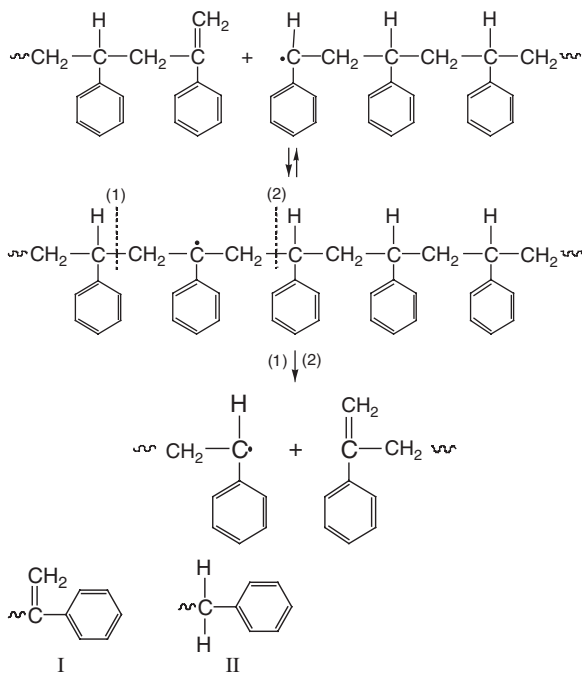
**Scheme 7.1** Main mechanism of propagating PS chain length in the case of high-temperature polymerization [64]

Further, it appeared [60–63] that formed polymeric chains with terminal double bonds are capable of reacting with the chain carrier radical according to the mechanism of the so-called addition-fragmentation: Scheme 7.1

It was found [64] that all polymers (oligomers) with different values of molecular weight that are formed under different conditions of polymerization have an identical ratio of terminal groups of different types: predominant concentration of chains with group I (Scheme 7.2) on one end and II (Scheme 7.2) on the other end (the percentage of such chains is  $\approx 80\%$  at  $316^\circ\text{C}$  and  $\approx 90\%$  at  $288^\circ\text{C}$ ), while other chains have identical groups on both ends (either double bonds or 1-phenylvinyl



groups); the concentrations of such chains are approximately equal and in total their percentage is  $\approx 20\%$  (at  $316^\circ\text{C}$ ) and  $\approx 10\%$  (at  $288^\circ\text{C}$ ).



**Scheme 7.2** Mechanism of addition-fragmentation reactions PS chain with end double bond in the case of high-temperature polymerization [60–64]

The above-indicated data served as the basis for developing a HBP synthesis method via high-temperature copolymerization of styrene and divinyl benzene (DVB) because researchers managed to reduce the average length of oligo-styrene chains to several units by appropriate regulation of temperature and residence time in the reactor [59, 65–67]. HBP synthesis was carried out in the same flow reactor. By varying the values of  $T$ ,  $\tau$ , concentration ( $[M_2]$ , % by weight) of DVB (commercial mixture, 80% of isomers  $n$ -DVB and  $m$ -DVB with 20% styrene) and concentration of solvent (0/15% by weight of aromatic hydrocarbons with boiling temperature  $100^\circ\text{C}$ ), researchers have been selecting the optimal conditions of synthesis. Selection of  $[M_2]$  was carried out based on dependence of molecular weight of polymer  $M_w$  upon  $[M_2]$  with all other factors staying constant (unfortunately, values of  $M_w$  were determined using only GPC-1 method with refractometric detector and, therefore, obtained data are not strictly quantitative). Approaching to critical conversion  $C_{cr}$  (gel point) was manifested as a sharp increase in the rate of  $M_w$  growth with increasing  $[M_2]$ . The change of sign of the first derivative of function  $M_w = f([M_2])$  (“plus” for “minus”) at a certain concentration of branching monomer was observed in special experiments on GPC testing of sol fractions. This concentration (equal to 0.106% by weight of DVB at  $316^\circ\text{C}$ ,  $\tau = 15$  min, and 15% by weight of solvent) was identified with critical conversion  $C_{cr}$  (gel point).

One publication [59] gives systematic data on the influence of copolymerization conditions controlling the value of  $M_w$  for copolymers being formed in the form of several series of curves  $M_w = f([M_2])$ . Obviously, these data can serve as the base data both for optimization of HBP synthesis process and for forecasting synthesis results for prespecified conditions of the copolymerization process. The physical meaning of base data presented as dependences of  $M_w$  on  $[M_2]$  consists in the fact that movement by the abscissa to the right means an increase in the number of units of branching comonomer in HBP macromolecules and, hence, rise of branching degree. Therefore, the best option for the synthesis of HBP would be the one with which curve  $M_w = f([M_2])$  reaches its maximum in the region of highest  $[M_2]$ ; it can be seen that “getting closer” to the gel point recorded by sharp increase of curve slope represents backbiting. It is obvious that this physical meaning is inherent to the motion by abscissa only in the case when conversion is close to 100% (in the opposite case, growth of  $[M_2]$  in the initial mixture does not necessarily lead to respective increase in the number of branching comonomer units in the macromolecules). The authors [59] assert that conversion in all cases was more than 90%.

The same authors [59] showed that addition of only 15% solvent (aromatic hydrocarbons) provides a possibility to produce more highly branched copolymers in all cases. Increasing the temperature and residence time in a reactor gives a similar effect. The impact of temperature is quite understandable: if we assume that activation energy of limiting elementary stage of chain backbiting reaction  $E_a^\#$  is higher than chain propagation activation energy  $E_{pr}^\#$ , then the temperature should be acting exactly in this direction. And,  $E_a^\# > E_{pr}^\#$  follows from data on styrene polymerization at moderate temperature [36 (p. 113)] when no signs of special mechanism for chain backbiting are observed. The impact of time (observed in all cases) as a factor allowing raising the branching degree is not understandable if one assumes that conversion in all cases is actually higher than 90%. Indeed, if with  $\tau = 5$  min and  $[M_2] \leq 0.04$  gel formation already takes place, and in the next experiment with  $\tau = 30$  min, gel formation is not observed even with  $[M_2]$  that is two times higher than 0.04, then one has only to believe that with  $\tau = 5$  min, conversion is significantly lower than with  $\tau = 30$  min, because in the experiment with  $\tau = 30$  min (mixture with supercritical content of  $[M_2]$ ) gel would have been formed already during first minutes of mixture residence in the active zone of the reactor. In any case, regardless of interpretation, the data system presented [59] is extremely valuable and useful for practical application (plus it is quite universal enough and characterized by a high degree of generalization).

Measurements of copolymer MWD showed that it is broad for all degrees of branching and that it continuously broadens as the degree of branching goes up (i.e., as  $[M_2]$  increases). Taking the application of the GPC-1 method (without using a light-scattering detector) into account, which underestimates measurement results from reduced hydrodynamic volumes of branched macromolecules as compared to linear analogues having the same molecular weight, it should be anticipated that in reality MWD of synthesized copolymers would be even broader owing to the shift in the high molecular region.

The authors of [59] showed that the HBP synthesis method (developed by them) is highly economically efficient and quite competitive to be implemented on an industrial scale [65–67]. However, data on valuable and useful properties of HBP of this class are still missing (at least, they have not yet been published).

### 7.2.4 Regulation of Chain Length Through the Use of Molecular Oxygen as an Inhibitor

Oxygen is an extremely efficient acceptor of carbon-centered free radicals: numeric value of reaction (7.5) rate constant lies within  $k_1 = 10^6\text{--}10^7\text{1}/(\text{mol}\cdot\text{s})$  [68 (p. 39); 69 (p. 55)].



In the case of radical polymerization of vinyl monomers M, oxygen performs the function of inhibitor, the efficiency of which depends upon reactivity of double bond of a given monomer in relation to radical  $\text{MO}_2^\bullet$ . As a rule, numeric value of reaction (7.6) rate constant,  $k_2$ , is 10–100 times lower than that for reaction (7.7),  $k_{pr}$  [32; 69 (p. 59)].



Obviously, the lower is the value of relationship  $k_2/k_{pr}$ , the higher is the efficiency of  $\text{O}_2$  as inhibitor. When  $k_2/k_{pr} = 1$ , the inhibiting effect of  $\text{O}_2$  disappears completely. When  $k_2/k_{pr} < 1$ , the presence of oxygen in a polymerization system reduces the length of chain, and therefore it could be used for this purpose in the HBP synthesis processes instead of chain transfer agents (of the cobalt macroheterocyclic complexes type) and instead of all other methods for chain shortening described in Sects. 7.2 and 7.3.

Moreover, in the presence of oxygen in a polymerization system such processes arise that are qualified as radically initiated oxidation and oxidative polymerization of vinyl monomers. These processes have been studied in detail [68, 69]. They lead to the formation of various oxygen-containing functional groups in polymers being created: namely, peroxide groups, hydroperoxide groups, hydroxyl groups, carboxyl groups, and so forth. The presence of formed peroxides and hydroperoxides in a polymerization system makes it possible to reduce the concentration of conventionally used initiators.

Consequently, the use of the widely available and most inexpensive reagent—air oxygen—as applied to HBP synthesis offers possibilities to concurrently regulate the chain length (and, hence, degree of branching) and form oxygen-containing functional groups in HBP macromolecules with concurrent reduction in the amounts of initiators.

The strategy of HBP synthesis in the presence of air oxygen was developed at the Institute of Chemical Physics Problems of the Russian Academy of Science (G.V. Korolev) on the basis of the mathematical model of three-dimensional oxidative polymerization.

A reactor for ideal mixing with regulated access of air oxygen was chosen. Polymerization conditions (i.e., temperature, monomer concentration, solvent type, type and amount of initiator) are selected based on calculations carried out according to the mathematical model of the process. Constants of rates (or their combinations) of elementary stages of polymerization processes [32–34, 36], oxidative polymerization [68–70], and oxidation [32, 35, 71–73] serve as base data for the mathematical model. These constants have been determined and verified throughout several decades by different groups of researchers. Rate constants, data on which are missing in scientific publications, were estimated according to the method proposed by E.T. Denisov [74, 75]. The mathematical model takes into account all basic elementary acts from known mechanisms of polymerization, oxidation, and oxidative polymerization.

### 7.3 Synthesis of Hyper-Branched Polymers Via Living Chains Free-Radical Three-Dimensional Polymerization

#### 7.3.1 *Living Chains Free-Radical Three-Dimensional Polymerization as Reaction for Hyper-Branched Polymers Synthesis*

The “living” chains conditions in radical polymerization change the mechanism of macromolecule propagation from chain like (“instantaneous”) to stepwise (“slow”). The term instantaneous means that chain development time  $\tau$ , i.e., time from origination (initiation) until “destruction” (irreversible termination, linear or quadratic) is incommensurably small as compared to the time of polymerization process development  $\Delta t$ , i.e., time from zero conversion to final conversion: i.e.,  $\tau \ll \Delta t$ . Therefore, the polymerization process proceeds as accumulation of chains of average length  $\bar{P}$  that are formed “instantaneously” ( $\tau \ll \Delta t$ ) after each act of initiation.

The term slow means that average chain propagation time, from origination until irreversible termination  $\tau_{\text{LRP}}$ , is commensurable with  $\Delta t$  (usually  $\tau_{\text{LRP}} \geq \Delta t$ ; index “LRP” here is the acronym for “living chains radical polymerization”). That is, the chain is elongated continuously in the course of the polymerization process, and an increment of conversion occurs not because of accumulation of chain of certain length  $P$ , but as a result of summing of increments of all chains that have originated virtually at one and the same time at  $t \rightarrow 0$  (“instantaneous” initiation). And, the most important: each act of increment chain propagation has a high activation barrier  $E_{\text{pr}}^{\#}$  commensurable with the activation barrier of the elementary act of initiation of chains  $E_i^{\#}$ , i.e.,  $E_i^{\#} \approx E_{\text{pr}}^{\#}$ . Therefore, each act of increment chain propagation occurs only after the reinitiation act. In this context, the macromolecule propagation reaction (which is, in essence, a chain reaction) is identical to the stepwise reaction of polyaddition of polycondensation type, migration polymerization, and the like.

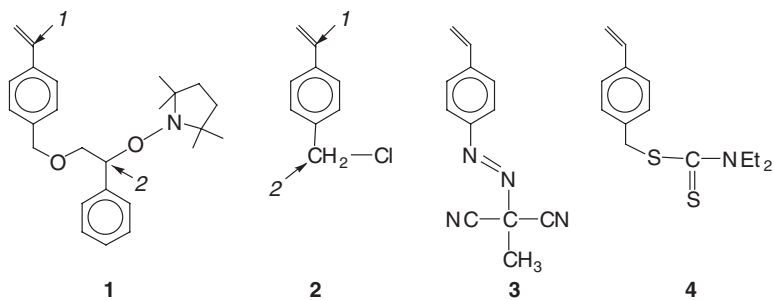
As it is just *stepwise* polymerization (polycondensation) of monomers of  $\text{AB}_2$  type that represents the simplest option of HBP synthesis, this fact makes employment of “living” radical polymerization for the production of HBP promising,

provided that such unsaturated monomer would be synthesized (either in advance or directly in the copolymerization system, in situ) that is polymerized similarly to  $AB_2$ .

It is easy to verify using formulas for determining critical conversion  $C_{cr}$  in the processes of living radical copolymerization (Chap. 5), but that simple combination of monounsaturated monomer ( $M_1$ ) with branching (polyunsaturated) comonomer  $M_m$  (where  $m$  = number of double bonds in a molecule) cannot solve the problem of HBP synthesis by the living radical polymerization method. Despite the clearly pronounced stepwise mechanism of the latter, the value of  $C_{cr}$  turns out to be unacceptably low ( $C_{cr} < 5\%$ ), if an acceptable value of copolymer branching degree is specified. With more or less acceptable values,  $C_{cr} < 50\%$ , the copolymer branching degree appears to be so low that the copolymers could no longer be qualified as HBP.

In 1995, Hawker and Frechet with their colleagues [76] were the first to solve the problem of synthesis of monomer  $AB_2$  that is polymerized according to the mechanism of "living" radical polymerization.

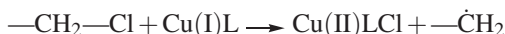
#### Functionalized styrenes for HBP synthesis by "living" radical polymerization method



Monomer **1** (synthesized by them) at  $T = 120\text{--}130^\circ\text{C}$  became polymerized according to the mechanism of living radical polymerization (similarly to  $AB_2$ ) by means of reversible homolytical dissociation of bond  $NO-C$  and subsequent reactions of stepwise addition of formed carbon-centered radical to the double bond of the next molecule of monomer **1**. These reactions are well known and have been studied in detail within the framework of the so-called alkoxyamine mechanism of living radical polymerization [77]. As a result, each molecule of monomer **1**, in the final end, appears to be included into the three-dimensional macromolecule as a branching fragment with two trifunctional junctions of the network (points *1* and *2* in the formula of monomer **1**). That is, a stepwise process of branched molecule formation from monomer **1** is identical to the similar process on the basis of monomers  $AB_2$ . In this case, the function of groups *A* is performed by the carbon-centered radical formed in point *2*, while the function of two groups *B* is formation of two free valences in point *1* after opening of a double bond [78, 79].

Later, HBP on the basis of monomer **2** were synthesized in a similar manner. Here another option of living radical polymerization was employed, namely, the ATRP

option (atom transfer radical polymerization) with the use of copper-containing organic complexes  $\text{Cu(I)L}$  ( $\text{L} = \text{ligands}$ ) that reversibly generate active free radical  $-\dot{\text{C}}\text{H}_2$  according to the following scheme:



This process results in the formation of branched macromolecules with trifunctional junctions in points 1 and 2 (formula of monomer **2**), while the HBP synthesis process is identical to stepwise polycondensation on the basis of monomers  $\text{AB}_2$ .

An interesting option of “living” radical polymerization for HBP synthesis was proposed by Voit in 2000 [80]. This option implies using compound **3** as an initial monomer of the  $\text{AB}_2$  type. Under the action of UV radiation this compound is capable of generating methyl(malonodinitrile) free radicals, performing the function of reversible inhibitor in this case.

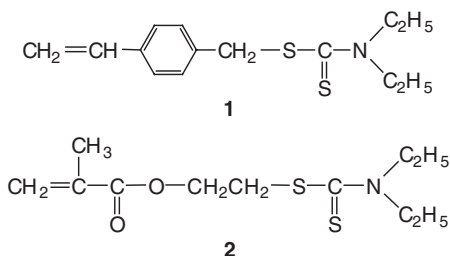
A direction implying the use of compounds of type **4** for the synthesis of HBP via living radical polymerization of functionalized styrenes was developed most of all in comparison to other directions. This direction is described in the next section.

### 7.3.2 Living Chains Polymerization of Vinyl Monomers with Diethyldithiocarbamate Groups

This direction of HBP synthesis appeared to be extremely successful and enabled scientists to develop a strategy of design of hyper-branched macromolecules of complicated topological architecture. A special term was introduced to denote such macromolecules: “nanostructured polymers.” These polymers find application in most advanced fields (e.g., in microelectronics). They are used in combination with nanoparticles of Ag or Cu as polymeric plasmons, etc.

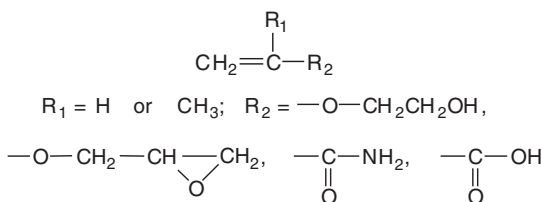
Otsu and his colleagues were the pioneers of living radical polymerization direction, which is based on the use of compounds with dialkyldithiocarbamate groups [81–83]. The main results of research conducted by this group throughout many years are presented in two surveys [84, 85].

A group of Japanese researchers under the leadership of K. Ishizu used the results of said research to develop a new direction for HBP synthesis [7, 23–31, 86–89]. As initial monomers, they have synthesized styrene and methyl(meth)acrylate with *N,N*-diethylamino-dithiocarbamate (DC) groups:



Photopolymerization (UV irradiation) of monomers **1** and **2** in 50% solutions (such as benzene) proceeding according to the mechanism of living radical polymerization discovered by Otsu [84, 85] enables synthesizing hyper-branched polystyrene and poly(methyl(meth)acrylate) with DC groups on chain ends.

As chains with end DC groups are living chains (according to the Otsu mechanism), an opportunity appears for their subsequent propagation through introduction of additives of any other vinyl monomers after initial monomers **1** or **2** have been exhausted. As a result, secondary nanostructured (e.g., star-shaped nanosized macromolecules with grafted chains [24, 29], nano-cylinders [23], and other nanostructured polymers of complicated topological architecture [7]) could be synthesized on the basis of primary HBP. In a number of cases, photopolymerization (as the first stage of the process) is not necessary for the synthesis of nanostructured polymers of complicated topological architecture. When subjected to photoirradiation, DC groups dissociate reversibly, and hence, branched macromolecules are necessarily formed. In those cases when a linear initial macromolecule with “living” points of propagation in the framing of carbon chains should be necessarily used as a matrix for nanostructured polymer (i.e., as in nano-cylinders), dark polymerization in the presence of conventional initiators is conducted (as indicated in [23]), and then photopolymerization of the matrix is conducted in the presence of any other monomer chosen for the formation of a given nano-structure. The approach analyzed herein has one more merit; namely, DC groups as agents of living radical polymerization are insensitive to the nature of the double bond in vinyl monomers in contrast to alkoxyamines, for example. This universality of DC groups allows combining monomers **1** and **2** for the purpose of HBP synthesis with vinyl monomers containing any functional groups in their molecules (e.g., hydroxyl groups, carboxyl groups, amine groups, amide groups), thus introducing these functional groups into HBP molecules:



As this direction has exceptional importance of potentiality in terms of both fundamental science and applied aspect, let us consider certain examples of synthesis and exploration into the properties of HBP and more complicated nanostructures on the basis of monomers **1** and **2** carried out by the team of researchers headed by K. Ishizu.

### 7.3.2.1 Hyper-Branched Polystyrenes [87, 88]

Polymers H1 (30%), H2 (40%), and H3 (50%) were obtained via UV irradiation of 50% solutions of monomer **1** in benzene. Conversions (C) corresponding to dif-

ferent irradiation times (2.5, 5, and 7.5 h, respectively) are given in parentheses. Analysis of synthesized polymers by the GPC method showed clearly expressed bimodality of MWD. By fractioning H1–H3 through deposition by methanol from benzene solutions, the authors managed to separate fraction F2, which corresponds to the lower molecular weight region. Fraction F1 (corresponding to higher molecular weight region) was studied in detail using different methods. The results are listed in Table 7.14.

Viscosimetric radius of macromolecules  $R_v$  was determined based on a known relationship:

$$R_v = \{3[\eta]M/(10\pi N_A)\}^{1/3} \quad (7.8)$$

where  $N_A$  = Avogadro number.

Parameter  $g'$  (which is a ratio of characteristic viscosity of branched polymer  $[\eta]$  to that of linear polymer  $[\eta]_L$ , with said polymers having identical molecular weights) was calculated by Zimm and Stockmayer [90] taking into account the relationship [91] for toluene solutions:

$$[\eta]_L = 17 \times 10^{-3} M_w^{0.69} \text{ cm}^2/\text{h} \quad (7.9)$$

Hydrodynamic radius of macromolecules  $R_h$  and gyration radius  $R_g$  were determined from data on light scattering in toluene solutions. It is known [92–96] that the ratio  $R_g/R_h$  is a characteristic parameter related to shape of macromolecules: for flexible coils (linear chains),  $R_g/R_h = 1.25$ – $1.37$  [92], while for densely packed spheres,  $R_g/R_h = 0.775$  [93–96]. The packing density is determined, all other things being equal, by degree of chain branching. Based on data listed in Table 7.14, the authors believe that quite highly branched macromolecules were synthesized.

Using the NMR method, the authors found that the ratio of aromatic protons to methyl protons of DC groups is very close to 2 : 3. This ratio should be exactly like this, provided that polymerization of monomer **1** proceeds strictly according to the Otsu mechanism and is not complicated by secondary reactions (of the chain transfer type and the like). However, MWD of nonfractionated polymers H1–H3 is very wide, which is not characteristic of living polymerization processes. Apparently, this is a consequence of the statistical character of macromolecule formation, not only via addition of new monomer units, but also via joining of propagating molecules

**Table 7.14** Properties of high polymeric fractions F1 isolated from polymers H1–H3 and designated as H1F1–H3F1

	$M_w^a \times 10^{-4}$	$M_w/M_n^b$	$[\eta]^c$ , ml · g <sup>-1</sup>	$g'^d$	$R_v$ , nm	$R_h$ , nm	$R_g$ , nm	$R_g/R_h$
H1F1	3.75	1.55	7.13	0.28	3.5	–	–	–
H2F1	6.10	1.17	9.90	0.26	4.6	5.0	4.3	0.860
H3F1	7.91	2.03	9.33	0.16	4.9	5.5	4.5	0.818

*Notes.* a, measured using universal GPC calibration in the THF solution at 38°C; b, calculated from chromatogram profiles; c, measured in toluene at 25°C;  $d-g' = [\eta]/[\eta]_L$ , degree of branching factor.



with one another as a result of relatively seldom, although still occurring, acts of recombination of polymeric chains.

Copolymerization of monomer **1** and styrene also allows synthesizing HBP [86]. In this case, by varying the composition of initial mixture “monomer **1**: styrene,” one can control the degree of branching and other topological parameters of formed copolymeric macromolecules with the proviso that constants of copolymerization  $r_1$  and  $r_2$  are known. Values  $r_1 = r_2 = 1$  were measured through determination of instantaneous composition of copolymer (having prespecified composition of initial mixture). That is, introduction of DC substitute into the styrene molecule does not influence the reactivity of the double bond.

Using maleic anhydride (incapable of homo-polymerization:  $r_2 = 0$ ) as comonomer, Ishizu et al. [30] managed to synthesize HBP having alternating units. Another option of HBP with alternating units was synthesized via copolymerization of monomer **1** and maleimide [28]. An attempt [27] to obtain a hyper-branched styrene methacrylate copolymer with alternating units using complex MMA with  $\text{ZnCl}_2$  as a comonomer (in this case,  $r_1 = 0.25$ ,  $r_2 = 0.056$ , and alternation of units should be observed) was not successful: the synthesized copolymer had statistical distribution of units. It appeared that Lewis acid  $\text{ZnCl}_2$  in this case becomes complexed not only with MMA but also with the DC group of molecules of monomer **1**, and this was the reason for the failure of the said attempt.

### 7.3.2.2 Hyper-Branched Poly(meth)acrylates [25, 26, 89]

Hyper-branched poly(meth)acrylates were synthesized from monomer **2** in the same manner as hyper-branched polystyrene from monomer **1**. It was established [26] that the photopolymerization rate of monomer **2** in benzene is proportional to the concentration of monomer, whereas  $M_n$  grows with increasing conversion. A mechanism of initiation and propagation of chains was studied with the use of appropriate low molecular substances that simulate these processes. As a result, it was shown that reversible dissociation of DC groups takes place mainly from the C–S bond in accordance with the “living” radical polymerization mechanism proposed by Otsu [84, 85].

Copolymerization of monomer **2** and ethyl(meth)acrylate gave HBP with a different degree of branching controlled by the composition of the initial mixture of comonomers [25]. Values of copolymerization constants  $r_1$  and  $r_2$  appeared to be equal to 1, as in the case of copolymerization of monomer **1** and styrene. That is, in this case the DC substitute in a molecule of monomer **2** does not influence the double bond reactivity. Therefore, copolymer composition will be identical to the composition of the initial mixture of comonomers. An exploration into properties of synthesized HBP was carried out using the same methodological scheme as for hyper-branched polystyrenes and gave similar results, namely, proof of higher compactness of macromolecules of branched poly(meth)acrylates as compared to the linear analogue [i.e., poly(ethyl)methacrylate] having the same molecular weight.

Exploration into the ability of hydrophilic comonomer 2-hydroxyethyl methacrylate (HEMA) to photopolymerize in the presence of DC-containing compounds according to the “living” radical polymerization mechanism [29] is of utmost interest. It was shown that polymer chains being formed include DC fragments as end units. When such chains (after they are isolated from the reaction mixture by precipitation and placed into a medium of another monomer, MMA) are subjected to UV irradiation, they are elongated through buildup of poly(methyl) methacrylate blocks; that is, they behave as living chains. In the context of synthesis of new hyper-branched structures, this opens a possibility for using HEMA as comonomer for monomer **2** with the aim to introduce hydroxyl groups into HBP macromolecules.

### 7.3.2.3 Nanostructured Polymers [7, 23, 24, 31]

We analyze here HBP of complicated molecular architecture in an example of macromolecules of nanocylinder type with hyper-branched side chains [23]. Such nanostructured polymers were synthesized in two stages. First, monomer **1** was polymerized at 35°C in the presence of dark initiator 2,2'-azo-bis-(2,2,4-trimethylvaleronitrile) in the THF solution (100 h). The formed linear polymer, according to NMR data (500 MHz, in  $\text{CdCl}_3$ ), consisted of styrene units that contained one DC group per unit and had, according to GPC data (with additional light-scattering detector of LALLS type), in one case (let us denote this polymer  $\text{PS}^{\text{DC}}\text{-1}$ )  $M_w = 1.14 \times 10^5$ ;  $M_w/M_n = 1.23$ , while in another case ( $\text{PS}^{\text{DC}}\text{-2}$ )  $M_w = 1.53 \times 10^5$ ;  $M_w/M_n = 1.26$ . Then followed the second stage: photopolymerization of monomer **1** in the presence of synthesized polymer  $\text{PS}^{\text{DC}}$  (in 50% THF solution, with molar composition of initial mixture  $\text{PS}^{\text{DC}} : \text{monomer } \mathbf{1} = 1 : 10$ ) at 25°C via UV irradiation (high-pressure mercury lamp, 250 W, at a distance of 20 cm) during a period of 4 h.

Analysis (GPC, NMR, and LALLS) of the reaction mixture showed that only 2% of monomer **1** has been added to  $\text{PS}^{\text{DC}}$  macromolecules. Increasing the polymerization time to 16 h had no influence upon the outcome. Therefore, further buildup of branched monomer **1** on pendent DC groups of  $\text{PS}^{\text{DC}}$  chains was conducted as a multistage process with isolation of target product from the reaction mixture (precipitation of benzene solutions into methanol), then the repeated addition of a new portion of monomer **1** to it at the end of each stage (each time, the proportion was 1 : 10) and repeated photopolymerization during a period of 4 h. Preformed polymer  $\text{PS}^{\text{DC}}\text{-1}$  was subjected to such procedure six times (resulting product, nc1-6f: nanostructured polymer on the basis of  $\text{PS}^{\text{DC}}\text{-1}$ , fractionized six times), preformed polymer  $\text{PS}^{\text{DC}}$ , two to four times (resulting product, nc2-4f). Each stage was conducted under the conditions of GPC-LALLS control: MWD of reaction mixture after photopolymerization was determined (polymodal, very wide), then MWD after fractionizing was determined (unimodal, narrow), and this sequence of steps was repeated four or six times.

Properties of typical products—nc1-6f and nc2-4f—are shown in Table 7.15.

**Table 7.15** Properties of initial preformed polymers and final products obtained on the basis of such preformed polymers

	$M_w^a \times 10^{-5}$	$M_w/M_n^a$	$R_h^b$ , nm	$[\eta]^c$ , ml g <sup>-1</sup>	$g'^d$	$R_g^e$	$R_{g,c}^f$
PS <sup>DC</sup> -1	1.14	1.23	–	30.18	–	–	–
nc1-6f	10.1	1.35	15.0	23.01	0.11	25.33	6.8
PS <sup>DC</sup> -2	1.53	1.26	–	38.32	–	–	–
nc2-4f	4.45	1.50	13.1	26.30	0.27	23.63	4.5

*Notes.* a, measured using GPC-LALLS method; b, measured using dynamic light-scattering method in THF solution at 25°C; c, measured in THF solution at 38°C; d,  $g' = [\eta]/[\eta]_L$ , branching factor; e, measured using statistical light-scattering method in THF solution at 25°C; f,  $R_{g,c}$ , gyration radius measured by small-angle scattering of X-ray method (monochromatized CuK $\alpha$  radiation,  $\lambda = 0.154$  nm) in THF solution.

Using the dynamic light-scattering method and varying the angle from 30° to 90°, the authors found that the shape of nc1-6f and nc2-4f macromolecules is anisometric. Rough estimate of macromolecule length ( $\approx 73$  nm for nc1-6f) was derived based on values of  $R_{g,c}$  and  $M_n$ . This estimation was conducted based on the assumption that they are of cylindrical shape, with degree of polymerization 349 (estimate by  $M_n$ ), and length of C–C bonds  $\approx 0.15$  nm taken into account. Direct electron microscopic measurement of nc1-6f size gave the following results: cylinder length, 70 nm, and cylinder diameter, 10 nm. Also, a clear electron microscopic image of individual macromolecules shaped as cylinders was obtained. Data listed in Table 7.15 agree well with the cylindrical shape of macromolecules. The ratio  $R_g/R_h = 1.69$ – $1.80$  differs strongly from  $R_g/R_h = 0.775$  as obtained for spheres [95]; for monodisperse rods,  $R_g/R_h > 2$  [96].

It also follows from Table 7.15 that the degree of branching of nano-cylindrical macromolecules (compare value of  $g'$  for nc1-6f with that for nc2-4f) increases sharply as  $M_w$  grows. The value of  $g'$  equal to the relationship of characteristic viscosities  $[\eta]/[\eta]_L$  of branched macromolecules and linear analogue (with their molecular weight being close) goes down with enhancing compactness of branched macromolecules of symbate degree of branching.

Measurements of interdiffusion coefficient of nc1-6f and nc2-4f macromolecules in THF at different concentrations showed independence of this coefficient from concentration in the range 0–25 g/l, which is indicative of absence of aggregation (macromolecules behave as discrete particles that do not interact with one another). A sharply impaired tendency for aggregation is a distinctive feature of HBP.

The theoretical significance of successful synthesis of nano-cylindrical macromolecules is obvious. From the standpoint of applied science, potentialities of HBP having complicated topological architecture are, of course, restricted by labor consumption of the synthesis process. However, the authors have no doubts that in modern microelectronics, which is currently rapidly progressing and transforming into “molecular electronics” that requires very small amounts of substances, although possessing exceptional properties, nano-cylinders would appear to be in demand.

## References

1. Korolev GV, Bubnova ML (2007) *Vysokomolekul Soedin A* **49**:1357–1388 (in Russian)
2. Kim YH (1998) *J Polym Sci Polym Chem* **36**:1685–1698
3. Burchard W (1999) *Adv Polym Sci* **143**:113
4. Ambade AV, Kumar A (2000) *Prog Polym Sci* **25**:1141–1170
5. Kakimoto M, Jikei M (2001) *Prog Polym Sci* **26**:1233–1285
6. Mori H, Müller AHE (2003) *Prog Polym Sci* **28**:1403–1439
7. Ishizu K, Tsubaki K, Mori A, Ushida S (2003) *Prog Polym Sci* **28**: 27–54
8. Aulenta F, Hayes W, Rannard S (2003) *Eur Polym J* **39**:1741–1771
9. Pyun J, Zhou H-Z, Drockenmüller E, Hawker CJ (2003) *J Mater Chem* **13**:2653–2660
10. Yates CR, Hages W (2004) *Eur Polym J* **40**:1257–1281
11. Korolev GV, Mogilevich MM, Golikov IV (1995) Cross-linked polyacrylates: micro-heterogeneous structures, physical networks, deformation-strength properties. *Khimiya, Moscow* (in Russian)
12. Kurochkin SA, Grachev VP, Korolev GV (2007) *Vysokomol Soedin A* **49**:347–353 (in Russian)
13. Korolev GV (2003) *Usp Khim* **72**:222–244 (in Russian)
14. O'Brien N, McKee A, Sherrington DC, Slark AT et al (2000) *Polymer* **41**:6027–6031
15. Costello PA, Martin IK, Slark AT et al (2002) *Polymer* **43**:245–254
16. Slark AT, Sherrington DC, Titterton A, Martin IK (2003) *J Mater Chem* **13**:2711–2720
17. Isaure F, Cormack PAG, Sherrington DC (2003) *J Mater Chem* **13**:2701–2710
18. Isaure F, Cormack PAG, Sherrington DC (2004) *Macromolecules* **37**:2096–2105
19. Mori H, Chang Seng D, Zhang M, Müller AHE (2004) In: Cabuil V, Levitz P, Treiner C (eds) *Prog Colloid Polym Sci* **126**:40–43
20. Zhang M, Muller AHE, Teissier P et al (2004) In: Cabuil V, Levitz P, Treiner C (eds) *Prog Colloid Polym Sci* **126**:35–39
21. Zhang M, Estournès C, Bietsch W, Müller AHE (2004) *Adv Funct Mater* **14**:871–882
22. Bohrisch J, Eisenbach CD, Jaeger W, Mori H et al (2004) In: Schmidt M (ed) *New polyelectrolyte architectures*. *Adv Polym Sci* **165**:1–41
23. Ishizu K, Ohta Y (2003) *J Mater Sci Lett* **22**:647–650
24. Ishizu K, Kojima T, Ohta Y, Shibuya T (2004) *J Colloid Interface Sci* **272**:76–81
25. Ishizu K, Shibuya T, Park J, Uchida S (2004) *Polym Int* **53**:259–265
26. Ishizu K, Shibuya T, Kawauchi S (2003) *Macromolecules* **36**:3505–3510
27. Ishizu K, Park J, Ohta Y, Shibuya T (2003) *J Appl Polym Sci* **89**:2490–2495
28. Ishizu K, Takashimizu C, Shibuya T, Uchida S (2003) *Polym Int* **52**:1010–1015
29. Ishizu K, Khan RA, Ohta Y, Furo M (2004) *J Polym Sci Polym Chem* **42**:76–82
30. Ishizu K, Mori A, Shibuya T (2001) *Polymer* **42**:7911–7914
31. Ishizu K, Tsubaki K, Mori A et al (2003) *Prog Polym Sci* **28**:27–54
32. Denisov ET (1971) *Liquid-phase reaction rate constants*. Nauka, Moscow (in Russian)
33. Lipatov YuS, Nesterov AS, Gritsenko TM, Veselovskiy RA (1971) *Reference book on chemistry of polymers*. Naukova Dumka, Kiev (in Russian).
34. Bamford CH, Tipper CFH (1976) *Free radical polymerization: comprehensive chemical kinetics*, vol. 14A. American Elsevier, New York
35. Denisov ET, Azatyan VV (1997) *Inhibition of chain reactions*. Institute of Chemical Physics, Chernogolovka (in Russian)
36. Bagdasaryan XS (1966) *Radical Polymerization Theory*. Nauka, Moscow (in Russian)
37. Odian G (1974) *Principles of polymerization*. Moscow, Mir (Russian translation)
38. Behera GC, Ramakrishnan S (2004) *Macromolecules* **37**:9814–9820
39. Sato T, Sato N, Seno M, Hirano T (2003) *J Polym Sci Polym Chem* **41**:3038–3047
40. Sato T, Hashimoto M, Seno M, Hirano T (2004) *Eur Polym J* **40**:273–282
41. Sato T, Higashida N, Hirano T, Seno M (2004) *J Polym Sci Polym Chem* **42**:1609–1617
42. Sato T, Arima Y, Seno M, Hirano T (2004) *Polym Int* **53**:1138–1144

43. Sato T, Ihara H, Hirano T, Seno M (2004) *Polymer* **45**:7491–7498
44. Gao C, Yan D (2004) *Prog Polym Sci* **29**:183–275
45. Smirnov BR, Marchenko AP, Korolev GV et al (1981) *Vysokomol Soedin A* **23**:1042–1050 (in Russian)
46. Smirnov BR, Morozova IS, Puschayeva LN et al (1980) *Dokl Acad Nauk USSR* **255**:603–607 (in Russian)
47. Smirnov BR, Ponomarev GV, Marchenko AP (1980) *Dokl Acad Nauk USSR* **254**:127–130 (in Russian)
48. Gridnev A, Ittel S (2001) *Chem Rev* **101**:3611–3660
49. Matsumoto A, Matami D, Aota H (2000) *Polymer* **41**:1321–1324
50. Matsumoto A (1995) *Adv Polym Sci* **123**:41–80
51. Matsumoto A, Okuno S, Aota H (1996) *Angew Makromol Chem* **240**:275–284
52. Miller G, Alumbaugh R, Bratheston R (1952) *J Polym Sci* **9**:453–462
53. Pravednikov AN, Medvedev SS (1955) *Dokl Acad Nauk USSR* **103**:461–464 (in Russian)
54. Pravednikov AN, Medvedev SS (1956) *Dokl Akad Nauk USSR* **109**:579–581 (in Russian)
55. Hui A, Hamielec AE (1972) *J Appl Polym Sci* **16**:749–769
56. Hussain A, Hamielec AE (1978) *J Appl Polym Sci* **22**:1207–1223
57. Hamielec AE, MacGregor JF, Webb S, Spychaj T (1986) In: Reichert KH, Geisler W (eds) *Polymer reaction engineering*. Hüthig Wepf, New York
58. Spychaj T, Hamielec AE (1991) *J Appl Polym Sci* **42**:2111–2119
59. Campbell JD, Teymour F, Morbidelli M (2005) *Macromolecules* **38**:752–760
60. Fisher JP, Luders W (1972) *Makromol Chem* **155**:239–257
61. Meijs GF, Rizzardo E, Thang SH (1988) *Macromolecules* **21**:3122–3124
62. Meijs GF, Rizzardo E (1990) *Makromol Chem* **191**:1545–1553
63. Meijs GF, Morton TC, Rizzardo E, Thang SH (1991) *Macromolecules* **24**:3689–3695
64. Campbell JD, Allaway JA, Teymour F, Morbidelli M (2004) *J Appl Polym Sci* **94**:890–908
65. Campbell JD, Teymour F (1999) Hyperbranched polymers. US Patent 5.986.020
66. Campbell JD, Teymour F (2001) Hyperbranched polymers. US Patent 6.265.511 (S/C/Johnson Commercial Markets, Inc.)
67. Guan Z (1998) Synthesis of multi-functional hyperbranched polymers by polymerization of di- or tri-vinyl monomers in the presence of a chain transfer catalyst. US Patent 5.767.211 (E/I/du Pont de Nemours and Company)
68. Mogilevich MM (1977). Oxidative polymerization in film-formation processes. *Khimia (Chemistry)*, Leningrad
69. Mogilevich MM, Pliss EM (1990) Oxidation and oxidative polymerization: unsaturated compounds. *Khimia (Chemistry)*, Moscow (in Russian)
70. Mogilevich MM (1979) *Usp Khim* **48**:362–386 (in Russian)
71. Kucher RV, Timokhin VI, Shevchuk IP et al (1986) Liquid-phase oxidation of unsaturated compounds in olefin oxide. *Naukova Dumka*, Kiev (in Russian)
72. Rubailo VL, Maslov SA (1989) Liquid-phase oxidation of unsaturated compounds. *Nauka*, Moscow (in Russian)
73. Denisov ET, Denisova TG (2003) *Handbook of free radical initiators*. Wiley, New Jersey
74. Denisov ET (2000) *Usp Khim* **69**:166–177 (in Russian)
75. Denisov ET, Denisova TG (2002) *Usp Khim* **71**:477–499 (in Russian)
76. Hawker CJ, Frechet JMJ, Grubbs RB, Dao J (1995) *J Am Chem Soc* **117**:10763–10764
77. Korolev GV, Marchenko AP (2000) *Usp Khim* **69**:447–475 (in Russian)
78. Weimer MW, Frechet JMJ, Gitsov I (1998) *J Polym Sci Polym Chem* **36**:955–970
79. Gaynor SG, Edelman S, Matyjaszewski K (1996) *Macromolecules* **29**:1079–1081
80. Voit B (2000) *J Polym Sci Polym. Chem* **38**:2505–2525
81. Otsu T, Yoshida M, Kuriyama A (1982) *Polym Bull* **7**:45–50
82. Endao K, Murata K, Otsu T (1992) *Macromolecules* **25**:5554–5556
83. Kuriyama A, Otsu T (1984) *Polym Bull* **16**:511–514
84. Otsu T, Matsumoto A (1998) *Adv Polym Sci* **136**:75–137
85. Otsu T (2000) *J Polym Sci Polym Chem* **38**:2121–2136

86. Ishizu K, Mori A (2001) *Polym Int* **50**:906–910
87. Ishizu K, Mori A (2000) *Macromol Rapid Commun* **21**:665–668
88. Ishizu K, Ohta Y, Kawauchi S (2002) *Macromolecules* **35**:3781–3784
89. Ishizu K, Shibuya T, Mori A (2002) *Polym Int* **51**:424–428
90. Zimm H, Stockmayer WH (1949) *J Chem Phys* **17**:1301–1314
91. Roovers A, Zhou L-L, Toporowski PM et al (1993) *Macromolecules* **26**:4324–4331
92. Roovers J, Martin JE (1989) *J Polym Sci Polym Phys* **27**:2513–2524
93. Yamakawa H (1971) *Modern theory of polymer solutions*. Harper Row, New York
94. Schmidt M, Neger D, Burchard W (1979) *Polymer* **20**:582–588
95. Antonietti M, Bremser W, Schmidt M (1990) *Macromolecules* **23**:3796–3805
96. Schmidt M (1984) *Macromolecules* **17**:553–560

## Chapter 8

# Properties and Application of Hyper-Branched Polymers

**Abstract** Chapter 8 does not presume to describe a variety of hyper-branched polymer (HBP) properties and examples of HBP application. This chapter is based on those studies and publications in which an interrelationship between the unique HBP properties and morphology and topology of HBP structure has been revealed. Special attention is given to industrially produced HBP—Boltorn<sup>®</sup> and Hybrane<sup>®</sup>. Problems to be solved in the near future have been formulated—theoretical problems plus analytical and synthetic concerns. Finding solutions to these problems would move us closer to the practical application of HBP. The progress associated with HBP application is so significant that one has grounds to assert that a revolution has occurred in polymeric material science.

As has been indicated earlier (Chap. 7), hyper-branched polymers (HBP) possess unique properties distinguishing them from polymers belonging to other classes. The unusual topological structure, the “core-shell” characterized by a very high local concentration of chain ends in the peripheral layer (shell) of macromolecules and a very high local concentration of branching points in the core, represents a source of these unique properties. As a result, the hydrodynamic volume of HBP macromolecules stops increasing after a certain degree of branching has been reached and, starting from a certain value  $M_n$  (usually starting from  $M_n > 10^4$ ), the volume becomes significantly less than the hydrodynamic volume of linear macromolecules with the same value  $M_n$ . Such compact packing of HBP macromolecules and the large number of free chain ends at the periphery represent the primary structural and physical reasons for the manifestation of the unique HBP properties.

At the macroscopic level, the topological features of HBP are manifested as properties such as high solubility and thermodynamic compatibility, and high sorption capacity in combination with the ability to transport sorbates in those media in which the sorbate is insoluble (this ability allows using HBP as Ners with a high local concentration of reagents). All these properties appeared to be in demand in polymer material science, in medicine, in biology, in electronics, and in other fields of application. It should be pointed out that the HBP application efficiency was so high (improvement in properties by 100–200%!) that it led to a *revolution in polymer material science*.

## 8.1 “Structure–Property” Relationship and Purposeful Generation of Hyper-Branched Polymer Properties That Are in Demand in Practice

An extremely wide variety of options for practical application of HBP (which is reflected in Table 8.3, later in this chapter) is based on the equally wide variety of HBP used, because each specific option of practical application requires that HBP has quite specific properties determined by the chemical and topological structure of hyper-branched macromolecules. For this reason, much attention is given to studies related to identification of those chemical and topological structural elements of HBP that control one or another property. The “structure–property” relationship is studied in HBP families with successively varied parameters in the first place, such as type of functional groups, length and flexibility of interjunction chains, number of branching generations (see Fig. 7.1), and molecular mass characteristics of polymers, exactly with this aim. A large body of information has been already accumulated on this issue, and this information enables the authors to draw certain generalizations that would be useful for developing methods for creating exactly those properties that HBP should have to be successfully used in a specific field of practical application [1].

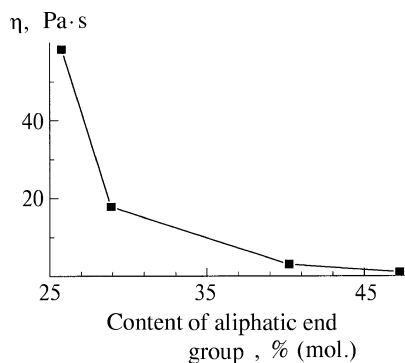
HBP are described quite adequately by two parameters: the chemical and the topological structure of macromolecules. The chemical structure is a set of atomic groups in HBP macromolecules. The topological structure is determined by the number of chains (arms) outgoing from the symmetry center of macromolecules, by number of branching (generation) cascades, by number of branching points (junctions) in each cascade, and by length of chain sections between adjacent junctions (i.e., interjunction chains). Modern research methods (namely, chemical analysis, spectroscopy, PMR,  $^{13}\text{C}$ -NMR, and others) enable us to identify the above-indicated characteristic parameters of HBP with quite a high degree of accuracy, i.e., the chemical and topological structure regulating the main macroscopic properties of hyper-branched macromolecules.

Such information is given below in an example of base HBP of two types that are produced industrially—namely, Boltorn<sup>®</sup> (Perstorp Speciality Chemicals AB, Sweden, with a subsidiary in the USA: Perstorp Polyols Inc.) [2] and Hybrane<sup>®</sup> (DSM Fine Chemicals, Netherlands) [3].

HBP of Boltorn<sup>®</sup> type [2] are polyesters synthesized via polycondensation of monomer  $\text{AB}_2$ , 2,2-dimethylol-propionic acid (A, COOH; B, OH), by esterification reaction and, hence, carrying hydroxyls as end functional groups that form a “shell.” The analyzed basic series includes brands H20, H30, and H40 that differ in terms of number of generations ( $Z = 2, 3$ , and  $4$ , respectively), number of functional groups OH ( $F = 16, 32$ , and  $64$ ), value of  $M_w$  (2100, 3500, and 5100), polydispersity  $M_w/M_n$  (1.3, 1.5, and 1.8), glass-transition temperature  $T_g$  ( $31^\circ$ ,  $38^\circ$ , and  $42^\circ\text{C}$ ), and viscosity ( $\eta$ ) of melt at  $110^\circ\text{C}$  (7, 40, and  $110 \text{ Pa} \cdot \text{s}$ ). The combined impact of factors  $Z$ ,  $F$ ,  $M_w$ , and  $M_w/M_n$  is manifested in insignificant (but, nevertheless, systematic) increase of  $T_g$  and in very drastic growth of viscosity with concurrent increase of  $Z$ ,  $F$ ,  $M_w$ , and  $M_w/M_n$ . Considerable variation



**Fig. 8.1** Influence of partial substitution of hydroxyls in Boltorn<sup>®</sup> H20 polyester with aliphatic end groups upon viscosity at 23°C



of  $T_g$ ,  $\eta$ , and solubility values for HBP of “H” series was observed in the case of partial substitution of other functional groups for hydroxyls. For instance, partial esterification of OH groups in H20 by aliphatic monocarboxylic acid results in very steep decline of  $T_g$  and  $\eta$ . Quantitatively, the dependence of measured viscosity upon the content of esterified hydroxyls (%mol) is shown in Fig. 8.1 and Table 8.1.

Substitution of long aliphatic chains (capable of crystal formation) for hydroxyls in HBP of “H” series leads to the formation of a clearly distinct melting temperature instead of  $T_g$ , and this melting temperature is indicative of the crystalline phase appearance. The melt of initial polyester Boltorn<sup>®</sup> H20 behaves as a pseudo-thixotropic (non-Newtonian) liquid. Destruction of thixotropic structure occurs only under the conditions of very high strain rates. Obviously, the reason for thixotropy consists in strong intermolecular interaction resulting from hydrogen bonds formed by hydroxyls. Substitution  $\approx 50\%$ (mol) of nonpolar aliphatic chains for hydroxyls results in ideally Newtonian behavior. It was found that the deviation from Newtonian behavior decreases with increasing  $Z$ ,  $F$ , and  $M_w$  (with transition from H20 polyester to H40 polyester). The main reason for this may consist of extension of potential conformations of macromolecular branches (that carry OH groups) when these branches are elongated (and, hence, their flexibility enhances) by the growth of  $Z$ . In this case, accumulation of a large number of hydroxyls on the periphery of HBP macromolecules gives additional opportunity of intramolecular realization of hydrogen bonds (instead of intermolecular realization) because of the “pull-in” of peripheral hydroxyls inside macromolecules.

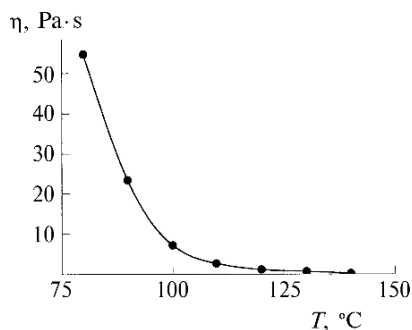
As a result of partial substitution of hydroxyls in HBP of the Boltorn<sup>®</sup> “H” series, scientists manage to vary their properties within a wide range to match specific fields of application. Main directions of such variation are shown in Scheme 1.

**Table 8.1** Influence of partial substitution of aliphatic end groups for hydroxyls in Boltorn<sup>®</sup> H20 polyester on  $T_g$

Substitution, % (mol)	0	10	25	50	60
$T_g$ , °C	31	12	5	-15	-30



**Fig. 8.2** Rheological properties of base HBP Hybrane<sup>®</sup> modified by esterification of octadecanoic acid (esterification degree, 50% mol)



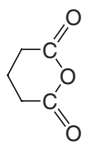
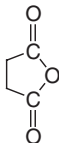
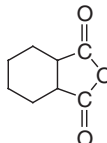
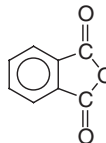
in water at pH = 5–9, and they possess expressed capability to biodegradation. By varying the set of functional groups  $F$ , chemical structure of repeating unit and value of  $M_n$  one can influence the following properties: solubility and thermodynamic compatibility,  $T_g$ , surface activity (when using as surfactant) and rheological properties. Variation of the set of functional groups  $F$  is effected via esterification of hydroxyls of base HBP by following acids: fatty acids, benzoic acid, methacrylic acid, and functionalized acids. In those cases when solubility in water is required, HBP with end functional groups  $-\text{N}(\text{CH}_3)_2$  or  $-\text{COOH}$  are specially synthesized. Substitution of hydroxyls in the base HBP via esterification of fatty (dodecanoic) acid sharply lowers the value of  $T_g$ .

Partial substitution (~50%) of hydroxyl via esterification by octadecanoic acid leads to an extremely sharp drop of melt viscosity (Fig. 8.2).

The influence of chemical “BB + BE” structure upon properties of Hybrane<sup>®</sup> family HBP was studied by varying one of its two initial components—namely, fragment of anhydride—in the following series: anhydrides of 1,4-cyclohexane dicarboxylic acid, succinic acid, and phthalic acid, as well as anhydride of succinic acid with substituents  $\text{C}_{12}\text{H}_{29}$  and more complex ones (Table 8.2).

It appeared that composition of the anhydride fragments (building blocks) of “BB + BE” structure strongly influences the solubility of HBP in water: successive substitution of anhydride of succinic acid for anhydride of 1,4-cyclohexane dicarboxylic acid in the initial composition (by 20%, 40%, 60%, 80%, and 100%) facilitates the gradual transition from complete insolubility to poor swelling, then to strong swelling, then to partial and complete solubility, and, finally, to good solubility.

**Table 8.2** Influence of chemical structure of repeating unit on glass-transition temperature of Hybrane<sup>®</sup> polyesteramides

Anhydride of dicarboxylic acid				
$T_g, ^\circ\text{C}$	19	41	70	95

Viscosity in solutions and compounds also appeared to be a parameter that is well regulated via “building block” variation: a record-breaking low viscosity of 50% solution of HBP was achieved exactly through building block variation. Low viscosity of Hybrane<sup>®</sup> polyesters as compared to their linear analogues (which is a common property inherent to all known HBP to a greater or lesser extent) offers strong possibilities for practical application of these HBP, especially in varnishes and paints and in polymeric composites.

Variation of the nature of end functional groups for HBP of Hybrane<sup>®</sup> type also resulted in record-breaking values of certain parameters. With certain proportion of hydrophilic and hydrophobic groups  $F$  in macromolecules of Hybrane<sup>®</sup> family polyesteramides, the latter acquire properties of very active surfactants. For instance, in the case of esterification of a part of hydrophilic groups (hydroxyl groups) in base polyesteramide with fatty acid having hydrophobic chain  $C_{11}$  (dodecanoic), this polyesteramide becomes an extremely active surfactant.

Activity of surfactant of a given type (surface tension serves as a measure of this activity) is extremely high: the effect of twofold reduction of the surface tension is obtained even at surfactant concentration  $\approx 10^{-2}\%$  (!). High efficiency of hyper-branched surfactants (in contrast to surfactants of other types) is determined by the following factors: very high local concentration of polar and nonpolar groups in the volume of one macromolecule, possibility to control the proportion of these groups in a macromolecule to provide the optimum balance, and low critical concentration of micelle formation (CCM parameter).

A proportion of hydrophilic and hydrophobic groups in macromolecules represents the main factor for another property of HBP belonging to Hybrane<sup>®</sup> family, namely, for capability for adsorbing on the surface of solid bodies (including polymers) in the form of extremely high-density films (density of surface filling is meant here). Continuous filling of the surface (i.e., without defects of bare micro-area type) controlled by modern methods is observed starting from film thickness of 7–10 nm. The same degree of filling for linear polymer is observed starting from film thickness of 10–20  $\mu\text{m}$ , that is,  $\approx 1000$  times greater.

## 8.2 Hyper-Branched Polymers as Modifiers of Polymeric Materials

The problem of HBP interaction with polymeric matrices emerged (as it often happens with fundamental scientific problems) from the development of one direction in polymer material science. This direction involves application of HBP additives as highly efficient modifiers and is broken down into two subdirections that are rapidly developing at present [1]. The first subdirection implies introduction of HBP additives into structural polymeric materials with the aim to improve their physical and mechanical characteristics (mainly to degrade brittleness by upgrading the impact elasticity) and making the material production procedure more streamlined (mainly by reducing the viscosity of the initial mixture from which the product is fabricated). The second subdirection concerns the use of HBP additives for producing functional

polymeric materials. In this case, HBP macromolecules are used as nano-containers (hosts) filled with “guest” molecules of functional substances (chromotropes such as spiropyrans, scintillators, aurum clusters and other metals including several atoms, dyeing agents, and so forth). Said nano-containers ensure ideally uniform distribution of contained substances in the volume of materials such as organic “chameleon glass,” radiation detectors, polymeric plasmons, and dyed organic glasses.

In any case, especially when using HBP as nano-containers, it is necessary to know whether the level of molecular mobility inside HBP macromolecules changes after these macromolecules are confined into a glass-like or semicrystalline polymeric matrix. In other words, it is necessary to know the character of the interaction of HBP macromolecules (or their aggregates, if HBP aggregation is inevitable during matrix formation) with matrices because the efficiency of modification by HBP additives depends heavily upon the degree of preservation of HBP macromolecule self-sufficiency. Indeed, if self-sufficiency of HBP macromolecules is retained, the latter (or their aggregates) would be able to create nanosized centers in the matrix, and these centers would have a predetermined set of properties specified by chemical and topological structure of selected HBP.

Multiple data on modification of polymeric matrices by HBP additives indirectly prove the retention of self-sufficiency. Direct proofs of this fact are also available [4, 5]; these were obtained after measuring the glass-transition temperature of HBP proper ( $T_{g1}$ ), poly-epoxy polymeric matrices ( $T_{g2}$ , with  $T_{g2} > T_{g1}$ ), and polymeric matrices with HBP additives. It appeared that in the latter case two clearly distinguishable areas of  $\alpha$ -transition were observed on temperature scale (measurements were taken using the dynamic mechanical method for temperature dependence  $\text{tg } \delta$ ): a low temperature near  $T_{g1}$  and a high temperature near  $T_{g2}$ . Also, the intensity of peak  $\text{tg } \delta$  (corresponding to  $T_{g1}$ ) was increasing with growing HBP additive concentration. As values of  $T_g$  are determined by molecular mobility level, the authors can assert (based on data presented in [4, 5]) that HBP (polyesters with end hydroxy groups) in polymeric (poly-epoxy) matrices maintain their inherent level of molecular mobility, that is, retain their self-sufficiency.

Regularities of HBP interaction with glass-like polymeric matrices were systematically studied in detail, mainly in an example of poly-epoxy matrices [4–7].

An extremely interesting and unusual type of interaction with HBP is observed for semicrystalline polymeric matrices: small additives of HBP introduced into a melt of crystallizing polymers (poly(olefins) and poly(carbonates)) [8, 9] led, in the course of crystallization, to the formation of very small spherulites (of almost identical size) instead of those of large and different size that are formed in the absence of HBP. As a consequence, physical and mechanical properties of matrices were improved quite radically. Reduction in melt viscosity (considerably facilitating the process of product processing) represented an additional positive effect.

Analysis of all the aforementioned publications related to problems of HBP interaction with glass-like polymeric matrices leads to the following main conclusion.

In the process of matrix formation [via polymerization in the case of reactive plastics or from solutions (melts) in the case of thermoplastics], an HBP additive can either stay in dissolved state (if HBP concentration is low, and thermodynamic

compatibility to matrix polymer is high), or, as a result of micro-phase separation, become aggregated in part or completely (depending on concentration and thermodynamic compatibility level) in the form of sufficiently small (2–5 μm) monodispersed spherical particles evenly distributed in the matrix volume. Each and all authors believe (providing convincing argumentation) that it is exactly these particles that are responsible for the effect of matrix brittleness degrading. Micro-phase separation processes are inherent to polymeric modifiers of any type (not only to HBP), but a morphological structure having the most uniform volume distribution of dispersed phase is formed exactly in the case of HBP (as follows from electron microscopy data). Obviously, it is such uniformity (being a distinctive feature of HBP interaction with a matrix) that provides incommensurably higher efficiency of HBP additives as modifiers in comparison to other types of polymeric modifiers.

The merits of HBP as highly effective and efficient modifiers are manifested to the maximum extent in polymeric composites characterized by high degree of filling with dispersed particles or fibers and in nano-composites [10, 11]. Indeed, when finely dispersed fillers (mineral particles, carbon microfibrinous dispersions, etc.) are used for composite reinforcement, aggregation of nano-filler particles represents the main problem to be handled. Such aggregation leads, on the one hand, to undesirable increase in size of the dispersed phase (filler efficiency goes down with increasing size of particles) and, on the other hand, to its nonuniform distribution in polymeric matrix of a composite. Both said increase in size and nonuniformity of distribution degrade the reinforcement effect. Aggregation is enhanced as filler concentration increases. Filler aggregation promotes the growth of initial composition viscosity at the stage preceding the polymeric matrix procession, which makes required technological steps more complicated.

Application of HBP represents an ideal approach for suppressing aggregation due to the upgraded level of thermodynamic compatibility of HBP and a wide range of opportunities for varying the set of functional groups on the periphery of macromolecules with the aim to ensure optimal interaction both with filler surface and with polymeric matrix of a composite having the best rheology of initial mixture (as compared to other polymeric additives).

HBP merits are multiplied when they are used in nano-composites because nano-sized fillers are characterized by an incommensurably higher tendency for clustering (i.e., aggregation) because of the more extended surface of such fillers.

### 8.3 Major Fields for Hyper-Branched Polymers Application

It is almost impossible to find an area in which HBP are not used at present. The efficiency of HBP is especially high when they are employed as modifiers of polymeric materials (structural and paint and varnish materials, organic glass, polymeric nano-composites, and the like), as polymeric base materials in electronics, micro-electronics, and current sources of new generation (insulators with extremely low dielectric permeability, polymeric electrolytes, semiconductors, polymeric plasmons),

**Table 8.3** Major fields of HBP application

Field of application	Achieved objective	Reference
1. Structural polymeric materials		
1.1. Highly cross-linked polymers (poly-epoxides, polyesters, etc.)	Degrading brittleness of cured polymeric matrices; improvement of rheology of initial uncured reaction system	[12, 13]
1.2. Highly filled composites (including dental composites); polymer–polymer composites (blends); porous materials	Surface modification of fillers, improvement of rheological properties of initial compositions, increasing the content of filler in a composite; improvement of morphological structure of polymer–polymer composites by enhancement of thermodynamic compatibility of components	[14, 15]
1.3. Organic glass (including polymeric optical materials)	Nanosized local reservoirs for functional additives (phototropic substances, dyestuffs, and so forth); superthin-layer functional coatings for organic glass surface; modification of morphological structure of glass via radical polymerization by using polyunsaturated HBP as cross-linking agents	[12, 16, 17]
2. Paints and varnishes, protective coatings; hermetics (sealing materials); laminates; thin-layer packaging materials, including nonimpact printing inks	Ecologically friendly (i.e., without organic solvents) materials, including water-based paints, photocuring, adhesion enhancement, degrading brittleness and level of internal stresses, improvement of properties (glossiness, etc.)	[14, 18, 19]
3. Printing paints	Flush cure effect as a result of UV radiation, improvement of properties	[19]
4. Highly efficient current sources of new generation	Highly efficient polymeric electrolytes; extremely thin (monomolecular, $\approx 10$ nm) antipolarization coatings for electrodes	[15, 20]
5. Polymeric nano-composites	Prevention of aggregation of nanoparticles (or metal particles) and, as a consequence, extremely uniform distribution of particles over material volume; improvement of properties	[21, 22]
6. Metal polymers		
7. Polyolefins, polycarbonates, and other crystallizing polymers	Nanosized nuclei of crystallization that are uniformly distributed within a polymer volume; these nuclei provide reduction of spherulite size, narrowing the function of their distribution within volume, and, as a consequence, enhancement of strength; reduction of melt viscosity; dyeing	[8, 9]

**Table 8.3** (continued)

Field of application	Achieved objective	Reference
8. Lubricant oils	Nano-containers dissolvable in oils and filled with nonsoluble additives (such as antioxidants)	[23]
9. Holography	Improvement of resolution capability when recording information by laser beam in a polymer volume in the form of holograms	[24]
10. Production of polymeric articles of microscopic size by means of radiation tools (micro-fabrication) for microelectronics and other fields of application	Upgrading the accuracy of micro-fabrication	[24]
11. Medicine, cosmetics, biology, biotechnology	HBP-based nano-containers for pharmacological preparations that provide either prolongation of preparation action or transportation of medications inside the human body	[14, 23, 25, 26]
12. Electronics		
12.1. Semiconductors, superconductors, ferromagnetic materials, insulation materials, electro-optical materials, light guides, materials for three-dimensional nano-electronics	Production of monolithic articles with very good volume distribution of functional particles; extending the potentialities of monolithization; production of functional materials in the form of HBP (hyper-branched copolymers with linking system on the basis of phenyl acetylene, and others)	[12, 16, 17, 27]
12.2. Polymeric plasmons and supersensitive analyzers on the basis of such plasmons	Production of polymeric plasmons from nanodispersed particles of Ag or Au synthesized by decomposition of organic compounds of these metals in nano-containers (micro-reactors) on the basis of HBP	[28]
13. Chemistry; chemical technology; supramolecular chemistry	Employment of HBP: (1) as initial polymers for the synthesis of technologically complicated nanostructured polymers; (2) as highly efficient reagents with increased local concentration of functional groups in organic synthesis; (3) as nano-containers in phase-transfer processes; (4) as carriers of catalytically active nano-clusters of metals (Pt, Au, Pd, etc.); (5) as agents for living radical polymerization and cross-linking agents; (6) instead of conventional micelles in supramolecular chemistry	[29–32]
14. Polymeric sensors	Enhancement of sensor sensitivity owing to creation of extremely thin sensor films with improved uniformity	[33, 34]

*Note.* Reviews and articles that contain generalizations are listed in this table.



as nanosized containers for functional additives (dyestuffs, phototropic substances, and the like for optical organic glass), as pharmacological nanosized containers in medicine, and as sensors for supersensitive analyzers for chemical and biochemical purposes. Various fields of practical application are listed in Table 8.3.

#### **8.4 HBP: Main Achievements and Problems to Be Solved Without Delay**

Discovery of the unique properties of hyper-branched macromolecules has led to rapid development of the HBP field during the past decade. So far, numerous options of synthesis of various HBP and methods of their identification have been developed. Topological specifics of HBP macromolecules responsible for their most important peculiar properties have been studied. Among those are high level of solubility and thermodynamic compatibility, low viscosity of solutions, resistance to aggregation in solutions (including concentrated solutions), and ability to function as nano-containers for substances sorbed inside macromolecules. The main topological feature of HBP is high-volume concentration of chain units inside macromolecules as a consequence of branching without cross-linking. Also, this volume concentration increases as the degree of branching increases. Hence, HBP are characterized by weak dependence (as compared to linear polymers) of hydrodynamic volume of macromolecules upon molecular weight, because the higher is the molecular weight, the more compact is the molecular packing. Such compact packing of HBP macromolecules and the large number of free ends of chains with functional groups on their periphery represent the main structural and physical reason for the unique properties of HBP.

Currently, in the field of HBP synthesis scientists have managed to successfully solve the main key problems using stepwise polymerization methods (polycondensation). As a result, unified synthesis options have been developed—some of them are so reliable and technologically streamlined that businessmen were able to quickly launch industrial production in Europe of certain HBP types: aliphatic polyesters and polyesteramides having different number of branching generations and a variable set of end functional groups (hydroxy in base types) and with different degree of substitution of aliphatic, epoxy, and other groups in modifiers for hydroxy groups.

In a very short period of time, HBP found application in various branches of industry. The scale of progress associated with HBP application is so large that one has grounds to state that a revolution has happened in polymeric material science [1].

Despite the huge array of data already obtained for HBP, the following problems still remain unsolved.

1. Development of those methods for chemical designing of HBP macromolecules of prespecified topology that provide synthesis of a wide range of HBP with purposefully varying the degree of branching, functionality, length, and nature of

interjunction bonds. Of special note is the tendency of developing HBP synthesis processes using methods of radical (chain) polymerization, which, in contrast to stepwise polymerization, allows varying both the topological structure of macromolecules and the set of functional groups over much wider limits.

2. Search for simple and well-controlled reactions of addition to functional groups of HBP (already produced industrially) for the purpose of their chemical modification. Also, using a comparatively narrow range of industrially produced HBP, it is also necessary to expand this range for specific conditions of practical application.
3. Development of methods for the identification of chemical and topological structure, as well as molecular parameters of HBP macromolecules.
4. Establishment of correlation between properties of HBP molecular level (chemical and topological structure, molecular parameters, functionality) with macroscopic properties (thermodynamic compatibility, sorption capacity, resistance to associative interaction, etc.).
5. Problem of HBP macromolecule interaction with glass-like (polyester, polyeoxy, polymethacrylate, etc.) and semicrystalline (polyolefin, polyamide, etc.) polymeric matrices. Solving this problem represents a necessary condition for the development of a scientific basis for the modification of polymeric materials by HBP additives.

## References

1. Korolev GV, Bubnova ML (2007) *Vysokomolek Soedin A* **49**:1357–1388 (in Russian)
2. Properties and applications of Boltorn<sup>®</sup> (2001) In: Pettersson B (ed) *Dendritic polymers*. Perstorp Speciality Chemicals AB, SE-284 80 Perstorp, Sweden. Boltorn<sup>®</sup>: Advancing performance & comfort. Perstorp Corp. [http://www.perstorp.com/upload/boltorn\\_002.pdf](http://www.perstorp.com/upload/boltorn_002.pdf). Accessed 22 June 2008.
3. Hybrane, DCM's hyperbranched polymer platform. DCM Corp. [http://www.dsm.com/en\\_US/downloads/hybrane/hybrane\\_molecule.pdf](http://www.dsm.com/en_US/downloads/hybrane/hybrane_molecule.pdf). Accessed 22 June 2008
4. Ratna D, Varley R, Singh Raman RK, Siman GP (2003) *J Mater Sci* **38**:147–154
5. Ratna D, Siman GP (2001) *Polymer* **42**:8833–8839
6. Ratna D, Varley R, Siman GP (2003) *J Appl Polym Sci* **89**:2339–2345
7. Flohlich J, Kautz, Thoman R et al (2004) *Polymer* **45**:2155–2164
8. Bergbreiter DE, Boren D, Kippenberger AM (2004) *Macromolecules* **37**:8686–8691
9. Xu G, Shi WF, Gong M et al (2004) *Eur Polym J* **40**:483–491
10. Ratna D, Becker O, Krishnamurthy R et al (2003) *Polymer* **44**:7449–7457
11. Rodlert M, Plummer CJG, Garamszegi L et al (2004) *Polymer* **45**:949–960
12. Granick S, Kumar SK, Amis EJ et al (2003) *J Polym Sci Polym Phys* **41**:2755–2793
13. Seiler M (2002) *Chem Eng Technol* **25**:237–253
14. Voit B, Beyerlein D, Eichhorn KJ et al (2002) *Chem Eng Technol* **25**:704–707
15. Hong CY, You YZ, Decheng WU et al (2005) *Macromolecules* **38**:2606–2611
16. Crooks RM (2001) *Chem Phys Chem* **2**:644–654
17. Kou HG, Shi WF (2004) *Eur Polym J* **40**:1337–1342
18. Dzunuzovic E, Tasic S, Bozic B et al (2005) *Prog Org Coat* **52**:136–143
19. Hu G, Shi WF (2005) *Prog Org Coat* **52**:110–111
20. Kong H, Luo P, Gao C et al (2005) *Polymer* **46**:2472–2485

21. Zou JH, Zhao YB, Shi WF et al (2005) *Polym Adv Technol* **16**:55–60
22. Abd-El-Aziz AS (2002) *Macromol Rapid Commun* **23**:995–1031
23. Gao F, Schricker SR, Tong YH et al (2002) *J Macromol Sci Pure Appl Chem* **39**:267–286
24. Kou HG, Asif A, Shi WF et al (2004) *Polym Adv Technol* **15**:192–196
25. Albertsson A-C (ed) (2002) *Adv Polym Sci* **157**:1–179
26. Siriba S, Frey H, Haag R (2002) *Angew Chem Int Ed* **41**:1329–1334
27. Kang SH, Luo JD, Ma H et al (2003) *Macromolecules* **36**:4355–4359
28. Siergers C, Biesalski M, Haag R (2004) *J Chem Eur* **10**:2831–2838
29. Jesberger M, Barner L, Stenzel MH et al (2003) *J Polym Sci Polym Chem* **41**:3847–3861
30. Kaanumalle LS, Gibb CLD, Gibb BC, Ramamurthy V (2004) *J Am Chem Soc Commun* **126**:14366–14367
31. Tomalia DA (2005) *Progr Polym Sci* **30**:294–324
32. Teertstra SJ, Gauthier M (2004) *Progr Polym Sci* **29**:277–327
33. Thompson CH, Hu J, Kaganove SN et al (2004) *Chem Mater* **16**:5357–5364
34. Belge G, Beyerlein D, Betsch C et al (2002) *Anal Bioanal Chem* **374**:403–411

## Appendix: Chapter 9

# Methods for Studying Three-Dimensional Free-Radical Polymerization and Cross-Linked Polymers

**Abstract** Chapter 9 will be useful for those who are wishing to master the field of three-dimensional free-radical copolymerization because it contains a general description of applicability of various methods used in analytical and physical chemistry for specific tasks: studying the kinetics and peculiarities of cross-linked polymers formation using the TFRP method.

Conventional and widely known methods for high-molecular compound chemistry that are described in detail in scientific publications are inapplicable for three-dimensional free-radical polymerization (TFRP) with formation of cross-linked polymers because the reaction medium is strongly structured, starting from small degrees of conversion (from the gel point), and produces polymers that are nonfusible and insoluble. Therefore, this chapter gives a brief description of well-proven experimental methods used to study TFRP kinetics and the mechanism as well as the structure and properties of cross-linked polymers.

### 9.1 Calorimetry

Precision isothermal microcalorimetry with the use of Calve calorimeters [1–3] appeared to be the most effective method for kinetic measurements for TFRP. The use of nonisothermal Differential Scanning Calorimetry (DSC) calorimeters followed by complex mathematical calculations of experimental data is less reliable.

Values of molar heat of polymerization are quite high ( $\Delta H = 42\text{--}49\text{ kJ/mol}$  [4]), and they are practically independent of conversion. Therefore, it is possible to continuously measure the rate of heat release  $dQ/dt$  in the course of polymerization with high accuracy, identifying this rate with the process rate  $W$ :

$$W = -\frac{d[M]}{dt} \equiv \frac{dQ}{dt} \quad (9.1)$$

The difference between the initial concentration of a monomer and its current concentration  $[M_0] - [M_t]$  is equal to the amount of released heat divided by molar heat of polymerization  $\Delta H$  of a given monomer. Taking into account that

$W = dC/dt$ , where  $C$  = conversion, we obtain  $C = \frac{G\Delta T}{\Delta H}$ , where  $G$  = thermal capacity of the reaction system, and  $\Delta T$  = heating value. Thus, from experimental curves of heat release  $\Delta T = f_1(t)$ , one can easily obtain kinetic curves:

$$C = \frac{G}{\Delta T} \cdot f_2(t)$$

In the case of copolymerization, when  $[M] = \sum_i [M_i]$  and  $\Delta H = \sum_i \Delta H_i$ , application of calorimetry for kinetic measurements is limited by azeotropic systems, because compositions of the monomer mixture and copolymer remain constant for these systems during copolymerization.

The majority of data published on kinetics of TFRP in block, solutions, and films were obtained through the use of calorimetric methods [1–3, 5–7].

The application of precision fast-response photocalorimeters [8] in combination with a monochromatic light delivery system enables one to take successive measurements after several seconds and, hence, to record kinetics of rapid TFRP processes not only in the stationary mode (i.e., under photoinitiation), but also in the posteffect mode at all stages of polymerization (especially in the area of high conversions) (photo-DSC). Such combination of stationary kinetic measurements and nonstationary measurements is necessary for calculating constants of elementary stages of chain propagation and termination rates ( $k_{pr}$  and  $k_{ter}$ , respectively) as a function of conversion. Results of calculations of this kind represent a component of a database required for the macromolecular design.

The application of DSC enabled researchers to identify local glass transition in the course of TFRP [9].

## 9.2 IR Spectroscopy

The method of infrared (IR) spectroscopy for determining the current concentration of double bonds has become the second most powerful method (after calorimetry) in terms of potentialities in the field of kinetic studies of TFRP. The RTIR (real-time infrared) version of this method appeared to be even more effective in terms of measurement speed than photocalorimetry. This method enables researchers to solve the same problems of stationary and nonstationary kinetics with time resolution being  $10^{-2}$ – $10^{-3}$  s [10–12].

The main source of error in the IR spectroscopy method as applied to TFRP is the distortion of spectrum shape resulting from growth of conversion due to matrix cross-linking, which is equivalent to calibration variation in the course of polymerization. Usually this problem is eliminated to a certain extent by choosing such spectral lines (as a basis) that are least susceptible to distortion with increasing conversion.

The application of the internal standard method makes it possible to avoid difficulties associated with measurement of film thickness [2].

The IR spectroscopy method could be effectively employed for studying kinetics of three-dimensional copolymerization and composition of cross-linked copolymers [7, 8, 11].

### 9.3 Other Methods of Kinetic Measurements

Densitometric methods for kinetic measurements appeared to be very convenient for TFRP purposes, especially for the case implying flotation and titration [13]. The gravimetric method, chemical analysis method (determination of double bond concentration), dilatometric method, and some other methods [1] have proved themselves to be very effective for studying radical polymerization. However, significant modification of these methods was required to adapt them for studying TFRP. The first two methods deal with monomers isolated from a reacting system. These methods require isolation procedure modification because conventional precipitation of the polymer is impossible because of cross-linking, while extraction may turn out to be incomplete due to the presence of “pendent” double bonds. Therefore, the isolation stage should be preceded by a stage of destruction [14, 15], which is a very labor-consuming and insufficiently selective process of destruction of inter-chain cross-links (e.g., via hydrolysis, if ester groups or other bonds, which are broken as a result of hydrolysis, are present in cross-links). The classical version of the dilatometric method is unsuitable for TFRP exploration because of loss of system fluidity at early stages of polymerization (with conversion being less than 1%). Dilatomers of special design are used, e.g., dilatomers in the form of long thin glass tubes (with a diameter of 2–3 mm and height of 500–1000 mm), elastic dilatomers, and others. Differential dilatometric installation [16] having two elastic cells and a displacement-detection precision sensor (of mechanotron type) appeared to be the most effective design option (although very complex in terms of hardware components). It was exactly this installation that enabled researchers to take the first nonstationary kinetic measurements of TFRP processes [1 (p. 148); 17].

Recently, specific methods have gained acceptance in which TFRP development is detected based on indirect features associated with viscosity growth, which leads to retardation of molecular mobility of reaction system components, e.g., unreacted monomer [the nuclear magnetic resonance (NMR) method] [18, 19], or additives of substances specially introduced as a molecular probe (fluorescent methods [20, 21]). Also, substances capable of isomerization during TFRP [22] are used as a molecular probe. If the activation volume during isomerization is large enough, the isomerization rate can serve as a measure of free volume in the polymerization system and, hence, characterize conversion indirectly. The application of such isomerizing substances as azobenzene and stilbene as photochromic probes has allowed us not only to monitor the growth of conversion during TFRP but also to draw conclusions regarding the character of function of free volume distribution in a system as well as identifying the microheterogeneous structure of the formed polymeric network [22].

## 9.4 Light Scattering

Methods that are based on light scattering play a special role in studying the TFRP mechanism because they enable researchers to observe the evolution of structural microheterogeneity in the course of TFRP [6, 23–25]. Methods of static and dynamic light scattering are employed for estimating the size of highly branched macromolecules and microgels in pre-gel state [26–28].

## 9.5 EPR

Free radicals  $R^\bullet$  in structured reaction media are characterized by long lifetimes ( $\tau_R$ ), which is why direct measurement of  $R^\bullet$  concentrations by the EPR method is possible for TFRP [3, 6, 29–43]. The application of the EPR method appeared to be most effective for the following scientific directions: studying the kinetics of accumulation and decay of free radicals and structural and physical studies.

### 9.5.1 Studying the Kinetics of Free-Radical Accumulation in Nonstationary Mode [33, 34]

In the case of thermal decomposition of initiators (organic peroxides) in partially cured oligo(acrylate) (with conversion being within 30–70%), it is possible to select such an experimental temperature at which the EPR method is capable of recording (during a period of 10–20 min) the  $R^\bullet$  accumulation kinetics described for the nonstationary mode by the following classical formula:

$$\sqrt{\frac{W_i}{k_{ter}}} \operatorname{th}(W_i k_{ter} t) \quad (9.2)$$

For small values of time  $t \leq 0,3/\sqrt{W_i k_{ter}}$ , this formula is approximated by the following relationship

$$[R^\bullet] \approx W_i t \quad (9.3)$$

while for high values of time  $t > 1/\sqrt{W_i k_{ter}}$ , by relationship

$$[R^\bullet] \approx \sqrt{\frac{W_i}{k_{ter}}} \quad (9.4)$$

which allows calculating  $W_i$  and  $k_{ter}$  based on obtained experimental data. If initiator and temperature were selected so that upon attainment of stationary value of  $[R^\bullet]$  a slow decline of  $[R^\bullet]$  is observed (for high values of time) due to initiator

consumption, then, knowing the kinetics of this decline, one can in addition find the constant of thermal decomposition rate of initiator  $k_{dec}$ . In this case it would be also possible to estimate the initiation efficiency:

$$f = \frac{k_i}{k_{dec}} = \frac{W_i}{[I]k_{dec}} \quad (9.5)$$

where  $[I]$  = initiator concentration; and  $k_i$  = initiation rate constant determined by relationship  $W_i = k_i [I]$ .

Thus, this method enables researchers to determine the values of  $k_i$ ,  $k_{dec}$ ,  $k_{ter}$ , and  $f$  for TFRP in the case of high conversion and, hence, to evaluate the influence of cross-linking on the processes of chain initiation and termination. It appeared that for oligo(acrylates), as conversion increases from 0 to 70–90%, the value of  $k_{ter}$  decreases 106–107 fold, while  $f = 25$ –50 fold for organic peroxides and 250–500 fold for initiators of azonitrile type [33, 34].

### 9.5.2 Studying the Kinetics of Decay of Accumulated Free Radicals [35]

Photochemical or radiative initiation is used for studying the kinetics of accumulated (trapped) free radicals to avoid undesirable thermal generation of  $R^\bullet$  during EPR measurements. Important regularities have been established through the use of the EPR method. First, it was found that kinetics of  $R^\bullet$  decay is described by complex dependence  $[R^\bullet] = f(t)$ , the graph of which has bends in points  $t_1, t_2, \dots, t_i (i = 2-4)$ . Kinetics of curve sections between bends is well described by the following classical expression:

$$-\frac{d[R^\bullet]}{dt} = (k_{ter})_i [R^\bullet]^2 \quad (9.6)$$

where  $(k_{ter})_1 > (k_{ter})_2 > \dots > (k_{ter})_i$ .

Second, the numerical value of  $(k_{ter})_i$  correlates with conversion value and depends on the nature of molecules of the initial network-forming monomer (oligomer). Factors controlling flexibility of oligomeric blocks play the main role in these correlations. In a macromolecular network, oligomeric blocks function as interjunction chains connecting long carbon chains—that is, they perform the function of interchain cross-links. The most important among these factors are length of oligomeric block and presence of interatomic bonds characterized by lowered barriers of rotation (e.g., substitution of C—O—C groups for C—C groups) lead to flexibility enhancement. The analysis of kinetics of trapped  $R^\bullet$  decay not only allows exploring the TFRP mechanism, but also enables obtaining structural and physical information: bends on curves  $[R^\bullet] = f(t)$  are indicative of microheterogeneity of the highly cross-linked polymeric matrix, and numerical values of  $(k_{ter})_i$  serve as a measure of network structure relaxation at the molecular level [1, 35].



### 9.5.3 Method of Synchronous Comparison of Continuously Recorded Kinetic Curves $[R^\bullet] = f_1(t)$ and $W = f_2(t)$ [37]

Any continuous method (preferably, the method of precision kinetic calorimetry) is used to measure polymerization rate  $W = f_2(t)$ .

$$W = k_{pr}[R^\bullet][M] \quad (9.7)$$

The current concentration of free chain carrier radicals can be calculated from current TFRP rate and current concentration of monomer  $[M]$  as follows:

$$[R^\bullet]_2 = \frac{W}{k_{pr}[M]} \quad (9.8)$$

The value of  $[R^\bullet]_2$  may appear to be arbitrarily lowered in comparison to the value of  $[R^\bullet]_1$  determined using the EPR method because  $[R^\bullet]_2$  is the concentration of only those radicals that at this moment in time are capable of participating in the chain propagation reaction  $R^\bullet + M \rightarrow RM^\bullet$ .

If a certain fraction of radicals by this moment has lost the ability to participate in the reaction for any reasons (e.g., due to fixation in a highly cross-linked polymeric matrix), synchronous comparison of  $[R^\bullet]_1$  measurement results by the EPR with results of calculations using kinetic data  $[R^\bullet]_2$  enables one to determine the fraction of radicals that have lost their activity in a wide range of conversions and, hence, to establish regularities of  $\gamma_R$  variation in the course of TFRP.

$$\gamma_R = \frac{[R^\bullet]_1 - [R^\bullet]_2}{[R]_1} \quad (9.9)$$

### 9.5.4 Structural and Physical Studies Using EPR

The spin-probe version of the EPR method is successfully applied for studying the structure of cross-linked polymers that are TFRP products, the microredistribution phenomenon, and topological features of deep stages of TFRP.

Paramagnetic probing is based on introducing molecules of stable radical (as a rule, nitroxyl radical) into a medium to be studied (these molecules serve as a probe) and taking measurements of correlation time  $\tau_c$  of rotational oscillations of these molecules in terms of EPR spectrum shape. The value of  $\tau_c$  depends upon medium properties regulated by molecular mobility, and, hence, it is a carrier of information on intensity of molecular motion in those micro-volumes, where paramagnetic probe molecules are localized. Stable nitroxyl radicals were introduced into cross-linked polymer via sorption from vapor or into initial oligomer before the beginning of polymerization followed by regeneration of probe molecules in the polymer from adduct  $\text{>NO}^\bullet\text{-M-}$ , where  $\text{-M-}$  = a fragment of the polymeric chain.

The spin-probe version of the EPR method enabled us to establish microheterogeneity of cross-linked oligo(acrylates) polymer structure [38, 39], to demonstrate structural heterogeneity of the intergrain layer material [40], to find microredistribution of initiator [41] and adduct  $\text{>NOB}_i$  of stable nitroxyl radical and cyanisopropyl radical  $\text{R}^\bullet$  during TFRP of various oligomers [42], and to discover a phenomenon of selective inhibition of radical polymerization by nitroxyl radicals at the monolithization stage [43].

## 9.6 NMR

Nuclear magnetic resonance (NMR) appeared to be an effective method for studying the chemical structure, molecular mobility, and intermolecular interaction in high molecular weight compounds. However, application of this method for TFRP products is limited because of the insolubility and infusibility of these products. Pulse NMR, broadband NMR, and  $^{13}\text{C}$ -NMR characterized by high resolution with cross-polarization and under magic angle spinning appeared to be the most effective among the small number of NMR options [18, 19, 21, 31, 44–46].

Usually the broadband NMR method is used for determining temperature dependence of the second moment of NMR spectrum lines in a wide range of temperatures. Analysis of this dependence enables us to draw conclusions on the presence of relaxation transitions and make an estimate of the corresponding energies of activation. Studying the model set of oligo(acrylates) polymers with prespecified modification of structure by the  $^{13}\text{C}$ -NMR method characterized by high resolution with cross polarization and under magic angle spinning gave data on configuration of units in a polymeric network and on structural microheterogeneity, manifested as shown in broadening of spectral lines [6, 45].

## 9.7 Physicomechanical and Thermo-Mechanical Methods

When TFRP products are deformed ( $\epsilon$ ) in the axial compression mode under low rate ( $\dot{\epsilon} = 10^{-4} - 10^{-3} \text{c}^{-1}$ ), researchers can record deformation curves in the range  $0 \leq \epsilon \leq 0.5$  that includes region of transition from Hooke's deformation to the forced-elastic one. Analysis of deformation curves in this transition region allows drawing substantiated conclusions about structural features of highly cross-linked polymers (including microheterogeneity). Thermos-mechanical curves  $\epsilon = f(T)$  in the area of  $\alpha$ -transition are also suitable for the similar analysis.

For oligo(acrylates), physicomechanical and thermo-mechanical measurements were taken using precision installations of special design [47] intended for exploring mini-samples (weighing  $\approx 0.1 \text{ g}$ ). A large number of oligo(acrylates) of various types (including those oligo(acrylates) the synthesis of which is possible only in laboratory conditions and which could be synthesized only in small amounts) were explored via such measurements.

Dynamic physicochemical measurements are also very useful for structural studies of TFRP products. In this case, researchers usually analyze spectra of relaxation times. It was found that a degree of structure microheterogeneity correlates with spectra width in a certain frequency domain [48].

## 9.8 Volumetric Method

The volumetric method was employed for studying kinetics of oxidative polymerization (oxidation) of compounds of vinyl (allyl) type by absorption of oxygen at low conversions in block and in solutions, and also in films (including deep stages of TFRP). A design of volumetric installation for taking measurements at low conversion [49] and design of improved circulation volumetric installation for taking measurements during TFRP in films under specified conditions of partial pressure of oxygen, temperature, and film thickness [50] appeared to be the most suitable designs.

## 9.9 Complex Methods

Three-dimensional free-radical polymerization involves concurrently proceeding chemical transformation (radical polymerization) and a number of physical transformations (aggregation, microsineresis, etc.) actively influencing the chemical process. Therefore, complex methods are most effective for studying TFRP because they allow both taking kinetic measurements and identifying structural variation stages in the course of polymerization or structural features of final polymeric products [3, 6, 8, 21, 26–28, 36, 51–60].

Successes in studying TFRP mechanism and its main feature, namely, microheterogeneity, are mainly determined by the development and application of a set of methods including more than 10 kinetic and structurally physical methods [3, 6]. For instance, such combined techniques as application of spectrum turbidimetry together with calorimetry, use of a modified calorimeter equipped with a cell intended for taking measurements of dielectric permeability, and molecular labels and employment of IR spectrometric monitoring of three-dimensional copolymerization kinetics [36, 55] have been developed to obtain structurally physical and kinetic information directly during polymerization. In some cases, in addition to combining known methods, researchers also developed unique methods. Detection of local microredistribution of initiator via radiation probing in combination with diffusion probing by molecules of paramagnetic NO [3, 6, 39, 41] represents one of such methods.

Exploration into TFRP using complex methods is becoming more and more intensive nowadays [8, 21, 26–28, 56–58, 61–64]. The combinations of various methods employed to study three-dimensional free-radical copolymerization are presented in a review [65].

## References

1. Berlin AA, Kefeli TYa, Korolev GV (1967) Poly(esteracrylates). Nauka, Moscow (in Russian)
2. Mogilevich MM (1977) Oxidative polymerization in film-formation processes. *Khimiya (Chemistry)*, Leningrad
3. Berlin AA, Korolev GV, Kefeli TYa, Sivergin YuM (1983) Acrylic oligomers and materials on the acrylic oligomers. *Khimiya*, Moscow (in Russian)
4. Bagdasaryan XS (1966) Radical polymerization theory. Nauka, Moscow (in Russian)
5. Mogilevich MM, Pliss EM (1990) Oxidation and oxidative polymerization unsaturated compounds. *Khimiya (Chemistry)*, Moscow (in Russian)
6. Korolev GV, Mogilevich MM, Golikov IV (1995) Cross-linked polyacrylates: micro-heterogeneous structures, physical networks, deformation-strength properties. *Khimiya*, Moscow (in Russian)
7. Korolev GV (2003) *Usp Khim* **72**:222–244 (in Russian)
8. Wen M, Scriven E, McCormick AV (2002) *Macromolekules* **35**:112–120
9. Semyannikov VA, Belgovskiy IM, Mogilevich MM et al (1989) *Vysokomolek Soedin A* **31**:1602–1607 (in Russian)
10. Decker C (1994) *Acta Polymer* **43**:333–347
11. Decker C (2002) *Polym Int* **51**:1141–1150
12. Decker C (1998) *Polym Int* **45**:133–141
13. Houben-Weyl (1955) *Method Org Chem* **3/1**:188
14. Mogilevich MM, Arkhipov MI (1962) *J LKM* **1**:57–60 (in Russian)
15. Azo G (1959) *J Polym Sci* **39**:475–486
16. Tvorogov NN, Korolev GV (1964) *Vysokomolek Soedin* **6**:877–883 (in Russian)
17. Tvorogov NN, Korolev GV (1964) *Vysokomolek Soedin* **6**:1006–1011 (in Russian)
18. Baidin IS, Budanov NA, Shapiro YuE et al (1989) *Vysokomolek Soedin A* **31**:1394–1397 (in Russian)
19. Budanov NA, Baidin IS, Shapiro YuE et al (1988) *Vysokomolek Soedin A* **30**:1544–1550 (in Russian)
20. Okay O, Kayo D, Pekcon O (1999) *Polymer* **40**:6179–6187
21. Jager WF, Lungu A, Chen DY, Neckers DS (1997) *Macromolekules* **30**:780–791
22. Anseth KS, Rothenberg MD, Bowmav CN (1994) *Macromolekules* **27**:2890–2892
23. Volkova MV, Belgovskiy IM, Mogilevich MM et al (1987) *Vysokomolek Soedin A* **29**:435–440 (in Russian)
24. Vasilyev DK, Belgovskiy IM, Mogilevich MM et al (1989) *Vysokomolek Soedin A* **31**:1233–1237 (in Russian)
25. Rey L, Galy J, Soutereau H (2000) *Macromolekules* **33**:6780
26. Sun X, Chiu YY, Lee LJ (1997) *Ind Eng Chem Res* **36**:1343–1351
27. Lin L, Yu TL, Cheng CH (1999) *Macromolekules* **32**:690–696
28. Szuromi E, Berka M, Borbely J (2000) *Macromolekules* **33**:3993–3998
29. Doetschman DC, Mehlenbacher RC (1996) *Macromolekules* **29**:1807–1815
30. Selli E, Oliva C (1996) *Macromol Chem Phys* **197**(2):497
31. Kamachi M, Kajiwara A (1996) *Macromolekules* **29**:2378–2382
32. Schlick S, Pilar J, Kweon S-C et al (1995) *Macromolekules* **28**:5780–5788
33. Korolev GV, Smirnov BR (1964) *Vysokomolek Soedin* **6**:1140–1144 (in Russian)
34. Korolev GV, Smirnov BR, Bashkirova SG et al (1964) *Vysokomolek Soedin* **6**:1256–1260 (in Russian)
35. Korolev GV, Smirnov BR, Bolkhovitinov AB (1962) *Vysokomolek Soedin* **4**:1660–1664. (in Russian)
36. Pereira SG, Telo JP, Nunes TD (2008) *J Mater Sci Mater Med* doi: 10.1007/s10856-008-3434-1
37. Korolev GV, Smirnov BR, Makhonina LI (1965) *Vysokomolek Soedin* **7**:1417–1421 (in Russian)

38. Golikov IV, Berezin MP, Mogilevich MM et al (1979) *Vysokomolek Soedin A* **21**:1824–1830 (in Russian)
39. Lagunov VM, Smirnov BR, Korolev GV et al (1987) *Vysokomolek Soedin A* **27**:1442–1446 (in Russian)
40. Lagunov VM, Berezin MP, Korolev GV et al (1981) *Vysokomolek Soedin A* **23**:2747–2751 (in Russian)
41. Lagunov VM, Berezin MP, Korolev GV et al (1985) *Vysokomolek Soedin A* **27**:2056–2060 (in Russian)
42. Ilyin AA, Golikov IV, Korolev GV (1990) *Vysokomolek Soedin A* **32**:243–250 (in Russian)
43. Lagunov VM, Golikov IV, Korolev GV (1982) *Vysokomolek Soedin A* **24**:131–137 (in Russian)
44. Volkova NN, Sosikov AI, Korolev GV et al (1988) *Vysokomolek Soedin A* **30**:2133–2140 (in Russian)
45. Sivergin YuM, Kireyeva SM, Grishina IN (2001) *Khim Phys* **20**:50–54
46. Heatley F, Platsitsip Y, Mellugh N et al (1995) *Polymer* **36**:1859–1867
47. Berezin MP, Korolev GV (1980) *Vysokomolek Soedin A* **22**:1872–1878 (in Russian)
48. Kannurpatti AR, Anseth JW, Bowman CN (1998) *Polymer* **39**:2507–2513
49. Tsepalov VF (1964) *Zavodsk Labor* **30**:111 (in Russian)
50. Mogilevich MM, Sukhanov GA (1973) *J LKM* **2**:53–55 (in Russian)
51. Rostchupkin VP, Ozerkovskiy BV, Kalmykov YuB et al (1977) *Vysokomolek Soedin A* **19**:699–706 (in Russian)
52. Rostchupkin VP, Kocheryavinskiy VV, Selskaya OG et al (1971) *Vysokomolek Soedin B* **13**:317–318 (in Russian)
53. Kocheryavinskiy VV, Karapetyan ZA, Rostchupkin VP et al (1975) *Vysokomolek Soedin A* **17**:2425–2433 (in Russian)
54. Rostchupkin VP, Ozerkovskiy BV, Karapetyan ZA (1977) *Vysokomolek Soedin A* **19**:2239–2245 (in Russian)
55. Kurmaz SV, Rostchupkin VP (1977) *Vysokomolek Soedin A* **19**:1557–1564 (in Russian)
56. Jager WF, Norder B (2000) *Macromolekules* **33**:8576–8582
57. Kannurpatti AK, Bowman CN (1998) *Macromolekules* **31**:3311–3316
58. Bowman CN, Peppas NA (1991) *J App Polym Sci* **42**:2013–2018
59. Lu H, Lovell LG, Bowman CN (2001) *Macromolekules* **34**:8021–8025
60. Cardona F, Rogers D, Van Erp G (2007) *J Thermoplast Comp Mater* **20**:601–615
61. Morgan DR, Kalachandra S, Shobha HK et al (2000) *Biomaterials* **21**:1897–1903
62. Drozdowski M, Lapsa K et al (1998) *J Mod Struct* **450**:129–134
63. Havad N, Dargent E, Lebaudy P et al (2000) *J Therm Anal Calor* **61**:701–709
64. Fitz BD, Mijovic I (1999) *Macromolekules* **32**:4134–4140
65. Rostchupkin VP, Kurmaz SV (2004) *Usp Khim* **73**:247–273 (in Russian)

# Index

- Alkoxyamines, as initiators in living TFRP, 87–93
- Associates  
computer modeling, 38, 41  
kinetically active, 35, 37, 38, 39, 40, 54  
in TFRP, 35–41
- Auto-acceleration  
living TFRP, 97  
oxidative polymerization, 55–56, 59  
TFRP, 41–46  
TFRP equation, 76  
TFRP-gel-effect comparison, 152–154
- Auto-deceleration  
TFRP, 19, 41–46  
TFRP equation, 76  
TFRP, solvent effect, 51
- Avrami equation, 7, 8
- Boltorn<sup>®</sup>, HBP, 243, 244, 245, 246
- Cage effect, in living TFRP, 91
- Carrier network, 176, 177, 178, 182, 184
- Chains length regulation by  
CTC, 212, 213  
inhibitors, 17, 205, 212, 230–231  
initiation rate, 206–211  
intrachain reactions, 226–230
- Chains length regulation, 205–231
- Computer modeling of liquid associates, *see*  
Associates, computer modeling
- Constant(s)  
copolymerization, 87, 111, 118, 123, 127,  
188, 190, 191, 221, 222, 236  
initiation, 35, 83, 130, 134  
propagation, 35, 36, 41, 77, 132, 142  
termination, 35, 36, 37, 144  
transfer, 130, 134
- Copolymer, cross-linked  
elasticity moduli equation, 15, 103, 106,  
170, 172, 175, 179, 180
- forced-elastic state, 102, 106, 172–181,  
182, 183, 184, 193–195
- glassy state, 42, 102, 104, 108, 172, 176,  
177, 178, 179, 180, 181, 182, 184,  
186, 189
- high-elastic state, 185–195
- oligo(acrylate)-MMA, 35, 36, 158–166,  
260
- oligo(carbonate)-MMA, 159, 160, 163,  
164
- snake-cage structure, 180, 188, 192, 194
- styrene, 87–93, 173, 174
- tEGdMA-BA, 112, 188, 193
- tEGdMA-BMA, 116
- tEGdMA-DDMA, 116
- tEGdMA-MMA, 116, 199
- tEGdMA-styrene, 108, 115, 197
- tEGdMA-VA, 192
- Copolymerization  
constants variability, 111–112  
glass-transition effect, 120–121  
kinetic peculiarities, 111–118  
kinetic study, 111–127  
in living chains conditions, 87–93  
microheterogeneity, 5, 27, 47, 75, 77, 78,  
100, 107, 116, 117, 184, 185, 186, 190,  
191, 196, 260, 261, 263, 264  
with oxygen, 230–231  
steric effect, 38, 112, 117, 145, 146, 159  
topological peculiarity, 4, 14, 100, 104,  
106, 130, 177, 180, 181, 182, 186,  
234, 236
- Critical conversion  
for copolymerization, 136–145, 154–155  
experimental detection, 141, 152–155  
experimental verification, 97–98, 132,  
133, 137  
Flory–Stockmayer equation, 153, 154

- for living chain radical polymerization, 136–143
  - for living TFRP, 136–143
  - novel equation for TFRP, 133–136
  - for TFRP, 131–133
  - traditional equation for TFRP, 137
- Cross-linked poly(acrylates), 157–199
  - degree of micro-nonhomogeneity, 171
  - network model, *see* Network model; Model of, networks of physical and chemical bonds in polymeric solid structure, 166–181
- CTC, 212
  - co-macrocycles, 212
- Cyclization in TFRP
  - copolymerization, 181
  - DB parameter, 201
  - in HBP, 204
  - in living chains mode, 191
- Dendrimers, 109, 201, 202
- Design of macromolecules, *see* Macromolecular design
- Diffusion control
  - oxidative polymerization, in, 55
  - rate constants, on, 41–42
- Dimethacrylates
  - copolymerization, 87–93
  - inhibited TFRP, 46–47
  - TFRP kinetics, 108, 144
- Divinyl benzene, copolymerization, 154–155
- Flory–Stockmayer critical conversion for polycondensation, 131
- Frank-Rabinovich cage, 91
- Gel effect
  - local in TFRP, 23
  - for monounsaturated, 117, 181
  - for poly(unsaturated), 4, 13, 130, 145, 151
- Glass transition
  - cross-linked copolymer, 4, 17, 170
  - cross-linked polymer, 186, 192
  - HBP effect, 249
  - living TFRP, 4, 30, 77, 258
  - local, 4, 6–7, 23–24, 170, 186, 258
- Grains, 5, 29
  - accretion, 4, 12–17
  - cores, 24
  - growth, 7–12
  - layers intergrains, 20, 30–31
  - penetrating chains, 4, 23
  - shell, 10, 51
  - structural parameters, 10, 11
  - structure, 30, 76
  - zones of contacts, 4, 10, 17, 25, 49
- HBP, applications, 243, 250
  - fillers stabilizer, 250
  - modification of substrate structure, 246, 248
  - nano-containers, 249, 252, 253
- HBP, problems for solution, 253–254
- HBP, properties, 243–248
  - sorption, 243, 248
  - surface, 247
- HBP, structure, 243, 244–248
  - core-shell, 243
  - DB parameter, 201
  - generations number, 244–245
  - gyration radius, 208, 214, 235, 238
  - hydrodynamic radius, 209, 235
  - Mark–Houwink parameter, 208
  - polymer chain length, 55, 205–231
  - viscosimetric radius, 235
- HBP, synthesis
  - TFRP via living polymerization, 231–238
  - TFRP via regulation of chains length, 205–231
- HBP, viscosity, *see* Viscosity, HBP solutions
- Highly cross-linked polymer particles, *see* Grains
- Hybrane<sup>®</sup>, HBP, 244, 246, 247, 248
- Inhibitor
  - effective, 46–47, 112
  - in HBP synthesis, 230
  - ideal, 48–49, 50
  - local, for TFRP study, 46
  - low-effective, 49, 50
  - nitroxyl radical, 15, 24, 263
  - oxygen, 60, 230–231
  - synergist, 50–51
  - TNT, 14, 49, 153
- Intergrains layers, 27–31
  - effect on properties, 29
  - structure, 11
- Intermolecular interactions system, *see* Network model, physical bonds network
- Intramolecular cross-linking, *see* Cyclization in TFRP
- Junctions of physical network
  - breaking, 177
  - stabilization/cooperation, 176
  - strong, 175, 176
  - weak, 176

- Kharasch, M.S., 85
- Kinetic regularities  
of living TFRP, 97, 100  
of TFRP, 42–43, 75, 97, 100
- Living chains conditions  
for anionic polymerization, 82  
for radical polymerization, 3
- Living chains radical polymerization  
atom transfer, 81, 85, 233  
nitroxide-mediated, 81, 83  
reversible addition, 81, 83, 84, 94, 97
- Living TFRP  
comparison with conventional, 152–155  
comparison with stepwise, 262  
copolymerization, 87–93, 136, 143, 154  
initiators for, 206  
peculiarities, 46, 75, 82, 103–104, 106, 180, 184, 190  
products properties, 20, 69, 73  
tool for macromolecular design, 75–78
- Macromolecular design  
living TFRP, 99–109  
TFRP, 75–78
- Mechanism of  
auto-acceleration, 41–46  
auto-deceleration, 41–46  
chain transfer catalysis, 211–226  
intrachains reactions of chain carrier radicals, 226–230  
oxygen effect, 60–61, 67, 70  
physical and chemical bond networks  
effect on properties, 159, 166  
polycondensation, 129, 133  
solvent effect, 51, 52
- Mechanism of polymerization  
living TFRP, 81–99  
radical, 3–29  
study method, 257–264  
TFRP, 3–29
- Medium of TFRP  
at late stage, 51  
in oxidative polymerization, 66, 67, 76  
solvent, 51  
structured, 46, 49
- Metal transitions complexes, *see* Transition metals complexes, as initiators in living TFRP
- Method of calculation of copolymer composition  
novel, 133–136  
traditional, 131–133
- Method calculation of critical conversion  
generating functions, 134, 135, 136  
moments in numerical form, 130
- Method of calculation of TFRP  
microheterogeneity, 3–29  
computer, 38, 75
- Method, experimental  
densitometry, 100–101, 174, 178, 181, 259  
dilatometric, 185, 259  
DSC, 23, 24, 30, 257, 258  
EPR, 260–263  
fluorescent spectroscopy, 259  
GPC, 154, 209, 214, 228, 229  
IR spectroscopy, 258–259  
light scattering, 260  
mass spectrometry, 226–227  
microcalorimetry, 257–258  
NMR, 263  
physicomechanical, 263–264  
radiation probing, 107, 264  
selective inhibition, 15, 259, 263  
spectroturbidometry, 7  
thermo-mechanical, 263–264  
transmission electron microscopy, 210  
vapor sorption, 25, 26, 108, 199  
viscosimetry, 131, 209, 214, 220  
volumetry, 264
- Microheterogeneity  
inhibited TFRP, 46–51  
living TFRP, 81–99  
solvent effect, 51  
TFRP, 3–29  
TFRP model, *see* Model of, microheterogeneous TFRP
- Microheterogeneous reaction medium, *see* Medium of TFRP, structured
- Micro-nonhomogeneous reaction medium, *see* Medium of TFRP, structured
- Microredistribution, 22–23, 49  
of initiator, 22–23, 86–87, 263
- Microsyneresis, 17–20
- Model of  
layered for oxidative polymerization, *see* Oxidative polymerization, layered model  
microheterogeneous, 4  
microheterogeneous experimental proof, 3  
microheterogeneous TFRP, 3, 46  
microheterogeneous TFRP, computer, 33, 40–41, 77, 78  
networks of physical and chemical bonds in polymeric solid, 166, 173, 176–177



- Smolukhovsky, 77
- three-dimensional oxidative polymerization, 230
- Monolithization, *see* Grains, accretion
- Morphological structure
  - living TFRP, 107, 181, 250, 251
  - in TFRP, 107
- Nano-containers, HBP, 201, 249, 252, 253
- Nanostructured polymers, 237–238
- Network model
  - chemical bonds network, 166–172
  - model verification, 38, 60, 61, 157, 182, 231
  - physical bonds network, 158
  - with the regard of cyclization, 181–185
  - structure–property relations, 244–248
- Oligo(acrylates)
  - copolymerization, 55, 118–127
  - inhibited TFRP, 46
  - oxidative copolymerization, 55
  - oxidative polymerization, 55, 59
  - physicomechanical properties of polymeric solid, 263
  - polymerization, 35
  - TFRP kinetics, 33–78
- Oligo(carbonates)
  - copolymerization, 88, 159, 164
  - copolymerization in living chains mode, 85, 87–93
  - physicomechanical properties of polymeric solid, 158–166, 263
- Oxidative polymerization
  - allyl compounds, 66–75
  - allyl–vinyl comparison, 66
  - autocatalysis, 55, 56–57, 59
  - layered model, 57, 59, 60, 68, 71
  - vinyl compounds, 55–60
- Pendent double bonds, 4, 42, 46, 99, 106, 133, 145–150, 151, 152, 153, 181, 190, 216, 225, 259
- Peripheral surface layers, *see* Grains, shell
- Polymer coils, 4, 5, 6, 23
- Polymerization rate
  - anomalies, 35–41, 180
  - equation, 8
  - in films, 54–75
  - influence on, 34, 35
  - inhibition mode, 152–153
  - initial stage, 7–12, 34
  - solvent effect, 51–54
- Polymeric grains, *see* Grains
- Probing molecules
  - AIBN, 48
  - comonomer, 38, 78, 100
  - nitrogen oxide, 22
  - oxygen, 230
  - photochromic, 259
  - regenerating radicals, 25, 26–27
  - solvent, 222
  - stable radicals, 97, 262
  - surfactants, 9, 54, 248
  - TEMPO, 15, 87, 88
  - vapor sorption, 24–25, 108, 199
- Properties, mechanical
  - copolymers, 157–199
  - living TFRP products, 94, 97
  - polymer, 157–199, 244
  - TFRP, final stage, 9, 12–17, 107
  - TFRP, initial stage, 4
- Properties sorption
  - TFRP, final stage, 9, 107
  - TFRP, initial stage, 77–78, 100, 145, 259
- Scheme
  - allyl oxidative polymerization, 66
  - atom-transfer living chains radical polymerization, 85
  - HBP Boltorn<sup>®</sup> modification, 246
  - living TFRP, 81–109
  - living TFRP kinetic, 83
  - radical polymerization kinetic, 33–78
  - reversible addition living chains radical polymerization, 83, 97
  - vinyl oxidative polymerization, 55
- Self-contained micro-reactors, *see* Grains
- Semenov, N., 37
- Stable radical, nitroxyl, as initiator, 23
- State
  - forced elastic, 102, 172–181
  - glassy, 42, 102, 108, 172, 175, 176, 177, 178, 179, 180, 181, 182, 184, 186, 189
  - highly elastic, 193–195
- Steric effect, in copolymerization, 112, 117
- Szwarc, Michael, 82
- TFRP
  - general kinetic scheme, 112
  - general regularities, 189
  - in living chains conditions, *see* Living TFRP
  - peculiarities, 16, 40, 46
  - topology formation, 81, 106, 206, 216
- Transition metals complexes, as initiators in living TFRP, 85, 86

Tri(ethylene glycol) dimethacrylate  
copolymerization, 87–93  
in living TFRP, 93–97  
polymeric solid, 174, 184  
polymerization, 10, 13, 21, 22, 48, 54, 93  
polymerization inhibited, 47, 48  
solvent effect, 51

Viscosity  
HBP solutions, 209  
local, 4  
oligomers, 34–35, 54

Zones of grains contact, *see* Grains, accretion